



# RESEARCH

2009-14

Implementation of Intelligent Compaction  
Performance Based Specifications in Minnesota

Take the



steps...

*Research...Knowledge...Innovative Solutions!*



**Transportation Research**

## Technical Report Documentation Page

1. Report No. MN/RC 2009-14	2.	3. Recipients Accession No.	
4. Title and Subtitle Implementation of Intelligent Compaction Performance Based Specifications in Minnesota	5. Report Date July 2009		6.
	7. Author(s) David White, Pavana Vennapusa, Jiake Zhang, Heath Gieselman, Max Morris		
9. Performing Organization Name and Address Earthworks Engineering Research Center Dept. of Civil, Construction and Environmental Engineering Iowa State University 2711 South Loop Drive, Suite 4700 Ames, Iowa 50010-8664	8. Performing Organization Report No. EERC 09-02		10. Project/Task/Work Unit No.
	11. Contract (C) or Grant (G) No. (c) 89256 (wo) 2		
12. Sponsoring Organization Name and Address Minnesota Department of Transportation 395 John Ireland Boulevard Mail Stop 330 St. Paul, Minnesota 55155	13. Type of Report and Period Covered Final Report		14. Sponsoring Agency Code
	15. Supplementary Notes <a href="http://www.lrrb.org/PDF/200914.pdf">http://www.lrrb.org/PDF/200914.pdf</a>		
16. Abstract (Limit: 250 words) <p>This study documents relationships between intelligent compaction measurement values (IC-MVs) and various in-situ point measurement techniques for monitoring compaction of non-granular and granular materials. Factors affecting correlations are discussed (e.g., soil type, moisture contents, stress level, etc.). Measurements from earth pressure cells document the relationship between in-ground stresses for rollers and various in-situ test methods.</p> <p>Comparisons were made between test roller rut depth measurements and IC-MVs and various point measurements as a quality assurance (QA) check for the subgrade pavement foundation layer. It was concluded that IC-MVs and in-situ point measurements can serve as reliable alternatives to test rolling. Site specific target values were calculated for IC-MVs, dynamic cone penetrometer (DCP), light weight deflectometer, (LWD), and shear strength.</p> <p>Measurement error and protocols for field testing were evaluated for LWDs. Laboratory compacted samples were used to assess an approach for determining LWD field target values. Future research is recommended to evaluate this approach for materials on a state-wide basis.</p> <p>Results from field studies were used to develop four IC specification options. Three specifications do not require on-site roller calibration. One specification option requires on-site calibration of IC-MVs and in-situ point measurements. This specification option has the advantages of quantifying risk, establishing a framework for a performance specification, providing information for incentive-based pay, and better linking as-built quality to long-term performance. An IC training/certification program, new IC field data analysis tools, and additional pilot projects will assist with greater implementation of these technologies.</p>			
17. Document Analysis/Descriptors Earthwork quality, intelligent compaction, geostatistics, in-situ testing, laboratory compaction testing, resilient modulus		18. Availability Statement No restrictions. Document available from: National Technical Information Services, Springfield, Virginia 22161	
19. Security Class (this report) Unclassified	20. Security Class (this page) Unclassified	21. No. of Pages 337	22. Price

# **Implementation of Intelligent Compaction Performance Based Specifications in Minnesota**

## **Final Report**

*Prepared by*

David J. White  
Pavana KR. Vennapusa  
Jiake Zhang  
Heath Gieselman  
Max Morris

Earthworks Engineering Research Center  
Department of Civil, Construction and Environmental Engineering  
Iowa State University

**July 2009**

*Published by*

Minnesota Department of Transportation  
Research Services Section  
Transportation Bldg.  
395 John Ireland Boulevard, Mail Stop 330  
St. Paul, Minnesota 55155-1899

This report represents the results of research conducted by the authors and does not necessarily represent the views or policies of the Minnesota Department of Transportation or the Iowa State University Department of Civil, Construction and Environmental Engineering. This report does not contain a standard or specified technique.

The authors and the Minnesota Department of Transportation and the Iowa State University Department of Civil, Construction and Environmental Engineering do not endorse products or manufacturers. Trade or manufacturers' names appear herein solely because they are considered essential to this report.

## **Acknowledgements**

The Minnesota Department of Transportation (Mn/DOT) and the Federal Highway Administration (FHWA) sponsored this study. Numerous people assisted the authors in identifying and providing access to grading projects for testing, refining research tasks, providing review comments and targeting concepts to improve implementation of intelligent compaction technologies. Some of the contributors are listed in the following. Their support is greatly appreciated.

Input and review comments were provided from the Technical Advisory Panel members: John Siekmeier, Rebecca Embacher, Glenn Engstrom, Erland Lukanen, Clark Moe, Art Bolland, Tim Andersen, Perry Collins, Dan Ross, George Begelman, Kevin Kliethermes, Matt Oman, George Cochran, Curt Turgeon, and Jay Hietpas. These members were very helpful in directing the research tasks for this project.

Darren Nelson, Tom Ravn, Todd Davidson, Ted Sexton, Shiloh Wahl, Gary Troge, Bob Williams, Lonny White, Keith Bloomgren, David Rettner, Kaye Bieniek, Clint Larsen, Mike Sheehan, John Hager, Curt Bolles, and Steven Adamsky assisted with project coordination and field testing. Their timely response in identifying areas for testing, coordination with contractors and roller manufacturers, and supplying project information is greatly appreciated.

The roller manufacturers provided assistance with machine operations and data analysis. The authors acknowledge Dean Potts, Nick Oetken, Mario Souraty, Bryan Brady, Terry Rasmussen, Blake Aldrich, Mark Rinehart, and Allen DeClerk of Caterpillar and their dealer Ziegler Inc.

Mathiowetz Construction and Road Constructors provided support during field testing.

Luke Johanson, Rachel Goldsmith, Dan Enz, John Puls, Bradley Fleming, Peter Becker, Kevin McLaughlin, Andrew Weber, and Alexandra Buchanan from the Iowa State University research team provided assistance with the ISU Geotechnical Mobile Lab, field and lab testing, and assistance with data analysis.

# Table of Contents

Chapter 1 Introduction .....	1
1.1 Overview.....	1
1.2 Project Goals/Tasks .....	1
1.3 Research Methodology .....	2
1.4 Report Organization.....	3
1.5 Units Conversion .....	3
Chapter 2 Experimental Testing Methods .....	5
2.1 Roller-Integrated Compaction Measurements .....	5
2.1.1 Compaction Meter Value (CMV) and Resonant Meter Value (RMV).....	5
2.1.2 Machine Drive Power (MDP).....	7
2.2 In-Situ Testing Methods .....	8
2.2.1 Heavy Test Rolling .....	8
2.2.2 Light Weight Deflectometers.....	8
2.2.3 Falling Weight Deflectometer.....	9
2.2.4 Dynamic Cone Penetrometer .....	9
2.2.5 Piezocone Cone Penetration Test.....	10
2.2.6 Nuclear Gauge .....	10
2.2.7 Shelby Tube Sampling.....	10
2.2.8 Static Plate Load Test .....	10
2.2.9 Clegg Hammer .....	10
2.2.10 Soil Stiffness Gauge.....	11
2.2.11 Earth Pressure Cells .....	11
Chapter 3 Field Project Case Histories .....	15
3.1 Introduction.....	15

3.2 Overview of IC Pilot Specifications .....	16
3.3 Metro District TH 36, North St. Paul.....	18
3.3.1 Project Overview .....	18
3.3.2 Experimental Testing.....	19
3.3.3 Comparison of IC-MVs and In-Situ Point Measurements.....	20
3.3.4 Stresses in Pavement Foundation Layers.....	36
3.3.5 Project Level In-Situ QA/QC Test Results.....	46
3.3.6 Key Observations and Conclusions .....	52
3.4 District 2 US 10, Staples.....	54
3.4.1 Project Overview .....	54
3.4.2 Experimental Testing.....	54
3.4.3 Comparison between IC-MVs and in-situ point measurements .....	56
3.4.4 Stresses in Granular Subgrade Layers .....	81
3.4.5 Key Observations and Conclusions .....	89
3.5 District 7 TH 60, Bigelow.....	90
3.5.1 Project Overview .....	90
3.5.2 Experimental Testing.....	90
3.5.3 Field Observations and In-Situ QA Test Results from Mn/DOT .....	95
3.5.4 Comparison between IC and In-situ Point Measurements.....	104
3.5.5 Stresses in Non-granular Subgrade Layer.....	137
3.5.6 Discussion .....	140
3.5.7 Key Observations and Conclusions .....	141
3.6 CSAH 2, Olmsted County.....	142
3.6.1 Introduction.....	142
3.6.2 Analysis of Results .....	145

3.6.3 Key Observations and Conclusions .....	152
3.7 Repeatability and Reproducibility of IC-MVs.....	153
3.7.1 Analysis Approach.....	153
3.7.2 Analysis Results and Discussion .....	154
3.8 Key Findings from Field Studies .....	162
3.8.1 Granular Soils .....	162
3.8.2 Non-Granular Soils .....	164
Chapter 4 Guidance for Test Roller Specification Modification .....	166
4.1 Background.....	166
4.2 Experimental Testing.....	168
4.3 Correlations between Rut Depths and Different In-situ Measurements .....	169
4.4 Bearing Capacity Analysis on a Layered Non-granular Soil Stratum .....	172
4.5 Implementation Aspects.....	176
4.6 Conclusions and Recommendations .....	176
Chapter 5 LWD Evaluation and Target Value Determination.....	178
5.1 Introduction.....	178
5.2 Background.....	178
5.3 Experimental Comparison of LWD Devices .....	180
5.3.1 $E_{LWD}$ Comparison between Different LWD devices .....	184
5.3.2 Influence of Plate Diameter on $E_{LWD}$ .....	187
5.3.3 Influence of Applied Contact Stress on $E_{LWD}$ .....	189
5.3.4 Influence of Buffer Stiffness on $E_{LWD}$ .....	190
5.3.5 Influence of Confinement on In-Situ $E_{LWD}$ Measurements .....	191
5.4 Variability of $E_{LWD}$ Measurements.....	193
5.5 Laboratory Evaluation of Repeatability and Reproducibility of LWD Measurements ....	195

5.6 Guidance for LWD Testing Standard Protocol for Granular and Non-Granular Soils.....	201
5.7 Comparison between $E_{LWD}$ and CIV measurements.....	204
5.8 Target Value Determination Study .....	207
5.8.1 Background and Test Methods .....	208
5.8.2 Laboratory Approach.....	209
5.8.3 Experimental Test Results and Discussion.....	224
5.8.4 Field Approach to Target Value Determination .....	240
5.8.5 Linking Laboratory LWD-TVs to In-Situ LWD Measurements .....	241
5.8.6 Summary of Laboratory Target Value Determination Study .....	251
Chapter 6 IC Verification and Specification Options.....	253
6.1 Verification Procedures for IC Equipment .....	253
6.1.1 Determining IC-MV Measurement Error .....	253
6.1.2 Dedicated IC Verification Test Facility at MnROAD .....	256
6.1.3 Mechanical System to Simulate Ground Conditions.....	256
6.2 Recommendations for Future IC Specifications and Implementation Strategies .....	257
6.2.1 Option 1 – Use of IC-MV Map to Target In-situ QA Measurements.....	258
6.2.2 Option 2 – Assessment of IC-MV Change to Target In-situ QA Testing .....	259
6.2.3 Option 3 – Pre-selected IC-TVs and Mechanistic-Related QA-TVs.....	261
6.2.4 Option 4 – Concept for Statistically-Framed QA/QC Assessment Approach.....	261
6.3 Summary.....	270
Chapter 7 Summary and Conclusions.....	273
7.1 Summary .....	273
7.2 Key Findings from Field Projects.....	273
7.2.1 Granular Soils .....	273
7.2.2 Non-Granular Soils .....	274

7.3 Guidance for Test Roller Specification Modification.....	276
7.4 LWD Evaluation and Target Value Determination .....	276
7.4.1 Experimental Comparison of LWD Devices and Influencing Factors .....	276
7.4.2 Variability of $E_{LWD}$ Measurements and Measurement Error .....	277
7.4.3 Guidance for a Standard Test Protocol .....	278
7.4.4 Comparison between $E_{LWD}$ and CIV Measurements .....	280
7.4.5 Laboratory Target Value Determination Study .....	280
7.5 IC Verification and Specification Options.....	281
7.5.1 Verification .....	281
7.5.2 Specifications.....	282
Chapter 8 Recommendations for Implementation .....	284
8.1 Recommendations for Specification Development .....	284
8.2 Development of Training/Certification Program.....	284
8.3 Data Analysis/Report/Archiving.....	284
References.....	285
Appendix A: Repeatability and Reproducibility Analysis Procedure and Example Calculations for LWD and Roller Measurement Data	

## List of Tables

Table 1.1. Summary of unit conversions from Metric to English .....	4
Table 2.1. Summary of measurement values and settings on the machines used.....	6
Table 2.2. Observed modes of vibratory roller drum (Adam 1997).....	7
Table 2.3. In-situ test methods and procedures employed in this study .....	12
Table 2.4. Resilient modulus ( $M_r$ ) test loading sequences for subgrade materials (AASHTO T-307 test procedure).....	14
Table 3.1. Field testing summary (TH36).....	19
Table 3.2. Summary of soil index properties (TH36).....	20
Table 3.3. Summary of regression relationships (TH36 strip 1 – lift 1).....	23
Table 3.4. Summary statistics of IC-MVs and in-situ point measurements at surface (TH36 strip 1 – lift 1).....	23
Table 3.5. Summary of regression relationships for measurements at surface (TH36 strip 2).....	27
Table 3.6. Summary statistics of IC-MVs and in-situ point measurements (TH36 strip 2) .....	27
Table 3.7. Summary of roller passes (TH36 strip 4).....	30
Table 3.8. Summary of regression relationships (TH36 strip 4).....	34
Table 3.9. Summary statistics of IC-MVs and in-situ point measurements at surface (TH36 strip 4) .....	34
Table 3.10. Summary of Mn/DOT QA/QC test results for GN = 3.9 material .....	47
Table 3.11. Summary of Mn/DOT QA/QC test results for GN = 5.2 material .....	48
Table 3.12. Summary of Mn/DOT QA/QC test results for GN = 5.3 material .....	49
Table 3.13. Summary of Mn/DOT QA/QC test results for GN = 5.6 material .....	49
Table 3.14. Summary of measurement influence depth of different measurements – TH36 project .....	54
Table 3.15. Field testing summary (US10).....	55
Table 3.16. Summary of soil index properties from US 10 project.....	55
Table 3.17. Testing and compaction summary for test strip 1.....	58

Table 3.18. Summary statistics of IC-MVs and in-situ point measurements from test strip 1 .....	60
Table 3.19. Summary statistics of IC-MVs and in-situ point measurements on test strip 2.....	70
Table 3.20. Summary statistics of CMV and in-situ point measurements from test strip 3 .....	71
Table 3.21. Summary of regression relationships between IC-MVs and in-situ point measurements – US10 project test strips 1, 2, and 3 .....	75
Table 3.22. Summary of regression relationships between different in-situ point measurements – US10 project .....	76
Table 3.23. Summary of measurement influence depth of different measurements – US10 project .....	90
Table 3.24. Field testing summary (TH60).....	93
Table 3.25. Summary of soil index properties from US 60 project subgrade material .....	93
Table 3.26. E <sub>LWD</sub> test measurements by Mn/DOT during field survey by ISU .....	97
Table 3.27. QA test results from TH60 project by Mn/DOT field personnel.....	98
Table 3.28. Summary statistics of CCV and in-situ point measurements from test strip 1 .....	109
Table 3.29. Summary statistics of IC-MVs and in-situ point measurements after passes 8 and 15 – test strip 2.....	115
Table 3.30. Test Strips 3a, 3b, and 3c roller pass summary .....	119
Table 3.31. Summary statistics of in MDP* and in-situ point measurements – test strip 3 .....	124
Table 3.32. Summary of regression relationships – TH60 project .....	129
Table 3.33. Summary of roller passes – Olmsted County project .....	143
Table 3.34. Summary of regression relationships – Olmsted County project .....	151
Table 3.35. Summary of multiple regression analysis – Olmsted County data.....	152
Table 3.36. Summary of repeatability analysis results on MDP*, CMV, and RMV.....	160
Table 3.37. Summary of R&R analysis results on MDP* .....	161
Table 3.38. Summary of measurement influence depth of different measurements – granular soils .....	163
Table 4.1. Description of project locations with rut depth measurements.....	168

Table 4.2. Summary of QA target values alternative to heavy test rolling rut depth of 50 mm.	176
Table 5.1. Comparison between different LWD devices.....	179
Table 5.2. Summary of field studies and index properties of materials .....	183
Table 5.3. Summary of Zorn and Keros/Dynatest 3031 LWD test conditions.....	184
Table 5.4. Summary of modulus measurements from different field studies.....	195
Table 5.5. Summary of testing for repeatability and reproducibility evaluation on LWD measurements.....	198
Table 5.6. Summary of repeatability analysis results on LWD measurements .....	200
Table 5.7. Summary of R&R analysis on LWD measurements for change in device.....	201
Table 5.8 Summary of soil index properties – LWD-Clegg comparison studies .....	205
Table 5.9. Comparison of summary statistics for $E_{LWD-Z2}$ and $CIV_{20-kg}$ measurements .....	206
Table 5.10. Summary of experimental testing – laboratory target value determination study ...	211
Table 5.11. Summary of index properties of granular materials used in laboratory target value determination study and tests performed .....	212
Table 5.12. Summary of index properties of non-granular soils used in laboratory target value determination study.....	212
Table 5.13. Summary of laboratory determined $w-\gamma_d-DPI/s_u/E_{LWD}$ relationships .....	228
Table 5.14. Comparison of $M_r$ for 2:1 and 1:1 height to diameter ratio specimens – TH-60 soil 306 (USCS: CL).....	237
Table 5.15. In-situ $d_{LWD}$ measurements (TH60 project test strips 1 to 5) for Mn/DOT moisture content target limits.....	247
Table 5.16. In-situ $E_{LWD}$ measurements (TH60 project test strips 1 to 5) for Mn/DOT moisture content target limits.....	248
Table 5.17. Comparison between Mn/DOT and laboratory-determined $d_{LWD}$ and $E_{LWD}$ target values for different moisture ranges for materials from TH60 project test strips 1 to 5.....	249
Table 5.18. In-situ Mn/DOT QA $d_{LWD}$ and $E_{LWD}$ measurements at different moisture contents from the TH60 project .....	250
Table 6.1 Suggested pass sequence to assess measurement error .....	254
Table 6.2 Summary comparison between different specifications .....	258

Table 6.3. Summary of change in CCV between successive passes for non-granular subgrade soil (USCS classification: CL) test strip 3 – TH 60.....	261
--------------------------------------------------------------------------------------------------------------------------------------------------	-----

## List of Figures

Figure 2.1. 12-ton CS-563 smooth drum (left) and 19-ton CS-683 smooth drum rollers equipped with CMV/RMV systems and GPS .....	6
Figure 2.2. 12-ton CP-563 padfoot roller equipped with MDP* system and GPS .....	8
Figure 2.3. In-situ testing methods employed in this study: (a), (b) towed pneumatic dual-wheel test rollers with 650 kPa contact tire pressure, (c) Keros, Dynatest, and Zorn LWDs, (d) Mn/DOT Dynatest FWD, (e) DCP, (f) Mn/DOT CPT, (g) nuclear moisture-density gauge, (h) shelby tube sampler, (i) static plate load test, (j) 20-kg Clegg Hammer, (k), Humboldt SSG, and (l) Piezoelectric EPCs .....	13
Figure 2.4. Static plate load test data modulus scheme for subgrade, subbase, and base materials .....	14
Figure 3.1. Illustration of differences in measurement influence depths of different testing devices.....	16
Figure 3.2. Construction operations on test strip 1 .....	21
Figure 3.3. CMV map of test strip 1 (lift 1) and DPI profiles at spot test locations TH 36 .....	22
Figure 3.4. Comparison between CMV and in-situ point measurements (TH 36 strip 1 – lift 1; roller operation parameters (nominal): $a = 0.85$ mm, $f = 33$ Hz, $v = 4.0$ km/h) .....	22
Figure 3.5. Simple linear regression relationships between in-situ point measurements and CMV (TH 36 strip 1 – lift 1).....	23
Figure 3.6. Photographs showing LWD and Clegg hammer tests conducted in the 0.15 m deep excavation and plots showing comparison of in-situ point measurements obtained at the surface and at 0.15 m below the surface (TH 36 strip 1 – lift 2).....	24
Figure 3.7. CMV map of test strip 2 and DPI profiles at select spot test locations .....	25
Figure 3.8. Comparison between CMV and in-situ point measurements (TH 36 strip 2; roller operation parameters (nominal): $a = 0.85$ mm, $f = 33$ Hz, $v = 4.0$ km/h).....	26
Figure 3.9. Simple linear regression relationships between in-situ point measurements and CMV (TH 36 strip 2) .....	28
Figure 3.10. Plan view of TH36 strip 4 and photographs during rolling and testing operations..	30
Figure 3.11. Example CPTU profile from a test location in the test strip area describing the general foundation soil conditions (TH36 strip 4) (actual soil profile determined based on project drawings).....	31

Figure 3.12. CMV and RMV from test strip 4 with nominal $v = 3.2$ km/h and $f = 33$ Hz settings: (a) repeatability of CMV at two amplitude settings, (b) influence of RMV on CMV measurements.....	31
Figure 3.13. Comparison of CMV with in-situ mechanistic point measurements – DCP index, $q_t$ , and $E_{FWD}$ profiles at two select points (test strip 4).....	32
Figure 3.14. Relationships between different in-situ point measurements ( $E_{FWD-D3}$ at $F \sim 26.7$ kN).....	33
Figure 3.15. Relationships between CMV and point measurements ( $E_{FWD-D3}$ at $F \sim 53.4$ kN)....	35
Figure 3.16. Results of multiple regression analysis illustrating the effect of RMV.....	36
Figure 3.17. Plan and cross-sectional views of location of EPCs in the pavement foundation layers – test strip 3 .....	37
Figure 3.18. Pictures showing rolling pattern on test strip 3 .....	38
Figure 3.19. Installation of EPCs in a layer of silica sand at different depths on test strip 4 .....	39
Figure 3.20. Triaxial stresses developed under the roller at position A at different amplitude settings (top) and profile of peak stresses (bottom) (test strip 3).....	40
Figure 3.21. Triaxial stresses developed under the roller at position B at different amplitude settings (top) and profile of peak stresses (bottom) (test strip 3).....	41
Figure 3.22. Triaxial stresses developed under the roller at position C at different amplitude settings (top) and profile of peak stresses (bottom) (test strip 3).....	42
Figure 3.23. Total vertical and lateral stress measurements from test strip 4 under roller vibratory loading at $a = 0.85$ and $1.70$ mm nominal settings (note drum jumping at $a = 1.70$ mm) (test strip 4) .....	43
Figure 3.24. Peak vertical and lateral stress increase profiles (measured and theoretical Boussinesq curves) for roller induced vibratory loads, and FWD and LWD dynamic loads, and estimated residual stresses to calculate K from Duncan and Seed (1986) (test strip 4) .....	44
Figure 3.25. Comparison of total stress paths under roller vibratory load (Positions A to B loading and Positions B to C unloading), FWD and LWD dynamic loads, and stresses applied during laboratory $M_r$ tests on base/subbase materials (test strip 3) .....	45
Figure 3.26. Histograms of Mn/DOT QA/QC moisture content measurements from TH36 project (data includes both pass and fail measurements).....	50
Figure 3.27. Histograms of Mn/DOT QA/QC DPI measurements from TH36 project (data includes both pass and fail measurements).....	50

Figure 3.28. Histograms of Mn/DOT QA/QC $E_{LWD-Z2}$ and $d_{LWD-Z2}$ measurements from TH36 project (data includes both pass and fail measurements).....	51
Figure 3.29. Histograms of Mn/DOT QA/QC $E_{LWD-D2}$ and $d_{LWD-D2}$ measurements from TH36 project (data includes both pass and fail measurements).....	52
Figure 3.30. Test strip 1 area with spot test locations.....	57
Figure 3.31. Construction operations on test strip 1 .....	57
Figure 3.32. LWD testing performed by excavating loose material at the surface to a depth of about 0.15 m.....	58
Figure 3.33. Compaction growth curves of in-situ point measurements (no measurements at points A, B, 11 and 12 at pass 0) .....	59
Figure 3.34. CMV data from mapping passes 1 to 5 .....	59
Figure 3.35. Frequency distribution of CMV data (pass 2, $a = 0.85$ mm).....	60
Figure 3.36. Comparison between CMV and in-situ point measurements from test strip 1.....	61
Figure 3.37. Comparison of $E_{LWD-Z3}$ point measurements at surface and at different depths with DPI profiles.....	62
Figure 3.38. Photographs of test strip 2 after final pass (left) and in-situ testing (right).....	63
Figure 3.39. Plan view CMV map at two different amplitude ( $a = 0.85$ and $1.70$ mm) settings of test strip 2 compacted in six roller lanes.....	64
Figure 3.40. Frequency distribution of CMV data from test strip 2 ( $a = 0.85$ and $1.70$ mm) .....	64
Figure 3.41. Comparison of CMV ( $a = 0.85$ and $1.70$ mm) and $E_{LWD-D2}$ measurements from test strip 2 lanes 1 to 6 .....	65
Figure 3.42. Comparison of CMV ( $a = 0.85$ mm) and NG measurements from test strip 2 lanes 1 to 6 .....	66
Figure 3.43. Comparison of CMV ( $a = 1.70$ mm) and NG measurements from test strip 2 lanes 1 to 6 .....	67
Figure 3.44. Comparison of CMV ( $a = 0.85$ and $1.70$ mm) and $DPI_{300}$ measurements from test strip 2 lanes 1 to 6 .....	68
Figure 3.45. Comparison of CMV ( $a = 0.85$ and $1.70$ mm) and $DPI_{S-300}$ measurements from test strip 2 lanes 1 to 6 .....	69
Figure 3.46. Compaction operations on test strip 3 (left) and excavations performed for LWD testing.....	70

Figure 3.47. Comparison of CMV ( $a = 0.85$ and $1.70$ mm) and in-situ point measurements from test strip 3 .....	71
Figure 3.48. Compaction operations on test strip 4 with soft and uncompacted material .....	72
Figure 3.49. Compaction operations on test strip 5 with relatively uniform conditions across the test strip .....	72
Figure 3.50. Regression relationships between CMV ( $a = 0.85$ mm) and different in-situ point measurements.....	73
Figure 3.51. Regression relationships between CMV ( $a = 1.70$ mm) and different in-situ point measurements.....	74
Figure 3.52. Regression relationships between different in-situ point measurements .....	77
Figure 3.53. Semivariograms of IC-MVs and in-situ point measurements from test strip 2.....	79
Figure 3.54. Spatial comparison of IC-MVs and in-situ point measurement Kriged spatial maps from test strip 2 .....	80
Figure 3.55. EPC installation setup on test strips 1 and 5.....	82
Figure 3.56. Picture of EPC installed in orthogonal directions on test strip 1 (top view) .....	83
Figure 3.57. Plan view on roller and scraper passes on test strips 1 and 5 .....	83
Figure 3.58. Triaxial stress increase time histories at different depths under $a = 0.85$ mm (left) and $1.70$ mm (right) vibratory rolling operation – Test strip 1 .....	84
Figure 3.59. Triaxial stress increase time histories at different depths under scraper tire position A passes without load (left) and fully loaded (right) – Test strip 1 .....	85
Figure 3.60. Triaxial stress increase time histories at different depths under scraper tire position B passes without load (left) and fully loaded (right) – Test strip 1 .....	86
Figure 3.61. Triaxial stress increase time histories at different depths under scraper tire position C passes without load (left) and fully loaded (right) – Test strip 1 .....	87
Figure 3.62. Triaxial stress increase time histories for different passes at $a = 0.85$ mm (left) and $1.70$ mm (right) vibratory rolling operation – Test strip 5.....	88
Figure 3.63. Peak vertical and horizontal stress increase profiles (measured and theoretical Boussinesq curves) for roller induced vibratory loading and under scraper tire .....	89
Figure 3.64. Laboratory compaction test results for sample A.....	94
Figure 3.65. Laboratory compaction test results for test strip 1 sample .....	94

Figure 3.66. Laboratory compaction test results for test strip 2 sample .....	95
Figure 3.67. Scraper traffic contributing to compaction of fill materials .....	97
Figure 3.68. Histogram of moisture content, LWD, and MDP* test measurements .....	102
Figure 3.69. Simple linear regression relationships between QA measurements obtained by Mn/DOT field personnel.....	103
Figure 3.70. Plan view MDP* map of the test strip 1 area with selected lanes for compaction testing (production area mapped a few hours prior to testing) .....	105
Figure 3.71. Screen shots from the on-board AccuGrade compaction monitoring system showing number of passes and MDP* – Test strip 1 .....	106
Figure 3.72. Comparison between CCV ( $a = 1.87$ mm) and in-situ point measurements ( $E_{LWD}$ and DPI) from test strip 1.....	107
Figure 3.73. Comparison between CCV ( $a = 1.87$ mm) and in-situ point measurements (NG and DC) from test strip 1 .....	108
Figure 3.74. DCP profiles from test strip 1 (depth to the dashed line indicates the compacted compaction layer thickness) and histogram of estimated lift thickness – test strip1 .....	111
Figure 3.75. Laboratory moisture-density relationships and in-situ moisture density measurements from test strip 1 .....	112
Figure 3.76. Pictures from test strip 2 construction: fill placement, compaction, in-situ spot testing, and final compacted surface (top left to bottom right).....	113
Figure 3.77. IC-MVs and in-situ point measurements at several passes – test strip 2.....	114
Figure 3.78. Frequency distribution plot of IC-MVs for pass 8 – test strip 2.....	114
Figure 3.79. Laboratory and in-situ moisture-density measurements – test strip 2.....	115
Figure 3.80. Compaction growth curves for IC-MVs and in-situ point measurement values ....	116
Figure 3.81. Bar chart comparisons of average IC-MVs and in-situ point measurement values at different passes.....	116
Figure 3.82. DPI profiles and $s_u$ from UC testing on Shelby tube samples from test strip 2 subgrade after pass 15.....	117
Figure 3.83. Test strip 3 prepared in three lanes (lanes 3a, 3b, and 3c) for rolling (top left), picture of roller used on-site (top right), rolling operations (bottom left), and LWD testing (bottom right) in at the bottom of the padfoot penetration .....	118

Figure 3.84. Screen shots from AccuGrade showing change in elevation from pass 1 to final pass – test strip 3 .....	119
Figure 3.85. Screen shots from AccuGrade showing change in MDP*from pass 1 to pass 2 – test strip 3 .....	120
Figure 3.86. Screen shots from AccuGrade showing change in MDP*from pass 4 to pass 8 – test strip 3 .....	120
Figure 3.87. CCV and $E_{LWD}$ comparisons for test strip 3 .....	121
Figure 3.88. CCV and NG test measurements after final pass for test strip 3 .....	122
Figure 3.89. Bar charts comparing CCV and $E_{LWD}$ measurement values from strip 3a, 3b, and 3c .....	122
Figure 3.90. Laboratory Proctor and in-situ moisture-density measurements.....	123
Figure 3.91. Influence of amplitude on MDP*compaction curves on lanes 3a, 3b, and 3c – test strip 3 .....	123
Figure 3.92. Linear regression relationships between MDP* and $E_{LWD}$ measurements.....	126
Figure 3.93. Linear regression relationships between MDP* and $d_{LWD}$ measurements .....	127
Figure 3.94. Linear regression relationships between MDP* and in-situ point measurements..	128
Figure 3.95. Multiple linear regression relationships incorporating moisture content in predicting MDP* values.....	130
Figure 3.96. Screen shots from AccuGrade showing test strips 4 and 5 CMV and RMV maps	132
Figure 3.97. CMV map of test strip 4 ( $a = 0.85$ mm), photograph of the test area, and frequency distribution histograms of CMV and in-situ point measurements .....	133
Figure 3.98. CMV map of test strip 5 ( $a = 0.85$ mm) and photograph of the test area highlighting soft and stiff spot test locations.....	134
Figure 3.99. Frequency distribution histograms of CMV and in-situ point measurements from test strip 5.....	135
Figure 3.100. Linear regression relationships between CMV and in-situ point measurements .	136
Figure 3.101. Relationships between DPI, $s_u$ , $E_{LWD-Z2}$ , and $d_{LWD-Z2}$ .....	137
Figure 3.102. Installation of EPCs on test strip 2: (a) EPC placement in an excavated trench; (b) placement of thin clean sand layer; (c) GPS measurement on the top of EPC; (d) replacing the trench with hand-compacted fill material .....	138

Figure 3.103. Vertical stress increase under roller at multiple passes .....	139
Figure 3.104. IC padfoot roller (left) and LWD test preparation (right) by excavating to bottom of padfoot penetrations .....	143
Figure 3.105. AccuGrade screenshots from Olmsted County test strips 1 and 2 showing number of passes, elevation, MDP*, and average MDP* (shown as CCV) with pass .....	144
Figure 3.106. Influence of roller operation direction, amplitude and speed settings on average MDP* .....	145
Figure 3.107. Elevation change across the test strip – Olmsted County.....	146
Figure 3.108. Comparison of MDP* with $E_{LWD-Z2}$ measurements (one point measurement at the center of the drum) – Test strip 1 ( $a = \text{static}$ and $v = 3.2 \text{ km/h}$ and $6.4 \text{ km/h}$ ).....	146
Figure 3.109. Comparison of MDP* with $E_{LWD-Z2}$ measurements (one point measurement at the center of the drum) – Test strip 2 ( $a = 0.90 \text{ mm}$ and $v = 3.2 \text{ km/h}$ and $6.4 \text{ km/h}$ ) .....	147
Figure 3.110. Comparison of MDP* with $E_{LWD-Z2}$ measurements (one point measurement at the center of the drum) – Test strip 2 ( $a = 1.80 \text{ mm}$ and $v = 3.2 \text{ km/h}$ and $6.4 \text{ km/h}$ ) .....	147
Figure 3.111. Effect of change in elevation on MDP* values .....	148
Figure 3.112. Simple linear regression relationships ( $E_{LWD-Z2}$ and MDP*) – Olmsted County data .....	149
Figure 3.113. Simple linear regression relationships ( $d_{LWD-Z2}$ and MDP*) – Olmsted County data .....	150
Figure 3.114. Results of multiple regression analysis incorporating speed, direction, amplitude, and $E_{LWD-Z2}$ as prediction parameters.....	152
Figure 3.115. Comparison of averaged MDP* data from Iowa State University VB IC repeatability algorithm (spacing 0.3 m) and actual MDP* data – TH60 test strip 2 .....	153
Figure 3.116. Repeatability of MDP* measurements at $a = 0.85 \text{ mm}$ – TH60 test strip 2 .....	156
Figure 3.117. Repeatability of MDP* measurements in static mode – Olmsted County test strip 1 .....	157
Figure 3.118. Repeatability of MDP* measurements at $a = 0.90 \text{ mm}$ setting – Olmsted County test strip 2.....	158
Figure 3.119. Repeatability of MDP* measurements at $a = 1.80 \text{ mm}$ setting – Olmsted County test strip 2.....	159
Figure 3.120. Correlations between CMV and in-situ point measurements obtained from TH36 and US10 field projects with granular soils.....	164

Figure 4.1. Towed pneumatic dual-wheel test rollers with 650 kPa contact tire pressure used on TH14 (left), TH60 (left) and TH36 (right) project .....	167
Figure 4.2. DCP- $s_u$ profiles from compacted glacial till subgrade at US14 (from White et al. 2007a) .....	167
Figure 4.3. Regression relationships between rut depth, roller-integrated $k_s$ , and in-situ point measurements from US14 project.....	170
Figure 4.4. Relationship between rut depth and LWD measurements from TH36 project .....	171
Figure 4.5. Regression relationships between rut depth, roller-integrated CMV, and in-situ point measurements from TH60 project .....	171
Figure 4.6. Bearing capacity of a test roller wheel on a layered non-granular stratum .....	172
Figure 4.7. Comparison of DCP- $s_u$ profiles with rut depth measurements.....	174
Figure 4.8. (a) Relationship between calculated $q_{ult}$ and measured rut depth, and (b) influence of $s_u$ properties of top and bottom layers at different H to achieve a minimum $q_{ult} = 1050$ kPa.....	175
Figure 4.9. Comparison of estimated $q_{ult}$ from layered bearing capacity analysis and static plate load test .....	175
Figure 5.1. Relationship between deflection measurements and calculated $E_{LWD}$ .....	180
Figure 5.2. Dynatest 3031, Keros, and ZFG Zorn LWD devices (left to right) .....	180
Figure 5.3. Schematic with example output of LWD devices used in this study (a) Zorn ZFG 2000 (b) Keros (c) Dynatest 3031 .....	181
Figure 5.4. Zorn LWD device with 300, 200, 150, and 100 mm plate diameters .....	184
Figure 5.5. Relationships between $E_{LWD}$ values from different devices: (a) 200-mm Keros and Zorn, (b) 300-mm Keros and Zorn, (c) 200-mm Dynatest and Zorn, and (d) 200-mm Dynatest and Keros .....	185
Figure 5.6. Relationships between $d_{LWD}$ values from different devices: (a) 200-mm Keros and Zorn, (b) 200-mm Dynatest and Zorn, and (c) 200-mm Dynatest and Keros .....	186
Figure 5.7. Frequency distribution of impact force at drop height 50 cm by Keros and Dynatest LWD devices and comparison to Zorn assumed impact force (Field Study No. 4).....	186
Figure 5.8. Influence of plate diameter and applied stress on Zorn ELWD from field studies 3 and 4.....	188
Figure 5.9. Influence of applied stress and effect of buffer stiffness on $E_{LWD}$ with different plate diameters from Field Study No. 5.....	188

Figure 5.10. Relationship between material stiffness and diameter of bearing plate .....	189
Figure 5.11. Effect of buffer type and stiffness on applied force for different LWD devices....	190
Figure 5.12. Pictures of LWD testing performed in the excavation – US10 project.....	191
Figure 5.13. DPI profiles and LWD tests at different depths from US10, Staples, MN .....	192
Figure 5.14. Normalized $E_{LWD}$ versus depth with best fit power model to show general trend. 193	
Figure 5.15. Comparison of 90% confidence limits for target value based on eleven $E_{LWD-Z2}$ and $E_{LWD-D2}$ measurement points with mean values calculated from random selection of three points (Field Study 3a granular subbase layer).....	194
Figure 5.16. Schematic and pictures of soft and stiff pad setups.....	197
Figure 5.17. Static plate load test applied stress-displacement curves for soft and stiff pads ....	198
Figure 5.18. Box plots of $d_{LWD-Z2}$ , $E_{LWD-Z2}$ , $d_{LWD-D2}$ and $E_{LWD-D2}$ measurements for different models from 33 repeated drops.....	199
Figure 5.19. LWD test in an excavation by removing loose material at the surface to a depth of about 100 to 200 mm for cohesionless materials.....	203
Figure 5.20. Level surface at the bottom of the padfoot impression for non-granular materials	203
Figure 5.21. Simple linear regression relationships between $E_{LWD-Z2}$ and $CIV_{20\text{-kg}}$ .....	207
Figure 5.22. AFGB1A gyratory compactor (left) and pressure distribution analyzer (PDA) ....	209
Figure 5.23. Approach for laboratory mechanistic target value determination using gyratory compacted specimens.....	210
Figure 5.24. Dry unit weight growth curves with number of gyrations at different target moisture contents – US10 granular material (USCS: SP-SM) .....	213
Figure 5.25. Dry unit weight growth curves with number of gyrations at different target moisture contents – TH 36 granular material (USCS: SM).....	214
Figure 5.26. Dry unit weight growth curves with number of gyrations at different target moisture contents – TH 36 silty clay material (USCS: ML) .....	215
Figure 5.27. Dry unit weight growth curves with number of gyrations at different target moisture contents – TH60 soil 301 (USCS: CL).....	216
Figure 5.28. Dry unit weight growth curves with number of gyrations at different target moisture contents – TH60 soil 303 (USCS: CL) .....	217

Figure 5.29. Dry unit weight growth curves with number of gyrations at different target moisture contents – TH 60 soil 305 (USCS: CL) .....	218
Figure 5.30. Dry unit weight vs. No. of gyrations for TH 60 soil 306 (USCS: CL) .....	219
Figure 5.31. Dry unit weight vs. No. of gyrations for Iowa loess (USCS: ML).....	220
Figure 5.32. Comparison of moisture-dry unit weight relationships using Proctor and gyratory compaction (at 900, 600, 300, and 100 kPa vertical pressures) methods: (a) US10 granular (USCS: SP-SM), (b) TH 36 granular (USCS: SM), (c) TH 36 silty clay (USCS: ML), (d) Iowa loess (USCS: ML), (e) TH 60 soil 301 (USCS: CL). (f) TH 60 soil 303 (USCS: CL), (g) TH 60 soil 305 (USCS: CL), (h) TH 60 soil 306 (USCS: CL) .....	221
Figure 5.33. 150 mm (left) and 100 mm (right) plate diameter Zorn LWD tests on gyratory compacted specimens.....	222
Figure 5.34. LWD testing with four different boundary conditions: (a) no boundary, (b) soft polyurethane (Durometer = 20A), (c) stiff polyurethane (Durometer = 50A), and (d) rigid gyratory compaction mold .....	222
Figure 5.35. Schematic representation of LWD testing with different boundary conditions: rigid gyratory mold and flexible mold.....	223
Figure 5.36. PDA (left) and unconfined compression test (right) on gyratory compacted specimen .....	223
Figure 5.37. Resilient modulus testing on 1:1 and 2:1 gyratory compacted specimens.....	224
Figure 5.38. Procedure for inserting Shelby tube into gyratory compacted specimen to generate 2:1 height to diameter ratio specimens .....	224
Figure 5.39. $E_{LWD-Z1}$ contours in relationship with moisture and dry unit weight – US 10 granular material (USCS: SP-SM) ( $d_{LWD-Z1} = 85/E_{LWD-Z1}$ ) .....	225
Figure 5.40. $E_{LWD-Z1}$ contours in relationship with moisture and dry unit weight – TH36 silty clay material (USCS: ML) ( $d_{LWD-Z1} = 59.4/E_{LWD-Z1}$ ).....	226
Figure 5.41. $E_{LWD-Z1}$ contours in relationship with moisture and dry unit weight – TH60 soil 301 material (USCS: CL) ( $d_{LWD-Z1} = 49.8/E_{LWD-Z1}$ ).....	226
Figure 5.42. $E_{LWD-Z1}$ contours in relationship with moisture and dry unit weight – TH60 (301, 303, and 305 combined) non-granular material (USCS: CL) ( $d_{LWD-Z1} = 49.8/E_{LWD-Z1}$ ) .....	227
Figure 5.43. DPI contours in relationship with moisture and dry unit weight – TH60 non-granular material (301, 303, and 305 combined) (USCS: CL) .....	227

Figure 5.44. $s_u$ contours in relationship with moisture and dry unit weight – TH60 non-granular material (301, 303, and 305 combined) (USCS: CL) ( $s_u$ determined from empirical relationship with DPI).....	228
Figure 5.45. Shear resistance versus number of gyrations ( $\sigma_o = 300$ kPa) for TH 60 soil 306 (USCS: CL).....	230
Figure 5.46. Shear resistance versus number of gyrations for US10 granular material (USCS: SP-SM) ( $\sigma_o=300$ kPa).....	230
Figure 5.47. Influence of moisture content on $\tau_G$ for TH60 – soil 306 non-granular (USCS: CL) and US 10 granular (USCS: SP-SM) materials .....	231
Figure 5.48. Influence of boundary conditions on LWD measurements on gyratory compacted specimens at different moisture contents – TH 60 soil 306 (USCS: CL).....	231
Figure 5.49. Relationships between LWD measurements and $\tau_G$ for different boundary conditions – TH 60 soil 306 (USCS: CL).....	232
Figure 5.50. Influence of boundary conditions on LWD measurements on gyratory compacted specimens at different moisture contents – US10 granular material (USCS: SP-SM).....	232
Figure 5.51. Relationship between LWD measurements and $\tau_G$ for different boundary conditions – US10 granular material (USCS: SP-SM).....	233
Figure 5.52. $\tau_G$ G versus number of gyrations for loess (USCS: ML) .....	234
Figure 5.53. $s_u$ and $\tau_G$ versus moisture content for gyratory compacted specimens after 100 gyrations at $\sigma_o = 100, 300,$ and $600$ kPa for loess (USCS: ML).....	235
Figure 5.54. Relationship between $s_u$ and $\tau_G$ for loess (USCS: ML).....	235
Figure 5.55. Effect of height to diameter ratio ( $H/D = 1$ and $2$ ) on $M_r$ of gyratory compacted specimens at $\sigma_o = 100, 300$ and $600$ kPa at 100 gyrations –TH-60 soil 306 (USCS: CL) .....	238
Figure 5.56. Relationship between $H/D = 2:1$ and $1:1$ $M_r$ results on gyratory compacted specimens – TH60 soil 306 (USCS: CL).....	239
Figure 5.57. $\tau_G$ versus number of gyrations for $\sigma_o = 100, 300,$ and $600$ compacted specimens TH60 soil 306 (USCS: CL).....	239
Figure 5.58. Correlation between $s_u, M_r$ and $\tau_G$ for samples with $H/D = 1$ and $2$ – TH 60 soil 306 (USCS: CL).....	240
Figure 5.59. Results from in-situ LWD tests showing $E_{LWD}$ increase and $d_{LWD}$ decrease with number of blows at locations with different in-situ moisture contents – TH60 soil 306 (test strips 4 and 5 of Chapter 3 TH60 project).....	241

Figure 5.60. $E_{LWD-Z1}$ and $E_{LWD-Z1.5}$ contours in relationship with moisture and dry unit weight with stiff boundary conditions – TH60 soil 306 material (USCS: CL) .....	242
Figure 5.61. DPI and $s_u$ contours in relationship with moisture and dry unit weight with stiff boundary conditions – TH60 soil 306 material (USCS: CL).....	242
Figure 5.62. $\tau_G$ contours in relationship with moisture and dry unit weight with stiff boundary test – TH60 soil 306 material (USCS: CL).....	243
Figure 5.63. Correlations between $\tau_G$ and LWD/DPI measurements with different boundary conditions – TH60 soil 306 material (USCS: CL).....	244
Figure 5.64. Relationships between laboratory $E_{LWD-Z1}$ and $E_{LWD-Z2}$ measurements in comparison with Terzaghi’s theoretical relationships – TH60 soil 306 material (USCS: CL).....	245
Figure 5.65. Comparison between in-situ LWD measurements (from TH60 project test strip 3) and laboratory predicted LWD target values (TH60 soil 306 “stiff” boundary model) .....	245
Figure 5.66. Comparison between in-situ LWD measurements (from TH60 project test strips 1 and 4/5) and laboratory predicted LWD target values (TH60 soil 301, 302, 303 combined rigid boundary model) .....	246
Figure 5.67. Comparison between $E_{LWD}$ Mn/DOT and laboratory determined target values, and in-situ values (see Tables above for number of observations for each dataset).....	251
Figure 6.1. Proposed verification test beds with granular and non-granular materials .....	256
Figure 6.2. IC-MV compaction growth (left) and $\Delta$ IC-MV (right) between successive passes for non-granular subgrade soil test strip 3 – TH 60.....	260
Figure 6.3. Spatial map of $\Delta$ CCV between successive passes on non-granular subgrade soil test strip 3 – TH 60 .....	260
Figure 6.4. Illustration of combined specification options: lower portion IC-MVs used primarily for QC; upper 1 m with more stringent calibrations and use of IC-MVs for QC and QA .....	271

## **Executive Summary**

This report documents the field measurements from intelligent compaction (IC) project sites, summarizes results comparing test rolling rut measurements to various IC and in-situ point measurements, provides a detailed evaluation of light weight deflectometer (LWD) measurements and an approach to determine target values, includes recommendations for IC specification and verification procedures, and finally provides summary/conclusions and further recommendations for implementation of IC and LWD technologies. Building on the report *Field Validation of Intelligent Compaction Monitoring Technology for Unbound Materials*, Final Report MN/RC-2007-10 by White et al. (2007a), this project was initiated with a series of five educational/training seminars for Mn/DOT and contractor personnel.

### **Intelligent Compaction Technology Project Level Field Studies**

Four field projects were studied to investigate how IC specifications were being implemented and how IC technologies and LWD devices were being used in quality assurance/quality control (QA/QC) operations and testing. At each project site, test sections were constructed to investigate intelligent compaction measurement value (IC-MV) versus point measurement correlations and the influence of roller operating conditions on the IC-MVs. Test sections contained non-granular and granular materials. Detailed conclusions are reported in terms of empirical correlations between the IC-MVs and point measurements using LWD, falling weight deflectometer (FWD), dynamic cone penetrometer (DCP), Clegg hammer, and piezocone cone penetration test (CPTU) test devices. Results provide a basis for linking mechanistic-empirical pavement design to construction QA/QC. A procedure was developed for calculating the reproducibility and repeatability errors of IC-MVs. The analysis technique is independent of the IC technology and can also be applied to in-situ point measurement technologies.

### **Test Roller Evaluation in Relation to IC and Point Measurements**

Use of IC-MVs and DCP/LWD point measurements were used to evaluate bearing capacity in terms of rut depth under test rolling for non-granular and granular subgrade layers. Comparisons were made to test roller rut depth QA criteria for the upper subgrade layer of the pavement foundation. Correlations between compaction meter value (CMV) and machine drive power (MDP) IC-MVs and point measurements show positive trends, but with varying degrees of uncertainty. Scatter in the relationships was partly attributed to differences in the measurement influence depth.

At one project site involving compaction of non-granular soils, DCP- $s_u$  profiles showed significant vertical non-uniformity. Test rolling identified soft layers at and below the surface (rut depths  $\geq 50$  mm). Based on this finding, a chart solution using layered bearing capacity analysis was developed and linked to target shear strength values to predict test rolling rut failures. It was concluded that the IC-MVs and point measurements can serve as reliable indicators of compaction quality for non-granular and granular subgrades and as alternatives to test rolling. It is recommended, however, that development of a correlation database continue with future projects to improve confidence in target values.

## **LWD Analysis and Target Value Study**

Several operational aspects of LWD testing including factors influencing values and protocols for field practices were studied. Some of the key findings were that differences exist in the reported plate deflections and repeatability between manufacturers. Further, plate diameter, contact stress, and buffer stiffness affect the calculated elastic modulus values. Field testing protocols were developed to provide consistency in the field practices, and laboratory gyratory compacted specimens were tested to link moisture-density-modulus values together and as a means to establish soil specific field target values.

## **IC Verification and Specification Alternatives**

Integrating IC-MVs into QC and QA operations will benefit from standard protocols for verification procedures and quantifying measurement errors. Verification builds confidence in the IC-MVs; and specifications that link IC-MV's to traditional point measurements should be done with knowledge of measurement errors. Procedures suggested for verification of IC-MVs and quantifying measurement error are described in this report. One concept for verification involves a dedicated and controlled test bed at the MnROAD facility. This option would require an investment in the facility and personnel to regularly monitor the test bed values and perform maintenance as needed. A simple schematic of the test bed is provided. Another option would be to develop a highly mobile mechanical system that could simulate the range of soil conditions expected to be encountered on a project. It is envisioned that the device could be transported to a project periodically to verify the IC-MVs.

In accordance with the research tasks, three possible options are presented as alternatives to on-site calibration testing for IC machines. The premise of these options is to better assist the roller operator to target areas that need more compaction or re-work and the field engineer to target areas for QA testing. A statistically rigorous concept was also presented and is a new way to create a new way of defining quality of compacted fill materials. Some key features of these options are as follows:

- Option 1 – The final pass roller MV map of a production area is used to identify “weak” areas. The weak areas are targeted for in-situ QA testing. Acceptance of the production area is based on in-situ QA test measurements in the “weak” areas.
- Option 2 – This option requires evaluating the change in roller MV between successive passes over a production area. Production compaction should be performed until 90% of the production area achieves a percent change in MV of  $\leq 5\%$ . These percentages may be adjusted based on field conditions and experience.
- Option 3 – IC and QA target values for this option are pre-selected, which can be derived from a database of correlations from current study/literature, information from local projects, and calibration tests on test beds of known engineering properties. The contractor would use the pre-selected roller MV target values for QC, and QA is evaluated using a combination of roller data and in-situ QA test measurements.
- Option 4 – This specification approach is based on two goals: (1) that the overall level of critical soil engineering properties, over the entire site, achieve at least some specified minimal value (IC-TV), and (2) that the variability of critical soil engineering properties,

over the entire site, is no more than some specified maximal amount (e.g., %COV). These statements are quantified by determining the nature of uncertainty inherent in the measurement systems and then writing rules for defining degree of acceptable risk, (i.e., risk that a site which actually does not meet the goal is erroneously declared as meeting the goal based on the data.) The approach requires calibration of IC-MVs and point measurements. Site wide QA is then based on achievement of the defined critical soil engineering property based on the IC results. The advantage of this approach is that it allows for the assignment of acceptable risk and creates a framework for incentive-based pay. Although more rigorous mathematically, this option could provide a new way of characterizing compacted soils. This approach should be considered a concept and will require detailed pilot testing from multiple projects and conditions, but has the advantage of creating a consistent metric between different technologies and for defining quality. This report lays out the framework for the specification. A next step will be to evaluate this approach for large project level areas for different soil conditions and multiple roller IC systems.

A concept combining these options is presented to target more stringent compaction criteria (including uniformity) perhaps in the upper part of the embankment where it is more critical. In the long term, it is the authors' view, however, that option 4 is the approach that holds the most promise for specification development because it will be more easily linked to performance of the compacted fill materials than the other approaches. All four approaches provide a major advancement over traditional approaches. From a practice standpoint, option 4 will take the most effort and training to implement.

## **Recommendations**

The results of this study provided further evidence that IC technology has the potential to significantly improve construction process control and the resulting quality of compacted fill materials. To continue to make advancements and provide value to the process there are three recommendations suggested as outcomes of this study:

1. The statistically framed specification option for calibration and statistical analysis of risk is viewed as the building block of a future more robust and complete specification that is independent of IC machine technologies and point measurement technologies. Although the basic framework has been established some of the operational aspects of this specification will need to be developed. It is recommended that a specification task force take on the role to more fully developing the operational aspects. Future research is recommended to evaluate this approach for multiple material and IC rollers.
2. The general response from field inspectors and roller operators is that the IC technology brings value to projects and that it will improve construction efficiencies and quality. Much has been gained over the past few years in terms of experience and knowledge from the Mn/DOT field projects. This knowledge should be captured in the form of a formal training program for field inspectors and roller operators. A field inspector's guide should be developed for quick reference on roller operations, in-situ testing, data reporting, data analysis, and corrective actions.
3. Finally, challenges still exist with making use of the field data obtained during the construction process and archiving the data for future analysis. A critical next step in the

implementation process is to develop tools to provide real-time data analysis in conjunction with the specification criteria. This will benefit both the contractor and the field inspectors. It is recommended that the data analysis aspect be tied to the IC specification options and done external to the IC manufacturers' software.

# Chapter 1

## Introduction

### 1.1 Overview

Research conducted by Mn/DOT and others has indicated that intelligent compaction (IC) has tremendous potential to improve construction quality and efficiencies for contractors and field personnel. Several demonstration and pilot projects have been completed by Mn/DOT since 2005 (<http://www.dot.state.mn.us/materials/researchic.html>). Building on the knowledge gained from these demonstration projects, the first IC pilot specification in the U.S. was implemented on TH 64 in District 2 in 2006 which provided promising results in terms of IC measurements providing information for improved process control and quality assurance/quality control (QA/QC) (see White et al. 2007a, White et al. 2008). Additional pilot projects have since been performed by Mn/DOT that showed similar promising results. Some challenges and opportunities remain, however, to fully benefit from implementation of this technology. For example, although IC has been specified in the contract for pilot projects, traditional test requirements and procedures are being used for QA. A next step is to implement IC as both a QC tool for the contractor and to fully use the IC data as part of QA. In the future, it is possible that providing an incentive-based QC program could be established similar to pavement smoothness. To take the next step, improvements to selection of IC target values, linking results to test rolling rut depth measurements and mechanistic pavement design parameter values, understanding IC measurements for a wider range of materials, characterizing spatial non-uniformity, and improving data handling are some of the elements that were identified as needing work and constitute some of the key tasks of this research report. A parallel effort has been to implement light weight deflectometer (LWD) testing in lieu of traditional density testing as part of the QA/QC program for IC projects. LWD testing has advantages of being rapid and being empirically linked to pavement design parameters and IC measurement values (IC-MVs). LWD testing also has unique implementation challenges in terms of understanding modulus-based measurements, developing standard test protocols, creating suitable target values for QA/QC, and understanding influence from moisture content. This research report addresses many of these challenges and provides results and recommendations to further improve implementation of IC and LWD technologies including ideas for improvements to IC specifications.

### 1.2 Project Goals/Tasks

The overall goals of this research project were to:

- Provide educate and training opportunities to Mn/DOT staff and contractors on how to most effectively use IC and LWD technologies.
- Verify that the current IC specifications can be used on a wide range of materials and site conditions.
- Advance the implementation of IC specifically for use on non-granular materials.

- Refine the current IC specifications based on lessons learned from additional IC implementation.
- Develop the link between mechanistic empirical pavement design and construction QA/QC.

Specific tasks developed for the research effort were as follows:

- Develop procedures that could eliminate control strips prior to production compaction.
- Provide mechanistic empirical pavement design based target values for construction QA/QC use of IC and LWD.
- Develop guidance that could be used by Mn/DOT to modify or eliminate the existing test roller specification.
- Develop calibration procedures for IC and LWD equipment that could be adopted by Mn/DOT.

### 1.3 Research Methodology

This project was initiated after completion of the study *Field Validation of Intelligent Compaction Monitoring Technology for Unbound Materials*, Final Report MN/RC-2007-10, by White et al. (2007a), and builds on key findings from the study. A series of five educational/training seminars were conducted early in the project at the locations and on dates shown below to provide new information and experience with IC and LWD testing. Mn/DOT staff and contractors attended the seminars. Electronic files for all presentations are provided separate from this report.

1. *Mn/DOT Intelligent Compaction Implementation Seminar #1*, by David J. White, Ph.D. and Pavana Vennapusa, Mn/DOT Office of Materials, Maplewood, MN, April 23, 2007
2. *Mn/DOT Intelligent Compaction Implementation Seminar #2: Strategies for IC Data Management using ArcGIS, Correlations, and Geostatistical Analysis*, by David J. White, Ph.D. and Pavana Vennapusa, Mn/DOT Office of Materials, Maplewood, MN, April 23, 2007
3. *Mn/DOT Intelligent Compaction Implementation Seminar #3: Lessons Learned from IC and LWD Testing*, by David J. White, Mn/DOT District 4, Detroit Lakes, MN, May 30, 2007
4. *Mn/DOT Intelligent Compaction Implementation Seminar #4: Lessons Learned from IC, DCP and LWD Testing*, by David J. White, Mn/DOT District 4, Staples, MN, June 28, 2007
5. *Mn/DOT Intelligent Compaction Implementation Seminar #5: Lessons Learned from IC and LWD Testing*, by David J. White, Pavana Vennapusa, and Dan Enz, Mn/DOT District 4, Baxter, MN, November 14, 2007

In addition to the technology transfer efforts, a significant effort from this study also involved roller operation, test strip construction, in-situ testing, in-ground instrumentation, laboratory testing, and interviewing field personnel/constructor/technology manufacturers. Many individuals contributed to coordinating this work. Field studies were conducted on earthwork construction sites at the following project sites:

- TH 36, Metro District, North St. Paul, MN (S.P. 6211-81)
- US 10, District 2, Staples, MN (S.P. 7702-42)
- TH 60, District 7, Bigelow, MN (S.P. 5305-55)
- CSAH 2, Olmsted County, MN

At each site IC measurement values and in-situ point measurements were collected and compared to assess the relationships between the various measurements and also to examine the variability observed for the measurement systems. Laboratory soil index tests, compaction tests, strength, and resilient modulus tests were performed to characterize materials. LWD devices from two manufacturers (Zorn Stendal from Germany and Dynatest from Denmark) were evaluated in this study including devices with different plate diameters. Piezocone cone penetration testing (CPTU), dynamic cone penetration testing (DCP), plate load tests (PLT), falling weight deflectometers (FWD), Clegg impact tests (CIV), and nuclear moisture-density gauge tests (NG) were also used as part of the field investigations.

The findings from the field studies provide the basis for the IC and LWD specification recommendations and test protocols.

## **1.4 Report Organization**

This report is comprised of eight chapters. Chapter 2 describes the experimental laboratory and field testing methods used throughout the research project with test procedures referencing test standards, when applicable. Chapters 3 summarizes the field measurements from the above referenced project sites in case history format. Chapter 4 summarizes the results comparing test rolling rut measurements to various IC and in-situ point measurements. Chapter 5 provides a detailed summary of LWD measurements and an approach to determine target values for QA/QC. Chapter 6 provides recommendations for IC specification and verification procedures. Finally Chapter 7 and 8 provide summary/conclusions and further recommendations for implementation of IC and LWD technologies. Electronic files of raw data from field/laboratory measurements are provided separate from this report.

## **1.5 Units Conversion**

Per Mn/DOT report publishing guidelines, all measurements reported in this report are in Metric units. Conversions to appropriate English units for the measurements in this report are provided in Table 1.1, for reference.

Table 1.1. Summary of unit conversions from Metric to English

Measurement	Metric Unit	Multiply by	To obtain English Unit
Length	millimeter (mm)	0.03937	inches (in)
Length	millimeter (mm)	0.00328	feet (ft)
Length	centimeter (cm)	0.39370	inches (in)
Length	centimeter (cm)	0.03281	feet (ft)
Length	meter (m)	39.37	inches (in)
Length	meter(m)	3.281	feet (ft)
Velocity	kilometers per hour (km/h)	0.621	miles per hour (mph)
Weight	Gram (g)	0.0022	pound (lb)
Weight	Kilogram (kg)	2.205	pound (lb)
Force	Newton (N)	0.2248	Pound-force (lbf)
Force	kilo Newton (kN)	224.81	Pound-force (lbf)
Density	kilo gram per cubic meter (kg/m <sup>3</sup> )	0.0624	Pount per cubic feet (pcf)
Unit Weight	kilo Newton per cubic meter (kN/m <sup>3</sup> )	6.3659	pound per cubic feet (pcf)
Pressure	kilo Pascal (kPa)	0.145	pounds per square inch (psi)
Pressure	kilo Pascal (kPa)	20.89	pounds per square feet (psf)
Pressure	mega Pascal (MPa)	145.04	pounds per square inch (psi)
Pressure	mega Pascal (MPa)	20885.4	pounds per square feet (psf)

## Chapter 2

### Experimental Testing Methods

Two roller-integrated compaction monitoring technologies—Compaction Meter Value (CMV) and Machine Drive Power (MDP)—were evaluated in this research study. Several in-situ testing methods were employed in the field studies. This chapter provides a brief overview of the IC measurements and the in-situ testing procedures.

#### 2.1 Roller-Integrated Compaction Measurements

##### 2.1.1 Compaction Meter Value (CMV) and Resonant Meter Value (RMV)

Caterpillar 12-ton CS-563 and 19-ton CS-683 smooth drum rollers were used in this study. These rollers were instrumented with accelerometers to determine Geodynamik CMV and RMV by measuring drum accelerations in response to soil behavior during compaction operations. Settings available on the machines are summarized in Table 2.1.

CMV is defined as the ratio between the amplitude of the first harmonic and the amplitude of the fundamental frequency (Equation 2.1) (Thurner and Sandström, 1980). An increase in CMV indicates increasing compaction.

$$\text{CMV} = C \cdot \frac{A_1}{A_0} \quad (2.1)$$

where,  $C$  = constant,  $A_1$  = acceleration of the first harmonic component of the vibration, and  $A_0$  = acceleration of the fundamental component of the vibration (Sandström and Pettersson, 2004). CMV is a dimensionless parameter that depends on roller dimensions (i.e., drum diameter, weight) and roller operation parameters (i.e., frequency, amplitude, speed). CMV at a given point indicates an average value over an area whose width equals the width of the drum and length equal to the distance the roller travels in 0.5 seconds (Geodynamik ALFA-030).

Based on numerical investigations Adam (1997) identified five significant vibratory drum operation modes of motion (see Table 2.2) that are related to soil stiffness and roller operation parameters (i.e., vibration frequency and amplitude). These different operation modes influence the roller compaction measurements significantly and have to be considered in evaluating the data. Continuous contact occurs only for relatively uncompacted soils. Partial uplift and double jump are the most frequent drum operation modes. When the soil stiffness is very high the roller drum enters into a double jump rocking or chaotic motion. The roller compaction measurements are considered unreliable when the drum is in rocking or chaotic motion (Adam 1997). Results from earlier field investigations by the authors' (see Vennapusa and White 2009b, White et al. 2009, NCHRP 21-09 2009) indicate that double jump is likely to occur when roller is operated in high amplitude settings (e.g.,  $a > 1$  mm). The degree of double jump can be assessed using the

RMV which is calculated using Equation 2.2, where  $A_{0.5}$  = subharmonic acceleration amplitude caused by jumping (the drum skips every other cycle). According to Brandl and Adam (2004),  $RMV > 0$  indicates that the drum is a double jump, rocking or chaotic mode. For a CS-563 machine used on TH64 project (see Vennapusa and White 2009b),  $RMV > 2$  was used a practical cut-off value for transition between continuous contact and double jump.

$$RMV = C \cdot \frac{A_{0.5}}{A_0} \quad (2.2)$$

Table 2.1. Summary of measurement values and settings on the machines used

Parameter	Description
Measurement Value	CS563 and CS683: CMV CP563: MDP
Frequency	CS563 and CS683: 33 Hz (nominal) [31.8 ± 0.2 Hz measured] CP563: 30 Hz (nominal) [not reported in the output]
Amplitude	CS563 and CS683: nominal 0.85 mm (low amplitude) and 1.70 mm (high amplitude) CP563: nominal 0.85 mm (low amplitude) and 1.87 mm (high amplitude)



Figure 2.1. 12-ton CS-563 smooth drum (left) and 19-ton CS-683 smooth drum rollers equipped with CMV/RMV systems and GPS

Table 2.2. Observed modes of vibratory roller drum (Adam 1997)

Drum Motion	Drum-Soil Interaction	Operation Mode	Validity of compaction values	Soil Stiffness
Periodic	Continuous Contact	Continuous Contact	Yes	Low ↓ High
	Periodic loss of contact	Partial Uplift	Yes	
		Double Jump	Yes	
		Rocking Motion	No	
Chaotic	Non-periodic loss of contact	Chaotic Motion	No	

### 2.1.2 Machine Drive Power (MDP)

CP-563, CP-56, and CP-662 padfoot rollers equipped with MDP system (Figure 2.2) were used in this research study. Controlled field studies documented by White and Thompson (2008), Thompson and White (2008), and Vennapusa et al. (2009) verified that roller-integrated machine drive power (MDP) can reliably indicate soil compaction for granular and non-granular soils. The basic premise of determining soil compaction from changes in equipment response is that the efficiency of mechanical motion pertains not only to the mechanical system but also to the physical properties of the material being compacted. MDP is calculated using Equation 2.3.

$$MDP = P_g - WV \left( \sin \alpha + \frac{a}{g} \right) - (mV + b) \quad (2.3)$$

where,  $P_g$  = gross power needed to move the machine (kJ/s),  $W$  = roller weight (kN),  $a$  = machine acceleration ( $m/s^2$ ),  $g$  = acceleration of gravity ( $m/s^2$ ),  $\alpha$  = slope angle (roller pitch from a sensor),  $V$  = roller velocity (m/s), and  $m$  (kJ/m) and  $b$  (kJ/s) = machine internal loss coefficients specific to a particular machine (White et al. 2005). MDP is a relative value referencing the material properties of the calibration surface, which is generally a hard compacted surface ( $MDP = 0$  kJ/s). Positive MDP values therefore indicate material that is less compact than the calibration surface, while negative MDP values would indicate material that is more compacted than the calibration surface (i.e. less roller drum sinkage).

The MDP results presented in this research study (here after referred to as  $MDP^*$ ) are modified using Equation 2.4 and adjusted between 1 and 150. The calibration surface with  $MDP = 0$  (kJ/s) is scaled to  $MDP^* = 150$ , and a soft surface with  $MDP = 111.86$  (kJ/s) is scaled to  $MDP^* = 1$  (from email communication with Mario Souraty, Caterpillar, Inc. October 2007). Therefore, with increasing compaction MDP decreases and  $MDP^*$  increases.

$$MDP^* = 119.7 - 0.798(MDP) \quad (2.4)$$



Figure 2.2. 12-ton CP-563 padfoot roller equipped with MDP\* system and GPS

## 2.2 In-Situ Testing Methods

Table 2.3 lists the in-situ test methods employed in this research study along with the standard procedures followed. A brief overview of each of test method is presented below.

### 2.2.1 Heavy Test Rolling

Test rolling was performed using a pneumatic tire two-wheeled trailer with each wheel weighing 133.5 kN and is towed behind a tractor in accordance with Mn/DOT specification 2111 (Mn/DOT 2005). The depth of the rut beneath the roller wheels was measured from the top of the compaction surface. If measured rut depths are  $\geq 50$  mm, the area is considered unstable and corrective action is required (Mn/DOT 2005). Further description of test rolling operations is provided in Chapter 4.

### 2.2.2 Light Weight Deflectometers

Zorn, Keros, and Dynatest light weight deflectometers (LWDs) were used in this study. Zorn is manufactured by Gerhard Zorn in Germany, and Keros/Dyantest LWD devices are manufactured by Dynatest in Denmark. Zorn LWDs setup with 100, 150, 200, and 300 mm diameter plates and 50 to 72 cm drop heights were used. Keros/Dynatest LWDs setup with 200 and 300 mm diameter plates and 50 to 72 cm drop heights were used. Equation 2.5 was used to determine modulus from LWD measurements ( $E_{LWD}$ ). Further discussion on LWD measurements and factors affecting the  $E_{LWD}$  values is provided in Chapter 5.

$$E = \frac{(1 - \eta^2) \cdot \sigma_0 \cdot r}{d_0} \times F \quad (2.5)$$

where,  $d_0$  = measured settlement (mm),  $\eta$  = Poisson's ratio,  $\sigma_0$  = applied stress (MPa),  $r$  = radius of the plate (mm),  $E$  = Young's modulus (MPa);  $F$  = Shape factor depending on assumed contact stress distribution (see Vennapusa and White 2009a for discussion on shape factors). For calculations in this report  $F = 8/3$  was used for granular materials and  $F = \pi/2$  was used for non-granular materials. The calculated  $E_{LWD}$  values differ significantly with size of loading plate and type of LWD device (see Chapter 5). Therefore,  $E_{LWD}$  values are differentiated by using the following terminology between model, plate diameter, and diameter used.

- $E_{LWD-XY(Z)}$  = "X" denotes the model type (Z – Zorn, D – Dynatest, and K – Keros); "Y" denotes the plate diameter (1 – 100 mm, 1.5 – 150 mm, 2 – 200 mm, and 3 – 300mm), "Z" denotes the drop height in cm.

### 2.2.3 Falling Weight Deflectometer

FWD testing was performed by applying three seating drops using a nominal force of about 26.7 kN followed by three test drops each at 26.7 kN and 53.4 kN force ( $F$ ). The actual applied  $F$  was recorded using a load cell. The deflections were measured using geophones placed at the center of the plate and at 0.2 m, 0.3, 0.5, 0.6, 0.8, 0.9, 1.2, 1.52, and 1.8 m offsets from the center of the plate. A composite modulus value ( $E_{FWD-D3}$ ) was calculated using measured deflection at the center of the plate from Equation 2.5. Modulus values of the underlying layers were calculated using Equation 2.6, where  $D_i$  is the radial distance from the center of the plate to the  $i^{th}$  sensor and  $d_{0(i)}$  is the deflection measured at the  $i^{th}$  sensor.

$$E = \frac{(1-\eta^2) \cdot \sigma_0 \cdot r^2}{D_i d_{0(i)}} \times F \quad (2.6)$$

### 2.2.4 Dynamic Cone Penetrometer

DCP tests were performed in accordance with ASTM D 6951-03. The tests were performed extending to a depth of about 1 m using the typical DCP setup, and tests extending to a depth of about 2 m were conducted using extension rods. Dynamic penetration index (DPI) with units of mm/blow is reported from the tests. DPI is inversely related to soil strength/stiffness properties and is well discussed in the literature (see McElvanet and Djatnika 1991, Yoon and Salgado 2002). Weighted average DPI was calculated for the compaction layer thickness ( $z$ ) using two different approaches shown in Equations 2.7 and 2.8.

$$DPI_z = \frac{DPI_1 \cdot z_1 + DPI_2 \cdot z_2 + \dots + DPI_n \cdot z_n}{\sum z_n} \quad (2.7)$$

$$DPI_{s-z} = \frac{DPI_2 \cdot z_2 + \dots + DPI_n \cdot z_n}{\sum z_n} \quad (2.8)$$

where,  $DPI_z = DPI$  for compaction layer of thickness  $z$ ,  $DPI_{1,2,\dots,n} = DPI$  of blows 1 to  $n$ .  $DPI_{s-z} = DPI$  for compaction layer of thickness  $z$  excluding data obtained from first (seating) drop.

### **2.2.5 Piezocone Cone Penetration Test**

Piezocone cone penetration tests (CPTU) tests were performed by Mn/DOT personnel using a 30 ton rig. Tests were conducted using a cone with  $60^\circ$  taper angle and  $10 \text{ cm}^2$  area to measure tip resistance ( $q_t$ ), sleeve friction ( $f_s$ ), and pore pressure ( $u$ ) during penetration. A nominal rate of penetration of about  $2 \text{ cm/s}$  was used. The tip resistance values were corrected to account for unequal areas above and below the porous element with respect to pore pressure measurements to calculate  $q_t$  (Vertek 2005).

### **2.2.6 Nuclear Gauge**

A calibrated nuclear moisture-density gauge (NG) device was used to provide rapid measurements of soil dry unit weight and moisture content. Tests were performed following ASTM D2922. Generally, two measurements of moisture and dry unit weight were obtained at a particular location with the average value being reported. Probe penetration depths were selected based on the compaction layer thickness.

### **2.2.7 Shelby Tube Sampling**

Undisturbed samples of compacted subgrade material were obtained by hydraulically pushing 71 mm diameter thin-walled/Shelby tube samples into the compacted subgrade. The tube samples were sealed and transported to the laboratory for laboratory unconfined compressive (UC) strength, resilient modulus ( $M_r$ ), and unconsolidated-undrained (UU) testing.

### **2.2.8 Static Plate Load Test**

Displacement-controlled static plate load tests (PLTs) were conducted by applying a static load on a 300/200 mm diameter plates against a 62kN capacity reaction force. The applied load was measured using a 90-kN load cell and deformations were measured using three 50-mm linear voltage displacement transducers (LVDTs). The average of the three deflection measurements was used in the calculation. The load and deformation readings were continuously recorded during the test using a data logger. Initial ( $E_{v1}$ ) and re-load ( $E_{v2}$ ) modulus were determined using Equation 2.5 by using stress and deformation readings taken from 0.2 to 0.4 MPa for granular materials and 0.1 to 0.2 MPa for non-granular subgrade soils (see Figure 2.4).

### **2.2.9 Clegg Hammer**

Clegg impact hammers were developed by Clegg during the late 1970's for evaluating compacted fill and pavement materials. The Clegg hammer setup with 20 kg drop weight and

450 mm drop height was used in this study and tests were performed in accordance with ASTM D 5874-02. The Clegg impact value is derived from the peak deceleration of the free falling drop hammer in a guide sleeve for four consecutive drops.

### 2.2.10 Soil Stiffness Gauge

The soil stiffness gauge (SSG) was used for determining in-situ soil stiffness or modulus. The device is also referred to as the GeoGauge. The device produces small dynamic forces (vibrates at 25 frequencies ranging from 100 to 196 Hz) and soil deflections, from which soil modulus can be calculated using Equation 2.9 (Humboldt Mfg. Co. 2000):

$$E_{SSG} = \frac{Force}{\delta} \cdot \frac{(1-\eta^2)}{(1.77r)} \quad (2.9)$$

where, Force = dynamic force caused by the vibrating device,  $\delta$  = deflection measured,  $\eta$  = Poisson's ratio (assumed as 0.4), and  $r$  is the radius of the annular ring.

### 2.2.11 Earth Pressure Cells

Piezoelectric EPCs with a measurement range 0 to 600 kPa and 0 to 1000 kPa were used in this study to measure the total peak horizontal ( $\sigma_x$  and  $\sigma_y$ ) and vertical stresses ( $\sigma_z$ ) developed in the pavement foundation layers under roller, LWD, and FWD loading. Horizontal stresses were measured by installing EPCs parallel ( $\sigma_y$ ) and perpendicular ( $\sigma_x$ ) to the direction of roller compaction. The EPCs used in this study were manufactured by Geokon. They were 100 mm in diameter, 10 mm in thickness and were made of two stainless steel plates welded together around their periphery and filled with deaired hydraulic fluid. Wieler and Kulhawy (1982) indicated that stress measurements made using EPCs are affected by the type and density of the soil placed around the sensors. The EPCs used in the study were calibrated using an EPC calibration pressure chamber designed and fabricated at Iowa State University (see White et al. 2009). The cells were calibrated for compacted 50 mm thick dry Ottawa # 10 sand ( $\gamma = 1658\text{kg/m}^3$ ) placed above and below the sensors.

The EPCs were installed in the pavement foundation layers by excavating a trench. To represent the laboratory calibration conditions, approximately 50-mm thick layer of clean Ottawa #10 sand was placed around the EPCs installed. The excavated trench was then backfilled with hand tools using the trench spoil materials. Efforts were made to separate the spoil materials into soils type based on the layer it was excavated from and to cover the materials to prevent moisture loss.

Table 2.3. In-situ test methods and procedures employed in this study

In-situ Test Device	Measurement	Test Method/ Standard	Remarks
Heavy test Rolling	Rut Depth	Mn/DOT Specification 2111	Figure 2.3a,b
300/200 mm diameter plate Dynatest 3031LWD	$d_{LWD-D3}$ , $E_{LWD-D3}$ and $d_{LWD-D2}$ , $E_{LWD-D2}$	Dynatest (2004)	Figure 2.3c
200 mm diameter plate Keros LWD	$d_{LWD-D2}$ , $E_{LWD-K2}$	Dynatest (2004)	Figure 2.3c
100, 150, 200, and 300 mm diameter plate Zorn LWD	$d_{LWD-Z1}$ , $E_{LWD-Z1}$ , $d_{LWD-Z1.5}$ , $E_{LWD-Z1.5}$ , $d_{LWD-Z2}$ , $E_{LWD-Z2}$ , $d_{LWD-Z2}$ , and $E_{LWD-Z3}$	Zorn (2000)	Figure 2.3c
Dynatest 300 mm plate diameter FWD	$E_{FWD-D3}$	see text	Figure 2.3d
DCP	DPI	ASTM D6951-03	Figure 2.3e
CPTU	$q_t$ , $f_s$ , and $u$	see text	Figure 2.3f
Humboldt Nuclear Gauge	$\gamma_d$ and $w$	ASTM D2922	Figure 2.3g
Shelby tube sampling	UC, UU, and $M_r$ (in laboratory)	ASTM D2166-06 (UC), AASTHTO T- 307 (UU and $M_r$ )*	Figure 2.3h
Static PLT	$E_{V1}$ and $E_{V2}$	see text	Figure 2.3i
20-kg Clegg Hammer	$CIV_{20\text{-kg}}$	ASTM D5874-02	Figure 2.3j
Humboldt SSG	$E_{SSG}$	Humboldt Mfg. Co. (2000)	Figure 2.3k
Piezoelectric EPCs	Horizontal and vertical stresses	see text	Figure 2.3l

\*AASHTO T-307 loading sequences for subgrade materials are presented in Table 2.4.

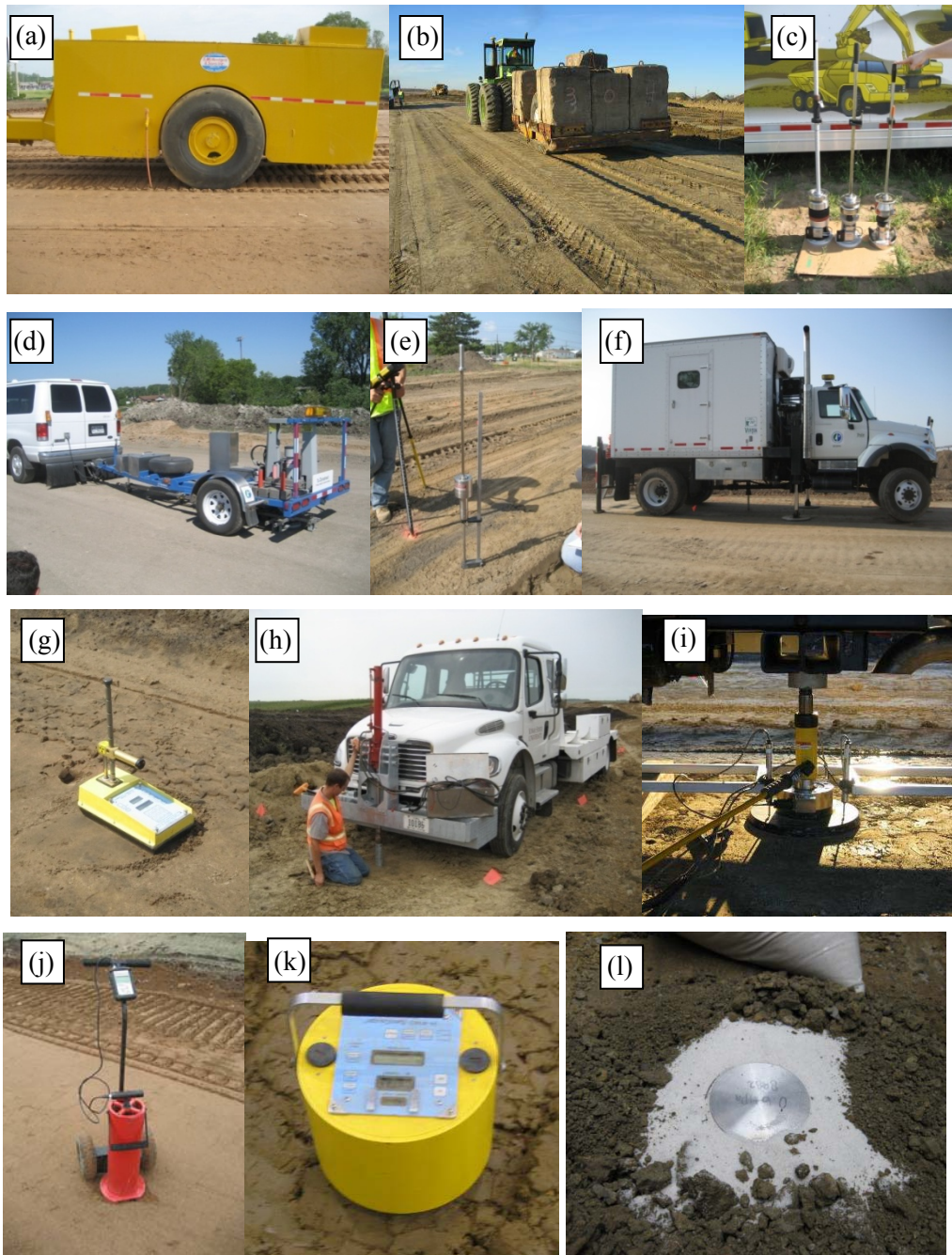


Figure 2.3. In-situ testing methods employed in this study: (a), (b) towed pneumatic dual-wheel test rollers with 650 kPa contact tire pressure, (c) Keros, Dynatest, and Zorn LWDs, (d) Mn/DOT Dynatest FWD, (e) DCP, (f) Mn/DOT CPT, (g) nuclear moisture-density gauge, (h) shelly tube sampler, (i) static plate load test, (j) 20-kg Clegg Hammer, (k), Humboldt SSG, and (l) Piezoelectric EPCs

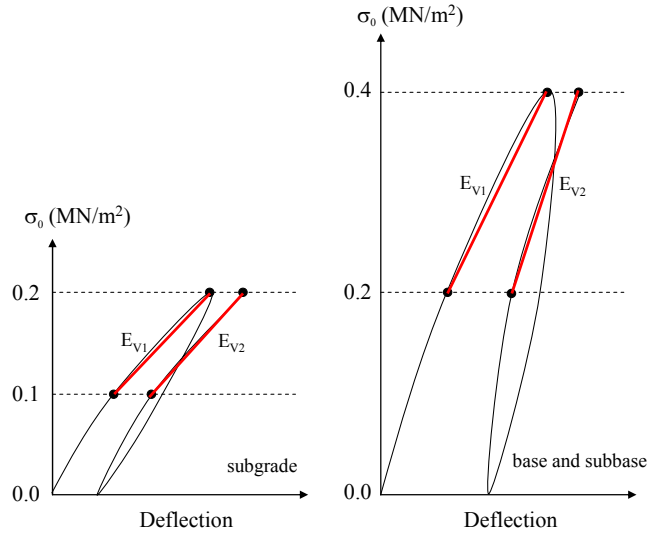


Figure 2.4. Static plate load test data modulus scheme for subgrade, subbase, and base materials

Table 2.4. Resilient modulus ( $M_r$ ) test loading sequences for subgrade materials (AASHTO T-307 test procedure)

Sequence No.	Confining Pressure		Max. Axial Stress		No. of cycles
	kPa	psi	kPa	psi	
0	41.4	6	27.6	4	500-1000
1	41.4	6	13.8	2	100
2	41.4	6	27.6	4	100
3	41.4	6	41.4	6	100
4	41.4	6	55.2	8	100
5	41.4	6	68.9	10	100
6	27.6	4	13.8	2	100
7	27.6	4	27.6	4	100
8	27.6	4	41.4	6	100
9	27.6	4	55.2	8	100
10	27.6	4	68.9	10	100
11	13.8	2	13.8	2	100
12	13.8	2	24.8	4	100
13	13.8	2	37.3	5	100
14	13.8	2	49.7	7	100
15	13.8	2	62.0	9	100

## Chapter 3

### Field Project Case Histories

#### 3.1 Introduction

Field investigations were conducted by the ISU research team at four earthwork construction projects in Minnesota where IC pilot specifications were implemented. These projects include: (a) Metro District TH36, North St. Paul (b) District 3 US10, Staples, (c) District 7 TH60, Bigelow, and (d) CSAH 2, Olmsted County. Caterpillar roller-integrated vibratory based CMV/RMV and vibratory and non-vibratory based MDP\* compaction monitoring technologies (referred to as IC-MVs hereafter) were evaluated on these project sites. Embankment materials at the TH36 and US10 projects were predominantly granular soils, whereas at the TH60 and CSAH 2 projects the materials were predominantly non-granular soils.

To date, the general approach followed in the IC pilot specifications has been constructing on-site calibration strips to develop target values and using the target values for QA/QC in production areas. One of the research tasks of this project was to identify alternatives to eliminate the construction of calibration strips. Utilizing target values from an existing database of relationships and experience is one alternative (see White et al. 2007a). To help populate the database, the field investigations for the case histories described herein involved performing a variety of traditional in-situ point measurements (LWD, FWD, PLT, SSG, DCP, CIV,  $w$ ,  $\gamma_d$ ) to develop correlations with IC-MVs. Previous work and experience indicates that the IC-MVs are better correlated with strength/stiffness based measurements (e.g., FWD, DCP, PLT, etc.) compared to relative compaction or dry unit weight measurements (see Thurner and Sandström 1980, Floss et al. 1991, NCHRP 21-09). Correlations presented in the literature show varying degrees of uncertainty in the relationships between IC-MVs, however. Factors contributing to uncertainties are: (a) differences in measurement influence depths between IC-MVs and in situ point measurements (see Figure 3.1), (b) difference in applied stresses during loading under roller and point measurements, (c) heterogeneity in the underlying layer stiffness, and (d) differences in volume of soil tested. These factors limit the potential of relying on a database of typical values. For accelerometer based measurement systems, measurement influence depths between 0.8 to 1.5 m under a 12-ton vibratory roller have been reported in the literature (see ISSMGE 2005, NCHRP 21-09, and White et al. 2009). MDP based measurements have measurement influence depths ranging from 0.3 m to 0.6 m depending on the variability of the underlying layer (see White et al. 2009). Conventional in-situ point measurements such as NG, SSG (Florida DOT, 2003), and LWD (Kudla et al. 1991) are believed to have influence depths < 300 mm. To investigate in-situ testing methods that provide deeper measurements, FWD, DCP, and CPTU were investigated as part of this study. Because in-situ soil properties are stress dependent, in-ground stress measurements in the pavement foundation layers under roller, LWD, and FWD loading were also obtained from the field investigations. In addition, field interviews were conducted with Mn/DOT and contractor personnel to obtain insights on the challenges with respect to improved implementation of IC and LWD technologies.

This chapter presents a brief overview of key elements of the IC pilot specifications implemented, experimental results, field observations, and significant findings and conclusions from each project site. Comparisons to test roller rut depth measurements were also obtained from these projects, but are presented separately in Chapter 4.

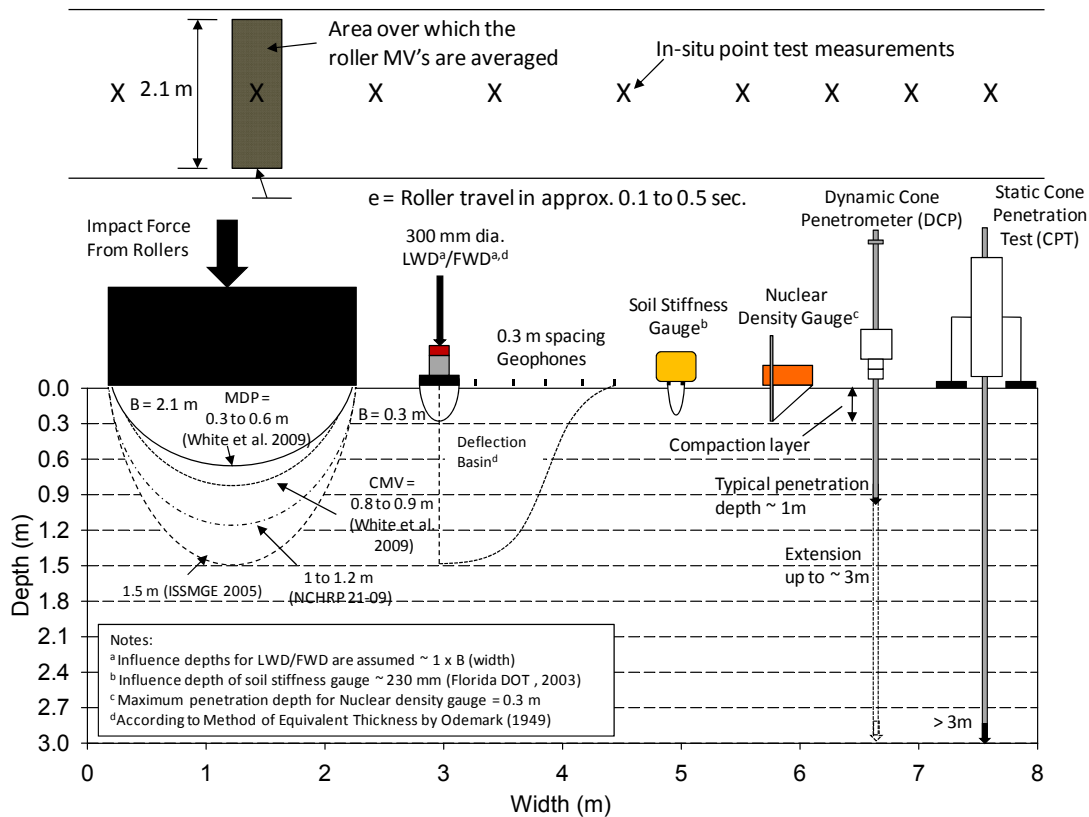


Figure 3.1. Illustration of differences in measurement influence depths of different testing devices.

### 3.2 Overview of IC Pilot Specifications

Mn/DOT 2106 – Excavation and Embankment – (QA/QC) IC Quality Compaction (Pilot Specification) for Granular and Non-Granular embankment grading materials was implemented on the project sites. Granular materials are defined in Mn/DOT specification 3149.2B. Some key elements of the specifications are provided below.

**Equipment Specifications:** Use a self propelled vibratory pad foot roller for compacting non-granular materials and a vibratory smooth drum roller for compaction of granular materials equipped with an IC measurement system and global positioning system (GPS) to allow continuous recording of roller location and corresponding compaction-related output. The contractor is required to complete an IC test pad on the project site using the embankment grading materials to demonstrate that the IC roller and its documentation system meets all the

specification requirements. The IC test pad requirements are same as the control strip requirement or as otherwise determined by the Engineer but cannot be one of the control strips.

**Compaction Process and Acceptance Specifications:** The contractor shall utilize data gathered from the control strip construction to develop a QC procedure including proper IC equipment and procedures, collecting and reporting IC compaction results, ensuring uniformity, confirming acceptable moisture limits, compaction pattern and speed of roller passes, etc.

Construct one control strip for each different type/source of grading material used on the construction site to determine the Intelligent Compaction – Target Value (IC-TV) and Light Weight Deflectometer Target Value (LWD-TV). IC-TV will be the optimum compaction value determined by the Engineer when optimum compaction is reached i.e., when additional compaction passes do not result in a significant increase in stiffness. Three (3) LWD tests will be performed by the Engineer on each layer of control strip (spaced 25 m apart or as modified by the Engineer) to determine the average and use as LWD-TV. Moisture should be 65%–95% of Optimum Moisture, as determined by the standard Proctor test method. Contractor shall add water or dry and/or perform blending as needed to meet the moisture requirements. To determine the moisture sensitivity correction for IC-TV and LWD-TV, the control strip shall be constructed at or near each extreme of 65% and 95% of optimum moisture content. This data will be utilized to produce a correction trendline showing a linear relationship of the IC-TV and LWD-TV at different moisture contents. As part of QC, the contractor will perform moisture content tests on the granular treatment at a minimum of 1 per 3,000 cubic meter for compliance.

QA is accomplished by constructing proof layers. For layers less than or equal to 0.75 m (2.5 ft) in thickness, the proof layer shall be designated as the top of the layer. For layer thickness greater than 0.75 m and less than 1.2 m (4 ft) in thickness, the proof layers shall be designated as the midpoint and the top of the layer. For layers equal to or greater than 1.2 m (4 ft) in thickness, the proof layers shall be successive 0.6 m (2 foot) layers in thickness from the bottom and up to the top of the final layer. All segments of proof layers shall be compacted so that at least 90% of the IC measurements are at least 90% of the IC-TV prior to placing the next lift. Areas less than 80% of IC-TV, the Contractor shall bring these areas to at least 90% of IC-TV prior to placing the next lift. If a significant portion of the grade is more than 20% in excess of the IC-TV, the Engineer shall re-evaluate the IC-TV. If an applicable IC-TV is not available, the contractor shall construct an additional control strip. The Engineer will perform one (1) LWD and moisture test per proof layer per 300 m (1000 feet) in length for the entire width of embankment. The LWD value shall be at least 90% but not more than 120% of the corrected LWD-TV. Areas that do not meet these requirements shall be re-compacted (and dry or add moisture as needed). The Engineer will perform moisture content tests at a minimum of 1 per 9,000 cubic meter of grading materials for QA.

**Location Specifications (including size, depth, and track overlap):** Each control (calibration) strip must be at least 100 m (300 ft) x 10 m (32 ft) at its base (or as determined by the Engineer). The lift thicknesses for the control strip and the constructed embankment shall be limited to the maximum lift thickness allowed in Mn/DOT 2106.3E. The total thickness should equal that of

the planned embankment grading materials thickness being constructed (maximum 1.2 m (4.0 ft)).

**Misc. Specs (moisture, speed, frequency, etc.):** Compaction and mixing of embankment grading materials shall be uniform from bottom to top and for the entire length and width of the embankment. Engineer grants final approval, based on observation of final compaction/stiffness recording pass, approval of Weekly QC Reports, LWD/moisture tests, and test rolling requirements. In addition to QA from IC measurements, TH 36 and TH 60 projects required QA following the Mn/DOT 2111 test rolling specification.

**Documentation Requirements:** The IC roller should be equipped with a location, measurement, and documentation system, which shall provide the results that:

- Enhance the ability of the roller operator and project inspectors to make real-time corrections to compaction process. Be available for the Engineer to review the IC screen located in the roller operator's cab when requested
- Be exportable into a comma delimited ASCII format or other approved data submittal format. Each ASCII data file shall contain: drum parameters including frequency, amplitude and acceleration, compaction parameters, position data including x,y,z coordinates for each side of the drum in UTM NAD 1983 zone 15 N format and a time stamp for each data point accurate to the frequency of the drum.
- Allow for a plan-view, color-coded plot of roller measured compaction parameters and roller pass number measurements throughout a designed section of roadway.

### **3.3 Metro District TH 36, North St. Paul**

#### **3.3.1 Project Overview**

The project involved reconstruction of TH 36 between White Bear Avenue and Century Avenue in North St. Paul, Minnesota. Reconstruction activities included a diamond interchange at TH 36 and McKnight Road intersection, and bridges for Margaret Street and pedestrian traffic over TH 36. Earthwork involved cuts and fills up to 5.5 m (18 ft) in height. Embankment materials used in the project were select granular base, granular subbase, and non-granular or granular "common" subgrade materials. The "common" subgrade material contained sandy soils with varying clay content. Moisture content tests were conducted as part of QC. IC measurements, test rolling (Mn/DOT standard specification 2111 only for granular soils), DCP (Mn/DOT modified DCP method, see Oman 2004), LWD, and "speedy" moisture content tests were conducted for QA tests. CP563 padfoot and CS563 smooth drum rollers equipped with IC technologies were used for compacting embankment materials. The padfoot roller was used for compacting non-granular subgrade materials on TH 36 mainline west of McKnight Road, and the smooth drum roller was used in the remaining areas for compacting granular materials.

In-situ point measurements (DCP, LWD, FWD, PLT, CPT, and CIV) in conjunction with IC-MVs to develop correlations, and in-ground instrumentation data to evaluate stresses in the pavement foundation layers under roller and FWD/LWD loading were obtained from the project.

### 3.3.2 Experimental Testing

A total of four test strips were constructed and tested as part of this project (see Table 3.1). Compaction on test strips 1 and 2 was performed by the contractor and on test strips 3 and 4 was performed by ISU personnel. Compaction and mapping passes on all test strips were performed using CS563 smooth drum roller. A summary of soil index properties of embankment materials in each strip is presented in Table 3.2.

Test strips 1, 2, and 4 involved performing in-situ testing to develop correlations between in-situ point measurements and IC-MVs. Real time kinematic (RTK) global positioning system (GPS) location coordinates (in UTM NAD 1983 zone 15 N format) with accuracy of about 2 cm were obtained at in-situ point measurement locations to match with the roller measurements. To better understand and interpret the relationships between IC-MVs and in-situ point measurements, test strips 3 and 4 were instrumented with calibrated piezoelectric earth pressure cells (EPCs) with a measurement range of 0-1000 kPa. The EPCs were used to measure the total peak horizontal and vertical stresses induced by the roller, LWD, and FWD loading.

Table 3.1. Field testing summary (TH36)

Date	Test Strip	Location	Operator	Surface Material	Lift	Remarks
05/23/2007	1	West end of project on WB lane exit ramp	Contractor	Granular subbase (0.3 m thick)	1	DCP, SSG, CIV <sub>20-kg</sub> , Zorn LWD <sup>§</sup>
			Contractor	Granular subbase (0.3 m thick)	2	DCP, Zorn LWD <sup>§</sup>
05/29/2007	2	West end of project on WB Lane exit ramp	Contractor	Select granular base	1	DCP, Zorn LWD, PLT <sup>§</sup>
05/31/2007	3	West end of project on WB Lane exit ramp	ISU	Select granular base	1	In-Ground Instrumentation <sup>§</sup>
07/26/2007 to 07/27/2007	4	East side of McKnight bridge approach on WB lane	ISU	Select granular base	1	CPTU, DCP, FWD, Dynatest and Zorn LWD, and EPCs <sup>§</sup>

Note: Compaction/mapping on all strips using smooth drum roller; <sup>§</sup>GPS measurements for point measurements.

Table 3.2. Summary of soil index properties (TH36)

Parameter	Strip 1/2	Strip 2/3	Strip 4		
Material Description	Granular subbase	Granular Base	Granular Base	Granular subbase	“Common” Subgrade
Maximum Dry Unit Weight (kN/m <sup>3</sup> ) and Optimum Moisture Content (%)					
Standard Proctor	18.8 (9.0)	20.0 (7.9)	20.0 (8.2)	18.7 (8.9)	18.5 (11.5)
Modified Proctor	—*	20.9 (7.0)	—*	—*	19.0 (9.2)
Gravel Content (%) (> 4.75mm)	15	20	38	0	10
Sand Content (%) (4.75mm – 75µm)	77	58	48	97	57
Silt Content (%) (75µm – 2µm)	5	14	10	0	19
Clay Content (%) (< 2µm)	3	8	4	2	13
Coefficient of Uniformity (c <sub>u</sub> )	4.8	109.1	83.2	2.9	—
Coefficient of Curvature (c <sub>c</sub> )	1.2	11.1	0.6	0.9	—
Liquid Limit, LL (%)	NP	NP	NP	NP	22
Plasticity Index, PI	NP	NP	NP	NP	9
AASHTO	A-1-b	A-2-4	A-1-b	A-1-b	A-2-4
USCS symbol	SP-SM	SM	SM	SP	SC
Specific Gravity, G <sub>s</sub>	2.70	2.68	2.64	2.69	2.70

NP – non-plastic; \* test not performed.

### 3.3.3 Comparison of IC-MVs and In-Situ Point Measurements

#### 3.3.3.1 Test Strip 1

The test strip was approximately 113 m long and was located on west bound TH36 along the exit ramp for White Bear Avenue. Two lifts of granular subbase material each about 0.3 m thick were placed over existing subgrade and compacted using a smooth drum IC roller. Index properties of the granular subbase layer material are provided in Table 3.2. Following compaction passes on lift 1, the layer was mapped with  $a = 0.85$  mm,  $f = 33$  Hz, and  $v = 4.0$  km/h nominal settings (Figure 3.2). Following mapping, in-situ point measurements ( $d_{LWD-Z2}$ ,  $E_{LWD-Z2}$ ,  $CIV_{20-kg}$ ,  $E_{SSG}$ , and DPI) were performed on lift 1 at the surface. IC-MVs were not available on lift 2. The point measurements were performed on lift 2 at the surface and at 0.15 m below the surface by excavating the material to investigate the effect of confinement on the measurement values.

A color-coded CMV map of lift 1 and DPI profiles at spot test measurement locations are shown in Figure 3.3. A concrete utility pipe was located beneath the subbase layer lift 1 at spot test location 2 (see Figure 3.3).

In-situ point measurements obtained on lift 1 in comparison with CMV measurements are presented in Figure 3.4. Variation observed in the CMV measurements along the test strip tracked well with the variation in point measurements. The CMV values were higher on top of the concrete pipe and lower along the edge suggesting poor compaction, which is a relatively common scenario when compacting material directly adjacent to large utility pipes or box culverts. Regression relationships obtained by pairing point measurement data with nearest point CMV data are presented in Figure 3.5 and are summarized in Table 3.3. Regression relationships showed good correlations with coefficient of determination ( $R^2$ ) values ranging from 0.5 to 1.0.  $E_{LWD-Z2}$ ,  $d_{LWD-Z2}$ , and  $E_{SSG}$  showed comparatively better correlations ( $R^2 > 0.8$ ) than  $CIV_{20\text{-kg}}$  and  $DPI_{300}$ . Summary statistics (mean  $\mu$  and coefficient of variation COV) of the measurements are presented in Table 3.4.

In-situ point measurements obtained on lift 2 at the surface and after excavating to 0.15 m below the surface are shown in Figure 3.6. Results indicate that the measurements obtained at 0.15 m depth are generally higher than obtained at the surface, which is typical for granular materials due to the effects of confinement (also documented in White et al. 2007a). DPI values in particular are much more uniform between point locations at 0.15 m depth than at the surface. CMV measurements were not available on lift 2 for comparison with point measurements because of machine data saving problems.



Figure 3.2. Construction operations on test strip 1

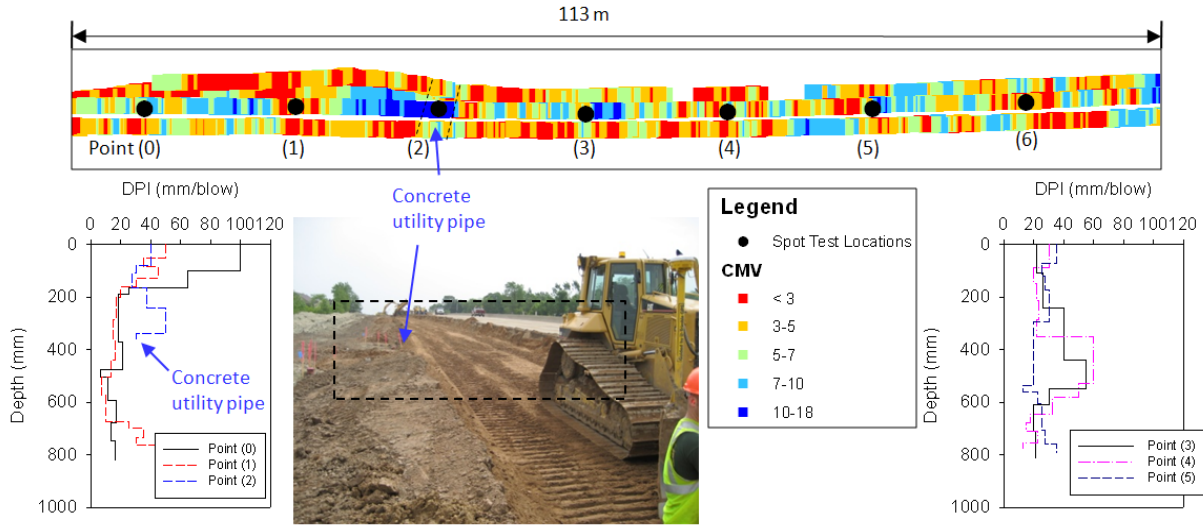


Figure 3.3. CMV map of test strip 1 (lift 1) and DPI profiles at spot test locations TH 36

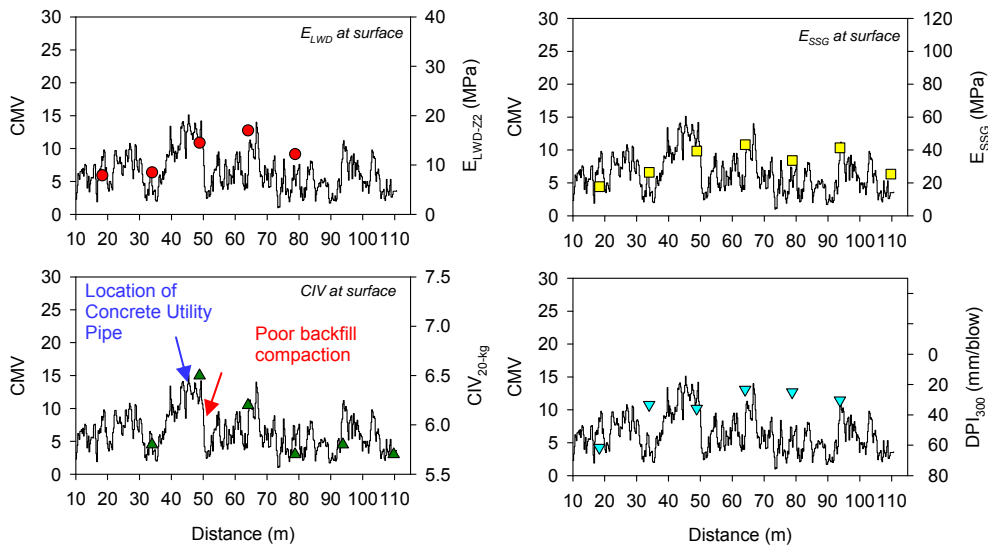


Figure 3.4. Comparison between CMV and in-situ point measurements (TH 36 strip 1 – lift 1; roller operation parameters (nominal):  $a = 0.85$  mm,  $f = 33$  Hz,  $v = 4.0$  km/h)

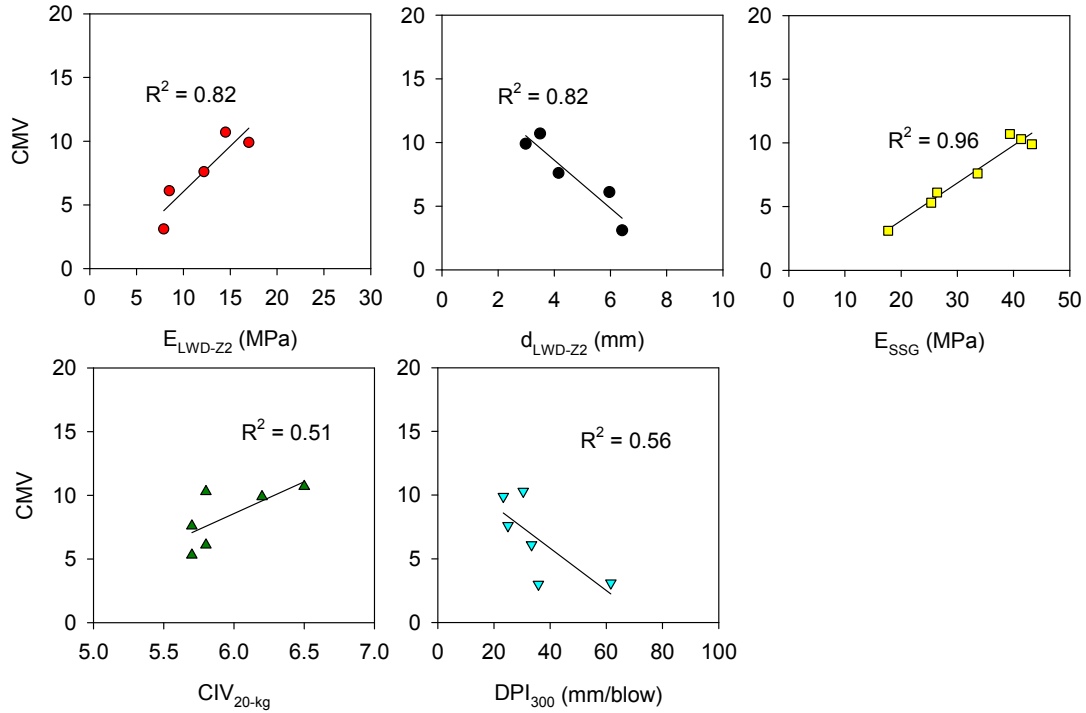


Figure 3.5. Simple linear regression relationships between in-situ point measurements and CMV (TH 36 strip 1 – lift 1)

Table 3.3. Summary of regression relationships (TH36 strip 1 – lift 1)

Relationship	n	R <sup>2</sup>
$CMV = -1.1 + 0.71 E_{LWD-Z2}$	5	0.82
$CMV = 16.2 - 1.89 d_{LWD-Z2}$	5	0.82
$CMV = -2.0 + 0.29 E_{SSG}$	7	0.96
$CMV = -21.4 + 4.98 CIV_{20-kg}$	6	0.51
$CMV = 13.5 - 0.16 DPI_{300}$	22	0.56

Table 3.4. Summary statistics of IC-MVs and in-situ point measurements at surface (TH36 strip 1 – lift 1)

Parameter	$\mu$	COV (%)
CMV ( $a = 0.85$ mm)	6.5	45
$E_{LWD-Z2}$ (MPa)	12.0	32
$d_{LWD-Z2}$ (mm)	4.6	33
$E_{SSG}$ (MPa)	33.9	30
$CIV_{20-kg}$	6.0	6
$DPI_{300}$ (mm/blow)	82	38

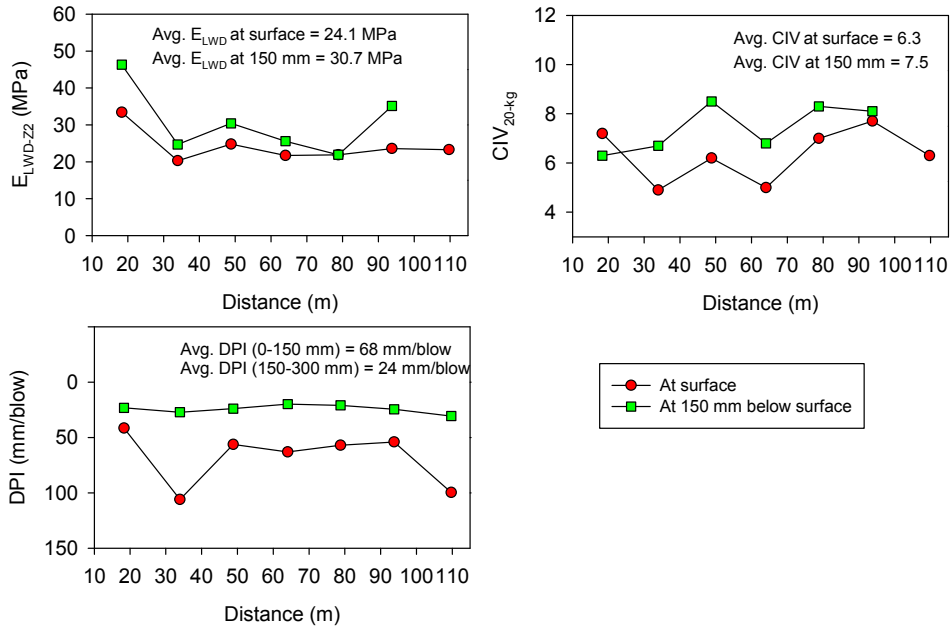


Figure 3.6. Photographs showing LWD and Clegg hammer tests conducted in the 0.15 m deep excavation and plots showing comparison of in-situ point measurements obtained at the surface and at 0.15 m below the surface (TH 36 strip 1 – lift 2)

### 3.3.3.2 Test Strip 2

This test strip was approximately 126 m long, located on the east side of White Bear Avenue on west bound TH36, and consisted of approximately 0.2 m thick select granular base material underlain by granular subbase layer. Index properties of the granular base material are provided in Table 3.2. The granular base layer was compacted and mapped with a smooth drum IC roller with  $a = 0.85$  mm,  $f = 33$  Hz, and  $v = 4.0$  km/h nominal settings. Following mapping, in-situ point measurements ( $E_{V1}$ ,  $E_{V2}$ ,  $d_{LWD-ZZ}$ ,  $E_{LWD-ZZ}$ , and DPI) were performed on the test strip. LWD tests were performed at the surface and at 0.2 m below the surface, i.e., on top of underlying

granular subbase layer. A color-coded CMV map of the test strip and DPI profiles at four select locations are shown in Figure 3.7.

In-situ point measurements in comparison with CMV measurements from strip 2 are presented in Figure 3.8. Comparatively,  $E_{LWD-Z2}$  measurements obtained at the surface tracked the variation in CMV measurements better than other measurements. CMV values were low at some locations but the point measurement values were not (e.g., point locations 9 and 12). DPI profiles at these locations are shown in Figure 3.7 along with profiles at locations 6 and 10 for reference. DPI profiles at point locations 9 and 12 indicated a soft zone below about 0.5 m from the surface, which likely have contributed to low CMV values at these locations. Results obtained from this study (presented later with test strip 4 results) and earlier studies (see Kudla et al. 1991), the 200-mm LWD typically has an influence depth of less than 0.3 m, therefore the  $E_{LWD-Z2}$  measurements are not expected to be influenced by the soft zone below about 0.5 m depth at point locations 9 and 12.

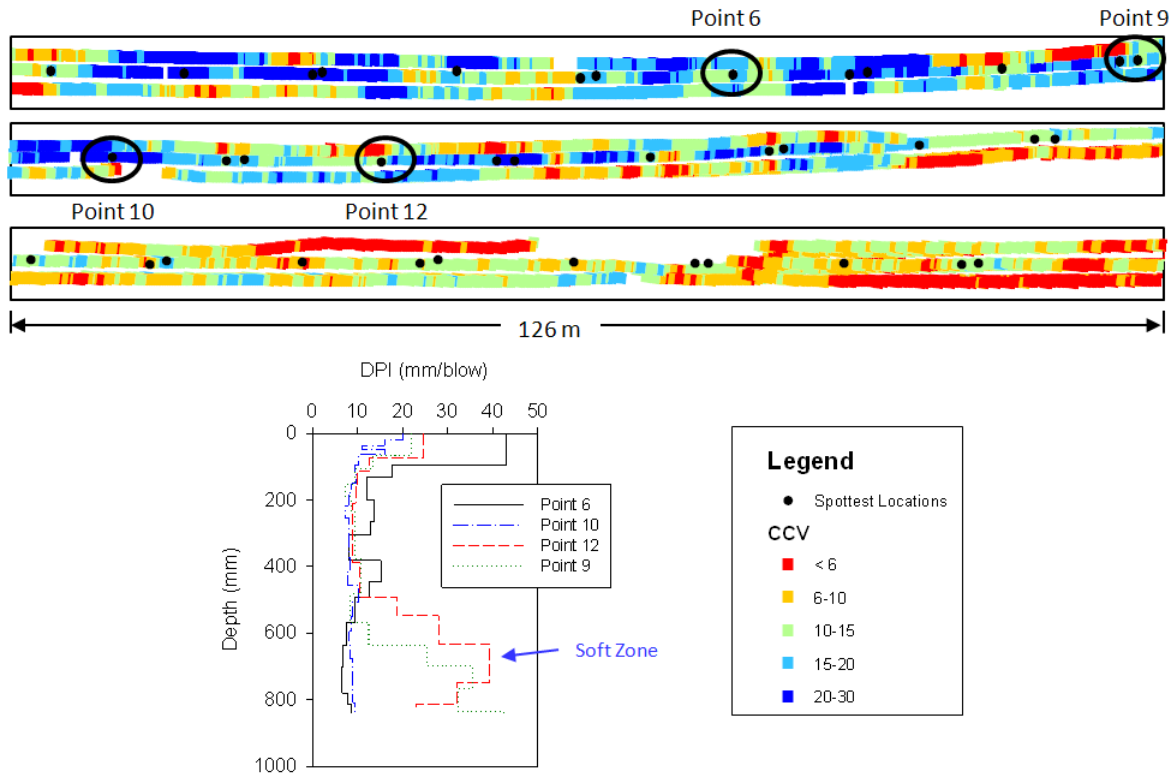


Figure 3.7. CMV map of test strip 2 and DPI profiles at select spot test locations

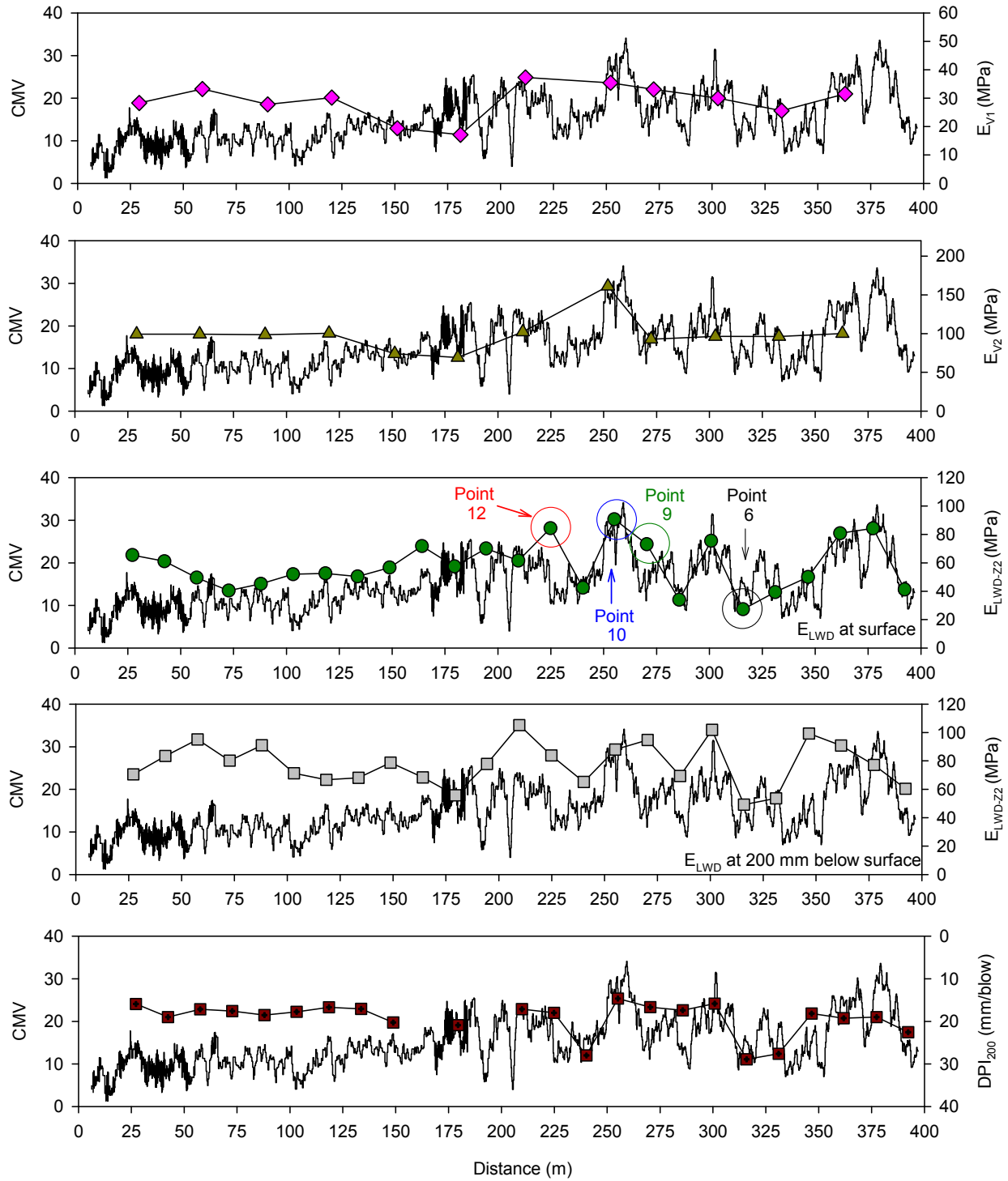


Figure 3.8. Comparison between CMV and in-situ point measurements (TH 36 strip 2; roller operation parameters (nominal):  $a = 0.85$  mm,  $f = 33$  Hz,  $v = 4.0$  km/h)

Regression relationships obtained by pairing point measurement data with nearest point CMV data are presented in Figure 3.9 and are summarized in Table 3.5. Regression relationships showed good correlations with coefficient of determination ( $R^2$ ) values greater than 0.6 for  $E_{LWD-Z2}$ ,  $d_{LWD-Z2}$ ,  $E_{V1}$ , and  $E_{V2}$  measurements obtained at the surface. Poor correlations ( $R^2 = 0.2$ ) were produced with  $DPI_{150}$ ,  $E_{LWD-Z2}$ , and  $d_{LWD-Z2}$  at 0.2 m depth. As the CMV values at point locations 9 and 12 were likely influenced by the soft zone at 0.5 m below surface (see Figure 3.7), these measurements were excluded from the regression analysis with the point measurements. CMV correlations with modulus measurements (i.e.,  $E_{LWD-Z2}$ ,  $E_{V1}$  and  $E_{V2}$ ) showed linear relationships while with deflection measurements showed non-linear power relationships (Figure 3.9). Summary statistics (mean  $\mu$  and coefficient of variation COV) of the measurements are presented in Table 3.6.

Table 3.5. Summary of regression relationships for measurements at surface (TH36 strip 2)

Relationship	n	$R^2$
$CMV = 0.11 + 0.31 E_{LWD-Z2}$	23	0.80
$CMV = 14.12 d_{LWD-Z2}^{-0.91}$	23	0.80
$CMV = 1.04 + 0.56 E_{V1}$	12	0.60
$CMV = 1.09 + 0.16 E_{V2}$	12	0.69
$CMV = 184.61 (DPI)^{-0.82}$	22	0.20

Table 3.6. Summary statistics of IC-MVs and in-situ point measurements (TH36 strip 2)

Parameter	$\mu$	COV (%)
CMV ( $a = 0.85$ mm)	15.0	41
$E_{LWD-Z2}$ (MPa) at surface	58.2	29
$d_{LWD-Z2}$ (MPa) at surface	0.85	32
$E_{LWD-Z2}$ (mm) at 200 mm depth	77.8	20
$d_{LWD-Z2}$ (mm) at 200 mm depth	0.59	22
$E_{V1}$ (MPa) at surface	29.1	21
$E_{V2}$ (MPa) at surface	99.2	22
$DPI_{150}$ (mm/blow)	19.3	20

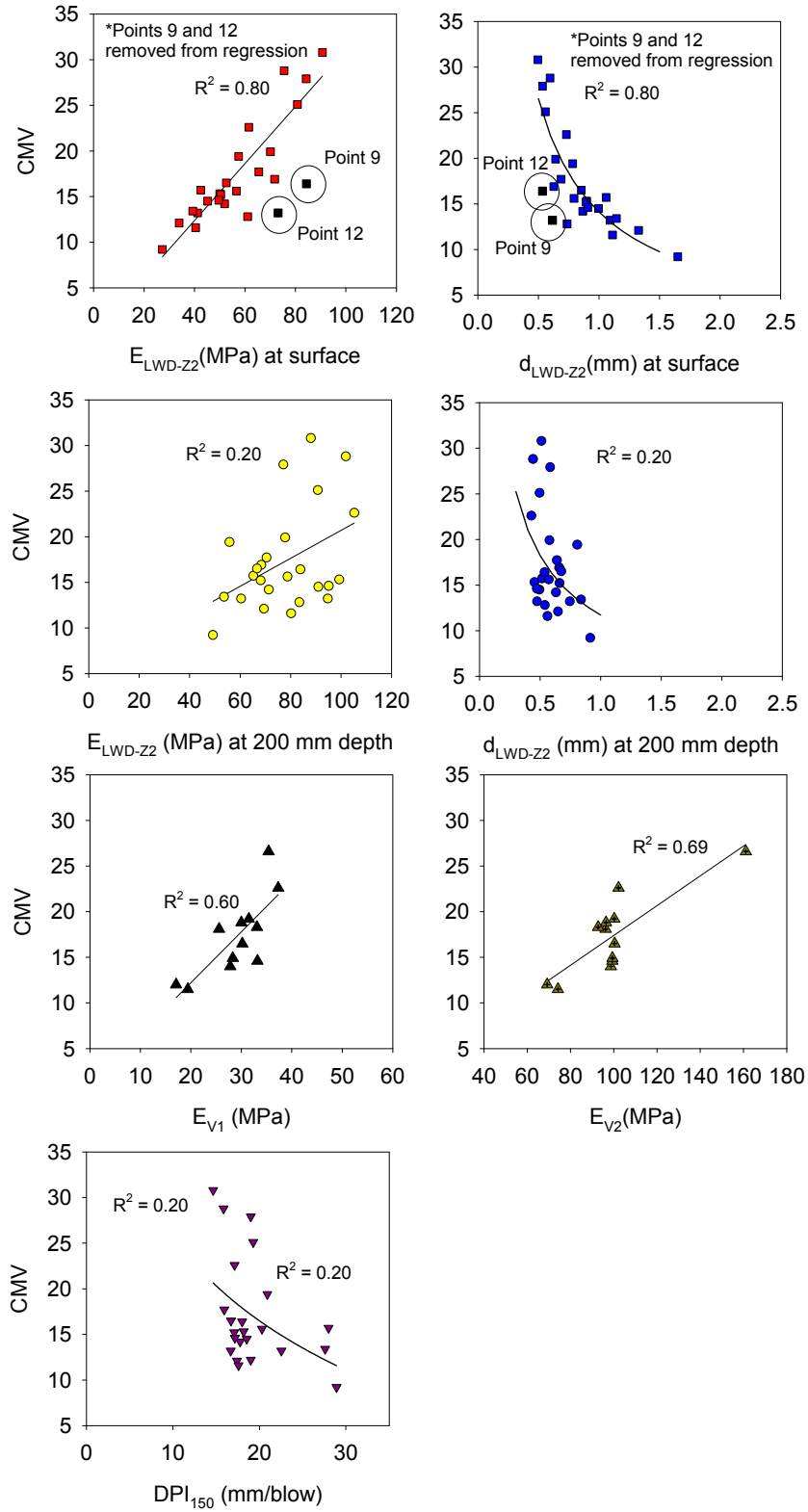


Figure 3.9. Simple linear regression relationships between in-situ point measurements and CMV (TH 36 strip 2)

### 3.3.3.3 Test Strip 4

Test strip 4 consisted of a two-dimensional area with plan dimensions of about 3 m x 35 m surfaced with select granular base layer underlain by granular subbase and granular subgrade layers down to a depth of about 2.8 m below surface (Figure 3.10). Index properties of the granular subbase, base, and subgrade materials are provided in Table 3.2. Figure 3.11 shows CPTU results from the test strip showing interpreted soil profile and behavior type down to a depth of about 6 m below surface. The subgrade was underlain by new embankment fill and rubble/cobbles/old reclaimed pavement and natural sandy glacial deposits at a depth of about 3.5 m below surface. The test strip was mapped for several roller passes using different amplitude settings (see Table 3.7) and nominal  $f = 33$  Hz, and  $v = 3.2$  km/h (note that the test area was reportedly fully compacted prior to mapping passes). Following mapping, in-situ test measurements (see Table 3.7) were conducted on the test strip at 11 test locations.

RMV and CMV measurements obtained from two different amplitude settings are presented in Figure 3.12 for passes 7 to 10. Figure 3.12a demonstrates the repeatability of CMV values under similar amplitude settings. Figure 3.12b shows the influence of RMV on CMV values at  $a = 1.70$  mm setting. At  $a = 0.85$  mm the RMV measurements were close to zero while at  $a = 1.70$  mm the RMV values were significantly greater than zero indicating that the roller drum was losing contact with the ground. This is referred to as drum double jumping (Adam 1997) and is confirmed from stress cell measurements described later in the chapter (see section 3.4.4). Results show a decrease in CMV with increasing RMV which is identified in the literature as a distinctive feature of this measurement system (see Adam 1997). This CMV-RMV behavior is related to ground stiffness. In-situ point measurements ( $E_{LWD-D2}$ ,  $E_{LWD-Z2}$ ,  $E_{FWD-D3}$ , and DPI) obtained from the test strip are presented in comparison with IC-MVs in Figure 3.13. DCP, CPTU, and  $E_{FWD}$  profiles from two select locations are also shown in Figure 3.13. Point A is located in the area where the RMV was lower and Point B is located in the area where RMV was greater when operated at  $a = 1.70$  mm. The profiles identify relatively stiff conditions at Point A compared to Point B.

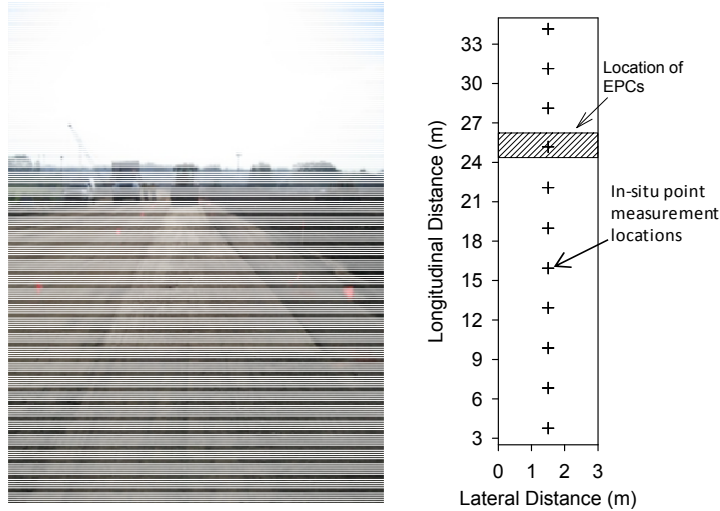


Figure 3.10. Plan view of TH36 strip 4 and photographs during rolling and testing operations

Table 3.7. Summary of roller passes (TH36 strip 4)

Date	Pass <sup>§</sup>	<i>a</i> (mm)	EPC sensor measurements	Remarks
07/26/07*	1, 2	0.85	None	CPT and 2 m DCP tests (after pass 6)
	3, 4	1.70		
	5, 6	Static		
07/27/07	1 – 4	0.85	Yes	300 mm FWD and Dynatest LWD, 200 mm Zorn and Dynatest LWD (after pass 12)
	5 – 6	Static		
	7 – 8	0.85		
	9 – 10	1.70		
	11 – 12	0.85		

\*Roller data from 07/26/07 was not available.

§ The test area was well compacted prior to pass 1 on 07/26/07.

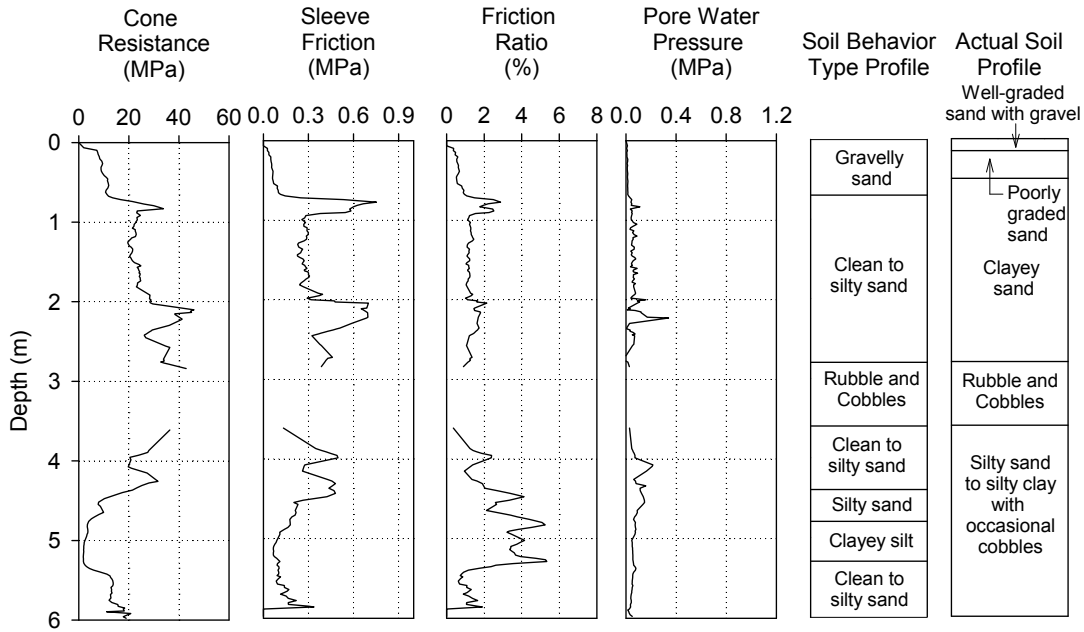


Figure 3.11. Example CPTU profile from a test location in the test strip area describing the general foundation soil conditions (TH36 strip 4) (actual soil profile determined based on project drawings)

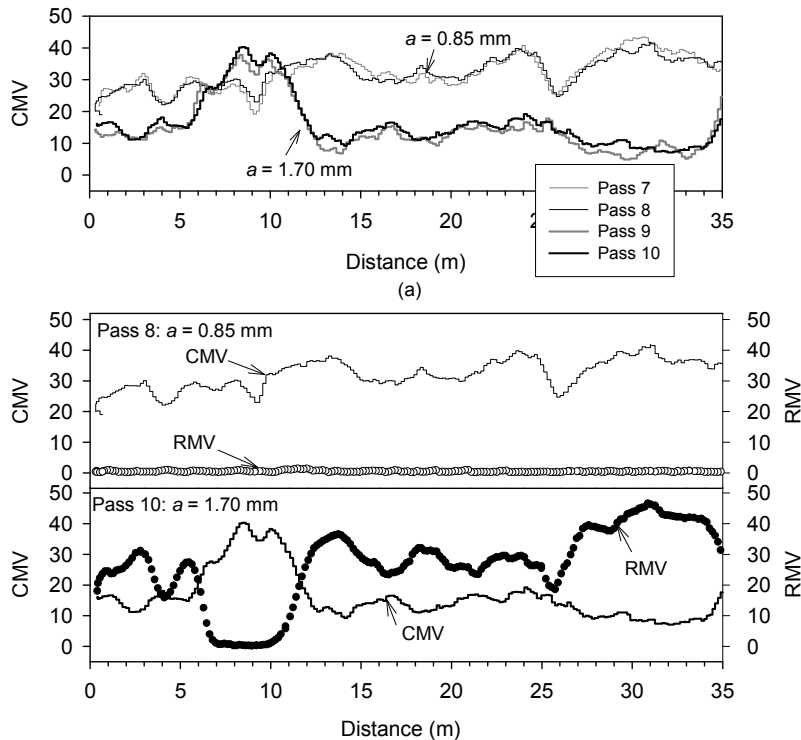


Figure 3.12. CMV and RMV from test strip 4 with nominal  $v = 3.2$  km/h and  $f = 33$  Hz settings: (a) repeatability of CMV at two amplitude settings, (b) influence of RMV on CMV measurements.

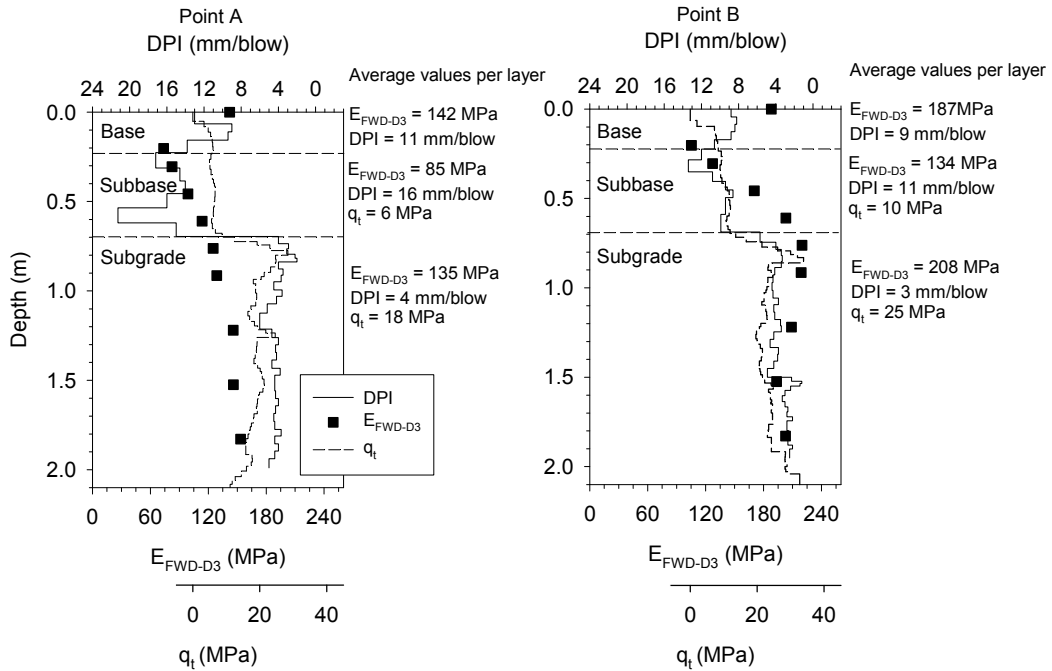
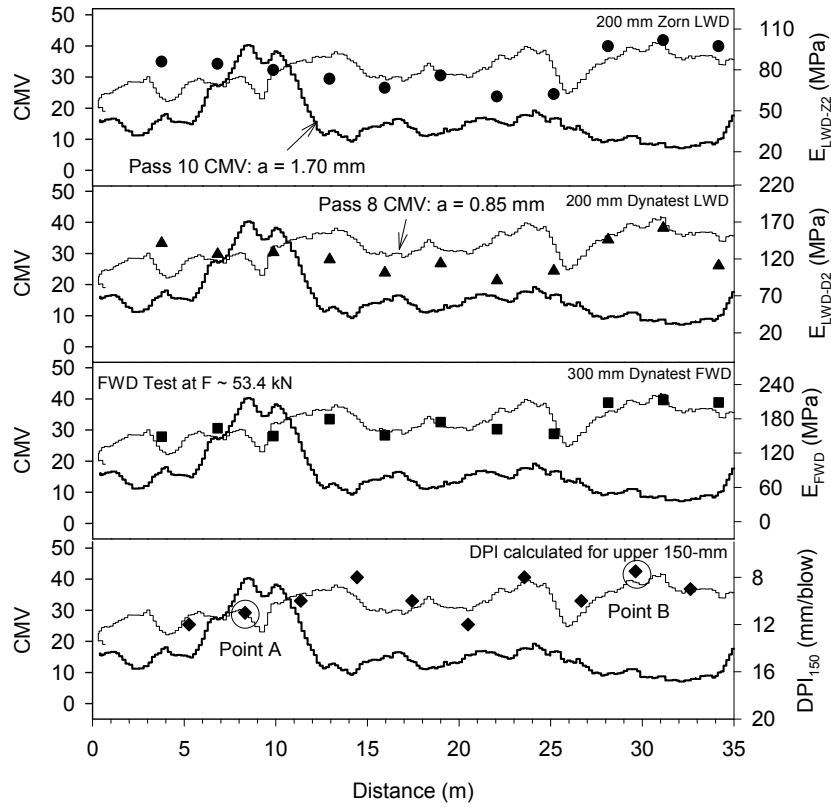


Figure 3.13. Comparison of CMV with in-situ mechanistic point measurements – DCP index,  $q_t$ , and  $E_{FWD}$  profiles at two select points (test strip 4).

Correlations obtained between different point measurements obtained from the test strip are provided in Figure 3.14 and Figure 3.15. The regression relationships are summarized in Table 3.8. Regression relationships are presented for  $E_{FWD}$  at two applied force levels (nominal  $F = 26.7$  kN and  $53.4$  kN). Comparatively, relationships for  $E_{FWD-D3}$  at  $F = 26.7$  kN were slightly better with other in-situ point measurements and at  $F = 53.4$  kN were slightly better with CMV. Summary statistics (mean  $\mu$  and coefficient of variation COV) of different measurements are summarized in Table 3.9.

Results showed relatively poor correlations between  $E_{FWD}$  and  $E_{LWD}$  with  $R^2$  values between 0.2 and 0.6, but with limited data. One factor that could contribute to scatter in the correlations is the differences in applied stresses and measurement influence depths of these measurement devices and is discussed further in section 3.2.3. The correlation between  $E_{FWD}$  and DPI fit a power relationship with  $R^2$  values of about 0.7 and is similar to the relationship proposed by Chen *et al.* (2005).  $E_{FWD}-q_t$  and DPI- $q_t$  relationships also showed power relationships with  $R^2$  of about 0.7. A different trend in  $E_{FWD}-q_t$  is observed compared to equations proposed by Konrad and Lachance (2001) and Schmertman (1970) for elastic modulus. The relationship presented by Konrad and Lachance (2001) was based on three data points and Schmertman's equation was based on correlations to static plate load modulus. To the authors' knowledge, this is the first study to document  $E_{FWD}-q_t$  and DPI- $q_t$  relationships.

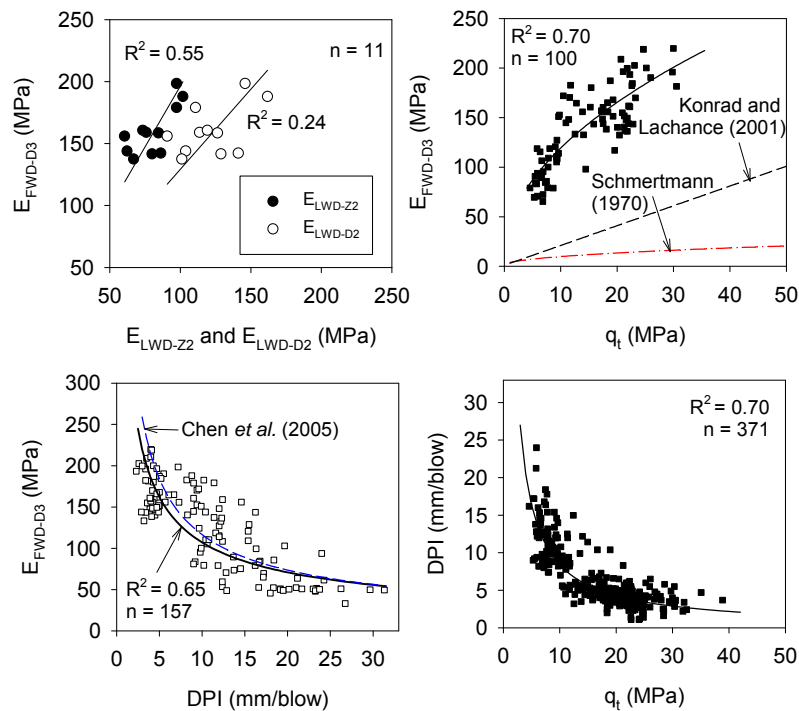


Figure 3.14. Relationships between different in-situ point measurements ( $E_{FWD-D3}$  at  $F \sim 26.7$  kN).

Table 3.8. Summary of regression relationships (TH36 strip 4)

Relationship	n	R <sup>2</sup>
FWD Applied Force, F ~ 26.7 kN		
$E_{\text{FWD-D3}}$ (MPa) = 76.31 + 1.04 $E_{\text{LWD-Z2}}$ (MPa)	11	0.55
$E_{\text{FWD-D3}}$ (MPa) = 99.88 + 0.50 $E_{\text{LWD-D2}}$ (MPa)	11	0.24
$E_{\text{FWD-D3}}$ (MPa) = 43.53 ( $q_t$ ) <sup>0.45</sup> (MPa)	100	0.70
$E_{\text{FWD-D3}}$ (MPa) = 422.84 (DPI) <sup>-0.60</sup> (mm/blow)	157	0.65
$E_{\text{FWD-D3}}$ (MPa) = 75.42 + 2.65 CMV	11	0.50
FWD Applied Force, F ~ 53.4 kN		
$E_{\text{FWD-D3}}$ (MPa) = 68.26 + 1.31 $E_{\text{LWD-Z2}}$ (MPa)	11	0.52
$E_{\text{FWD-D3}}$ (MPa) = 106.73 + 0.55 $E_{\text{LWD-D2}}$ (MPa)	11	0.20
$E_{\text{FWD-D3}}$ (MPa) = 37.11 ( $q_t$ ) <sup>0.49</sup> (MPa)	100	0.62
$E_{\text{FWD-D3}}$ (MPa) = 341.99 (DPI) <sup>-0.51</sup> (mm/blow)	157	0.52
$E_{\text{FWD-D3}}$ (MPa) = 59.87 + 3.56 CMV	11	0.59
DPI (mm/blow) = 22.42 – 0.39 CMV	10	0.69
DPI (mm/blow) = 78.35 ( $q_t$ ) <sup>-0.97</sup> (mm/blow)	371	0.69

Table 3.9. Summary statistics of IC-MVs and in-situ point measurements at surface (TH36 strip 4)

Parameter	$\mu$	COV (%)
Roller $a$ = 0.85 mm	32.1	15
Roller $a$ = 1.70 mm	16.7	49
$E_{\text{FWD-D3}}$ (MPa) (F ~ 26.7 kN)	160.4	13
$E_{\text{FWD-D3}}$ (MPa) (F ~ 53.4 kN)	173.8	15
$E_{\text{LWD-D2}}$ (MPa)	122.4	17
$d_{\text{LWD-D2}}$ (mm)	0.24	21
$E_{\text{LWD-Z2}}$ (MPa)	80.6	18
$d_{\text{LWD-Z2}}$ (mm)	0.62	24
DPI <sub>150</sub> (mm/blow)	9.7	16

Simple linear regression relationships between CMV and in-situ point measurements are presented in Figure 3.15, separately for low and high amplitude settings. The relationships were developed by pairing in-situ test measurements with spatially nearest roller measurement point. Despite limited data points, CMV relationships with  $E_{\text{FWD-D3}}$  and DPI<sub>150</sub> showed good

correlations with  $R^2$  in the range of 0.6 to 0.7. Relationships between CMV and  $E_{LWD-Z2}$  or  $E_{LWD-D2}$  showed weak correlations for these materials. Previous studies however have showed that a positive correlation between CMV and  $E_{LWD}$  can be developed (see White et al. 2007b). A relationship documented by White et al. (2007b) for a granular base material (classified as A-1-b) between CMV and the Keros 200-mm plate diameter LWD device ( $E_{LWD-K2}$ ) is presented in Figure 3.15 as a reference (Note that the  $E_{LWD-K2}$  and  $E_{LWD-D2}$  measurements are strongly correlated and are close to  $R^2 = 1$  line (see Vennapusa and White 2009a). Another regression line is plotted on Figure 3.15 for  $E_{LWD-Z2}$  based on a relationship documented by Vennapusa and White (2009a) between  $E_{LWD-K2}$  and  $E_{LWD-Z2}$  measurements ( $E_{LWD-K2} = 1.75 E_{LWD-Z2}$ ). Although there is scatter, the  $E_{LWD-D2}$  and  $E_{LWD-Z2}$  measurements match existing relationships. Regression relationships between CMV and in-situ point measurements are summarized in Table 3.8 and summary statistics (mean  $\mu$  and coefficient of variation COV) are summarized in Table 3.9.

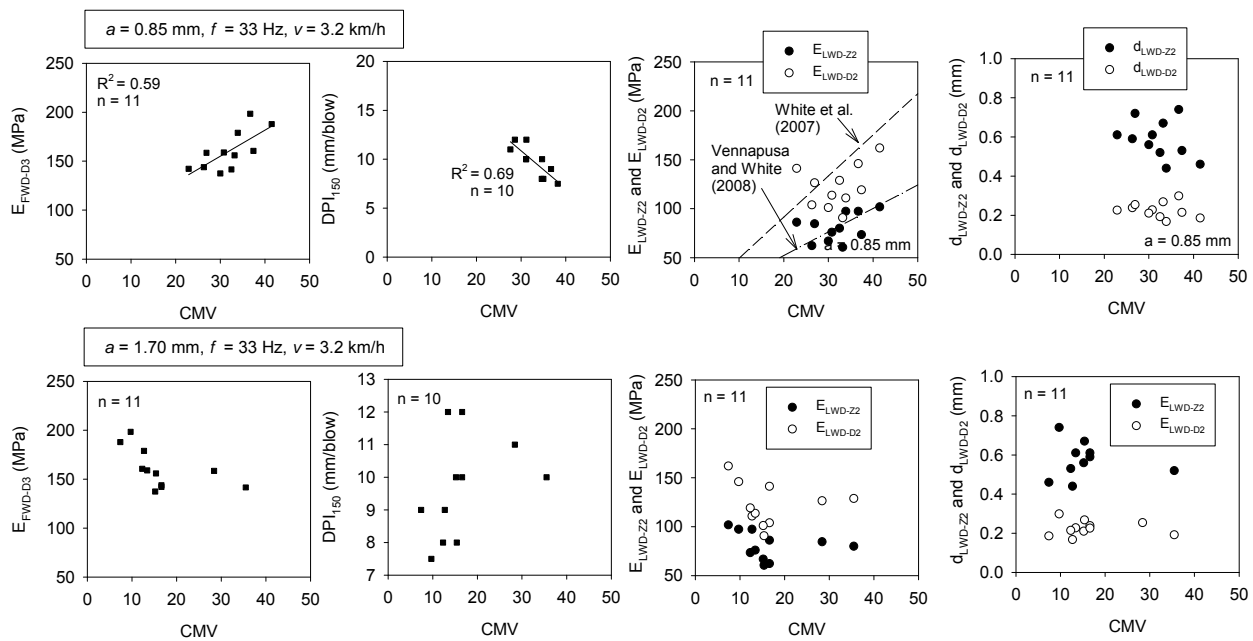


Figure 3.15. Relationships between CMV and point measurements ( $E_{FWD-D3}$  at  $F \sim 53.4$  kN).

Relationships between different point measurements and CMV at high amplitude setting are also shown in Figure 3.15. Due to the effect of RMV at high amplitude operation as described above, no trend was seen in the relationships. To statistically assess the influence of RMV on CMV, multiple regression analysis was performed as presented in Figure 3.16. The analysis was performed by incorporating amplitude, RMV, and  $E_{FWD-D3}$  measurements as independent variables into a multiple linear regression model to predict CMV. Statistical significance of each variable was assessed based on  $p$ - and  $t$ -statistics. The selected criteria for identifying the significance of a parameter included:  $p$ -value  $< 0.05$  = significant,  $< 0.10$  = possibly significant,  $> 0.10$  = not significant, and  $t$ -value  $< -2$  or  $> +2$  = significant. The  $p$ -value indicates the significance of a parameter and the  $t$ -ratio value indicates the relative importance (i.e., higher the absolute value greater the significance). Based on this criterion, analysis results presented in Figure 3.16 indicate a strong significance of RMV in predicting CMV, while  $E_{FWD-D3}$  was

somewhat significant. Amplitude was not found statistically significant; therefore, it was removed from the model. Statistically significant relationships were not found with other in-situ point measurements.

The effect of RMV on CMV has been discussed in the literature (e.g., Adam 1997, Adam and Kopf 2004) but has lacked attention in an implementation standpoint with guidance on how to account for RMV measurements during QA/QC operations. A statistically significant correlation was possible in this current study by incorporating RMV into a multiple regression model; however, it is preferable to perform calibration testing with low amplitude setting ( $a \leq 1$  mm) to avoid complex interpretation and analysis of results with roller jumping. The interpretation of CMV data thus must not be absent of evaluating or at least reviewing RMV. An example approach to evaluate CMV with RMV results in a specification/quality assurance standpoint is described in Vennapusa and White (2009b) using results from the TH 64 project.

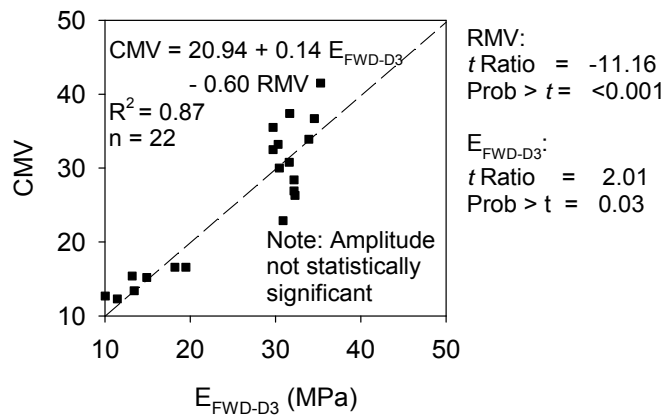


Figure 3.16. Results of multiple regression analysis illustrating the effect of RMV

### 3.3.4 Stresses in Pavement Foundation Layers

#### 3.3.4.1 Installation of EPCs

Peizoelectric 0-1000 kPa range EPCs were installed in the granular base, subbase, and subgrade foundation layers of test strips 3 and 4 by carefully excavating the material and embedding the cells in a layer of calibration sand material. The calibration sand material was carefully hand compacted in thin layers to achieve good compaction around the sensors. The excavation was backfilled using the excavated material and was hand compacted in thin lifts. The backfilled area was then compacted with eight to ten roller passes to ensure good compaction was achieved. LWD tests were performed as layers were placed and compacted to ensure stiffness values were similar the condition before excavation.

The plan and cross-sectional views of test strip 3 pavement foundation layers with location of EPCs are shown in Figure 3.17. Pictures taken on test strip 3 are shown in Figure 3.18. In-ground triaxial stresses (i.e.,  $\sigma_x$  = horizontal stress in direction perpendicular to the direction of

roller travel,  $\sigma_y$  = horizontal stress in direction parallel to the direction of roller travel, and  $\sigma_z$  = vertical stress) developed in the granular subbase and subgrade layers at depths of about 0.30 m, 0.60 m, and 0.90 m below surface were measured under static and vibratory rolling. Stress measurements were obtained by positioning the drum center at A, B, C, and D positions as shown in Figure 3.17.

Stresses developed under roller, LWD, and FWD loading were measured in test strip 4 by installing EPCs in the granular base, subbase, and subgrade layers at depths of about 0.15 m, 0.30 m, 0.50 m, 0.65, 0.80 m, 1.04, and 1.20 m below surface (see Figure 3.19). The EPCs installed at depths 0.30 m, 0.65m, and 1.04 m depths were placed perpendicular to the alignment of the test strip to measure stresses in horizontal direction ( $\sigma_x$ ). The remaining EPCs were installed to measure stresses in vertical direction ( $\sigma_z$ ).

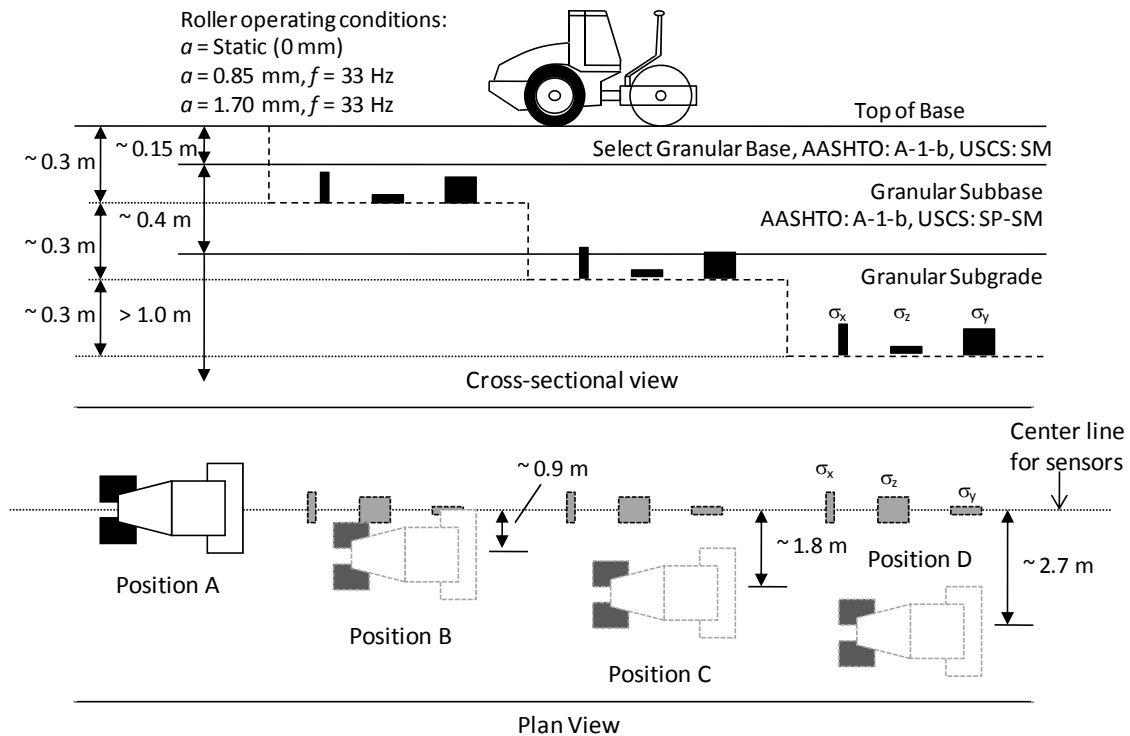


Figure 3.17. Plan and cross-sectional views of location of EPCs in the pavement foundation layers – test strip 3



Figure 3.18. Pictures showing rolling pattern on test strip 3

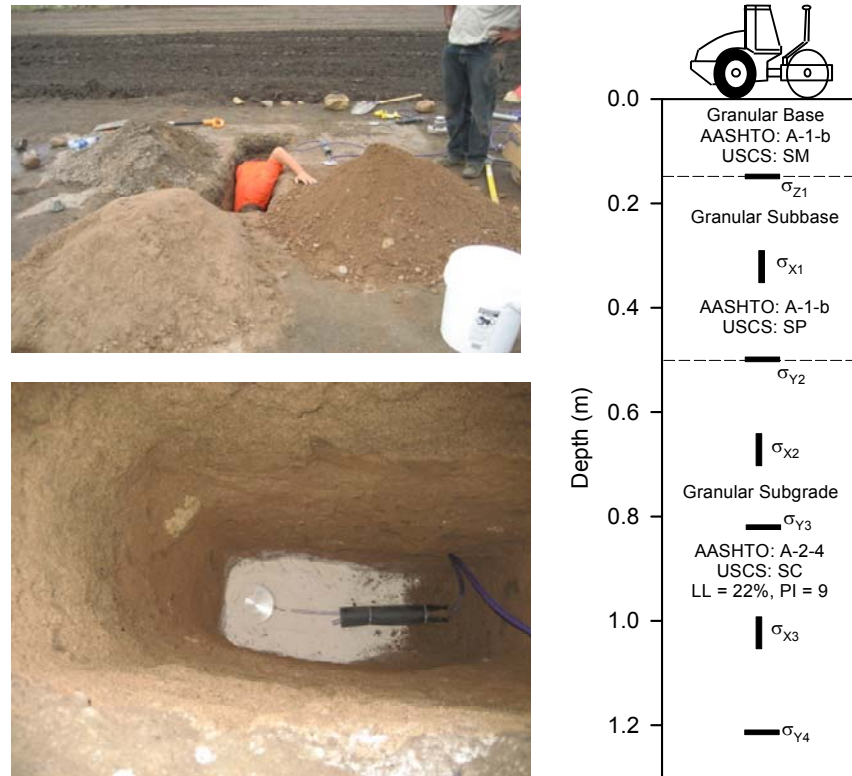


Figure 3.19. Installation of EPCs in a layer of silica sand at different depths on test strip 4

### 3.3.4.2 EPC measurements under roller, LWD, and FWD loading

EPC measurements obtained from test strip 3 under roller static and vibratory compaction and peak vertical and horizontal stresses developed under roller vibratory loading are presented in Figure 3.20, Figure 3.21, and Figure 3.22 for drum positions A, B, and C, respectively. Stress increase observed in the EPCs at position D (i.e., drum center being ~ 2.7 m away from the sensors) were significantly smaller (< 5 kPa) and therefore results are not presented herein. Theoretical vertical and horizontal stress distributions are plotted in Figure 3.20 for drum position A (i.e., drum center positioned above the sensors) based on Boussinesq elastic solutions. The stress distributions were determined assuming a uniformly loaded continuous strip footing with width  $B$ . The  $B$  and contact stress values were adjusted to obtain a best fit through the measured peak stresses. A contact width of 0.2 m was found to fit the theoretical vertical stress distributions well for both low and high amplitude loading. However, the horizontal stresses were not well predicted by the theoretical solutions.

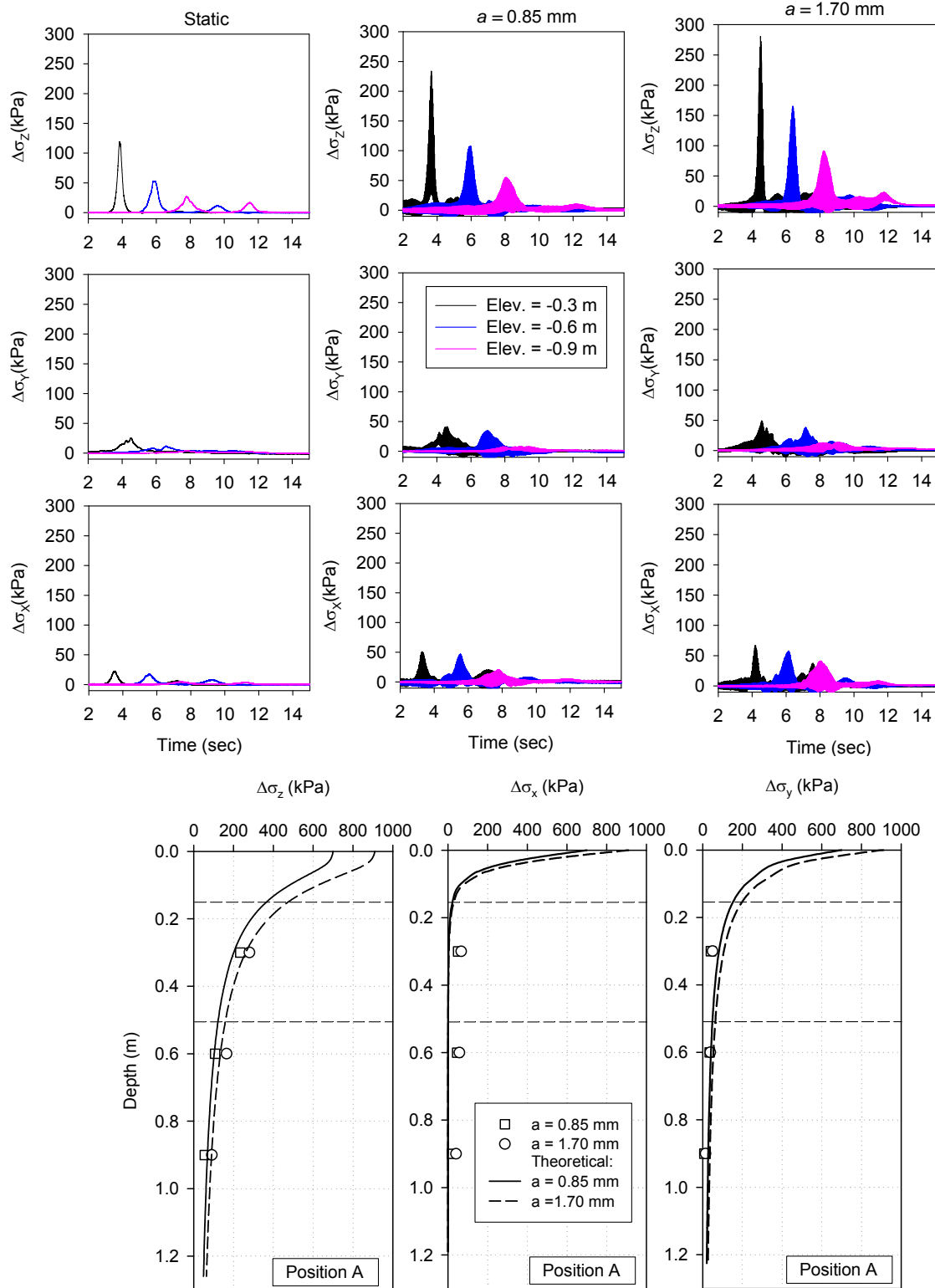


Figure 3.20. Triaxial stresses developed under the roller at position A at different amplitude settings (top) and profile of peak stresses (bottom) (test strip 3)

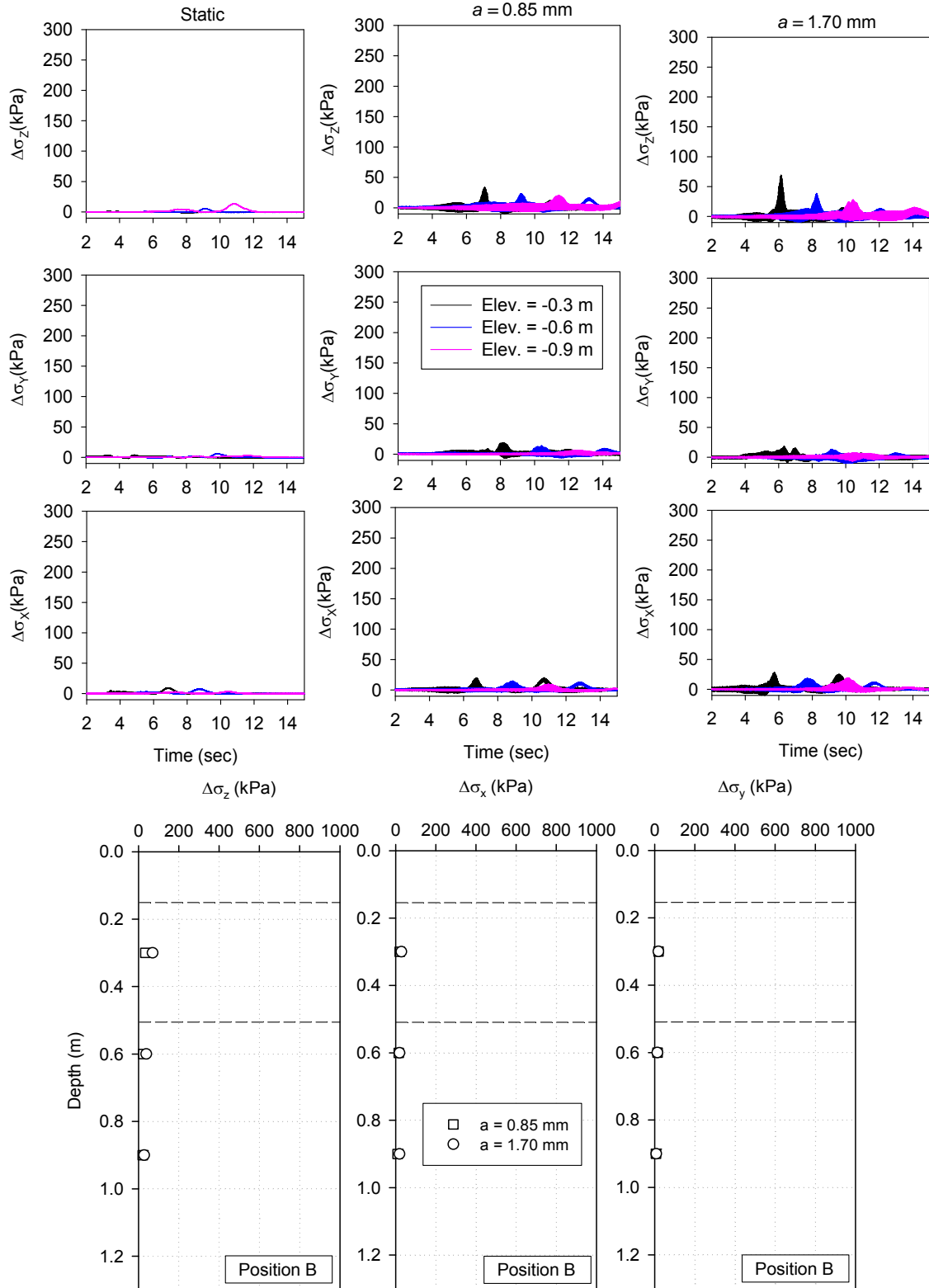


Figure 3.21. Triaxial stresses developed under the roller at position B at different amplitude settings (top) and profile of peak stresses (bottom) (test strip 3)

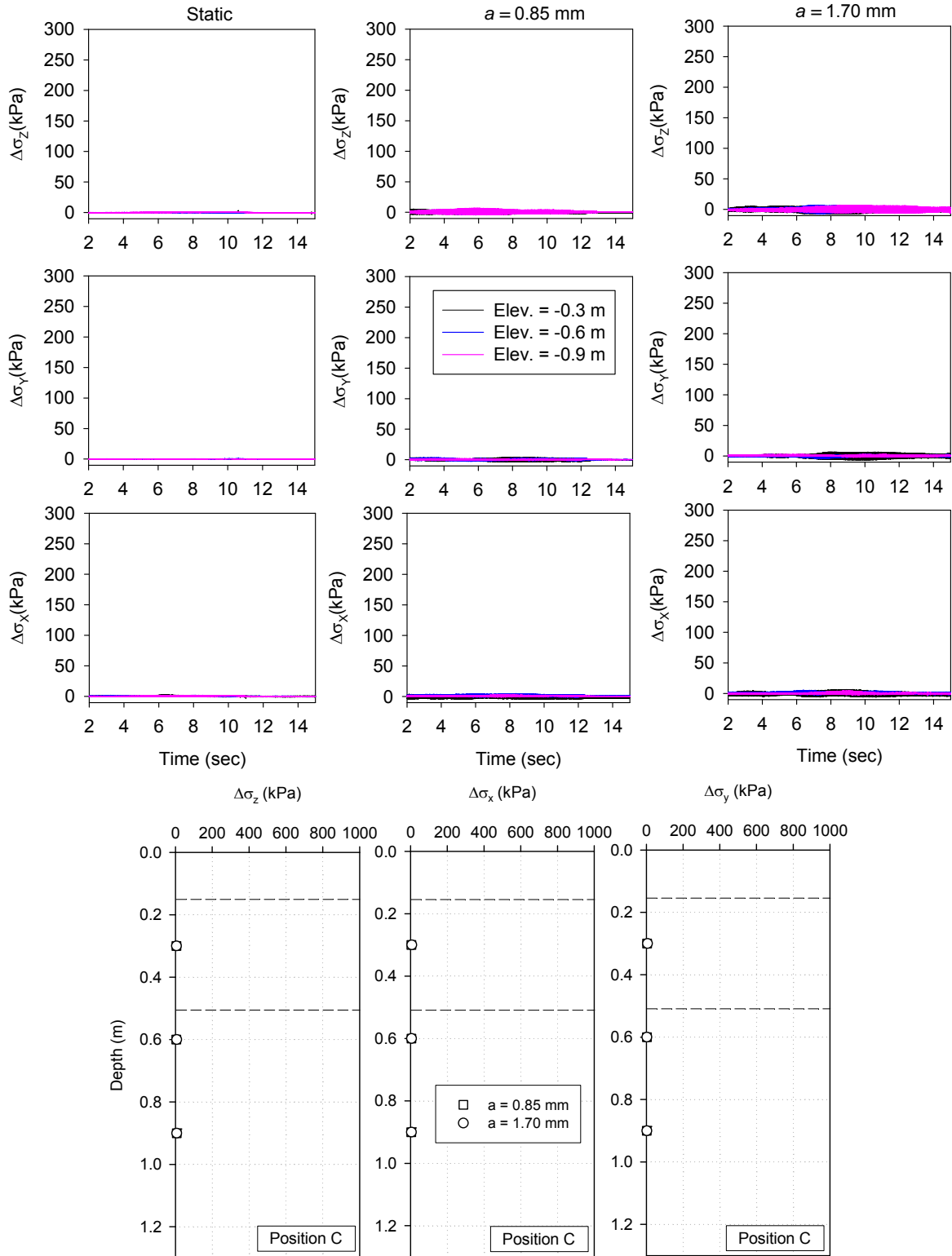


Figure 3.22. Triaxial stresses developed under the roller at position C at different amplitude settings (top) and profile of peak stresses (bottom) (test strip 3)

Figure 3.23 shows EPC measurements under roller vibratory compaction from test strip 4. The stress measurements represent an increase in stress under loading and do not include the geostatic stresses. Figure 3.24 shows peak vertical and horizontal stresses developed under the roller, 300-mm diameter FWD with applied  $F = 26.7$  kN and  $F = 53.4$  kN (shown as FWD(A) and FWD(B), respectively), and 200-mm LWD with  $F = 6.3$  kN from test strip 4. Figure 3.24 shows theoretical vertical and horizontal stress distributions under the roller and LWD/FWD plates based on Boussinesq elastic solutions. The stress distributions under the roller were determined assuming a uniformly loaded continuous strip footing with width  $B$ . The  $B$  and contact stress values were adjusted to obtain a best fit through the measured peak stresses. The stress distributions under the FWD/LWD plate were predicted using theoretical solutions for a uniformly loaded circular plate. The vertical stress distributions under roller, FWD and LWD loading were well predicted by the theoretical solutions but not the horizontal stress distributions.

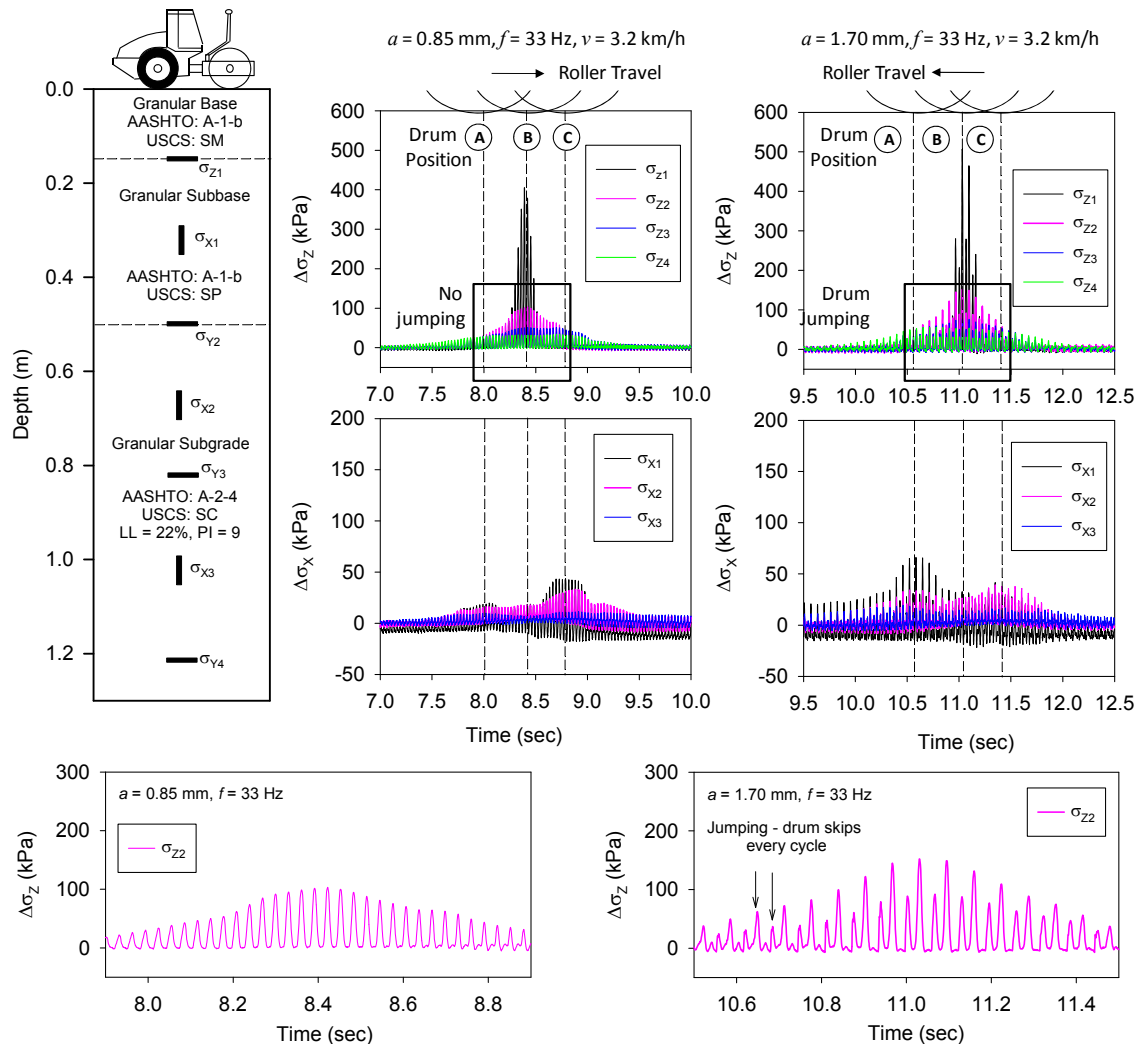


Figure 3.23. Total vertical and lateral stress measurements from test strip 4 under roller vibratory loading at  $a = 0.85$  and  $1.70$  mm nominal settings (note drum jumping at  $a = 1.70$  mm) (test strip 4)

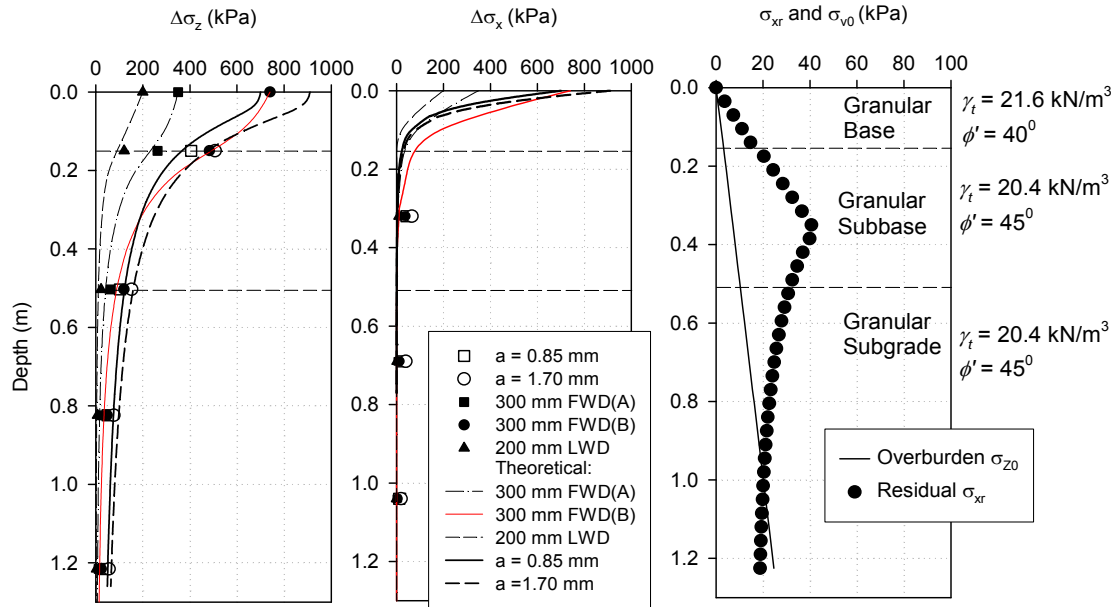


Figure 3.24. Peak vertical and lateral stress increase profiles (measured and theoretical Boussinesq curves) for roller induced vibratory loads, and FWD and LWD dynamic loads, and estimated residual stresses to calculate  $K$  from Duncan and Seed (1986) (test strip 4)

The horizontal and vertical loading regimes observed in Figure 3.23 indicate a rotation of principal stresses in the layers due to the moving roller load. To explain this behavior, three positions are identified on Figure 3.23 at locations of peak horizontal and vertical stresses (Note that the sensors are all positioned vertically at position B). When the roller drum is at position A, the magnitude of horizontal stress increase is more than the magnitude of vertical stresses ( $\Delta\sigma_x > \Delta\sigma_z$ ). When the moving load is directly above the sensor (position B), vertical stresses are significantly higher than the horizontal stresses ( $\Delta\sigma_z > \Delta\sigma_x$ ). As the roller travels away from position B, vertical stress decreases and horizontal stress increases ( $\Delta\sigma_x > \Delta\sigma_z$ ). After the roller loading, both vertical and horizontal stresses decrease. The horizontal stresses are not completely relieved in compacted fill materials due to residual “locked-in” stresses ( $\sigma_{xr}$ ) developed during compaction process (also observed by Duncan and Seed 1986). Residual stresses were estimated (see Figure 3.24) using the  $K_0$  hysteric model proposed by Duncan and Seed (1986) for free field conditions. The total unit weight ( $\gamma_t$ ) values of each layer were assumed to be at 100% standard Proctor density and 100%  $w_{opt}$  and the drained friction angle ( $\phi'$ ) values were estimated using empirical relationships between  $q_b$ , overburden stress ( $\sigma_{v0}$ ) and ( $\phi'$ ) proposed by Robertson and Campanella (1983). The vertical stresses induced under the roller showed “spreading” of the stresses with depth as expected, i.e, a vertical sensor at a deeper depth sensing greater vertical stresses than at shallow depths just before approaching position B (Figure 3.23). Also shown in Figure 3.23 is a close-up view of the vertical stresses under  $a = 0.85$  and  $1.70$  mm loading. During roller operation at  $a = 1.70$  mm, the vibratory stress cycles were reduced every other cycle which distinguishes a condition whereby the roller drum begins to lose contact with the ground. This is referred to as drum double jumping behavior (Adam

1997) which affects the CMV and RMV measurement values (discussed earlier in conjunction with roller-integrated measurements in section 3.3.3).

3.3.4.4 Stress paths under roller, LWD, and FWD loading

Using the calculated residual stresses, the K values at different depths are calculated as the ratio of  $\sigma_{xr}$  and  $\sigma_{vo}$  from Figure 3.24. Considering the three positions described in Figure 3.22 (Positions A, B, and C) as the main loading and unloading regimes under the roller load, and the estimated K values for the at-rest state, stress paths were developed for soil elements in the granular base layer (depth = 0.08 m) and subbase layers (depth = 0.32 m). The stress paths are shown in Figure 3.25 for the two amplitude loading conditions. Stress paths under the roller showed a hysteresis of extension and compression during loading and unloading phases due to rotation in principal stresses as described above. Stress paths for LWD and FWD dynamic loads, laboratory resilient modulus ( $M_r$ ) test loads following AASHTO T-307 and NCHRP 1-28 A procedures for base and subbase materials are also provided in Figure 3.25 for comparison. Slope coefficients  $m$  (ratio of  $q$  and  $p$ ) are determined for the stress paths as shown in Figure 3.25.

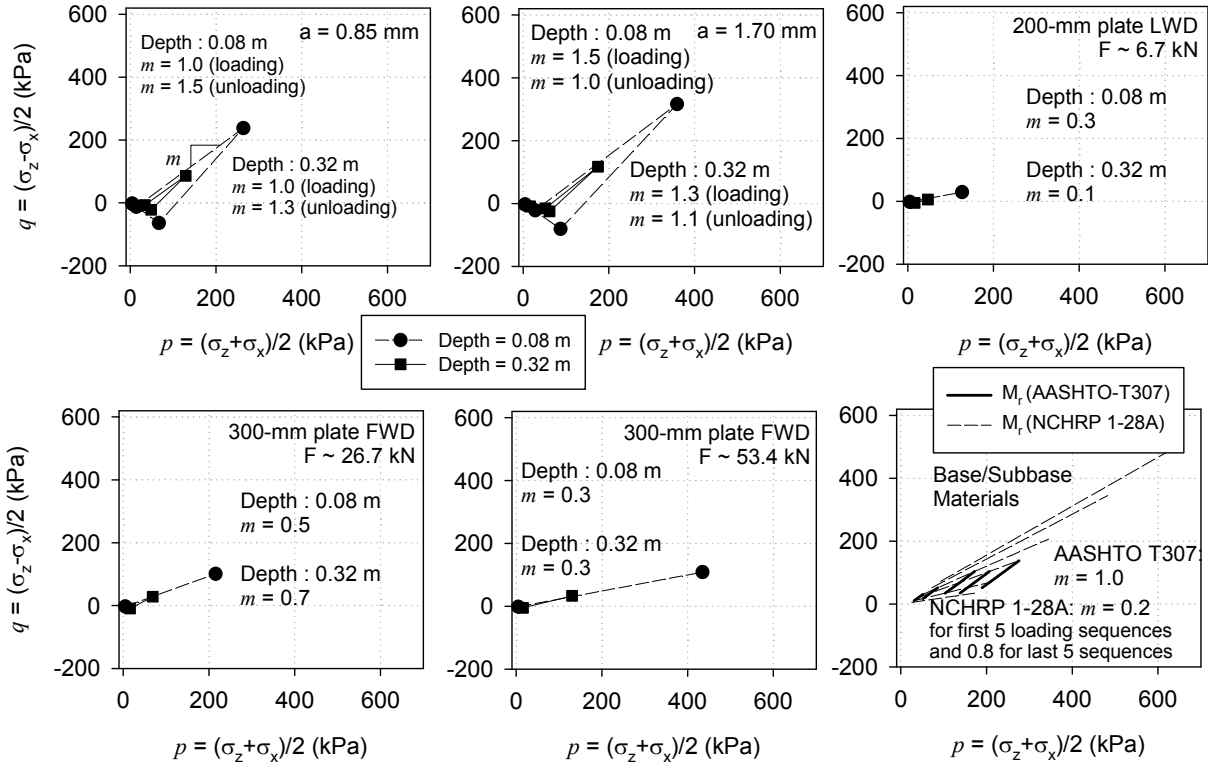


Figure 3.25. Comparison of total stress paths under roller vibratory load (Positions A to B loading and Positions B to C unloading), FWD and LWD dynamic loads, and stresses applied during laboratory  $M_r$  tests on base/subbase materials (test strip 3)

### 3.3.4.5 Discussion

The results presented above can be used to interpret (a) the measurement influence depths under roller, FWD, and LWD loading by using the peak vertical stress measurement profiles and (b) evaluating the differences in stresses induced in the foundation layer materials under different loading conditions from the stress paths.

One way to characterize the measurement influence depth is to assume depth at which only 10% of the surface vertical stress increment is reached (10% is arbitrary but provides a point of comparison herein). Using this criteria, the measurement influence depth under the roller for both  $a = 0.85$  mm and 1.70 mm loading conditions is estimated at about 0.9 m for the soil profiles tested in this study. The measurement influence depth under 300-mm FWD plate with  $F = 53.4$  kN and  $F = 26.7$  kN is about 0.6 m, and under 200-mm LWD plate is about 0.3 m.

Comparison of stress paths presented in Figure 3.25 revealed the following key observations for differentiating between measurement values: (a) the mean stresses developed under a 300-mm FWD plate with  $F = 53.4$  kN are similar to mean stresses developed under the roller for  $a = 1.7$  mm but the  $m$  coefficients for FWD loading is comparatively smaller than under roller loading, (b)  $m$  coefficients are similar for roller induced loads and the  $M_r$  loading procedure following AASHTO T-307 and final 5 sequences of NCHRP 1-28A, (c) applied mean stresses and  $m$  coefficients for LWD loading are significantly smaller than roller and FWD induced stresses and  $m$  coefficients (d) the magnitude of mean stresses and  $m$  coefficients for LWD loading are somewhat similar to AASHTO T-307  $M_r$  testing and initial sequences of NCHRP 1-28A testing for  $M_r$ , and (e) NCHRP 1-28A procedure captures a wide range of stress states with  $m$  values in the range of 0.2 to 0.8 and significantly higher normal and shear stresses than FWD, LWD, and roller measurements. The implication of these differences in the  $m$  values is that measurements with higher  $m$  values (1.0 to 1.5) induce comparatively high shear stresses resulting in non-linear behavior (i.e., compaction), whereas for measurements with lower  $m$  values (0.2 to 0.5) resulting in near linear elastic behavior.

The granular foundation materials tested herein are believed to exhibit non-linear stress dependency and are expected to be sensitive to the subjected stress paths under loading. To that end, these observations are of significance in interpreting the scatter observed in the regression relationships presented in section 3.3.4. Relating in-ground stress measurements with the non-linear behavior of the pavement foundation materials merits further research, especially in terms of directly linking IC measurement values to mechanistic pavement design parameters.

### 3.3.5 Project Level In-Situ QA/QC Test Results

Mn/DOT personnel conducted QA/QC tests including  $w$  from “speedy” moisture content tests,  $E_{LWD}$  using 200-mm Zorn and Dynatest LWD devices, and DPI following the modified Mn/DOT DCP procedure. Acceptance criteria for these measurement values were as follows:

- $w$  should be within 65% to 95% of  $w_{opt}$  as determined by the standard Proctor method.

- $E_{LWD}$  should be within 90% to 120% of the  $E_{LWD-TV}$  determined from a representative calibration strip.
- DPI should be less than the DPI-TV determined based on the Grading Number (GN) of the material and  $w$  measurement at the test location. GN is determined based on the material gradation properties and ranges between 0.0 and 7.0 (GN = 0.0 represents a predominantly coarse gravel material while GN = 7.0 represents a predominantly fine material) (see Davich et al. 2006).

The results obtained from the QA/QC tests are organized by the GN value. Four different materials were identified from the test data: GN = 3.9, 5.2, 5.3, and 5.6. The target values, point test measurements at different locations, and the pass/fail results are summarized in Table 3.10, Table 3.11, and Table 3.12 for these materials. The  $E_{LWD}$  values recorded by Mn/DOT personnel were calculated using  $\nu = 0.5$  and  $f = 2$  in the  $E_{LWD}$  calculations. These values were corrected for  $\nu = 0.4$  and  $f = 8/3$  for consistency and comparison with the results presented in this report. Histograms of  $w$ ,  $E_{LWD-Z2}$ ,  $d_{LWD-Z2}$ ,  $E_{LWD-D2}$ ,  $d_{LWD-D2}$ , and DPI measurement values for materials with different GNs are presented in Figure 3.26, Figure 3.28, Figure 3.29, and Figure 3.27 respectively.

Table 3.10. Summary of Mn/DOT QA/QC test results for GN = 3.9 material

Location	Station	$w_{opt}$ (%)	$w$ (%)		$E_{LWD}$ (MPa) and $d_{LWD}$ (mm)					DPI (mm/blow)		
			Value	Pass/ Fail	$E_{LWD-TV}$	Model	$d_{LWD-D2}$	$E_{LWD-D2}$	Pass/ Fail	TV	Value	Pass/ Fail
EB 36	563+11	7.0	5.6	Pass	66.0	Zorn	1.47	36.3	Fail	10.0	14.4	Pass
EB 36	564+62	7.0	5.6	Pass	66.0	Zorn	1.43	37.2	Fail	10.0	14.7	Fail
EB 36	563+11	7.0	7.0	Fail	66.0	Zorn	1.00	53.0	Fail	15.0	12.2	Pass
EB 36	564+62	7.0	7.0	Fail	66.0	Zorn	1.52	35.1	Fail	15.0	12.7	Pass
EB 36	563+34	7.0	7.1	Fail	66.0	Zorn	1.25	42.6	Fail	—	—	—
EB 36	594+90	6.9	5.5	Pass	66.0	Zorn	1.06	50.0	Fail	—	—	—
EB 36	576+94	6.9	4.8	Pass	66.0	Zorn	0.54	99.1	NR	—	—	—
EB 36	574+90	6.9	4.8	Pass	66.0	Zorn	0.67	79.8	Pass	10.0	11.0	Fail
EB 36	576+94	6.9	4.8	Pass	—	—	—	—	—	10.0	14.4	Fail
EB 36	577+27	6.9	4.4	Fail	—	Zorn	0.65	81.8	—	10.0	16.1	Fail
EB 36	576+46	6.9	4.4	Fail	—	Zorn	0.73	72.5	—	—	—	—
EB 36	575+73	6.9	4.4	Fail	—	Zorn	0.81	65.6	—	—	—	—

Note: NR – target value not representative (exceeds 120% of  $E_{LWD-TV}$ ).

Table 3.11. Summary of Mn/DOT QA/QC test results for GN = 5.2 material

Location	Station	w <sub>opt</sub> (%)	w (%)		E <sub>LWD</sub> (MPa) and d <sub>LWD</sub> (mm)					DPI (mm/blow)		
			Value	Pass/ Fail	E <sub>LWD-TV</sub>	Model	d <sub>LWD-D2</sub>	E <sub>LWD-D2</sub>	Pass/ Fail	TV	Value	Pass/ Fail
SW Ramp	17+68	9.8	6.4	Pass	—	Dyna	0.58	56.5	—	21.0	35.6	Fail
SW Ramp	16+87	9.8	6.6	Pass	—	Dyna	0.24	134.3	—	21.0	27.1	Fail
SW Ramp	16+10	9.8	4.8	Fail	—	Dyna	0.51	63.9	—	—	—	—
SW Ramp	17+68	9.8	6.4	Pass	—	Dyna	0.58	56.5	—	—	—	—
SW Ramp	16+87	9.8	6.6	Pass	—	Dyna	0.37	89.5	—	—	—	—
SW Ramp	16+10	9.8	4.8	Fail	—	Dyna	0.51	63.9	—	—	—	—
SW Ramp	17+93	9.8	6.4	Pass	—	Dyna	0.67	49.3	—	21.0	9.3	Pass
SW Ramp	17+52	9.8	6.8	Pass	—	Dyna	0.61	54.1	—	21.0	27.1	Fail
SW Ramp	16+92	9.8	6.4	Pass	—	Dyna	0.51	64.4	—	21.0	32.2	Fail
SW Ramp	15+92	9.8	4.8	Fail	—	—	—	—	—	17.0	27.1	Fail
EB 36	534+40	9.8	3.1	Fail	139.2	Dyna	0.22	151.6	NR	17.0	16.9	Pass
EB 36	542+87	9.8	3.3	Fail	139.2	Dyna	0.24	135.7	Pass	17.0	18.6	Fail
EB 36	524+68	9.8	3.5	Fail	139.2	Dyna	0.23	140.5	Pass	21.0	17.8	Pass
EB 36	538+94	9.8	8.5	Pass	139.2	Dyna	0.82	40.1	Fail	25.0	41.5	Fail
EB 36	548+39	9.8	—	—	—	Zorn	0.94	56.6	—	—	—	—
EB 36	548+69	9.8	—	—	—	Zorn	1.16	45.8	—	—	—	—
EB 36	549+40	9.8	—	—	—	Zorn	1.21	43.8	—	—	—	—
EB 36	550+03	9.8	—	—	—	Zorn	2.14	24.8	—	—	—	Fail
NW Ramp	19+82	9.8	4.6	Fail	64.1	Dyna	0.63	51.7	Pass	17.0	28.8	Fail
NW Ramp	20+73	9.8	4.4	Fail	64.1	Dyna	0.63	51.7	Fail	17.0	33.0	Fail
NW Ramp	21+63	9.8	4.2	Fail	64.1	Dyna	0.54	61.3	Pass	17.0	31.3	Fail
NW Ramp	24+20	9.8	3.6	Fail	64.1	Dyna	0.43	76.0	NR	17.0	28.8	Fail
NW Ramp	23+84	9.8	6.2	Fail	64.1	Dyna	0.24	136.6	NR	21.0	18.6	Pass
WB 36	525+71	9.8	5.4	Fail	139.2	Dyna	0.27	121.6	Pass	21.0	21.2	Fail
WB 36	535+44	9.9	8	Pass	—	Dyna	0.68	48.0	—	—	—	—
WB 36	537+73	9.9	8.9	Pass	—	Dyna	0.50	65.7	—	—	—	—
WB 36	536+92	9.9	8.5	Pass	—	Dyna	0.48	68.2	—	—	—	—
WB 36	536+07	9.9	4.3	Fail	—	Dyna	0.36	90.4	—	—	—	—
WB 36	552+00	7	—	—	66.0	Zorn	1.37	38.8	Fail	—	—	—
WB 36	549+95	7	7.5	Fail	—	Zorn	0.88	60.2	—	21.0	22.0	Fail
WB 36	549+16	7	7.6	Fail	—	Zorn	0.53	100.3	—	21.0	21.2	Fail
WB 36	548+30	7	7.6	Fail	—	Zorn	0.72	74.2	—	21.0	21.2	Fail

Note: NR – target value not representative (exceeds 120% of E<sub>LWD-TV</sub>).

Table 3.12. Summary of Mn/DOT QA/QC test results for GN = 5.3 material

Location	Station	$w_{opt}$ (%)	$w$ (%)		$E_{LWD}$ (MPa) and $d_{LWD}$ (mm)					DPI (mm/blow)		
			Value	Pass/Fail	$E_{LWD-TV}$	Model	$d_{LWD-D2}$	$E_{LWD-D2}$	Pass/Fail	TV	Value	Pass/Fail
NW Ramp	18+86	—	5.3	—	—	Dyna	0.56	59.1	—	21.0	13.5	Pass
NW Ramp	17+90	—	5.0	—	—	Dyna	0.27	121.6	—	21.0	11.9	Pass
NW Ramp	17+04	—	5.9	—	—	Dyna	0.29	113.2	—	21.0	13.5	Pass
NW Ramp	17+01	—	11.4	—	—	Dyna	0.21	153.9	—	25.0	9.3	Pass
SE Ramp	12+35	—	7.3	—	—	—			—	21.0	28.8	Fail
SE Ramp	11+55	—	4.8	—	92.6	Zorn	0.54	99.1	Pass	17.0	6.8	Pass
SE Ramp	13+06	—	4.2	—	92.6	Zorn	0.54	98.5	Pass	17.0	10.2	Pass
SE Ramp	12+32	—	7.3	—	92.6	Zorn	0.41	130.7	Pass	21.0	6.8	Pass
SE Ramp	12+38	—	7.3	—	92.6	Zorn	2.08	25.6	Fail	—	—	—
SE Ramp	12+38	—	7.3	—	92.6	Zorn	1.71	31.2	Fail	—	—	—

Note: NR – target value not representative (exceeds 120% of  $E_{LWD-TV}$ ).

Table 3.13. Summary of Mn/DOT QA/QC test results for GN = 5.6 material

Location	Station	$w_{opt}$ (%)	$w$ (%)		$E_{LWD}$ (MPa)					DPI (mm/blow)		
			Value	Pass/Fail	$E_{LWD-TV}$	Model	$d_{LWD-D2}$	$E_{LWD-D2}$	Pass/Fail	TV	Value	Pass/Fail
EB 36	556+06	9.2	8.9	Fail	—	Dyna	0.42	77.5	—	28.0	25.4	Pass
EB 36	557+10	9.2	7.5	Pass	—	Dyna	0.37	89.2	—	24.0	26.2	Fail
EB 36	559+77	9.2	12.6	Fail	—	Dyna	0.40	82.2	—	28.0	26.2	Pass
EB 36	559+37	9.2	7.8	Pass	—	Dyna	0.27	120.0	—	24.0	18.6	Pass
EB 36	560+06	9.2	8.9	Fail	—	Dyna	0.42	77.6	—	28.0	25.4	Pass
EB 36	560+87	9.2	9.2	Fail	—	Dyna	0.32	102.3	—	28.0	24.6	Pass
EB 36	561+07	9.2	6.8	Pass	—	Dyna	0.53	61.5	—	24.0	20.3	Pass
WB 36	513+24	9.2	5.7	Fail	118.3	Dyna	0.25	130.8	NR	24.0	16.9	Pass

Note: NR – target value not representative (exceeds 120% of  $E_{LWD-TV}$ ).

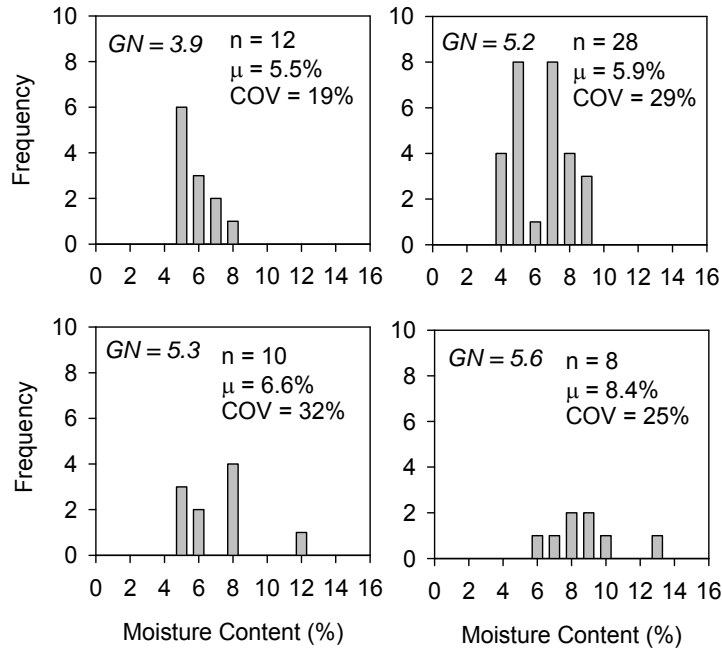


Figure 3.26. Histograms of Mn/DOT QA/QC moisture content measurements from TH36 project (data includes both pass and fail measurements)

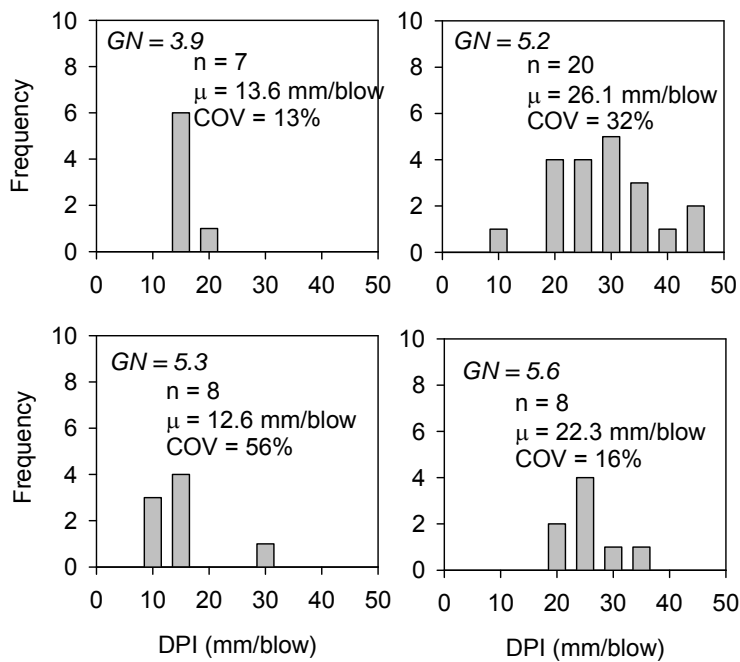


Figure 3.27. Histograms of Mn/DOT QA/QC DPI measurements from TH36 project (data includes both pass and fail measurements)

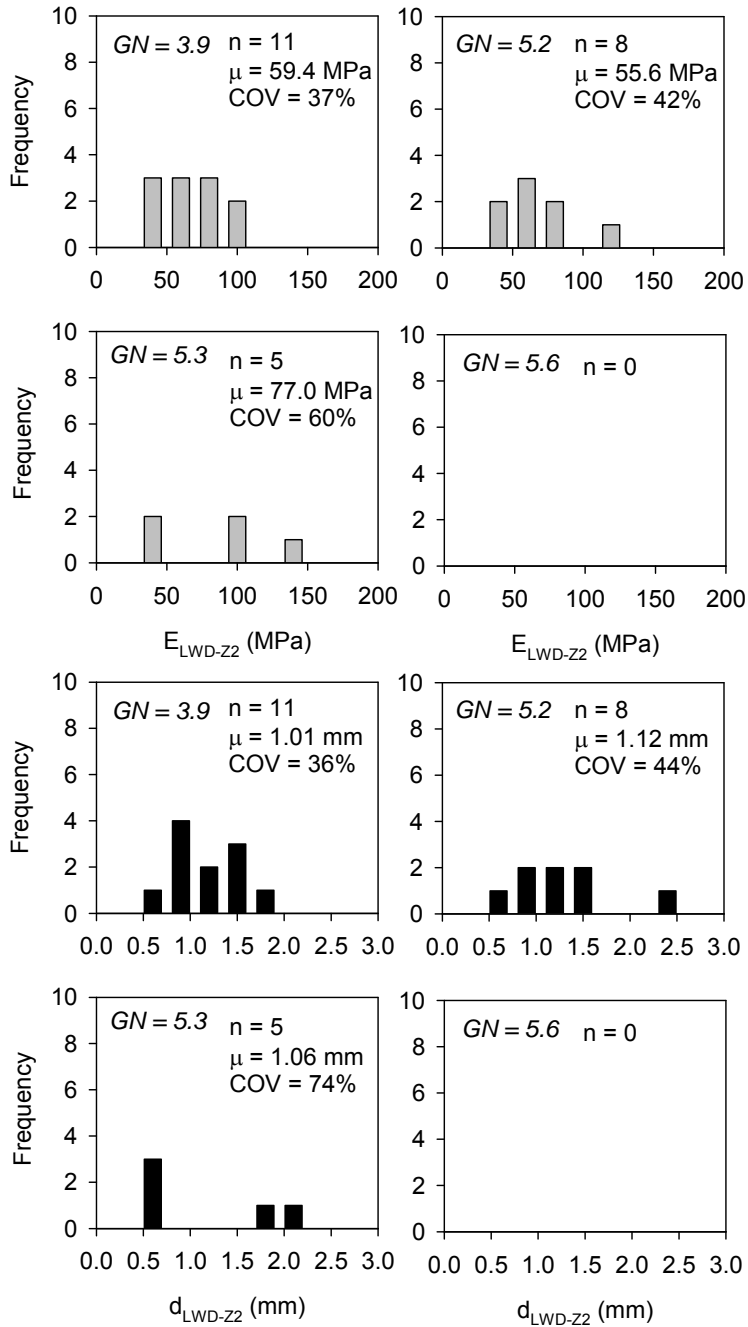


Figure 3.28. Histograms of Mn/DOT QA/QC  $E_{LWD-Z2}$  and  $d_{LWD-Z2}$  measurements from TH36 project (data includes both pass and fail measurements)

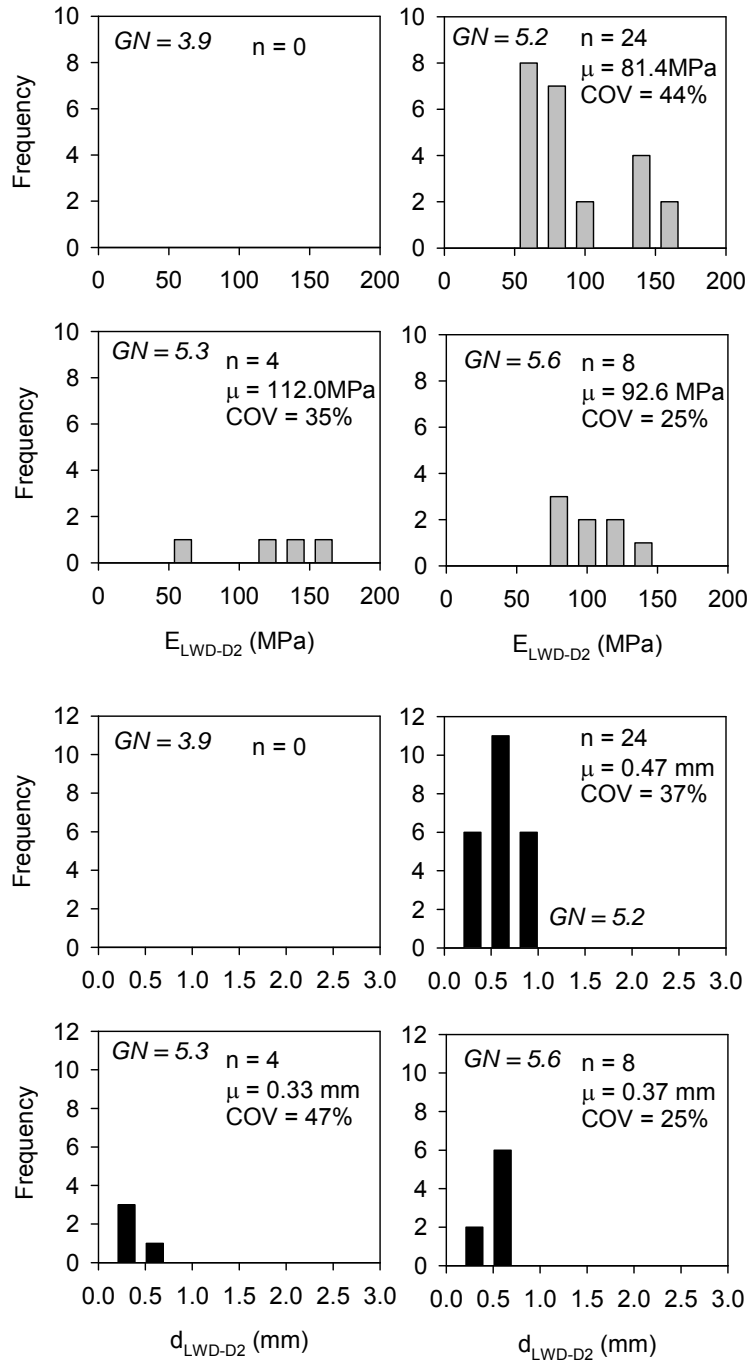


Figure 3.29. Histograms of Mn/DOT QA/QC  $E_{LWD-D2}$  and  $d_{LWD-D2}$  measurements from TH36 project (data includes both pass and fail measurements)

### 3.3.6 Key Observations and Conclusions

Experimental test results from four test strips on the TH36 project with granular pavement foundation layer (base, subbase, and subgrade) materials are presented above. Statistical

correlations between CMV measurements and in-situ point measurements were developed from the test strip studies. Further, results from instrumented embankment test sections of granular base, subbase, and subgrade layers with in-situ vertical and horizontal stresses induced under roller vibratory loading and LWD/FWD dynamic loading are presented. Some key findings from this project are as follows:

- IC-MVs were able to reliably indicate compaction quality of granular embankment materials.
- Correlations between CMV (obtained at  $a = 0.85$  mm) and different point measurements ( $E_{LWD}$ ,  $E_{FWD}$ ,  $E_{V1}$ ,  $E_{V2}$ ,  $E_{SSG}$ , CIV) showed positive relationships with  $R^2$  values  $> 0.5$ , with exception on one test strip (test strip 4). Data from test strip 4 showed poor correlations between CMV and  $E_{LWD}$  measurements; however, the data scatter closely matched the trends observed from previous studies. The primary factors contributing to low  $R^2$  values and scatter observed in the relationships is believed to be due to differences in measurement influence depths and applied stresses.
- Results obtained from one test strip (test strip 2) indicated that CMV is correlated with a linear regression relationship with modulus values (i.e.,  $E_{LWD-Z2}$ ,  $E_{V1}$  and  $E_{V2}$ ), while it is correlated with a non-linear power relationship with LWD deflection ( $d_{LWD-Z2}$ ) measurements.
- Comparison between CPTU, FWD, and DCP measurements showed good correlations with  $R^2$  values greater than 0.6. Comparison between FWD and LWD measurements showed poor correlations. The reasons are attributed partly due to limited data and partly due to significant differences in stress states in the material under FWD and LWD loading.
- Comparison between FWD, DCP, and CMV showed good correlations with  $R^2$  values around 0.6.
- Roller jumping (as measured by high RMV measurements) affected the CMV values and consequently the correlations. A statistically significant correlation was possible from test strip 4 by incorporating RMV into a multiple regression model to predict CMV. However, for practical purposes, it is preferable to perform calibration testing in low amplitude setting (about less than 1 mm) to avoid complex interpretation and analysis of results with roller jumping.
- Stress paths for loading under the roller showed a hysteresis of extension and compression during loading and unloading phases due to rotation in principal stresses under moving roller load. For the pavement foundation layers tested in this study, the mean stresses developed under a 300-mm FWD plate with  $F = 53.4$  kN are similar to mean stresses developed under the roller for  $a = 1.7$  mm but the stress path slope coefficient  $m$  for FWD loading is comparatively smaller than for roller loading. Applied mean stresses and  $m$  coefficients for LWD loading are significantly smaller than roller and FWD induced stresses and  $m$  coefficients – a likely contributor to scatter in relationships between roller and  $E_{LWD}$  measurements.

- Using criteria for characterizing measurement influence depth as the depth at 10% of the maximum stresses at the surface, the measurement influence depths under the roller, 300-mm FWD plate, and 200-mm LWD plate are summarized in Table 3.38. No significant difference was observed in the influence depth with change in amplitude or increasing dynamic load under the FWD plate. These results are expected to vary with soil stiffness and layering conditions, but provide a reference point for typical conditions.

Table 3.14. Summary of measurement influence depth of different measurements – TH36 project

Measurement	Depth below surface
Roller	0.9 m
300-mm FWD	0.6 m
200-mm LWD	0.3 m

### 3.4 District 2 US 10, Staples

#### 3.4.1 Project Overview

This project involved expansion and reconstruction of US 10 from about 3.1 km west of Junction TH 210 to 1.3 km east of Junction TH 210 in Staples, MN. Typical pavement foundation sections consisted of 0.23 m thick Mn/DOT class 6 aggregate base layer underlain by subcut backfill with “select” and “suitable” granular grading layers. The gradation requirements for the “select” and “suitable” granular materials are provided in Mn/DOT specification 3149. The subcut backfill layers varied in thickness from 0.15 m to 1.5 m. The subcut consisted of at least 0.6 m of “select” granular layer underlain by “suitable” granular layers. The granular grading materials were obtained from excavations on the project or from borrow sites. Moisture content tests were conducted as part of QC. IC measurements, DCP (Mn/DOT modified DCP method), LWD, and “speedy” moisture content tests were conducted for QA. CS563 smooth drum roller equipped with CMV/RMV measurement technologies, RTK GPS, and the AccuGrade compaction mapping system were used for compacting embankment materials.

In-situ point measurements (DCP, LWD, and PLT) in conjunction with roller measurements to develop correlations, and in-ground instrumentation data to evaluate stresses developed in the pavement foundation layers under roller and construction equipment (i.e., wheel tractor-scrappers), were obtained by the ISU research team from the project.

#### 3.4.2 Experimental Testing

A total of five test strips were constructed and tested during the field investigations on the project (see Table 3.15). Soil index properties of the materials encountered in each test strip are summarized in Table 3.16.

Table 3.15. Field testing summary (US10)

Date	Test Strip	Material	Operator	In-situ testing <sup>§</sup>
07/17to 18/2007	1	Select granular	ISU	LWD, PLT, NG, DCP, Instrumentation
07/19 to 20/2007	2	Select granular	ISU	LWD, DCP, NG
07/25/2007	3	Granular	ISU	LWD, DCP
07/25/2007	4	Granular with organics	ISU	LWD, DCP
07/25/2007	5	Select Granular	ISU	LWD, DCP, Instrumentation

<sup>§</sup>GPS measurements for point measurements.

Table 3.16. Summary of soil index properties from US 10 project

Parameter	Strip1	Strip 2	Strip 3	Strip4	Strip 5
Material Description	Poorly graded sand with silt	Silty sand	Silty sand	Silty Sand with organics	Silty Sand
Maximum Dry Unit Weight (kN/m <sup>3</sup> ) and Optimum Moisture Content (%)					
Standard Proctor	17.5 (11.8)	17.8 (10.2)	—	—	18.4 (10.0)
Modified Proctor	18.1 (9.6)	18.3 (9.1)	—	—	18.9 (7.9)
Gravel Content (%) (> 4.75mm)	5	1	0	2	5
Sand Content (%) (4.75mm – 75µm)	87	83	87	80	80
Silt Content (%) (75µm – 2µm)	4	10	5	9	8
Clay Content (%) (< 2µm)	4	6	8	9	7
Coefficient of Uniformity (c <sub>u</sub> )	3.2	5.1	7.7	52.5	23.5
Coefficient of Curvature (c <sub>c</sub> )	1.2	1.4	3.4	15.3	8.0
Atterberg limits	Non-Plastic				
AASHTO	A-3	A-2-4	A-2-4	A-2-4	A-2-4
USCS symbol	SP-SM	SM	SM	SM	SM
Specific Gravity, G <sub>s</sub>	2.68	2.57	2.61	2.60	2.60

Testing involved obtaining in-situ point measurements (i.e., DCP, LWD, PLT, and NG) in conjunction with IC-MVs for correlation analysis. LWD tests were conducted at the surface and at different depths to study the effect of confinement on the  $E_{LWD}$  values. In-ground stress measurements from EPCs installed in the foundation layers were obtained from test strips 1 and 5 under static and vibratory roller operations and scraper tires. Roller measurements obtained during compaction passes on test strips 1, 2, 4, and 5 were not recorded due to data memory card

issues that were discovered after completing the testing. Mapping passes were obtained on test strips 1 and 2 for comparison with final pass in-situ point measurements. No roller data is available for test strips 4 and 5. The data recording process on the machine was setup to create a \*.tag file for every 5 minutes of roller operation up to 999 files. Any data recorded after the memory card reached 999 files was over-written on the existing files. This issue was reported later to Mn/DOT, contractor, and roller manufacturer personnel. Description of construction and testing of each test strip, experimental test results and analysis are provided in the following sections.

### 3.4.3 Comparison between IC-MVs and in-situ point measurements

#### 3.4.3.1 Test strip 1

Test strip 1 consisted of select granular material and was constructed with plan dimensions of approximately 3 m x 55 m (Figure 3.30 and Figure 3.31). Approximately 32 m length of the area was scarified to a depth of about 0.3 m to create variations across the test strip as illustrated in Figure 3.30 with compacted and uncompacted sections. A summary of compaction operations and in-situ testing on the test strip is provided in Table 3.17. In-situ point measurements were obtained at 0, 8, 17, 22, and 27 passes at 15 test locations across the test strip. After pass 27, 300 mm Zorn LWD tests were conducted at the surface at one test location across the drum width and in an excavation by removing loose material at the surface to a depth of about 0.15 m (Figure 3.32) at three locations across the drum width. These tests were intended to check the influence of confinement on the  $E_{LWD-Z3}$  values and their correlations with IC-MVs. Unfortunately, roller measurements were not recorded for compaction passes 1 to 27 due to data memory card problems discussed in section 3.4.2. Mapping passes were performed after pass 27 to obtain IC-MVs from the test area. Reportedly, an IC-TV = 13 for  $a = 0.85$  mm nominal settings was used by Mn/DOT for QA/QC in the test strip area.

Compaction curve results from in-situ point measurements are presented in Figure 3.33. Data obtained from all test locations on the test strip is presented as open circles, and average per pass is presented as filled circles. Test measurements at pass 0 were obtained only from point locations 1 to 10, and measurements at 8, 17, and 22 passes were obtained at all point locations (A, B, and 1 to 12). On average, the  $E_{LWD-Z2}$  measurements showed compaction growth up to pass 22, with only minor increase from pass 17 to 22 (average  $E_{LWD-Z2} = 28$  MPa at pass 17 and 30 MPa at pass 22). The  $\gamma_d$  and  $DPI_{300}$  values showed compaction growth up to pass 8 and then no considerable growth after pass 22. The average  $\gamma_d$  was about 95% of standard Proctor maximum dry unit weight ( $\gamma_{dmax}$ ) after pass 22. The moisture content measurements after pass 22 were lower than the Mn/DOT 65% to 95% of  $w_{opt}$  limits.

CMV data obtained from mapping passes 1 to 5 with  $a = 0.85$  and 1.70 mm,  $f = 33$  Hz, and  $v = 3.2$  km/h nominal settings are presented in Figure 3.34. Summary statistics of CMV data are provided in Table 3.18. CMV data obtained at  $a = 0.85$  mm setting was on average about 1.5 times greater than CMV obtained at  $a = 1.7$  mm setting but the COV for the two settings were similar. Frequency distribution of CMV data for map pass 2 (see Figure 3.35) indicates that only 5% of the data was above the IC-TV used in this area. Conversation with contractor and

Mn/DOT personnel indicated that the material on the test strip tended to gain strength/stiffness if tested 24 hour after watering and compaction.

In-situ point measurements obtained from pass 27 in comparison with CMV data are presented in Figure 3.36. CMV data is presented as lines and in-situ point measurements are shown as discrete points.  $E_{LWD-Z3}$  data shows measurements taken at the surface and at a depth of about 0.15 m below surface after pass 27. Summary statistics of point measurements are provided in Table 3.18. Results indicate that  $E_{LWD-Z3}$  at 0.15 m depth is about 1.8 times greater than  $E_{LWD-Z3}$  at the surface, which illustrates the effect of confinement on the measurement values. The  $E_{LWD-Z3}$  measurements are plotted with depth along with DPI profiles obtained from pass 22 in Figure 3.37 further illustrating the effect of confinement on the strength/stiffness of granular materials. Interestingly, the  $E_{LWD-Z3}$  measurements obtained at 0.15 m depth tracked well with variations in CMV compared to the measurements obtained at the surface. Similarly, the  $E_{V1}$  and  $E_{V2}$  measurements obtained at 0.15 m depth tracked well with variations in CMV. Regression analysis results for CMV and in-situ point measurements are presented in section 3.5.3.4 combining data from other test strips.

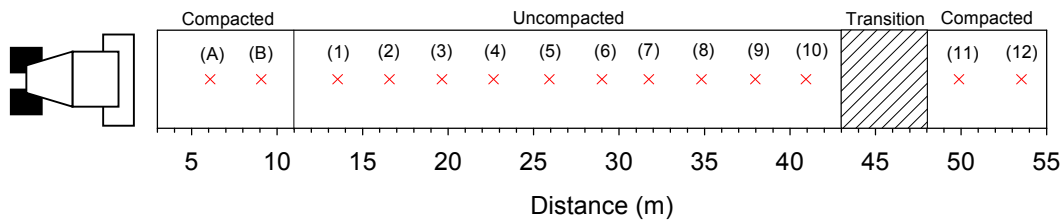


Figure 3.30. Test strip 1 area with spot test locations



Figure 3.31. Construction operations on test strip 1

Table 3.17. Testing and compaction summary for test strip 1

Pass*	<i>a</i> (mm)	Point Measurements	Remarks
0	—	x	NG, DCP, 200 mm Zorn LWD (at surface)
1 – 4	0.85	—	Moisture added with water truck after pass 4
5 – 6	Static	—	
7 – 8	0.85	x	NG, DCP, 200 mm Zorn LWD (at surface) after pass 8
9 – 10	0.85	—	
11 – 12	Static	—	
13 – 14	1.70	—	
15	0.85	—	
16	Static	—	
17	1.70	x	DCP, and 200 mm Zorn LWD
18 – 22	0.85	—	6 scraper <sup>§</sup> passes after pass 22 (3 loaded and 3 unloaded passes)
23 – 25	Static	—	
26	0.85	—	
27	1.70	x	After pass 27, 300 mm Zorn LWD (tests at surface at the center of the drum and at about 0.15 m depth at three points across the drum) and PLT (at 150 mm depth).
1 – 2 <sup>¥</sup>	0.85	—	
3 – 5 <sup>¥</sup>	1.70	—	

Note: Roller measurement data from pass 1 to 27 is not available; \* One pass represents a forwards pass with vibration on and reverse pass in static mode for passes 1-27; <sup>§</sup> Wheel-tractor scraper 627 B; <sup>¥</sup> Mapping passes



Figure 3.32. LWD testing performed by excavating loose material at the surface to a depth of about 0.15 m

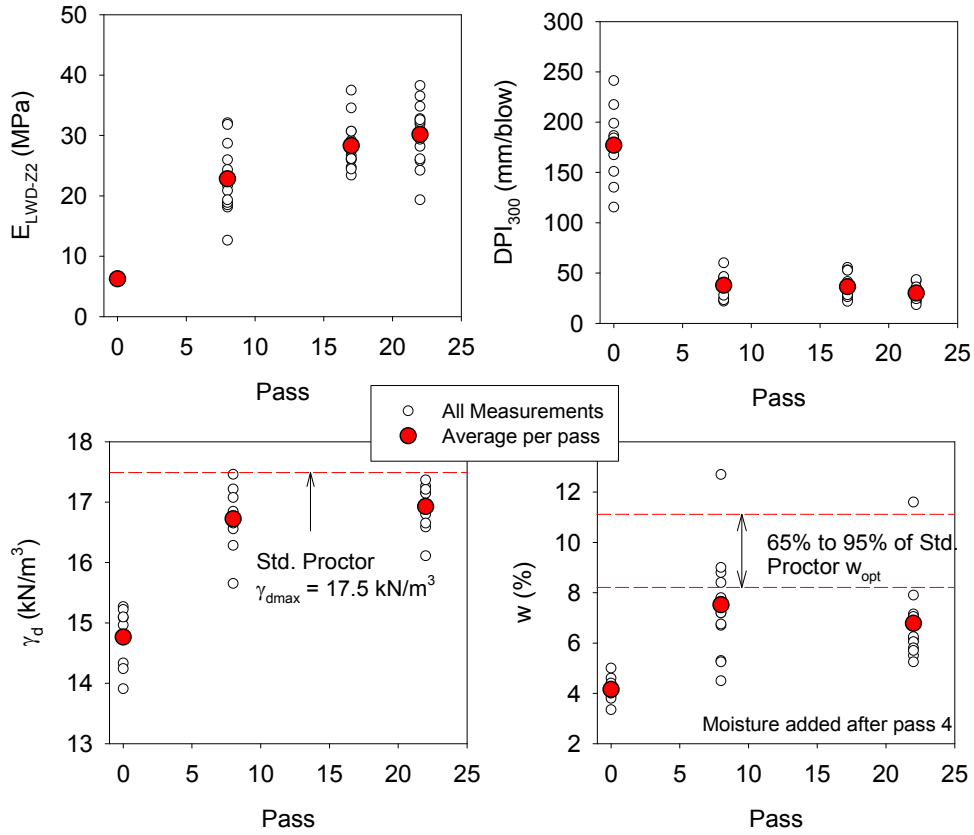


Figure 3.33. Compaction growth curves of in-situ point measurements (no measurements at points A, B, 11 and 12 at pass 0)

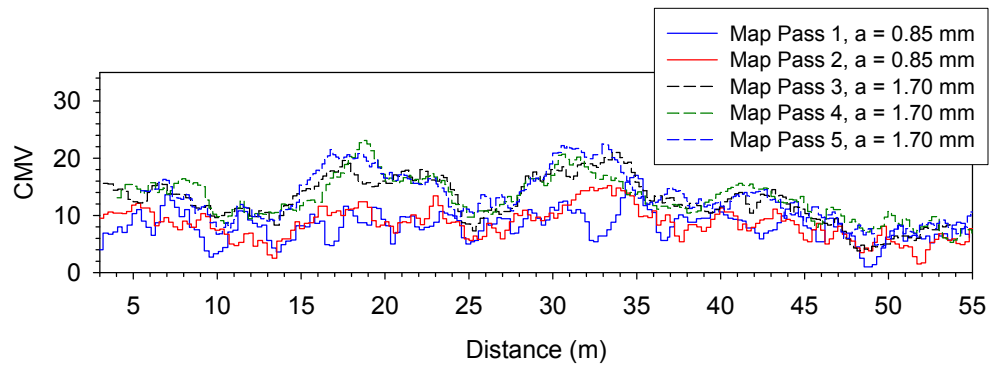


Figure 3.34. CMV data from mapping passes 1 to 5

Table 3.18. Summary statistics of IC-MVs and in-situ point measurements from test strip 1

Pass No.	Parameter	n	$\mu$	COV (%)
Map 1	CMV ( $a = 0.85$ mm)	194	8.2	34
Map 2	CMV ( $a = 0.85$ mm)	204	8.5	32
Map 3	CMV ( $a = 1.70$ mm)	213	12.7	32
Map 4	CMV ( $a = 1.70$ mm)	227	13.1	28
Map 5	CMV ( $a = 1.70$ mm)	299	12.9	34
27	Surface $E_{LWD-Z3}$ (MPa)	12	21.2	20
27	Surface $d_{LWD-Z3}$ (mm)	12	1.66	20
27	-150 mm $E_{LWD-Z3}$ (MPa)	36	37.6	21
27	-150 mm $d_{LWD-Z3}$ (MPa)	36	0.94	25
27	-150 mm $E_{V1}$ (MPa)	12	47.6	19
27	-150 mm $E_{V2}$ (MPa)	12	110.3	12

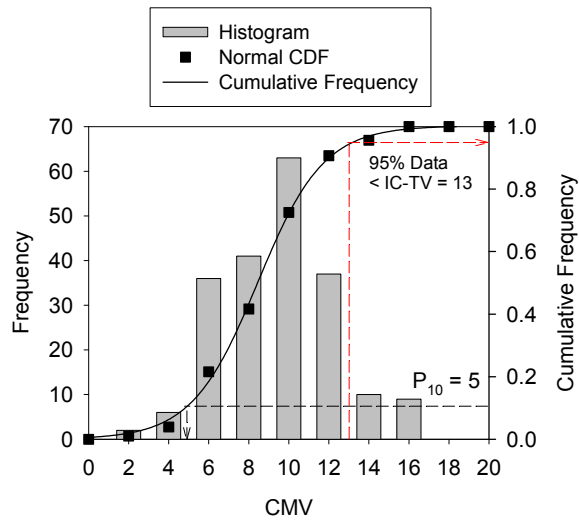


Figure 3.35. Frequency distribution of CMV data (pass 2,  $a = 0.85$  mm)

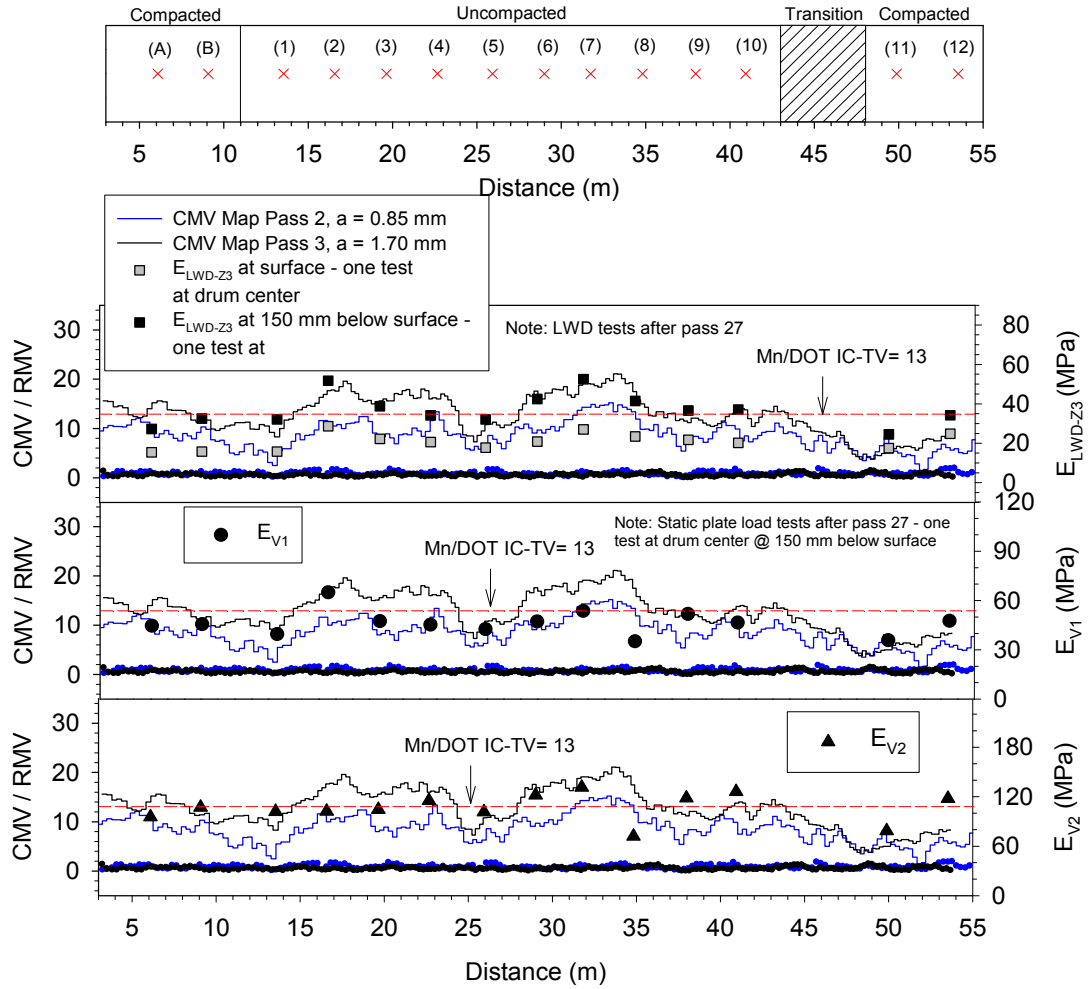


Figure 3.36. Comparison between CMV and in-situ point measurements from test strip 1

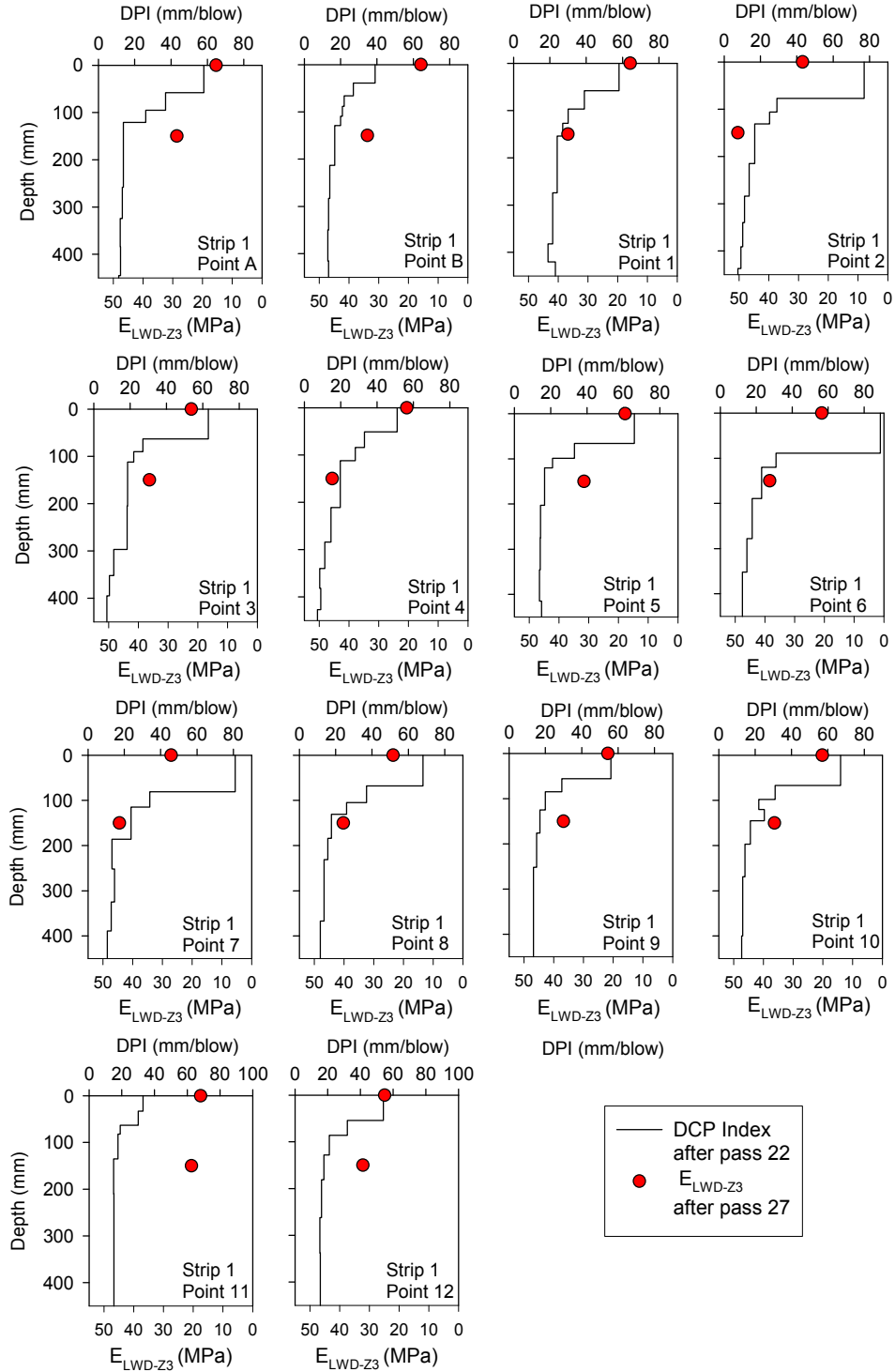


Figure 3.37. Comparison of  $E_{LWD-Z3}$  point measurements at surface and at different depths with DPI profiles

### 3.4.3.2 Test strip 2

Test strip 2 consisted of select granular material with plan dimensions of approximately 19 m x 55 m. The material was obtained from a borrow source and was placed with nominal loose lift thickness of approximately 0.3 m. The area was compacted in six roller lanes using different amplitude settings for eight roller passes. Following the final compaction pass, in-situ point measurements (NG, LWD, and DCP) were obtained at six test locations in each lane. Pictures of the final compacted layer and in-situ testing on the test area are shown in Figure 3.38. Due to data memory card issues described earlier, roller data from compaction passes were not recorded. The test area was mapped using  $a = 0.85$  and 1.70 mm,  $f = 33$  Hz, and  $v = 3.2$  km/h nominal settings. Similar to test strip 1, an IC-TV = 13 for  $a = 0.85$  mm nominal settings was used for QA/QC for this area.

CMV maps from the test area for the two amplitude settings are presented in Figure 3.39. Frequency distribution plots of CMV data presented in Figure 3.40 indicate that CMV obtained at  $a = 1.7$  mm is on average about 1.3 times greater than CMV obtained at  $a = 0.85$  mm but the COV was similar. This is consistent with observation from pass 1 where CMV was on average 1.5 times greater at  $a = 1.70$  compared to  $a = 0.85$  mm. Approximately 80% of the data was above the IC-TV.

In-situ point measurements obtained after the final compaction pass are plotted in comparison with CMV data in Figure 3.41, Figure 3.42, Figure 3.43, Figure 3.44, and Figure 3.45. CMV data is presented as lines and in-situ test measurements are shown as discrete points. Summary statistics of CMV and in-situ point measurements for the test strip are presented in Table 3.19. Results from the test strip indicate that the  $E_{LWD-D2}$  and DPI measurements tracked relatively well with variations observed in CMV measurements.  $\gamma_d$  measurements did not track well with variations in CMV. CMV was influenced by moisture variations at some locations, for example, increasing moisture showed a decrease in CMV for lanes 1, 2, and 3.  $DPI_{S-300}$  measurements captured the variations in CMV better than  $DPI_{300}$  measurements.



Figure 3.38. Photographs of test strip 2 after final pass (left) and in-situ testing (right)

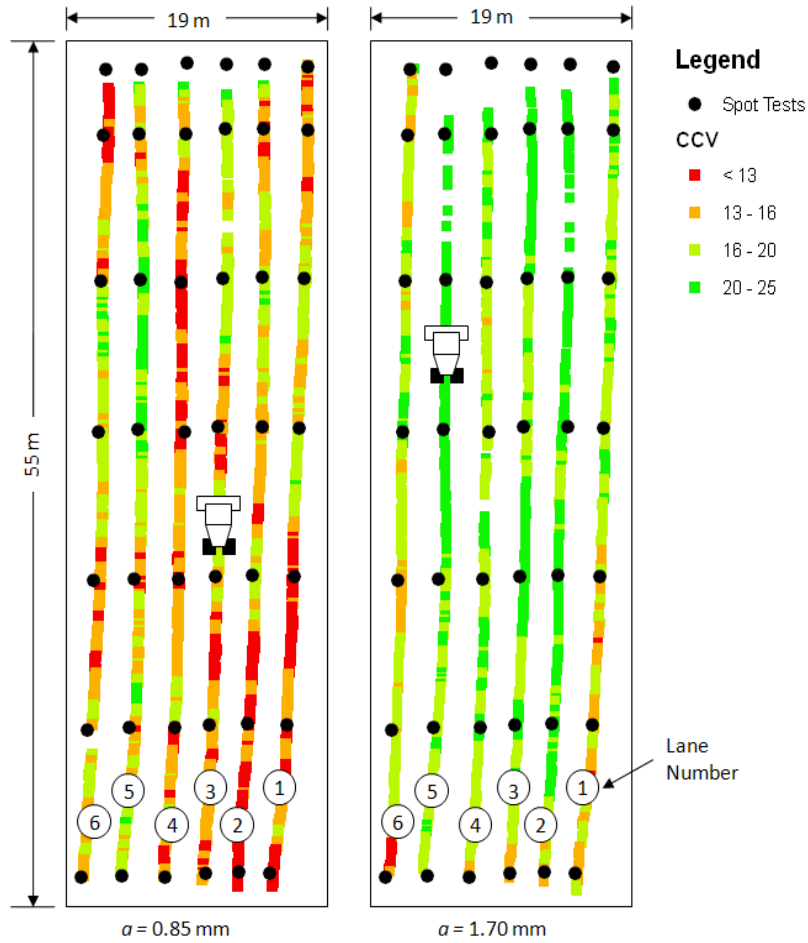


Figure 3.39. Plan view CMV map at two different amplitude ( $a = 0.85$  and  $1.70$  mm) settings of test strip 2 compacted in six roller lanes

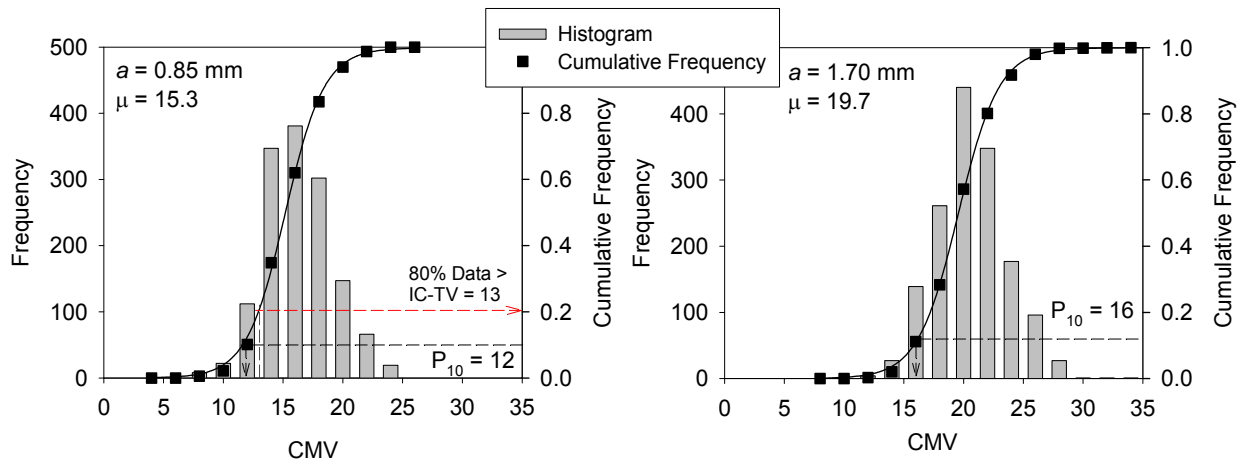


Figure 3.40. Frequency distribution of CMV data from test strip 2 ( $a = 0.85$  and  $1.70$  mm)

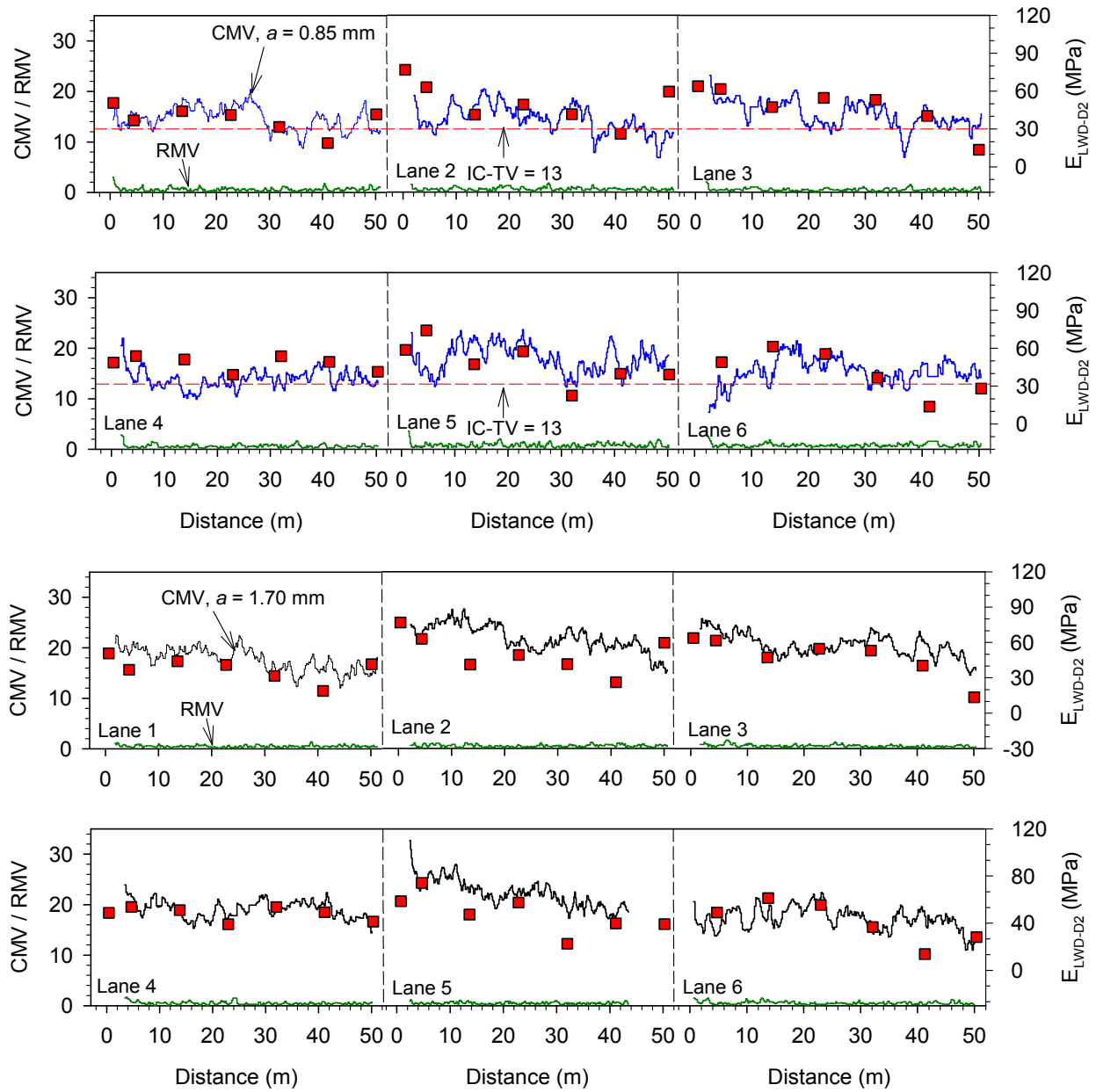


Figure 3.41. Comparison of CMV ( $a = 0.85$  and  $1.70$  mm) and  $E_{LWD-D2}$  measurements from test strip 2 lanes 1 to 6

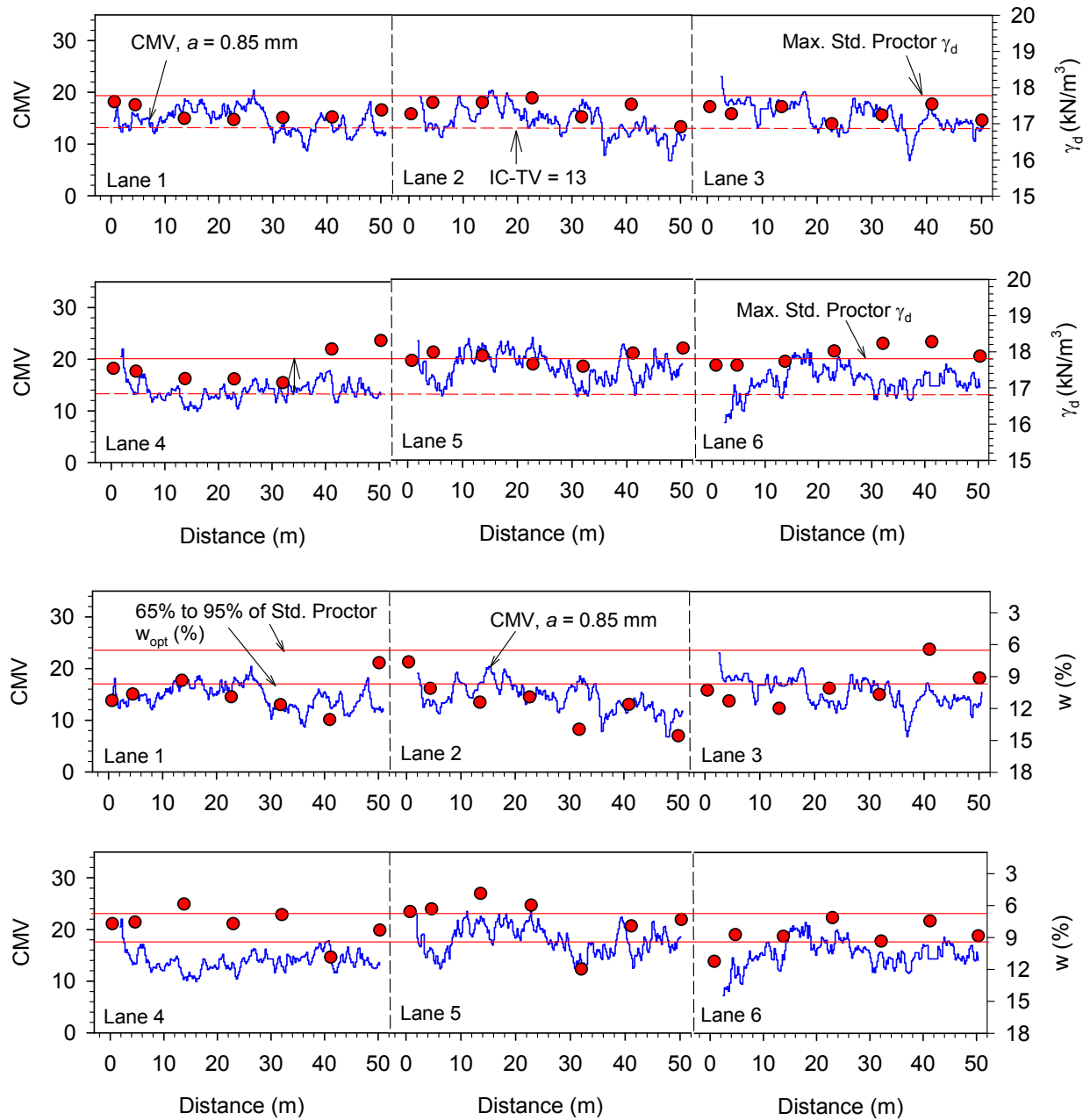


Figure 3.42. Comparison of CMV ( $a = 0.85$  mm) and NG measurements from test strip 2 lanes 1 to 6

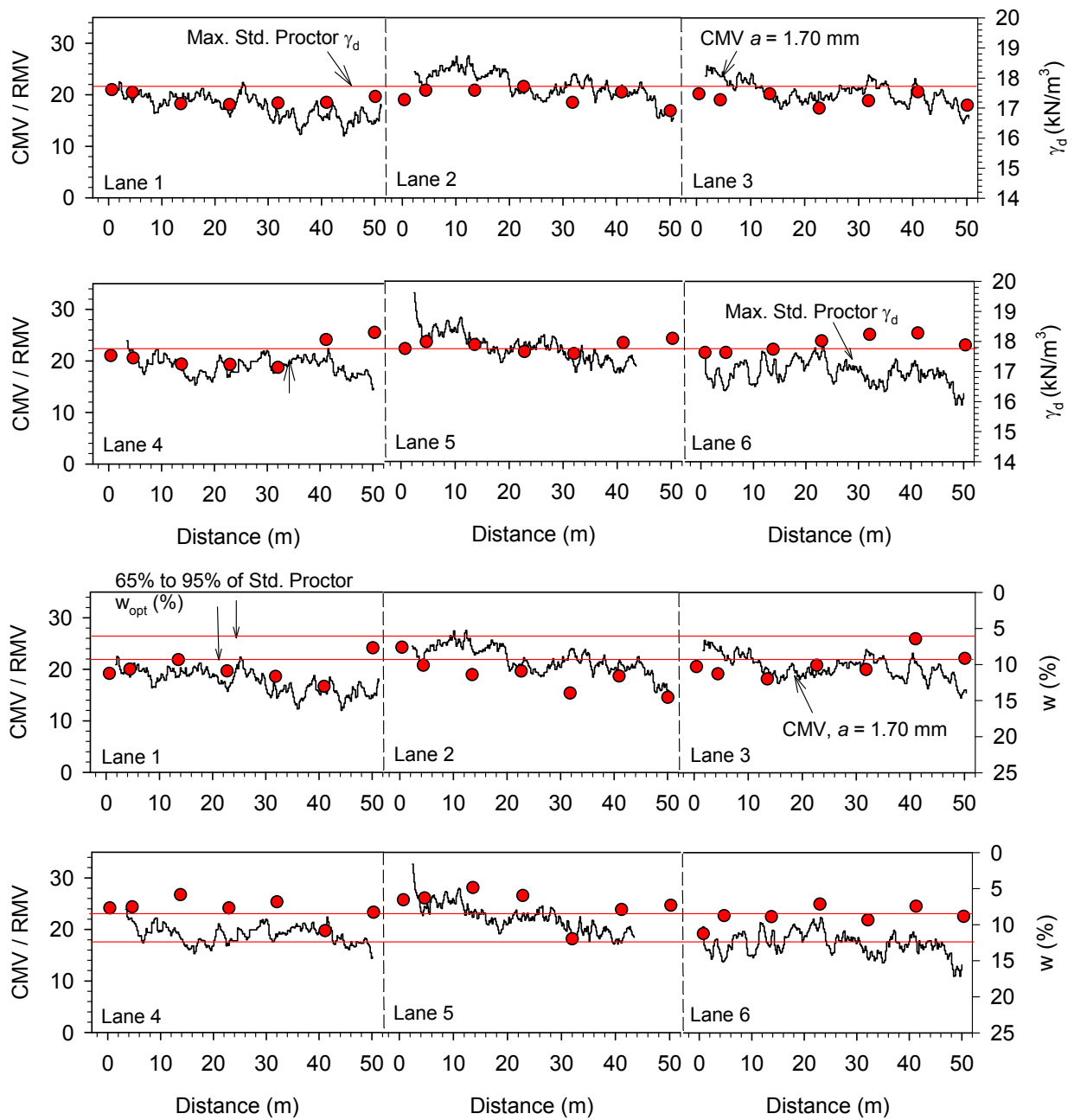


Figure 3.43. Comparison of CMV ( $a = 1.70$  mm) and NG measurements from test strip 2 lanes 1 to 6

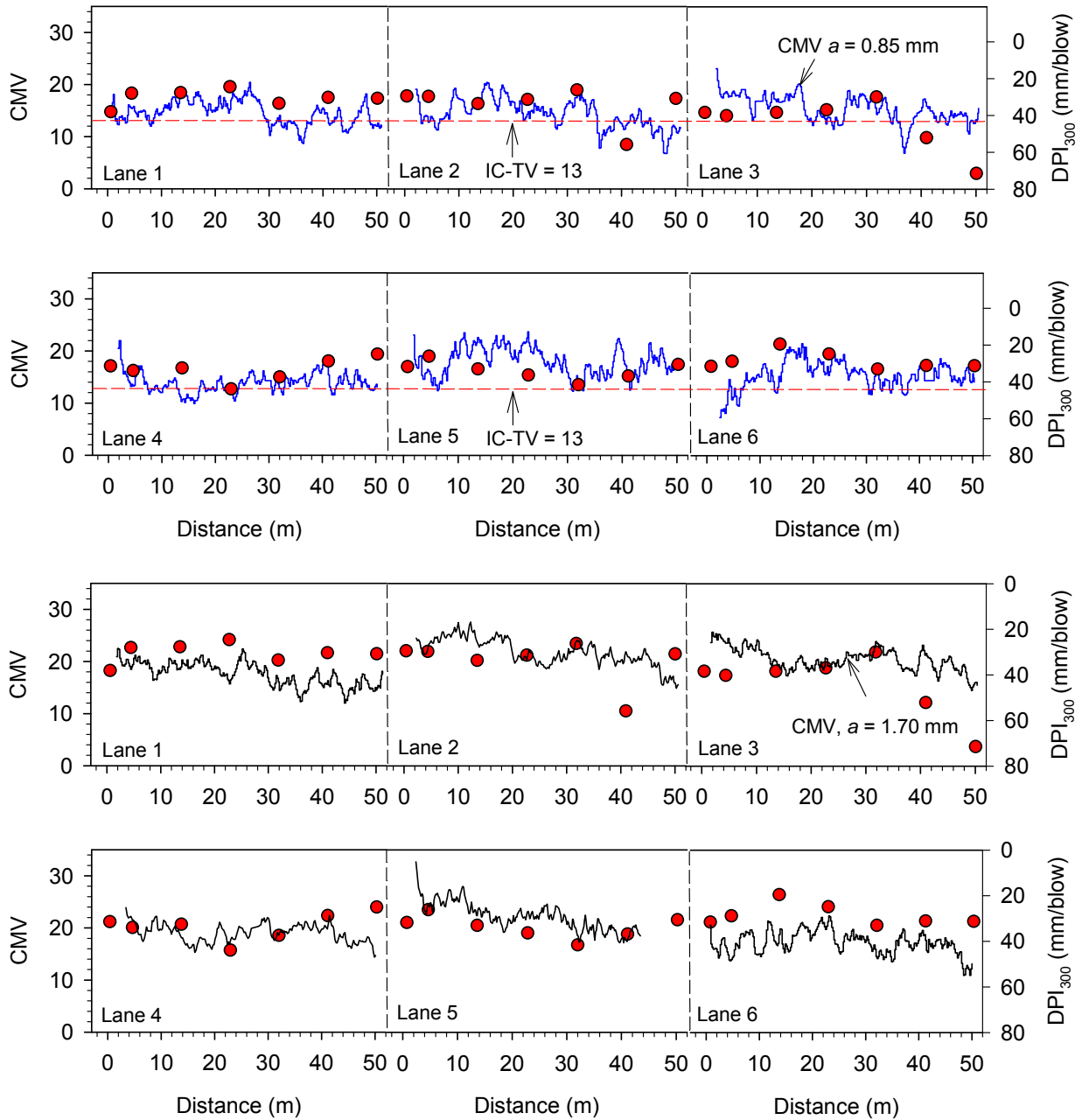


Figure 3.44. Comparison of CMV ( $a = 0.85$  and  $1.70$  mm) and  $DPI_{300}$  measurements from test strip 2 lanes 1 to 6

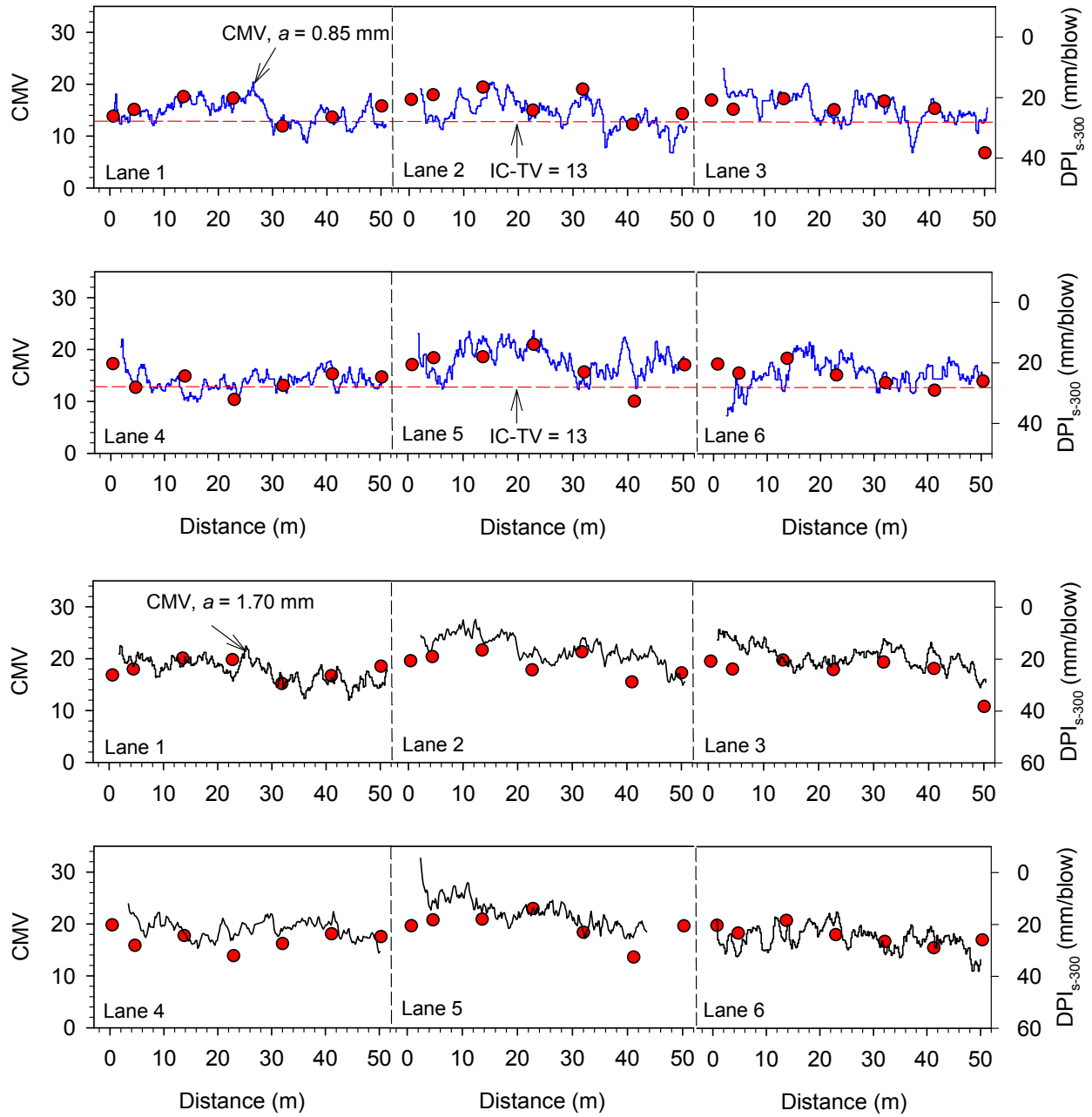


Figure 3.45. Comparison of CMV ( $a = 0.85$  and  $1.70$  mm) and  $DPI_{s-300}$  measurements from test strip 2 lanes 1 to 6

Table 3.19. Summary statistics of IC-MVs and in-situ point measurements on test strip 2

Parameter	n	$\mu$	COV (%)
CMV ( $a = 0.85$ mm)	194	15.3	19
CMV ( $a = 1.70$ mm)	204	19.7	15
$\gamma_d$ (kN/m <sup>3</sup> )	42	17.6	2
$w$ (%)	42	9.4	42
Surface $E_{LWD-D2}$ (MPa)	42	47.5	38
Surface $d_{LWD-D2}$ (mm)	42	0.70	52
DPI <sub>300</sub> (mm/blow)	42	33.6	28
DPI <sub>S-300</sub> (mm/blow)	42	23.6	20

### 3.4.3.3 Test strip 3

Test strip 3 consisted of granular subgrade material with variable conditions (i.e., soft and stiff locations) across the test strip and was located outside the US 10 main alignment (Figure 3.46). Plan dimensions of the test strip were approximately 3 m x 80 m. The area was mapped using  $a = 0.85$  and  $1.70$  mm,  $f = 33$  Hz, and  $v = 3.2$  km/h nominal settings. Following mapping passes in-situ point measurements (LWD and DCP) were obtained from 23 test locations along the test strip. LWD tests were conducted at the surface and at a depth of about 0.15 m below the surface. The excavation was performed to remove the loose soil at the surface. DCP tests were conducted in the excavation; therefore, the results are reported as DPI<sub>S-300</sub>. In-situ point measurements in comparison with CMV data are shown Figure 3.47. CMV data is presented as lines and in-situ test measurements are shown as discrete points. Summary statistics of CMV and in-situ point measurements for the test strip are presented in Table 3.20.  $E_{LWD-Z2}$  measurements at 0.15 m depth and DPI<sub>S-300</sub> tracked better with variations in CMV compared to  $E_{LWD-Z2}$  at the surface.



Figure 3.46. Compaction operations on test strip 3 (left) and excavations performed for LWD testing

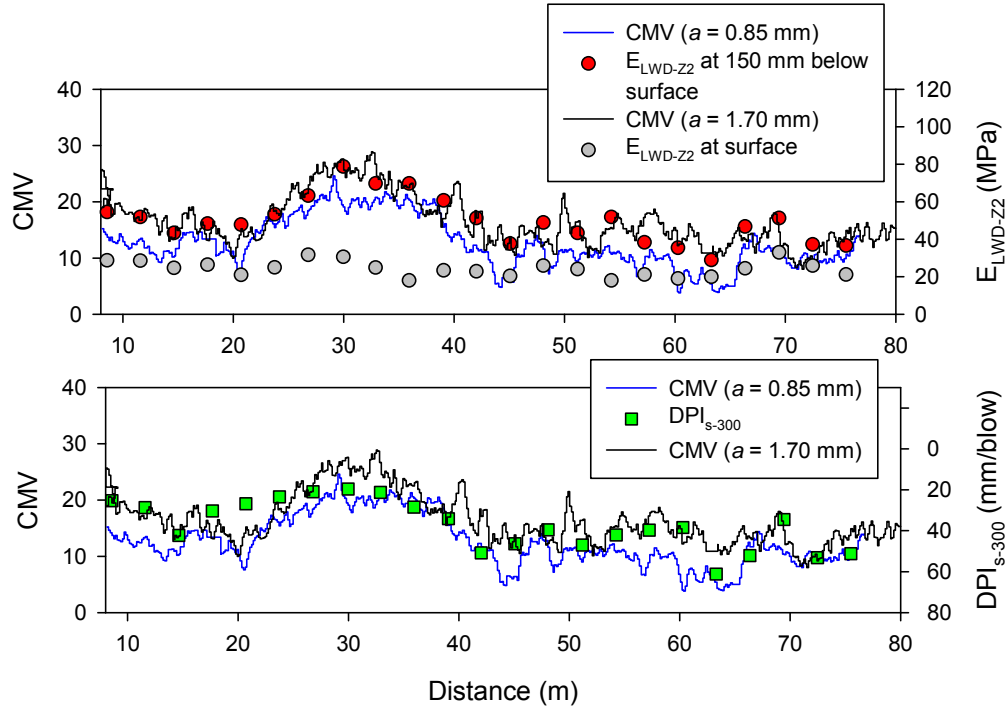


Figure 3.47. Comparison of CMV ( $a = 0.85$  and  $1.70$  mm) and in-situ point measurements from test strip 3

Table 3.20. Summary statistics of CMV and in-situ point measurements from test strip 3

Parameter	n	$\mu$	COV (%)
CMV ( $a = 0.85$ mm)	439	12.6	36
CMV ( $a = 1.70$ mm)	509	16.2	29
Surface $E_{LWD-Z2}$ (MPa)	23	24.3	17
Surface $d_{LWD-Z2}$ (MPa)	23	1.89	17
-150 mm $E_{LWD-Z2(50)}$ (MPa)	23	49.9	25
-150 mm $d_{LWD-Z2(50)}$ (MPa)	23	0.95	25
$DPI_{S-300}$ (mm/blow)	23	37.3	32

### 3.4.3.3 Test strips 4 and 5

Test strip 4 was located in a stockpile area and consisted of granular material with organics (Figure 3.48). The area was compacted with four roller passes. LWD and DCP tests were performed on the test strip. Test strip 5 consisted of select granular material (Figure 3.49). The area was compacted with 8 roller passes. LWD and DCP tests were performed on the test strip after the 8 compaction passes. LWD tests were conducted at a depth of about 0.1 m below the surface by removing the surficial loose material. The data from test strips 4 and 5 were used for correlation analysis between  $E_{LWD-Z2}$  and DPI presented later in the report.



Figure 3.48. Compaction operations on test strip 4 with soft and uncompacted material



Figure 3.49. Compaction operations on test strip 5 with relatively uniform conditions across the test strip

#### 3.4.3.4 Regression analysis between CMV and in-situ point measurements

Regression relationships derived from experimental testing on test strips 1, 2, and 3 are summarized in Figure 3.50 and Figure 3.51 for  $a = 0.85$  mm and 1.70 mm, respectively and are summarized in Table 3.21. These relationships were developed by spatially paring the nearest point data using GPS measurements. Results from regression analysis show linear relationships between  $E_{LWD}$  and CMV, and non-linear power relationships between DPI and CMV.  $E_{LWD}$  and  $d_{LWD}$  measurements obtained from 0.15 m below surface,  $DPI_{S-300}$ , and  $E_{V1}$  showed good correlations with CMV ( $R^2$  values  $> 0.6$ ). Relationships with  $E_{LWD}$  and  $d_{LWD}$  measurements at the surface and  $DPI_{300}$  showed correct trends but with  $R^2$  values  $< 0.3$ . No statistically valid correlations were found between  $\gamma_d$ ,  $w$ ,  $E_{V2}$ , and CMV. Similar to results described for a test strip under TH36 project, CMV correlations with modulus measurements (i.e.,  $E_{LWD-Z2}$ ,  $E_{V1}$ ,  $E_{LWD-D2}$ , and  $E_{LWD-Z3}$ ) showed linear relationships while with  $d_{LWD}$  measurements showed non-linear power relationships (Figure 3.50 and Figure 3.51).

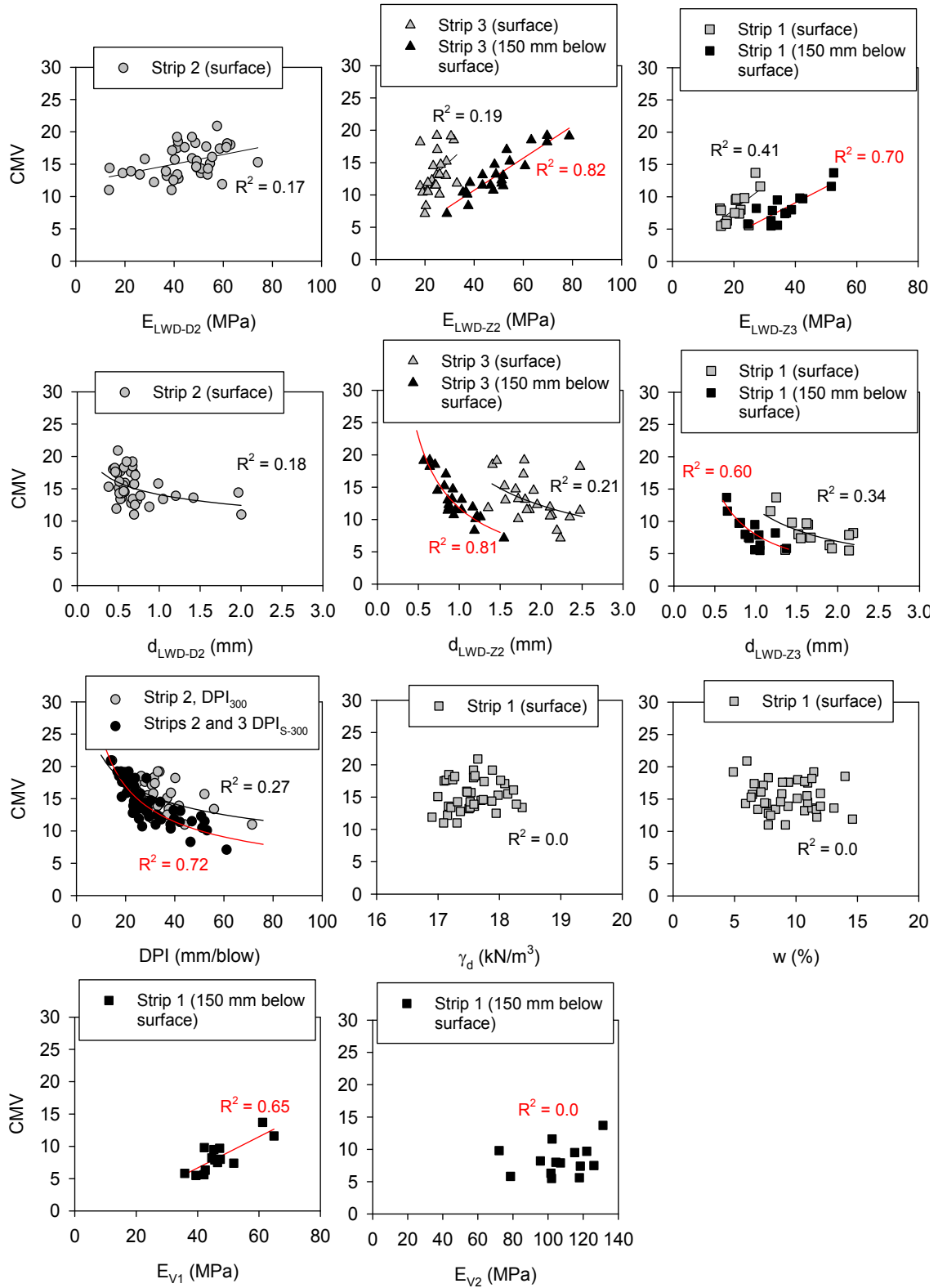


Figure 3.50. Regression relationships between CMV ( $a = 0.85$  mm) and different in-situ point measurements

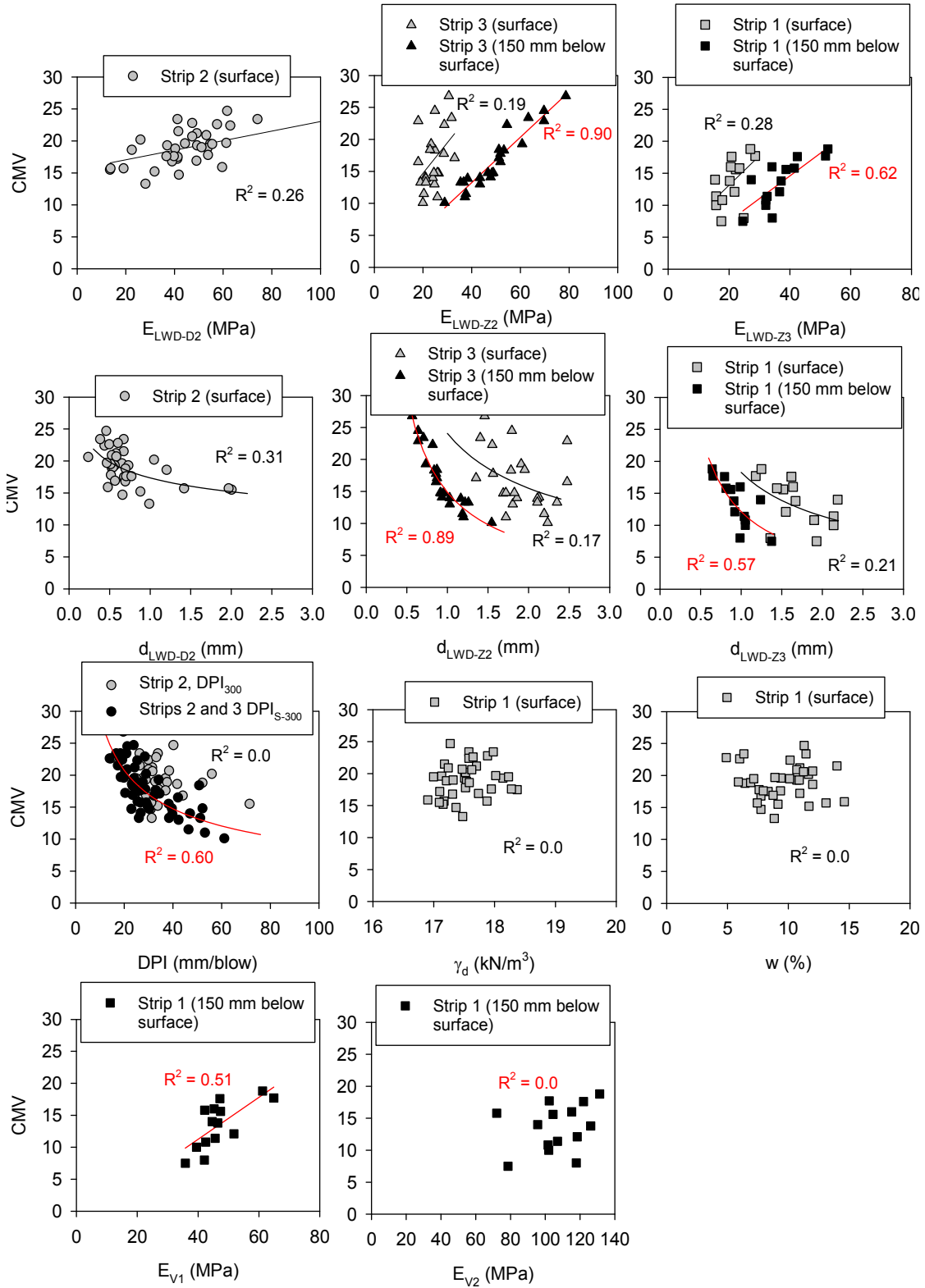


Figure 3.51. Regression relationships between CMV ( $a = 1.70$  mm) and different in-situ point measurements

Table 3.21. Summary of regression relationships between IC-MVs and in-situ point measurements – US10 project test strips 1, 2, and 3

Test strip(s)	Point Measurement	Relationship	<i>a</i> (mm)	n	R <sup>2</sup>	
1	Surface	CMV = 0.72 + 0.36 E <sub>LWD-Z3</sub>	0.85	15	0.41	
1		CMV = 11.96 (d <sub>LWD-Z3</sub> ) <sup>-0.80</sup>		15	0.34	
1	150 mm below surface	CMV = -0.79 + 0.24 E <sub>LWD-Z3</sub>		15	0.70	
1		CMV = 7.50 (d <sub>LWD-Z3</sub> ) <sup>-1.00</sup>		15	0.60	
3	Surface	CMV = 4.64 + 0.35 E <sub>LWD-Z2</sub>		23	0.19	
3		CMV = 19.50 (d <sub>LWD-Z2</sub> ) <sup>-0.68</sup>		23	0.21	
3	150 mm below surface	CMV = 0.78 + 0.25 E <sub>LWD-Z2</sub>		23	0.82	
3		CMV = 11.79 (d <sub>LWD-Z2</sub> ) <sup>-0.96</sup>		23	0.81	
2	Surface	CMV = 12.04 + 0.07 E <sub>LWD-D2</sub>		42	0.17	
2		CMV = 14.09 (d <sub>LWD-D2</sub> ) <sup>-0.18</sup>		42	0.18	
2	Surface	CMV = 44.18 (DPI <sub>300</sub> ) <sup>-0.31</sup>		42	0.27	
2, 3	After seating	CMV = 92.26 (DPI <sub>S-300</sub> ) <sup>-0.57</sup>		65	0.72	
1	150 mm below surface	CMV = -3.03 + 0.24 E <sub>V1</sub>		15	0.65	
1	Surface	CMV = 3.89 + 0.46 E <sub>LWD-Z3</sub>		1.70	15	0.28
1		CMV = 18.25 (d <sub>LWD-Z3</sub> ) <sup>-0.68</sup>			15	0.21
1	150 mm below surface	CMV = 0.42 + 0.35 E <sub>LWD-Z3</sub>			15	0.62
1		CMV = 12.12 (d <sub>LWD-Z3</sub> ) <sup>-1.03</sup>	15		0.57	
3	Surface	CMV = 5.24 + 0.48 E <sub>LWD-Z2</sub>	23		0.19	
3		CMV = 24.07 (d <sub>LWD-Z2</sub> ) <sup>-0.64</sup>	23		0.17	
3	150 mm below surface	CMV = -0.94 + 0.35 E <sub>LWD-Z2</sub>	23		0.90	
3		CMV = 14.87 (d <sub>LWD-Z2</sub> ) <sup>-1.03</sup>	23		0.89	
2	Surface	CMV = 15.55 + 0.07 E <sub>LWD-D2</sub>	42		0.26	
2		CMV = 17.35 (d <sub>LWD-D2</sub> ) <sup>-0.19</sup>	42		0.31	
2, 3	After seating	CMV = 91.49 (DPI <sub>S-300</sub> ) <sup>-0.50</sup>	65		0.59	
1	150 mm below surface	CMV = -1.89 + 0.33 E <sub>V1</sub>	15		0.51	

### 3.4.3.5 Correlations between different point measurements

Relationships between in-situ point measurements obtained from test strips 1, 2, 3, 4 and 5 are summarized in Table 3.22 and Figure 3.52. Regression analysis results showed non-linear power relationships between E<sub>LWD</sub> and DPI, and linear relationships between E<sub>LWD</sub> and E<sub>V1</sub>, and d<sub>LWD</sub>

and DPI measurements. Similar non-linear relationships between elastic modulus and DPI are reported by others (e.g. Chai and Roslie 1998). No statistically valid correlation was observed between  $E_{LWD-Z3}$  and  $E_{V2}$ .  $E_{LWD}$  measurements obtained from 0.1 to 0.15 m depth and  $DPI_{S-300}$  showed better correlations with  $R^2 > 0.6$  compared to  $E_{LWD}$  at surface at  $DPI_{300}$  ( $R^2 < 0.2$ ).

Table 3.22. Summary of regression relationships between different in-situ point measurements – US10 project

Test strip(s)	Relationship	n	R <sup>2</sup>
2 <sup>a</sup>	$E_{LWD-D2} = 70.62 - 0.69 DPI_{300}$	42	0.13
2 <sup>a</sup>	$d_{LWD-D2} = 0.08 - 0.02 DPI_{300}$	42	0.23
2 <sup>a</sup>	$E_{LWD-D2} = 92.03 - 1.88 DPI_{S-300}$	42	0.24
2 <sup>a</sup>	$d_{LWD-D2} = 0.36 - 0.05 DPI_{S-300}$	42	0.34
1 <sup>a</sup> , 3 <sup>a</sup> , 4 <sup>a</sup> , 5 <sup>a</sup>	$E_{LWD-Z2} = 393.48 (DPI_{300})^{-0.78}$	86	0.81
1 <sup>a</sup> , 3 <sup>a</sup> , 4 <sup>a</sup> , 5 <sup>a</sup>	$d_{LWD-Z2} = 0.71 + 0.03 DPI_{300}$	86	0.87
1 <sup>a</sup> , 3 <sup>a</sup> , 4 <sup>a</sup> , 5 <sup>a</sup>	$E_{LWD-Z2} = 238.76 (DPI_{S-300})^{-0.68}$	86	0.84
1 <sup>a</sup> , 3 <sup>a</sup> , 4 <sup>a</sup> , 5 <sup>a</sup>	$d_{LWD-Z2} = 0.89 + 0.03 DPI_{S-300}$	86	0.89
3 <sup>b</sup> , 4 <sup>b</sup> , 5 <sup>b</sup>	$E_{LWD-Z2} = 956.3 (DPI_{S-300})^{-0.92}$	42	0.87
3 <sup>b</sup> , 4 <sup>b</sup> , 5 <sup>b</sup>	$d_{LWD-Z2} = 0.04 DPI_{S-300}$	42	0.88
1 <sup>c</sup>	$E_{LWD-Z3} = 0.44 E_{V1}$	15	0.50
1 <sup>c</sup>	$d_{LWD-Z3} = 33.96 (DPI_{S-300})^{-0.79}$	15	0.48

<sup>a</sup>  $E_{LWD}$  measurements at surface

<sup>b</sup>  $E_{LWD}$  measurements at 150 mm below surface

<sup>c</sup>  $E_{LWD}$  and  $E_{V1}$  measurements at 100 to 150 mm below surface

Note:  $E_{LWD}$  in MPa,  $d_{LWD}$  in MPa, and DPI in mm/blow

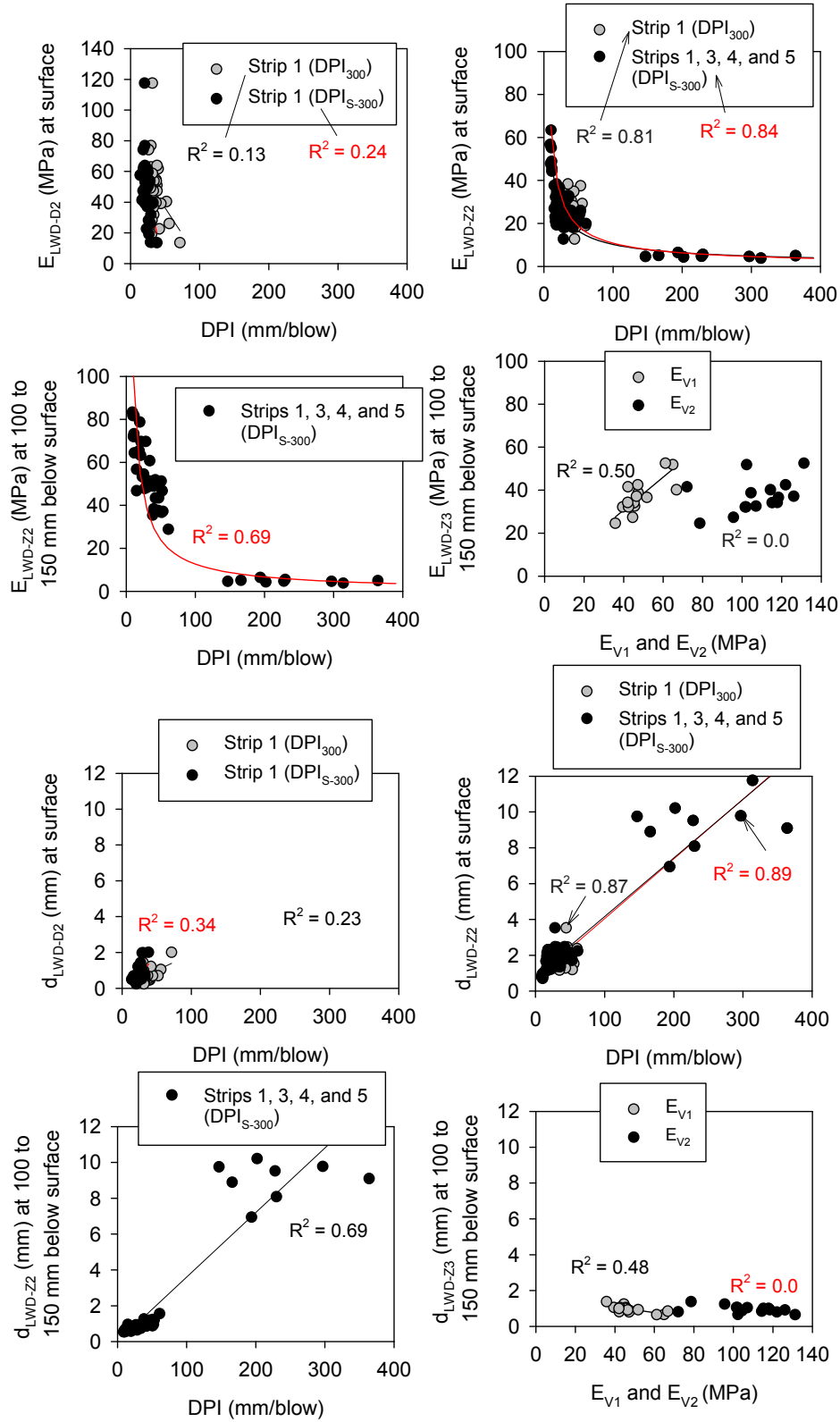


Figure 3.52. Regression relationships between different in-situ point measurements

### 3.4.3.5 Geostatistical Analysis of IC-MVs and in-situ point measurements

IC-MVs provide an opportunity to spatially visualize and quantify “non-uniformity” of compaction measurement values. This topic is slowly gaining popularity among IC researchers (see Petersen et al. 2007, White et al. 2008, Vennapusa and White 2009b). Vennapusa and White (2009b) demonstrated the use of semivariogram analysis in combination with conventional statistical analysis to effectively address the issue of non-uniformity in quality assurance during earthwork construction.

A semivariogram is a plot of the average squared differences between data values as a function of separation distance, and is a common tool used in geostatistical studies to describe spatial variation. Three important features of a semivariogram include: sill, range, and nugget. Sill is defined as the plateau that the semivariogram reaches, range is defined as the distance at which the semivariogram reaches the sill, and nugget is defined as the vertical height of the discontinuity at the origin which mostly represents sampling error or short scale variations (Srivastava, 1996). From a semivariogram model, a low “sill” and longer “range of influence” can represent best conditions for uniformity, while the opposite represents an increasingly non-uniform condition. Using these semivariogram parameters, theoretical models can be fit to the experimental semivariogram data. In the author’s experience, exponential or spherical model generally fits well with the IC-MVs and in-situ compaction measurements (see White et al. 2007a, White et al. 2007b, Vennapusa and White 2009b). Detailed descriptions of theoretical models can be found elsewhere in the literature (e.g., Clark and Harper 2002).

To evaluate the application of spatial analysis, spatially referenced CMV and in-situ point measurements obtained from test strip 2 were analyzed. The comparisons are shown using semivariogram models (Figure 3.53) and Kriged surface maps (Figure 3.54) generated for CMV and in-situ point measurements. Experimental semivariogram of CMV data showed good spatial structure. Experimental semivariogram of in-situ point measurements did not show spatial structure and the reason is attributed to limited measurements to characterize the spatial variability (number of in-situ point measurements = 42, and number of CMV measurements = 194 to 204). The Kriged surface maps of in-situ point measurements are provided herein only for visualization purposes and were not determined using a pre-defined variogram. The Kriged maps also point out the lack of spatial continuity in the data with contours as circles around the test points. Spherical semivariogram models were fit to the CMV experimental semivariograms by checking for its “goodness” using the modified Cressie goodness of fit approach suggested by Clark and Harper (2002) as well as the cross-validation process. A lower Cressie “goodness” factor and high  $R^2$  value from cross-validation indicates a better fit (see White et al. 2007a for additional details on model fitting process). The semivariograms of CMV for two different amplitude settings showed similar ranges of influence (13 m). The sill values for CMV data at  $a = 1.70$  mm was slightly lower than CMV data at  $a = 0.85$  mm, which indicates that the values at the high amplitude setting are less variable compared to the low amplitude setting. This is also reflected in the univariate statistics with COV of CMV at  $a = 1.70$  mm (15%) < than at  $a = 0.85$  mm (19%). Spatial visualization using Kriged contour maps presented in Figure 3.54 provide an alternative way to compare CMV and in-situ point measurement data.

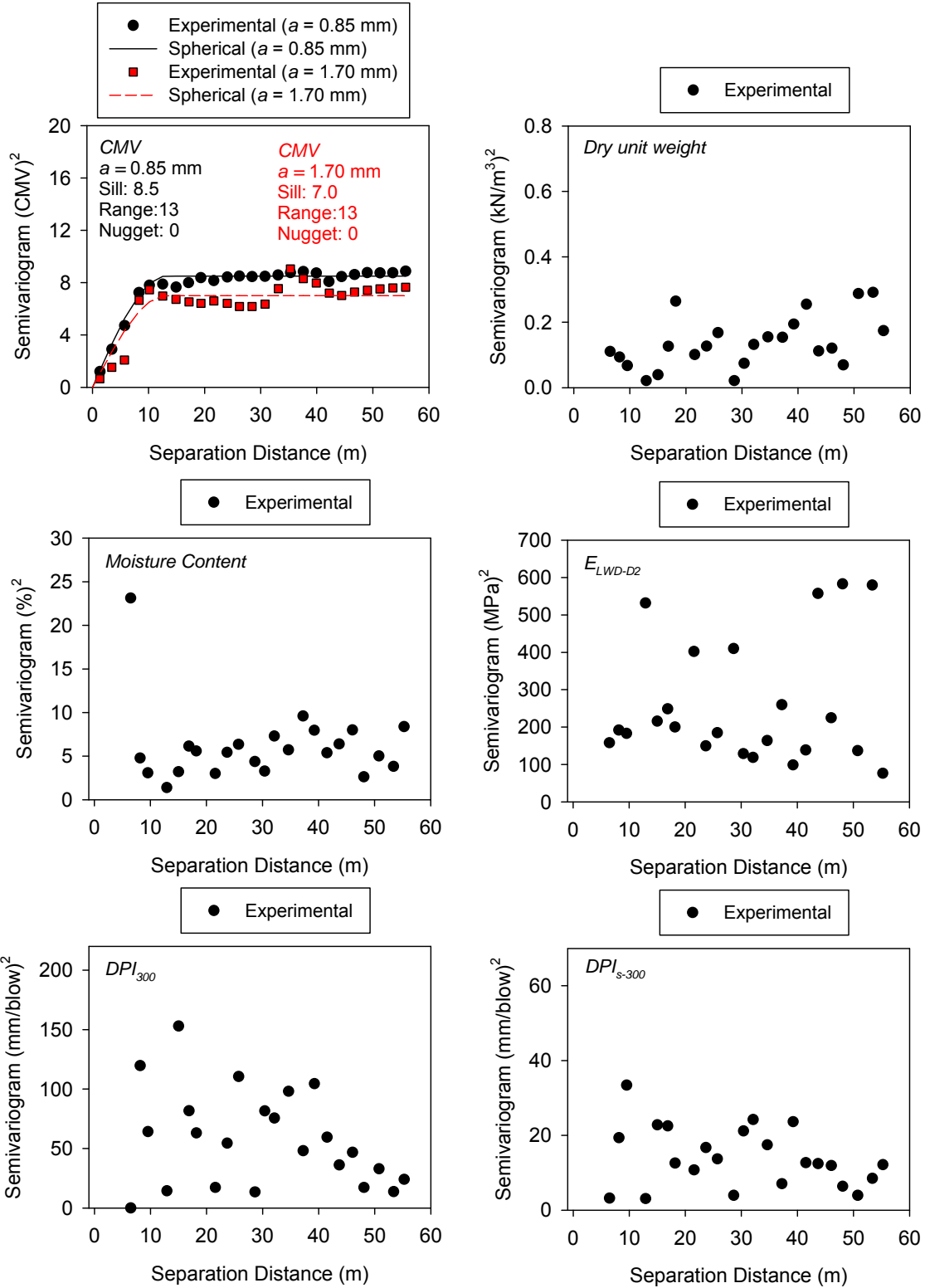


Figure 3.53. Semivariograms of IC-MVs and in-situ point measurements from test strip 2

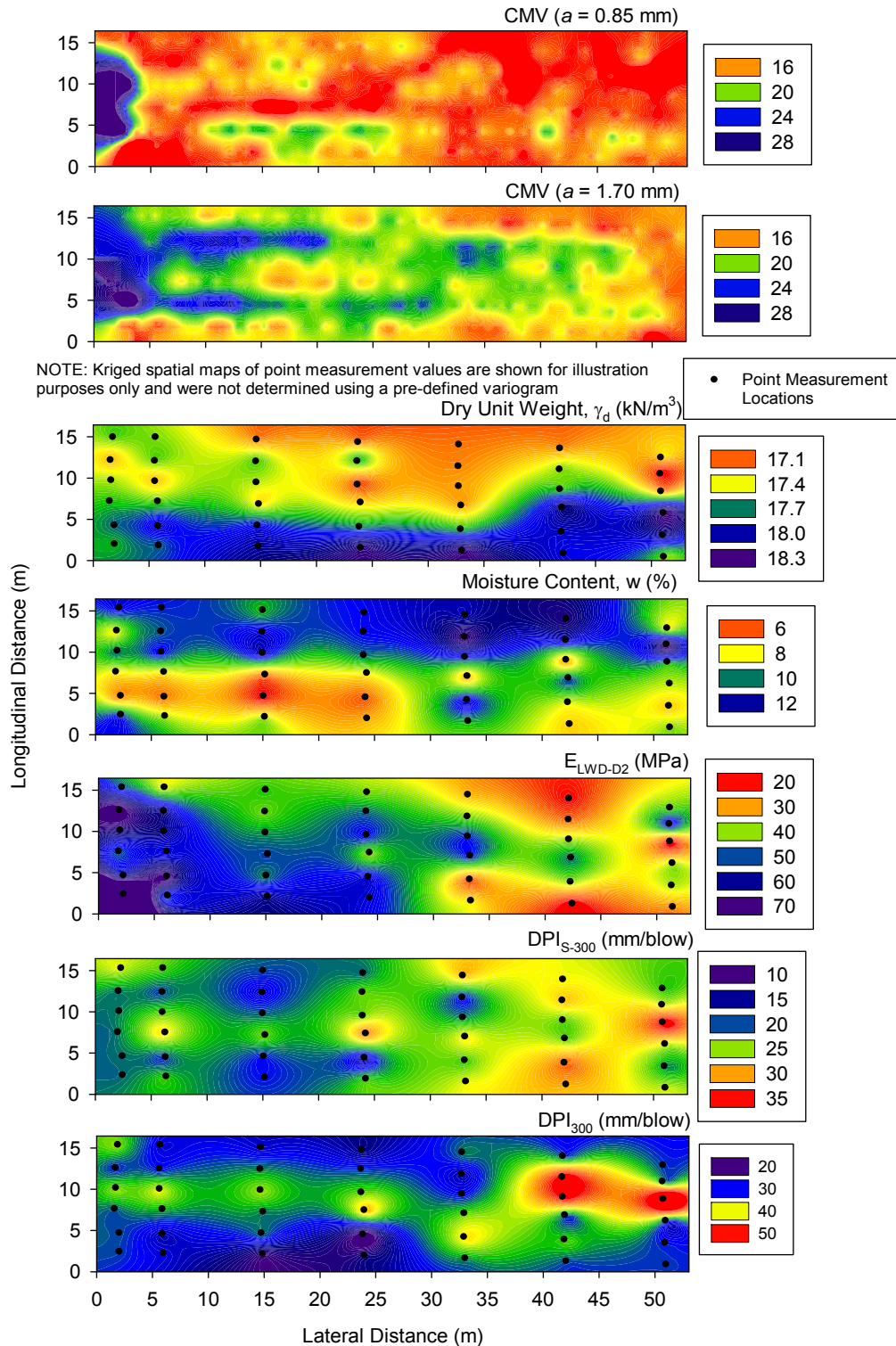


Figure 3.54. Spatial comparison of IC-MVs and in-situ point measurement Kriged spatial maps from test strip 2

### 3.4.4 Stresses in Granular Subgrade Layers

EPCs were installed in the granular subgrade layers of test strips 1 and 5. Figure 3.55 shows cross-sectional views of test strips 1 and 5 with locations where EPCs were installed. Installation was performed by carefully excavating the material and embedding the cells in the embankment sand material. The excavation was backfilled using the excavated material and was hand compacted in thin lifts. EPCs were installed in orthogonal directions to measure  $\sigma_x$ ,  $\sigma_y$ , and  $\sigma_z$  ( $\sigma_x$  = horizontal stress in direction perpendicular to the direction of roller travel,  $\sigma_y$  = horizontal stress in direction parallel to the direction of roller travel, and  $\sigma_z$  = vertical stress; see Figure 3.55 and Figure 3.56). Total stress increase under roller vibratory loading and scraper tires was measured (Figure 3.57). Roller was operated in such a manner that the EPCs were positioned at the center of the drum. Scraper passes were performed by positioning the tires at positions A, B, and C relative to the location of EPCs as shown in Figure 3.57.

EPC measurements obtained from test strips 1 and 5 are presented in Figure 3.58, Figure 3.59, Figure 3.60, Figure 3.61, and Figure 3.62. The stress measurements presented represent an increase in stress under loading and do not include the geostatic stresses. Figure 3.63 shows peak vertical and horizontal stresses developed under the roller at  $a = 0.85$  mm and 1.70 mm, and scraper tires. Theoretical vertical and horizontal stress distributions were fit to the data based on Boussinesq elastic solutions. The theoretical stress distributions under the roller were determined assuming a uniformly loaded continuous strip footing with width  $B$ . The  $B$  and contact stress values were adjusted to obtain a best fit curve through the measured peak stresses. A contact width of 0.4 m and maximum stress at the surface = 250 kPa for  $a = 0.85$  mm and 350 kPa for  $a = 1.70$  mm was found to fit well with the measured vertical stresses. The horizontal stress distributions could not be predicted well with the theoretical solutions, as discussed earlier in this report. The measured horizontal stresses were higher than theoretical predictions (Figure 3.63).

The maximum vertical and horizontal stress increase noted under the scraper tire (i.e., scraper pass in Position A) was higher than measured stresses under the roller vibratory loading. For example, the maximum vertical stress increase at  $a = 1.70$  mm setting at a depth of about 0.32 m was about 170 kPa, whereas it was about 470 kPa under the scraper tire. This is important to document as to how scraper and other construction traffic contribute to compaction of embankment fill materials. Field study conducted by the authors' on TH 64 (see White et al. 2008) documented that IC-MVs observed in areas subjected to construction traffic passes was much higher than areas with no construction traffic. Stresses measured under the scraper tire in a fully loaded condition (with 77 ton gross weight) showed lower stresses compared to no load condition (with 32 ton gross weight). The reason is attributed to the center of the scraper tire likely not positioned directly above the sensor locations. Scraper passes performed about 1.1 m away from the sensor alignment showed significantly low stresses (e.g., about 20 kPa vertical stress at a depth of about 0.32 m below surface).

Figure 3.61 shows EPC measurements from test strip 5 at a depth of about 0.28 m below surface for passes 1 to 8. Also shown in Figure 3.61 are close-up snap shots of vertical stress increase plots for each pass. Passes 1 and 2 were made at  $a = 0.85$  mm, 3 and 4  $a = 1.70$  mm, and 5 and 6  $a = 0.85$  mm nominal settings. As soil gets compacted with increasing pass, pass 4 showed

roller jumping as indicated by the stress cycles reducing every other cycle (see Figure 3.61). This is referred to as drum double jumping behavior (Adam 1997) which effects the CMV and RMV measurement values as discussed in the TH 36 project case history. Unfortunately, roller data was not available, again due to memory card issues, from this test strip to confirm the effect of double jump on the measurements.

Measurement influence depth under roller vibratory loading is characterized as the depth at which 10% of the surface vertical stress increment is reached (10% is arbitrary but provides a point of comparison herein). Using this criteria, the measurement influence depth under the roller for both  $a = 0.85$  mm and 1.70 mm loading conditions is estimated at about 1.5 to 1.6 m for the soil profile tested test strip 1. This is comparatively higher than the measurement influence depth interpreted from the data obtained from the TH 36 project site (0.9 m). The maximum contact stresses measured for test strip 1 at the surface were much lower than the maximum contact stresses measured from TH36 project ( $\sigma_z = 700$  kPa for  $a = 0.85$  mm at TH 36 versus  $\sigma_z = 250$  kPa for  $a = 0.85$  mm on test strip 1). This should be expected as the contact width of the roller for TH36 data was about 0.2 m where as the contact width of the roller for test strip 1 data is interpreted as 0.4 m. The reason for differences in contact area is attributed to the differences in soil type/shear strength. TH36 surface material consisted of very stiff granular base material while test strip 1 consisted of cohesionless sand with a loose condition at the surface.

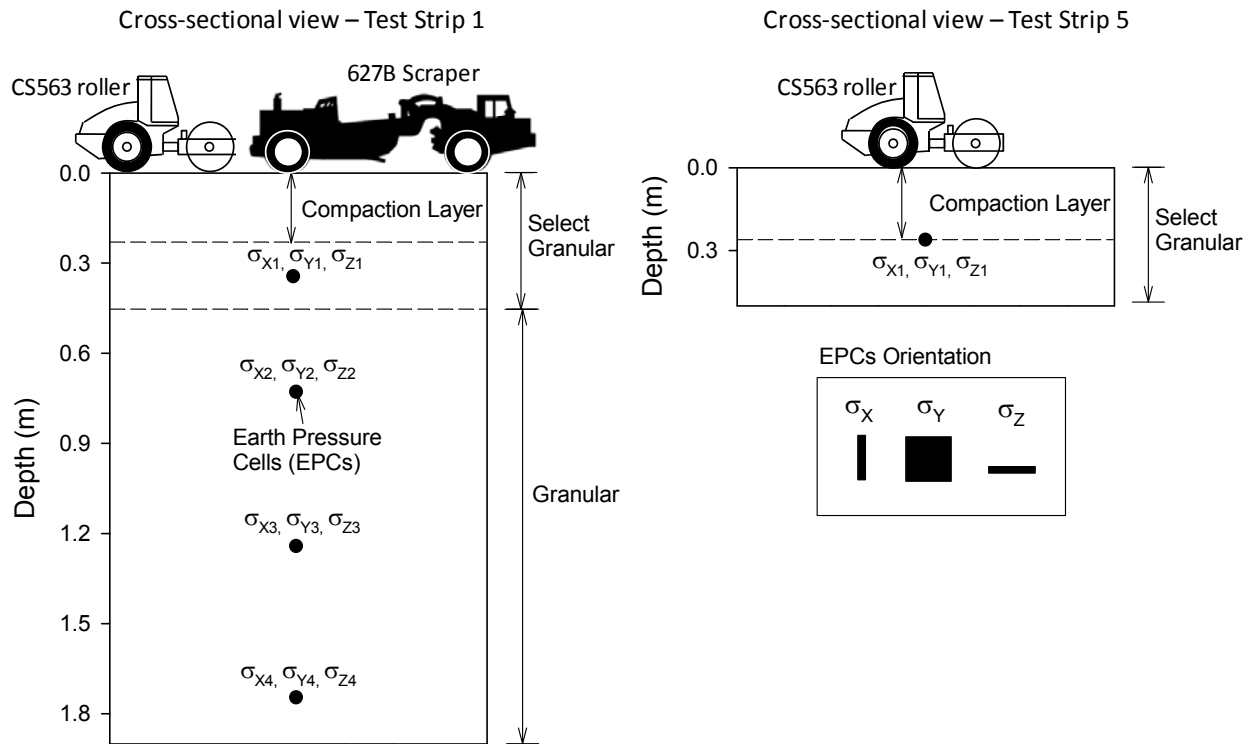


Figure 3.55. EPC installation setup on test strips 1 and 5

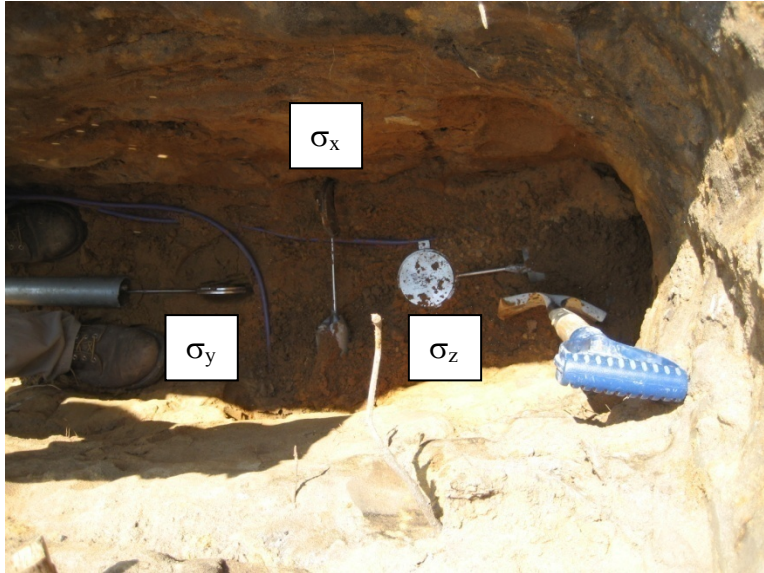


Figure 3.56. Picture of EPC installed in orthogonal directions on test strip 1 (top view)

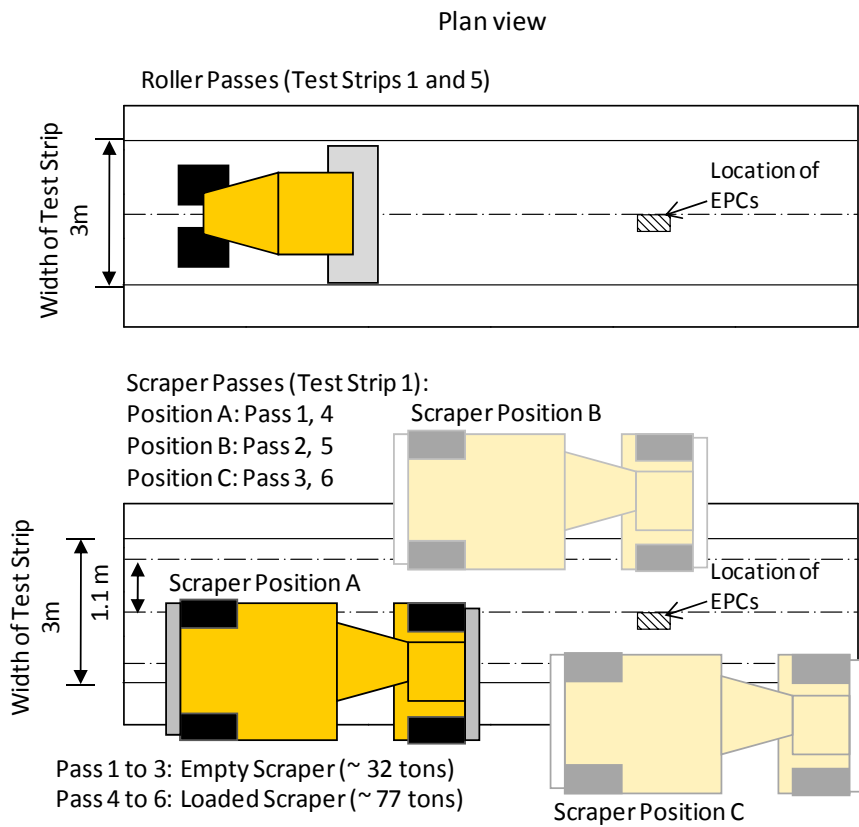


Figure 3.57. Plan view on roller and scrapper passes on test strips 1 and 5

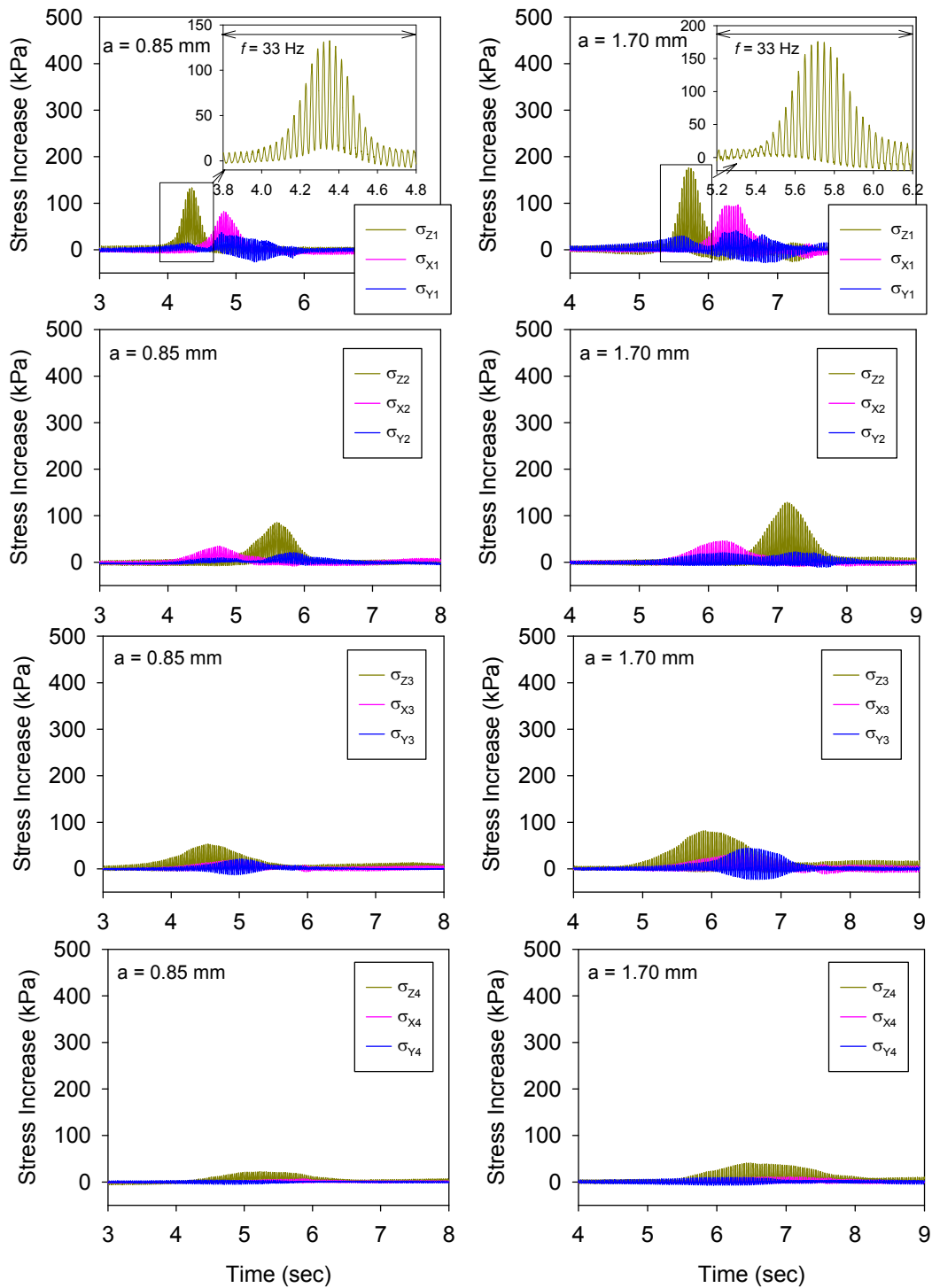


Figure 3.58. Triaxial stress increase time histories at different depths under  $a = 0.85$  mm (left) and  $1.70$  mm (right) vibratory rolling operation – Test strip 1

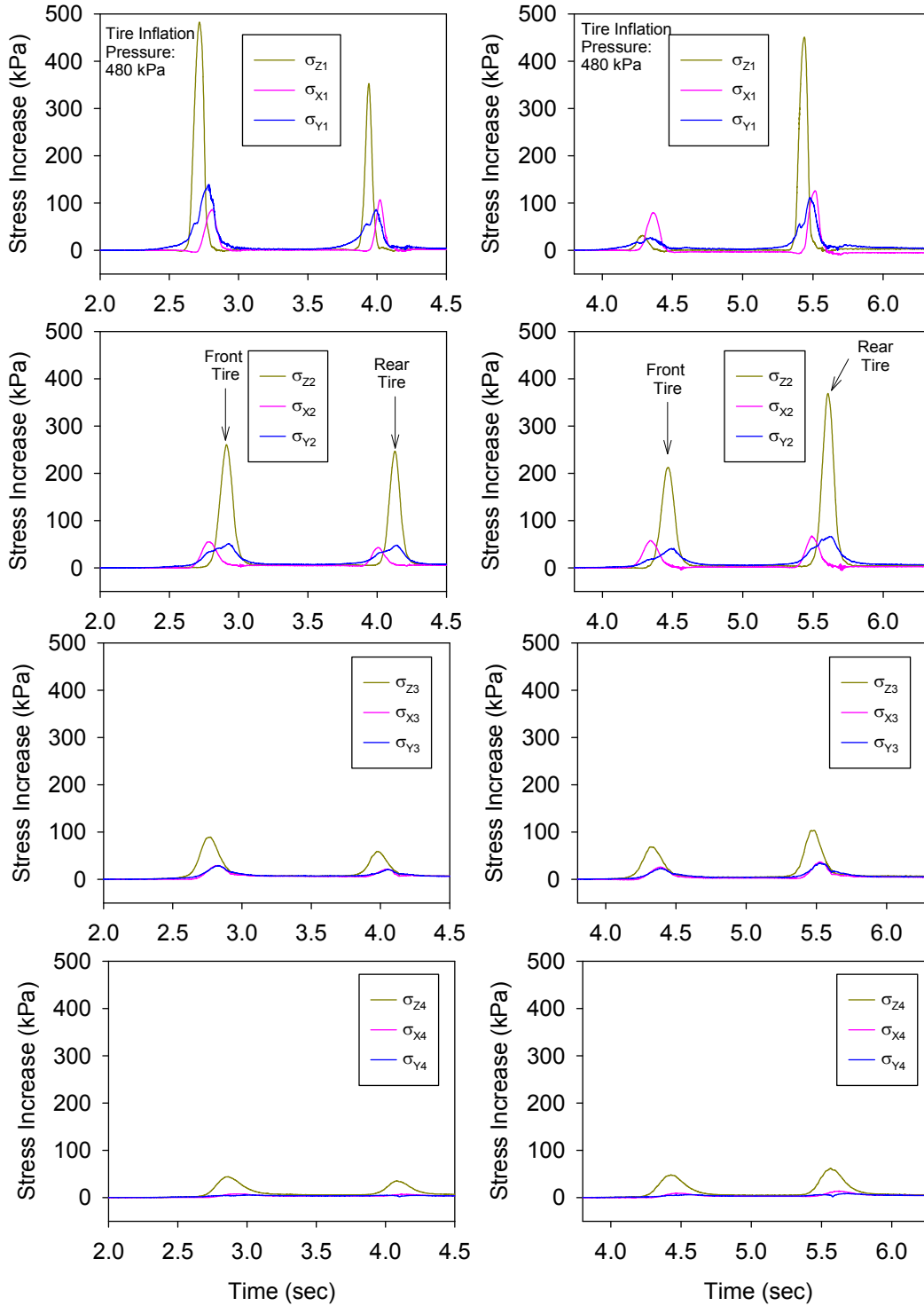


Figure 3.59. Triaxial stress increase time histories at different depths under scraper tire position A passes without load (left) and fully loaded (right) – Test strip 1

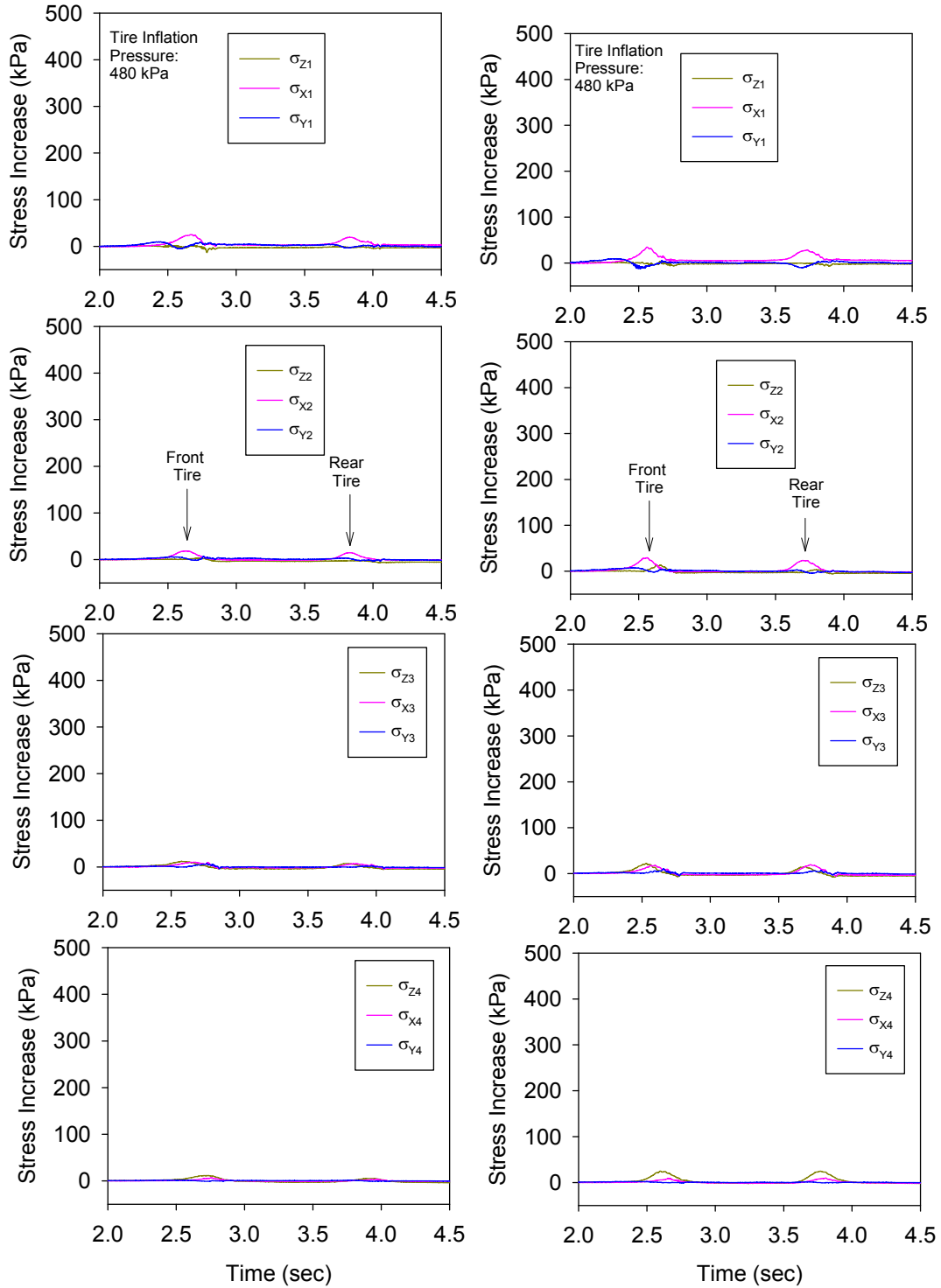


Figure 3.60. Triaxial stress increase time histories at different depths under scraper tire position B passes without load (left) and fully loaded (right) – Test strip 1

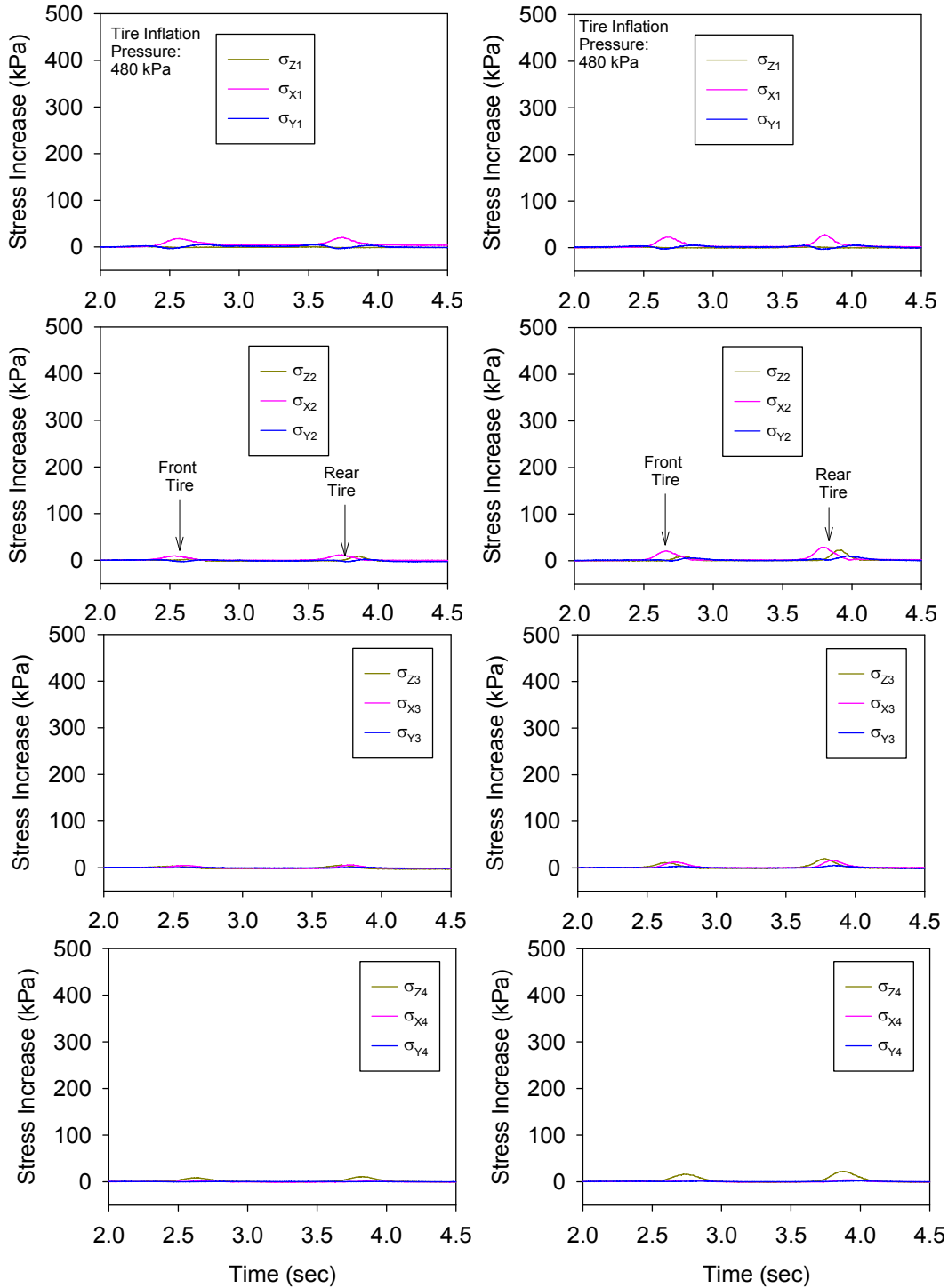


Figure 3.61. Triaxial stress increase time histories at different depths under scraper tire position C passes without load (left) and fully loaded (right) – Test strip 1

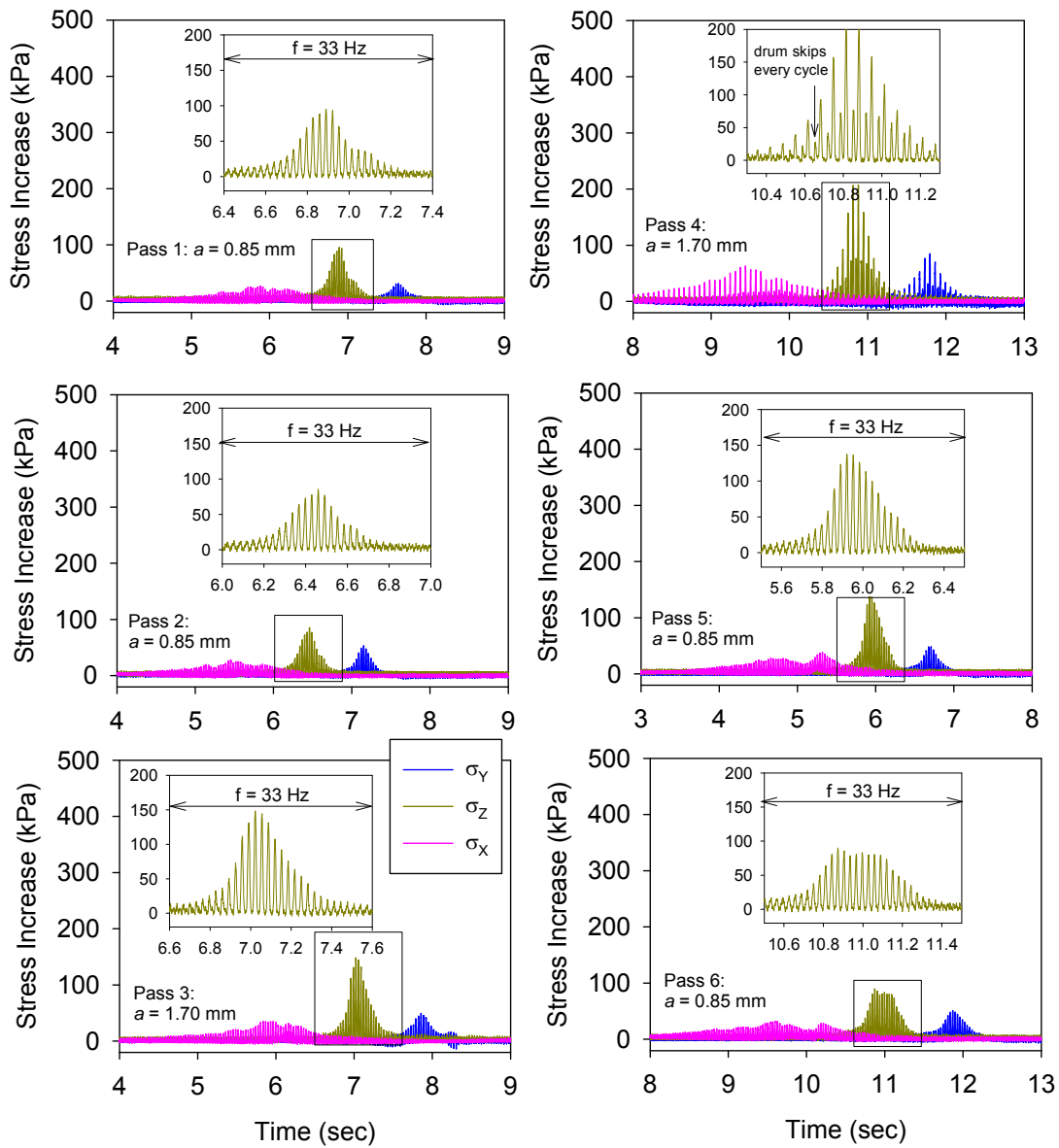


Figure 3.62. Triaxial stress increase time histories for different passes at  $a = 0.85$  mm (left) and  $1.70$  mm (right) vibratory rolling operation – Test strip 5

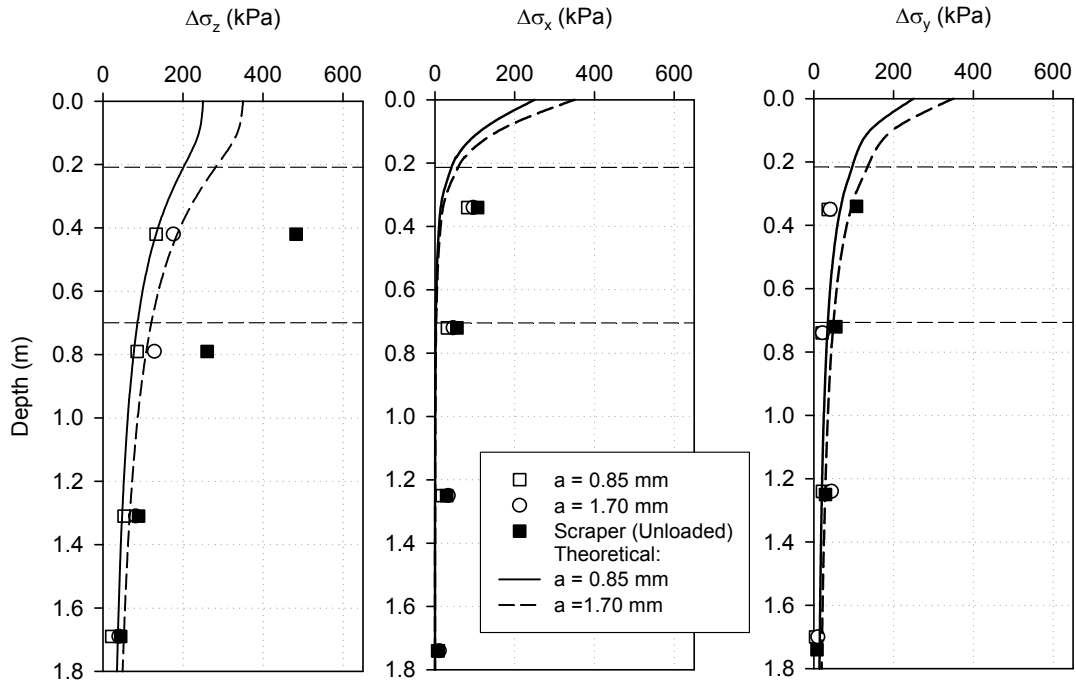


Figure 3.63. Peak vertical and horizontal stress increase profiles (measured and theoretical Boussinesq curves) for roller induced vibratory loading and under scraper tire

### 3.4.5 Key Observations and Conclusions

- Compaction growth curves from NG, DCP, and LWD show that increases in density taper off at lower pass counts than elastic modulus and strength.
- CMV values were higher at the high amplitude setting ( $a = 1.70$  mm) than the low setting ( $a = 0.85$  mm)
- Correlations between CMV and different in-situ point measurements showed regression relationships with varying degree of uncertainty ( $R^2$  value ranging from 0.2 to 0.9). The primary factors contributing to scatter are believed to be differences in measurement influence depths and applied stresses.
- Correlations between CMV and various in-situ test measurements improved using in-situ point measurements at about 150-mm below the compaction surface for cohesionless sand.
- Correlations between CMV and modulus values (i.e.,  $E_{LWD-Z2}$ ,  $E_{V1}$  and  $E_{V2}$ ) showed linear regression relationships, while correlations between CMV and LWD deflection measurements showed non-linear power relationships.
- In general, the COV values for CMV and LWD measurements are similar in the range of 20 to 40%.

- Spatial analysis of strip 2 demonstrated that the experimental variogram for the CMV measures was well defined, but that was not the case for the in-situ point measurements. Although the range values were similar the “sill” or variance was slightly lower for the high amplitude map compared to the low amplitude map.
- EPC measurements revealed that stresses under a motor scraper are much higher than the roller. Using criteria for characterizing measurement influence depth as the depth at 10% of the maximum stresses at the surface, the measurement influence depths under the roller at different amplitudes are summarized in Table 3.23. These results are different from observations on TH36 project due to variation in soil stiffness and layering conditions.

Table 3.23. Summary of measurement influence depth of different measurements – US10 project

Measurement	Depth below surface
Roller ( $a = 0.85$ mm)	1.5 m
Roller ( $a = 1.70$ mm)	1.6 m

### 3.5 District 7 TH 60, Bigelow

#### 3.5.1 Project Overview

This project involved construction of the new four-lane TH 60 bypass around Bigelow, MN. The highway construction extended from just north of 120th street in Iowa to about 1.6 km north of Nobles County Road 4 in Minnesota for a total length of about 8 km. The project involved construction of embankment fill sections varying from 1 m to 10 m in height. The embankment fill material on the project mostly consisted of non-granular materials derived from glacial deposits (lean clay to sandy lean clays). Moisture content tests were conducted as part of QC. IC measurements, test rolling (Mn/DOT standard specification 2111), LWD, and “speedy” moisture content tests were conducted for QA.

CP-56 and CP-663 padfoot rollers equipped with machine drive power (MDP) measurement technology (measurement reported as MDP\*; see discussion in Chapter 2), RTK GPS, and AccuGrade compaction mapping system were used on this project. A CS-683 smooth drum roller equipped with accelerometer based CMV/RMV measurement technologies was shipped to the site by Caterpillar at the request of the ISU research team during the July field visit for field evaluation.

#### 3.5.2 Experimental Testing

Six test strips were constructed and tested during the field investigations (see Table 3.24). Test strips 1 to 5 involved obtaining in-situ point measurements (i.e., DCP, LWD, NG, DC, and  $s_u$ ) in conjunction with IC-MVs for correlation analysis on non-granular embankment subgrade

materials. LWD and NG tests were conducted on a relatively flat surface by excavating material to the bottom of the padfoot penetration. In-ground stress measurements from EPCs installed in the subgrade were obtained from test strip 2 to evaluate stresses developed under the CP-56 roller pads. Repeated passes with similar amplitude and speed settings were performed on test strip 2 to assess the repeatability of MDP\* measurements. The contractor operated the roller for test strips 1 and 2, and ISU personnel operated the roller for test strips 3, 4, 5, and 6. Soil index properties of the materials from each test strip are summarized in Table 3.25. Experimental test results and analysis from each test strip are discussed in the following sections.

### 3.5.2.1 Laboratory Compaction Characteristics

A laboratory study was performed on three samples (sample A, samples from test strip 1 and test strip 2) obtained from the project site to develop relationships between laboratory impact compaction energy, moisture content, and dry unit weight. Soil index properties of these samples are summarized in Table 3.25. Due to insufficient quantities of material these samples were re-used during compaction testing. When samples were re-used they were extracted from the compaction mold, pulverized by hand, re-conditioned for moisture and allowed to mellow for at least 24 hours prior to compaction testing.

Results from laboratory compaction tests for sample A, test strip 1, and test strip 2 are presented in Figure 3.64, Figure 3.65, and Figure 3.66, respectively. The upper-left portion of the figures show the Proctor moisture-dry unit weight relationships for several compaction energies. As expected, the maximum dry unit weight increased and the optimum moisture content decreased with increasing compaction energy. Curves on the wet side of  $w_{opt}$  generally parallel the zero air void curve (100% saturation line). The points of  $w_{opt}$  at each energy level also tend to parallel the 100% saturation line. These relationships are common for fine-grained non-granular soils subjected to impact compaction.

The upper-right portion of Figure 3.64, Figure 3.65, and Figure 3.66, shows the dry unit weight growth curves as a function of compaction energy at the lower and upper Mn/DOT moisture specification limits (i.e., 65 to 95% of standard Proctor  $w_{opt}$ ), and at 120% of  $w_{opt}$ . These plots illustrate that at 65% of  $w_{opt}$  the dry unit weight is initially low but increases rapidly with increasing compaction energy. At 95%  $w_{opt}$  increases in dry unit weights are observed up to about 1000 kN-m/m<sup>3</sup> compaction energy (~2 times the standard Proctor energy), and minimal increase is observed beyond that energy level. At 120% of  $w_{opt}$ , minimal increase in dry unit weight is realized with increasing compaction energy.

The lower-left portion of Figure 3.64, Figure 3.65, and Figure 3.66 shows the laboratory compaction energy required to achieve selected target relative compaction values (95% and 100% standard Proctor and modified Proctor maximum dry densities) as a function of moisture content. Results plotted in such a manner allow for determination of the “compactability zone”. This zone represents the minimum required impact energy and its corresponding moisture content range to achieve the target relative compaction value. For example, for the soil samples tested the minimum energy required to achieving at least 95% of standard Proctor densities is approximately 60% of standard Proctor energy (356 kN-m/m<sup>3</sup>). Also indicated in the figures is the region of the plot where soil conditions are susceptible to “over-compaction”. In this zone,

applying additional compaction energy does not increase the relative compaction value of the soil and can often result in development of unwanted shear planes and excess pore pressures.

Table 3.24. Field testing summary (TH60)

Date	Test Strip	Test Area Description	Roller	IC-MV	Operator	In-situ testing <sup>§</sup>
08/13/2007	1	Production (Subgrade clay)	CP56 padfoot	MDP*	Contractor	LWD, DCP, NG, DC
08/14/2007	2	Calibration (Subgrade clay)			Contractor	LWD, NG, DCP, UC, M <sub>r</sub>
10/20/2007	3	Calibration (Subgrade clay)			ISU	LWD, NG
7/9/2008 and 7/10/2008	4/5	Production (Subgrade clay)	CS683 smooth drum	CMV and RMV	ISU	LWD, DCP, UC
7/10/2008	6	Median (Organic material)	—	—	—	DCP, LWD

<sup>§</sup>GPS measurements for point measurements.

Table 3.25. Summary of soil index properties from US 60 project subgrade material

Parameter	Sample A*	Strip 1	Strip 2	Strip 3	Strip 4/5	Strip 6
Maximum Dry Unit Weight (kN/m <sup>3</sup> ) and Optimum Moisture Content (%)						
Standard Proctor	18.8 (12.1)	18.7 (14.2)	16.35 (19.3)	17.19 (17.3)	18.24 (13.3)	16.72 (17.3)
Modified Proctor	20.5 (9.8)	20.4 (10.2)	18.2 (15.0)	19.4 (11.8)	—	—
Gravel Content (%) (> 4.75mm)	1	1	0	3	8	3
Sand Content (%) (4.75mm – 75µm)	35	37	18	30	44	34
Silt Content (%) (75µm – 2µm)	44	40	47	38	30	42
Clay Content (%) (< 2µm)	20	21	35	29	36	21
Liquid Limit, LL (%)	32	30	43	39	35	39
Plastic Limit, PL	16	16	27	20	19	18
Plasticity Index, PI	16	14	16	19	16	21
AASHTO Classification	A-6(8)	A-6(6)	A-7-6(14)	A-6(11)	A-6(4)	A-6-(6)
Unified Soil Classification (USCS)	CL	CL	CL	CL	SC	OL
Specific Gravity, G <sub>s</sub>	2.69	2.70	2.61	2.63	2.69	2.66

\*The sample was provided by the Contractor reportedly from Sta. 3115+00 NB

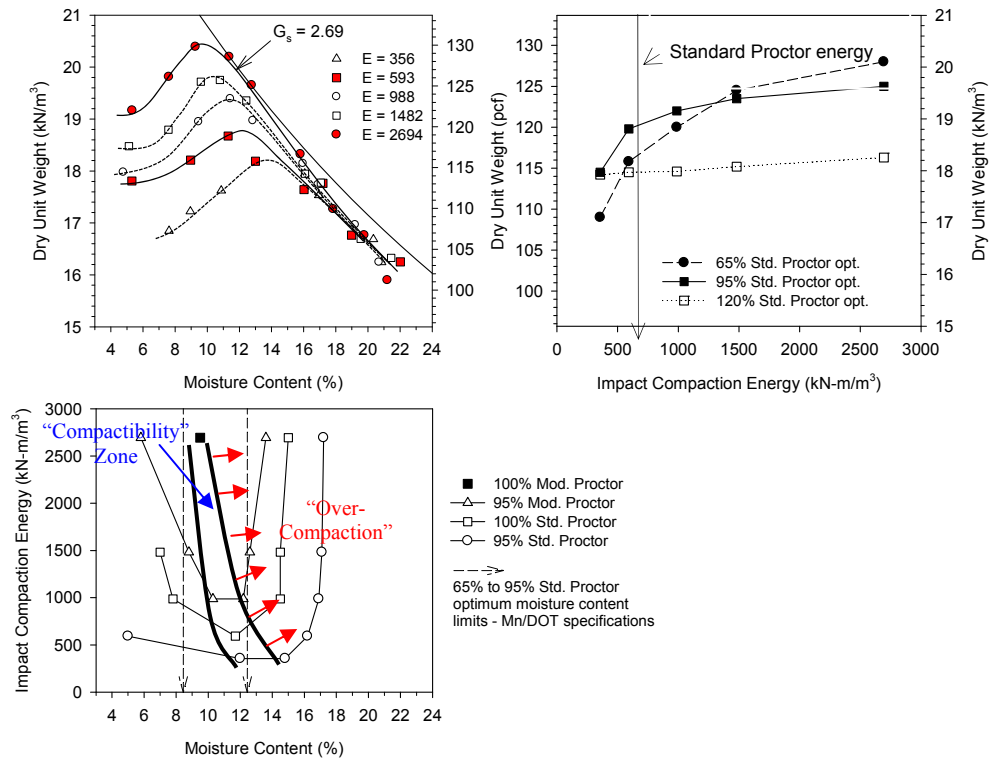


Figure 3.64. Laboratory compaction test results for sample A

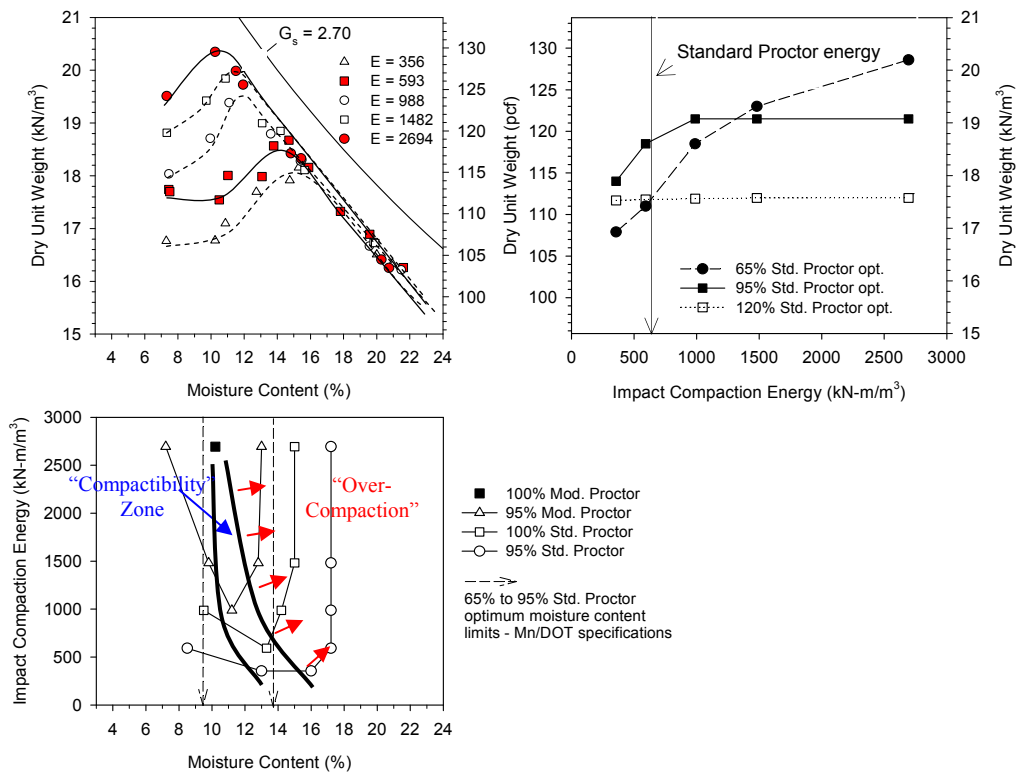


Figure 3.65. Laboratory compaction test results for test strip 1 sample

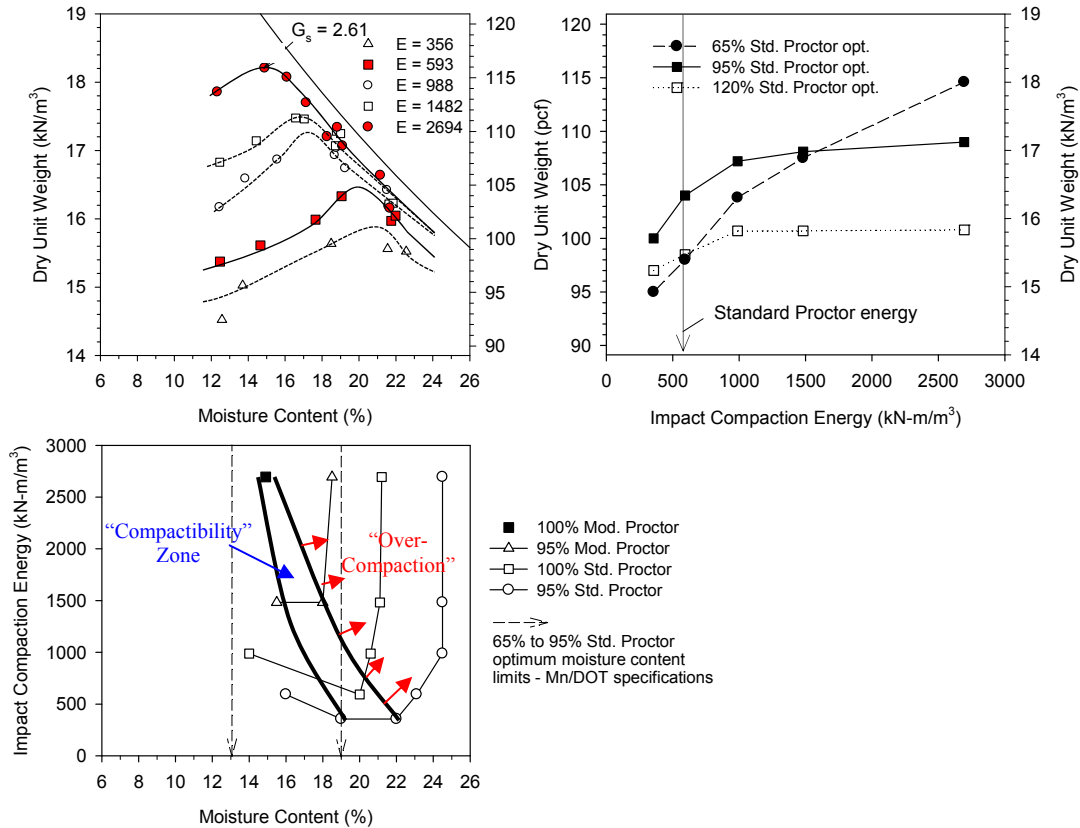


Figure 3.66. Laboratory compaction test results for test strip 2 sample

### 3.5.3 Field Observations and In-Situ QA Test Results from Mn/DOT

Field observations indicated that compaction material obtained from the borrow areas was generally wet due to prolonged rain events at the time of our field visits. Compaction of fill materials was achieved using padfoot roller and also by scraper traffic (Figure 3.67). The research team interviewed both Mn/DOT and contractor personnel to gain insights on challenges with respect to understanding the technology and implementing IC-TVs and LWD-TVs. Some of the findings are summarized below. Further, a summary and comparison of LWD, moisture content, and average IC values obtained from QA testing by Mn/DOT is provided.

#### 3.5.3.1 Selection of IC Target Values (IC-TVs)

Prior to the beginning of the project, the Mn/DOT field personnel and contractor/roller operator had limited experience with the MDP\* technology. For this project, minimum threshold values as opposed to target values were agreed to by the inspectors and the contractor. In general, the inspectors and contractors displayed a sense of goodwill toward developing the IC threshold values. This provided the flexibility required to develop acceptance values for the IC rollers on the fly to supplement information gathered from control strips. At the time of our field visit, a minimum threshold value of MDP\* = 138 was reportedly being used at the project site (Future

specifications need to address whether “target” or “minimum” should be used. If 150 is the maximum value (for hard surface) 90% of the target would be 135 – which is less than the established threshold value of 138).

### 3.5.3.2 Selection of LWD Target Values (LWD-TVs)

Two issues were raised by the field inspectors regarding LWD testing. One issue being the frequency of testing and the other being establishing target values (LWD-TV). For this project, LWD tests were performed about every 150 to 200 feet along the road alignment. Regarding LWD-TVs, similar to IC-TVs, there was limited information on what “target” values should be used for non-granular soils. Therefore, for this project some common sense and practicality contributed to developing LWD-TVs. Observing pad foot indentations and roller walkout was one of the elements to developing LWD-TVs. Materials difficult to trim with a motor grader produced  $E_{LWD-Z2}$  values in the range of 60 to 70 MPa, and materials with moisture contents that complied with the specifications produced  $E_{LWD-Z2}$  values in the range of 20 to 30 MPa. For relatively wet soils,  $E_{LWD-Z2}$  values were in the range of 5 to 15 MPa. When the inspector released the drop-weight, they also looked for “hard recoil” as an indicator of compaction quality. At the time of our field visit, a minimum acceptable threshold value of  $E_{LWD-Z2} = 18$  MPa was used for acceptance. When the  $E_{LWD-Z2}$  values at test locations were less than the threshold value, the field inspectors generally found that the in-place moisture content was relatively high. When the measurements were equal to or greater than the minimum threshold value, but the embankment layers appeared to be “spongy” under construction traffic or roller, an additional LWD reading was taken at a depth of about 100 to 150 mm below the surface. When additional compaction effort did not improve the LWD values, the embankment was disked, aerated and re-compacted. A summary of  $E_{LWD}$  test results obtained by Mn/DOT field inspectors at the time of our field survey is provided in Table 3.26.

### 3.5.3.3 Moisture Content QA/QC testing

Field inspectors indicated that moisture content measurements were typically only taken at the time of compaction (as part of QC). Since weather conditions changed throughout the construction phase of the project, it was difficult to maintain consistency in the moisture content. When utilizing 100 percent coverage of the IC measurements, it was noted that some difficulty developed in terms of determining the appropriate number of moisture content tests to execute. According to the field inspectors, moisture collection takes a lot of time and there tends to be some variation in the results obtained from the different test methods to determine moisture content.



Figure 3.67. Scraper traffic contributing to compaction of fill materials

Table 3.26.  $E_{LWD}$  test measurements by Mn/DOT during field survey by ISU

$E_{LWD-Z2}$ (MPa)*	Inspector Decision
35	Accept
14	Reject
18	Accept (but prefer 20)
14.9	Reject
31	Accept
15.4	Reject
20.1	Accept
20	Accept
20	Accept
18.7	Accept
11.8	Reject

\*values reported by Mn/DOT field engineers (using  $\nu = 0.5$  and  $f = 2$ )

### 3.5.3.3 In-situ QA test results in comparison with IC values by Mn/DOT

Mn/DOT field engineers conducted QA tests to determine  $w$  using “speedy” moisture content device and  $E_{LWD-Z2}$  tests and compared results with average IC values (i.e., average MDP\* per proof/calibration area). The  $E_{LWD}$  values recorded by Mn/DOT personnel on a project scale were calculated using  $\nu = 0.5$  and  $f = 2$  in the  $E_{LWD}$  calculations (default settings in Zorn LWD device). These values were corrected for  $\nu = 0.4$  and  $f = 8/3$  for consistency with the results presented in this report. The results obtained are summarized in Table 3.27. Histograms of  $w$ ,  $E_{LWD-Z2}$ ,  $d_{LWD-Z2}$ , and MDP\* are presented in Figure 3.68. Simple linear regression relationships developed for the QA test measurements are presented in Figure 3.69. Evaluation of the regression relationships and review of field notes indicate that the LWD and average MDP\* values were influenced by changes in moisture content (increasing moisture decreases  $E_{LWD-Z2}$

and MDP\*), MDP\* values are empirically correlated with  $E_{LWD-Z2}$  measurements, and  $E_{LWD-Z2}$  values are affected by wet/soft layers below the testing surface. Significant scatter was observed in these relationships with  $R^2$  values ranging from 0.1 to 0.2. Regression relationships between these parameter values are further explored in the test strip studies conducted by ISU research team and are described in the following sections of the report.

Table 3.27. QA test results from TH60 project by Mn/DOT field personnel

Station	Offset	Depth below final grade (m)	w (%)	$d_{LWD-Z2}$ (mm)	$E_{LWD-Z2}$ (MPa)	Avg. MDP*	Remarks
44+00	9' Lt	0.9	18.1	4.59	5.7	134	
41+50	C/L	4.0	11.5	2.29	11.4	141	
320+00	60 NB	0.8	15.7	5.69	4.6	128	
318+90	60 NB	0.6	11.6	1.48	17.8	140	
318+05	60 NB	0.9	12.6	2.96	8.9	135	
327+50 Lt	TH 60 NB	4.3	12.9	0.61	43.1		
331+25	12 Rt 60 NB	1.8	10.8	0.68	38.5		
318+00	6 Lt 60 NB	1.4		6.83	3.8		
319+00	12 Rt 60 NB	1.4		1.72	15.2		
337+15	8 Rt 60 NB	2.6	12.2	1.00	26.3		
320+00	6 Lt 60 NB	0.8	15.7	5.69	4.6	128	
318+90	Lt 4 60 NB	0.6	11.6	1.48	17.8	140	
318+05 C/L	60 NB	0.9	12.6	2.96	8.9	135	
325+25	6 Rt 60 NB	1.1	9.1	0.28	92.6	145	
327+75	60 NB	3.0	8.1	0.84	31.3	143	
333+00	60 NB	1.5	8.1	1.78	14.7	136	
322+85	12 Rt	0.8	10.6	0.71	37.1	143	
325+25	6 Rt NB	1.1	10	0.43	61.0	147	
326+60	1 Lt NB	1.8	10	0.48	54.2	150	
334+00	5 Lt	1.4	11.4	0.90	29.2	147	
336+75	7 Lt	1.8	10.8	1.03	25.5	140	
339+60	3 Rt	1.5	10.1	3.45	7.6	142	
343+10		0.5	10.2	0.74	35.5	144	
343+10		0.5	10.2	2.79	9.4	144	
346+10	9 Rt	1.7	13.2	3.80	6.9		
258+30	C/L	2.9	6.7	0.66	39.8	147	
258+00	2 Lt	3.0	12.1	1.31	20.0	140	
315+90	C/L	0.5	13.2	6.08	4.3		
258+00	9 Rt	3.4	13	1.20	21.9	145	
258+60 SB	9 Rt	2.4	13.1	1.24	21.1	142	
258+60 SB	9 Rt	2.4	13.1	1.73	15.1	142	

Station	Offset	Depth below final grade (m)	w (%)	d <sub>LWD-Z2</sub> (mm)	E <sub>LWD-Z2</sub> (MPa)	Avg. MDP*	Remarks
258+60 SB	9 Rt	2.4	13.1	1.57	16.7	142	
257+75 NB	2 Lt	2.4	14.1	1.03	25.4	150	
258 SB	C/L	1.8	14.1	1.52	17.2	148	
CSAH 4	C/L	Subcut		1.93	13.6	141	
255+00 NB	C/L			2.57	10.2	141	
255+00 NB	C/L			4.41	5.9	141	
257+90 NB	13 Lt			3.77	7.0	138	
255+50 NB	C/L			2.84	9.2	134	
256+20 NB	4 Lt			3.85	6.8	143	WET
256+60 NB	2 Rt			3.90	6.7	134	WET
331+10	NB 4 Rt	1.1	13.9	2.86	9.2	140	
330+70	NB 4 Rt	1.2	12.8	1.68	15.6	141	
337+75	NB 2 Lt	1.7	12.7	1.33	19.7		
349+75	NB C/L	2.7	12.6	1.16	22.6		
310+10	NB 3 Lt	1.2		2.05	12.8	133	
309+90	NB	1.2	14.1	2.22	11.8	131	
254+50	NB C/L	0.6	13.8	2.91	9.0	140	
256+10	NB 7 Rt	0.5		1.70	15.4	149	
258+70	NB 4 Rt	1.5		3.38	7.8	148	Wet
259+25	NB 8 Rt	0.6		2.21	11.9	140	Wet
257+70	SB 4 Lt	2.1		2.16	12.2	138	Wet
254+50	SB C/L	0.9		2.91	9.0	140	Wet
39+50	4 Rt	2.7		1.91	13.7		Avg
42+50	C/L	1.1		0.76	34.8		Dry
295+25	8 Lt	0.8	12.4	1.77	14.8	140	
304+50	7 Rt	0.5	13.2	4.75	5.5	140	
302+00	3 Rt	0.6		1.46	18.0	144	Dry
298+00	2 Rt	0.8		1.28	20.6	141	Avg
288+00	10 Lt	0.6		1.27	20.7	143	
288+00	8 Lt	0.6		2.30	11.4	143	
Unknown				1.08	24.2		
268+00	3 Rt			3.33	7.9	138	Wet*
266+00	C/L			0.73	36.0	150	
Unknown							
281+00	5 Rt	0.9		1.80	14.6	138	Avg
283+00	C/L	0.8		1.56	16.9	140	Avg
279+00	6 Rt	0.8		2.48	10.6	138	Avg
277+00	2 Rt	0.9		3.80	6.9	131	Wet*
277+10	10 Lt	0.9		1.42	18.5	131	Avg
272+00	5 Lt			2.32	11.3	135	Avg
264+25	7 Lt	1.2		3.12	8.4	140	Wet*
264+25	10 Lt	1.2		0.92	28.5	140	Avg
262+25	5 Lt	0.5		1.15	22.8	136	Avg
238+50	10 Lt			1.40	18.7	142	Dry
238+50	10 Lt			1.40	18.8	142	Dry
244+00	5 Lt			1.52	17.3	140	Dry
245+50	2 Lt	Final		2.30	11.4	140	Dry

251+25	10 Rt	Final		2.50	10.5	141	Avg
Station	Offset	Depth below final grade (m)	w (%)	d <sub>LWD-Z2</sub> (mm)	E <sub>LWD-Z2</sub> (MPa)	Avg. MDP*	Remarks
252+25	10 Lt	1.1		1.55	17.0	139	Dry crust
252+25	10 Lt	1.1		2.57	10.2	139	Wet*
255+00	2 Rt	0.6	18.9	3.67	7.2	144	
250+00	2 Rt	0.9	20	3.33	7.9	142	
258+00	6 Rt	1.5		2.62	10.0	144	Wet
257+25	4 Lt		16.2	1.00	26.4	140	
256+00	C/L			1.51	17.3	143	Dry
255+00	9 Lt		11.3	0.86	30.4	143	
255+00	8 Lt			1.00	26.3	143	Dry
254+00	C/L			0.63	41.5	150	Dry
255+30	8 Lt	0.6		0.49	53.2	147	Dry
255+80	2 Lt	0.6	11.1	0.67	39.1	147	
258+25	6 Lt	1.2		0.69	38.0	147	Dry
261+00	3 Rt	0.5		3.21	8.2	148	Wet
264+00	3 Rt	0.9		0.99	26.5	149	Dry
267+00	C/L	1.5		1.00	26.4	148	Dry
270+00	5 Rt	0.9		0.95	27.8	146	Dry
272+00	10 Rt	0.9		0.98	26.8	144	Dry
274+00	7 Lt	0.6		0.76	34.6	145	Dry
263+00	6 Rt	0.6	12.5	0.80	32.7	143	
265+00	8 Lt	0.9		1.59	16.5	143	Dry
267+00	1 Rt	0.9		0.86	30.4	143	Dry
271+25	7 Lt	0.6		1.28	20.5		Dry
262+00	7 Lt	0.9			17.5		Dry
260+00	2 Rt	1.1		1.50	17.0		Dry
254+25	3 Lt	0.5		1.55	9.0		Dry
230+00	14 Rt	1.2		2.92	16.5		Dry
232+00	9 Rt	0.9	18.9	1.59	7.5	139	
234+00	6 Rt	0.6		3.51	14.8	144	
236+00	3 Rt	0.9		1.77	12.9	146	
238+50	4 Rt	0.9		2.03	13.5	144	
Unkown	NBL			1.95	27.5		
Unkown	NBL			0.95	17.6		
Unkown	NBL			1.49	17.6		
Unkown	NBL			1.49	10.4		
Unkown	NBL			2.54	17.5		
Unkown	NBL			1.50	13.0		
255+00	SBL			2.02	10.6		
263+00	SBL			2.48	11.9		
265+00	2 Lt	0.6		2.21	12.7		
269+50	5 Rt	0.6		2.07	11.2		
271+00	8 Rt	0.9	13.8	2.34	22.2		
268+00	2 Lt	6.1		1.18	24.2		
265+00	4 Lt	6.1	12.5	1.09	20.6		
161+00	4 Lt	0.5	12.6	1.28	29.6	137	

Station	Offset	Depth below final grade (m)	w (%)	d <sub>LWD-Z2</sub> (mm)	E <sub>LWD-Z2</sub> (MPa)	Avg. MDP*	Remarks
NBL	4 Lt	1.2	19.7	0.99	26.5	139	
164+50	C/L	1.1	19.7	0.82	32.1	140	
165+75	6 Rt	1.2	19.7	1.32	19.9	137	
186+00	7 Lt	1.7	15	1.32	20.0	141	
188+25		1.1	15	0.91	28.8	140	
190+00	C/L	0.3	15	0.83	31.8	142	
171+50	4 Lt	1.8	18	1.84	14.2	144	
172+00	2 Rt	1.5	18	4.07	6.4	135	
174+00	6 Lt	0.8	18	1.86	14.1	139	
153+00	C/L	1.8		1.20	21.9	144	
155+00	9 Lt	0.6		5.58	4.7	140	
228+00	C/L	0.8	9.2	0.68	38.4	143	
234+00	4 Lt	0.2	9.2	0.56	46.8	145	
236+00	8 Rt	0.9	9.2	0.75	34.9	148	
239+00	7 Rt	1.2	9.2	0.76	34.5	150	
245+00	2 Lt	0.5	9.2	0.74	35.3	148	
250+00	4 Rt	0.9	9.2	1.12	23.3	149	
252+00	6 Rt	Final		0.66	39.9	144	
254+00	C/L	0.3		1.35	19.4	148	Dry
256+00	8 Lt	0.9		2.15	12.2	146	Dry
258+00	10 Rt	1.1		1.76	14.9	145	Dry
260+00	10 Rt	0.5		1.93	13.6	149	Dry
262+00	4 Lt	0.2	10.9	1.22	21.6	145	
264+00	6 Lt	0.6		3.89	6.7	146	Dry
186+00	6 Rt	2.1		1.01	26.0	139	
188+00	10 Rt	1.4	11.3	1.41	18.7	138	
190+00	4 Rt	0.8		0.83	31.5	143	
195+00	8 Rt	1.2		1.61	16.3	141	
198+00	8 Rt	0.9		3.05	8.6	142	
140+00	5 Rt			2.89	9.1	138	
142+00	5 Lt	0.9	18.3	1.97	13.3	140	
144+00	5 Rt	0.6	18.3	2.02	13.0	140	
146+00	10 Lt	1.2	18.3	1.13	23.2	143	
148+00	8 Lt	2.1	18.3	1.92	13.7	144	
165+00	8 Rt	0.3	12.6	0.89	29.6	140	
108+00	3 Lt	0.6	12.6	1.71	15.4	140	
170+00	10 Rt	0.6	12.6	0.94	27.9	140	
172+00	10 Lt	0.6	12.6	1.51	17.4	137	
213+00	8 Lt	1.5		1.04	25.2	149	
214+00	15 Lt	1.2		1.03	25.6	149	
215+00	C/L	1.2	7.3	2.48	10.6	141	
216+00	6 Rt	1.2		1.71	15.4	140	
218+80	4 Rt	1.2		0.82	32.0	145	
222+16	4 Lt	0.9		0.63	41.7	140	

Station	Offset	Depth below final grade (m)	w (%)	d <sub>LWD-Z2</sub> (mm)	E <sub>LWD-Z2</sub> (MPa)	Avg. MDP*	Remarks
146+00	3 Rt	1.4		1.77	14.8	148	
148+00	6 Lt	2.1		1.27	20.7	146	
149+50	C/L	2.4		0.34	77.7	150	
150+00	7 Rt	2.7		0.37	70.2	148	
152+00	7 Lt	1.8		1.08	24.4	144	
154+00	3 Rt	0.8		0.86	30.5	146	
207+50	4 Lt	0.9		0.79	33.2	147	
209+00	6 Rt	1.4		1.25	21.0	148	
211+00	12 Lt	1.7		1.24	21.2	147	
170+50	10 Rt	1.7	13.6	1.88	13.9	150	
171+00	4 Lt	1.7		1.51	17.4	149	
174+50	6 Rt	1.5		2.09	12.5	149	
140+00	2 Lt	0.6		1.32	19.9	146	
143+00	5 Lt	0.3		1.44	18.3	149	
145+00	C/L	0.3		2.21	11.9	140	
149+00	6 Rt	0.6		1.36	19.3	144	
149+00	6 Lt	0.6	11	2.87	9.1	138	
151+00	10 Lt	0.6		0.85	30.9	146	
153+00	4 Lt	0.6		1.27	20.6	143	

\*Wet/soft below compaction surface

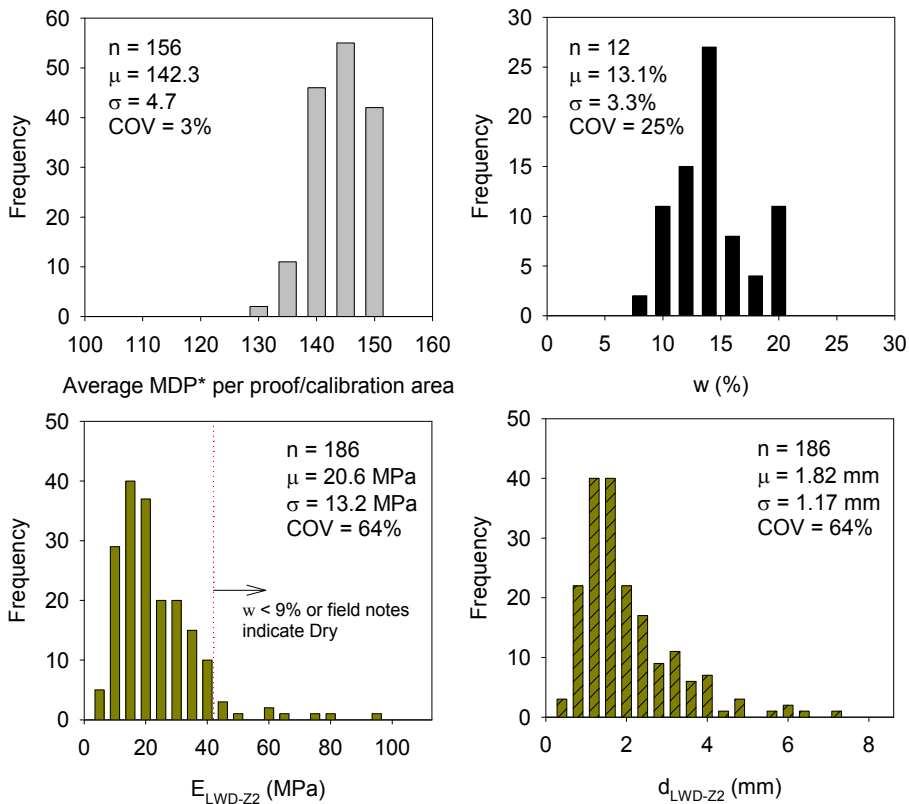


Figure 3.68. Histogram of moisture content, LWD, and MDP\* test measurements

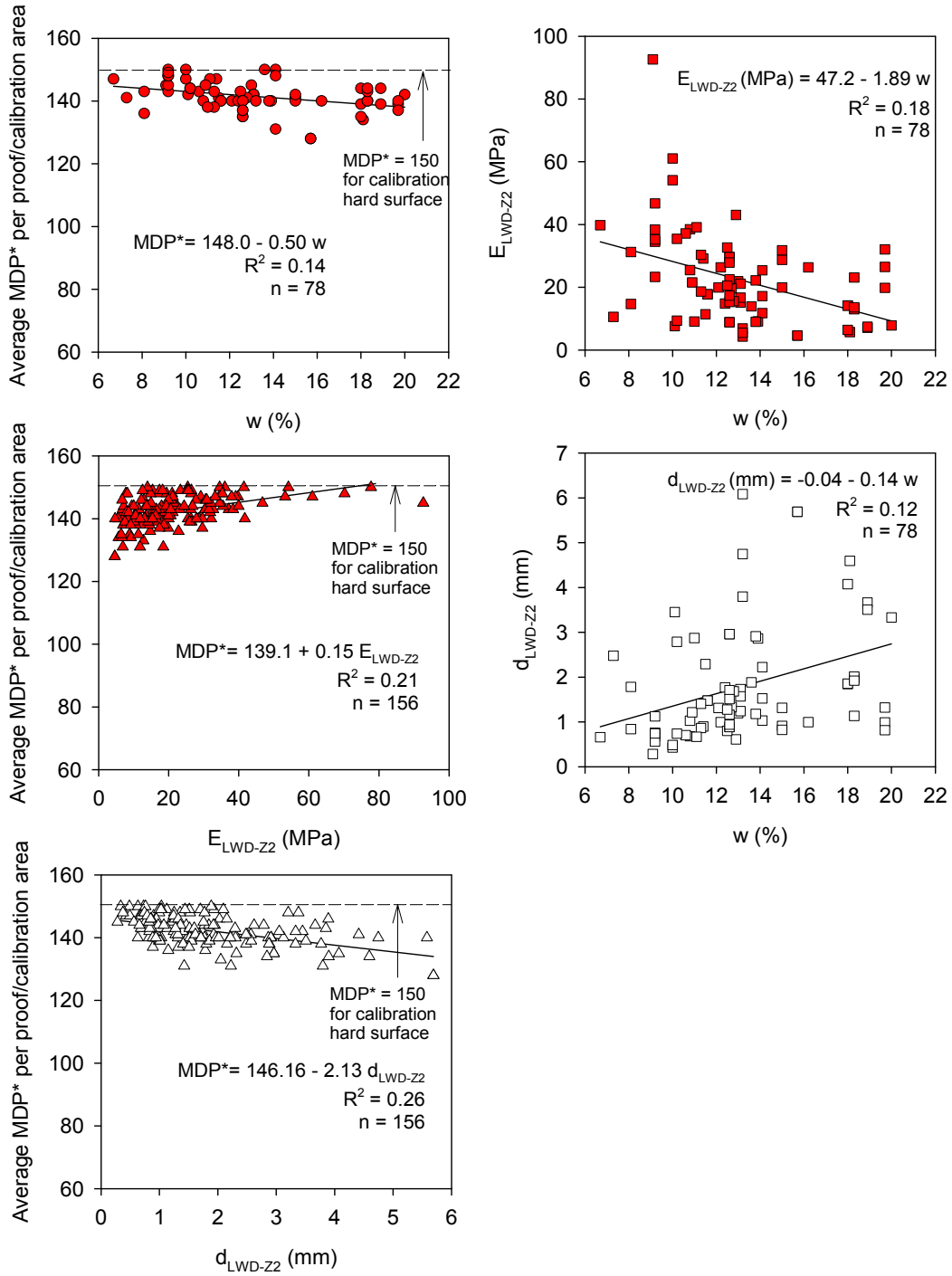


Figure 3.69. Simple linear regression relationships between QA measurements obtained by Mn/DOT field personnel

### 3.5.4 Comparison between IC and In-situ Point Measurements

#### 3.5.4.1 Test strip 1

Test strip 1 was located in a production area between Sta. 258+00 and 257+00 and consisted of three lanes approximately 3 m x 38 m in plan dimensions (Figure 3.70). A plan view MDP\* map is presented in Figure 3.70 and a screen shot from on-board AccuGrade compaction monitoring system showing number of passes and MDP\* are presented in Figure 3.71. Three lanes were randomly selected from the production area to obtain in-situ point measurements using 200-mm LWD (Dynatest, Keros, and Zorn), DCP, NG, and DC tests. This area was compacted prior to our arrival at the project site with aid of loaded scrapers and CP-56 IC roller. MDP\* data obtained from the final pass on the three lanes (at nominal  $a = 1.87$  mm and  $v = 4$  km/h) were used for comparison with in-situ point measurements. A target minimum MDP\* of 138 (IC-TV) and minimum  $E_{LWD-Z2}$  value of 18 MPa (LWD-TV) were reportedly used in this production area for QA.

The MDP\* data plots and the corresponding in-situ point measurements for the three lanes are shown in Figure 3.72 and Figure 3.73, and summary statistics of the measurements are provided in Table 3.28. The IC-TV, 65% to 95% of  $w_{opt}$  limits, and 100% standard Proctor density values are provided on the figures for reference. Low MDP\* measurements were recorded on Lane 2 and the reason is likely due to the operator using the wrong throttle or gear setting during roller operation. While this reason cannot be confirmed, a similar situation was experienced on test strip 3 (discussed later in this section) compaction passes where low MDP\* measurements were recorded with a low throttle setting. The roller manufacturer recommendation is that the roller should be operated at high throttle and low gear settings to obtain reliable MDP\* measurements.

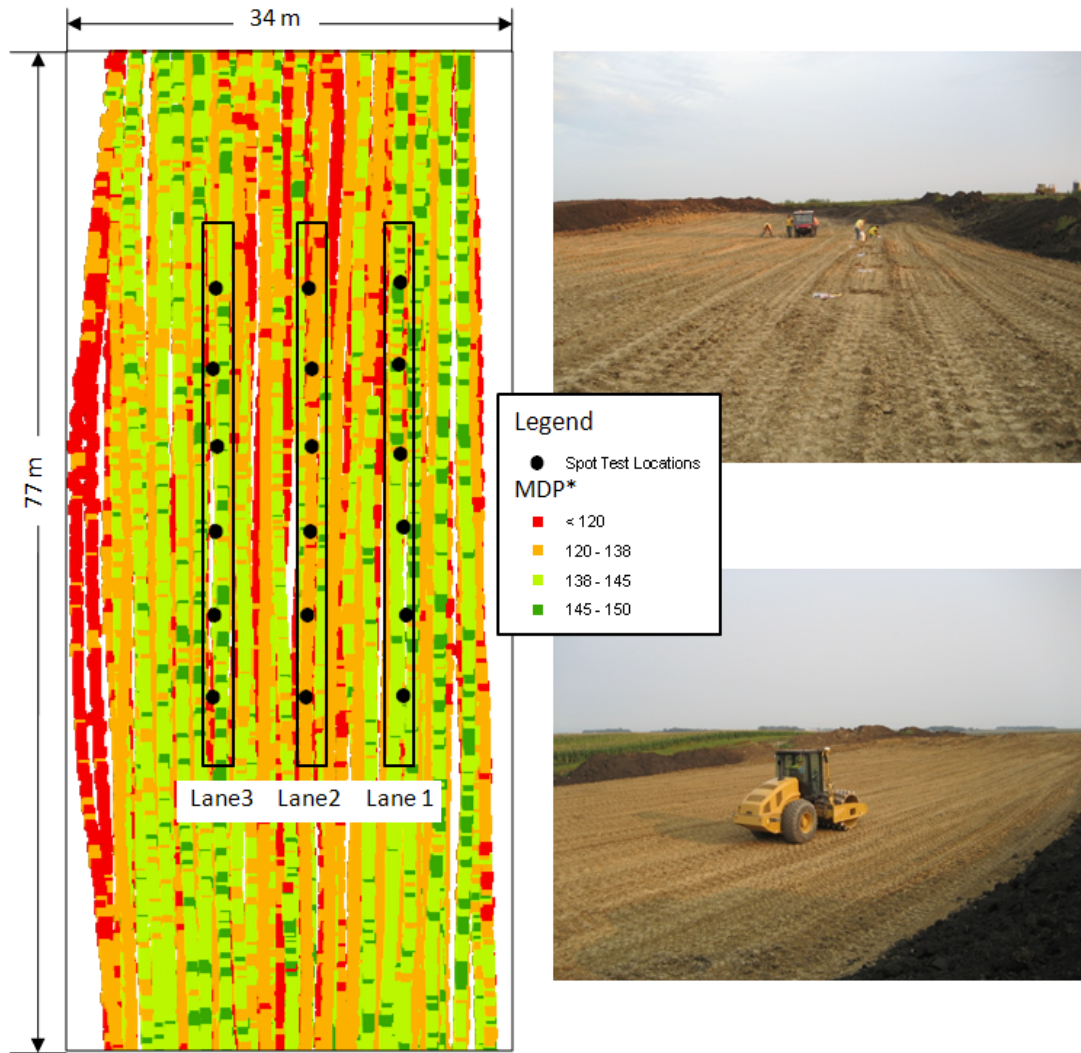


Figure 3.70. Plan view MDP\* map of the test strip 1 area with selected lanes for compaction testing (production area mapped a few hours prior to testing)

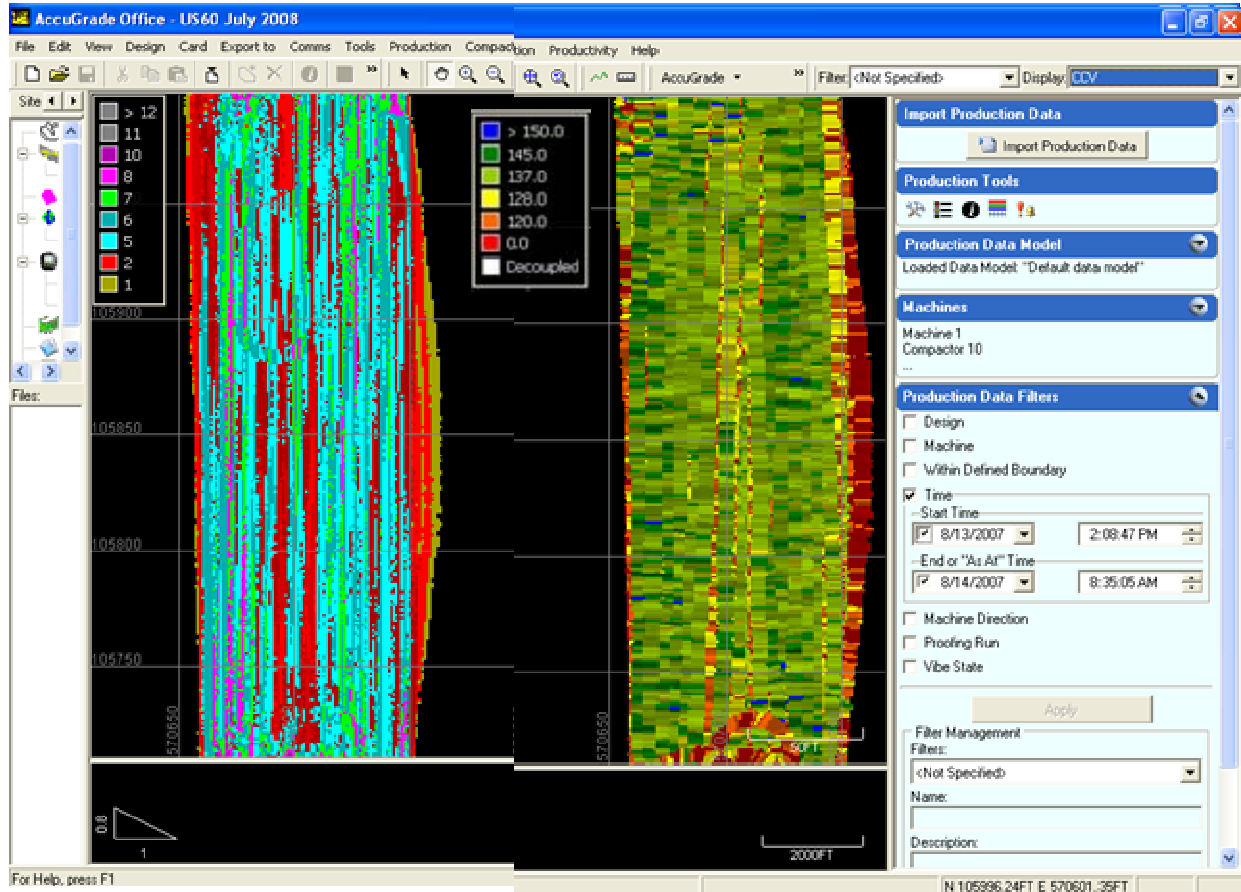


Figure 3.71. Screen shots from the on-board AccuGrade compaction monitoring system showing number of passes and MDP\* – Test strip 1

With the exception of measurements on lane 2, Figure 3.72 and Figure 3.73 show that the in-situ point measurement values generally coincide well with the variations in MDP\* measurements along each lane. Drive core samples for dry unit weight measurements were slightly higher (1.1 times) and moisture content measurements were slightly lower (0.9 times) than NG dry unit weight and moisture content measurements, respectively. It should be noted that the DC samples were obtained from the upper 80-mm of the compaction layer while NG measurements were obtained using 200-mm probe penetration depth. From lanes 1 and 2, the average MDP\* = 142.7 and the average  $E_{LWD-Z2} = 14.5$  MPa. MDP\* values along the test strip mostly exceeded the IC-TV; however, the  $E_{LWD-Z2}$  was less than the LWD-TV at many locations. Figure 3.74 shows DPI profiles extending to a depth of about 0.7 to 0.8 m below surface from lanes 1 to 3. The DPI profiles indicate that the thickness of the compaction layer varies from about 0.45 to 0.75 m (~1.5 to 2.5 ft). The moisture content measurements were mostly greater than 95% of  $w_{opt}$  (see Figure 3.75). The DPI profiles indicate significant vertical non-uniformity in soil properties which is a consequence of thicker lifts and variable moisture content. The average relative compaction based on NG measurements was about 86% of standard Proctor  $\gamma_{dmax}$  with an average moisture content of 123% of standard Proctor  $w_{opt}$  (17.6%).

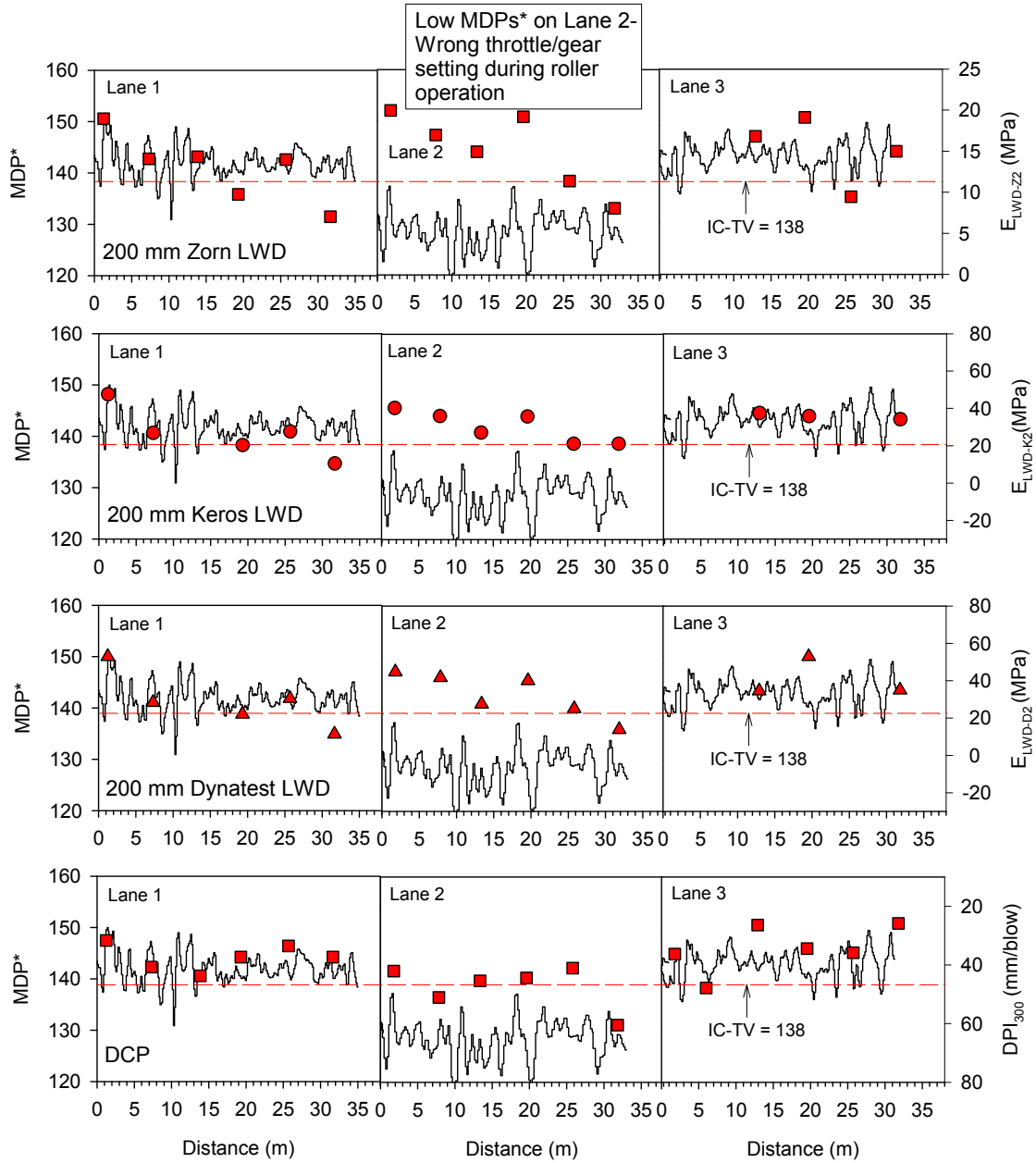


Figure 3.72. Comparison between CCV ( $a = 1.87$  mm) and in-situ point measurements ( $E_{LWD}$  and DPI) from test strip 1

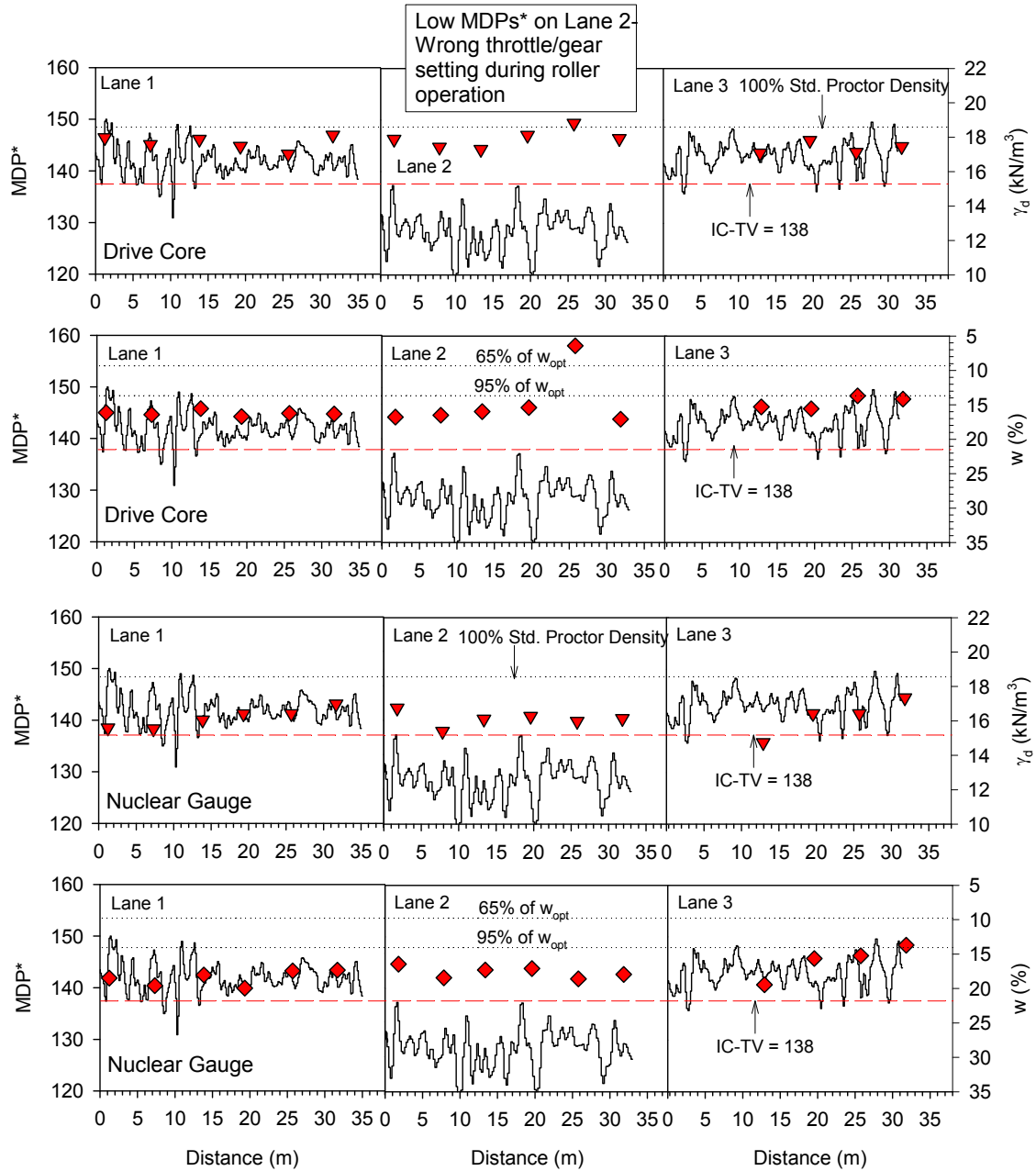
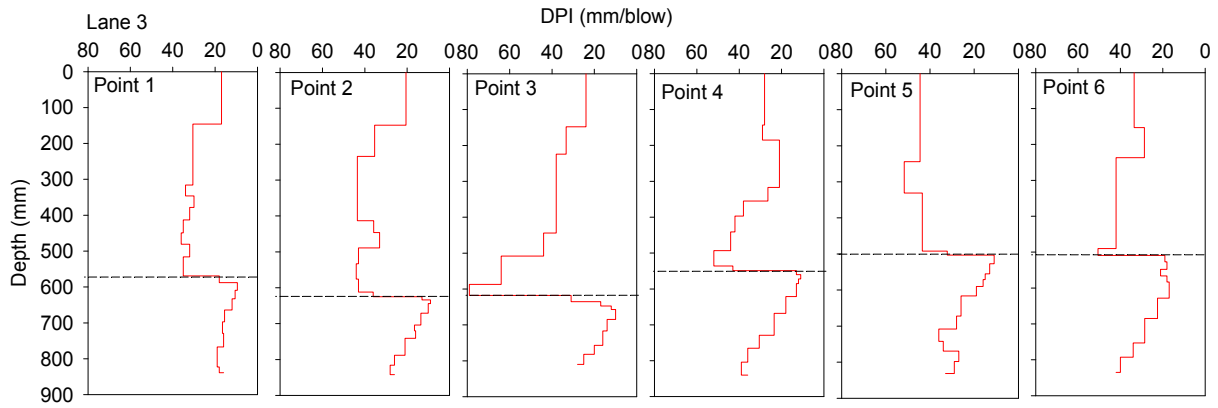
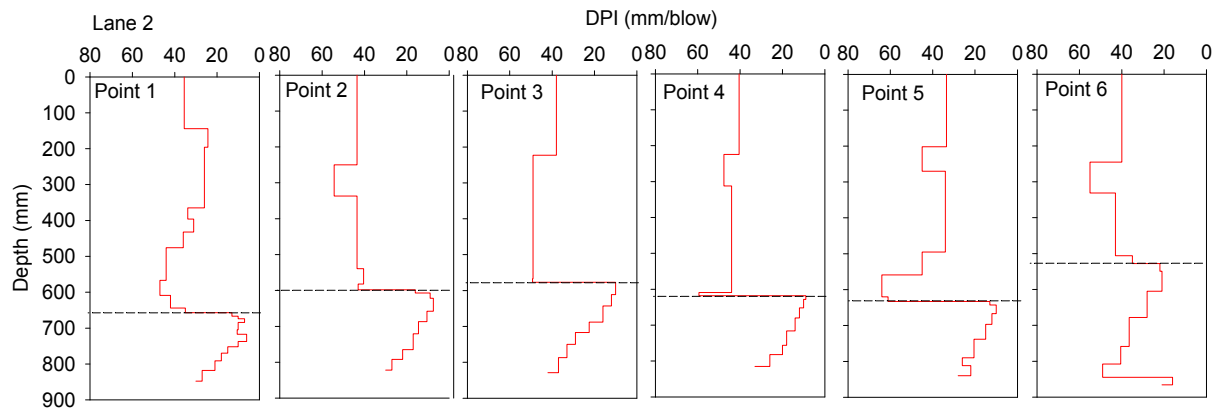
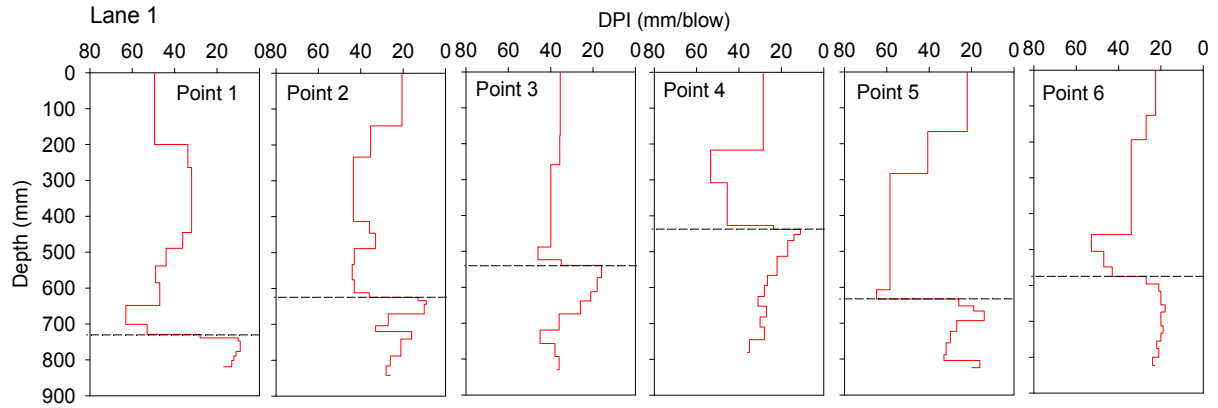


Figure 3.73. Comparison between CCV ( $a = 1.87 \text{ mm}$ ) and in-situ point measurements (NG and DC) from test strip 1

Table 3.28. Summary statistics of CCV and in-situ point measurements from test strip 1

Lane	Parameter	n	$\mu$	COV (%)
1	MDP* ( $a = 1.87$ mm)	249	142.2	2
	$E_{LWD-Z2}$ (MPa)	6	13.2	31
	$d_{LWD-Z2}$ (mm)	6	2.10	38
	$E_{LWD-D2}$ (MPa)	5	28.7	53
	$d_{LWD-D2}$ (mm)	5	0.61	66
	$E_{LWD-K2}$ (MPa)	5	26.5	51
	$d_{LWD-K2}$ (mm)	5	1.03	62
	DPI <sub>300</sub> (mm/blow)	6	37.6	11
	Nuclear Gauge, $w$ (%)	6	18.6	5
	Nuclear Gauge, $\gamma_d$ (kN/m <sup>3</sup> )	6	16.12	3
	Drive Core, $w$ (%)	6	16.0	2
	Drive Core, $\gamma_d$ (kN/m <sup>3</sup> )	6	17.63	2
	2	MDP* ( $a = 1.87$ mm)	Not reported	
$E_{LWD-Z2}$ (MPa)		6	15.1	31
$d_{LWD-Z2}$ (mm)		6	1.83	39
$E_{LWD-D2}$ (MPa)		6	32.2	37
$d_{LWD-D2}$ (mm)		6	0.57	50
$E_{LWD-K2}$ (MPa)		6	30.4	27
$d_{LWD-K2}$ (mm)		6	0.84	26
DPI <sub>300</sub> (mm/blow)		6	42.6	16
Nuclear Gauge, $w$ (%)		6	17.6	4
Nuclear Gauge, $\gamma_d$ (kN/m <sup>3</sup> )		6	16.10	3
Drive Core, $w$ (%)		6	14.7	26
Drive Core, $\gamma_d$ (kN/m <sup>3</sup> )		6	17.91	3
3		MDP* ( $a = 1.87$ mm)	301	143.2
	$E_{LWD-Z2}$ (MPa)	4	15.1	27
	$d_{LWD-Z2}$ (mm)	4	1.78	34
	$E_{LWD-D2}$ (MPa)	3	40.8	26
	$d_{LWD-D2}$ (mm)	3	0.40	23
	$E_{LWD-K2}$ (MPa)	3	35.8	5
	$d_{LWD-K2}$ (mm)	3	0.86	3
	DPI <sub>300</sub> (mm/blow)	6	34.4	21
	Nuclear Gauge, $w$ (%)	6	16.0	13
	Nuclear Gauge, $\gamma_d$ (kN/m <sup>3</sup> )	6	16.23	6

	Drive Core, $w$ (%)	4	14.7	5
	Drive Core, $\gamma_d$ (kN/m <sup>3</sup> )	4	17.37	2



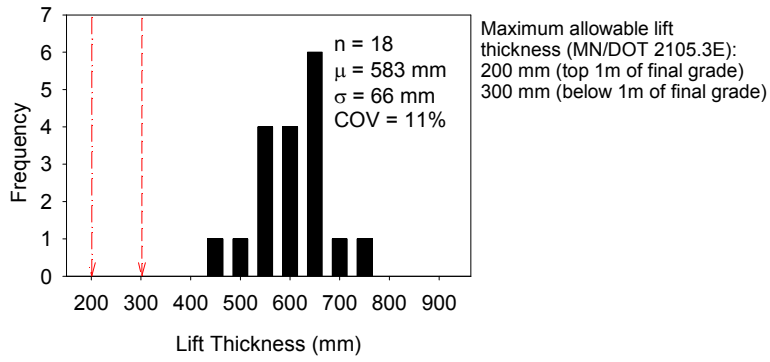


Figure 3.74. DCP profiles from test strip 1 (depth to the dashed line indicates the compacted compaction layer thickness) and histogram of estimated lift thickness – test strip 1

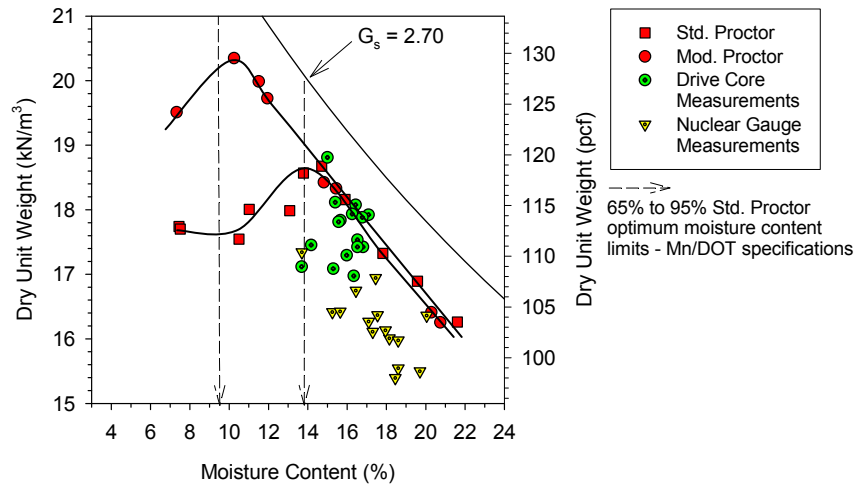


Figure 3.75. Laboratory moisture-density relationships and in-situ moisture density measurements from test strip 1

### 3.5.4.2 Test strip 2

Test strip 2 was a 36 m long one-dimensional test strip constructed as a calibration test strip. Rolling operations were performed using a CP-56 padfoot roller by the Contractor personnel. Motor scrapers were used to place the fill material and a dozer was used to level the material in the test strip area (see Figure 3.76). The uncompacted lift thickness of the fill was in the range of 0.3 to 0.5 m (~ 1.0 to 1.7 ft). The test strip was compacted with 15 roller passes with two nominal vibration amplitude settings: Pass 1 to 8 at  $a = 1.87$  mm and Pass 9 to 15 at  $a = 0.85$  mm. In-situ point measurements were obtained using NG, DCP, and 200-mm Zorn LWD test devices at 0, 4, 8, and 15 roller passes. After 15 passes, Shelby tube samples were obtained by hydraulically pushing the tubes to a depth of about 0.75 m (2.5 ft) into the compacted subgrade for UC and  $M_r$  testing. A picture of the final compacted surface is shown in Figure 3.76.

Figure 3.77 presents MDP\* data plots along the test strip length and corresponding point measurement values for 1, 4, 8, and 15 roller passes. Point measurements show variations that generally coincide well with variations in MDP\* along the test strip. The target minimum  $E_{LWD-22}$  and MDP\* values used for QA are also shown in Figure 3.77, for reference. Summary statistics of MDP\* and in-situ compaction measurement values for passes 8 and 15 are presented in Table 3.29. Figure 3.78 shows a frequency distribution plot and a normal cumulative distribution function of MDP\* for pass 8. White et al. (2007a) demonstrated that the minimum threshold value for quality acceptance can be selected by analyzing the data in this manner and using the tenth percentile ( $P_{10}$ ), for example (the tenth percentile represents the value above which 90% of measurement data may be found). For pass 8, the MDP\*  $P_{10}$  value is equal to 138, which is same as the IC-TV used by Mn/DOT in this area of the project.

In-situ moisture content and dry unit weight measurements obtained using NG and Shelby tube samples are shown in relationship to the standard Proctor curve and specified Mn/DOT moisture specification limits in Figure 3.79. This figure shows that the soil moisture content and dry unit weight are variable across the test strip and many of the moisture measurements are out of the moisture specification limits. Compaction growth curves for in-situ point measurements and MDP\* are provided in Figure 3.80. Bar charts of average MDP\* and average DPI,  $\gamma_d$ , and  $E_{LWD-Z2}$  values are presented in Figure 3.81. On average, some increase in compaction is observed up to pass 4 in MDP\* as well as point measurements, and then no considerable increase is observed with additional roller passes. On average after pass 15, relative compaction = 94% with average  $w = 20\%$  (104%  $w_{opt}$ ), and average  $E_{LWD-Z2} = 13.9$  MPa.

Laboratory unconfined compressive strength (UCS) tests were conducted on relatively undisturbed soil samples extracted from Shelby tubes collected from the subgrade. The  $s_u$  values are presented along with DPI profiles across the test strip in Figure 3.82. An empirical relationship was developed between  $s_u$  and DPI based on these results and results from test strip 5 presented later in this chapter. Laboratory resilient modulus ( $M_r$ ) and UU shear strength tests were performed on one Shelby tube sample following AASHTO T-307 standard procedure. The sample was obtained from a depth of about 25 mm (~ 2 in.) below the compacted surface. During  $M_r$  testing, 1000 loading cycles were applied on the confined sample during the conditioning phase followed by 15 sequences of 100 loading cycles each at different confining and deviator stress combinations. The test resulted in average  $M_r = 12.6$  MPa with standard deviation of 0.7 MPa. This value is comparable to Zorn  $E_{LWD-Z2}$  value of 10.5 MPa obtained at the surface of the Shelby tube sample location. The UU test resulted in  $s_u = 109.6$  kPa. Note that the peak vertical applied stress under the Zorn 200-mm diameter plate LWD is about 200 kPa while the peak axial stress during the  $M_r$  test is about 69 kPa (see Table 2.4).



Figure 3.76. Pictures from test strip 2 construction: fill placement, compaction, in-situ spot testing, and final compacted surface (top left to bottom right)

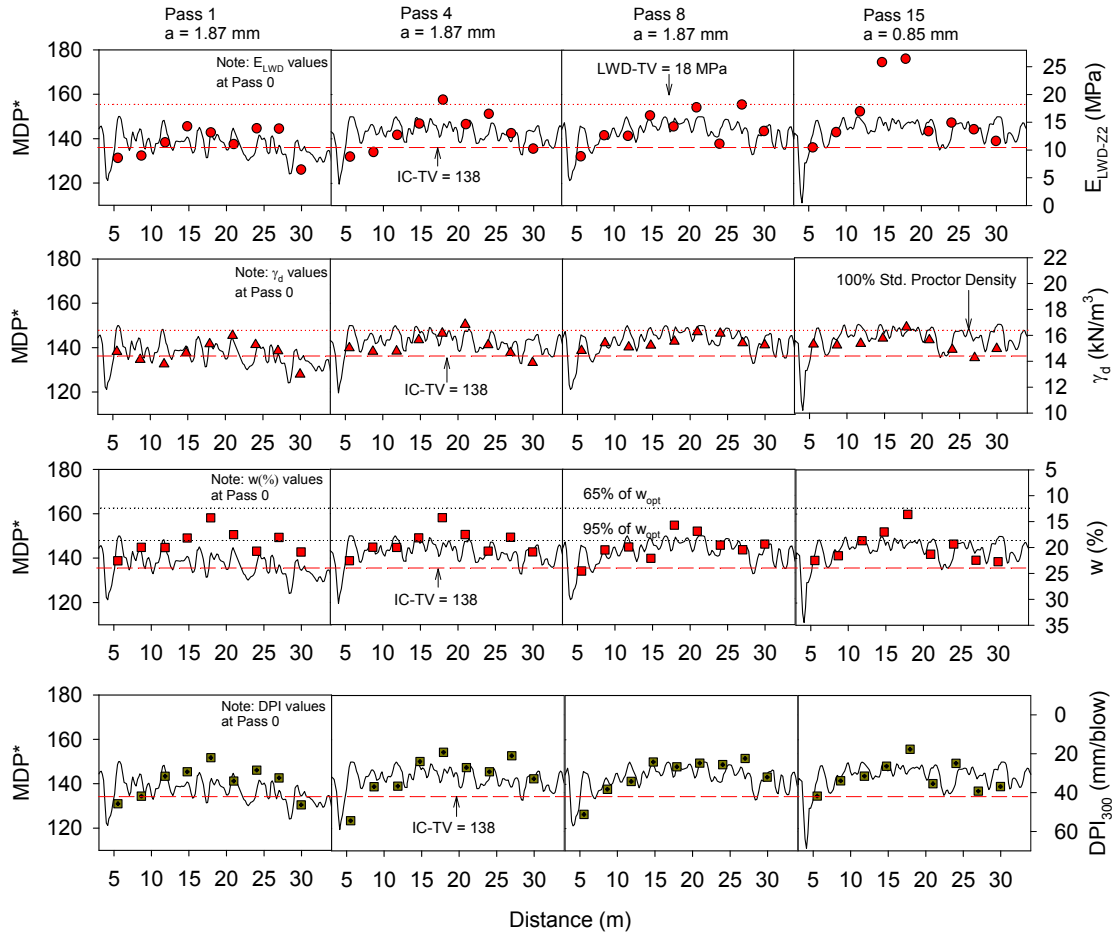


Figure 3.77. IC-MVs and in-situ point measurements at several passes – test strip 2

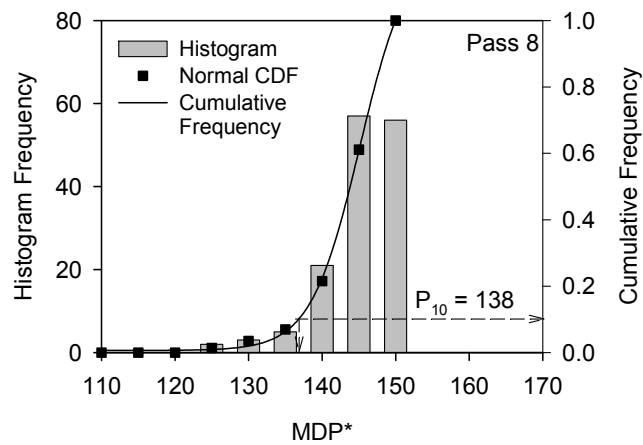


Figure 3.78. Frequency distribution plot of IC-MVs for pass 8 – test strip 2

Table 3.29. Summary statistics of IC-MVs and in-situ point measurements after passes 8 and 15 – test strip 2

Pass No.	Parameter	n	$\mu$	COV (%)
8	MDP* ( $a = 0.85$ mm)	144	142.9	4
	$E_{LWD-Z2}$ (MPa)	9	13.9	21
	$d_{LWD-Z2}$ (mm)	9	1.89	24
	DPI <sub>300</sub> (mm/blow)	9	31.1	28
	w (%)	9	20.0	12
	$\gamma_d$ (kN/m <sup>3</sup> )	9	15.6	3
15	MDP* ( $a = 1.87$ mm)	171	143.8	4
	$E_{LWD-Z2}$ (MPa)	9	16.3	36
	$d_{LWD-Z2}$ (mm)	9	1.69	29
	DPI <sub>300</sub> (mm/blow)	9	32.0	23
	w (%)	9	19.9	15
	$\gamma_d$ (kN/m <sup>3</sup> )	9	15.3	4
	$S_u$ (kPa)	15	77.5	28

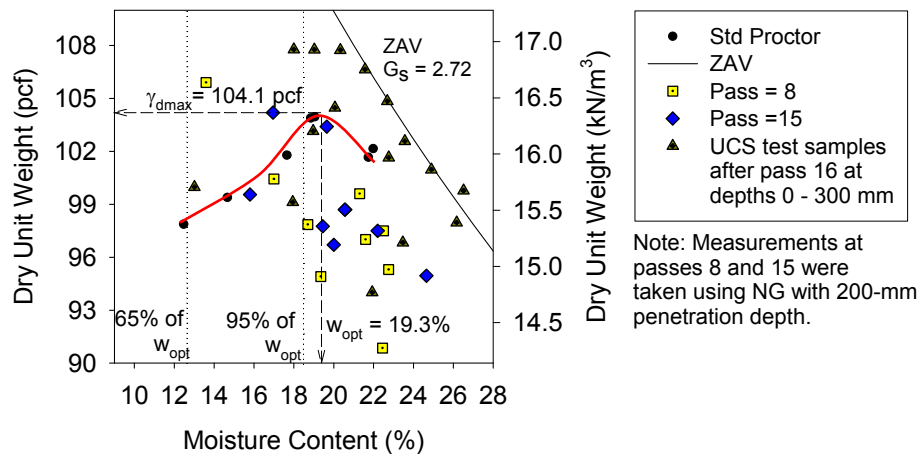


Figure 3.79. Laboratory and in-situ moisture-density measurements – test strip 2

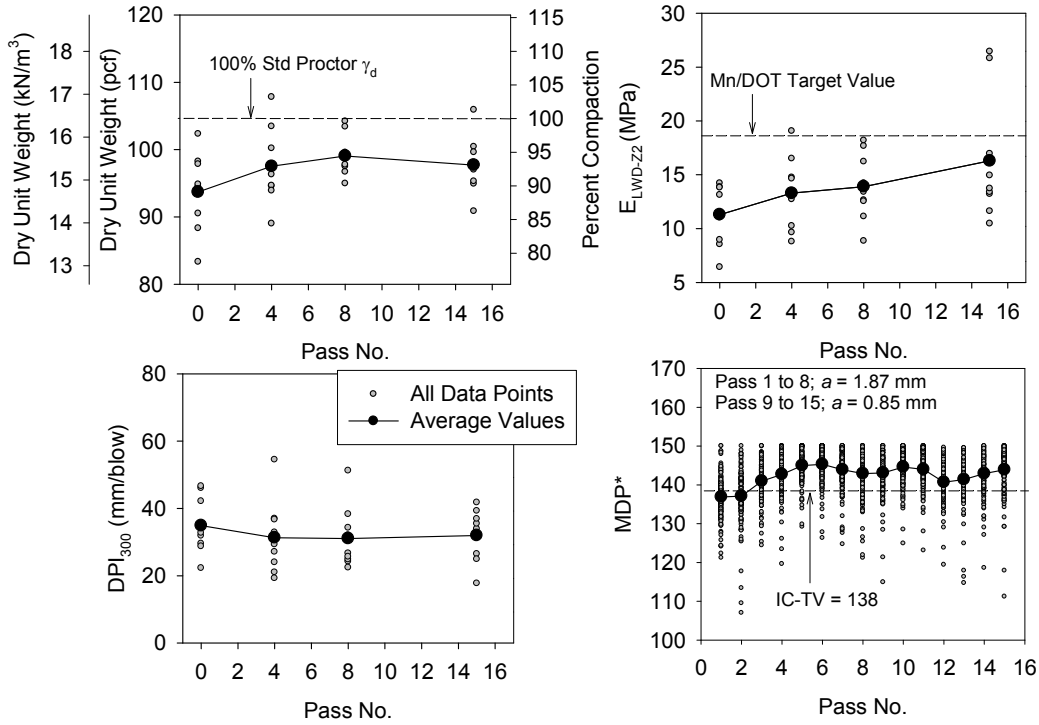


Figure 3.80. Compaction growth curves for IC-MVs and in-situ point measurement values

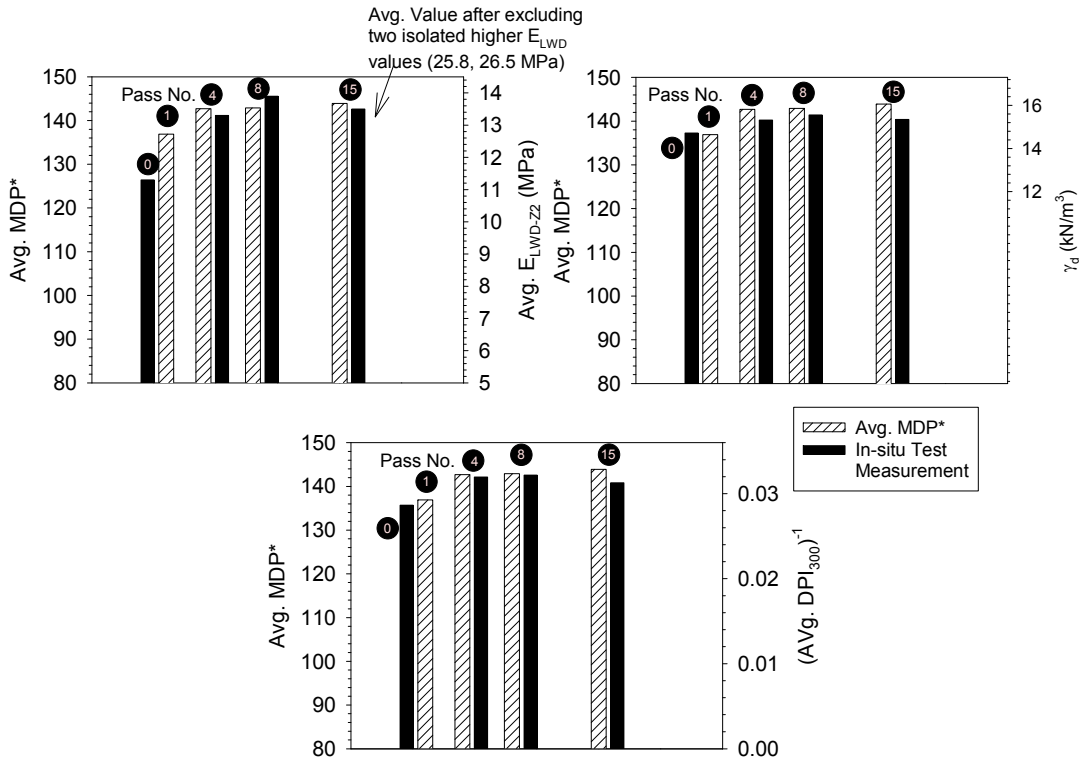


Figure 3.81. Bar chart comparisons of average IC-MVs and in-situ point measurement values at different passes

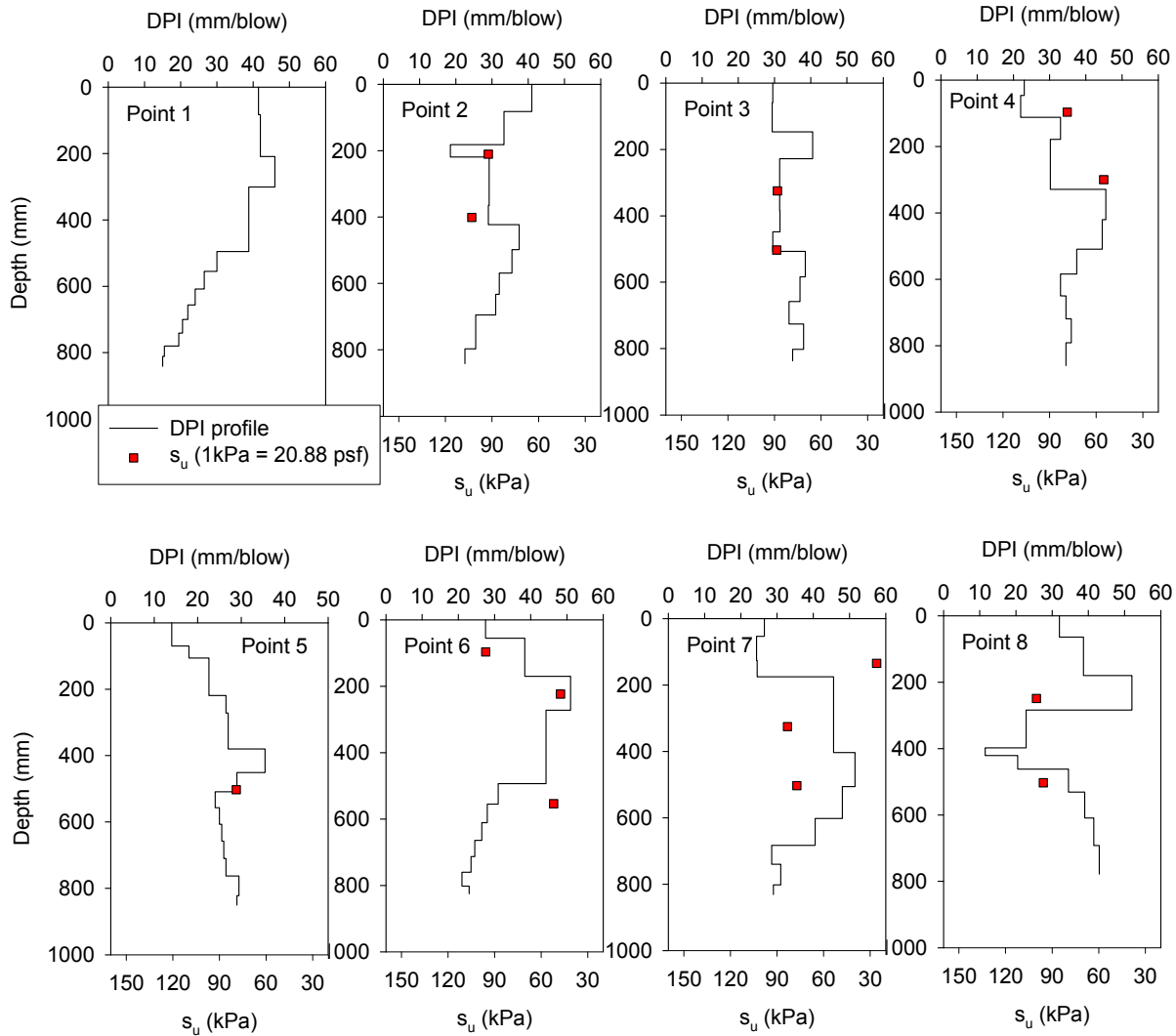


Figure 3.82. DPI profiles and  $s_u$  from UC testing on Shelby tube samples from test strip 2 subgrade after pass 15

### 3.5.4.3 Test strip 3

Test strip 3 was constructed with plan dimensions of approximately 9 m x 45 m. The test strip was constructed shortly after a period of significant rainfall in the project area. Therefore, most areas of the project were relatively wet. Few hours prior to our testing, the test area was disked by scarifying to a depth of about 0.25 to 0.3 m. The area was compacted in three lanes (lanes 3a, 3b, and 3c) using different amplitude settings (see Figure 3.83 and Table 3.30). LWD tests were conducted after 1, 2, 4, 8, and 12 roller passes, and NG tests were conducted after 12 passes at five test locations across each lane. GPS measurements at point measurement locations were not obtained for this test strip due to satellite signal problems. Therefore, the MDP\* and point measurement values are matched approximately based on reference measurements obtained from the field. The objectives of this test strip were to study the influence of amplitude on the MDP\* values and obtain data for correlation analysis.

Figure 3.84 shows the AccuGrade output indicating that the roller elevation decreased from the initial pass through the final pass suggesting compaction. Elevation change as an indicator to compaction has not been thoroughly analyzed and may have potential to provide useful information. Figure 3.85 and Figure 3.86 show the color-coded MDP\* spatial maps for the three compaction lanes (left side of figures) indicating increasing MDP\* values with successive passes.



Figure 3.83. Test strip 3 prepared in three lanes (lanes 3a, 3b, and 3c) for rolling (top left), picture of roller used on-site (top right), rolling operations (bottom left), and LWD testing (bottom right) in at the bottom of the padfoot penetration

Table 3.30. Test Strips 3a, 3b, and 3c roller pass summary

Lane	<i>a</i> (mm)	Pass	Spot Testing (No.)
3a	Static	1 – 2	LWD (5)
3a	Static	3 – 4	LWD (5)
3a	Static	5 – 8	LWD (5)
3a	1.87	9 – 10	–
3a	0.85	11 – 12	LWD, NG (5)
3b	0.85	1 – 2	LWD (5)
3b	0.85	3 – 4	LWD (5)
3b	0.85	5 – 8	LWD (5)
3b	1.87	9 – 10	–
3b	Static	11 – 12	LWD, NG (5)
3c	1.87	1 – 2	LWD (5)
3c	1.87	3 – 4	LWD (5)
3c	1.87	5 – 8	LWD (5)
3c	0.85	9 – 10	–
3c	Static	11 – 12	LWD, NG (5)

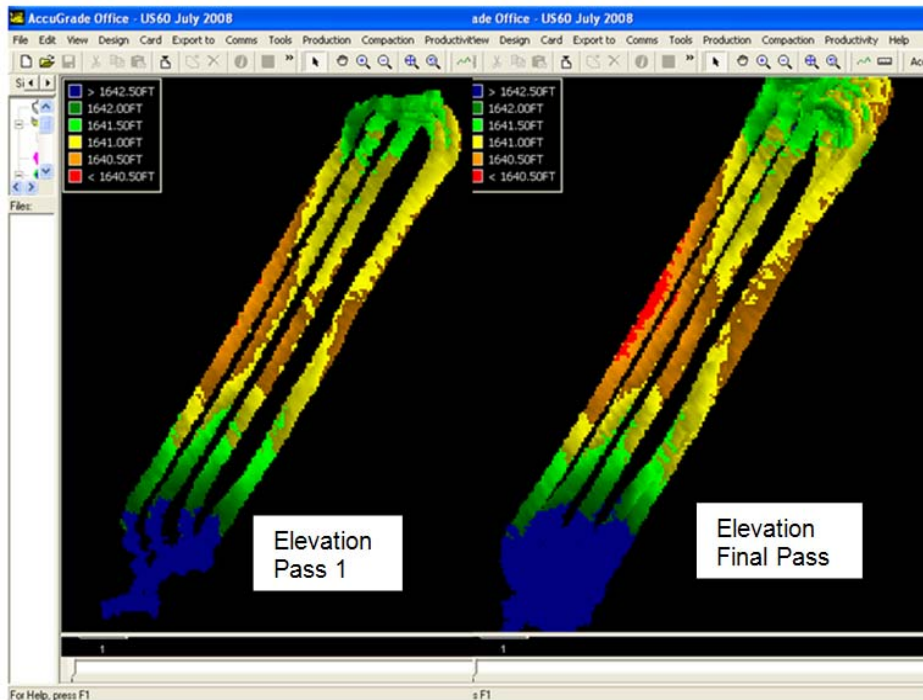


Figure 3.84. Screen shots from AccuGrade showing change in elevation from pass 1 to final pass – test strip 3

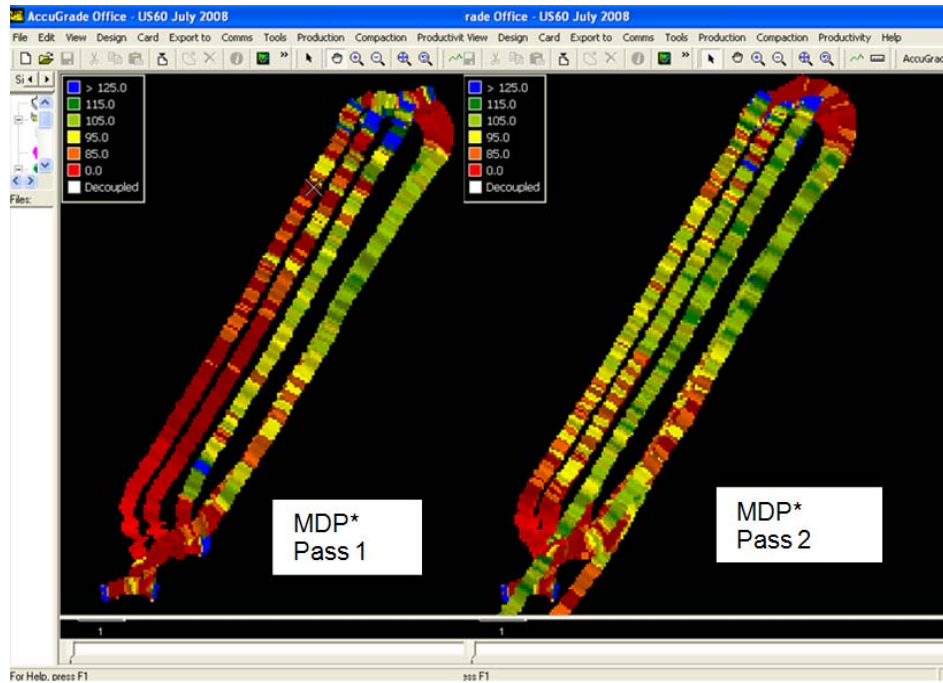


Figure 3.85. Screen shots from AccuGrade showing change in MDP\* from pass 1 to pass 2 – test strip 3

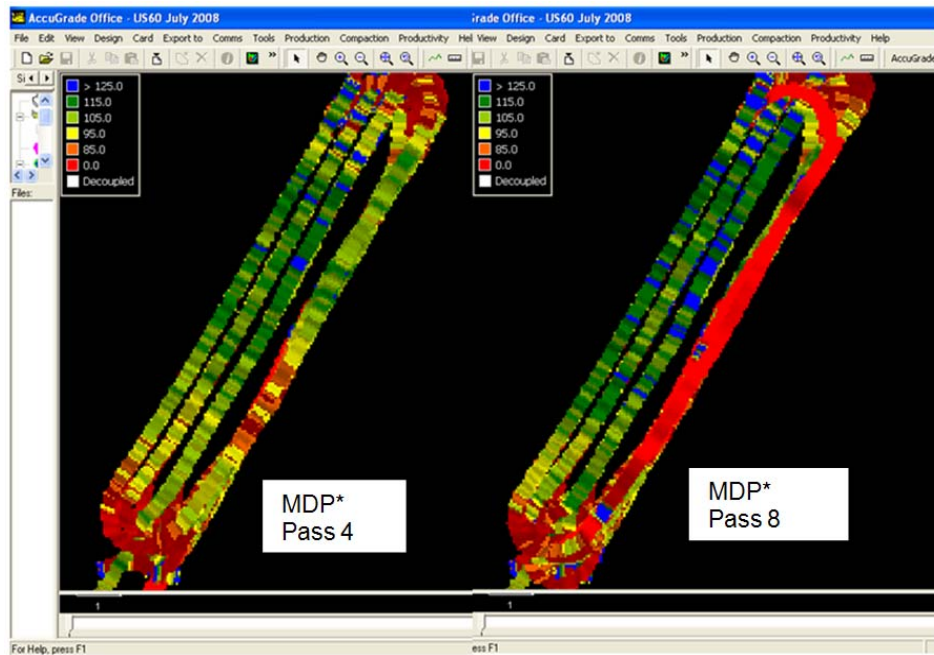


Figure 3.86. Screen shots from AccuGrade showing change in MDP\* from pass 4 to pass 8 – test strip 3

Figure 3.87 present MDP\* data plots along each lane and corresponding  $E_{LWD-Z2}$  point measurement values for 1, 2, 4, 8/9, and 12 roller passes. Figure 3.88 show MDP\* data plots from pass 12 and corresponding moisture and dry unit weight point measurements along each lane. Bar charts of average MDP\* and average  $E_{LWD-Z2}$  values for each lane are presented in Figure 3.89, which show that both measurements increase correspondingly with each pass. The in-situ moisture and dry unit weight measurements are plotted in relation to the laboratory standard and modified Proctor curves in Figure 3.90. Similar to the materials encountered in the previous test strips, the fill material in this test strip was also close to or wet of 95% standard Proctor  $w_{opt}$ . Summary statistics of MDP\* and point measurement values from the test strip are provided in Table 3.31.

MDP\* compaction growth curves for each lane are presented in Figure 3.91. The amplitude settings associated with each pass on the test strips are also shown in Figure 3.91. The compaction curves for all lanes followed the same path of increasing average MDP\* with pass up to pass 7, some decrease in MDP\* after pass 8 and 9, and then slight increase in MDP\* and/or relatively constant MDP\* after pass 10. Low MDP\* values were recorded for pass 9 on lane 3b (Figure 3.91), which is a result of a low throttle setting during roller operation similar to the results observed in test strip 1. Again, the manufacturer's recommendation is that the roller should be operated at the high throttle setting to obtain meaningful MDP\* values. The results presented in Figure 3.91 show no evidence of the influence of vibration amplitude on MDP\* on this test strip. However, the material was generally wet of  $w_{opt}$  and variable.

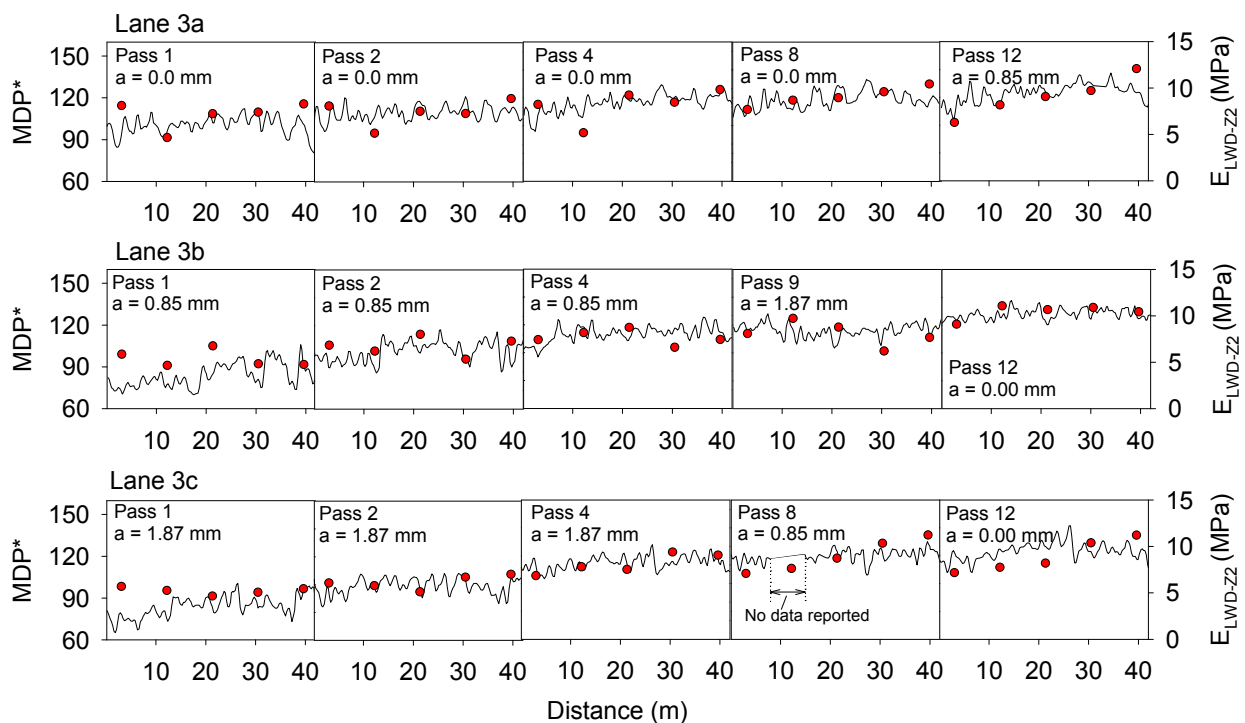


Figure 3.87. CCV and  $E_{LWD}$  comparisons for test strip 3

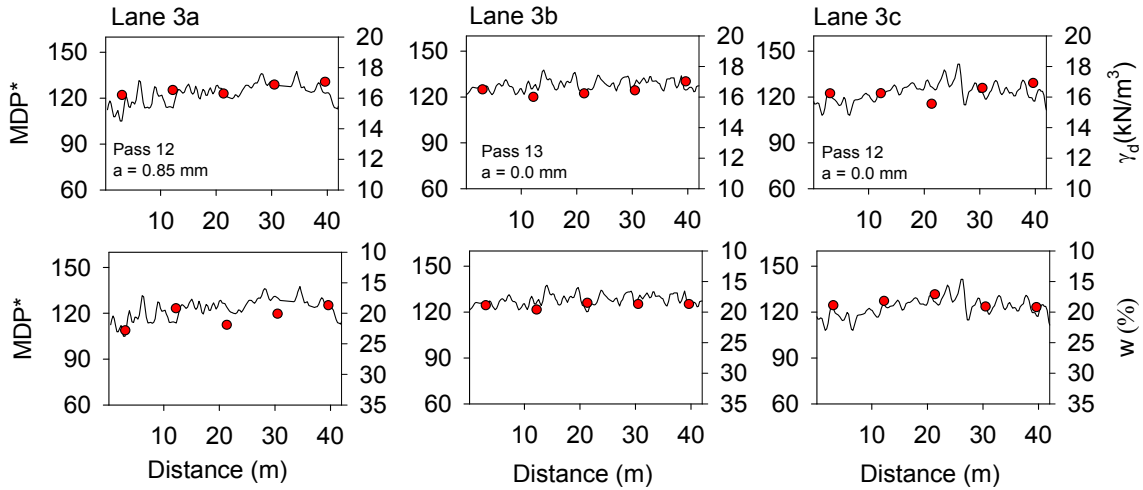


Figure 3.88. CCV and NG test measurements after final pass for test strip 3

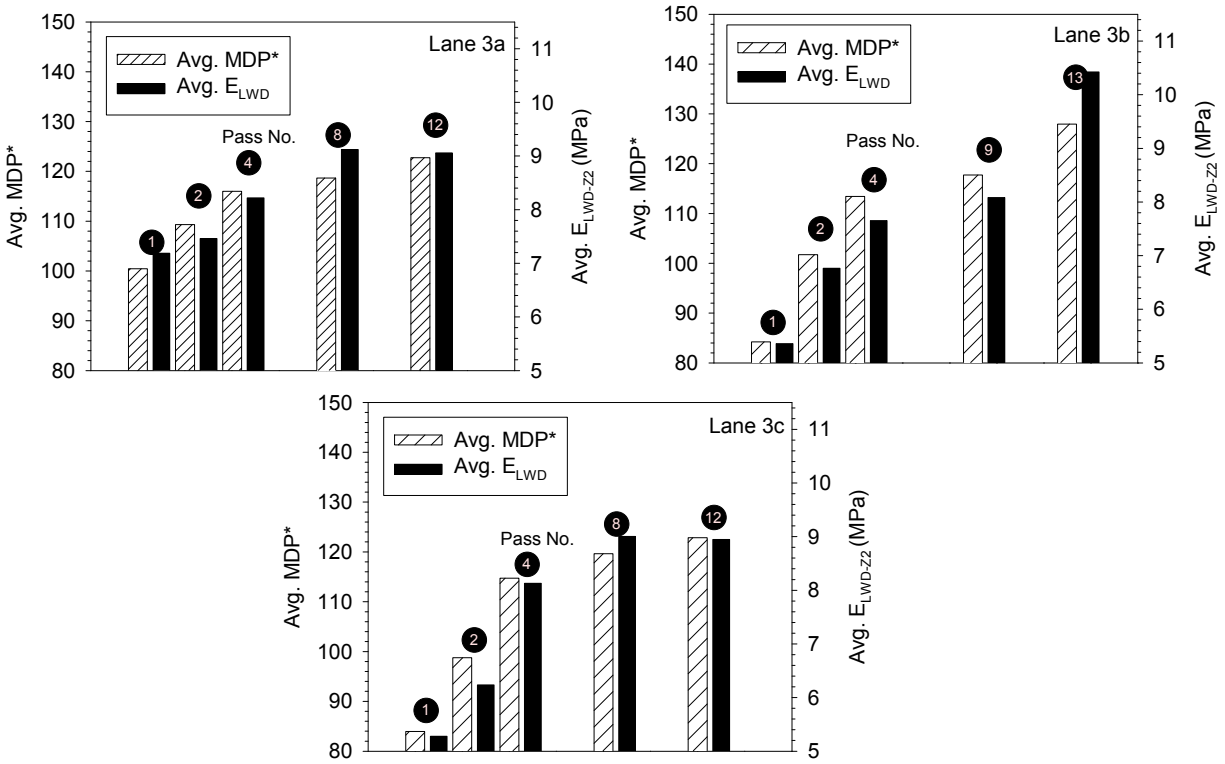


Figure 3.89. Bar charts comparing CCV and  $E_{LWD}$  measurement values from strip 3a, 3b, and 3c

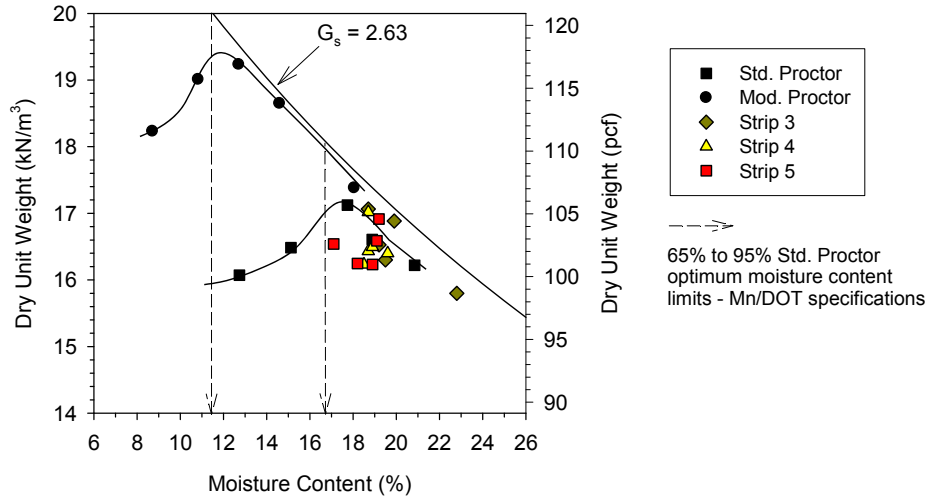


Figure 3.90. Laboratory Proctor and in-situ moisture-density measurements

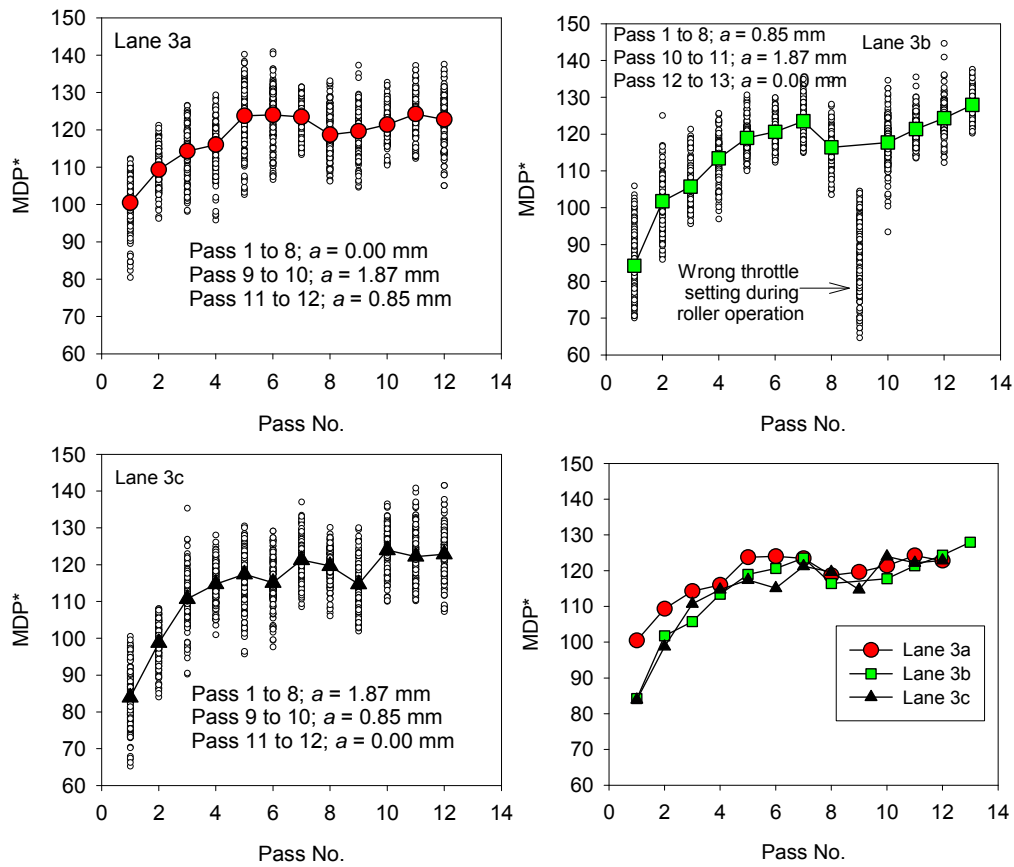


Figure 3.91. Influence of amplitude on MDP\*compaction curves on lanes 3a, 3b, and 3c – test strip 3

Table 3.31. Summary statistics of in MDP\* and in-situ point measurements – test strip 3

Lane	Pass	Parameter	n	$\mu$	COV (%)
3a	8	MDP* (static)	152	118.7	5
		$E_{LWD-Z2}$ (MPa)	5	9.1	10
		$d_{LWD-Z2}$ (mm)	5	2.77	10
	12	MDP* ( $a = 0.85$ mm)	153	123.7	7
		$E_{LWD-Z2}$ (MPa)	5	9.1	21
		$d_{LWD-Z2}$ (mm)	5	2.89	22
		$\gamma_d$ (kN/m <sup>3</sup> )	5	16.60	2
		$w$ (%)	5	20.5	9
3b	9	MDP* ( $a = 0.85$ mm)	163	116.4	4
		$E_{LWD-Z2}$ (MPa)	5	8.1	15
		$d_{LWD-Z2}$ (mm)	5	3.17	16
	13	MDP* (static)	168	127.9	3
		$E_{LWD-Z2}$ (MPa)	5	10.4	7
		$d_{LWD-Z2}$ (mm)	5	2.41	7
		$\gamma_d$ (kN/m <sup>3</sup> )	5	16.44	2
		$w$ (%)	5	18.9	2
3c	8	MDP* ( $a = 1.87$ mm)	138	119.7	4
		$E_{LWD-Z2}$ (MPa)	5	9.0	18
		$d_{LWD-Z2}$ (mm)	5	2.87	17
	12	MDP* (static)	159	122.8	5
		$E_{LWD-Z2}$ (MPa)	5	8.9	18
		$d_{LWD-Z2}$ (mm)	5	2.88	17
		$\gamma_d$ (kN/m <sup>3</sup> )	5	16.31	3
		$w$ (%)	5	18.5	5

#### 3.5.4.4 Regression analysis between MDP\* and in-situ point measurements

Regression relationships derived from experimental testing on test strips 1, 2, and 3 are summarized in Figure 3.92, Figure 3.93,

Figure 3.94, and Table 3.32. These relationships were developed by spatially paring the nearest point data using GPS measurements. Data obtained from lane 2 of test strip 1 was not included

in the regression analysis (recall that the readings were likely recorded in a wrong throttle setting).

Relationships between LWD and MDP\* measurement values are presented separately for data obtained at different amplitude settings and also by combining all the data (see Figure 3.92 and Figure 3.93). MDP\* data obtained from test strips 1 and 2 and test strip 3 showed different trends in the relationships with  $E_{LWD-Z2}$  and  $d_{LWD-Z2}$  measurement values. MDP\* values tend to reach an asymptotic value of 150. The MDP\*- $E_{LWD-Z2}$  and MDP\*- $d_{LWD-Z2}$  relationships show improved correlations for the trends observed with MDP\* values less than 138 ( $R^2 > 0.4$ ) than greater than 138 ( $R^2 < 0.3$ ). Despite limited data ( $n = 8$ ), MDP\* relationship with  $E_{LWD-K2}$  and  $E_{LWD-D2}$  showed good correlations with  $R^2 > 0.6$ . Relationships with  $d_{LWD-K2}$  and  $d_{LWD-D2}$  showed relatively poor correlations with  $R^2$  values  $< 0.5$ .

MDP\* and  $\gamma_d$  relationships presented in  
Figure 3.94 generally show poor correlations with  $R^2$  values between 0.0 and 0.3. Relationship obtained from strip 3 with  $a = 0.85$  mm setting showed good correlation with  $R^2 > 0.7$ . Similar to  $E_{LWD-Z2}$  measurements at MDP\* values greater than 138, MDP\* and  $DPI_{300}$  relationships presented in

Figure 3.94 show relatively poor correlations with  $R^2$  of about 0.3.

Multiple regression analysis was performed on the data to assess the influence of moisture content and amplitude on relationships between MDP\*- $E_{LWD-Z2}$ , MDP- $\gamma_d$ , and MDP- $DPI_{300}$ . The analysis was performed to predict MDP\* (i.e., treating MDP\* as a dependent variable) using in-situ point measurements (i.e., treating point measurements as independent variables). The following criteria were used for establishing statistical significance of a parameter based on  $p$  and  $t$  statistics:  $p$ -value  $< 0.05$  = significant,  $< 0.10$  = possibly significant,  $> 0.10$  = likely not significant, and  $t$  values  $< -2$  and  $> +2$ . Multiple regression analysis results and relationships from test strips 1, 2, and 3 are summarized in Figure 3.95. Findings from the analysis are as follows:

- Amplitude was not statistically significant in predicting MDP\*
- Moisture content was statistically significant in predicting MDP\* from  $E_{LWD-D2}$  and  $DPI_{300}$  measurements. Regression relationships for  $E_{LWD-Z2}$  and  $DPI_{300}$  improved from 0.37 to 0.48 and 0.30 to 0.45 respectively, by incorporating moisture content in the analysis.
- Moisture content was not statistically significant in predicting MDP\* from  $\gamma_d$  measurements for this dataset.

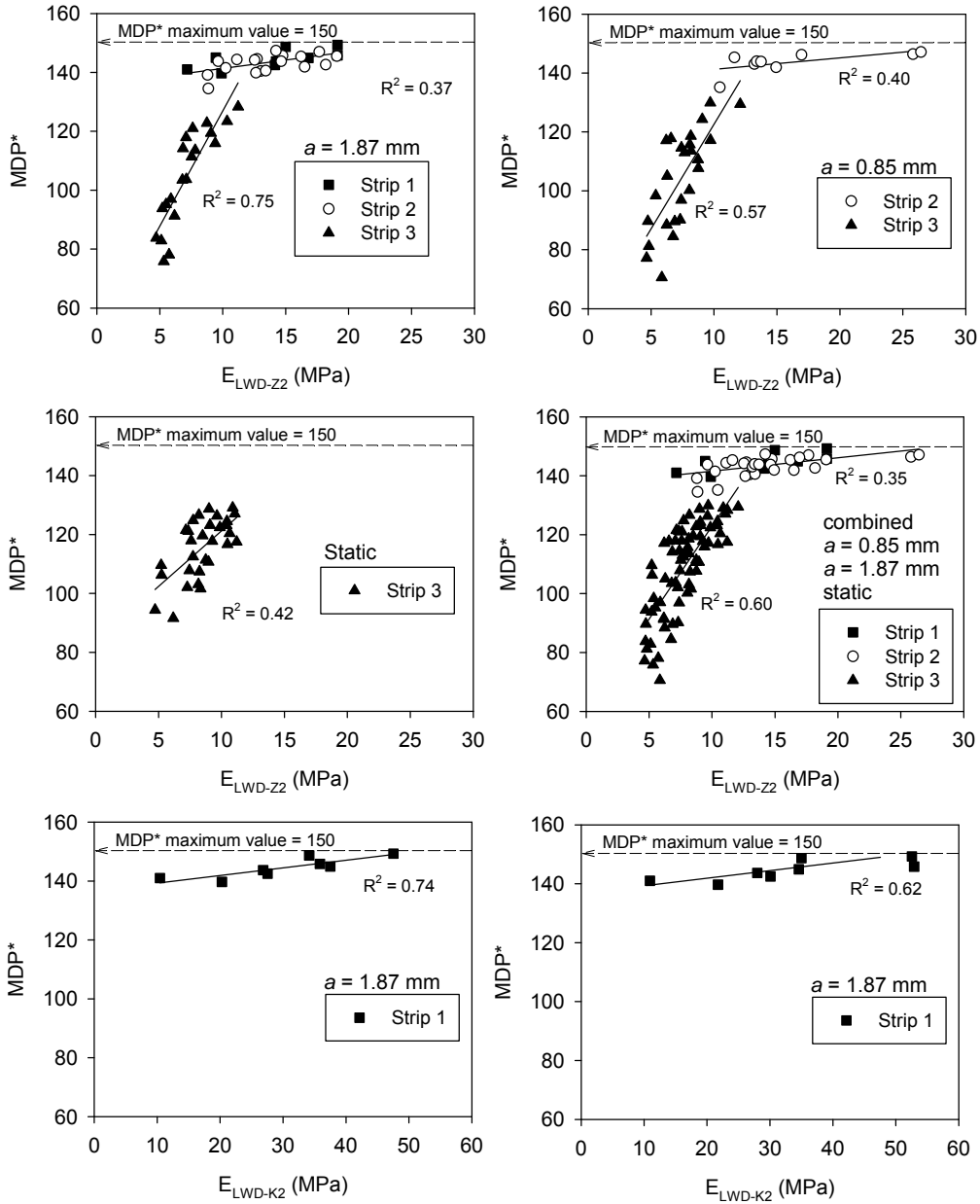


Figure 3.92. Linear regression relationships between MDP\* and E<sub>LWD</sub> measurements

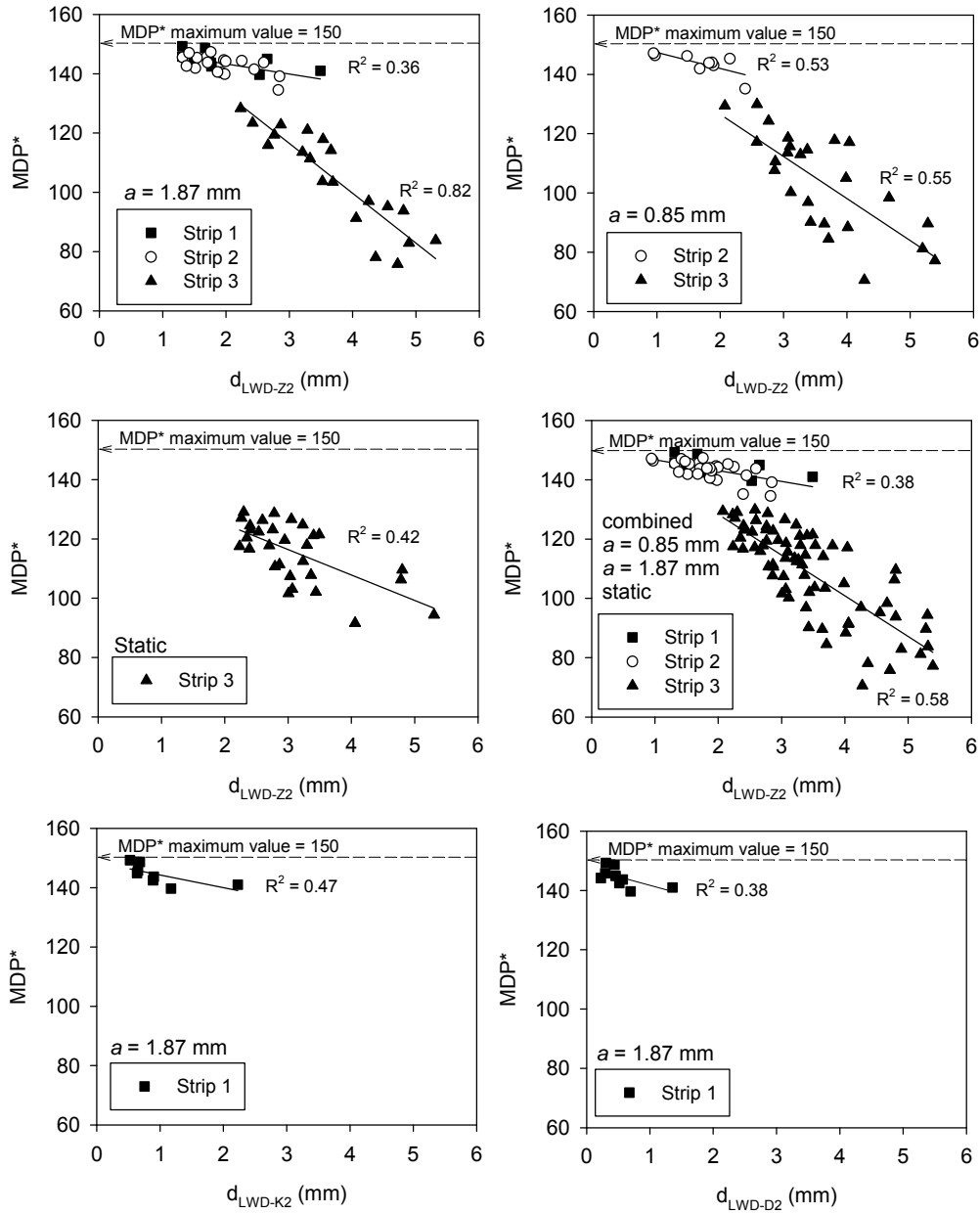


Figure 3.93. Linear regression relationships between MDP\* and  $d_{LWD}$  measurements

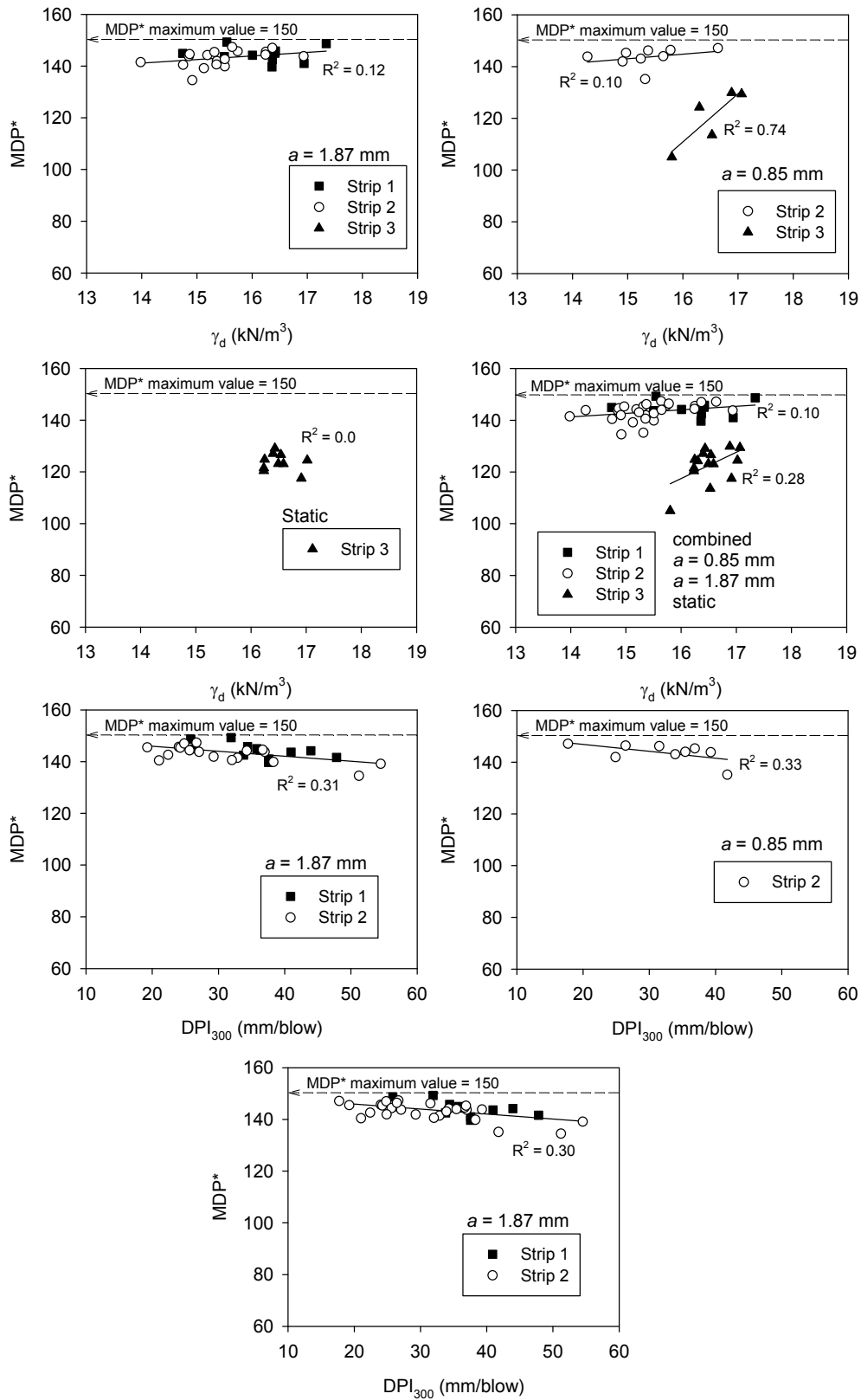


Figure 3.94. Linear regression relationships between MDP\* and in-situ point measurements

Table 3.32. Summary of regression relationships – TH60 project

Test strip(s)	Relationship	<i>a</i> (mm)	n	R <sup>2</sup>
1, 2	MDP* = 0.57 E <sub>LWD-Z2</sub> + 135.7	1.87	28	0.37
1, 2	MDP* = -3.43 d <sub>LWD-Z2</sub> + 150.2		28	0.36
3	MDP* = 7.81 E <sub>LWD-Z2</sub> + 48.7		20	0.75
3	MDP* = -16.81 d <sub>LWD-Z2</sub> + 166.9		20	0.82
2	MDP* = 0.39 E <sub>LWD-Z2</sub> + 137.3	0.85	9	0.40
2	MDP* = -5.37 d <sub>LWD-Z2</sub> + 152.7		9	0.53
3	MDP* = 7.11 E <sub>LWD-Z2</sub> + 51.6		25	0.57
3	MDP* = -14.20 d <sub>LWD-Z2</sub> + 154.9		25	0.55
3	MDP* = 3.78 E <sub>LWD-Z2</sub> + 83.5	static	30	0.42
3	MDP* = -8.57 d <sub>LWD-Z2</sub> + 142.1		30	0.42
1, 2	MDP* = 0.46 E <sub>LWD-Z2</sub> + 137.0	static, 0.85, and 1.87	37	0.35
1, 2	MDP* = -3.66 d <sub>LWD-Z2</sub> + 150.4		37	0.38
3	MDP* = 6.32 E <sub>LWD-Z2</sub> + 59.7		75	0.59
3	MDP* = -12.75 d <sub>LWD-Z2</sub> + 153.2		75	0.58
1	MDP* = 0.26 E <sub>LWD-K2</sub> + 136.7	1.87	8	0.74
1	MDP* = -4.26 d <sub>LWD-K2</sub> + 148.5		8	0.47
1	MDP* = 0.19 E <sub>LWD-D2</sub> + 138.2	1.87	8	0.62
1	MDP* = -5.82 E <sub>LWD-D2</sub> + 147.6		8	0.38
1, 2	MDP* = 1.39 γ <sub>d</sub> + 121.7	1.87	28	0.12
1, 2	MDP* = 1.75 γ <sub>d</sub> + 116.8	0.85	9	0.10
3	MDP* = 18.62 γ <sub>d</sub> - 187.14	0.85	5	0.74
3	— <sup>§</sup>	static	10	0.0
1, 2	MDP* = 1.37 γ <sub>d</sub> + 122.1	static, 0.85, and 1.87	39	0.10
3	MDP* = 10.13 γ <sub>d</sub> + 44.7		15	0.28
1, 2	MDP* = -0.19DPI <sub>300</sub> + 149.8	1.87	30	0.30
2	MDP* = -0.27DPI <sub>300</sub> + 152.3	0.85	7	0.33
1, 2	MDP* = -0.21DPI <sub>300</sub> + 150.3	0.85, 1.87	39	0.30
1, 2 <sup>¥</sup>	MDP* = 0.27 E <sub>LWD-Z2</sub> - 0.54 w + 150.0	0.85, and 1.87	39	0.48
1, 2 <sup>¥</sup>	MDP* = -0.55 DPI <sub>300</sub> - 0.11 w + 157.7		39	0.45
4 <sup>¥¥</sup>	CMV = 0.22 E <sub>LWD-Z2</sub> + 7.3	0.85	43	0.41
5	CMV = 0.22 E <sub>LWD-Z2</sub> + 7.3	0.85	10	0.84
4 <sup>¥¥</sup>	CMV = 12.85 (d <sub>LWD-Z2</sub> ) <sup>-0.36</sup>	0.85	43	0.31
5	CMV = 20.90 (d <sub>LWD-Z2</sub> ) <sup>-0.79</sup>	0.85	10	0.87
4 <sup>¥¥</sup>	— <sup>§</sup>	0.85	43	0.00
5	— <sup>§</sup>	0.85	10	0.00
5	— <sup>§§</sup>	0.85	10	0.00

<sup>§</sup>No correlation with γ<sub>d</sub>, <sup>§§</sup>No correlation with DPI<sub>300</sub>, <sup>¥</sup>amplitude was not statistically significant;

<sup>¥¥</sup> five data points excluded from regression (see discussion in text for test strip 4)

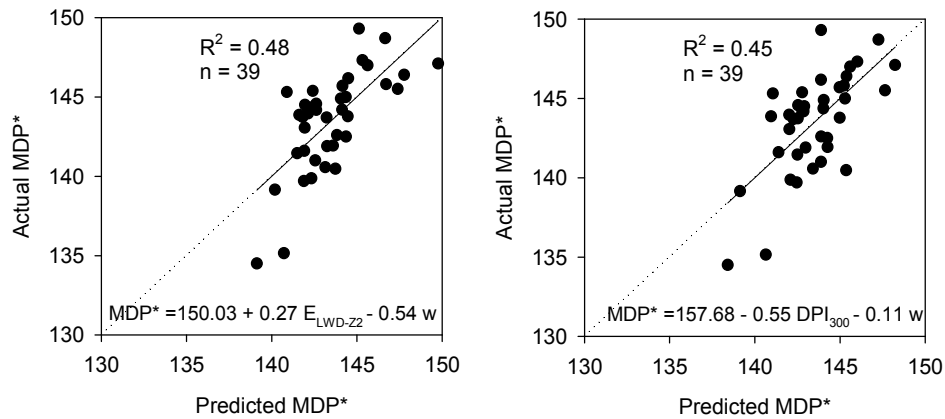
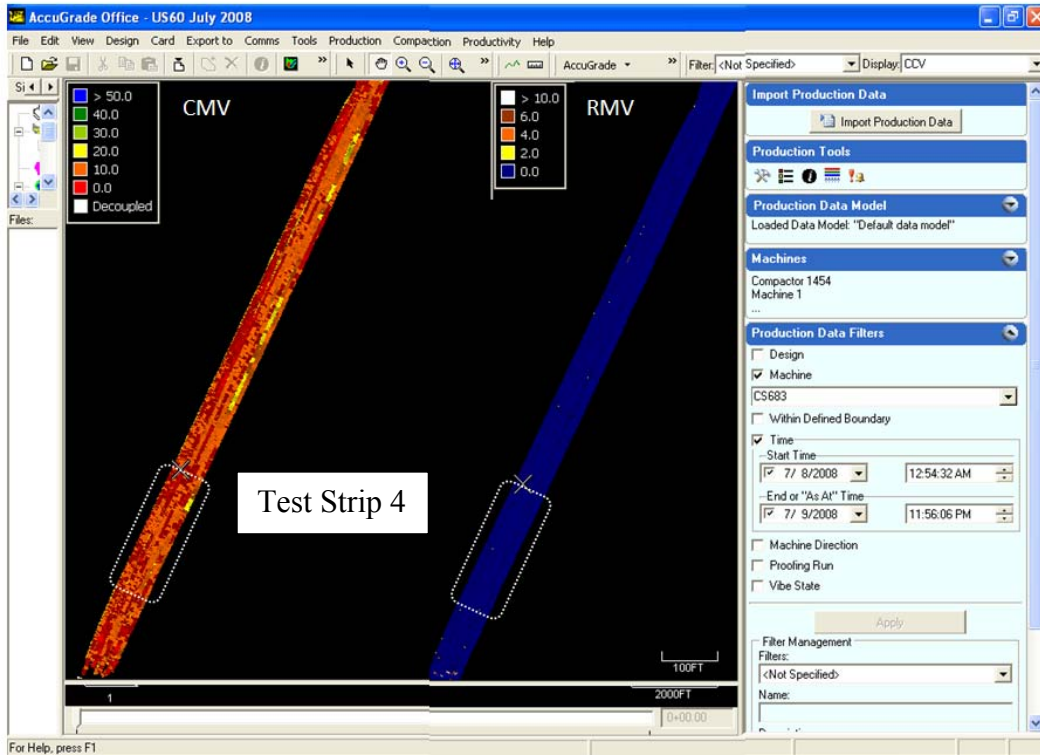


Figure 3.95. Multiple linear regression relationships incorporating moisture content in predicting MDP\* values

#### 3.5.4.5 Test strips 4 and 5

Test strip 4 was a production area on the project with plan dimensions of about 15.5 m x 764 m and 9 m x 39 m. Test strip 4 was compacted prior to our arrival at the project site with CP-663 roller. The area was first mapped using the CS-683 smooth drum roller at nominal  $a = 1.87$  mm,  $f = 30$  Hz, and  $v =$  km/h settings to smooth the area from padfoot indentations, and mapped again at nominal  $a = 0.85$  mm,  $f = 30$  Hz, and  $v =$  km/h settings. The measurements obtained from  $a = 0.85$  mm setting were used for analysis. 200-mm Zorn LWD and NG tests were conducted on the test area at 49 random test locations. Following mapping on test strip 4, the area was reportedly compacted using CP-663 roller and scraper traffic. The area was mapped the next day as test strip 5. Screen shots of CMV and RMV measurements from test strips 4 and 5 are shown in Figure 3.96. The CMV map of test strip 4 with point measurement locations and a photograph of the test area are shown on Figure 3.97. The production area CMV map shown in Figure 3.97 was split into two sections for better visualization of results. Also shown on Figure 3.97 are frequency distribution plots of CMV and in-situ point measurements.



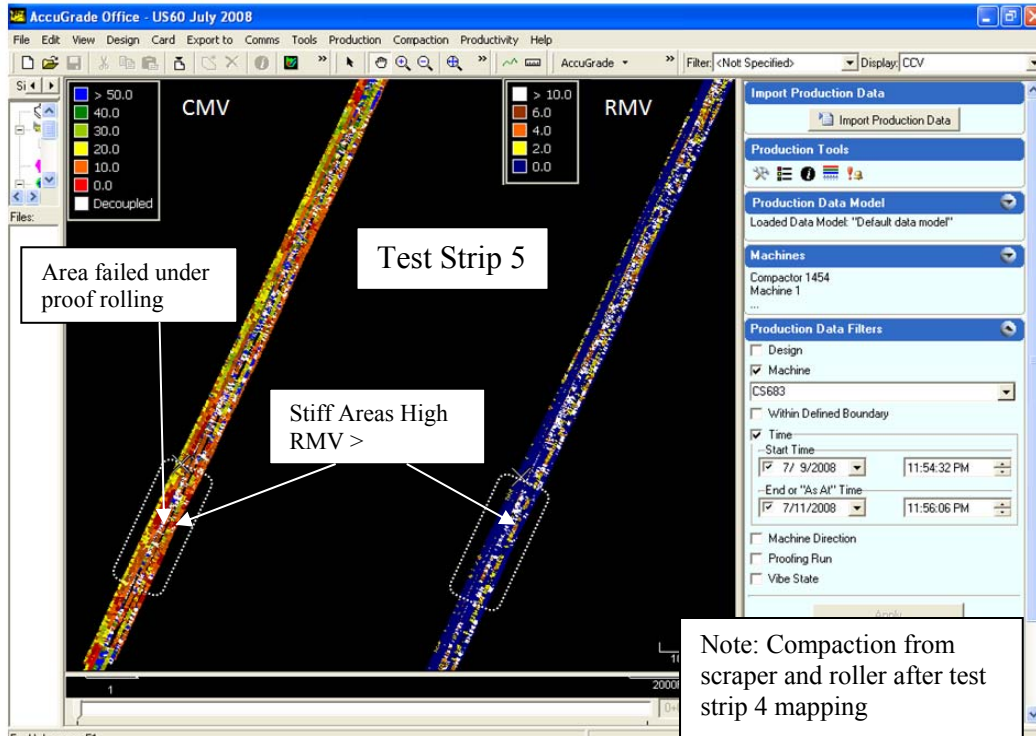


Figure 3.96. Screen shots from AccuGrade showing test strips 4 and 5 CMV and RMV maps

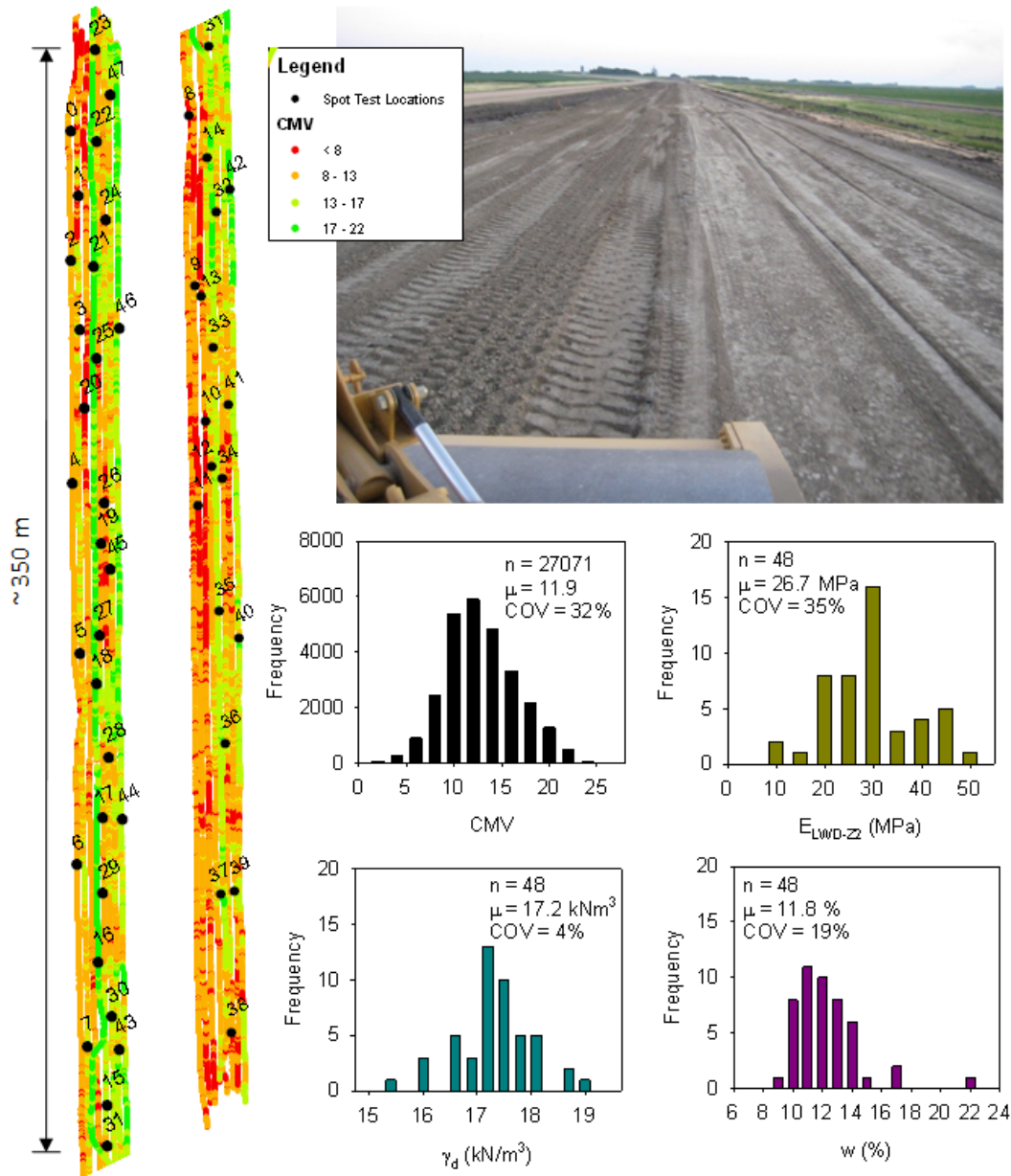


Figure 3.97. CMV map of test strip 4 ( $a = 0.85$  mm), photograph of the test area, and frequency distribution histograms of CMV and in-situ point measurements

A portion of test strip 5 was test rolled by the contractor in accordance with Mn/DOT 2111 specification. Following test rolling, the area was mapped using the CS-683 smooth drum roller with  $a = 0.85$  mm,  $f = 30$  Hz, and  $v =$  km/h nominal settings and 200-mm Zorn LWD, NG, and DCP measurements were obtained at 10 random test locations. The CMV map with point measurement locations and a photograph of the test area are shown on Figure 3.98. Few locations (near point measurement location 11) “failed” under test roller due to excessive ruts (rut depth measurements and analysis are presented later in Chapter 4). Prior to mapping, the



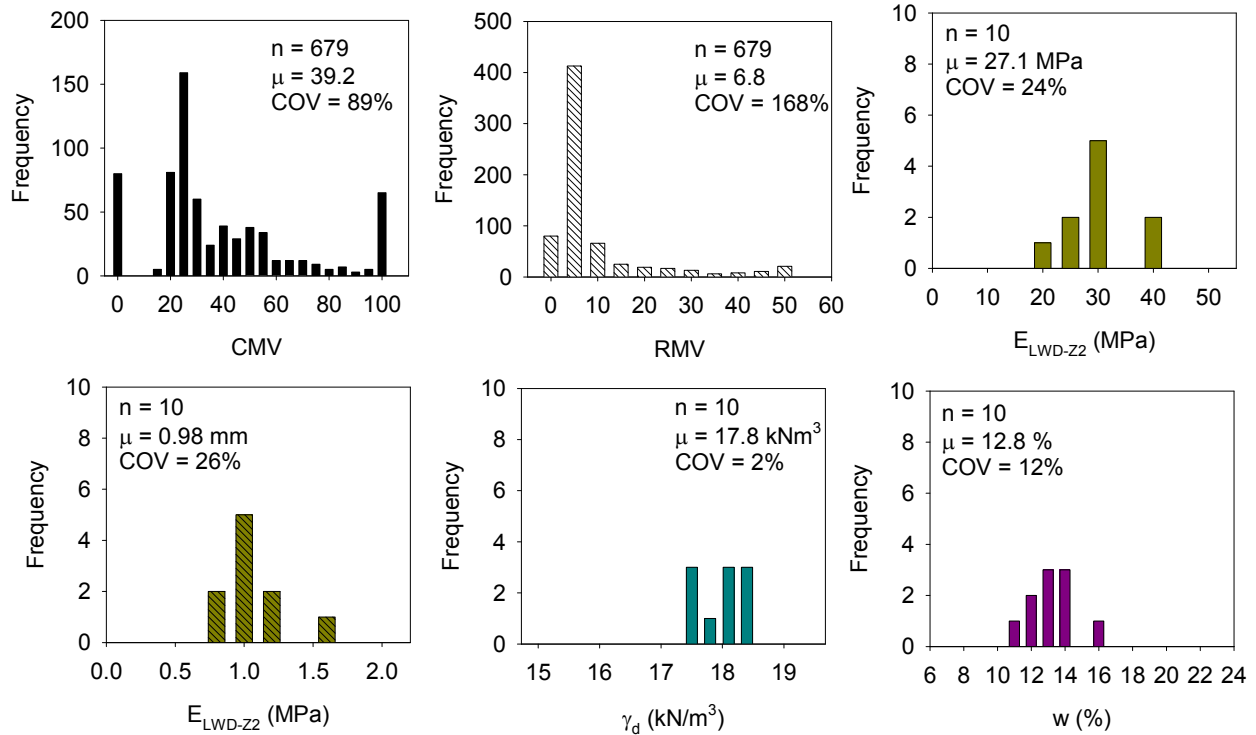


Figure 3.99. Frequency distribution histograms of CMV and in-situ point measurements from test strip 5

Regression relationships derived from experimental testing on test strips 4 and 5 are provided in Figure 3.100. These relationships were developed by spatially paring the nearest point data using GPS measurements. Five measurements from test strip 4 showed high  $E_{LWD-z2}$  corresponding to low CMV and were out of the general trend observed in the data. These measurements were excluded from the regression analysis as the low CMVs likely because of “weak” underlying layers at those locations. This was not confirmed, however. Additional tests (e.g., DCP) would be needed to further assess those locations. Relationships with  $\gamma_d$  and  $DPI_{300}$  did not show statistically significant correlations. The relationships presented in Figure 3.100 show separate trends between CMV and LWD measurements for test strips 4 and 5.

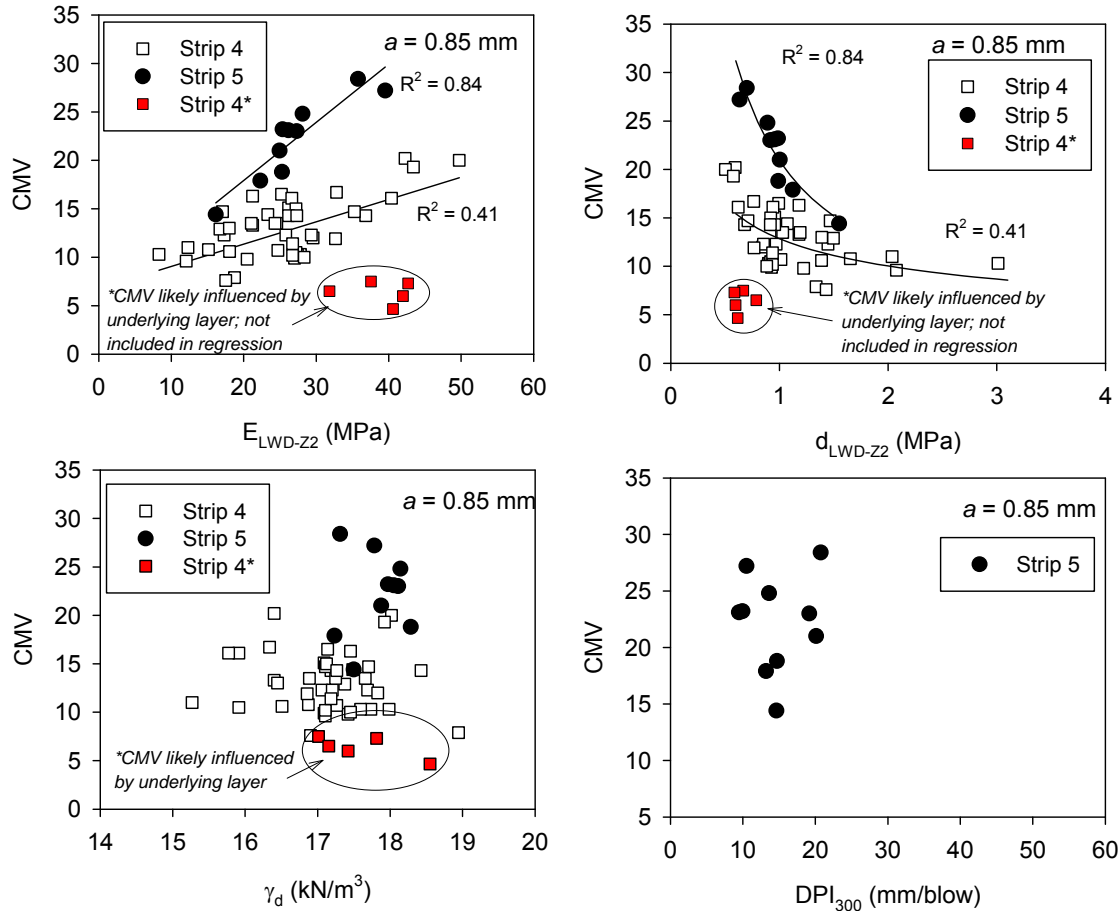


Figure 3.100. Linear regression relationships between CMV and in-situ point measurements

### 3.5.4.6 Correlations between different point measurements

Relationships between  $DPI_{300}$ ,  $E_{LWD-Z2}$ ,  $d_{LWD-Z2}$  and  $s_u$  derived from experimental testing from this project are summarized in Figure 3.101. A non-linear log relationship was developed between  $DPI$  and  $s_u$  and was developed based on UC tests performed on samples obtained from different depths at the DCP test locations from test strips 2 and 5. The relationship provides a good correlation with  $R^2 = 0.6$ . A similar relationship published by McElvanet and Djatnika (1991) for lime-stabilized materials is shown in Figure 3.101 for reference. Data obtained from this project fall slightly below the trend observed by McElvanet and Djatnika (1991).

Similarly, a non-linear log relationship was developed between  $E_{LWD-Z2}$  and  $DPI_{300}$  and a non-linear power relationship was developed between  $d_{LWD-Z2}$  and  $DPI_{300}$  with  $R^2 > 0.7$  (Figure 3.101). The relationships were developed based on data collected from test strips 2, 5, and 6. Test strip 6 was in a roadway median with organic material where comparison  $DPI_{300}$  and LWD measurements were obtained. Similar non-linear relationships between elastic modulus and  $DPI$  are reported by others (e.g. Chai and Roslie 1998).

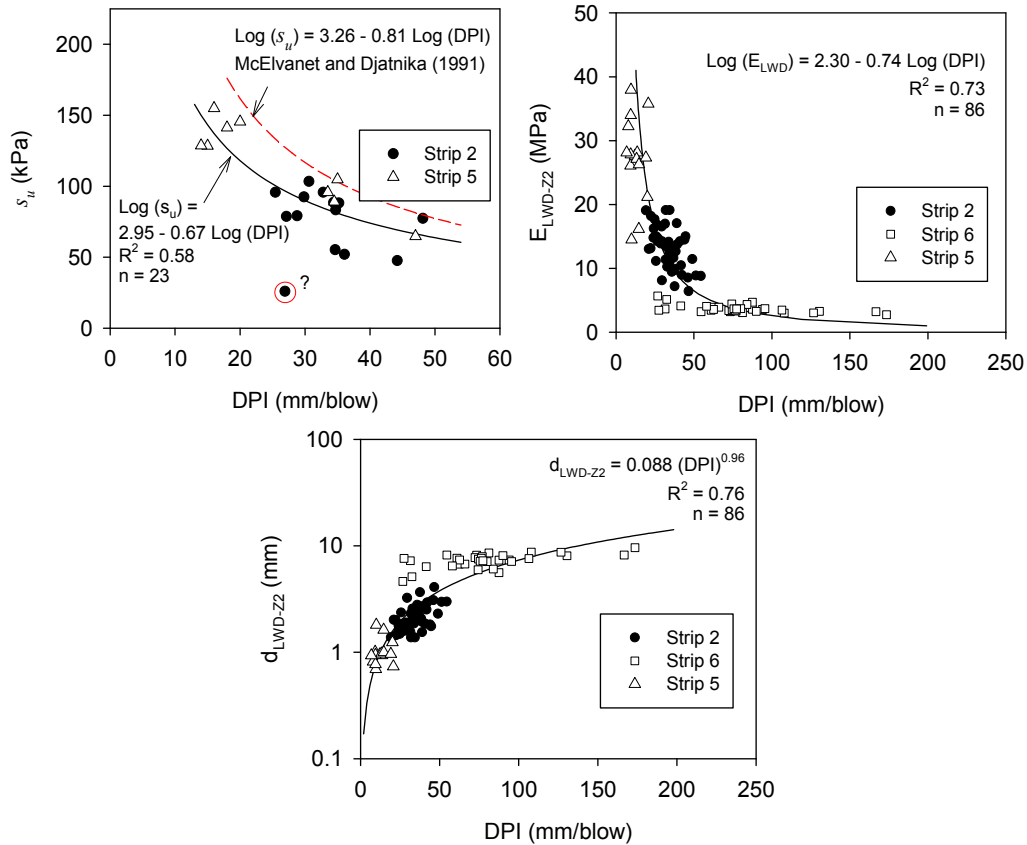


Figure 3.101. Relationships between DPI,  $s_u$ ,  $E_{LWD-Z2}$ , and  $d_{LWD-Z2}$

### 3.5.5 Stresses in Non-granular Subgrade Layer

Two piezoelectric EPCs of range 0-2500 kPa were installed in the test strip 2 subgrade layer after pass 8 to measure the vertical stress increase under roller pads and rear tires during compaction. The EPCs were placed in an excavated trench along the rear tire tracks of the machine (Figure 3.102) at a depth of about 0.15 m below surface and at a horizontal spacing of about 0.18 m apart. GPS measurements were obtained at the top of the sensors for exact location and elevation information of the sensors.

To represent the laboratory calibration conditions for EPCs approximately 50-mm thick layer of clean Ottawa #10 sand was placed above, below and around the EPCs installed in the excavation. The trench was then backfilled with hand-compacted fill material used on the test strip (see Figure 3.102). Later, seven roller passes were made on the test strip and the stress measurements associated with each pass is presented in Figure 3.103. The peak stresses measured are variable with each pass as it depends on location of the pad contact to the ground relative to the sensor location. Maximum stresses can be observed only if the pad is located directly on top of the sensor. Theoretical maximum stresses under the roller pad are calculated using the centrifugal

force applied by the roller (centrifugal force = 133 kN at  $a = 0.85$  mm), pad contact area ( $89.4 \text{ cm}^2$ ), and number of pads in contact with the soil (10 pads in a row).

Visual observations on the test strip indicated that the roller “walked” out after eight roller passes, which represents a no bearing capacity failure condition under the roller pads. Therefore, only 10 roller pads are assumed to be in contact with the soil and a theoretical maximum stress of about 1490 kPa (216 psi) is estimated under the roller pad. Hilf (1991) noted that bearing capacity failure under a sheepsfoot roller pad occurs at approximately 6 times (slight foot penetration) to 10 times (deep foot penetration) the shear strength of the material. Based on laboratory UCS strength, the average  $s_u$  of the samples obtained within the upper 300-mm depth of the compaction layer is 80 kPa. By assuming a factor of 6 the ultimate bearing capacity of the material is about 480 kPa, which is less than the maximum theoretical stress applied by the roller pad. This suggests that the material achieved sufficient compaction in the upper 300-mm for the roller to “walk” out. The maximum stresses measured by the EPCs were only about 350 kPa under the roller at pass 7 at about 15 cm below the roller. Variability in the maximum stress measurements are attributed to the location of roller pad relative to the sensor locations.

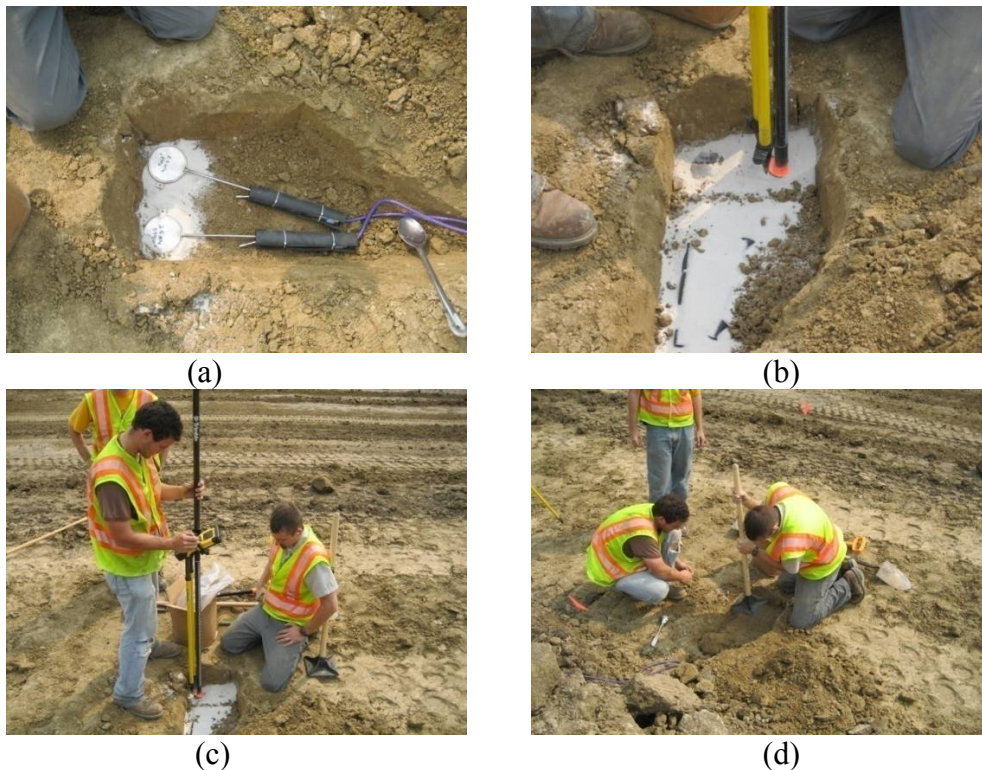


Figure 3.102. Installation of EPCs on test strip 2: (a) EPC placement in an excavated trench; (b) placement of thin clean sand layer; (c) GPS measurement on the top of EPC; (d) replacing the trench with hand-compacted fill material

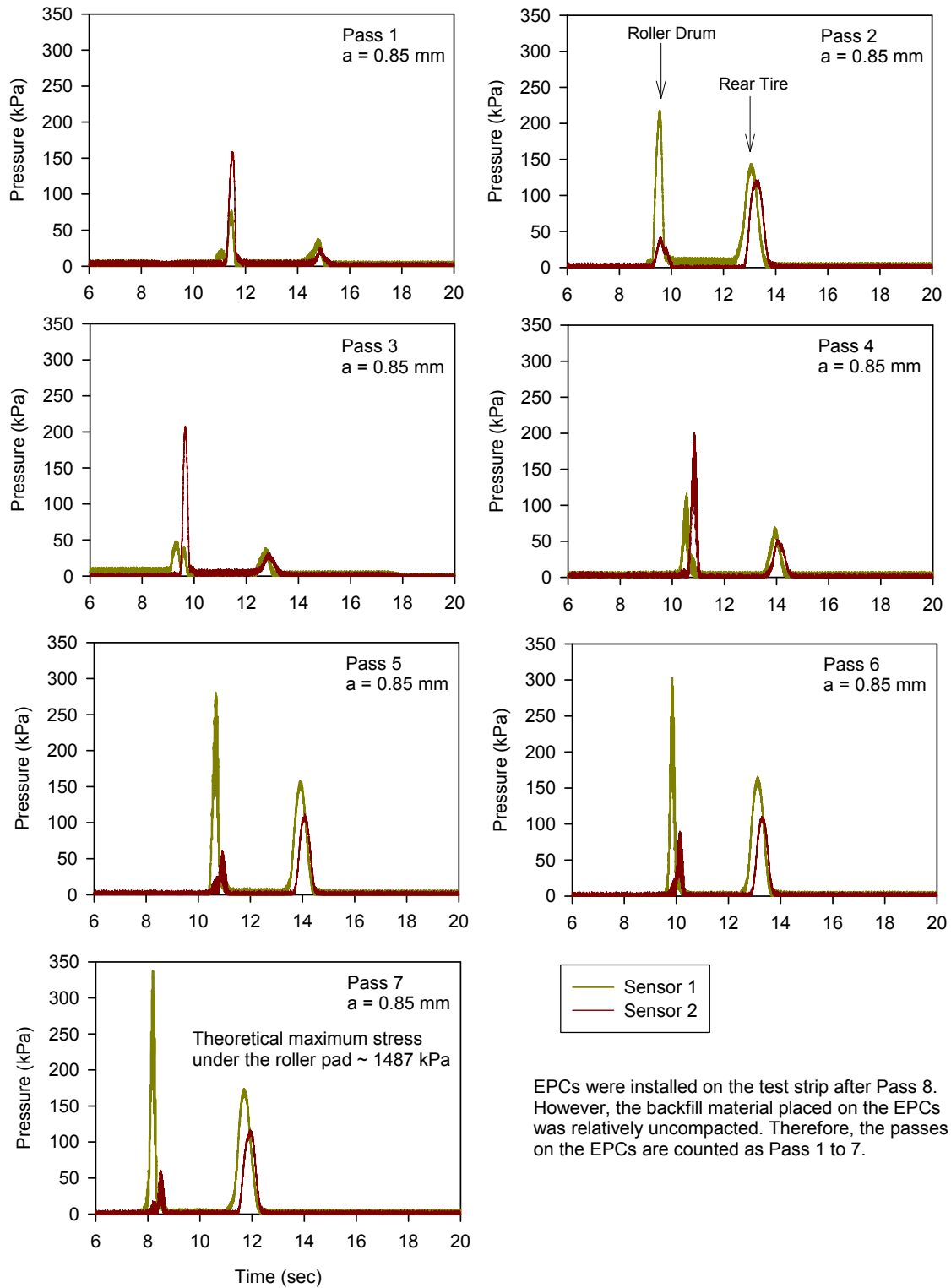


Figure 3.103. Vertical stress increase under roller at multiple passes

### 3.5.6 Discussion

MDP\* measurements demonstrated good repeatability in both  $a = 0.85$  and  $1.87$  mm settings and showed positive correlations with surface  $E_{LWD}$  and compaction layer DPI measurements. Statistical repeatability and reproducibility analysis results on the data are presented later in this chapter. The regression relationships between MDP\* and in-situ point measurements showed varying degrees of uncertainty with  $R^2$  values varying from about 0.3 to 0.8. This scatter is because of the various factors that generally influence the relationships including: (a) differences in stress states the material is subjected to under different loading conditions (a maximum contact stress of 340 kPa was recorded under roller pad while  $E_{LWD}$  measurements were obtained under contact stresses ranging from 100 to 200 kPa); (b) range of values over which measurements were obtained, (c) influence of moisture content, (d) position error from pairing point test measurements and IC-MV data, and (e) soil variability. Multiple regression analysis on test strips 1 and 2 measurements show that MDP\* measurements are sensitive to moisture content and that the regression relationships improve if moisture content is included in the analysis to predict MDP\* from  $E_{LWD}$  and DPI. Amplitude was not statistically significant in the multiple regression analysis. Relatively “weak” layers at depths below about 0.25 m on test strips 1 and 2 (as identified in DPI profiles) did not affect the MDP\* measurements. MDP\*- $E_{LWD-Z2}$  relationships showed separate trends for MDP\* values  $> 140$  and  $< 140$  in correlations with  $E_{LWD}$ . MDP\* values greater than about 140 were less sensitive with increasing compaction compared to values less than 140 (see Figure 3.92) and MDP\* values tend to reach an asymptotic value of 150 (Figure 3.92) (recall that  $MDP^* = 150$  was the maximum value set on the machine for a calibration hard surface). These separate trends in MDP\* present a challenge in implementing the QA requirement of production area meeting 90% to 120% of IC-TV as the limits are applicable only with a linear trend in MDP\* with increasing compaction.

Experimental results from test strips 1 and 2 indicate that although the test strips met the IC-TVs used on the project (i.e.,  $MDP^* = 138$ ), the  $E_{LWD-Z2}$  was often less than the LWD-TV (18 MPa). Moisture content measurements at several locations on test strips 1, 2, and 3 did not meet the Mn/DOT specifications (65% to 95% of  $w_{opt}$ ) at the time of testing. Comparisons to laboratory standard Proctor curves show that in-situ moisture contents were mostly close to or wet of the 95% of  $w_{opt}$ . Laboratory moisture-density-compaction energy relationships for these materials indicate that at such moisture contents applying additional compaction energy does not contribute to increasing relative compaction. Further, the DPI profiles at several test locations showed softer zones at the time of testing generally at about 0.25 m below the surface, which are a consequence of 0.3+ m thick loose lifts placed during compaction. Despite the use of these advanced technologies, proper control of construction methods in using appropriate lift thicknesses relative to the ability of the compaction equipment and effective moisture control are important to implement to obtain better results in the performance of the compacted embankment materials. Non-granular soils combined with poor weather conditions remain a challenge.

CMV and RMV from the CS-683 machine were evaluated on two production test strips. Regression relationships with  $E_{LWD-Z2}$  derived from experimental testing on test strips 4 and 5 showed good correlations but with separate trends for the two test strips. Statistically significant correlations were not developed with DPI and  $\gamma_d$  measurements, which is typical of

accelerometer based CMV measurements (see Thurner and Sandström 1980, Floss et al. 1991, NCHRP 21-09). Areas with low  $E_{LWD-Z2}$  values were well captured by low CMV measurements, however some stiff locations showed variable CMV measurements due to roller jumping as noticed with high RMV measurements. The effect of RMV on CMV is well-documented in the literature (see discussion in section 3.3 of this report); however, it lacked attention in a practical standpoint. It is important that the CMV measurements be evaluated in conjunction with RMV measurements for a meaningful interpretation.

### 3.5.7 Key Observations and Conclusions

- Test strips 1 and 2 met the IC-TV requirement of  $MDP^* = 138$ , but the minimum LWD-TV requirement of  $E_{LWD-Z2} = 18$  MPa did not at many test locations.
- $MDP^*$  measurements showed positive correlations with surface  $E_{LWD}$  and compaction layer DPI measurements. The regression relationships however showed varying degree of uncertainty with  $R^2$  values varied from about 0.3 to 0.8. Relationships between  $MDP^*$  and  $\gamma_d$  generally showed poor correlations ( $R^2 < 0.3$ ) with exception of one test strip with  $R^2 > 0.7$ . Soft or uncompacted zones at depths below about 0.25 m on tests strips 1 and 2 did not affect the  $MDP^*$  measurements.
- Regression relationships improve in predicting  $MDP^*$  from  $E_{LWD}$  and DPI when moisture content is included in the regression analysis ( $R^2$  value from 0.39 to 0.48 for  $E_{LWD}$  and 0.30 to 0.45 for DPI). This illustrates the sensitivity of soil moisture content in interpreting  $MDP^*$  values.
- Separate trends were observed in  $MDP^*$  correlations with  $E_{LWD}$  which present a challenge in implementing the QA requirement of production area meeting 90% to 120% of IC-TV as the limits are applicable only with one linear trend in the data with increasing compaction.
- At the time of testing in-situ moisture content measurements at several locations were wet of the upper 95%  $w_{opt}$  Mn/DOT specification limit. Laboratory moisture-density-compaction energy relationships indicate that at high moisture contents applying additional compaction energy does not increase the relative compaction value.
- The wrong throttle and gear settings used during roller operations invalidated IC measurement values for some sections. The roller manufacturer recommendation is that the roller should be operated at a high throttle and low gear setting during compaction operations.
- DCP profiles at several locations showed soft/uncompacted zones at about 0.25 to 0.3 m below the compaction layer surface which was a consequence of 0.3+ m thick lifts placed for compaction.
- DPI and  $s_u$  determined from UC testing on undisturbed samples, and surface  $E_{LWD}$  and compaction layer  $DPI_{300}$  are empirically correlated.

- Average resilient modulus  $M_r = 12.6$  MPa was measured on an undisturbed sample collected from the compacted subgrade. This value was comparable to the  $E_{LWD-Z2}$  value of 10.5 MPa obtained from the same point measurement location. (Note that the peak vertical applied stress under the Zorn 200-mm diameter plate LWD is about 200 kPa while the peak axial stress during the  $M_r$  test is about 69 kPa).
- Using multiple pass data from test strip 2 and performing statistical analysis, the MDP\* measurement error was characterized as 3.0 at  $a = 1.87$  mm and 1.8 at  $a = 0.85$  mm settings.
- No evidence of influence in vibration amplitude on MDP\* was for the material tested on tests strips 2 and 3. On test strip 3, the average MDP\* achieved on all lanes was almost the same by pass 8. The material was close to or wet of  $w_{opt}$ .
- CMV-  $E_{LWD-Z2}$  and CMV-  $d_{LWD-Z2}$  relationships derived from experimental testing on test strips 4 and 5 showed good correlations but with separate trends for the two test strips. Statistically significant correlations were not found with DPI and  $\gamma_d$ .
- Soft areas were well captured with low CMV, however some stiff locations showed variable CMV measurements due to roller jumping as noticed with high RMV measurements. It is important that the CMV measurements be evaluated in conjunction with RMV measurements for a meaningful interpretation.

## 3.6 CSAH 2, Olmsted County

### 3.6.1 Introduction

On September 5, 2008 a field visit was conducted to the CSAH 2 grading project in Olmsted County. The project had been in operation for several weeks and was part of an LWD implementation study conducted by Mn/DOT (see Siekmeier et al. 2009). The project created an opportunity to discuss progress with the roller operator in terms of how the IC machine was working and also to meet with Mn/DOT field personnel. In general, discussions were positive in the sense that the project was moving forward and IC technology was adding value to the project in terms of improving quality control. The roller operator mentioned that the IC-MVs were affected by machine speed and the slope of the grade. The ISU research team developed an experimental plan involving a detailed repeatability and reproducibility study on IC-MVs to evaluate machine operation parameters. LWD tests were also performed along the test strip at about 3 m intervals. Table 3.33 summarizes the experimental test plan, machine operations, and LWD testing. The test area consisted of non-granular material and the roller was operated in static and vibratory modes ( $a = 0.90$  and 1.80 mm) at two different speeds ( $v = 3.2$  and 6.4 km/h). Figure 3.104 shows the roller operations and LWD test preparation. Figure 3.105 shows the number of roller passes on the test strip, elevation profile, and corresponding IC-MVs for the full number of measurements passes.

Table 3.33. Summary of roller passes – Olmsted County project

Test Strip	Pass	$a$ (mm)	$v$ (km/h)	Direction	Point Measurements
1	1, 3, 5, 7	Static	3.2	East to West	LWD @ 5 locations after pass 16
	2, 4, 6, 8			West to East	
	9, 11, 13, 15		6.4	East to West	
	10, 12, 14, 16			West to East	
2	1, 3, 5, 7	0.90	3.2	East to West	LWD @ 8 locations after pass 16 [three measurements across the drum width at each test location]
	2, 4, 6, 8			West to East	
	9, 11, 13, 15		6.4	East to West	
	10, 12, 14, 16			West to East	
	17, 19, 21, 23	1.80	3.2	East to West	
	18, 20, 22, 24			West to East	
	25, 27, 29, 31		6.4	East to West	
	26, 28, 30, 32			West to East	



Figure 3.104. IC padfoot roller (left) and LWD test preparation (right) by excavating to bottom of padfoot penetrations

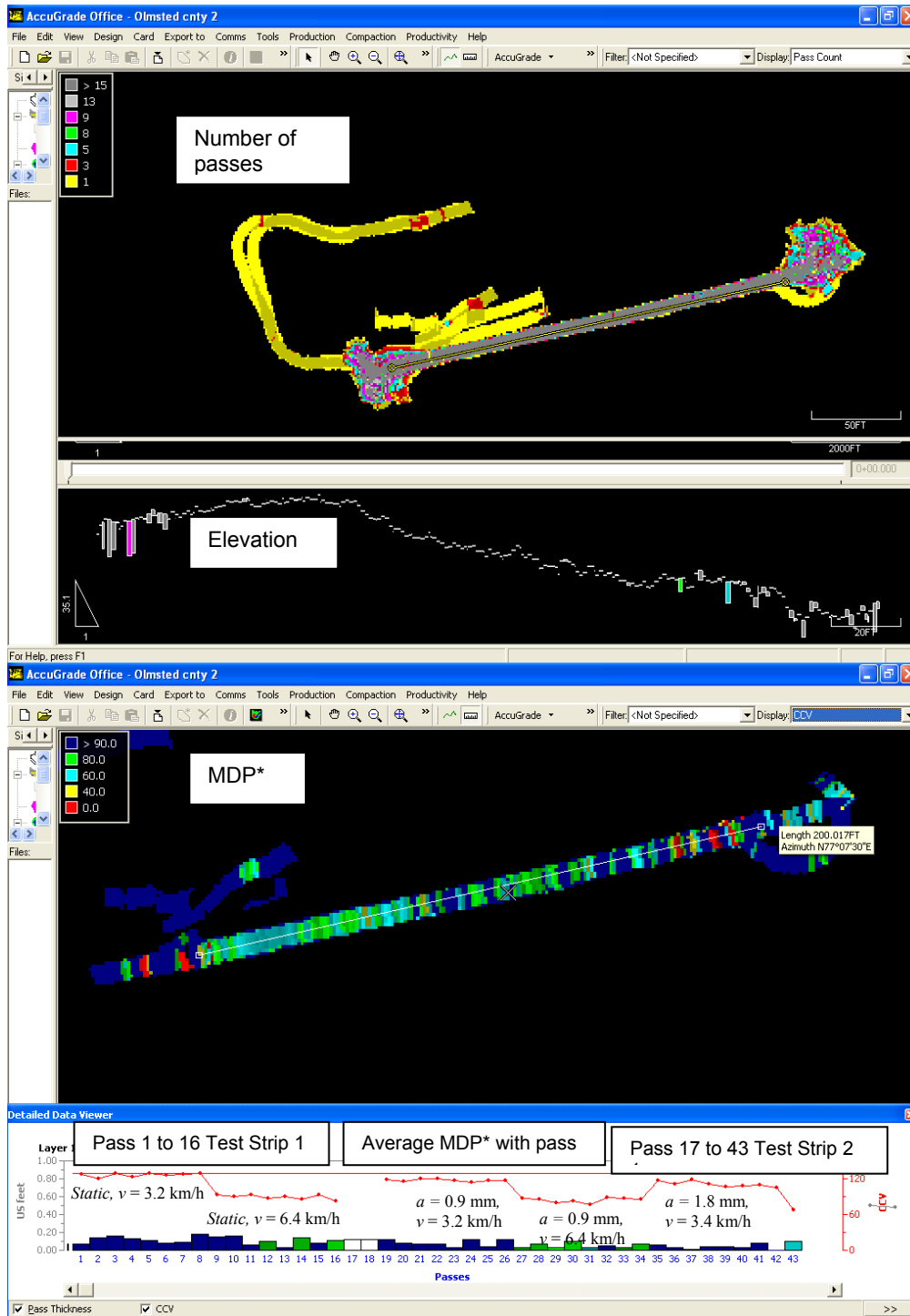


Figure 3.105. AccuGrade screenshots from Olmsted County test strips 1 and 2 showing number of passes, elevation, MDP\*, and average MDP\* (shown as CCV) with pass

### 3.6.2 Analysis of Results

Figure 3.106 provides the average MDP\* value for each roller pass with respect to travel direction (east or west), vibration mode, and travel speed. Roller passes alternated east to west between each pass. Results show that the MDP\* values were influenced by travel direction (e.g. slope), speed, and vibration setting. Figure 3.107 provides the elevation along the length of the test strip, which equates to about 0.2 m elevation change over 45 m length. Inspection of the results shows that the MDP\* values are comparatively higher in the uphill travel direction. Figure 3.108, Figure 3.109, and Figure 3.110 provide the MDP\* results along the length of the test strip for select pass numbers. Results show that the MDP\* values provide an out of phase interference that corresponds to travel direction and likely localized slope changes. Figure 3.111 shows the regression relationship between MDP\* and travel direction indicating that from a statistical standpoint (as assessed by *t*- and *p*-values), travel direction impacts the measurement values. Figure 3.112 and Figure 3.113 shows relationships between MDP\* for each machine operation mode and  $E_{LWD-Z2}$  and  $d_{LWD-Z2}$  measurement values. Overall, strong statistical correlations exist, but again the relationships are closely linked to machine operations. This finding is of consequence for on-site calibration and target value determination. In an attempt to develop a more robust calibration, the described machine operation parameters were lumped into a multiple regression model that include machine speed, vibration amplitude, and travel direction. The results are presented in Figure 3.114 and Table 3.35. Findings show that a model can be developed to account for these factors; however, it is preferable that these factors be controlled through upfront machine calibrations and internal machine compensations.

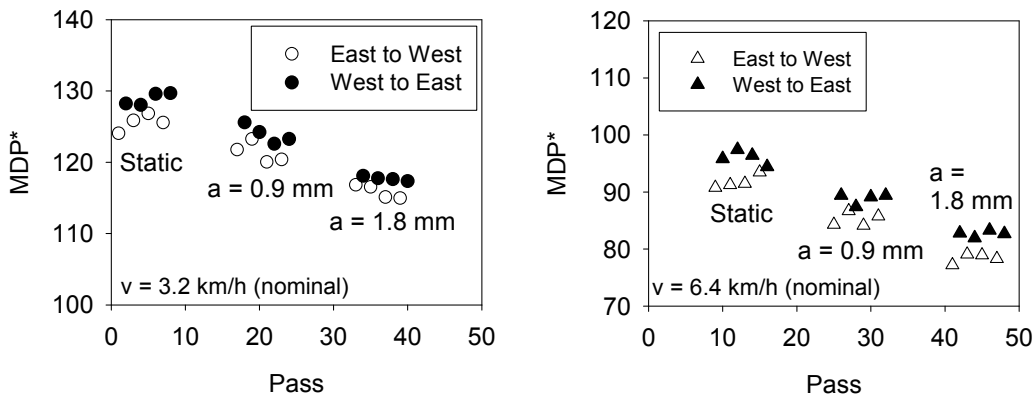


Figure 3.106. Influence of roller operation direction, amplitude and speed settings on average MDP\*

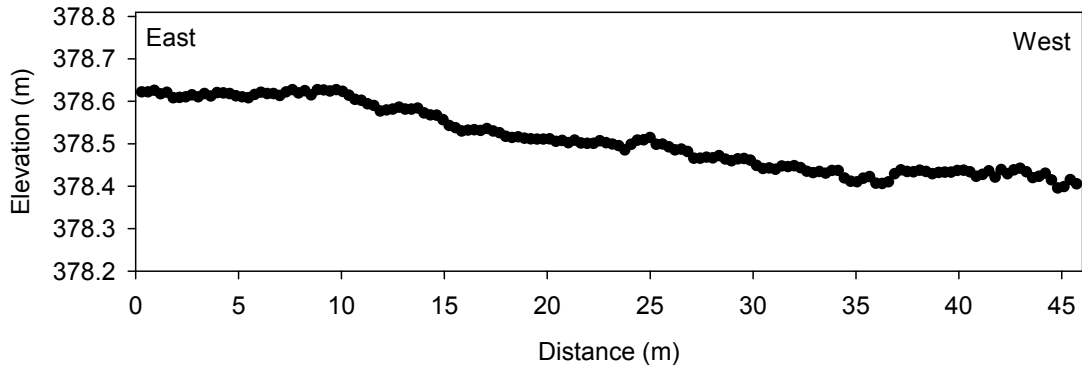


Figure 3.107. Elevation change across the test strip – Olmsted County

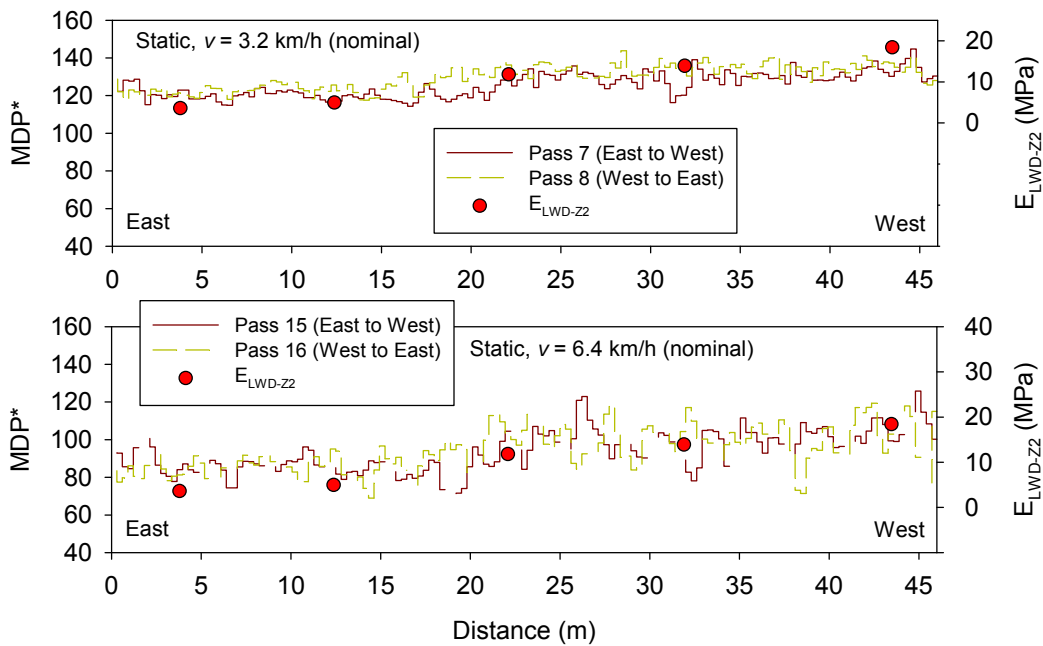


Figure 3.108. Comparison of MDP\* with  $E_{LWD-zz}$  measurements (one point measurement at the center of the drum) – Test strip 1 ( $a = \text{static}$  and  $v = 3.2$  km/h and 6.4 km/h)

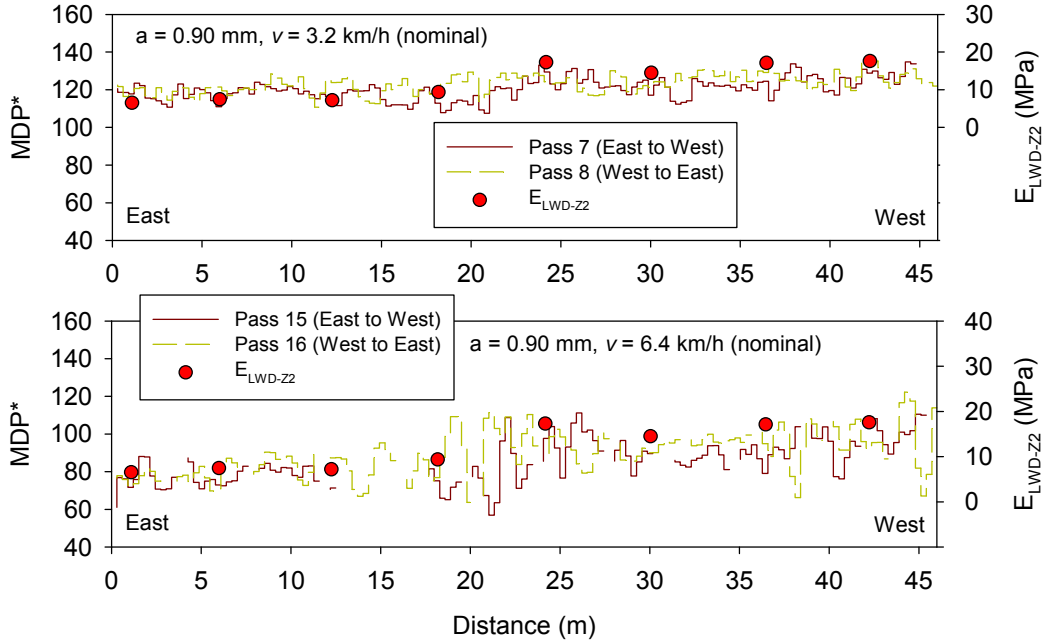


Figure 3.109. Comparison of MDP\* with  $E_{LWD-zz}$  measurements (one point measurement at the center of the drum) – Test strip 2 ( $a = 0.90$  mm and  $v = 3.2$  km/h and  $6.4$  km/h)

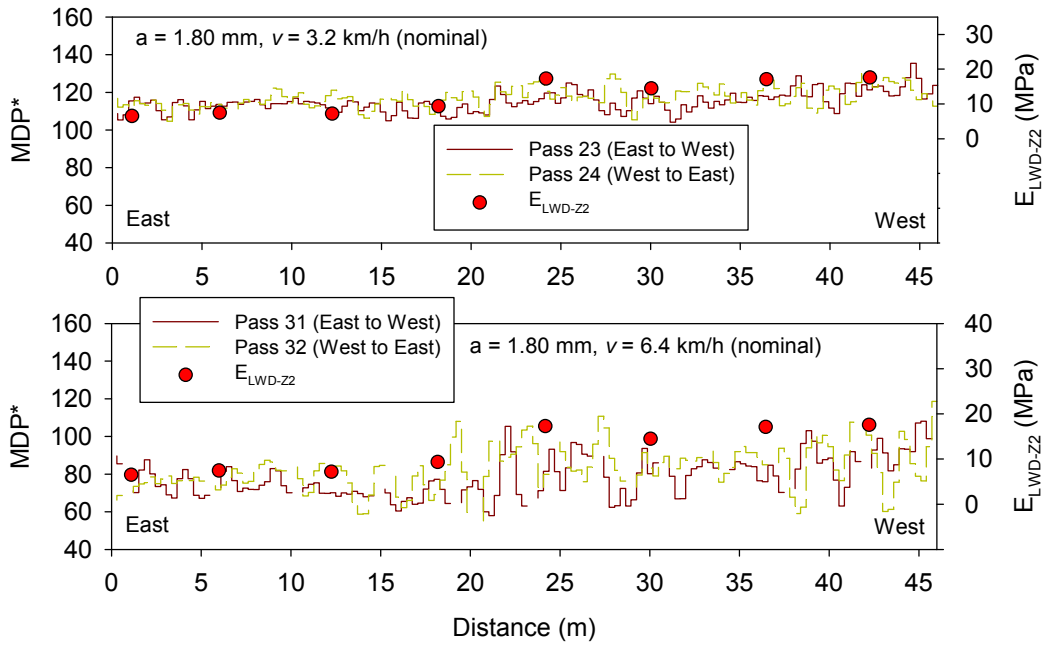


Figure 3.110. Comparison of MDP\* with  $E_{LWD-zz}$  measurements (one point measurement at the center of the drum) – Test strip 2 ( $a = 1.80$  mm and  $v = 3.2$  km/h and  $6.4$  km/h)

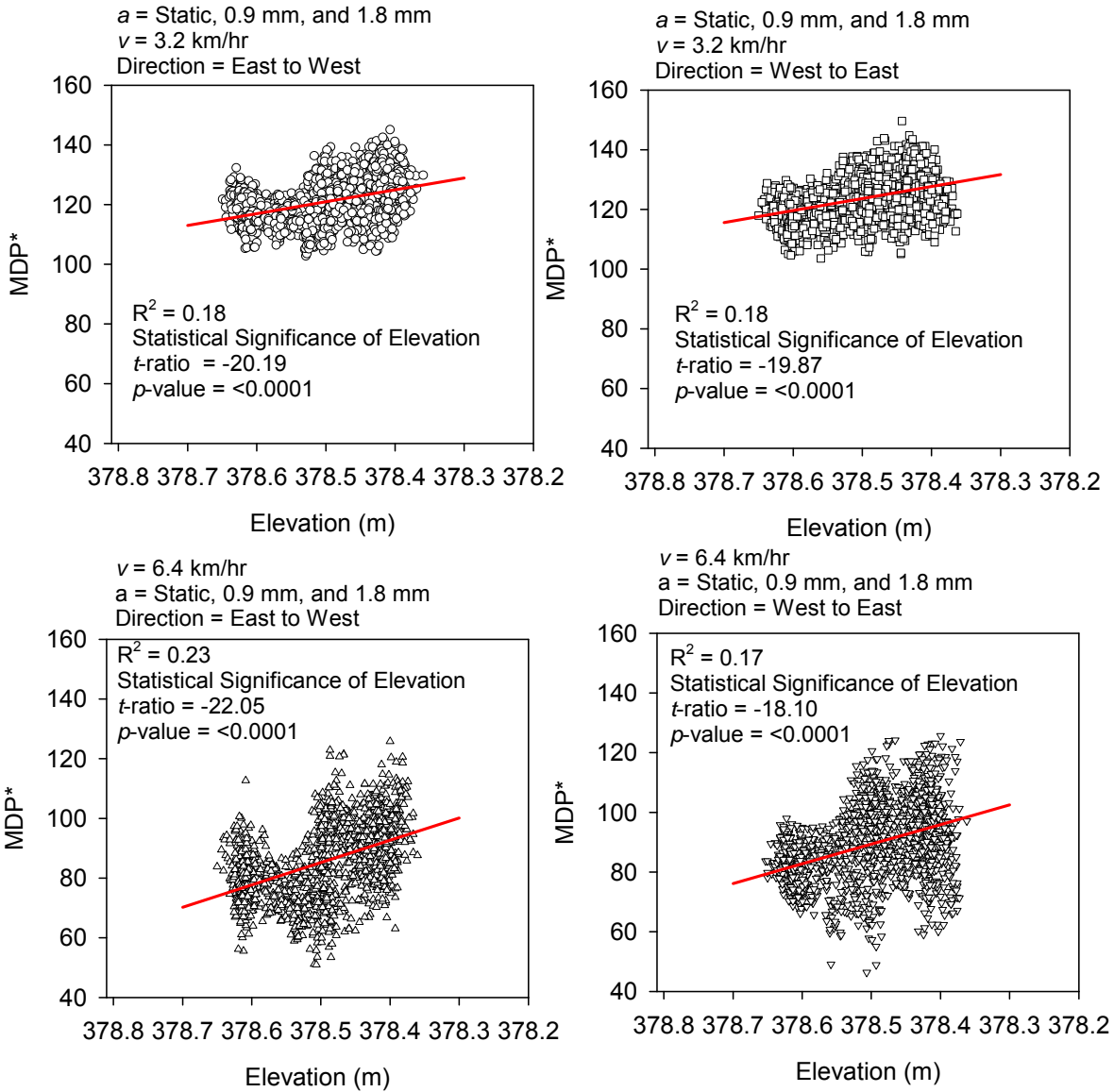


Figure 3.111. Effect of change in elevation on MDP\* values

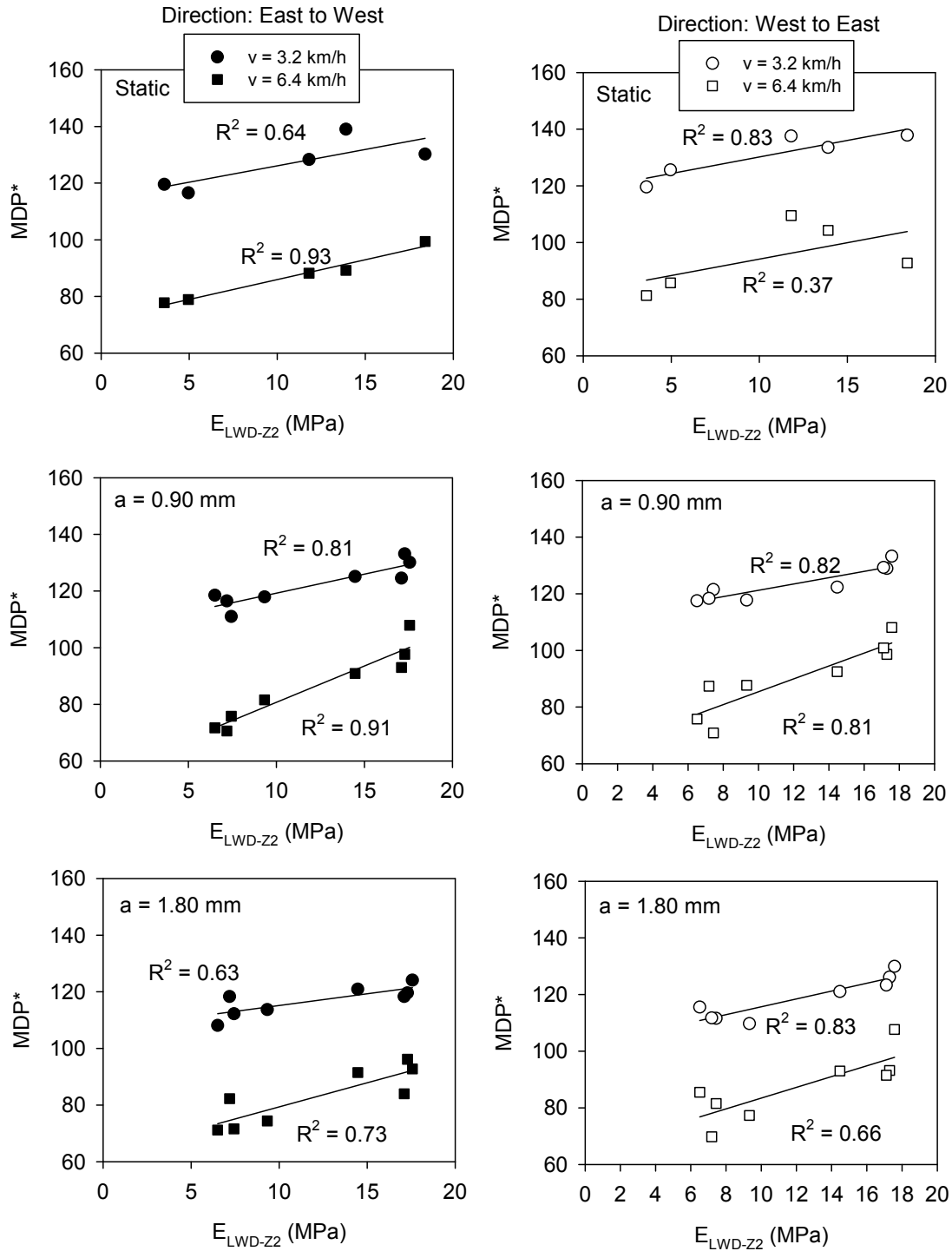


Figure 3.112. Simple linear regression relationships ( $E_{LWD-Z2}$  and  $MDP^*$ ) – Olmsted County data

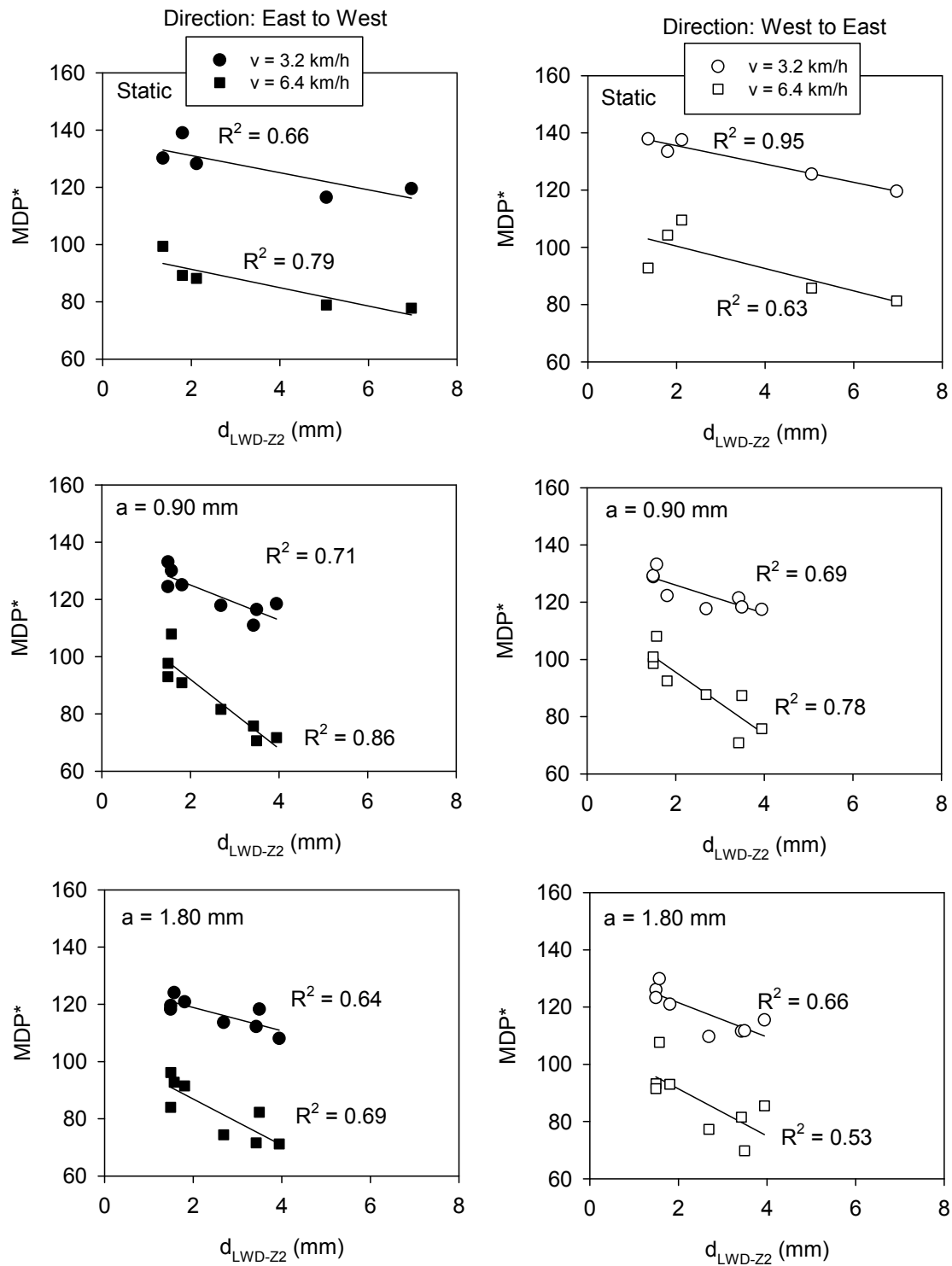


Figure 3.113. Simple linear regression relationships ( $d_{LWD-Z2}$  and  $MDP^*$ ) – Olmsted County data

Table 3.34. Summary of regression relationships – Olmsted County project

Test strip	Relationship	$a$ (mm)	Direction	$v$ (km/h)	$n$	$R^2$
1	$MDP^* = 114.6 + 1.15 E_{LWD-Z2}$	Static	East to West	3.2	5	0.64
	$MDP^* = 137.1 - 3.00 d_{LWD-Z2}$	Static	East to West	3.2	5	0.66
	$MDP^* = 118.5 + 1.17 E_{LWD-Z2}$	Static	West to East	3.2	5	0.83
	$MDP^* = 141.9 - 3.20 d_{LWD-Z2}$	Static	West to East	3.2	5	0.95
	$MDP^* = 72.0 + 1.40 E_{LWD-Z2}$	Static	East to West	6.4	5	0.93
	$MDP^* = 97.8 - 3.21 d_{LWD-Z2}$	Static	East to West	6.4	5	0.79
	$MDP^* = 82.5 + 1.16 E_{LWD-Z2}$	Static	West to East	6.4	5	0.37
	$MDP^* = 108.3 - 3.91 d_{LWD-Z2}$	Static	West to East	6.4	5	0.63
2	$MDP^* = 105.8 + 1.34 E_{LWD-Z2}$	0.90	East to West	3.2	8	0.81
	$MDP^* = 137.3 - 6.11 d_{LWD-Z2}$	0.90	East to West	3.2	8	0.71
	$MDP^* = 110.1 + 1.11 E_{LWD-Z2}$	0.90	West to East	3.2	8	0.82
	$MDP^* = 135.9 - 4.93 d_{LWD-Z2}$	0.90	West to East	3.2	8	0.69
	$MDP^* = 55.0 + 2.57 E_{LWD-Z2}$	0.90	East to West	6.4	8	0.91
	$MDP^* = 116.3 - 12.10 d_{LWD-Z2}$	0.90	East to West	6.4	8	0.86
	$MDP^* = 62.7 + 2.27 E_{LWD-Z2}$	0.90	West to East	6.4	8	0.81
	$MDP^* = 117.2 - 10.82 d_{LWD-Z2}$	0.90	West to East	6.4	8	0.78
	$MDP^* = 106.8 + 0.83 E_{LWD-Z2}$	1.80	East to West	3.2	8	0.63
	$MDP^* = 127.0 - 4.07 d_{LWD-Z2}$	1.80	East to West	3.2	8	0.64
	$MDP^* = 101.8 + 1.38 E_{LWD-Z2}$	1.80	West to East	3.2	8	0.83
	$MDP^* = 133.5 - 5.99 d_{LWD-Z2}$	1.80	West to East	3.2	8	0.66
	$MDP^* = 62.3 + 1.70 E_{LWD-Z2}$	1.80	East to West	6.4	8	0.73
	$MDP^* = 103.1 - 8.07 d_{LWD-Z2}$	1.80	East to West	6.4	8	0.69
	$MDP^* = 64.4 + 1.9 E_{LWD-Z2}$	1.80	West to East	6.4	8	0.66
	$MDP^* = 107.9 - 8.22 d_{LWD-Z2}$	1.80	West to East	6.4	8	0.53

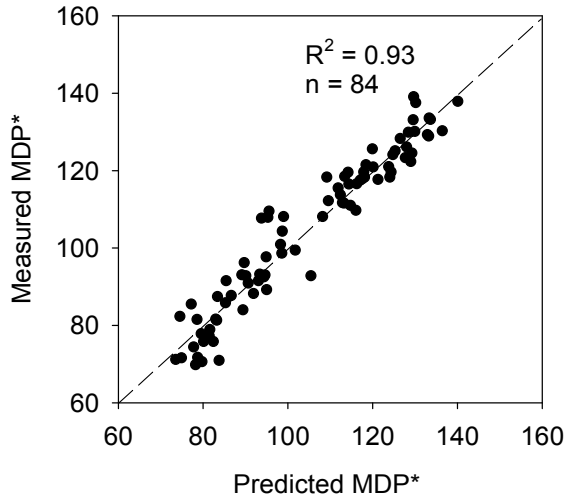


Figure 3.114. Results of multiple regression analysis incorporating speed, direction, amplitude, and  $E_{LWD-Z2}$  as prediction parameters

Table 3.35. Summary of multiple regression analysis – Olmsted County data

Relationship	Term	Estimate	Std Error	<i>t</i> Ratio	Prob > <i>t</i>	$R^2$
$MDP^* = b_0 + b_1 E_{LWD-Z2} + b_2 a + b_3 (\text{Direction}) + b_4 v$	$b_0$	139.8	3.04	45.95	< 0.0001	0.93
	$b_1$	1.50	0.12	12.33	< 0.0001	
	$b_2$	-5.78	0.86	-6.72	< 0.0001	
	$b_3$	3.68	1.19	3.09	0.0027	
	$b_4$	-10.83	0.37	-29.13	< 0.0001	

Note: For direction, a numerical value of 1 – East to west and 2 – West to East was used; parameters with  $t < -2$  or  $> 2$ , and  $p < 0.05$  are statistically significant.

### 3.6.3 Key Observations and Conclusions

The key findings from the Olmsted County project were as follows:

- The project was progressing well and feedback from the roller operator and Mn/DOT field personnel was that the IC roller was bringing value to the construction operations and QA/QC operations.
- The roller operator comments on the machine operations (velocity, amplitude, and travel direction) affecting the MDP values.
- A detailed test strip study and statistical analysis demonstrated that machine operation parameters and travel direction are statistically significant parameters and should be accounted for when developing target values.
- The  $E_{LWD}$  values were strongly correlated to the MDP\* values at this site.

### 3.7 Repeatability and Reproducibility of IC-MVs

Variability in IC-MVs is believed to be one source of scatter in relationships with in-situ point measurements. The measurement variability is quantified in this section in a repeatability and reproducibility context for MDP\*, CMV, and RMV measurements. Repeatability refers to variation observed in the measurement values (also referred to as measurement error) obtained over a test area from consecutive passes under identical operating conditions (i.e., using same operator, amplitude, speed, direction of travel, etc.). Reproducibility refers to the variation in measurements obtained from consecutive passes under changing conditions. The changing conditions may be due to different measurement methods, machines used, operators, or speed and amplitude settings (see section 3.6 above).

Data obtained from TH60 test strip 2 (MDP\*), Olmsted County test strips 1 and 2 (MDP\*), and TH36 test strip 4 (CMV/RMV) were analyzed. In this study, the repeatability variation was quantified from repeated passes made using a single operator maintaining constant amplitude and speed settings, and direction of travel during operation. The reproducibility variation was determined from repeated measurements using a single operator by changing amplitude, or speed, or direction of travel.

#### 3.7.1 Analysis Approach

One challenge with evaluating repeatability of roller measurement values is that the data points obtained from different passes are not collected at the exact same location. To overcome this problem, the data was processed in such a way that an average data is assigned to a preset grid point along the roller path. The grid point was set at 0.3 m along the roller path which represented an average of IC-MVs that falls within a window of size 0.15 m in forward and backward directions (the actual data was reported every 0.15 to 0.3 m). To validate the approach, an example dataset comparing the average and actual values is presented in Figure 3.115 based on data collected from TH60 test strip 2. The figure shows excellent agreement between the actual and average values. Following the same procedure, roller data used for the analysis were filtered and organized using a customized VB program called as *IC-REPEAT* developed at Iowa State University.

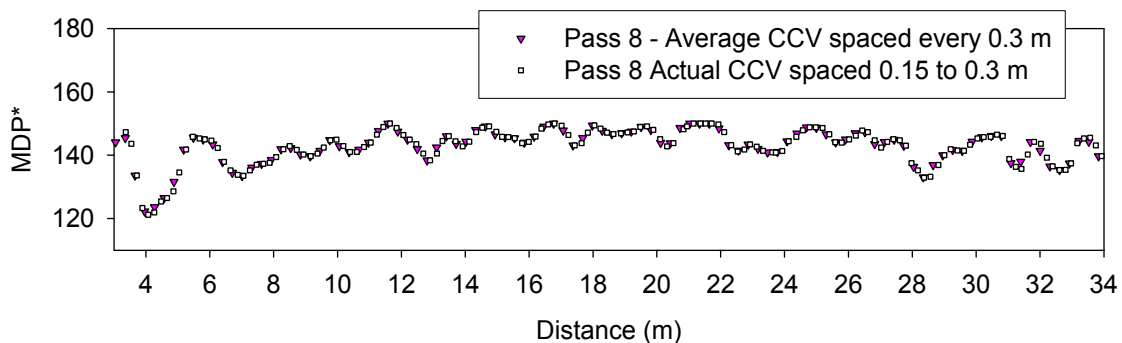


Figure 3.115. Comparison of averaged MDP\* data from Iowa State University VB IC repeatability algorithm (spacing 0.3 m) and actual MDP\* data – TH60 test strip 2

Repeatability analysis was performed on measurements obtained from several consecutive passes (at least three passes) under identical operating conditions (i.e., same amplitude, nominal speed, and direction). Although repeated passes were performed on “compacted” surfaces, some systematic change in soil properties with each pass is expected. Therefore, the effect of pass on IC-MVs was also considered in the analysis. This was accomplished by performing Two-Way Analysis of Variance (ANOVA), by taking both pass and measurement location as random effects (Vardeman and Jobe 1999). The parameter of interest from this analysis is the root mean squared error ( $\sqrt{MSE}$ ) which represents the measurement error (also called as  $\sigma_{\text{repeatability}}$ ). Procedure for calculating  $\sigma_{\text{repeatability}}$  is provided in Appendix D.

Reproducibility analysis was performed on measurements obtained from several passes with change in operating conditions,  $\sigma_{\text{reproducibility}}$  (i.e., change in amplitude, speed, and direction of travel). Each change in operating condition is treated separately to evaluate its influence on the overall variability. Similar to described above, increasing pass would have some systematic effect on the measurement values. One way to approach this is to include pass effect into the ANOVA along with the measurement location and operating condition effects. This would involve performing a Three-Way ANOVA. An alternate approach is to check statistical significance of the pass effect on the IC-MVs. If the pass effect is statistically insignificant (as assessed by statistical  $t$ -ratio and  $p$ -value), then it is justified to perform the ANOVA without including the pass effect. For the data analyzed, data obtained from at least three consecutive passes with negligible pass effect were selected. Procedure for calculating  $\sigma_{\text{reproducibility}}$  from a Two-Way ANOVA results are provided in Appendix D. Further,  $\sigma_{\text{R\&R}}$  which is a measure of overall variability (the two R’s represent repeatability and reproducibility) is calculated using Equation 3.1 (Vardeman and Jobe 1999). To quantitatively consider that there is no effect of change in operating conditions on the roller measurement values, the contribution of  $\sigma_{\text{reproducibility}}$  to the overall variability  $\sigma_{\text{R\&R}}$  should be about 50% (i.e.,  $\sigma_{\text{reproducibility}} \sim \sigma_{\text{repeatability}}$ ) or less.

$$\sigma_{\text{R\&R}} = \sqrt{\sigma_{\text{repeatability}}^2 + \sigma_{\text{reproducibility}}^2} \quad (3.1)$$

### 3.7.2 Analysis Results and Discussion

TH60 test strip 2 MDP\* data from consecutive passes at  $a = 1.87$  and  $0.85$  mm settings (nominal  $v = 3.2$  km/h) are presented in Figure 3.116. Olmsted county MDP\* data obtained consecutive passes at  $a = \text{static}$ ,  $0.90$ , and  $1.80$  mm settings are presented in Figure 3.117, Figure 3.118, and Figure 3.119 respectively. TH36 test strip 4 CMV and RMV data was presented earlier in Figure 3.12. Repeatability analysis results for the data is summarized in Table 3.36 and R&R analysis results are summarized in Table 3.37. Following are some key points based on the analysis:

Repeatability Analysis:

- The MDP\* results appear repeatable with measurement error in the range of 2 to 4 from the Olmsted County data and 2 to 3 from the TH60 data when operated at a nominal

speed of 3.2 km/h. The results show relatively high measurement error in the range of 4 to 14 when operated at 6.4 km/h nominal speed.

- The CMV results also appear repeatable with measurement error  $< 3$ . Similar measurement error value was estimated by White et al. (2009) based on data obtained on compacted granular base material.

#### R&R Analysis:

- The MDP\* results from TH60 project show that the values are reproducible with change in amplitude (from  $a = 0.85$  to  $1.87$  mm). In contrast, the results from Olmsted County project show that the values are not reproducible with change in amplitude (from  $a =$  static to  $1.80$  mm). A study conducted by White et al. (2009) also indicated that MDP values are influenced by change in amplitude.
- Similarly, results from Olmsted County indicate that MDP\* is generally not reproducible with change in direction of travel and speed (from 3.2 to 6.4 km/h).

Considering the nature of MDP\*, CMV and RMV calculation procedures and the various factors that influence their calculations, the estimated repeatability variations when operated at a nominal speed of  $v = 3.2$  km/h is considered minimal. Measurement error is greater for MDP\* when operated at nominal  $v = 6.4$  km/h, and therefore, should be avoided. CMV was not evaluated at different speeds in this study. However, study conducted by White et al. (2009) indicated that CMV is reproducible with variation in nominal speeds between 3.2 and 4.8 km/h. MDP\* and CMV (see White et al. 2009) obtained at different amplitude settings must be treated separately as they are not reproducible. MDP\* measurements are affected by travel direction, especially when the ground slope changes with direction (i.e., driving uphill or downhill). Olmsted County test strip showed sloping down from E-W direction (see Olmsted County case history discussion), the results were affected by the slope, and therefore, were not reproducible for change in direction.

Currently, there are no specifications on the acceptable limits of measurement error for the roller measurement values. However, it should be considered as an important element of the specification for evaluating the usefulness of a machine prior to its use or even periodically during the course of project, which will help build confidence in the measurements. The repeatability and reproducibility analysis procedure outlined in this section is applicable for any IC technology. As observed in the results above, the magnitude of measurement error (for the range of IC-MVs) is different for different IC-MVs. This is of consequence in a specification standpoint as it affects the regression relationships and anticipated variability in MVs. This is further addressed in Chapter 7.

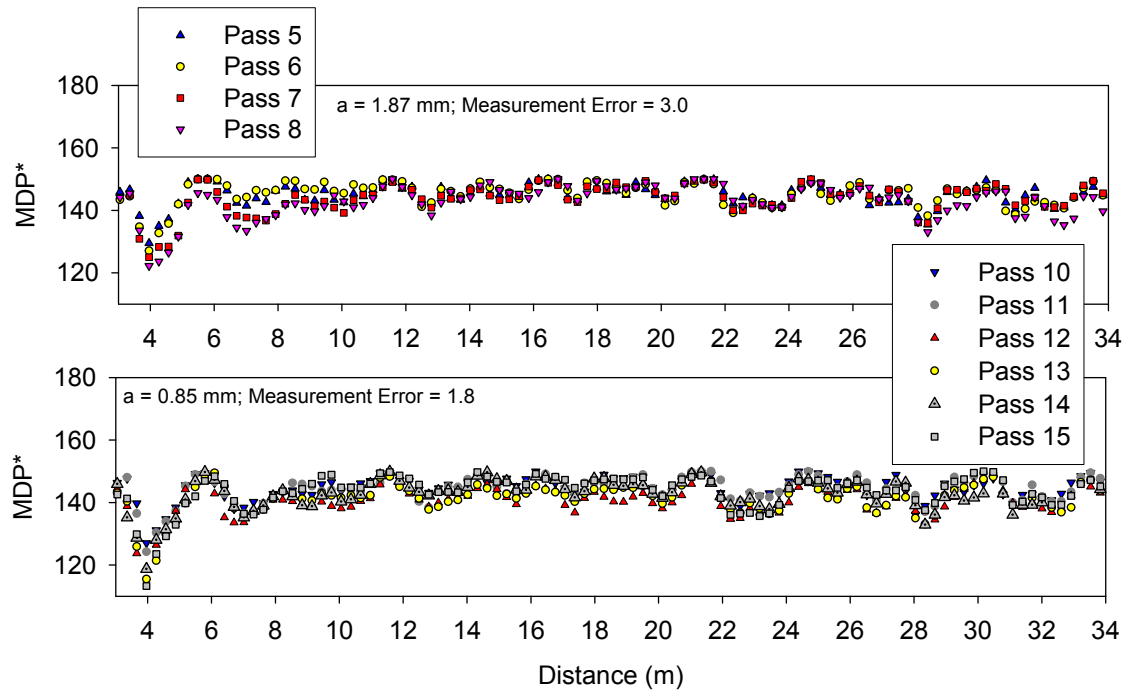


Figure 3.116. Repeatability of MDP\* measurements at  $a = 0.85$  mm – TH60 test strip 2

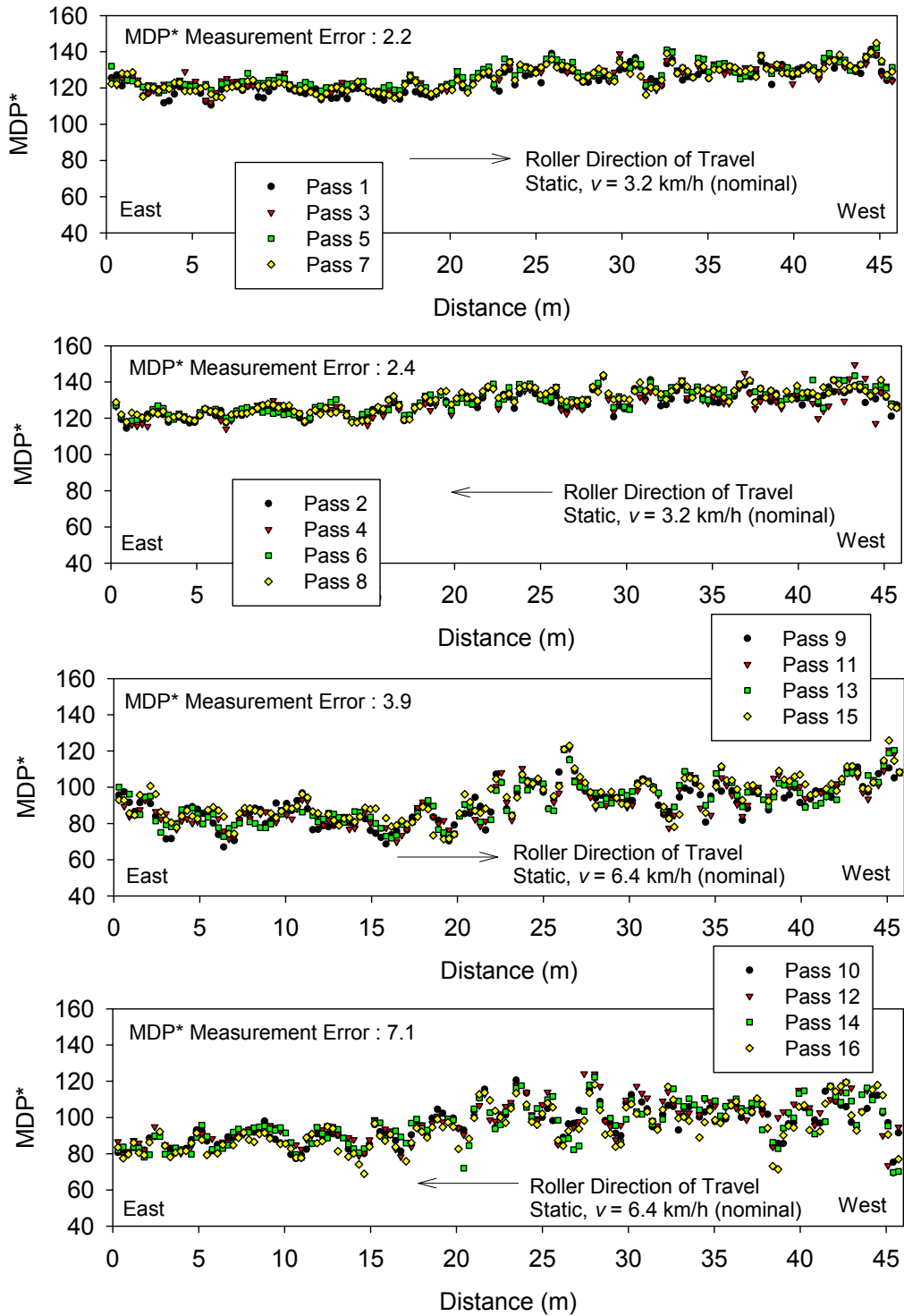


Figure 3.117. Repeatability of MDP\* measurements in static mode – Olmsted County test strip 1

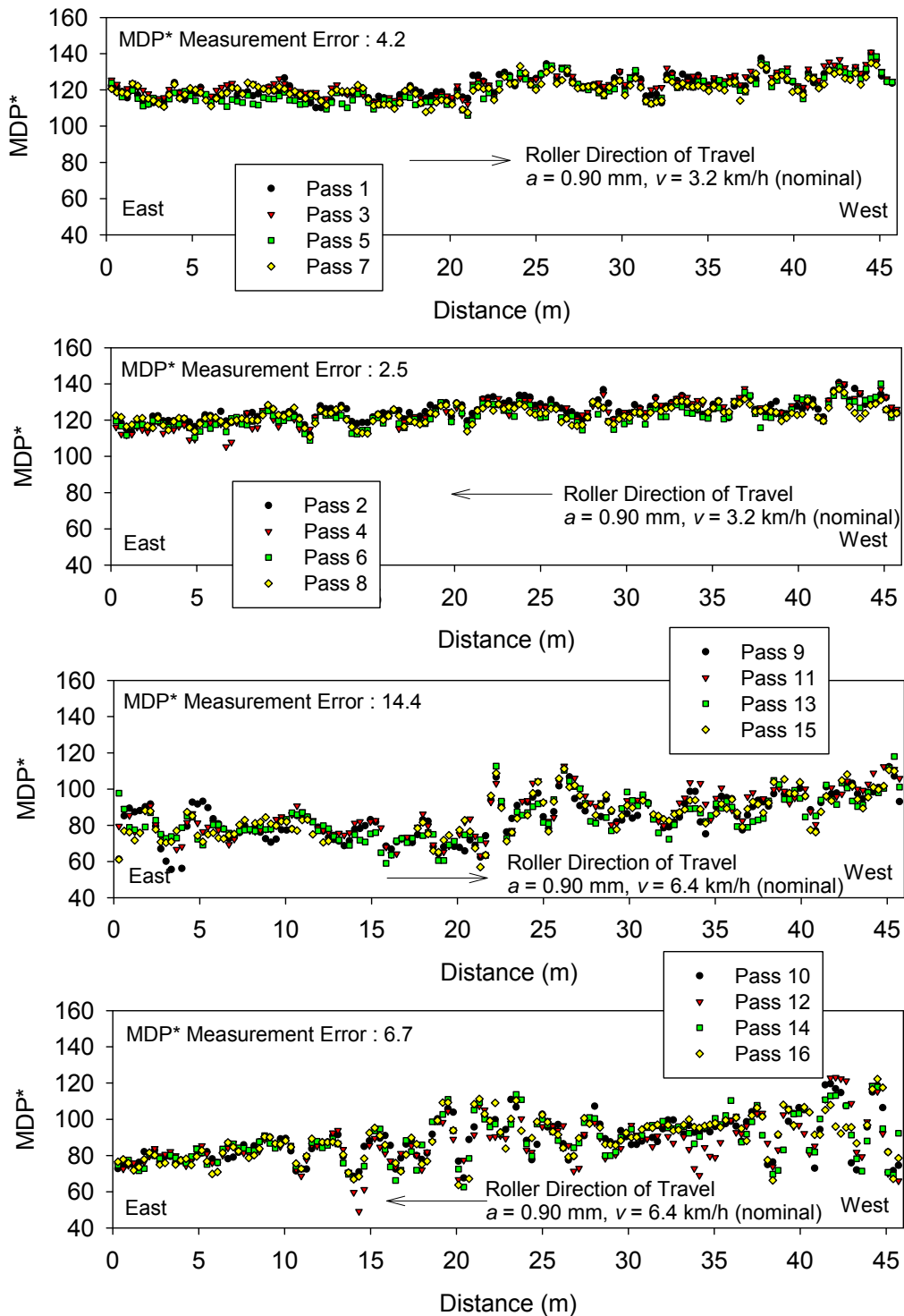


Figure 3.118. Repeatability of MDP\* measurements at  $a = 0.90 \text{ mm}$  setting – Olmsted County test strip 2

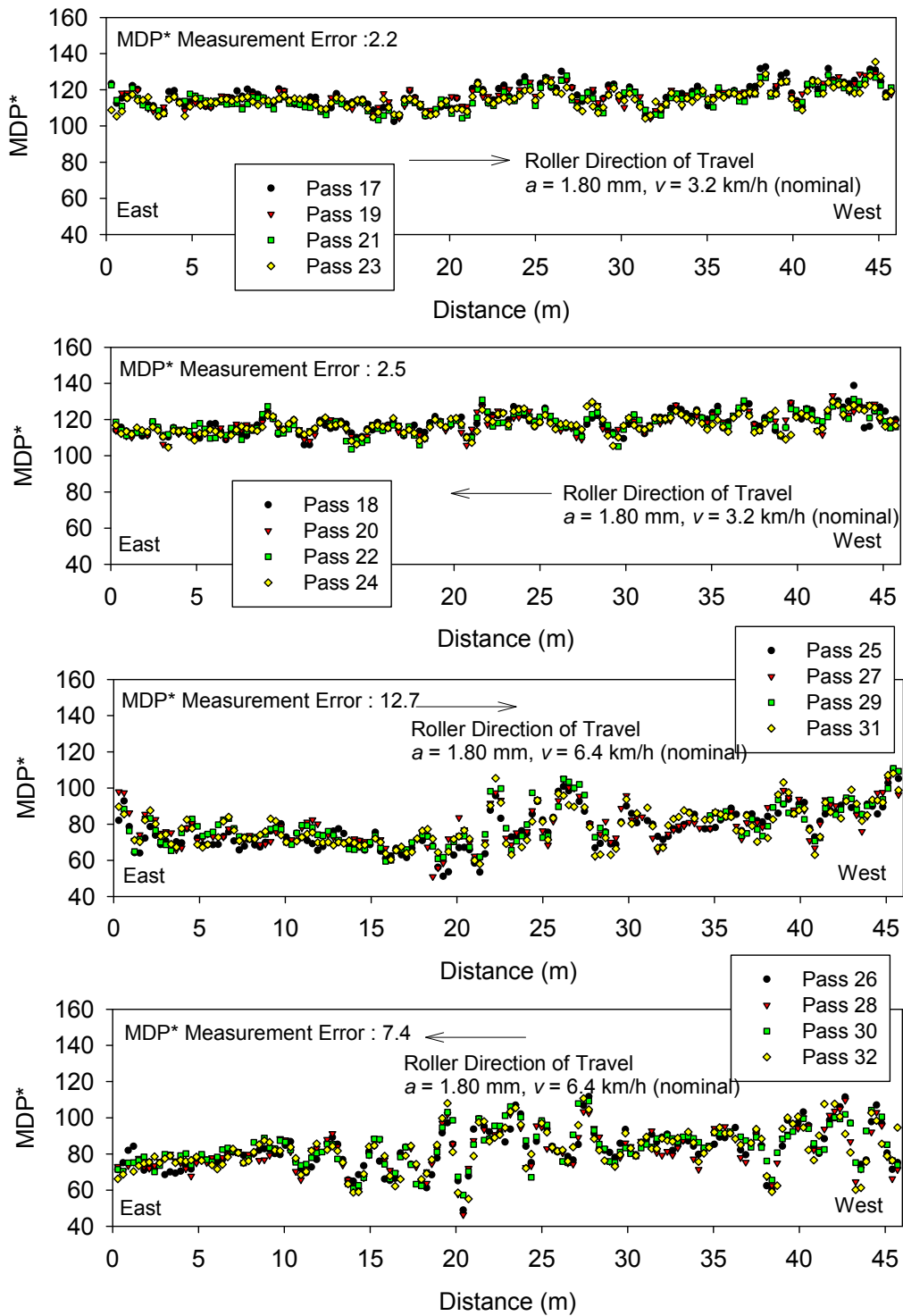


Figure 3.119. Repeatability of MDP\* measurements at  $a = 1.80 \text{ mm}$  setting – Olmsted County test strip 2

Table 3.36. Summary of repeatability analysis results on MDP\*, CMV, and RMV

Project/ Test Strip	Roller	Drum Type	Direction	<i>a</i> (mm)	<i>v</i> (km/h)	$\sigma_{\text{repeatability}}$		
						MDP*	CMV	RMV
TH60 Strip 2	CP-563	Padfoot	Forward	0.85	3.2	1.8	—	—
				1.87	3.2	3.0	—	—
Olmsted County, Test Strip 1	CP-563	Padfoot	Forward (East to West)	Static	3.2	2.2	—	—
					6.4	3.9	—	—
			Backward (West to East)	Static	3.2	2.4	—	—
					6.4	7.1	—	—
Olmsted County, Test Strip 2	CP-563	Padfoot	Forward (East to West)	0.9	3.2	4.2	—	—
					6.4	14.4	—	—
			Backward (West to East)	0.9	3.2	2.5	—	—
					6.4	6.7	—	—
			Forward (East to West)	1.8	3.2	2.2	—	—
					6.4	12.7	—	—
			Backward (West to East)	1.8	3.2	2.5	—	—
					6.4	7.4	—	—
TH36 test strip 4	CS-563	Smooth	Forward	0.85	3.2	—	2.7	0.3

Table 3.37. Summary of R&R analysis results on MDP\*

Project/ Test Strip	Description of change in conditions	Parameter	Measurement Variability			Percent contribution* of $\sigma_{\text{reproducibility}}$	Impact of change in machine operating parameters ( $a$ , $v$ , <i>direction</i> ) on measurement values
			$\sigma_{\text{repeatability}}$	$\sigma_{\text{reproducibility}}$	$\sigma_{\text{R\&R}}$		
TH60	Change in amplitude ( $v = 3.2$ km/h)	MDP*	2.36	0.83	2.49	11	Low Significance
Olmsted County	Change in direction (static and $v = 3.2$ km/h)	MDP*	2.39	5.34	5.85	83	High Significance
	Change in direction (static and $v = 6.4$ km/h)	MDP*	11.78	9.21	14.96	38	Low Significance**
	Change in direction ( $a = 0.90$ mm and $v = 3.2$ km/h)	MDP*	4.25	4.84	6.45	56	High Significance
	Change in direction ( $a = 0.90$ mm and $v = 6.4$ km/h)	MDP*	7.68	10.06	12.66	63	High Significance
	Change in direction ( $a = 1.80$ mm and $v = 3.2$ km/h)	MDP*	2.87	4.88	5.66	74	High Significance
	Change in direction ( $a = 1.8$ mm and $v = 6.4$ km/h)	MDP*	11.97	9.04	15.00	36	Low Significance**
	Change in amplitude (E to W, $v = 3.2$ km/h)	MDP*	3.36	4.90	5.94	68	High Significance
	Change in amplitude (W to E, $v = 3.2$ km/h)	MDP*	2.71	5.13	5.80	78	High Significance
	Change in amplitude (E to W, $v = 6.4$ km/h)	MDP*	13.68	8.84	16.29	29	Low Significance**
	Change in amplitude (W to E, $v = 6.4$ km/h)	MDP*	7.75	7.81	11.00	50	Low Significance**
	Change in speed (E to W, static)	MDP*	4.35	18.02	18.54	95	High Significance
	Change in speed (W to E, static)	MDP*	5.20	18.03	18.77	92	High Significance
	Change in speed (E to W, $a = 0.90$ mm)	MDP*	5.90	18.18	19.11	91	High Significance
	Change in speed (W to E, $a = 0.90$ mm)	MDP*	5.47	18.97	19.74	92	High Significance
	Change in speed (E to W, $a = 1.80$ mm)	MDP*	5.44	18.48	19.26	92	High Significance
Change in speed (W to E, $a = 1.80$ mm)	MDP*	5.32	19.19	19.92	93	High Significance	

\*  $100 \times \sigma_{\text{repeatability}}^2 / \sigma_{\text{R\&R}}^2$ ; \*\* comparatively high  $\sigma_{\text{repeatability}}$

### 3.8 Key Findings from Field Studies

Results and observations from the field studies indicate that IC technology has significant potential to improve construction process control and resulting quality of compacted granular and non-granular materials. Detailed test results and project level findings and conclusions are provided in the sections above. The purpose of this section is to summarize key general findings from the field studies differentiating granular and non-granular soils and discuss their significance with respect to specifications and implementation. Results obtained from TH36 and US10 field projects are considered for granular soils and results obtained from TH60 and Olmstead County field projects are considered for non-granular soils.

#### 3.8.1 Granular Soils

- Results indicated positive correlations between IC-MVs and modulus (i.e.,  $E_{LWD}$ ,  $E_{FWD}$ , etc.)/strength (i.e., DPI) based in-situ test measurements. Correlations between dry unit weight and IC-MVs (US10 project) showed poor correlations.
- Modulus measurements obtained on granular subgrade materials (i.e., fine sand as encountered in US10 project) correlated well with IC-MVs when tests are performed in a carefully excavated trench of about 100 to 150 mm depth. Similarly, compaction layer DPI measurements obtained on granular subgrade materials correlated well with IC-MVs when the first DCP blow is regarded as a seating blow. For granular base materials (i.e., aggregate base material as encountered in TH36 project), modulus/strength based in-situ measurements obtained at the surface correlated well with the IC-MVs. These are important practical aspects of in-situ LWD and DCP testing to note when correlating with IC-MVs.
- Regression relationships between CMV and  $E_{LWD}$ ,  $d_{LWD}$ ,  $E_{V1}$ , and DPI in-situ test measurements from TH36 and US10 projects are combined to obtain regression relationships and are presented in Figure 3.120. An important point to note in these relationships is that CMV is correlated with a linear regression relationship with modulus values, while it is correlated with a non-linear power relationship with LWD deflection values. This is of consequence as Mn/DOT is currently considering implementing  $d_{LWD}$  as part LWD QC/QA specification instead of  $E_{LWD}$  values. It must be noted that the current 90% to 120% of target values criteria needs to be reviewed for implementing  $d_{LWD}$  values due to the non-linear nature in the relationship with CMV.
- The primary factors contributing to low  $R^2$  values and scatter observed in the regression relationships is believed to be due to (a) differences in measurement influence depths, (b) stress state during loading and applied stresses, and (c) roller jumping (only for data obtained at high amplitude settings).
- Results from TH36 project demonstrated significantly different stress paths for loading under roller, FWD, and LWD loading which is a likely contributor to scatter in relationships between IC-MVs and  $E_{LWD}$  measurements.

- Using criteria for characterizing measurement influence depth as the depth at 10% of the maximum stresses at the surface, the measurement influence depths under the roller, 300-mm FWD plate, and 200-mm LWD from TH36 and US10 projects are summarized in Table 3.38. No significant difference was observed in the influence depth with change in amplitude under roller or increasing dynamic load under the FWD plate. The measurement influence depths under roller varied between TH36 and US10 projects due to variation in soil stiffness and layering conditions.
- Roller jumping (as measured by high RMV measurements) affected the CMV values and consequently the correlations. Influence of RMV in CMV-point measurement correlations can be accounted for through multiple regression analysis. However, for practical purposes, it is recommended to perform calibration testing in low amplitude setting (about less than 1 mm) to avoid complex interpretation and analysis of results.
- Field observations and discussion with contractor indicated that scraper traffic contributes to compaction of fill materials. EPC measurements from US10 project indicated that stresses under scraper tire are significantly higher (2.2 to 2.6 times greater) than stresses observed under roller vibratory loading. Results presented by White et al. (2008) from TH64 granular subgrade project showed high CMV values in areas with construction traffic.
- CMV data obtained from repeated passes indicated that the measurements are repeatable (CMV measurement error < 3), but are not reproducible with change amplitude. The measurements obtained at different amplitudes must be treated separately. Effect of speed on CMV was not evaluated as part of this study. However, a study conducted by White et al. (2009) indicated that CMV is reproducible with variation in nominal speeds between 3.2 and 4.8 km/h.

Table 3.38. Summary of measurement influence depth of different measurements – granular soils

Measurement	Depth below surface
TH36 Project	
Roller ( $a = 0.85$ and $1.70$ mm)	0.9 m
300-mm FWD	0.6 m
200-mm LWD	0.3 m
US10 Project	
Roller ( $a = 0.85$ mm)	1.5 m
Roller ( $a = 1.70$ mm)	1.6 m

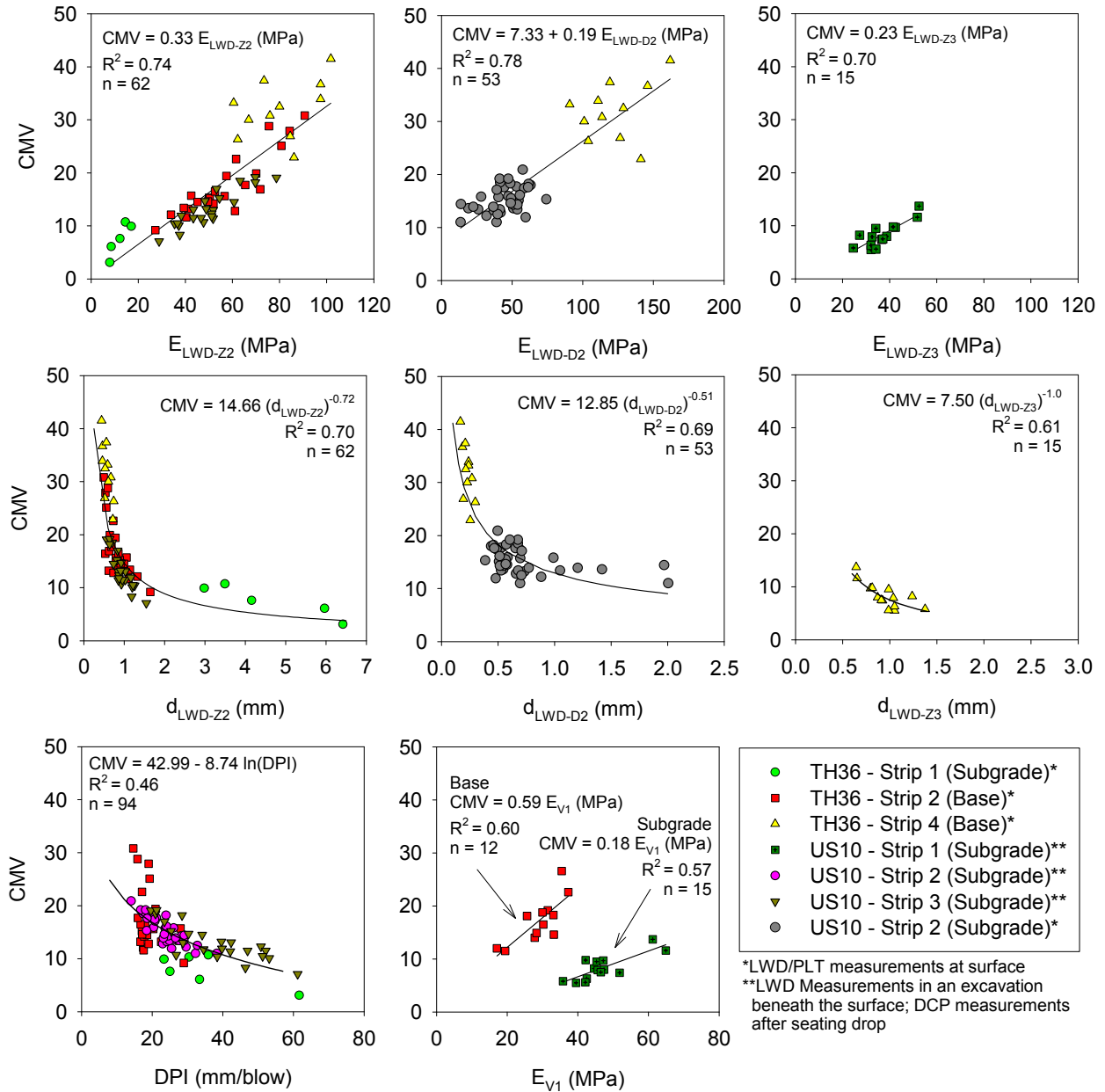


Figure 3.120. Correlations between CMV and in-situ point measurements obtained from TH36 and US10 field projects with granular soils

### 3.8.2 Non-Granular Soils

- Results and observations from TH60 project showed instances where IC-TV (MDP\* = 138) established at the project being met and not the  $E_{LWD-TV}$  at many test locations.
- Relationships between MDP\* measurements with surface  $E_{LWD}$  and compaction layer DPI measurements showed positive correlations, however, with varying degree of

uncertainty (i.e.,  $R^2$  values varied from about 0.3 to 0.8). Relationships between MDP\* and dry density generally showed relatively poor correlations. Soft or uncompacted zones at depths below about 0.25 m on some test strips did not affect the MDP\* measurements.

- Regression relationships showed improved  $R^2$  values in predicting MDP\* from  $E_{LWD}$  and DPI when moisture content is included in the regression analysis. This demonstrates the sensitivity of soil moisture content in interpreting MDP\* values.
- Separate trends were observed in MDP\*- $E_{LWD}$  correlations for MDP\* values  $< 140$  and  $> 140$ . This presents a challenge in implementing the QA requirement of production area meeting 90% to 120% of IC-TV as the limits are applicable only with one linear trend in the data with increasing compaction.
- Results from some test strips indicated that wrong throttle and gear settings used during roller operations produce invalid IC-MVs. The roller manufacturer recommendation is that the roller should be operated at a high throttle and low gear setting during compaction operations.
- MDP\* results obtained from repeated passes indicated that MDP\* values are repeatable with measurement error in the range of 2 to 5 when operated at a nominal speed of 3.2 km/h. The results showed relatively high measurement error in the range of 10 to 15 when operated at 6.4 km/h nominal speed.
- MDP\* results from TH60 project indicated that the values are reproducible with change in amplitude (from  $a = 0.85$  to 1.87 mm) (note that the material was mostly at wet of optimum moisture content). In contrast, the results from Olmsted County project indicated that the values are not reproducible with change in amplitude (from  $a =$  static to 1.80 mm). A study conducted by White et al. (2009) also indicated that MDP values are influenced by change in amplitude.
- MDP\* results from Olmsted County indicated that the values are affected by driving grade slope and therefore are not reproducible with change in direction of travel.
- CMV-  $E_{LWD-Z2}$  and CMV-  $d_{LWD-Z2}$  relationships derived from two test strips on the TH60 project showed good correlations but with separate trends. Statistically significant correlations were not found with DPI and dry density.
- Roller jumping (as measured by high RMV measurements) occurred at locations with very stiff conditions which affected the CMV values. It is recommended that the CMV measurement values be evaluated in conjunction with RMV values.

## **Chapter 4**

### **Guidance for Test Roller Specification Modification**

Heavy test rolling has been widely utilized by Mn/DOT as a QA technique on earthwork construction projects. Test rolling has the advantage of providing a continuous visual record; however, it can be difficult and expensive to setup and operate the test rolling equipment, and involves safety risks (Mn/DOT 2008). As part of this research, IC-MVs, and in-situ LWD, DCP, and NG point measurements were evaluated as alternatives to heavy test rolling to assess support conditions of compacted granular and non-granular subgrade materials. Experimental test results obtained from US 14 project (from White et al. 2007a) in Janesville, MN and TH 60 project in Bigelow, MN on non-granular subgrades, and TH 36 project in North St. Paul, MN on granular subgrade materials are presented in this chapter.

In brief, results indicate empirical relationships exist between IC-MVs, various in-situ point measurements, and rut depths. The IC-MVs and LWD/DCP point measurements can reliably indicate the rut depth under test rolling. DCP profiles on compacted non-granular subgrade layers show vertical non-uniformity typically with a stiff layer underlain by a soft layer. Support capacities of non-granular subgrades under the heavy test roller were analyzed using a layered bearing capacity solution and compared to measured rut depths at the surface. A simple chart solution is presented to determine target shear strength properties of compacted subgrade from DCP profiles to ensure heavy test rolling rut depths are less than the acceptable limit.

#### **4.1 Background**

Test rolling is performed using a pneumatic wheel roller (e.g. shown in Figure 4.1) on a compacted surface and the ruts observed beneath the wheels are measured to assess the support conditions. According to Mn/DOT test roller specification (Mn/DOT 2005), the test roller should be a tractor towed two-wheeled trailer with each wheel weighing approximately 133.5 kN and operated at speeds not less than 4 km/h nor more than 8 km/h. The two wheels on the trailer are required to be spaced 1.8 m apart and inflated to approximately 650 kPa air pressure. The contact width of the wheel is specified as 0.46 m. The rut depth beneath the roller wheels was measured from the top of the subgrade. If measured rut depths are  $\geq 50$  mm, the subgrade is considered unstable and corrective action is required (e.g., diskings and recompacting).

Using analytical solutions and numerical simulations, Hambleton and Drescher (2008) indicated that the influence depth of the Mn/DOT specified test roller varies from 0.6 m to 1.2 m depending on the soil stratigraphy (i.e., stiff over soft or soft over stiff layers). Recent field studies assessing the compaction quality for non-granular embankment subgrades in Minnesota and Iowa (see White et al. 2007a, Larsen et al. 2008) documented significant vertical non-uniformity in soil strength/stiffness properties for compacted non-granular soils. This condition is generally a result of poor moisture control, overly thick lift placement, and poor compaction. An example of vertical non-uniformity from US 14 project in Janesville, MN (from White et al.

2007a) on compacted glacial till material is presented in Figure 4.2. DCP tests conducted at five select locations in an area of compacted subgrade showed significant vertical non-uniformity based on undrained shear strength profiles at each point (undrained shear strength  $s_u$  values estimated from DPI using a correlation presented in Chapter 3; see Figure 3.101). Heavy test rolling performed in this area (in accordance with Mn/DOT 2005 specification) showed rut depths  $> 50$  mm at points 1, 2, and 4 and minimal rutting at points 3 and 5. The comparatively wet moisture content at the surface and low undrained shear strength conditions are believed to have contributed to poor stability under the test roller at points 1, 2, and 4 (see Gupta et al. 2007 for further discussion on the influence of water content on soil stiffness and strength). The influence of vertical non-uniformity in the support conditions of non-granular subgrades on bearing capacity (as assessed by rut depths) under the test roller are analyzed using DCP profiles and layered bearing capacity analysis later in this chapter.



Figure 4.1. Towed pneumatic dual-wheel test rollers with 650 kPa contact tire pressure used on TH14 (left), TH60 (left) and TH36 (right) project

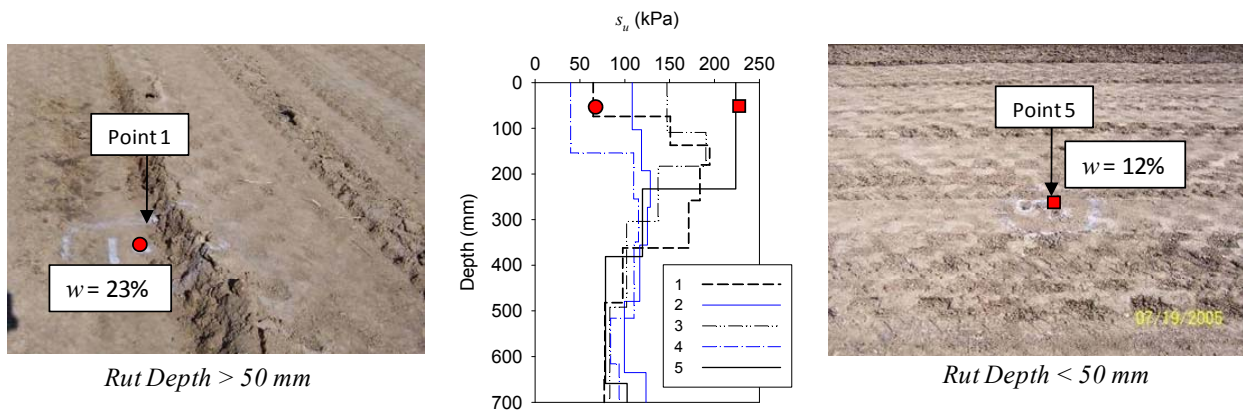


Figure 4.2. DCP- $s_u$  profiles from compacted glacial till subgrade at US14 (from White et al. 2007a)

The primary objectives of experimental results from field investigations presented in this chapter are to: (a) evaluate empirical relationships between rut depth measurements from heavy test

rolling and IC-MVs, and LWD, DCP, and NG point measurement values, (b) demonstrate an approach to develop target values for IC-MVs and point measurement values relating to conventionally accepted rut depth measurements, and (c) evaluate the effect of vertical non-uniformity in soil shear strength properties on bearing capacity of the test roller wheel.

## 4.2 Experimental Testing

Heavy test roller rut depth measurements in conjunction with roller-integrated compaction measurements and in-situ point measurements from three project sites (see Table 4.1) are presented in this chapter. The US 14 project data obtained from an earlier study by the authors on non-granular subgrade materials (White et al. 2007a) is presented herein for comparison with the current study. Ammann  $k_s$  IC measurement values were evaluated at that project (see White et al. 2007a and Thompson et al. 2007 for description of  $k_s$  measurement system). Experimental testing on TH 36 and TH 60 projects with select granular subbase and non-granular subgrade layers, respectively, were conducted as part of the current study. USCS classification of the materials and in-situ testing performed at each project site are summarized in Table 4.1. IC-MVs on the TH 60 project were obtained using 19 ton CS-683 smooth drum roller operated using  $a = 0.85$  mm,  $f = 30$  Hz, and  $v = 3.2$  km/h nominal settings. Test rolling on these projects was performed in accordance with Mn/DOT (2005) standard specifications. Figure 4.1 shows pictures of the test rollers used on the project sites.

Rut depth measurements obtained from the US14 project were obtained as depth of rut from the top of the heave developed due to tire indentation. From the TH 36 and TH 60 projects, rut depth measurements were obtained as depth of rut from the top of the subgrade similar to Mn/DOT (2005) specifications.

Table 4.1. Description of project locations with rut depth measurements

Date	Project Location	Layer	USCS Symbol	IC-MV	In-situ testing <sup>§</sup>
November 2005 (White et al. 2007a)	US14, Janesville, MN	Non-granular Subgrade	CL	$k_s$	Rut Depth*, NG, Clegg, DCP, LWD
May 2007	TH36, North St. Paul, MN	Select Granular Subbase	SP-SM	—	Rut Depth**, LWD
July 2008	TH60, Bigelow, MN	Non-granular Subgrade	CL	CMV	Rut Depth**, NG LWD, DCP

<sup>§</sup>GPS measurements for point measurements; \*Rut depth measurements from the top of the heave around the rut; \*\*Rut depth measurements from the top of the subgrade.

### 4.3 Correlations between Rut Depths and Different In-situ Measurements

Relationships derived from experimental testing on US 14, TH 36, and TH 60 projects are presented in Figure 4.3, Figure 4.4, and Figure 4.5, respectively. From the US 14 project, relationships between roller-integrated  $k_s$  and in-situ point measurements show positive trends (i.e., decreasing strength/stiffness/density and increasing moisture shows increasing rut depths); however with  $R^2$  values ranging from 0.2 to 0.5. Relationships from the TH 36 project showed a power relationship between rut depth and  $E_{LWD-Z2}$  measurements with  $R^2 = 0.5$ . Relationships between rut depth measurements with  $E_{LWD-Z2}$  and CMV on TH60 project produced  $R^2$  of about 0.6. Correlation with dry unit weight produced  $R^2$  of about 0.2 and no correlation was found with moisture content. The scatter observed in the relationships is partly attributed to the soil variability and the differences in the influence depth between roller, heavy test roller, and point measurements. IC-MVs are integrated over the width of the drum and have influence depths ranging from 0.6 to 1.5 m (see Chapter 3), a heavy test roller has an influence depth ranging from 0.6 to 1.2 m (Hambelton and Drescher 2008), and point measurements are mostly affected by compaction layer properties. An approach to analyze support capacities of the subgrade under the roller wheel using layered bearing capacity analysis from DPI profiles is described in the following section.

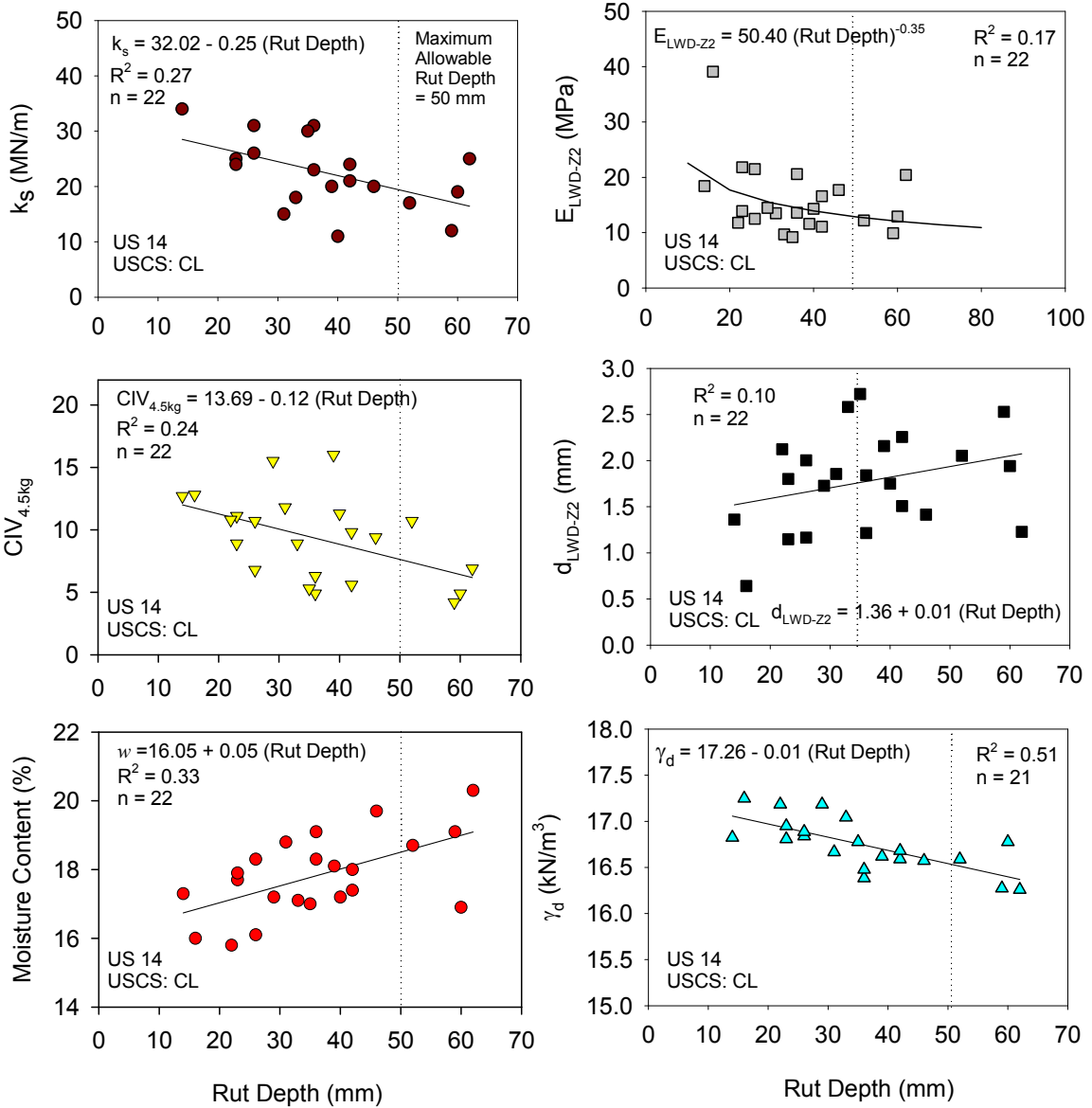


Figure 4.3. Regression relationships between rut depth, roller-integrated  $k_s$ , and in-situ point measurements from US14 project

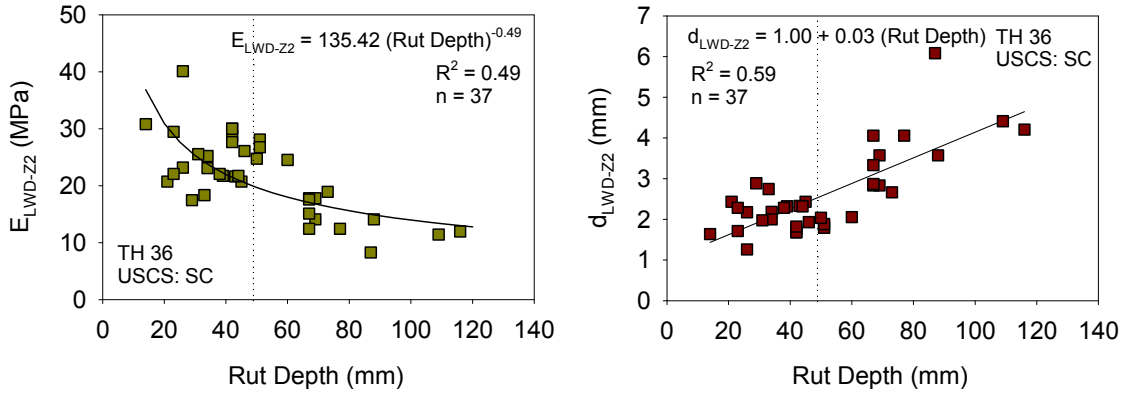


Figure 4.4. Relationship between rut depth and LWD measurements from TH36 project

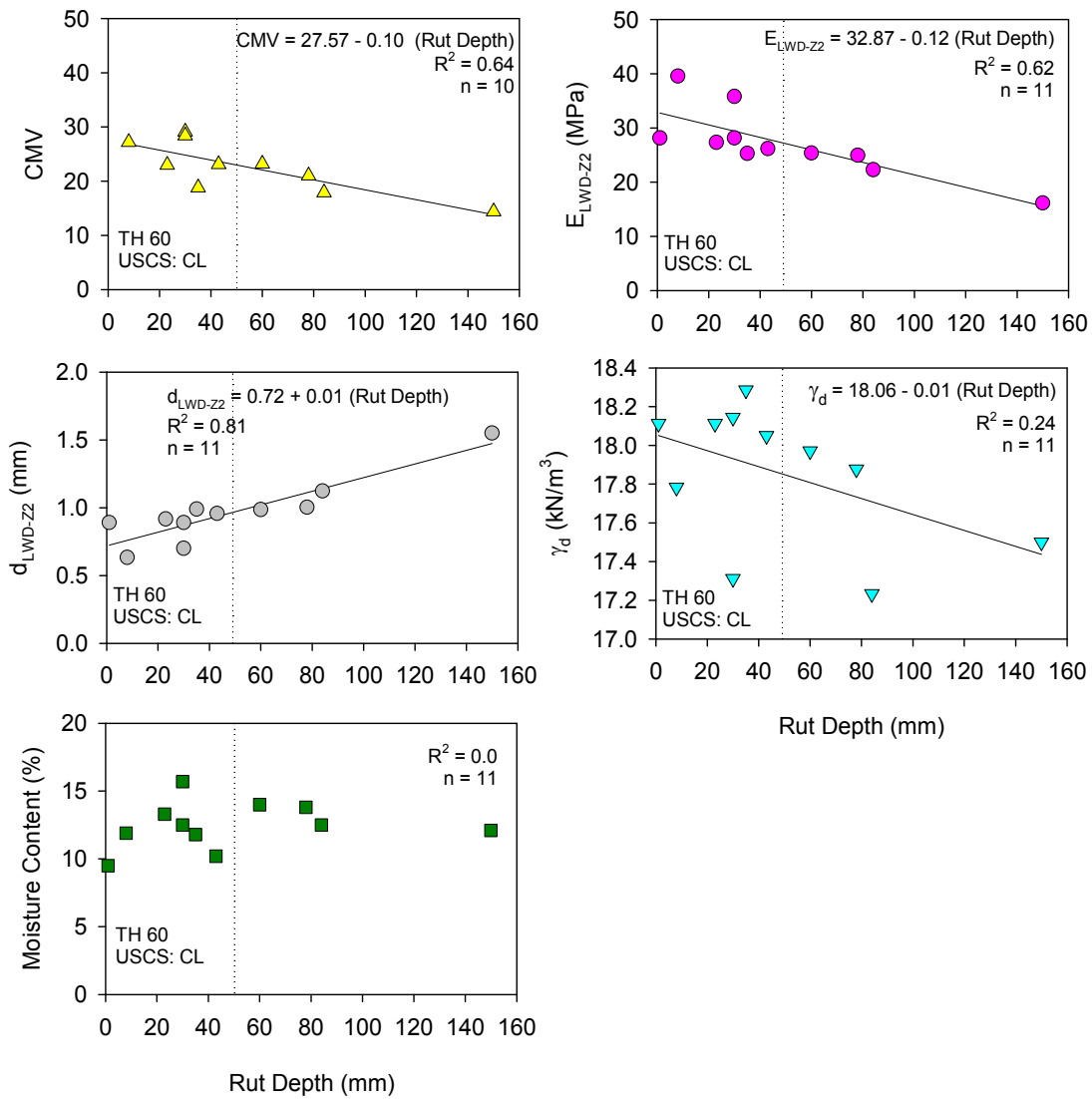


Figure 4.5. Regression relationships between rut depth, roller-integrated CMV, and in-situ point measurements from TH60 project

#### 4.4 Bearing Capacity Analysis on a Layered Non-granular Soil Stratum

DCP profiles were analyzed for bearing capacity under the test roller wheel using analytical layered bearing capacity solutions proposed by Meyerhof and Hanna (1978). For the analysis, the contact area under the tire is assumed as a rigid rectangular flat footing of size 0.45 m x 0.46 m (contact width dimension obtained from Mn/DOT 2005 and length calculated to equal 650 kPa contact pressure under 113.5 kN applied force), the contact pressure under the tire is assumed to be uniform (i.e. 650 kPa), and the load application is assumed to be vertical. The behavior of soil beneath a wheel is assumed analogous to soil behavior beneath a footing under undrained loading conditions. The footing is assumed to be rigid to simplify the analysis and is considered a reasonable assumption with the relatively high tire inflation pressure and tire carcass stiffness compared to the deformability of the soil (see Bekker 1960). The analysis can be fine tuned by solving theoretical equations to determine contact area under the roller, considering a possible inclination in footing shape and load, and accounting for flexibility of the rubber tire (see Hambleton and Drescher 2008). Hambleton and Drescher 2008 summarized theoretical solutions to determine contact area as a function of wheel sinkage which is a sum of both elastic (rebound after the load application) and plastic deformations (measured rut depth) under the wheel. Although plastic deformation is predominant at locations with greater rut depths, locations with minimal rut depths can have considerable elastic rebound, but is difficult to measure. The analysis is simplified herein with an objective of analyzing the effect of vertical non-uniformity on the subgrade bearing capacity under the wheel and obtaining insights on approximate target shear strength properties required to overcome rut failures under the test roller.

Meyerhof and Hanna (1978) proposed analytical solutions to estimate bearing capacity of a two-layered soil stratum with stronger soil underlain by weaker soil of known soil mechanical properties. The bearing capacity under the test roller wheel for a stiff over soft soil stratum is illustrated in Figure 4.6.

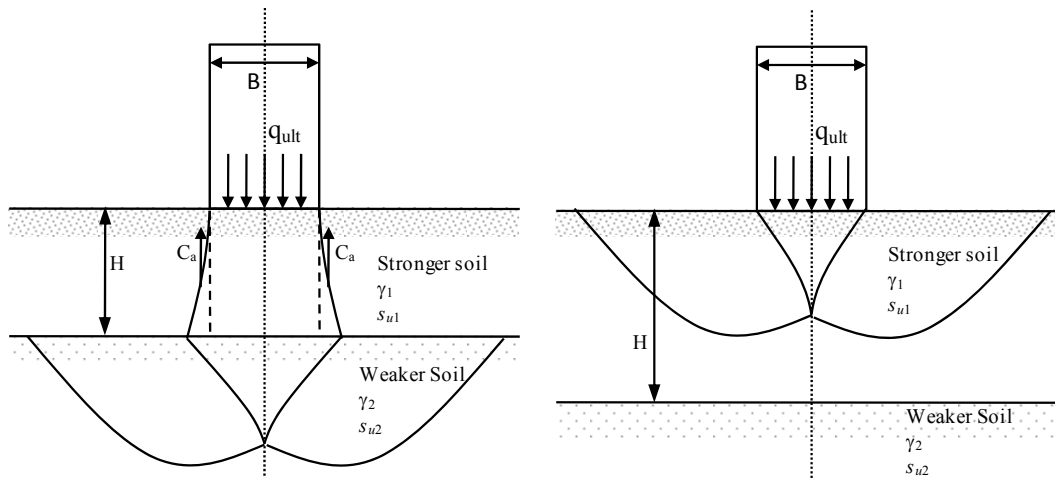


Figure 4.6. Bearing capacity of a test roller wheel on a layered non-granular stratum

If the thickness of the stronger layer (H) is relatively small, a punching shear failure is expected in the top stronger soil layer, followed by a general shear failure in the bottom weaker soil layer. In that case the ultimate bearing capacity  $q_{ult}$  is a function of the  $s_u$  properties (for  $\phi' = 0$  condition) of both top ( $s_{u1}$ ) and bottom layers ( $s_{u2}$ ) and is calculated using Equation 4. If the thickness H is relatively large, then the failure envelope lies within the top layer only. For that case,  $q_{ult}$  is a function of top layer  $s_u$  using Equation 4.2.

$$q_{ult} = \left(1 + 0.2 \frac{B}{L}\right) 5.14 s_{u2} + \left(1 + \frac{B}{L}\right) \left(\frac{2c_a H}{B}\right) \leq q_t \quad (4.1)$$

$$q_t = \left(1 + 0.2 \frac{B}{L}\right) 5.14 s_{u1} \quad (4.2)$$

where B = contact width, L = contact length,  $s_{u1}$  = undrained shear strength of the top layer,  $s_{u2}$  = undrained shear strength of the bottom layer,  $c_a$  = adhesion determined using theoretical relationship between  $c_a/s_{u1}$  and  $s_{u2}/s_{u1}$  by Meyerhof and Hanna (1978).

Rut depth measurements at 11 test locations in comparison with DCP- $s_u$  profiles at each location are presented in Figure 4.7. The  $s_u$  values were determined using the DPI- $s_u$  relationship presented in Chapter 3 for TH 60 non-granular subgrade soil. Similar to previous findings by White et al. (2007a) and Larsen et al. (2008), significant vertical non-uniformity in soil shear strength properties is evident from the DCP- $s_u$  profiles. The reason for this non-uniformity at this project is attributed to variable and thick lifts and variable moisture content (see discussion in Chapter 3 TH60 case history).

The soil profile at each test location was analyzed as a two-layered soil system using weighted average  $s_u$  values for each layer to determine the  $q_{ult}$  value at each location. The relationship between  $q_{ult}$  values and measured rut depth measurements from the test locations is shown in Figure 4.8a and shows a strong non-linear correlation with  $R^2 = 0.9$ . Based on the acceptable rut depth value = 50 mm, a target  $q_{ult} = 1050$  kPa was calculated. This target value can be interpreted as the minimum value required at a location with a two-layered non-granular soil stratum to avoid rut depth failures, i.e. rut depths  $\geq 50$  mm. This approach makes the assumption that  $q_{ult}$  is developed at 50 mm, which may not always be the case.

The graph presented in Figure 4.8b shows relationship between  $s_{u1}$  and  $s_{u2}$  at different H values to achieve the target  $q_{ult}$  value. The advantage of viewing the results in this manner is that if  $s_u$  values of the two layers ( $s_{u1}$  and  $s_{u2}$ ) are known (for example from DCP test), it can be determined rut depth failures at a given location are expected or not. An alternate way of interpretation is that if  $s_{u2}$  is known, the minimum required  $s_{u1}$  to avoid rut depth failures (as shown in the calculation in Figure 4.8b) can be estimated. A target  $s_u$  value for a homogenous condition (i.e. H = 0,  $s_{u1} = s_{u2}$ ) can be readily determined from Figure 4.8b which is = 170 kPa.

$q_{ult}$  values calculated from DCP- $s_u$  profiles shown in Figure 4.7 are plotted on Figure 4.8b to demonstrate the use of the graphical “pass”/“fail” evaluation procedure. A test location is determined as “fail” if the measured rut depth was  $\geq 50$  mm and checked if the calculated  $q_{ult}$  value was  $<$  target  $q_{ult}$ . Nine out of eleven test locations complied with the pass/fail criteria, and

the two test locations that did not comply produced  $q_{ult} = 989$  kPa with a rut depth = 23 mm and  $q_{ult} = 1093$  kPa with a rut depth = 84 mm. Similarly,  $q_{ult}$  determined from DCP- $s_u$  profiles from the US 14 project (results presented in Figure 4.2) are also plotted in Figure 4.8b for comparison. The test points from that project did not have corresponding rut depth measurements but had visual confirmation of whether or not significant rutting was observed at the test locations. Three out of five test locations from that project complied with the pass/fail criteria. Considering the simplifications and assumptions made in the analysis and inevitable statistical uncertainty associated with empirical relationships used in the analysis, the pass/fail estimations are considered practically acceptable and useful for establishing alternative method for QA target values. As with any geotechnical engineering application, a chart like this cannot replace thorough testing/analysis and engineering judgment but it can serve as a quick reference guide for field engineers.

The validity of the layered bearing capacity analysis was verified by performing 300 mm plate diameter static PLTs at hard and soft test locations. Applied stress –plate deformation curves from the PLTs are presented in Figure 4.9. Point B was relatively soft ( $E_{LWD-Z2} = 3.2$  MPa) and Point A was relatively stiff ( $E_{LWD} = 26.1$  MPa). The applied load was increased at point B until a bearing capacity failure was induced and at point A until the maximum capacity of the PLT system was reached. DCP- $s_u$  profile data was used to determine  $q_{ult}$  under the plate (assuming  $B = L = 0.3$  m). The calculated  $q_{ult} = 120$  kPa at point B was close to the measured  $q_{ult} = 130$  kPa. The calculated  $q_{ult} = 980$  kPa at point A appears to fall in line with the trend observed in the stress-deformation curve up to an applied stress of about 650 kPa (tire contact pressure).

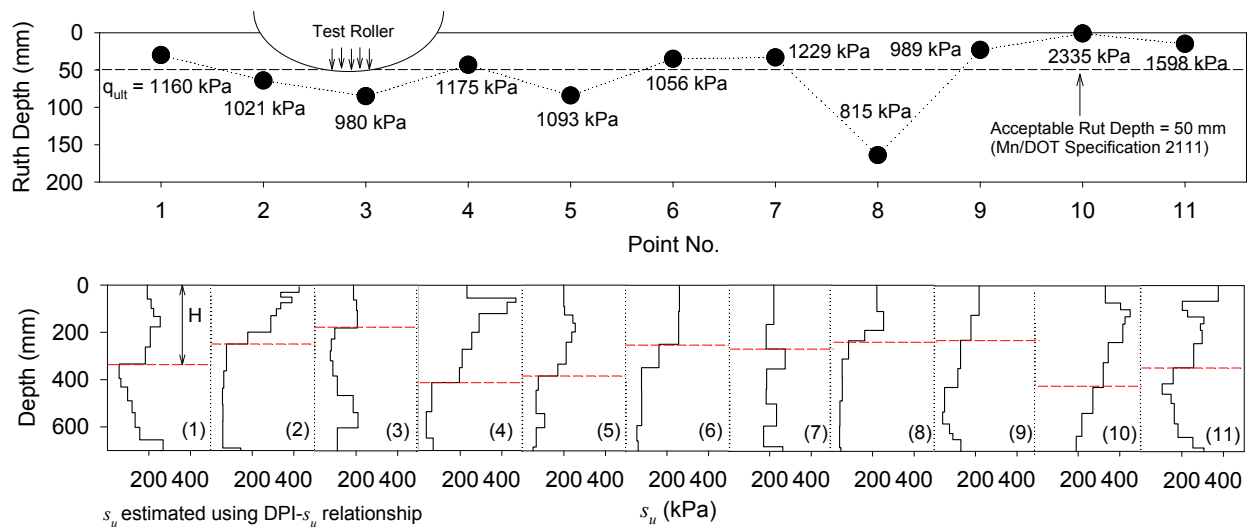


Figure 4.7. Comparison of DCP- $s_u$  profiles with rut depth measurements

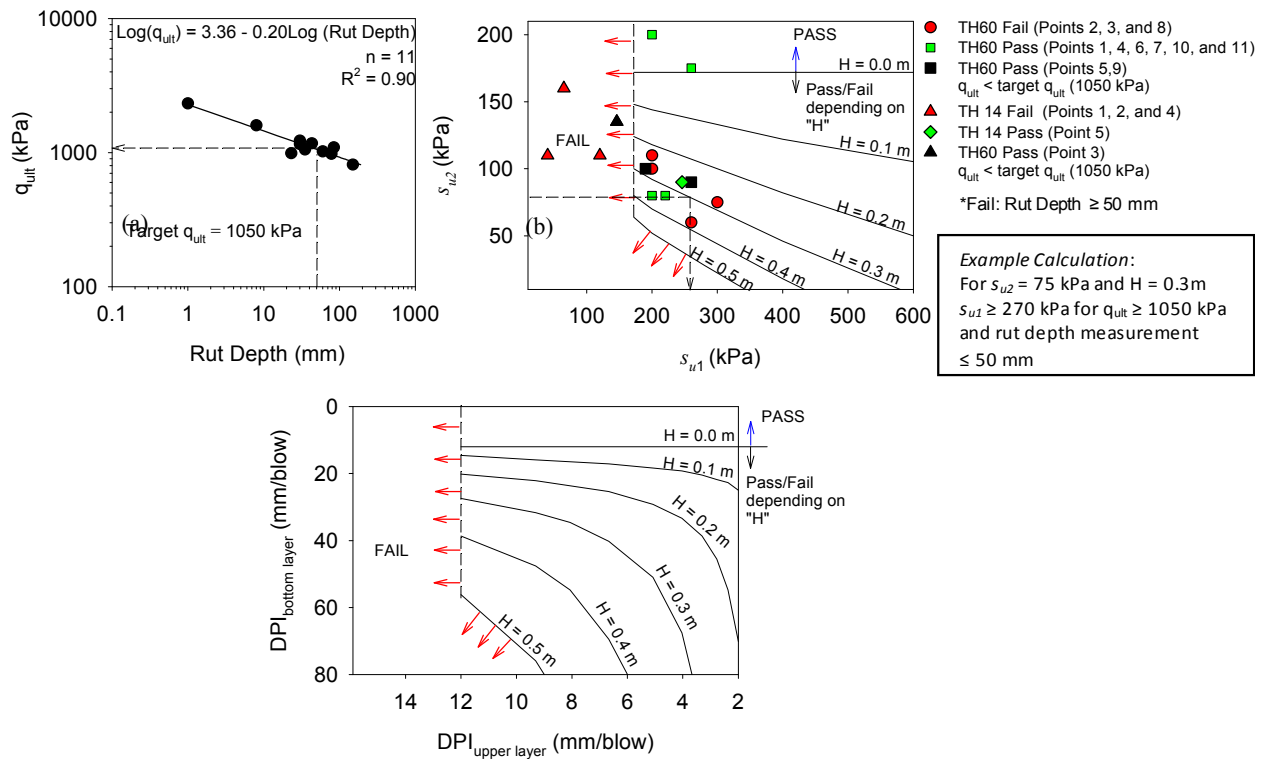


Figure 4.8. (a) Relationship between calculated  $q_{ult}$  and measured rut depth, and (b) influence of  $s_u$  properties of top and bottom layers at different  $H$  to achieve a minimum  $q_{ult} = 1050$  kPa

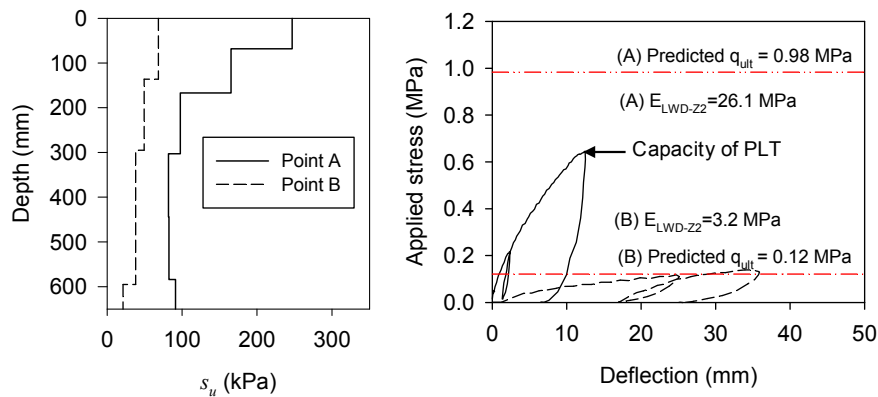


Figure 4.9. Comparison of estimated  $q_{ult}$  from layered bearing capacity analysis and static plate load test

## 4.5 Implementation Aspects

An alternate approach to heavy test rolling is to develop regression relationships (as presented above) and target values for other measurements. A summary of QA target values developed based on the empirical relationships are shown in Table 4.2. The target  $E_{LWD-Z2}$ ,  $\gamma_d$ ,  $CIV_{4.5kg}$ ,  $k_s$ , and IC-MVs were derived from relationships with rut depth measurements corresponding to a rut depth of 50 mm. The target  $s_u$  value was determined based on the layered bearing capacity analysis. The regression relationships, however, have some uncertainty which can be accounted for using statistical prediction limits at a selected percent confidence. For example, values in a relationship corresponding to the least-squared fit regression line will provide about 50% confidence in the predicted target value. These relationships should be considered specific to the material and project conditions and could vary considerably for other conditions.

Table 4.2. Summary of QA target values alternative to heavy test rolling rut depth of 50 mm

Parameter	Target values <sup>§</sup>
<i>US 14 Non-granular Subgrade</i>	
$k_s$ (MN/m) <sup>†</sup>	20
$CIV_{4.5kg}$	7.7
DPI (mm/blow)	12
$s_u$ (kPa)	170
<i>TH 36 Granular Subbase</i>	
$E_{LWD-Z2}$ (MPa)	20
$d_{LWD-Z2}$ (mm)	1.25
<i>TH 60 Non-granular Subgrade</i>	
CMV ( $a = 0.85, f = 30$ Hz)	23
DPI (mm/blow)	12
$s_u$ (kPa)	170
$E_{LWD-Z2}$ (MPa)	27

<sup>§</sup>based on empirical relationships; <sup>†</sup>Correlations showed  $R^2$  values < 0.3

## 4.6 Conclusions and Recommendations

Use of IC-MVs (CMV and  $k_s$ ) and DCP/LWD point measurements to evaluate the support capacities of non-granular and granular subgrade layers in-situ are discussed above. Comparisons were made to test roller rut depth QA criteria specified by Mn/DOT for the upper subgrade layer of a pavement foundation. Correlations developed between IC-MVs and point measurements show positive trends but with varying degrees of uncertainty in relationships. The scatter in the relationships is partly attributed to differences in the measurement influence depth.

DCP- $s_u$  profiles on compacted subgrades showed significant vertical non-uniformity with depth. Test rolling identified deep soft layers with excessive rutting (rut depths  $\geq 50$  mm) at the surface. Bearing capacities under the heavy roller wheel were evaluated using layered bearing capacity analytical solutions and DCP- $s_u$  profiles. The ultimate bearing capacities determined were empirically related to the measured rut depths at the surface. A chart solution was developed for using the layered bearing capacity analysis to determine target shear strength properties of a layered soil to avoid rut failures under the test roller.

Considering the significant advantage of IC technology with 100% coverage and positive trends in the relationships, it is concluded that the measurements can serve as a reliable indicator of compaction quality of non-granular and granular subgrades and serve as an alternative to heavy test rolling. It is recommended however, that development of this correlation database continue with future projects to improve confidence in these technologies.

## Chapter 5

### LWD Evaluation and Target Value Determination

#### 5.1 Introduction

Implementation of LWD test measurement values is considered an important step towards using a mechanistic-based parameter value that can potentially be related to performance of the compacted fill materials. Some of the identified challenges with implementation of LWD devices include differences between manufactures systems, unquantified test variability, lack of standard protocols, and methods for determination of target values. Each of these potential obstacles is discussed in this chapter. Results build on the previous research study by White et al. (2007a) and a recent work in Minnesota by their Local Road Research Board by Siekmeier et al.(2009).

#### 5.2 Background

Modulus from LWD test measurements is determined using Equation 5.1, which is derived from the Boussinesq elastic solution relating applied stresses, displacement in the soil, and contact stress distribution under the plate.

$$E = \frac{(1-\eta^2) \cdot \sigma_0 \cdot r}{d_0} \times F \quad (5.1)$$

where:  $d_0$  = measured settlement (mm),  $\eta$  = Poisson's ratio,  $\sigma_0$  = peak applied stress (MPa),  $r$  = radius of the plate (mm),  $E$  = Young's modulus (MPa);  $F$  = Shape factor depending on assumed contact stress distribution (see Vennapusa and White 2009a for discussion on shape factors). For calculations in this report  $F = 8/3$  was used for granular materials and  $F = \pi/2$  was used for non-granular materials. Figure 5.1 shows the relationship between  $E_{LWD}$  and deflection measurement values. Table 5.1 summarizes some of the key features of eight LWD devices identified in the literature. Vennapusa and White (2009) provide a summary of correlations reported in the literature between  $E_{LWD}$  from different devices and other in-situ modulus test measurements, i.e., initial or reload modulus from static plate load test ( $E_{V1}$  or  $E_{V2}$ ) and modulus from falling weight deflectometer test ( $E_{FWD}$ ) measurements. Variations in  $E_{LWD}$  for different devices have been documented in the literature (see Fleming et al. 2000, Hildebrand 2003, White et al. 2007a, Vennapusa and White 2009a). These differences are partly attributed to different load pulse durations and to differences in type and location of deflection transducers (Fleming et al. 2000). Several other factors that could however affect the  $E_{LWD}$  values include: size of loading plate, plate contact stress, plate rigidity, loading rate, buffer stiffness, and measurement of load versus assumption of load based on laboratory calibration from a standardized drop height. A detailed discussion on how these factors influence the  $E_{LWD}$  values is provided in Vennapusa and White (2009a). Experimental test results illustrating the influence of plate contact stress, buffer stiffness, and type and location of deflection transducers on  $E_{LWD}$  measurement values are presented in this chapter.

Table 5.1. Comparison between different LWD devices

Device <sup>§</sup>	Plate Diameter (mm)	Plate Thickness (mm)	Falling Weight (kg)	Maximum Applied Force (kN)	Load Cell	Total Load Pulse (ms)	Type of Buffers	Deflection Transducer		
								Type	Location	Measuring Range (mm)
Zorn	100, 150, 200, 300	124, 45, 28, 20	10, 15	7.07	No	18 ± 2	Steel Spring	Accelerometer	Plate	0.2 to 30 (± 0.02)
Keros	150, 200, 300	20	10, 15, 20	15.0	Yes	15 – 30	Rubber (Conical shape)	Velocity	Ground	0 to 2.2 (± 0.002)
Dynatest 3031	100, 150, 200, 300	20	10, 15, 20	15.0	Yes	15 – 30	Rubber (Flat)	Velocity	Ground	0 to 2.2 (± 0.002)
Prima	100, 200, 300	20	10, 20	15.0	Yes	15 – 20	Rubber (Conical shape)	Velocity	Ground	0 to 2.2 (± 0.002)
Loadman	110, 132, 200, 300	— <sup>†</sup>	10	17.6	No	25 – 30	Rubber	Accelerometer	Plate	— <sup>†</sup>
ELE	300	— <sup>†</sup>	10	— <sup>†</sup>	No	— <sup>†</sup>	— <sup>†</sup>	Velocity	Plate	— <sup>†</sup>
TFT	200, 300	— <sup>†</sup>	10	8.5	Yes	15 – 25	Rubber	Velocity	Ground	— <sup>†</sup>
CSM	200, 300	— <sup>†</sup>	10	8.8	Yes	15 – 20	Urethane	Velocity	Plate	— <sup>†</sup>

Notes: <sup>§</sup>Light Drop Weight Tester ZFG2000 by Gerhard Zorn, Germany; Keros Portable FWD and Dynatest 3031 by Dynatest, Denmark; Prima 100 Light Weight Deflectometer by Carl Bro Pavement Consultants, Denmark; Loadman by AL-Engineering Oy, Finland; Light Drop Weight Tester by ELE; TRL Foundation Tester (TFT) – a working prototype at the Transport Research Laboratory, United Kingdom; Colorado School of Mines (CSM) LWD device. <sup>†</sup>Unknown.

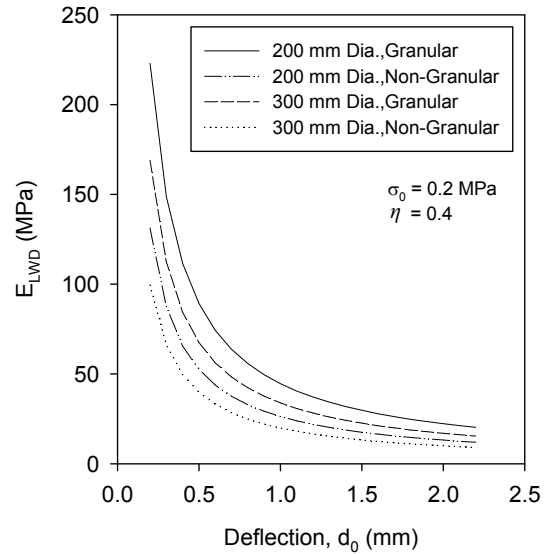


Figure 5.1. Relationship between deflection measurements and calculated  $E_{LWD}$

### 5.3 Experimental Comparison of LWD Devices

ZFG 2000 Zorn, Keros, and Dynatest 3031 LWD devices were investigated in this study (Figure 5.2) building upon the findings from an earlier study by the authors (White et al. 2007a). A schematic of each of these devices is provided in Figure 5.3.



Figure 5.2. Dynatest 3031, Keros, and ZFG Zorn LWD devices (left to right)

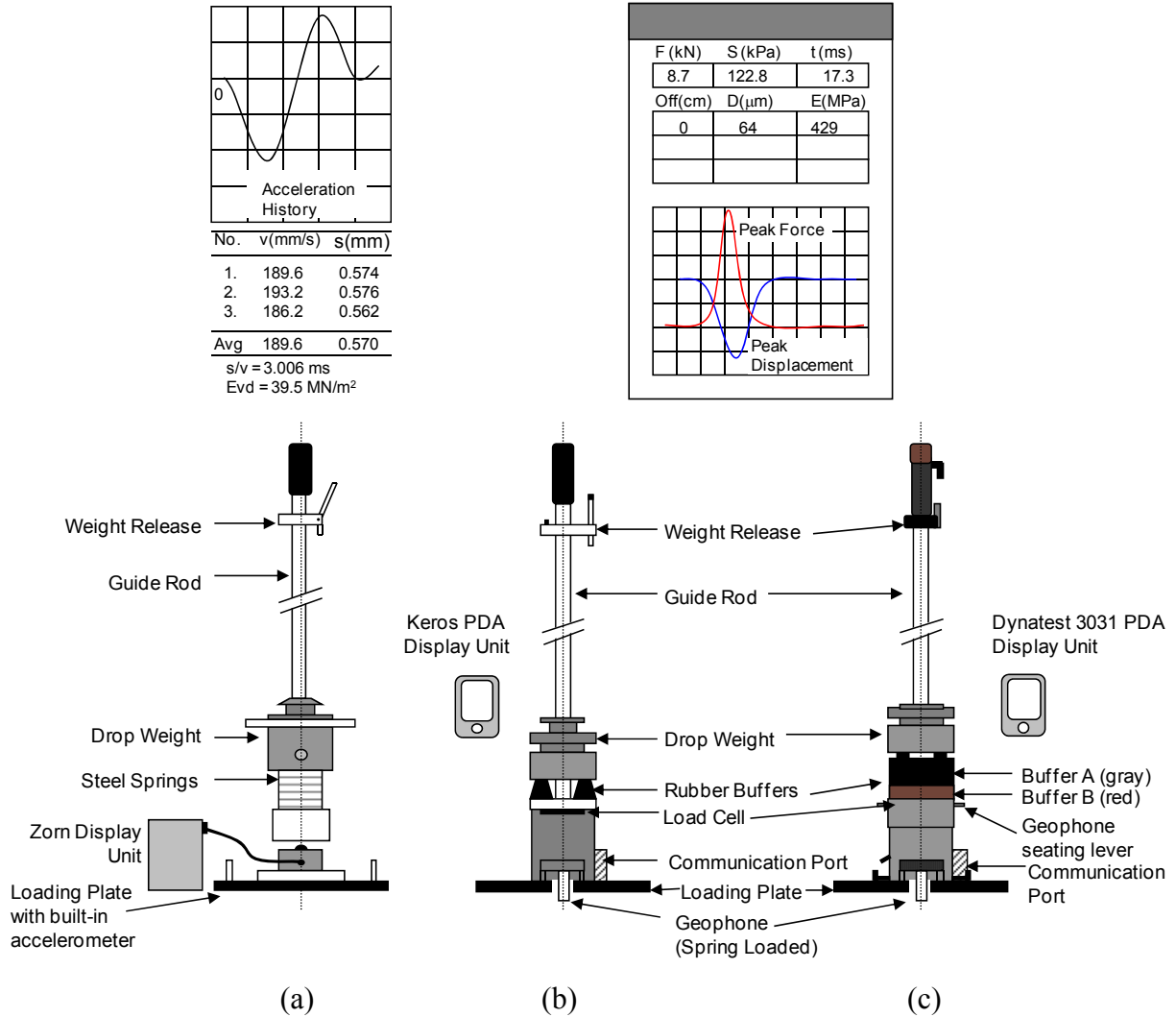


Figure 5.3. Schematic with example output of LWD devices used in this study (a) Zorn ZFG 2000 (b) Keros (c) Dynatest 3031

The Zorn device is programmed for  $v = 0.5$  and  $f = 2$  for  $E_{LWD}$  determination. Applied force is assumed constant for a drop height and is based on manufacturer's calibration tests. The force is estimated using Equation 5.2 with a spring stiffness constant  $C = 362396$  N/m (M. Weingart, personal communication, November 2006). Further technical details of the device are summarized in Table 5.1. Differences between the theoretical and experimental applied force will exist if the spring buffers behave non-linearly during loading.

$$F = \sqrt{2 \times m \times g \times h \times C} \quad (5.2)$$

where:  $F$  = Peak force in the spring (N);  $m$  = mass of falling weight (kg);  $g$  = acceleration due to gravity,  $9.81$  (m/s<sup>2</sup>);  $h$  = drop height (m);  $C$  = material stiffness constant (N/m).

The Keros and Dynatest 3031 LWD devices are manufactured by Dynatest, Denmark. The Dynatest 3031 LWD model is a recently produced version by Dynatest. These devices are equipped with a load cell to measure the impact force from the falling weight and a geophone to measure induced deflections at the ground surface. Software provided with the device allows the user to enter  $\nu$  and  $f$  values for  $E_{LWD}$  calculation. Primary differences between the two models are the type and stiffness of rubber buffers. Conical-type rubber buffers are used in the Keros device, while two layered flat rubber buffers are used in the Dynatest 3031 device (Buffer A and B, see Figure 5.3). The conical buffers used in the Keros device can be used in combinations of two or four. Laboratory tests were performed to determine the buffer stiffnesses. The rubber buffer stiffness is non-linear with increasing load. For a force range of 1 to 7 kN, the stiffness for the Keros two buffer setup ranges between 170 N/mm to 440 N/mm, and the four buffer setup ranges between 290 N/mm and 700 N/mm. For the Dynatest 3031 device, if only Buffer A was used, the stiffness range was between 150 N/mm to 700 N/mm, and if both Buffers A and B were combined, the range was between 90 N/mm to 500 N/mm for a force range of 1 kN and 7 kN, respectively. Further technical details of the two models are summarized in Table 5.1.

Comparison tests using the ZFG 2000 Zorn, Keros, and Dynatest 3031 LWD devices were performed at different project sites. A summary of soil index properties at each project site is provided in Table 5.2. Results obtained from three field studies by White et al. (2007a) (Field studies 1a, 1b, and 2) are also included here for comparison. Comparison tests were performed within a spacing of approximately 0.7 m or less to minimize variation in soil properties between test locations. Tests were performed by preloading each testing area with three load pulses and measuring the average deflection for the succeeding three load pulses. To investigate the differences in  $E_{LWD}$  values, assumptions made in the calculations (e.g.,  $\nu$  and  $f$  values) and the test procedures were kept identical. Table 5.3 lists the field test procedures and the parameters used in the calculations. Modulus values were estimated (using Equation 5.1) for the last three drops by using the measured applied force and deflection values for the Keros and Dynatest devices, and an assumed constant force depending on the drop height (see Equation 5.2) and measured deflection values for the Zorn device. The average estimated modulus of the last three drops was reported as the  $E_{LWD}$  value at a test point.

Zorn LWD was setup with 100, 150, 200, and 300 mm diameter plates (Figure 5.4) and  $E_{LWD}$  measurements were obtained by performing side-by-side testing at different applied stresses to evaluate the influence of plate diameter and applied stress. Similar tests were performed with Dynatest LWD setup with 200 and 300 mm diameter plates. Buffer stiffnesses on Dynatest and Zorn LWD devices were varied to evaluate its influence on the  $E_{LWD}$  values.

In brief, the primary objectives of the field investigations were to evaluate: (a) differences between LWD devices of similar plate diameters, (b) the influence of plate diameter (100, 150, 200 and 300 mm) and applied stress on  $E_{LWD}$ , and (c) the influence of buffer stiffness of  $E_{LWD}$ .

Table 5.2. Summary of field studies and index properties of materials

Parameter	Field Study No. 1a	Field Study No. 1b	Field Study No. 2	Field Study No. 3a	Field Study No. 3b	Field Study No. 3c	Field Study No. 4	Field Study No. 5	Field Study No. 6
Location	Mn/ROAD (White et al. 2007a)		TH64 (White et al. 2007a)	TH36, North St. Paul,, MN			US10, Staples, MN	Spangler Lab, Ames, IA	US60, Bigelow, MN
Device	Zorn and Keros		Zorn and Keros	Dynatest 3031 and Zorn		Zorn	Zorn, Keros, and Dynatest 3031		
Testing Layer	Subgrade	Class 5 Base	Granular subgrade and capping	Select granular subbase	Granular base	Gravel road	Granular subgrade	Gravel road	Subgrade
$c_u^*$	—	22.07	2.67 to 7.67	4.54	4.82	3.05	23.54	262.08	—
$c_c^*$	—	0.90	0.12 to 0.71	1.42	1.23	1.23	7.97	1.94	—
LL (%)	31	Non-plastic	Non-plastic	Non-plastic	Non-plastic	Non-plastic	Non-plastic	Non-plastic	30
PI	13	Non-plastic	Non-plastic	Non-plastic	Non-plastic	Non-plastic	Non-plastic	Non-plastic	14
AASHTO Classification	A-6 (5)	A-1-b	A-3	A-1-b	A-1-b	A-1-a	A-2-4	A-1-b	A-6(6)
USCS Classification and Material Description (ASTM D2487-00)	CL	SP-SM	SP to	SP	SP-SM	GP	SM	SM	CL
	Sandy lean clay	Poorly graded sand with silt and gravel	SW-SM	Poorly graded sand	Poorly graded sand with silt	Poorly graded gravel	Silty sand	Silty sand	Sandy lean clay

\* $c_u$  – coefficient of uniformity,  $c_c$  = coefficient of curvature

Table 5.3. Summary of Zorn and Keros/Dynatest 3031 LWD test conditions

Description	Keros/Dynatest 3031	Zorn ZFG 2000
Drop Weight	10 kg	10 kg
Diameter of Plate	200 and 300 mm	100, 150, 200 and 300 mm
Load Sensor	Load Cell Range: 0 – 19.6 kN	None (constant applied force using Equation 5.2)
Modulus Estimation Assumptions*	$\nu = 0.4$ (for all soils) $f = \pi/2$ for Field Study Nos. 1a, 6 (clay subgrade) $f = 2$ for Field Study No. 1b (granular base underlain by clay subgrade) $f = 8/3$ for field studies 2, 3a, 3b, 3c, 4, and 5.	

\*LWD plates and plate used for static PLT tests are assumed as truly rigid

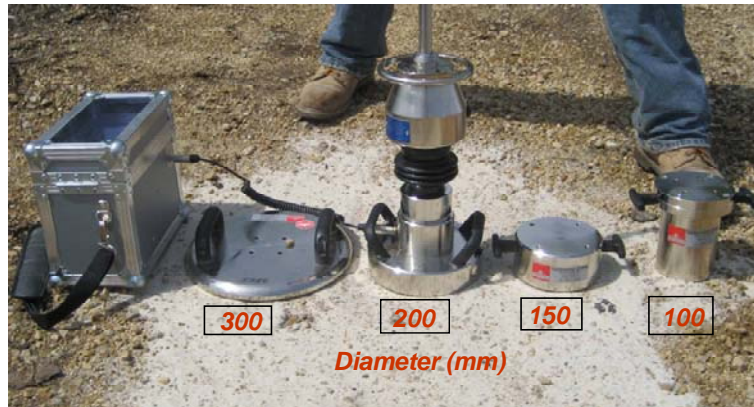


Figure 5.4. Zorn LWD device with 300, 200, 150, and 100 mm plate diameters

### 5.3.1 $E_{LWD}$ Comparison between Different LWD devices

Comparison results between modulus and deflections measured by different LWD devices are shown in Figure 5.5 and Figure 5.6, respectively. Linear regression relationships and associated  $R^2$  values are also presented in Figure 5.5. On average,  $E_{LWD-K2}$  and  $E_{LWD-D2}$  are approximately 1.75 and 1.56 times greater than  $E_{LWD-Z2}$ , respectively, with  $R^2$  values around 0.8 to 0.9 (Figure 5.5a,c); while  $E_{LWD-K3}$  is approximately 2.16 times greater than  $E_{LWD-Z3}$  with a relatively poor  $R^2$  value of 0.5 (Figure 5.5b). A similar trend of lower modulus (by factor of about 2 times) from the Zorn device was observed in a study conducted by the Danish Road Directorate (Hildebrand 2003) when compared with the Keros. Others have also reported that the moduli from Zorn is generally in the range of about 0.5 to 0.6 times lower, compared to other LWD devices and FWD that employ load cell and geophone displacement sensors (e.g. Fleming et al. 2000, 2002). Comparison between applied force values and deflection measurements by White et al. (2007a)

revealed that the primary contributor to differences in  $E_{LWD}$  values from Keros and Zorn is the difference in deflection values.

Figure 5.5d presents comparison between  $E_{LWD}$  values by Dynatest and Keros devices that were set up with 50-cm drop height. A best-fit linear regression with a slope of 1 and an  $R^2$  value of about 0.93 is observed between the two measurements. Note that although the drop height is similar, due to differences in buffer stiffnesses, the applied impact force was not the same. A frequency distribution plot of measured impact force by the two devices for test measurements from Field Study No. 4 is shown in Figure 5.7. On average, the Dynatest impact force was about 0.63 times lower than the Keros impact force. The estimated impact force for Zorn at 50-cm drop height is also shown on Figure 5.7 for reference. Despite differences in the impact force between the two devices, no pronounced difference was observed between the calculated  $E_{LWD}$  values. The influence of applied stress and buffer stiffness is discussed later in this chapter.

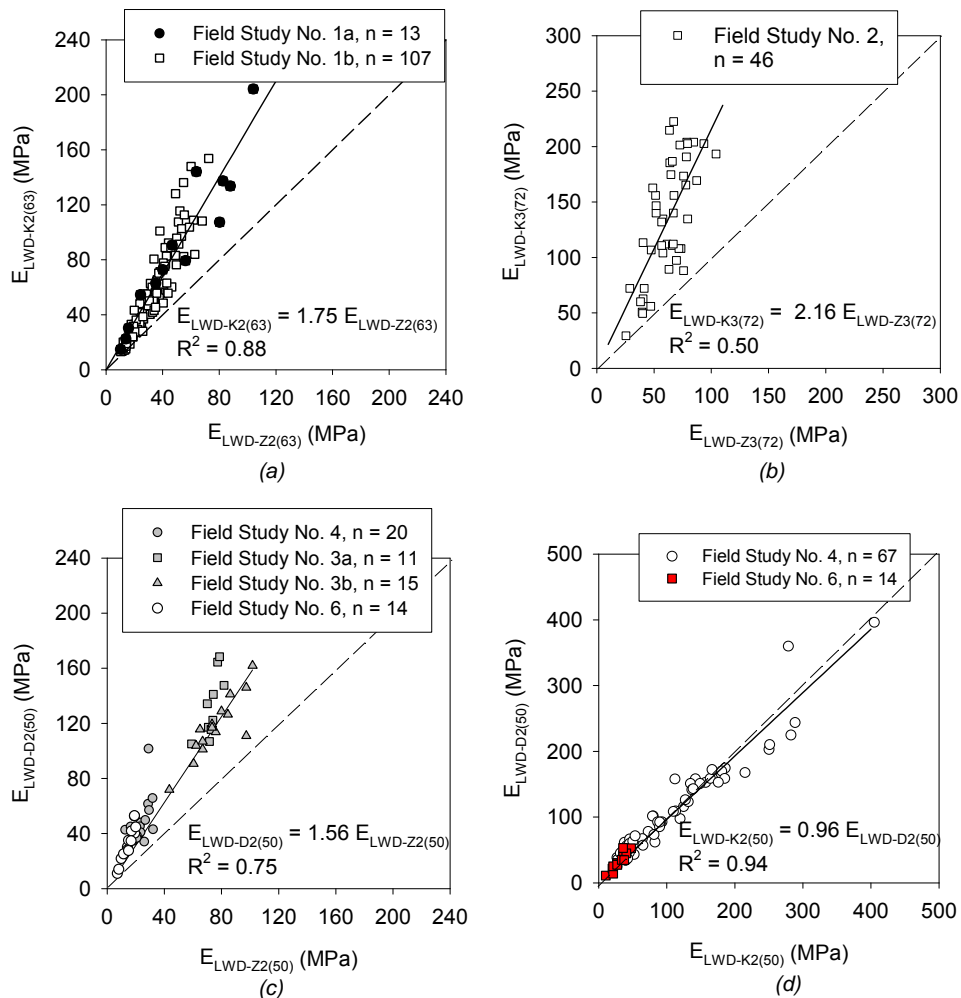


Figure 5.5. Relationships between  $E_{LWD}$  values from different devices: (a) 200-mm Keros and Zorn, (b) 300-mm Keros and Zorn, (c) 200-mm Dynatest and Zorn, and (d) 200-mm Dynatest and Keros

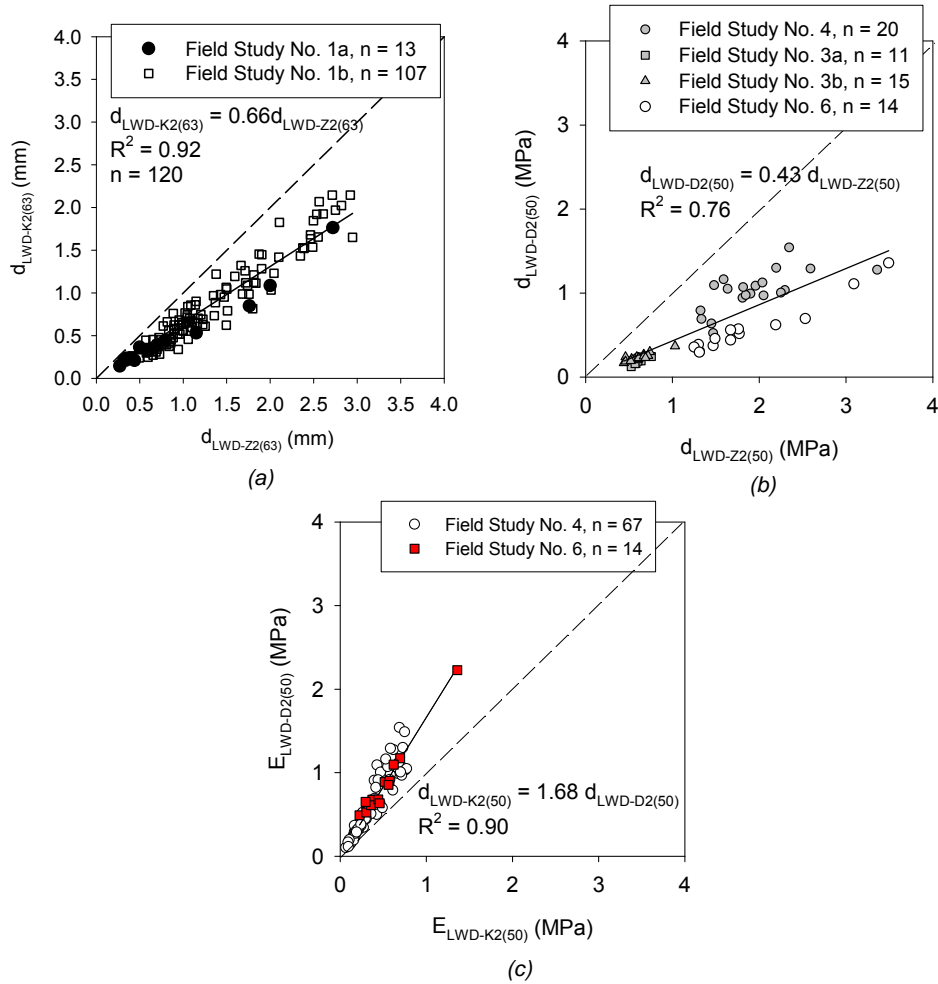


Figure 5.6. Relationships between  $d_{LWD}$  values from different devices: (a) 200-mm Keros and Zorn, (b) 200-mm Dynatest and Zorn, and (c) 200-mm Dynatest and Keros

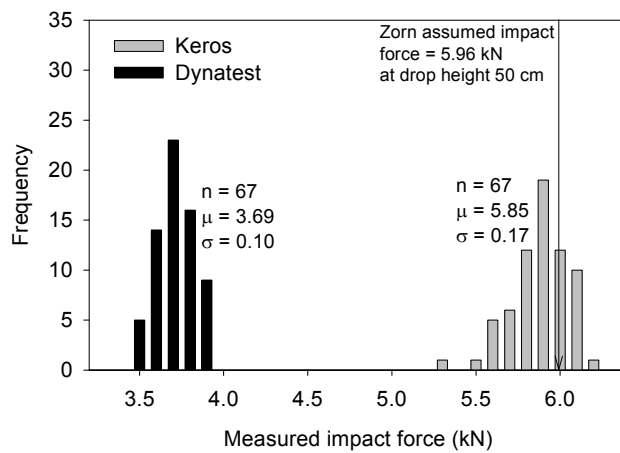


Figure 5.7. Frequency distribution of impact force at drop height 50 cm by Keros and Dynatest LWD devices and comparison to Zorn assumed impact force (Field Study No. 4)

### 5.3.2 Influence of Plate Diameter on $E_{LWD}$

White et al. (2007a) documented comparison results between Zorn LWDs setup with 200- and 300-mm diameter plates (Field Study 2) which showed that on average, the  $E_{LWD}$  with 200-mm is approximately 1.4 times greater than that with 300-mm plate. To further investigate the influence of plate diameter, Zorn LWD was tested with four different plate sizes (100-, 150-, 200-, and 300-mm diameter) in field studies 3c and 4, while Zorn, Keros, and Dynatest LWD devices were tested with 200- and 300-mm plate sizes in Field Study No. 5. Tests were conducted with each plate size, using drop heights varying from 10 to 80 cm at increments of 10 cm.

Results from Field Study Nos. 3c and 4 are presented in Figure 5.8. The trends indicate that at any level of applied contact stress, the calculated  $E_{LWD}$  values increase with decreasing plate size. On average, results from Field Study No. 3c show that the  $E_{LWD-Z2}$ ,  $E_{LWD-Z1.5}$ , and  $E_{LWD-Z1}$  are about 1.3, 1.5, and 1.9 times greater than  $E_{LWD-Z3}$ . In Field Study No. 4 the average  $E_{LWD-Z2}$ ,  $E_{LWD-Z1.5}$ , and  $E_{LWD-Z1}$  are about 1.2, 1.3, and 1.3 times greater than that of  $E_{LWD-Z3}$ .

Comparison results between Zorn, Dynatest, and Keros devices with 200- and 300-mm plate sizes from Field Study No. 5 are presented in Figure 5.9. Similar to findings from Field Study No. 4, Zorn  $E_{LWD}$  values increased with decreasing plate diameter from 300 to 200 mm. On average, the  $E_{LWD-Z2}$  is about 1.2 and 1.4 times greater than  $E_{LWD-Z3}$  for locations 1 and 2, respectively. On the other hand,  $E_{LWD}$  measured by Keros and Dynatest devices increased with decreasing plate diameter at location 1, while an opposite trend was observed at location 2. The  $E_{LWD-K2}$  and  $E_{LWD-D2}$  are about 1.3 and 1.2 times  $E_{LWD-K3}$  and  $E_{LWD-D3}$ , respectively, for location 1, while for location 2 the  $E_{LWD-K2}$  and  $E_{LWD-D2}$  are about 0.8 times  $E_{LWD-K3}$  and  $E_{LWD-D3}$ .

Based on the above field studies, a general conclusion can be made that the  $E_{LWD}$  values increase with decreasing plate diameters, which is consistent with experimental results presented by others (see Figure 5.10). Theoretical relationships presented by Terzaghi and Peck (1967) for footings on clay and sand are also presented in Figure 5.10 for comparison. For most cases, the ratio of  $E_{LWD}$  from a 200 to 300 mm plate is about 1.2 to 1.4. As an exception, in Field Study No. 5, the Keros and Dynatest device showed a ratio of  $\leq 1.0$  (see Figure 5.9). On the other hand, the ratio of  $E_{LWD}$  from 150-mm and 100-mm plates to  $E_{LWD}$  from the 300-mm plate showed considerable differences between field studies 3c and 4 (see Figure 5.8). These differences can be attributed to the difference in material stiffness; i.e., the ratio generally appears to increase with increasing material stiffness.

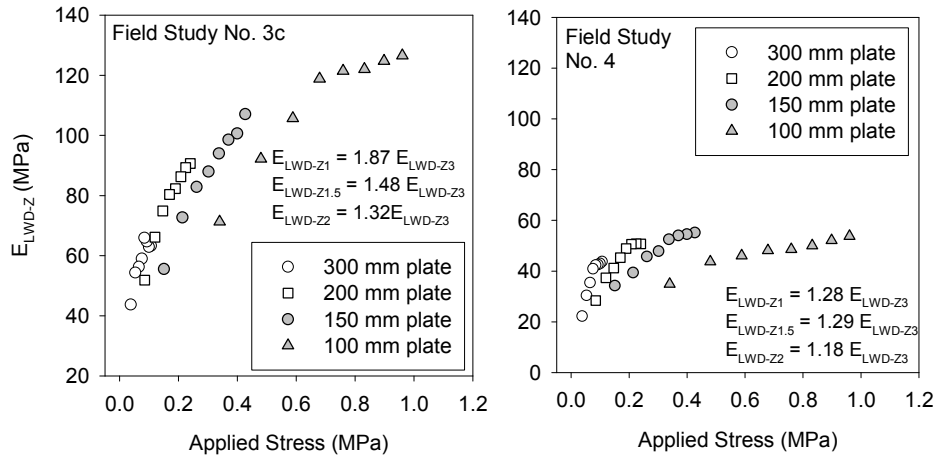


Figure 5.8. Influence of plate diameter and applied stress on Zorn ELWD from field studies 3 and 4

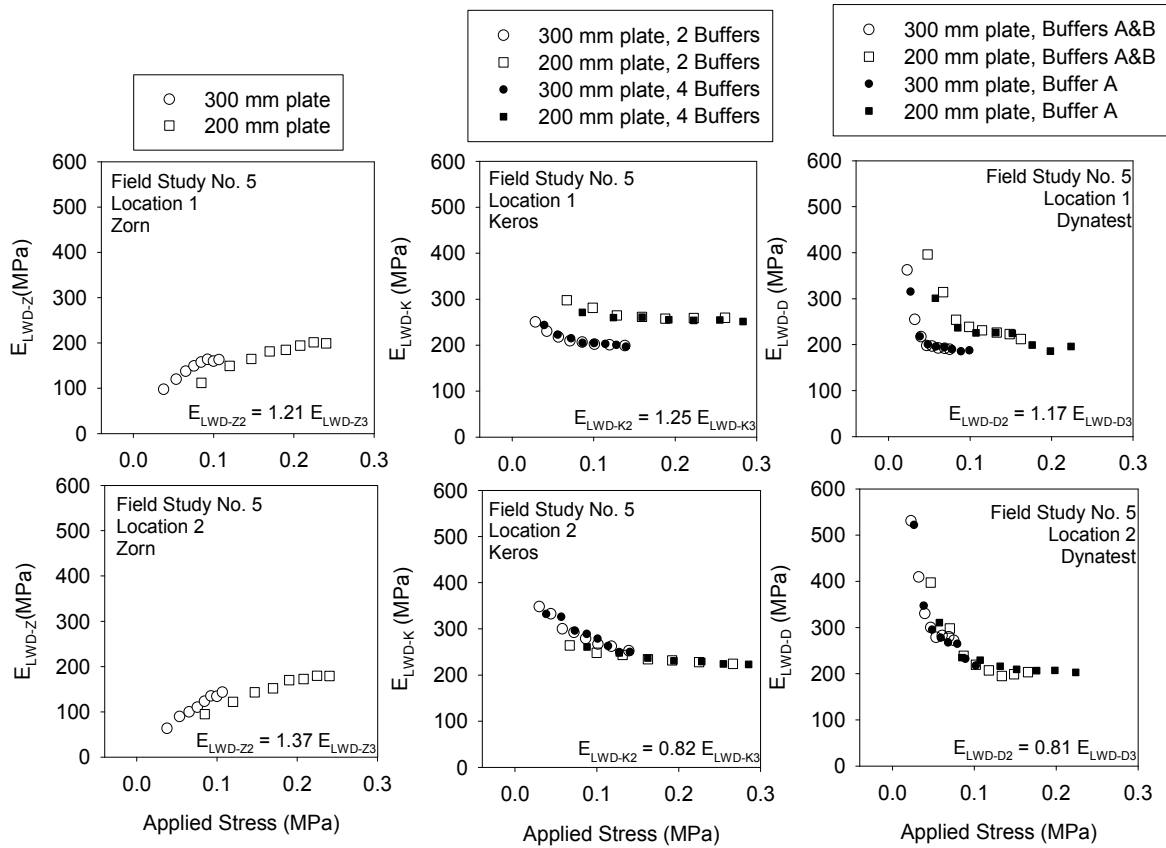


Figure 5.9. Influence of applied stress and effect of buffer stiffness on  $E_{LWD}$  with different plate diameters from Field Study No. 5

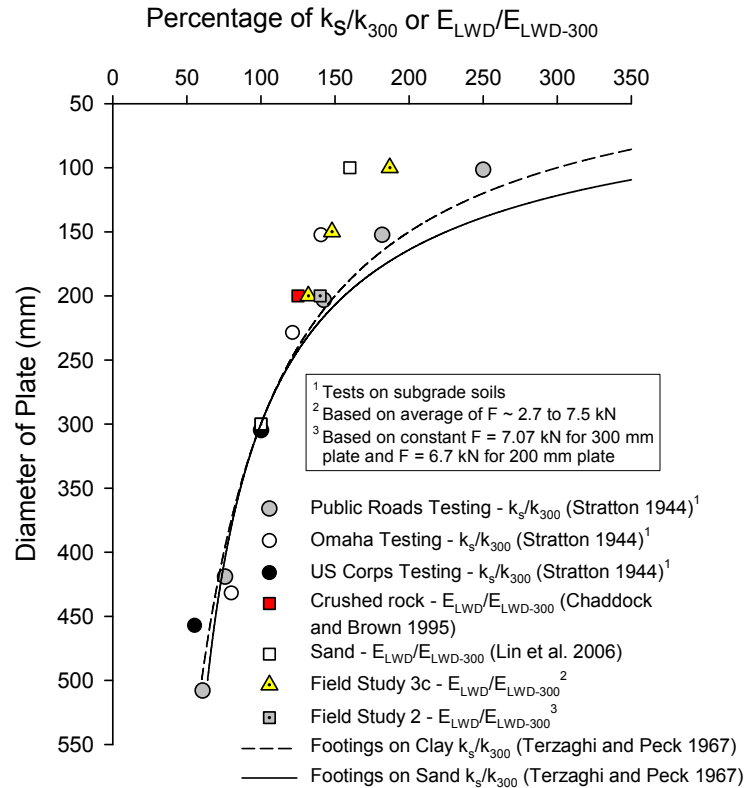


Figure 5.10. Relationship between material stiffness and diameter of bearing plate

### 5.3.3 Influence of Applied Contact Stress on $E_{LWD}$

Figure 5.8 and Figure 5.9 show relationships between applied contact stress and  $E_{LWD}$ . Figure 5.8 shows a strong stress dependency with a consistent increase in  $E_{LWD-Z}$  with increasing contact stress for all plate diameters. For Field Study No. 3c, an increase in drop height from 10 to 80 cm increased  $E_{LWD}$  by 45%, 75%, 93%, and 77%, for 300, 200, 150, and 100 mm diameter plates, respectively. At Field Study No. 4, an increase in  $E_{LWD}$  by 97%, 79%, 61%, and 54% was observed for 300, 200, 150, and 100 mm diameter plates, respectively.

Figure 5.9 shows comparison test results from Field Study No. 5 with  $E_{LWD}$  from Zorn, Keros, and Dynatest LWD devices. Similar to findings from Field Study No. 4, the  $E_{LWD-Z}$  increased with increasing applied contact stress for both 300 and 200 mm diameter plates. In contrast, both Keros and Dynatest devices showed a decrease in  $E_{LWD}$  with increasing contact stress. From the two test locations, on average the  $E_{LWD-K}$  decreased by about 32% and 17% with increasing contact stress from 30 to 139 kPa and 67 to 300 kPa for 300-mm and 200-mm plates, respectively. Similarly, on average from two test points, the  $E_{LWD-D}$  decreased by about 93% and 91% with increasing contact stresses from 22 to 75 kPa and 48 to 162 kPa for 300 mm and 200 mm plates, respectively.

The results presented above indicate that for the granular materials tested, Zorn  $E_{LWD}$  increases with increasing plate contact stresses. The rate of increase in  $E_{LWD}$ , however, is dependent on the

stiffness of the material; i.e., stiffer materials yielded a greater increase in modulus with increasing contact stress. Conversely, the Keros and Dynatest device measurements produced the opposite trend. However, the effect of applied stress on Keros and Dynatest  $E_{LWD}$  appears to have a comparatively reduced influence (less than about 10%) with increasing contact stresses above 100 kPa (for most QA/QC testing, applied stresses >100 kPa are typically used).

### 5.3.4 Influence of Buffer Stiffness on $E_{LWD}$

Steel spring buffers (e.g., Belleville washers) are used in the Zorn LWD device and conical/flat rubber buffers are used in Keros/Dynatest LWD devices (see Table 5.1). As discussed earlier, these different buffers vary in their stiffness. The Keros device is setup to use two or four rubber conical buffers, and the Dynatest device uses a two-piece, flat rubber buffer (Buffer A and B, see Figure 5.3). The effect of buffer stiffness on applied load at different drop heights is illustrated in Figure 5.11. On average, the applied force on Dynatest LWD increased by about 25% by increasing the buffer stiffness (i.e., by removing Buffer B), while the applied force on the Keros LWD increased by about 20% by increasing the buffer stiffness (i.e., adding two additional buffers (total four buffers)) under the impact load.

The effect of change in buffer stiffness on  $E_{LWD}$  measurements is presented in Figure 5.11. Tests with Keros LWD were conducted by adding two additional buffers to the existing two, and tests with Dynatest LWD were conducted by removing Buffer B to alter the buffer stiffnesses. If the measurement values at same drop height are compared, the  $E_{LWD-D}$  and  $E_{LWD-K}$  measurement values varied on average by about 8% and 2%, respectively, with change in buffer stiffnesses. However, if the results are compared for similar applied contact stresses, the change in  $E_{LWD}$  values are insignificant (<1%).

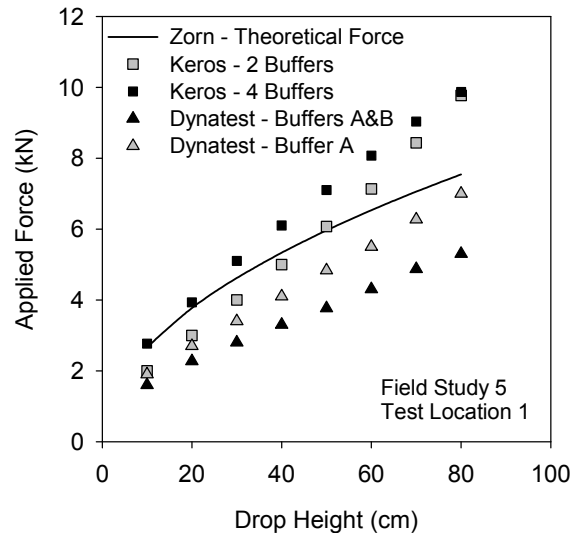


Figure 5.11. Effect of buffer type and stiffness on applied force for different LWD devices

### 5.3.5 Influence of Confinement on In-Situ $E_{LWD}$ Measurements

LWD tests on granular (cohesionless, e.g., fine sand) materials from US 10 and TH 36 projects discussed in Chapter 3 indicate that  $E_{LWD}$  measurement values in an excavation (at 100 to 200 mm depth) are significantly higher than  $E_{LWD}$  values at the surface. This is of consequence and important to address as it affects the determined “target values” during calibration testing. To investigate the issue, LWD measurements were performed at the compaction layer surface and at depths ranging from 100 to 800 mm below the surface at several test locations on the project. Figure 5.12 shows pictures of LWD tests performed in the excavations. At each test location, DCP tests were conducted to create continuous profiles of DPI as shown in Figure 5.13 (note that DPI is inversely related to soil modulus; see correlations presented in Chapter 3). For granular materials, it is generally believed that soil strength and stiffness/modulus is generally affected by the relative density and confining pressure. According to Lambe and Whitman (1969), as confining pressure ( $\sigma_c$ ) increases, elastic modulus increases as  $\sigma_c^n$  where  $n$  varies from 0.4 to 1.0.

Results presented in Figure 5.13 indicate that the penetration resistance generally decrease and  $E_{LWD}$  values generally increase with depth. Figure 5.14 shows a composite trend illustrating the influence of confinement neglecting any influence of relative density, moisture, or gradation changes and is expressed as Equation 5.3, where  $E_{LWD}(Z) = E_{LWD}$  value at depth  $Z$ ,  $E_{LWD}(0) =$

$E_{LWD}$  at surface ( $Z = 0$ ),  $\lambda =$  regression factor, and  $n = 0.4$ . Although there is significant scatter,

the general trend shows an increase in  $E_{LWD}$  values ( $\sim 150\%$  increase) at a depth of about 150 mm.

$$E_{LWD}(Z) = \lambda[E_{LWD}(0)](Z)^n \quad (5.3)$$



Figure 5.12. Pictures of LWD testing performed in the excavation – US10 project

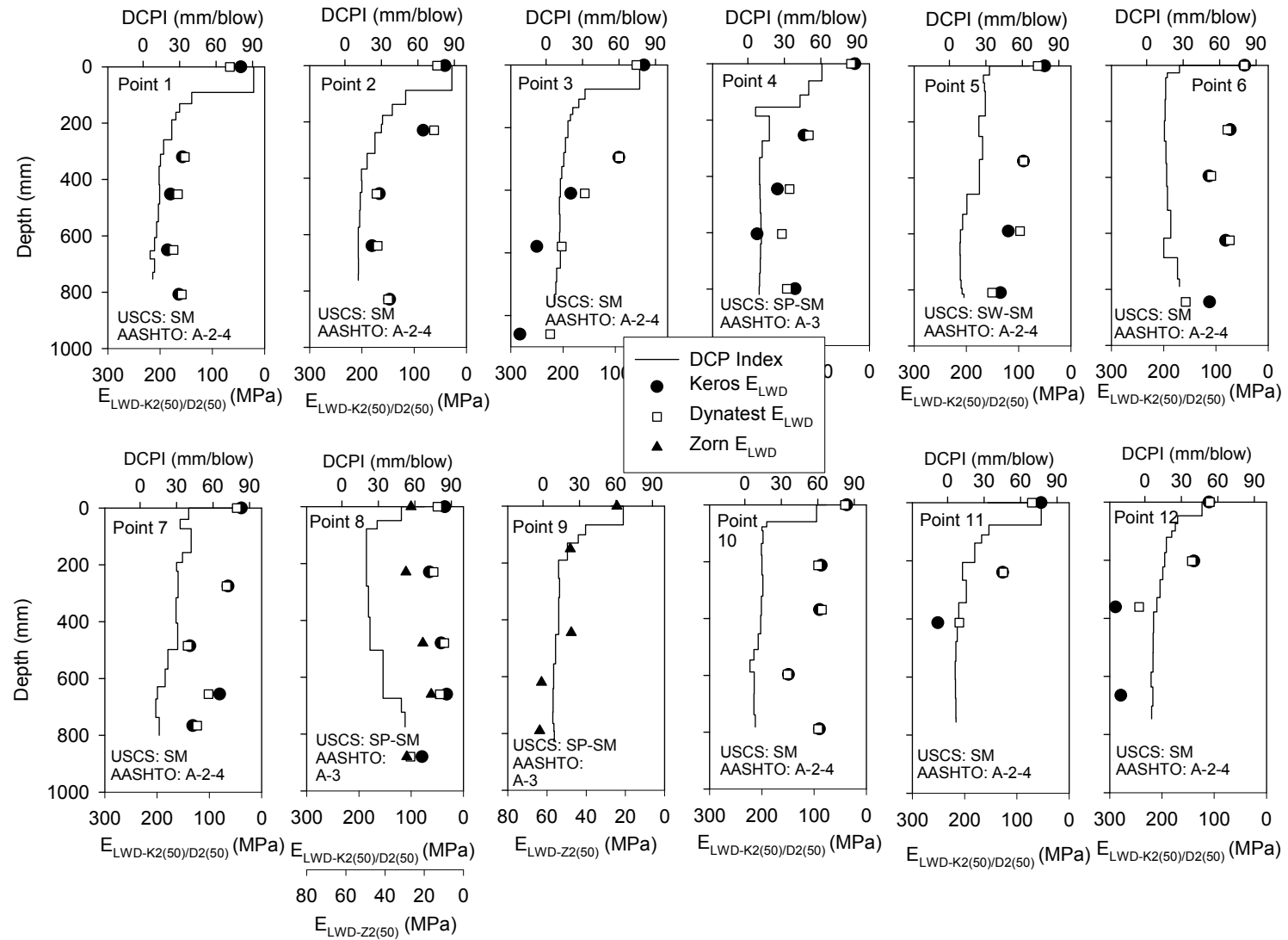


Figure 5.13. DPI profiles and LWD tests at different depths from US10, Staples, MN

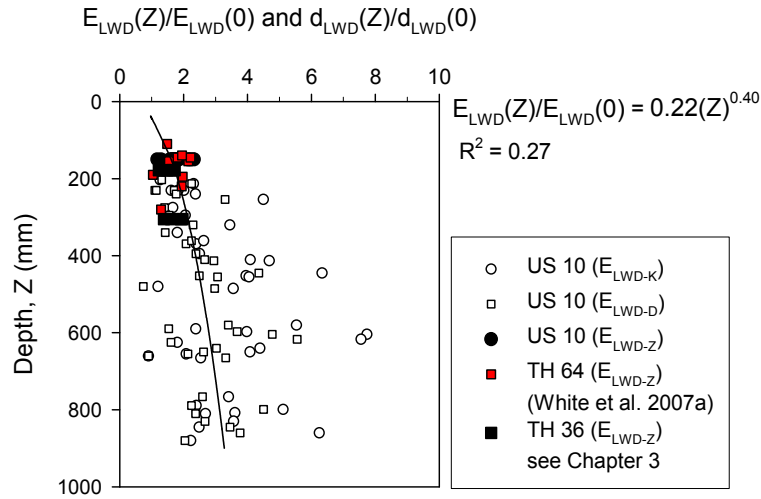


Figure 5.14. Normalized  $E_{LWD}$  versus depth with best fit power model to show general trend

#### 5.4 Variability of $E_{LWD}$ Measurements

An advantage of LWD testing is that many tests can be performed in a short period of time – perhaps as many as 10 or more compared to conventional sand cone density tests in the same time period. Simple and rapid field tests increase the efficiency of field engineers, and also have the advantage of better characterizing the soil variability. The COV values for  $E_{LWD}$  are generally higher than for density measurements (see Chapter 3 and White et al. 2007a).

Based on experimental LWD test results from projects described in Chapter 3 and White et al. (2007a), a summary of  $E_{LWD}$  measurement statistics ( $\mu$ ,  $\sigma$ , and COV) is presented in Table 5.4. In earthwork acceptance testing, to achieve good reliability and confidence in test measurements, it is important to plan and calculate the number of tests depending on the variability of the measurements. The sources of this variability generally include inherent variability in soil properties, sensitivity of the device, and repeatability and reproducibility of the measurements. Soil variability is often the dominating factor when it comes to measurement variability. The COV values from field testing indicate that the COV of Zorn  $E_{LWD}$  is generally lower, compared to Keros or Dynatest  $E_{LWD}$  values, with one exception at Field Study No. 3b. Some field studies showed considerable differences in the COV (e.g. Field Study Nos. 2 and 3a). As an example,  $E_{LWD-Z2}$  and  $E_{LWD-D2}$  measurements obtained from Field Study 3a are evaluated and compared. A simple statistical relationship shown in Equation 5.5 was used as a means to determine the number of tests needed to select a “target” value or to determine if a “target” value is achieved, with a selected statistical confidence.

$$L = y \pm t_{\alpha} \sqrt{\frac{s^2}{n}} \quad (5.5)$$

where  $L$  is the confidence limit of the average (target) value,  $t_{\alpha}$  is the Student’s  $t$  with  $(n - 1)$  degrees of freedom,  $\alpha$  is the probability level and  $s^2$  is the variance.

Field Study 3a consisted of a 30 m long test section with eleven test measurements. Prior to our testing, using the eleven test measurements, the 90% confidence limits for the  $E_{LWD-Z2}$  and  $E_{LWD-D2}$  measurements are  $49 \pm 2.5$  MPa and  $93 \pm 12.0$  MPa, respectively for the same material and test locations (see Figure 5.15). By randomly sampling three of the eleven measurements, the calculated average values could fall outside the 90% confidence limits for both devices resulting in selection of a target value that exceeds or under predicts the “true” value. Using this dataset and three random samples there is a 1:4.5 and 1:2.8 chance for Zorn and Dynatest, respectively that the selected target values are outside the 90% confidence limits.

From analyzing the variability of LWD measurement values, increasing the number of test measurements improves the statistical confidence in the limits. More analysis and work is needed to evaluate an approach for applying confidence limits to the selected target values. However, the implication is that with better defining the target value, pass/fail decisions can be made with improved confidence in the production tests areas. Further the number of test measurements must also consider the test variability itself. A laboratory study was performed on the LWD devices to specifically evaluate the test variability of the measurements and is discussed in the following section. Additional database development will also contribute to improving selection of appropriate target values.

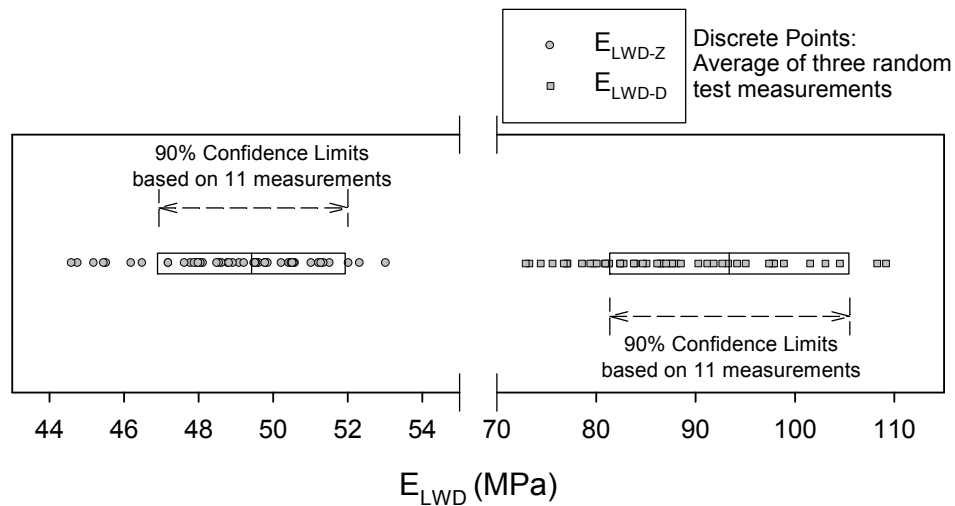


Figure 5.15. Comparison of 90% confidence limits for target value based on eleven  $E_{LWD-Z2}$  and  $E_{LWD-D2}$  measurement points with mean values calculated from random selection of three points (Field Study 3a granular subbase layer)

Table 5.4. Summary of modulus measurements from different field studies

Field Study	Measurement (MPa)	n	$\mu$	$\sigma$	COV (%)
Field Study No. 1a Mn/ROAD Subgrade (White et al. 2007a)	$E_{LWD-Z2(63)}$	13	50.9	31.0	61
	$E_{LWD-K2(63)}$	13	88.8	55.2	62
Field Study No. 1b Mn/Road Base (White et al. 2007a)	$E_{LWD-Z2(63)}$	124	33.5	18.0	54
	$E_{LWD-K2(63)}$	124	56.8	36.6	64
Field Study No. 2 TH64 Granular Base (White et al. 2007a)	$E_{LWD-Z2(63)}$	46	87.8	28.0	32
	$E_{LWD-Z3(72)}$	46	62.2	16.7	27
	$E_{LWD-K3(72)}$	46	140.1	58.8	42
Field Study No. 3a TH36 Granular Subbase	$E_{LWD-Z2(50)}$	11	74.2	6.9	9
	$E_{LWD-D2(50)}$	11	139.8	33.0	24
Field Study No. 3b TH36 Granular Base	$E_{LWD-Z2(50)}$	15	75.7	15.9	21
	$E_{LWD-D2(50)}$	15	117.0	22.3	19
Field Study No. 4 Granular Subgrade	$E_{LWD-Z2(50)}$	20	23.2	5.3	23
	$E_{LWD-D2(50)}$	20	46.9	15.5	33
	$E_{LWD-K2(50)}$	20	42.9	12.5	29
Field Study No. 6 US60 Subgrade	$E_{LWD-Z2(50)}$	14	14.7	4.2	29
	$E_{LWD-D2(50)}$	14	32.8	12.9	39
	$E_{LWD-K2(50)}$	14	30.2	9.8	33

### 5.5 Laboratory Evaluation of Repeatability and Reproducibility of LWD Measurements

To quantify the test variability (e.g., repeatability and reproducibility) of LWD plate deflection ( $d_0$ ), applied contact stress ( $\sigma_0$ ), and calculated  $E_{LWD}$  measurements, a laboratory study was conducted using five Zorn LWD models (4 from Mn/DOT and 1 from ISU) and three Dynatest LWD models (2 from Mn/DOT and 1 from ISU). The LWDs were setup with 200 mm plate diameter. The Zorn devices were setup at a calibrated height ranging from 54 cm to 56 cm to produce a constant applied stress of 0.2 MPa. The Dynatest device was setup at 50 cm drop height.

Repeatability refers to variation observed in LWD measurements when repeated measurements are made by the same operator and device following the same test method at a test location with negligible change in material property. This is also termed as measurement error ( $\sigma_{\text{repeatability}}$ )

and is equal to the standard deviation ( $\sigma$ ) of the repeated measurements. Reproducibility refers to the variations observed in LWD measurements under changing conditions, e.g., change in device, operator, test method, etc. In this study, LWD measurements were obtained on rubber pads with varying stiffnesses (stiff and soft pad setups; see Figure 5.16) by a single operator using different devices. Reproducibility variation ( $\sigma_{\text{reproducibility}}$ ) for change in device type is determined by performing Two-Way Analysis of Variance (ANOVA) with device and condition of test (stiff or soft) as random effects. Detailed procedures for calculating  $\sigma_{\text{repeatability}}$  and  $\sigma_{\text{reproducibility}}$  are presented in the Appendix. Further,  $\sigma_{\text{R\&R}}$  which is a measure of overall variability is calculated using Equation 5.4 to assess the contribution of reproducibility variation to the overall variation (Vardeman and Jobe 1999).

$$\sigma_{\text{R\&R}} = \sqrt{\sigma_{\text{repeatability}}^2 + \sigma_{\text{reproducibility}}^2} \quad (5.4)$$

Static plate load tests conducted on stiff and soft pads showed  $E_{V1}$  of about 3 MPa and 64 MPa, respectively (Figure 5.17). Rubber pads were elastic and therefore, no significant change in material properties with repeated drops is expected. A summary of experimental testing performed using different devices is provided in Table 5.5. For each condition, a total of 36 repeated drops were performed using each device. The first three drops were considered seating drops and therefore excluded from the analysis. The LWD tests were performed by following manufacturer recommendations (Dynatest 2004 and Zorn 2000).

Box plots of  $d_{\text{LWD}}$  and  $E_{\text{LWD}}$  measurements for each device are presented in Figure 5.18. Summary statistics from repeatability and reproducibility analysis are presented in Table 5.6 and Table 5.7. Percentage contribution of reproducibility due to model change on  $d_{\text{LWD}}$  and  $E_{\text{LWD}}$  measurements are summarized in Table 5.7. To quantitatively consider that there is no effect of model change on the measurement values, the contribution of  $\sigma_{\text{reproducibility}}$  to the overall variability  $\sigma_{\text{R\&R}}$  should be about 50% (i.e.,  $\sigma_{\text{reproducibility}} \sim \sigma_{\text{repeatability}}$ ) or less. The results are summarized separately for the Zorn and Dynatest LWD devices below:

- For the five Zorn LWD devices evaluated in this study,  $\sigma_{\text{repeatability}}$  in the  $d_{\text{LWD-Z2}}$  and  $E_{\text{LWD-Z2}}$  measurements increased with increasing measurement value, e.g.,  $\sigma_{\text{repeatability}}$  range for  $d_{\text{LWD-Z2}}$  for soft pad = 0.06 to 0.08 mm whereas for stiff pad  $\sigma_{\text{repeatability}}$  is around 0.01 mm. The COV values summarized in Table 5.6 show that  $d_{\text{LWD-Z2}}$  and  $E_{\text{LWD-Z2}}$  values for both stiff and soft pads are in the range of 2 to 3%. The contribution of variation attributed due to change in device on the  $d_{\text{LWD}}$  measurement values has low significance as the  $\sigma_{\text{reproducibility}}$  is less than  $\sigma_{\text{repeatability}}$  values (or in other words percent contribution less than 50%, see Table 5.7).
- For the three Dynatest LWD devices evaluated in this study,  $\sigma_{\text{repeatability}}$  in  $E_{\text{LWD-D2}}$  measurements increased with increasing measurement value, whereas no statistically significant trend was observed for  $d_{\text{LWD}}$  measurements. The COV values summarized in Table 5.6 show that  $d_{\text{LWD-D2}}$  and  $E_{\text{LWD-D2}}$  values for soft pads are in the range of 2 to 4%, while for stiff pads they are in the range of 18 to 72%. The contribution of variation

attributed due to change in device on the measurement values is significant for  $d_{LWD-D2}$  and  $\sigma_0$  measurements due to higher  $\sigma_{reproducibility}$  than  $\sigma_{repeatability}$  values.

A question can be raised here as to whether using  $\sigma_{repeatability}$  (or sometimes range) alone is appropriate from a specification stand point to verify the measurements are “repeatable”. The answer is that it is not appropriate to use  $\sigma_{repeatability}$  for the case where it increases with increasing measurement values as observed for  $d_{LWD-Z2}$ ,  $E_{LWD-Z2}$ , and  $E_{LWD-D2}$ . For this case, the COV parameter is more appropriate as the variation is interpreted in the context of the mean of the data. Currently, there is no standard on acceptable limits for repeatability and reproducibility variations on the LWD measurements. However, it is important to emphasize here that these variations must be accounted for in selecting the number of test measurements to be made in-situ for developing target values with adequate statistical confidence as described in 5.4. Further, a detailed laboratory investigation is warranted to further quantify the repeatability and reproducibility of LWD measurements over a wide range of material stiffnesses and independent verification of deflection measurements using precise measurement methods. Reproducibility must also be quantified in a context of change in operator.

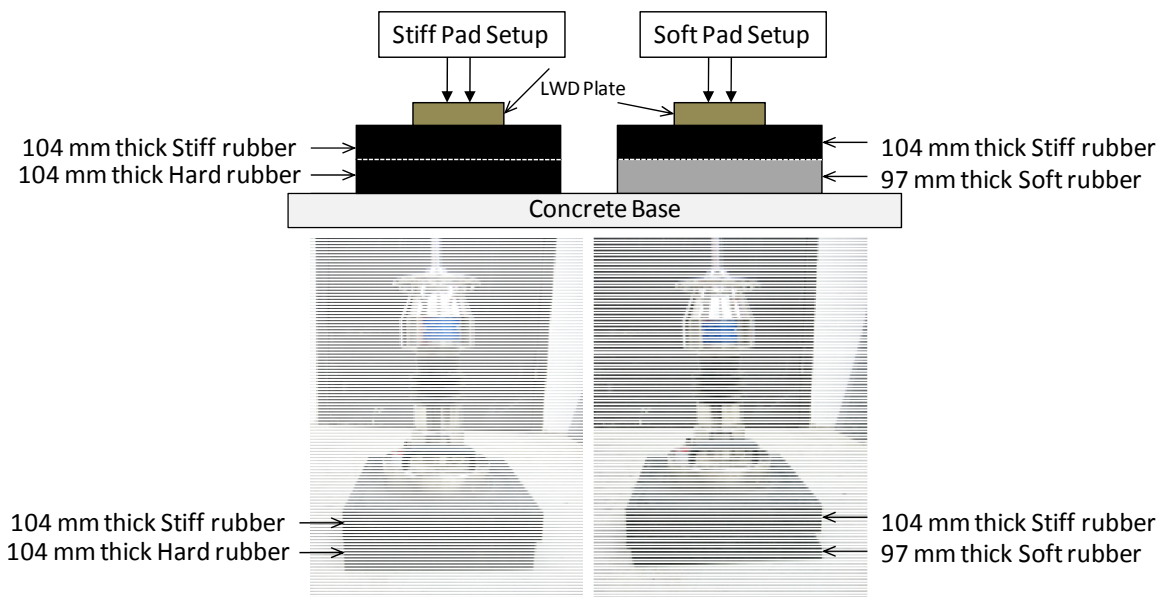


Figure 5.16. Schematic and pictures of soft and stiff pad setups

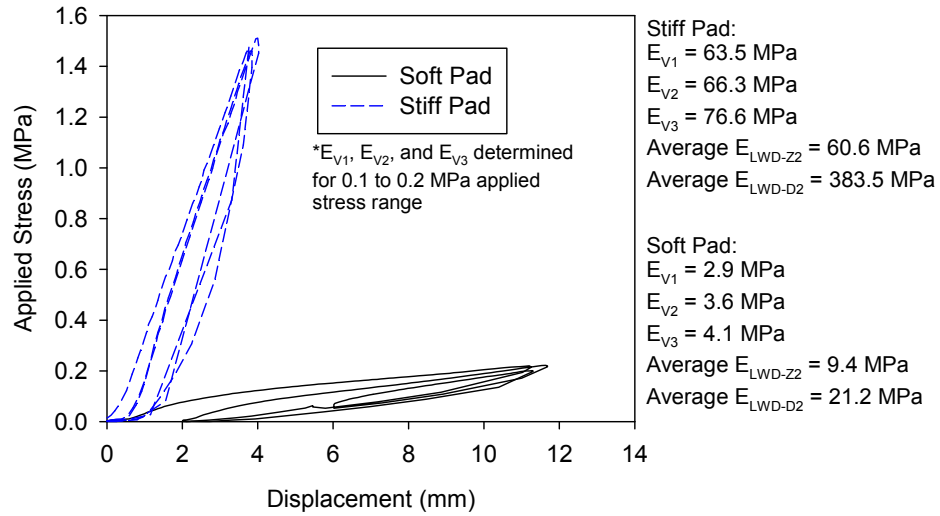


Figure 5.17. Static plate load test applied stress-displacement curves for soft and stiff pads

Table 5.5. Summary of testing for repeatability and reproducibility evaluation on LWD measurements

Model*	Devices	Material	Number of drops**	Measurements
Zorn	4457, 4321, 3480, and 4420 (Mn/DOT), and 3936 (ISU)	Soft Pad and Stiff Pad	33	$d_{LWD-Z2}$ and $E_{LWD-Z2}$
Dynatest	0021 and 0041 (Mn/DOT) and 0042 ISU)	Soft Pad and Stiff Pad	33	$d_{LWD-D2}$ , $\sigma_0$ , and $E_{LWD-Z2}$

\*LWD devices setup with 200 mm plate diameters; \*\*Excluding 3 seating drops

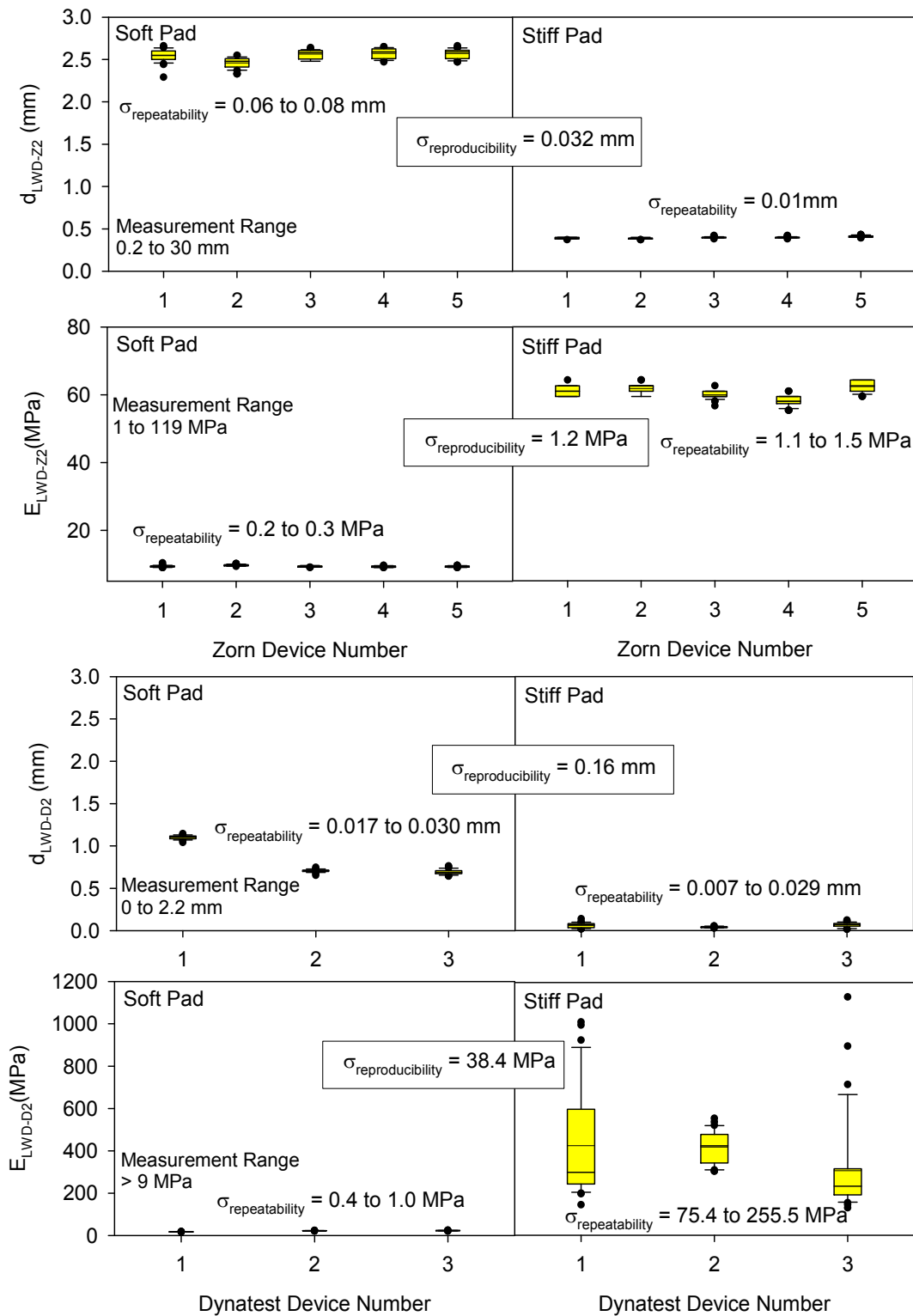


Figure 5.18. Box plots of  $d_{LWD-ZZ}$ ,  $E_{LWD-ZZ}$ ,  $d_{LWD-D2}$  and  $E_{LWD-D2}$  measurements for different models from 33 repeated drops

Table 5.6. Summary of repeatability analysis results on LWD measurements

Device	Material	$d_{LWD}^*$			Applied Stress*			$E_{LWD}^*$		
		$\mu$ (mm)	$\sigma$ (mm)	COV (%)	$\mu$ (kPa)	$\sigma$ (kPa)	COV (%)	$\mu$ (MPa)	$\sigma$ (MPa)	COV (%)
<i>Zorn LWD</i>										
4457 (Mn/DOT)	Soft Pad	2.55	0.08	3	Assumed as constant (200 kPa) (Based on Equation 5.2)			9.3	0.3	3
	Stiff Pad	0.39	0.01	2				61.0	1.4	2
4321 (Mn/DOT)	Soft Pad	2.46	0.06	3				9.7	0.3	3
	Stiff Pad	0.39	0.01	2				61.7	1.3	2
3480 (Mn/DOT)	Soft Pad	2.56	0.05	2				9.3	0.2	2
	Stiff Pad	0.40	0.01	2				59.9	1.1	2
4420 (Mn/DOT)	Soft Pad	2.57	0.06	2				9.2	0.2	2
	Stiff Pad	0.41	0.01	2				58.0	1.4	2
3936 (ISU)	Soft Pad	2.57	0.06	2				9.3	0.2	2
	Stiff Pad	0.38	0.01	2				62.3	1.5	2
<i>Dynatest LWD</i>										
0021 (Mn/DOT)	Soft Pad	1.102	0.023	2	149.3	0.9	1	17.9	0.4	2
	Stiff Pad	0.063	0.029	47	152.3	1.3	1	425.4	255.5	60
0041 (Mn/DOT)	Soft Pad	0.707	0.017	2	120.7	1.3	1	22.5	0.5	2
	Stiff Pad	0.040	0.007	18	122.2	0.9	1	418.4	75.4	18
0042 (ISU)	Soft Pad	0.691	0.030	4	121.7	1.0	1	23.3	1.0	4
	Stiff Pad	0.068	0.026	39	121.2	1.7	1	306.7	222.3	72

\* $\sigma$  represents measurement error

Table 5.7. Summary of R&R analysis on LWD measurements for change in device

Model	Measurement (Units)	$\sigma_{\text{repeatability}}$	$\sigma_{\text{reproducibility}}$	$\sigma_{\text{R\&R}}$	Percent contribution* of $\sigma_{\text{reproducibility}}$	Impact of device change on measurement values
Zorn	$d_{\text{LWD-Z2}}$ (mm)	0.043	0.032	0.050	35	Low significance
Dynatest	$d_{\text{LWD-D2}}$ (mm)	0.023	0.158	0.160	98	High significance
	Applied stress (kPa)	1.2	16.1	16.2	99	High significance

\* $100 \times \sigma_{\text{repeatability}}^2 / \sigma_{\text{R\&R}}^2$

## 5.6 Guidance for LWD Testing Standard Protocol for Granular and Non-Granular Soils

ASTM and Mn/DOT are developing standard test protocols for performing LWD testing. Following a standard protocol is important as  $E_{\text{LWD}}$  measurements are sensitive to localized disturbance, confinement, geophone/plate seating, levelness, and plate contact stress. Some key points providing guidance for development of the protocol are described below based on experience from experimental studies described above, a review of manufacturer manuals, and a detailed literature review (Vennapusa and White 2009a, White et al. 2007a, Beyer et al. 2006, draft ASTM Standard for LWD testing). Based on field studies documented in Chapter 3 and results presented above, a standard plate diameter of 20 cm and drop height of about 50 cm (contact stress = 0.2 MPa) is determined as adequate for the range of materials tested in Minnesota.

Following are some of the key points for LWD verification tests:

1. Quantify repeatability of LWD measurements prior to use on a project site. This is performed using the following procedure:
  - Select at least three test materials – low, medium, and stiff within the limits of measurement of the device. Perform three seating drops followed by nine consecutive measurement drops and record deflection, applied stress, and  $E_{\text{LWD}}$  measurements. The COV in the measurements at each test location should be less than a specified value (a detailed laboratory investigation is warranted to develop specifications on acceptable COV for the measurements).
2. Quantify reproducibility of LWD measurements. This should be done in a context of change in operator and device, especially if multiple operators and devices are utilized for a project. This procedure has the added benefit of being a training exercise for field engineers. The procedure to quantify reproducibility is as follows and can be combined with the repeatability measurements:

- Select at least three materials with varying stiffness for LWD testing following the procedure described under step 1. Tests should be performed by each operator on at least one device for the three materials, and by one operator on all the devices for the three materials. Perform three seating drops followed by nine consecutive measurement drops and record deflection, applied stress, and  $E_{LWD}$  measurements. Compute repeatability and reproducibility standard deviations. The reproducibility standard deviation should be similar or less than the repeatability standard deviation.

A detailed procedure for repeatability and reproducibility analysis is presented in the Appendix.

Following are some of the key points during in-situ LWD testing:

1. The test surface should be level and smooth. Levelness can be checked with a bubble level. The LWD plate should not translate laterally with successive drops.
2. Tests on cohesionless materials (e.g., USCS: SW, SP, SM), should be performed in a test pit by excavating surficial loose material (e.g., Figure 5.19). Based on experience, the excavation depth may vary between 100 to 150 mm. As a rule-of-thumb, the diameter of the test pit should be approximately 2 times the plate diameter (i.e. 400 mm for 200 mm plate).
3. Tests on non-granular materials (e.g., CL, CH) compacted with padfoot rollers should be at or lower than the bottom of the padfoot penetration (see Figure 5.20). (Preparation of a quality test surface often requires more time than performing the LWD test.)
4. Tests on granular base/stabilization layer materials should be at the surface of the compaction layer and may require a thin layer of leveling sand to ensure uniform contact of plate with the testing surface. Excess sand can cause seating problems, especially with geophones and should be minimized.
5. Perform three seating drops before collecting data for consistent measurements. If noticeable deflection or bearing capacity failure occurs, the material needs further compaction or is too wet. For stiff materials, one or two seating drops may be sufficient and can be determined by collecting data and demonstrating that successive seating drops do not change the  $d_{LWD}$  by more than about 5%.
6. Following the seating drops, perform three measurement drops of the falling weight for a given drop height recording data for each drop. If  $d_{LWD}$  values successively decrease with each drop exceeding 10% of the previous measurement, additional compaction is likely needed (this criteria will be helpful to the field engineer to quickly identify problem areas).
7. Record  $d_{LWD}$  from the last three measurement drops and compute the average.

8. If desired, record  $E_{LWD}$  by using appropriate shape factor,  $F$  in the calculation ( $F = \pi/2$  for non-granular materials,  $F = 8/3$  for granular materials, and  $F = 2$  for intermediate materials). A Poisson's ratio value of 0.4 is suggested.
9. Report the following from each test location:
  - Material/Layer
  - Test location identification (e.g., station, offset, etc.)
  - Excavation depth if tested on granular materials
  - Air temperature
  - $d_{LWD}$  measurements from three measurement drops
  - Applied stress measurements (if provided in the output)
  - Assumptions used in  $E_{LWD}$  calculation, if  $E_{LWD}$  values are reported (i.e., Poisson's ratio and shape factor used)



Figure 5.19. LWD test in an excavation by removing loose material at the surface to a depth of about 100 to 200 mm for cohesionless materials



Figure 5.20. Level surface at the bottom of the padfoot impression for non-granular materials

## 5.7 Comparison between $E_{LWD}$ and CIV measurements

There has been some interest among Mn/DOT field personnel on comparing Clegg hammer devices with LWD devices due to its portability and ease of use. Clegg hammer testing and determination of CIV is described in ASTM D5874-02. The CIV is considered a strength index parameter that has been correlated with CBR and elastic modulus. Theoretically derived relationships between CIV and elastic modulus are provided by the manufacturer (Newsletter #14, 1995).

Experimental test results correlating 200 mm plate diameter Zorn LWD measurements ( $E_{LWD-Z2}$  and  $d_{LWD-Z2}$ ) with 20-kg Clegg hammer ( $CIV_{20\text{-kg}}$ ) measurements on two project sites with granular material (TH64 and TH36 projects) and one project site with non-granular material (MnROAD project) are presented in the discussion that follows. Soil index properties at each project site are summarized in Table 5.8. TH 64 and MnROAD projects are described in White et al. (2007a). The Zorn LWD device was setup with a drop height of 63 cm on the TH64 and MnROAD projects and with a drop height of 71 cm on the TH36 project LWD tests were conducted in accordance with manufacturer recommendations and  $E_{LWD}$  was determined using Equation 5.1. Clegg hammer tests were conducted in accordance with ASTM D5874-02. At each test location, the LWD and Clegg device were performed within a spacing of approximately 0.3 m or less to minimize variation in soil properties between the test locations. For tests at the TH 36 and TH 64 project sites, measurements were performed at the surface and at approximately 150 mm to 300 mm below the surface. For tests at the MnROAD site, measurements were performed on a flat excavated surface at the bottom of the foot penetration of padfoot rollers (no leveling sand was used).

Summary statistics of  $E_{LWD-Z2}$  and  $CIV_{20\text{-kg}}$  from different proof layers at each project site are provided in Table 5.8. Figure 5.21 shows correlations between  $E_{LWD-Z2}$ ,  $d_{LWD-Z2}$  and  $CIV_{20\text{-kg}}$  separately for granular and non-granular materials.

Results from the TH 64 and TH36 projects with granular subgrade materials showed strong correlations between LWD measurements and  $CIV_{20\text{-kg}}$  values with  $R^2 = 0.76$ . The COV values of the two measurement values for each proof layer are generally comparable (see Table 5.9). Considering data from TH 64 and TH 36 projects,  $E_{LWD-Z2}$  is on average 4.2 times higher than  $CIV_{20\text{-kg}}$  for the range of values and the granular materials tested.

Results from the MnROAD project site with non-granular materials produced weaker correlation with  $R^2 = 0.35$ . The COV of the two measurement values on the final compacted layer are comparable (17% for  $E_{LWD-Z2}$  and 18% for  $CIV_{20\text{-kg}}$ ), however. On average, the  $E_{LWD-Z2}$  was about 2.6 times higher than  $CIV_{20\text{-kg}}$  for the range of measurements and the non-granular material tested.

With regard to use of the Clegg impact hammer in lieu of the LWD, some advantages would be that the device is relatively simply to operate, the cost is lower than the LWD, the results generally correlate to CBR and  $E_{LWD}$ , and the ASTM standard provides guidance on selecting target values. Further, the maximum measurable CIV is about 100 (or 1000g), which is

representative of a soil with an elastic modulus of about 2000 MPa for the 20-kg Clegg hammer (Newsletter # 14, 1995). On the other hand, the maximum measurable  $E_{LWD-Z}$  is about 120 MPa for 200 mm diameter plate (with drop height of 50 cm). To be brief, for materials with high stiffness (e.g. stabilized materials) the Clegg device would still be within the measurement range.

Some disadvantages in using the Clegg hammer would be that the maximum particle size of the material tested will be limited by the smaller plate diameter, and multiple devices of different drop weight may be needed to test the range of strengths and stiffnesses in the field, especially for soft materials, whereas the drop height can be adjusted for the LWD. In addition, more detailed and statistically reliable empirical correlations between CIV and mechanistic parameter values are warranted for a range of soil types as further evaluation.

Table 5.8 Summary of soil index properties – LWD-Clegg comparison studies

Location	Testing Layer	$c_u$	$c_c$	LL (%)	PI	Soil Classification	
						AASHTO	USCS
TH 64 Akeley, MN (White et al. 2007a)	Granular Subgrade	2.67 to 7.67	0.12 to 0.71	Non-Plastic		A-3	SP to SW-SM
TH 36 North St. Paul, MN (this study)	Granular Subgrade	—	—	13	Non - Plastic	A-2-4	SM
MnROAD Albertville, MN (White et al. 2007a)	Subgrade	—	—	31	13	A-6(5)	CL

Table 5.9. Comparison of summary statistics for  $E_{LWD-Z2}$  and  $CIV_{20\text{-kg}}$  measurements

Location	Parameter	n	$\mu$	$\sigma$	COV* (%)
TH 64 Proof 1 (surface)	$E_{LWD-Z2}$ (MPa)	54	28.3	5.0	18
	$CIV_{20\text{-kg}}$	54	6.9	1.4	20
TH 64 Proof 2 (surface)	$E_{LWD-Z2}$ (MPa)	36	23.1	3.6	15
	$CIV_{20\text{-kg}}$	36	5.0	1.0	19
TH 64 Proof 3 (surface)	$E_{LWD-Z2}$ (MPa)	6	26.0	3.9	15
	$CIV_{20\text{-kg}}$	6	5.5	0.7	12
TH 64 Proof 4 (surface)	$E_{LWD-Z2}$ (MPa)	11	33.5	5.2	15
	$CIV_{20\text{-kg}}$	11	8.1	2.4	31
TH 64 Proof 4 (~150mm below surface)	$E_{LWD-Z2}$ (MPa)	11	55.7	10.2	18
	$CIV_{20\text{-kg}}$	11	12.9	2.2	17
TH 36 Proof 1 (surface)	$E_{LWD-Z2}$ (MPa)	7	27.2	4.9	18
	$CIV_{20\text{-kg}}$	7	6.3	1.1	17
TH 36 Proof 1 (~150mm below surface)	$E_{LWD-Z2}$ (MPa)	6	41.0	6.1	15
	$CIV_{20\text{-kg}}$	6	7.5	1.0	13
TH 36 Proof 1 (~300mm below surface)	$E_{LWD-Z2}$ (MPa)	4	49.1	5.4	11
	$CIV_{20\text{-kg}}$	4	8.8	1.4	16
MnROAD (surface – bottom of padfoot penetration)	$E_{LWD-Z2}$ (MPa)	10	43.4	7.2	17

\*Clegg impact value COV for uniform condition is about 4% and variable condition is about 20% (ASTM D5874-02)

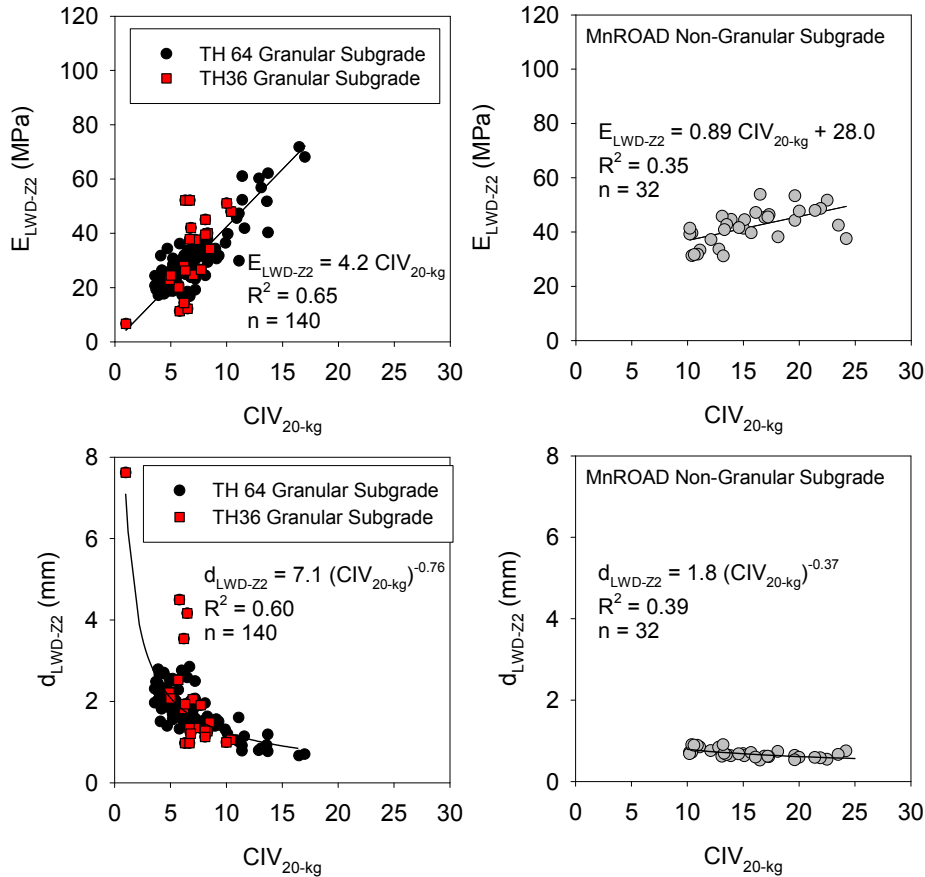


Figure 5.21. Simple linear regression relationships between  $E_{LWD-zz}$  and  $CIV_{20-kg}$

### 5.8 Target Value Determination Study

Establishing  $E_{LWD}$  target values is considered an obstacle to wider implementation and creates some uncertainty with QA/QC operations. Current practices rely to some degree on field experience and determination of values from representative field test sections that have been prepared within the range of acceptable moisture content limits and after several roller passes. Field observations indicate that the  $E_{LWD}$  values are heavily influenced by water content and confinement/depth of embedment, especially for non-granular materials and sandy granular materials, respectively.  $E_{LWD}$  values are also dependent on the factors discussed in previous sections in terms of the device configuration and loading conditions. In this section,  $E_{LWD}$  values are compared to traditional QA/QC parameters — water content and dry unit weight — based on laboratory measurements. Laboratory test specimens were developed using a gyratory compactor which produce relatively larger specimens (150 mm diameter x 150 mm high) compared to Proctor specimens (102 mm diameter by 116 mm high) and providing complete density and shear resistance curves versus number of gyrations for each specimen. By performing LWD and other measurements on the test specimens, relationships between moisture content, density, shear

resistance,  $E_{LWD}$ , undrained shear strength, and resilient modulus were developed. Although results show how these parameter values interrelate, some limitations were identified with the approach in terms of the influence of boundary conditions and sample size.

### 5.8.1 Background and Test Methods

With developments in compaction equipment technology and increasing use of heavy rollers, researchers have introduced concerns over laboratory Proctor and vibratory compaction methods in developing moisture-density relationships that simulate field conditions. The Army Corps of Engineers (Coyle and West 1956, McRae 1965) introduced the gyratory compaction test procedure for soils based on extensive testing on silty sand material in the Mississippi area. Measurements have shown that gyratory compaction can simulate field compaction characteristics better than impact compaction with standard Proctor energy. Recent work by Kim and Labuz (2006) and Gupta et al. (2009) on recycled granular materials in Minnesota provided similar conclusions. Based on testing fine sand and silty sand materials, Ping et al. (2003) found that the optimum moisture and maximum densities achieved in the field were closer to gyratory compaction results than both impact (modified Proctor) and vibratory compaction. According to Browne (2006) the gyratory compaction method produced maximum dry unit weights greater than modified Proctor method for three different types of soils (A-1-a, A-3, and A-7-6), but depends on the number of gyrations and compaction pressure.

The gyratory compaction method was standardized by ASTM (ASTM D-3387) based on the work by McRae (1965) for its use for subgrade, base and asphalt mixtures. This method, however, has not been widely implemented for compaction of subgrade and base materials. One reason for slow implementation may be that no standard gyratory variables (e.g. gyration angle, number of gyrations, normal stress, or rate of gyrations) have been developed for subgrade and subbase materials. For the results presented in the following sections of the report, a thoroughly mixed, loose, moist sample was placed into the cylindrical mold, and then a controlled vertical stress ( $\sigma_v$ ) (ranging from 100 to 900 kPa) was applied to both the top and bottom of the sample at a constant rate (gyrations per minute = 30). Number of gyrations was varied depending on the testing objective. The applied vertical stress is supplemented with kneading action or gyratory motion at an angle (gyration angle = 1.25 degrees) to compact the material. AFGB1A Brovold gyratory compactor (manufactured by Pine Instrument Company) shown in Figure 5.22 was used in this study.

Guler et al. (2000) recently reported on the Pressure Distribution Analyzer (PDA) to evaluate the stability of asphalt mixtures during compaction in a gyratory mold. The PDA is a device (see Figure 5.22) that can be placed above or below the sample in the gyratory compaction mold to capture the pressure distribution across the sample during compaction. The data output from the PDA includes total resultant force ( $R$ ) and the eccentricity ( $e$ ) at which the resultant force is acting. Using the  $R$  and  $e$  measurements, the frictional resistance or shear resistance ( $\tau_G$ ) of the compaction material can be calculated using Equation 5.5:

$$\tau_G = \frac{R \cdot e}{A \cdot H} \quad (5.5)$$

where  $R$  = resultant force,  $e$  = eccentricity,  $A$  = sample cross-sectional area, and  $H$  = sample height at any gyration cycle. The relationships between  $\tau_G$  and  $M_r$ ,  $s_u$ , and  $E_{LWD}$  are explored in this report.

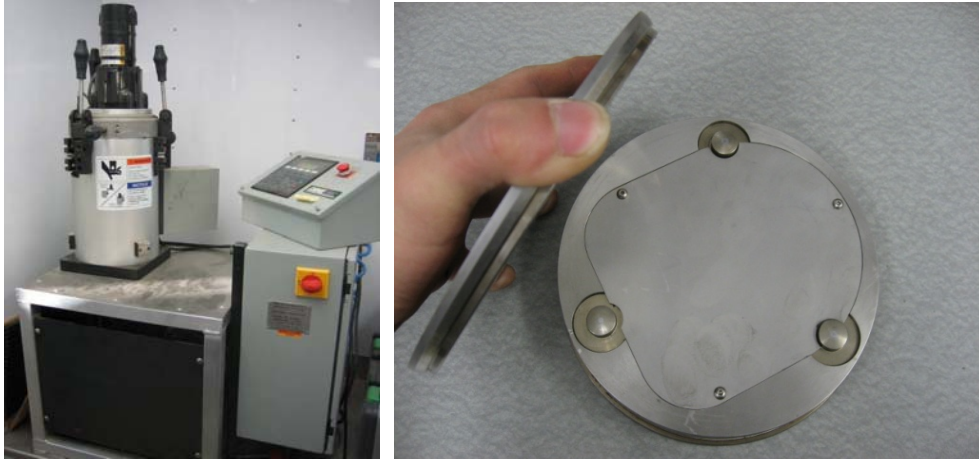


Figure 5.22. AFGB1A gyratory compactor (left) and pressure distribution analyzer (PDA)

### 5.8.2 Laboratory Approach

A brief overview of the approach followed in this research to determine  $E_{LWD}$  and other mechanistic related parameter ( $M_r$ ,  $s_u$ , and DPI) target values is summarized in Figure 5.23. Specimens were compacted using the gyratory compactor at  $\sigma_o = 100$  to 900 kPa along with PDA measurements. Later, LWD, DCP,  $M_r$ , and  $s_u$  tests were conducted on the compacted specimens. The goal was to link these parameter values using one type of specimen to moisture and density values.

The main objectives of the laboratory testing phase are categorized into five areas and are summarized in Table 5.10. Soil index properties of materials evaluated in this study are summarized separately for non-granular and granular materials in Table 5.11 and Table 5.12, respectively.

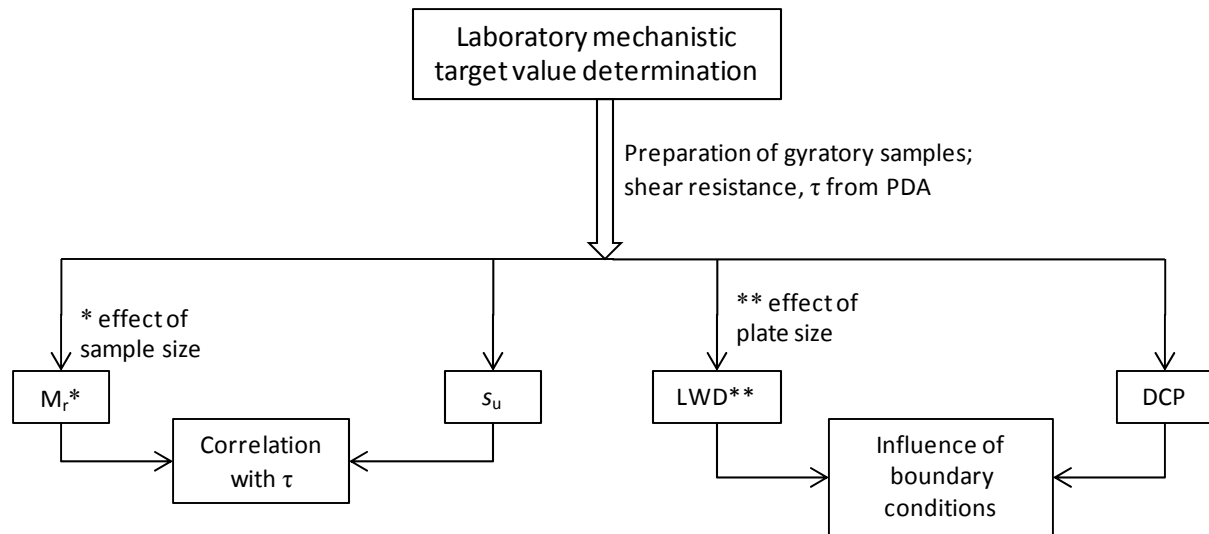


Figure 5.23. Approach for laboratory mechanistic target value determination using gyratory compacted specimens

Figure 5.24 to Figure 5.31 show the dry unit weight versus number of gyration compaction curves for all materials. Comparisons between moisture content-dry unit weight relationships from Proctor compaction tests using standard and modified procedures for eight different materials are provided in Figure 5.32.

Generally, results show that optimum moisture contents are at higher degrees of saturation for the gyratory specimens compacted to the Proctor specimens and that  $\sigma_o = 300$  kPa produced maximum dry densities at 100 gyrations between standard and modified Proctor.

Zorn LWD setup with a 100 mm diameter plate and DCP tests were conducted on gyratory compacted samples prepared at various target moisture and dry unit weights. Tests were initially conducted by testing the specimens as compacted in the gyratory mold. These results were used to evaluate the  $w-\gamma_d$  and  $E_{LWD-ZI}$  and DPI relationships. Using the DPI- $s_u$  relationship developed from TH 60 field testing (see Chapter 3), relationships between  $w-\gamma_d$  and  $s_u$  were also developed.

The rigid boundary condition of the gyratory mold creates a stiffer response from the in-mold LWD testing compared to no boundary. The true boundary conditions experienced in the field are somewhere in the middle and variable. To evaluate the effects of boundary conditions and effect of plate diameter on the  $E_{LWD}$  values, Zorn LWD tests using 100 and 150 mm plate diameters (Figure 5.33) were conducted with four different boundary conditions as shown in Figure 5.34: (a) no confinement, (b) confinement with a soft polyurethane (Durometer = 20A) sleeve, (c) confinement with a stiff polyurethane (Durometer = 50 A) sleeve, and (d) the aforementioned rigid confinement in the gyratory mold. For “soft” and “stiff” boundary conditions, the compacted samples were extracted from the rigid gyratory mold into the respective polyurethane sleeves. This procedure is illustrated in Figure 5.35.

Unconfined compression (UC) (ASTM D 2166), resilient modulus ( $M_r$ ) (AASHTO T-307), and unconsolidation undrained (UU) (AASHTO-T307) tests were performed on extracted gyratory compacted specimens. Pictures from the UC and  $M_r$  testing on 150 mm diameter gyratory samples are shown in Figure 5.36 and Figure 5.37. According to the standard test procedures, these tests should be performed on samples with height (H) to diameter (D) ratio = 2. The gyratory compacted specimens have a H:D = 1. To investigate the influence of H:D ratio,  $M_r$  and UU tests were conducted on gyratory compacted samples with H:D = 1 and 2. The H:D = 2 samples were obtained by hydraulically pushing a 72 mm diameter thin-walled Shelby tube into the gyratory mold (see Figure 5.38).

The PDA device was used during gyratory compaction testing to provide obtain  $\tau_G$  and compared with  $E_{LWD}$ ,  $s_u$ ,  $M_r$ , and UU test results.

Table 5.10. Summary of experimental testing – laboratory target value determination study

Objective	Materials	Soil ID	Project location	Remarks
Evaluate $w$ - $\gamma_d$ -DPI/ $s_u$ / $E_{LWD}$ relationship	Non-granular	TH36 silty clay	North St. Paul, MN	Samples were tested in gyratory compaction mold (rigid boundary condition). Applied vertical stresses during gyratory compaction = 100, 300, 600, and 900 kPa
		TH60 – soil 301, soil 303, soil 305	Bigelow, MN	
	Granular	US10	Staples, MN	
		TH36 silty clay	North St. Paul, MN	
Effect of boundary condition on $E_{LWD}$ (100 and 150 mm plate diameter LWDs)	Non-granular	TH 60 soil 306	Bigelow, MN	Samples were tested using with four different boundary conditions (rigid, stiff, soft, no confinement). Applied vertical stress during gyratory compaction = 300 kPa. Effect of plate size on $E_{LWD}$ is evaluated
	Granular	US10	Staples, MN	
Correlation between $\tau_G$ , $s_u$ and $E_{LWD-Z}$	Non-granular	Loess	Western Iowa	Applied vertical stress during gyratory compaction = 100, 300, and 600 kPa
		TH60 soil 306	Bigelow, MN	
	Granular	US10	Staples, MN	
Effect of sample size on $M_r$	Non-granular	TH 60 soil 306	Bigelow, MN	$M_r$ test on 2:1 and 1:1 height (H) to diameter (D) ratio gyratory compacted specimens. Applied vertical stress during gyratory compaction = 300 kPa

Table 5.11. Summary of index properties of granular materials used in laboratory target value determination study and tests performed

Parameter	Test Method	US10	TH36
Material Description	—	Granular	Granular
Standard Proctor $\gamma_{dmax}$ (kN/m <sup>3</sup> )	ASTMD 698-00	17.5	18.5
Optimum $w$ (%)		11.8	11.6
Modified Proctor $\gamma_{dmax}$ (kN/m <sup>3</sup> )	ASTMD 1557-00	18.1	18.9
Optimum $w$ (%)		9.6	8.9
Liquid Limit, LL	ASTMD 4318-05	NP	—
Plasticity Index, PI		NP	—
USCS group symbol	ASTMD 2487-00	SP-SM	SM
USCS group name		Poorly graded sand with silt	Silty sand
Tests performed	—	LWD	LWD

Table 5.12. Summary of index properties of non-granular soils used in laboratory target value determination study

Parameter	Test Method	Iowa	TH36	TH60			
		Loess	Silty clay	Soil 301	Soil 303	Soil 305	Soil 306
Standard Proctor $\gamma_{dmax}$ (kN/m <sup>3</sup> )	ASTMD 698-00	15.9	18.1	18.8	18.7	17.8	17.1
Optimum $w$ (%)		18.6	15.0	12.1	14.2	16.0	17.3
Modified Proctor $\gamma_{dmax}$ (kN/m <sup>3</sup> )	ASTMD 1557-00	—	20.1	20.5	20.4	19.7	19.4
Optimum $w$ (%)		—	9.8	9.8	10.2	9.6	11.8
Liquid Limit, LL	ASTMD 4318-05	29	—	27	26	32	39
Plastic Limit, PL		23	—	19	17	18	20
Plasticity Index, PI		6	—	8	9	14	19
USCS group symbol	ASTMD 2487-00	ML	ML	CL	CL	CL	CL
USCS group name		Silt	Silt	Sandy lean clay	Sandy lean clay	Sandy lean clay	Sandy lean clay
Tests performed	—	UC, PDA	LWD	LWD, DCP	LWD, DCP	LWD, DCP	PDA, LWD, M <sub>r</sub>

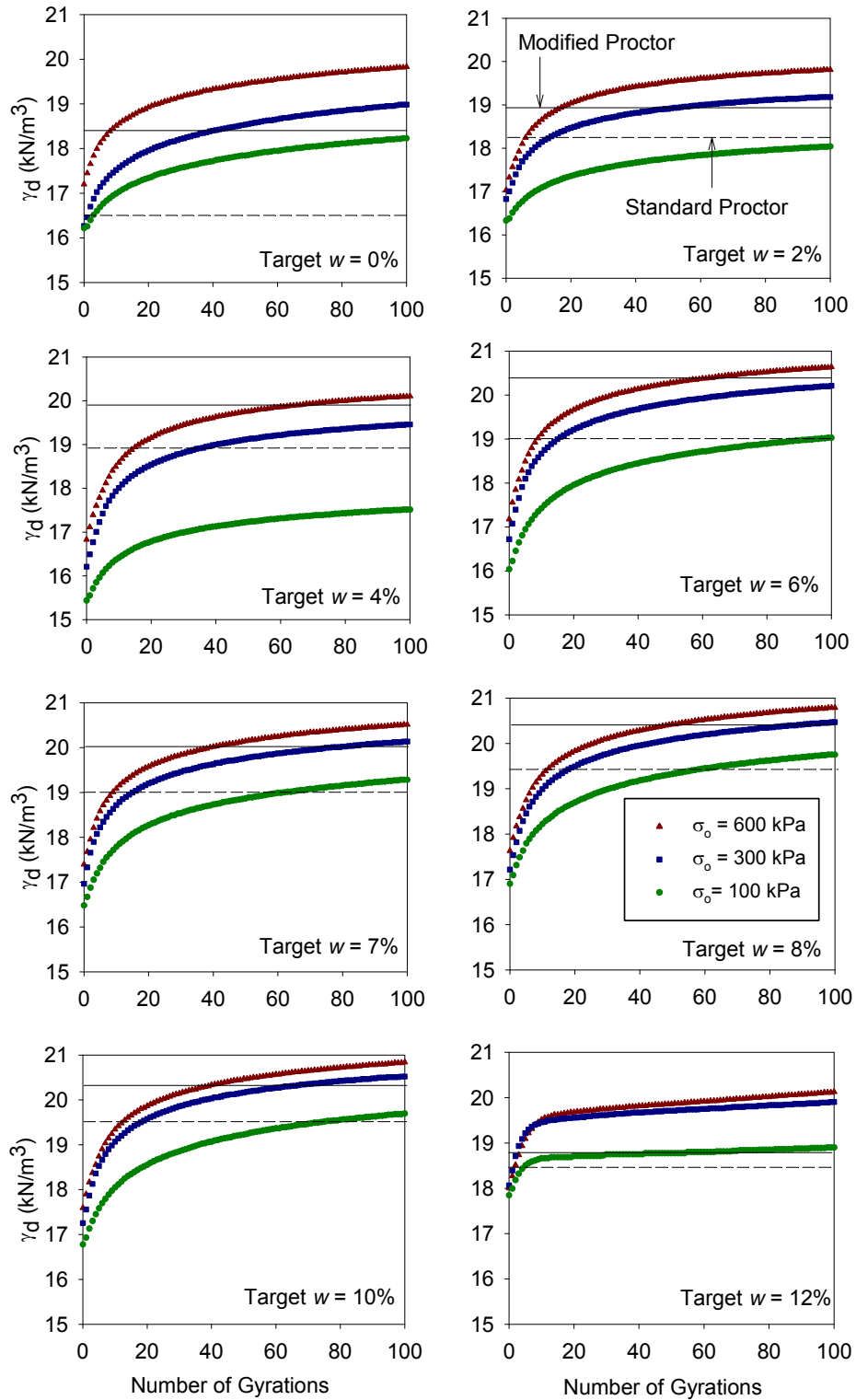


Figure 5.24. Dry unit weight growth curves with number of gyrations at different target moisture contents – US10 granular material (USCS: SP-SM)

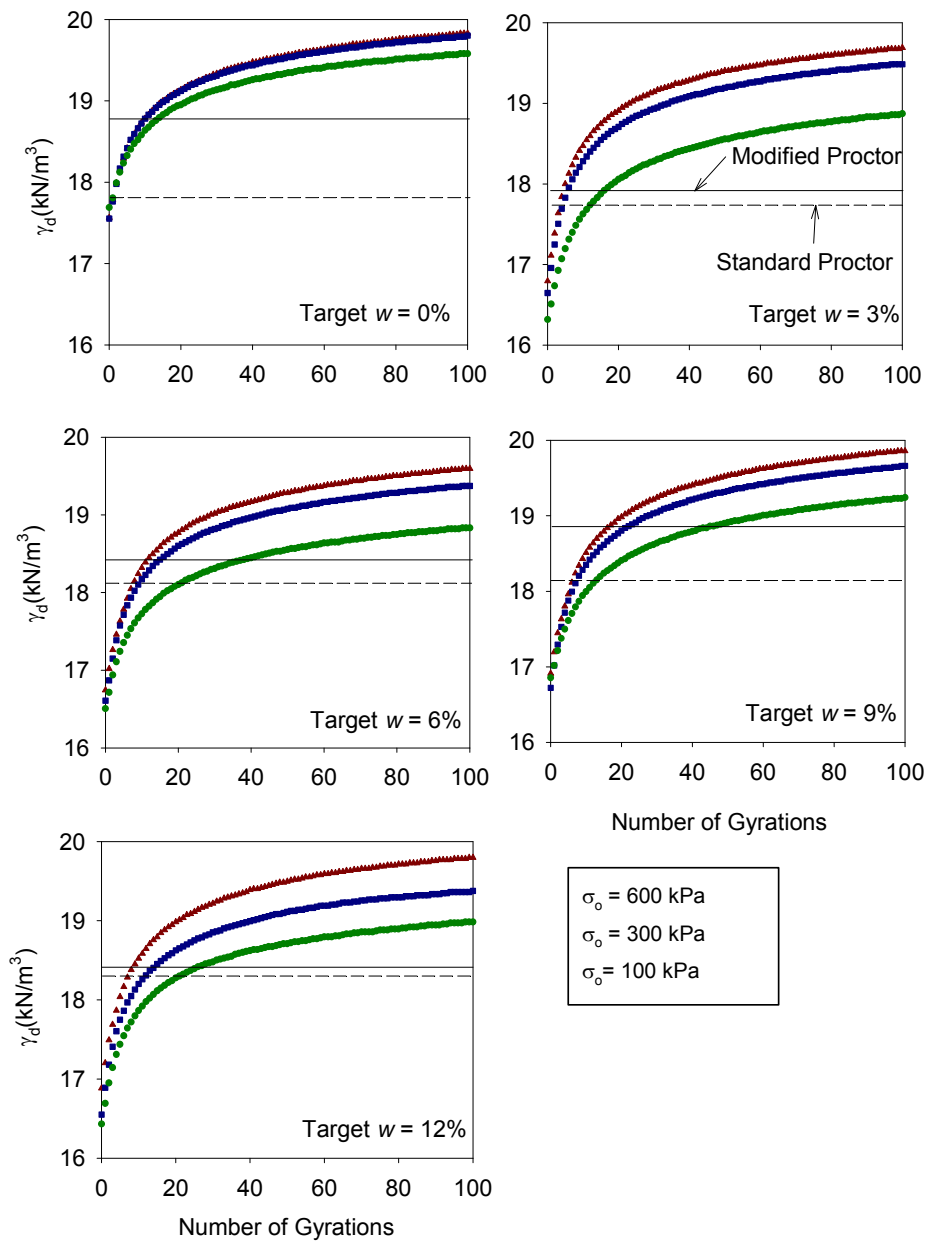


Figure 5.25. Dry unit weight growth curves with number of gyrations at different target moisture contents – TH 36 granular material (USCS: SM)

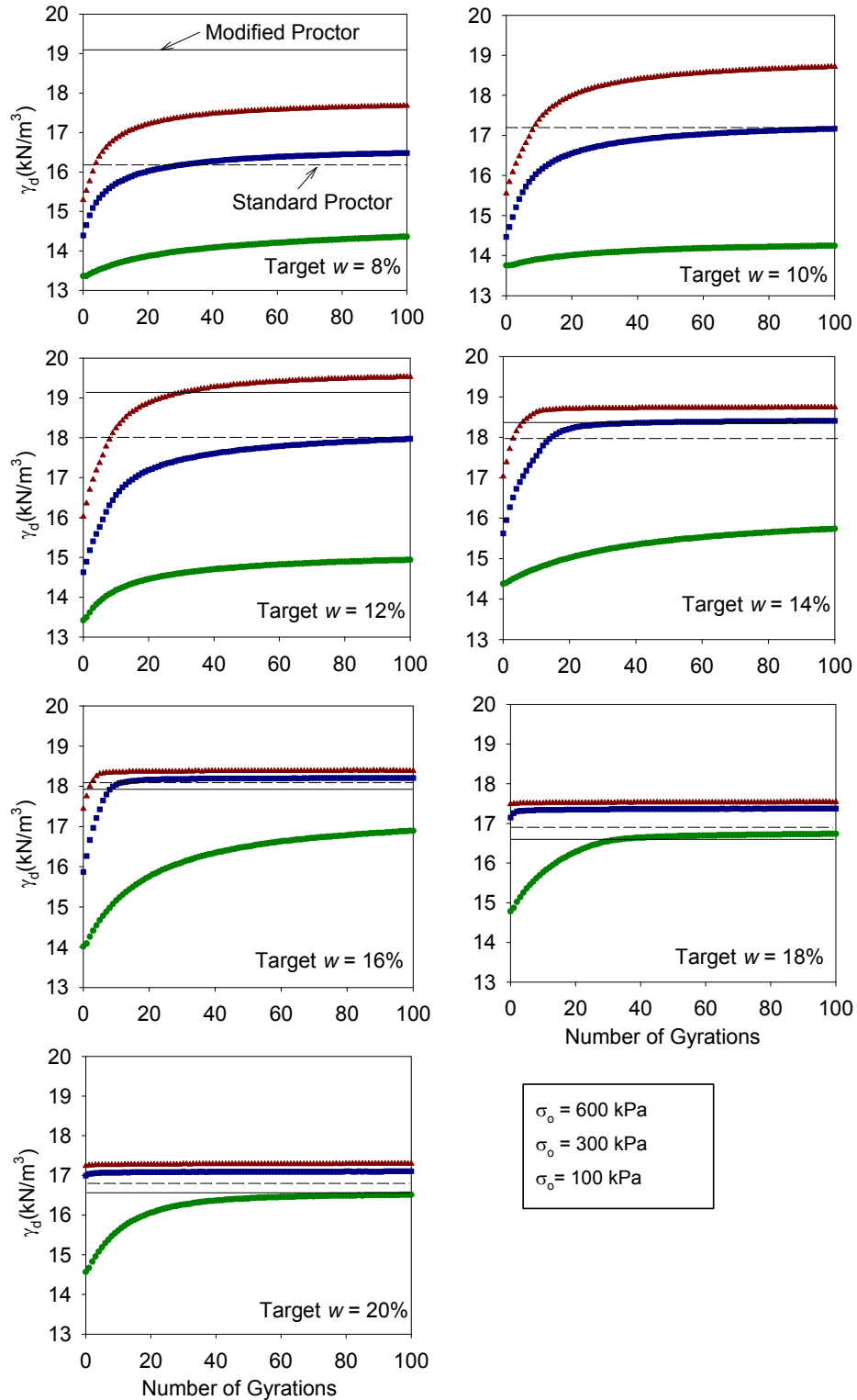


Figure 5.26. Dry unit weight growth curves with number of gyrations at different target moisture contents – TH 36 silty clay material (USCS: ML)

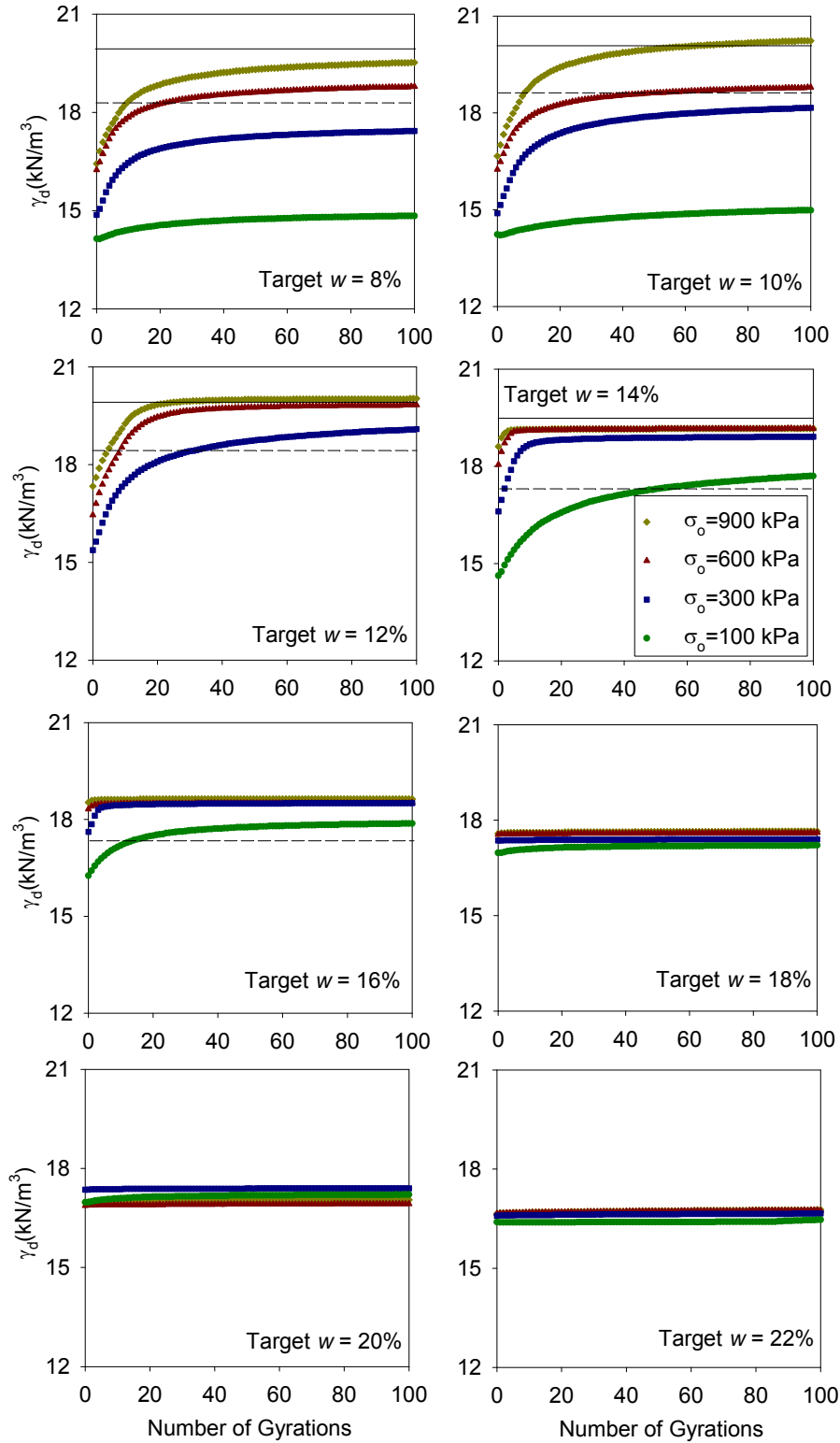


Figure 5.27. Dry unit weight growth curves with number of gyrations at different target moisture contents – TH60 soil 301 (USCS: CL)

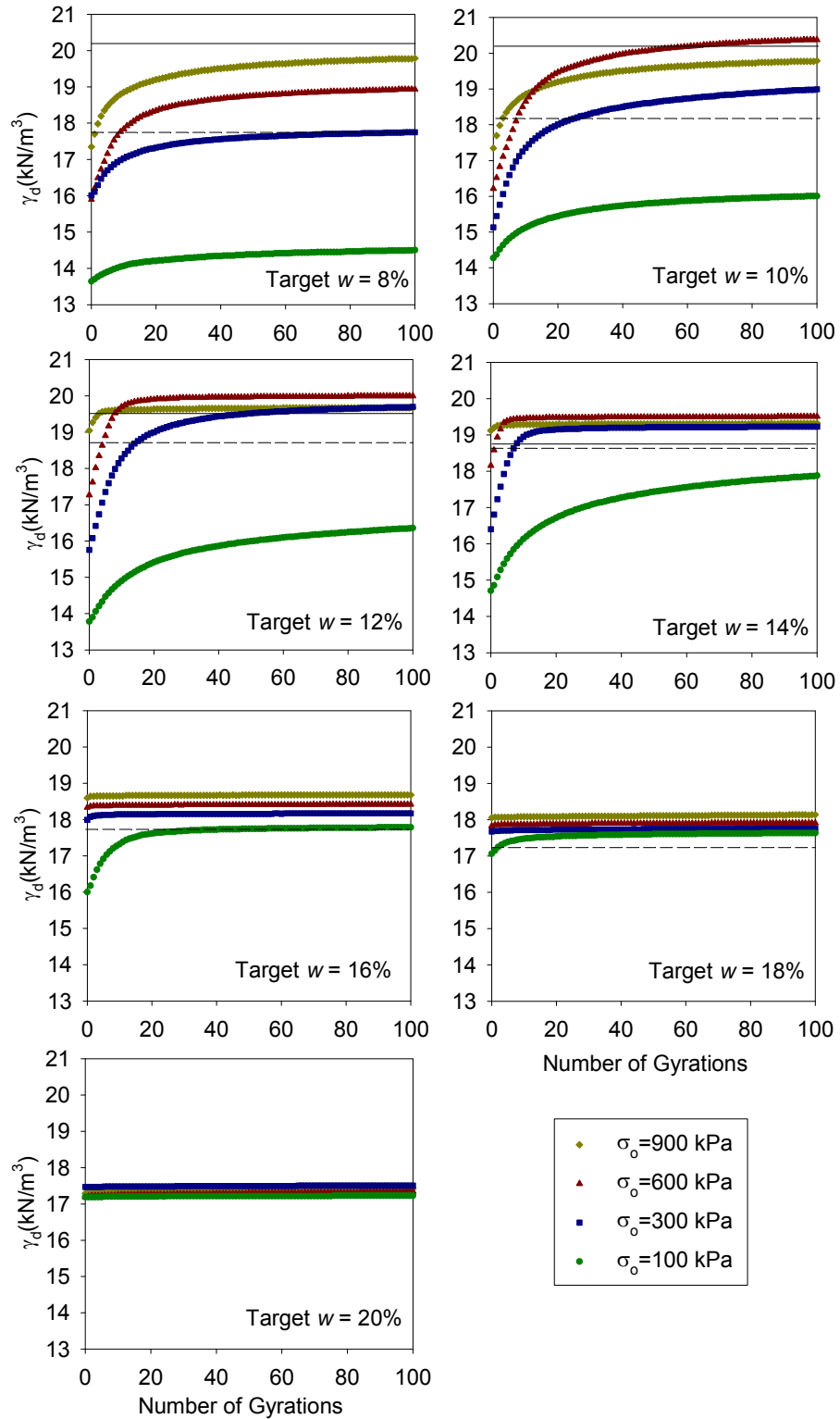


Figure 5.28. Dry unit weight growth curves with number of gyrations at different target moisture contents – TH60 soil 303 (USCS: CL)

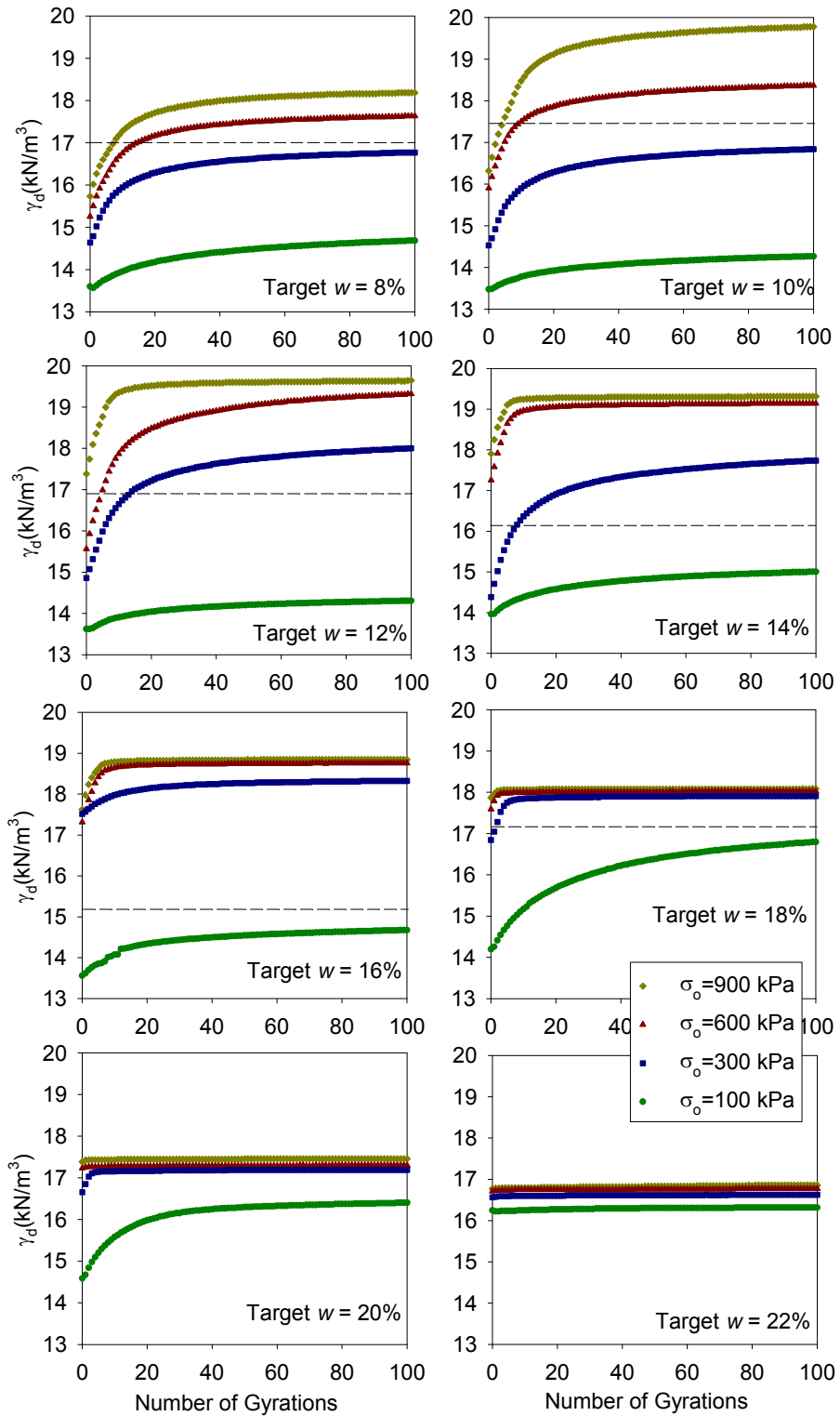


Figure 5.29. Dry unit weight growth curves with number of gyrations at different target moisture contents – TH 60 soil 305 (USCS: CL)

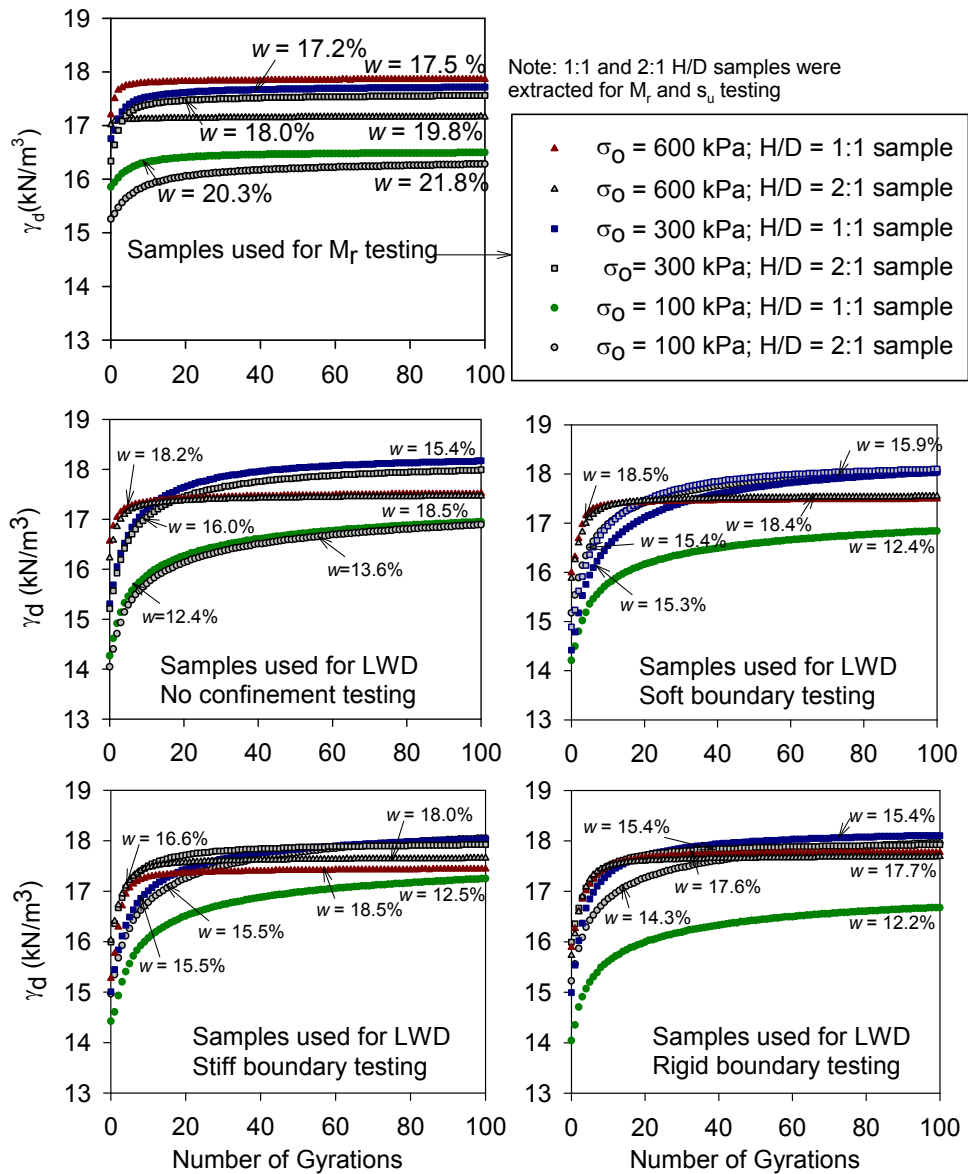


Figure 5.30. Dry unit weight vs. No. of gyrations for TH 60 soil 306 (USCS: CL)

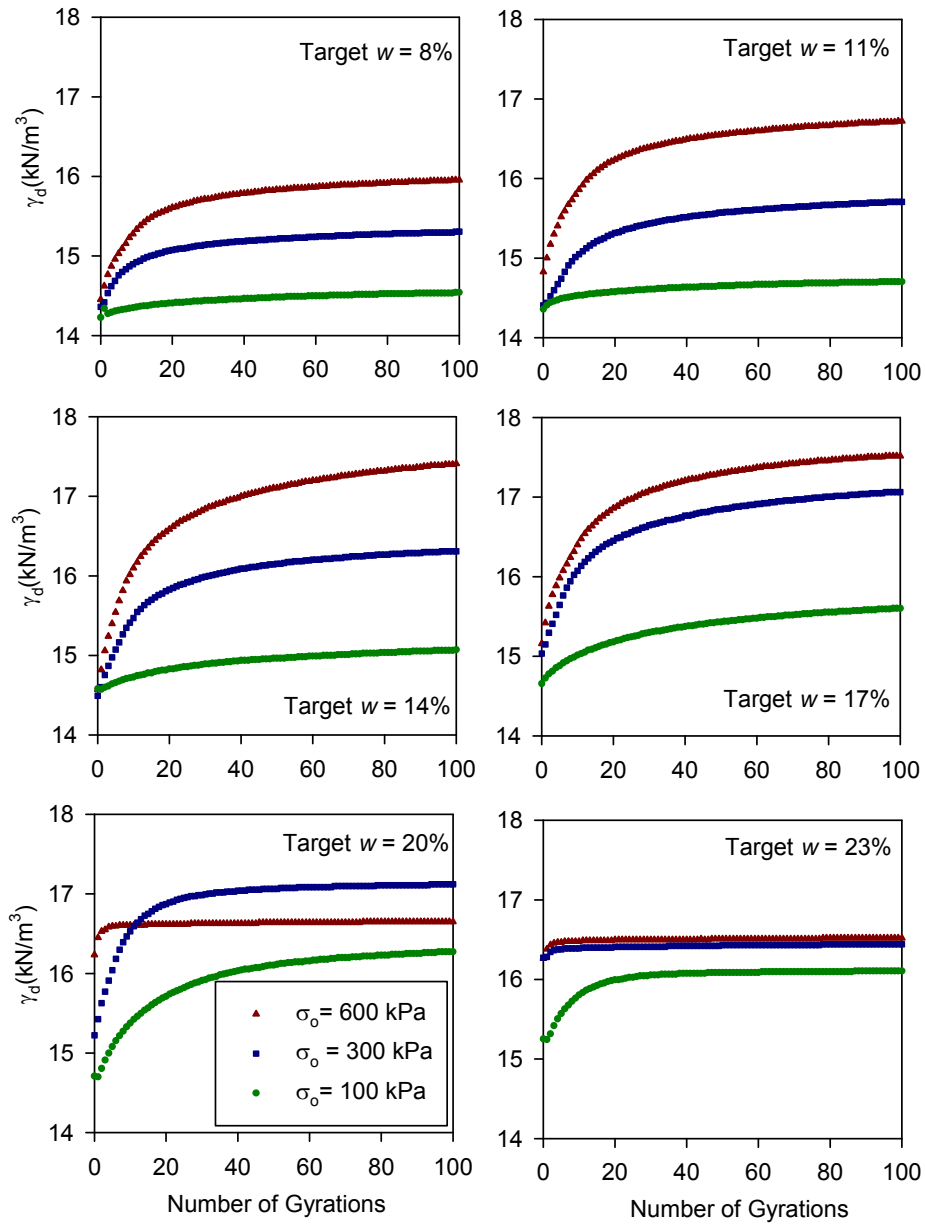


Figure 5.31. Dry unit weight vs. No. of gyrations for Iowa loess (USCS: ML)

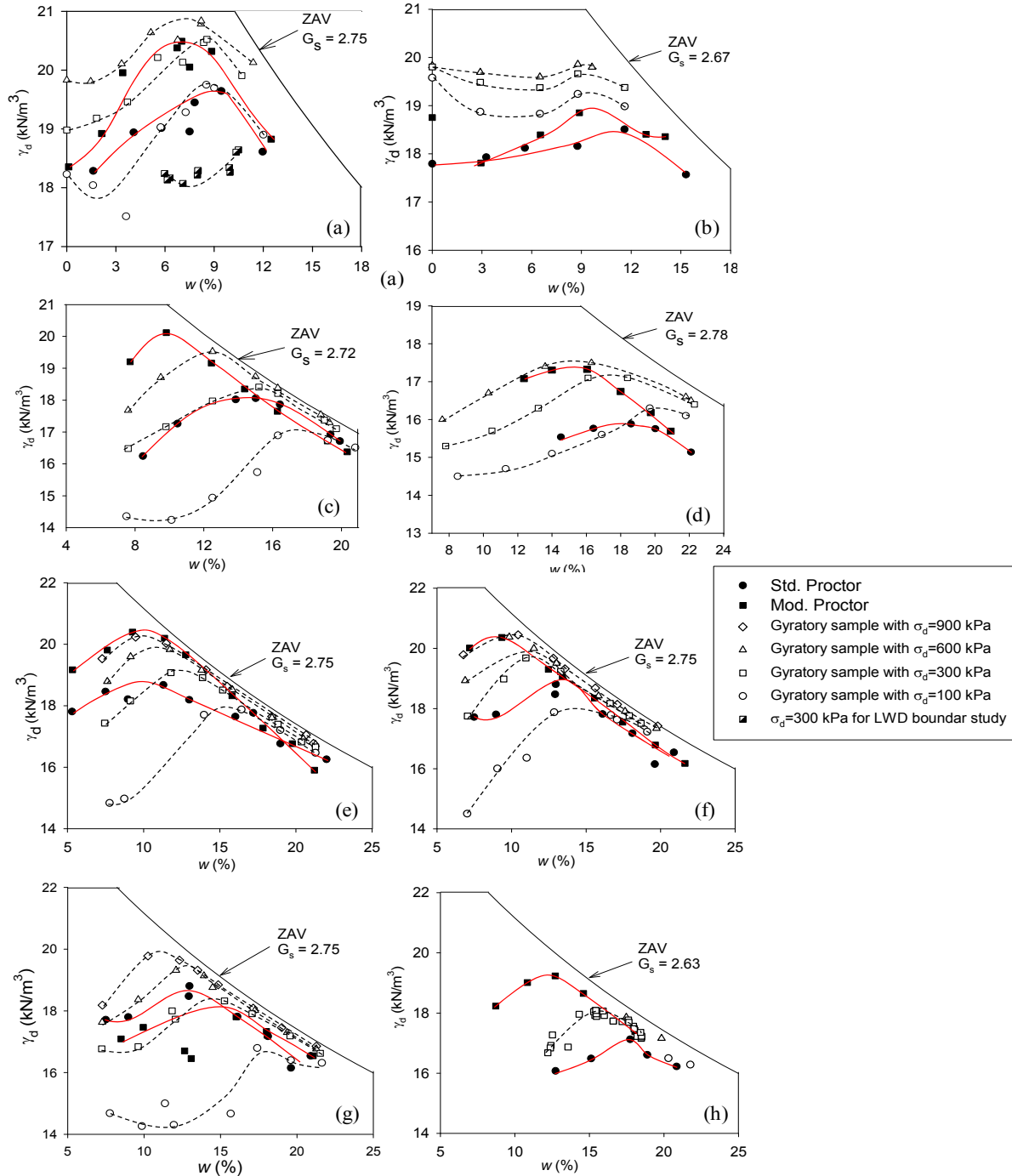


Figure 5.32. Comparison of moisture-dry unit weight relationships using Proctor and gyratory compaction (at 900, 600, 300, and 100 kPa vertical pressures) methods: (a) US10 granular (USCS: SP-SM), (b) TH 36 granular (USCS: SM), (c) TH 36 silty clay (USCS: ML), (d) Iowa loess (USCS: ML), (e) TH 60 soil 301 (USCS: CL), (f) TH 60 soil 303 (USCS: CL), (g) TH 60 soil 305 (USCS: CL), (h) TH 60 soil 306 (USCS: CL)

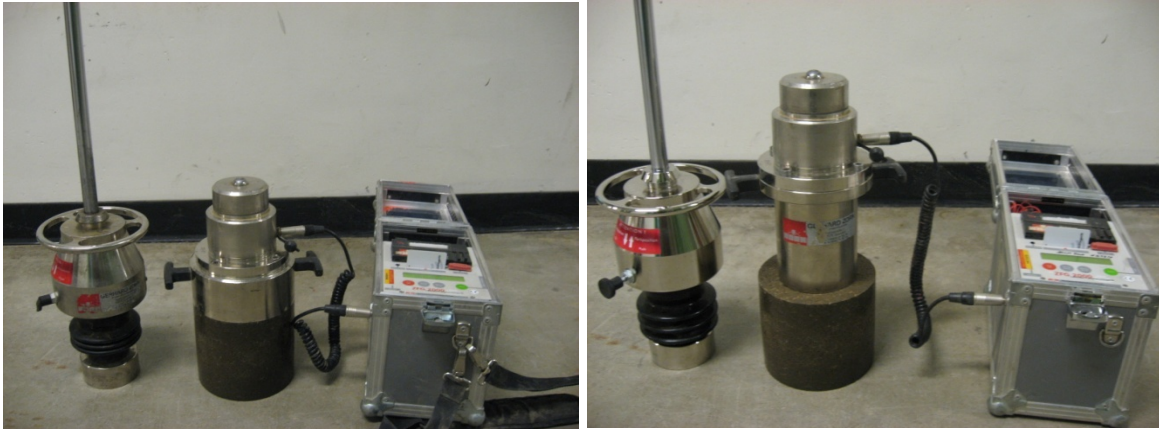


Figure 5.33. 150 mm (left) and 100 mm (right) plate diameter Zorn LWD tests on gyratory compacted specimens



Figure 5.34. LWD testing with four different boundary conditions: (a) no boundary, (b) soft polyurethane (Durometer = 20A), (c) stiff polyurethane (Durometer = 50A), and (d) rigid gyratory compaction mold

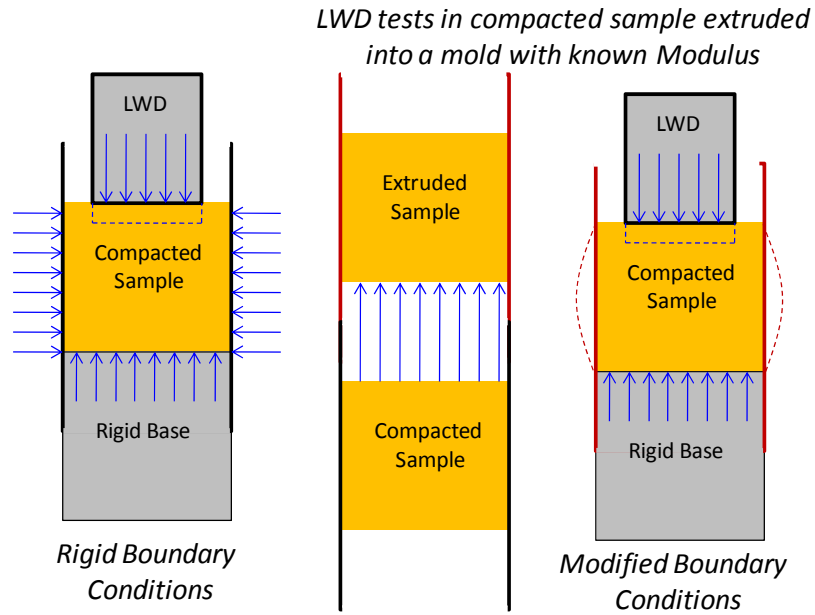


Figure 5.35. Schematic representation of LWD testing with different boundary conditions: rigid gyratory mold and flexible mold



Figure 5.36. PDA (left) and unconfined compression test (right) on gyratory compacted specimen



Figure 5.37. Resilient modulus testing on 1:1 and 2:1 gyratory compacted specimens



Figure 5.38. Procedure for inserting Shelby tube into gyratory compacted specimen to generate 2:1 height to diameter ratio specimens

### 5.8.3 Experimental Test Results and Discussion

#### 5.8.3.1 Evaluation of $w$ - $\gamma_d$ -DPI/ $s_u$ / $E_{LWD}$ relationships with rigid boundary conditions

DPI,  $s_u$  (determined from empirical relationship with DPI; see TH60 project results from Chapter 3), and  $E_{LWD}$  measurements obtained on gyratory compacted specimens confined with the rigid boundary condition were analyzed using multiple regression analysis to determine relationships with  $w$  and  $\gamma_d$ . Multiple regression analysis was performed by incorporating  $w$ ,  $\gamma_d$ , and interaction terms as indicated in Equation 5.6. Statistical significance of each variable was assessed based on  $p$ - and  $t$ -values. The selected criteria for identifying the significance of a

parameter included:  $p$ -value  $< 0.05$  = significant,  $< 0.10$  = possibly significant,  $> 0.10$  = not significant, and  $t$ -value  $< -2$  or  $> +2$  = significant. The  $p$ -value indicates the significance of a parameter and the  $t$ -ratio value indicates the relative importance (i.e., higher the absolute value greater the significance).

$$E_{LWD} \text{ or DPI or } s_u = b_0 + b_1 w + b_2 \gamma_d + b_3 w^2 + b_4 \gamma_d^2 + b_5 w\gamma_d \quad (5.6)$$

where:  $b_0$  = intercept,  $b_1, b_2, b_3, b_4,$  and  $b_5$  = regression coefficients

The multiple regression relationships obtained are presented as contour plots in relationship with Proctor  $w$  and  $\gamma_d$  relationships for different granular and non-granular soils in Figure 5.39 to Figure 5.44. The regression relationships are summarized in Table 5.13 including  $R^2$  values which range from 0.7 to 0.9. An advantage of presenting the results in contour format is that the  $E_{LWD}$  or DPI “target” values with respect to acceptable  $w$  and  $\gamma_d$  (or relative compaction) can be graphically determined and the influence of moisture content is clearly evident. The contours indicate that increasing  $w$  and decreasing  $\gamma_d$  generally decreases the  $E_{LWD}$ , DPI, and  $s_u$  values. Because of differences in boundary conditions between the lab and field, the aforementioned four different boundary conditions (“soft” and “stiff”) were evaluated and are discussed next.

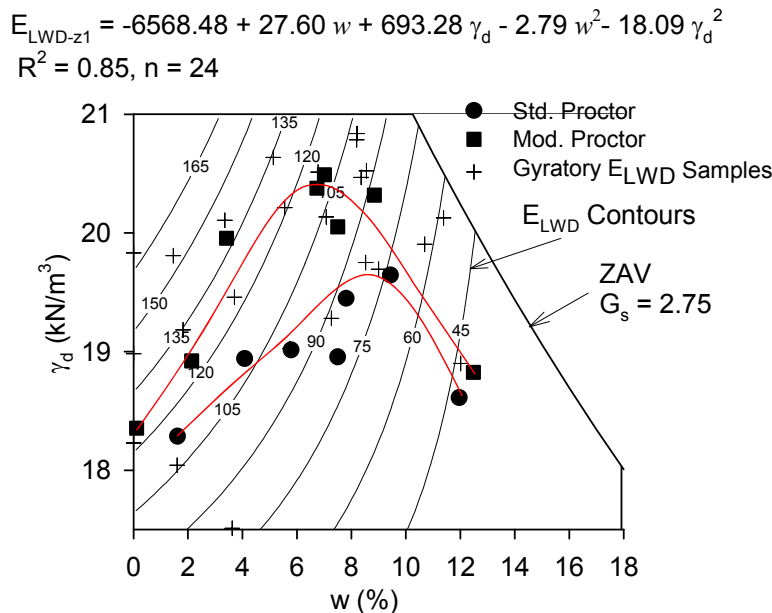


Figure 5.39.  $E_{LWD-Z1}$  contours in relationship with moisture and dry unit weight – US 10 granular material (USCS: SP-SM) ( $d_{LWD-Z1} = 85/E_{LWD-Z1}$ )

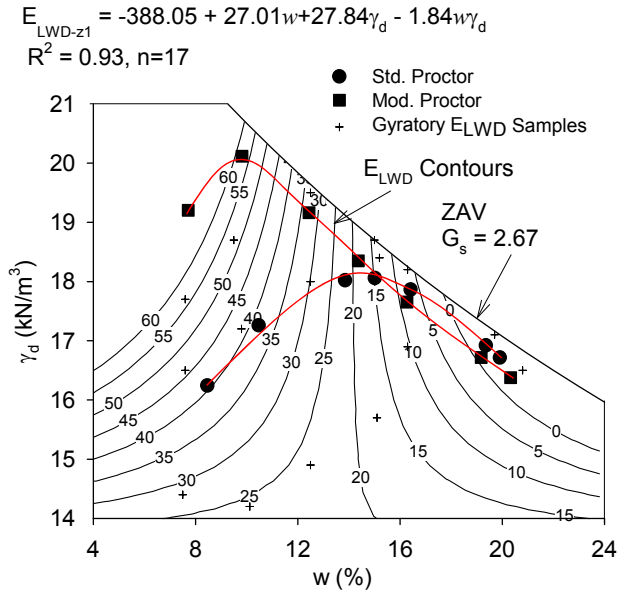


Figure 5.40.  $E_{LWD-Z1}$  contours in relationship with moisture and dry unit weight – TH36 silty clay material (USCS: ML) ( $d_{LWD-Z1} = 59.4/E_{LWD-Z1}$ )

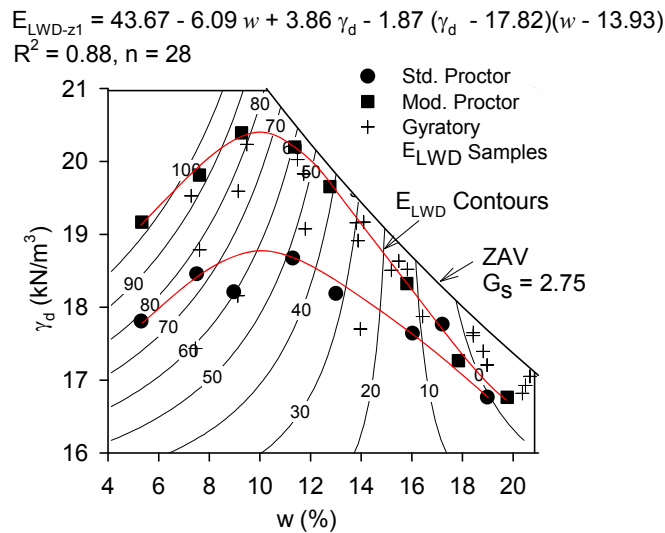


Figure 5.41.  $E_{LWD-Z1}$  contours in relationship with moisture and dry unit weight – TH60 soil 301 material (USCS: CL) ( $d_{LWD-Z1} = 49.8/E_{LWD-Z1}$ )

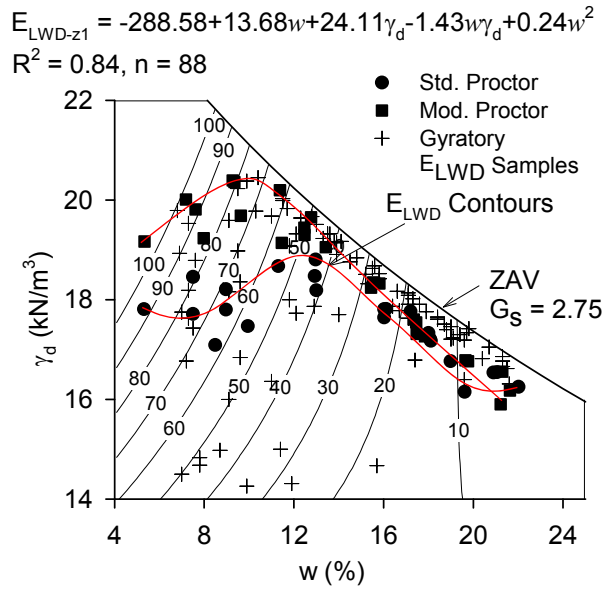


Figure 5.42.  $E_{LWD-Z1}$  contours in relationship with moisture and dry unit weight – TH60 (301, 303, and 305 combined) non-granular material (USCS: CL) ( $d_{LWD-Z1} = 49.8/E_{LWD-Z1}$ )

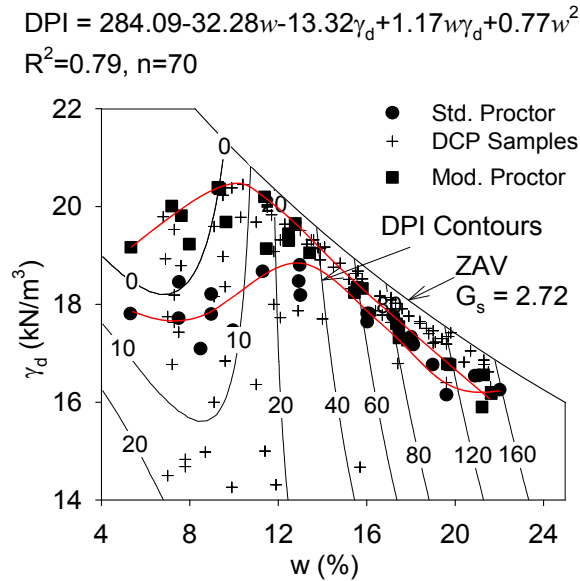


Figure 5.43. DPI contours in relationship with moisture and dry unit weight – TH60 non-granular material (301, 303, and 305 combined) (USCS: CL)

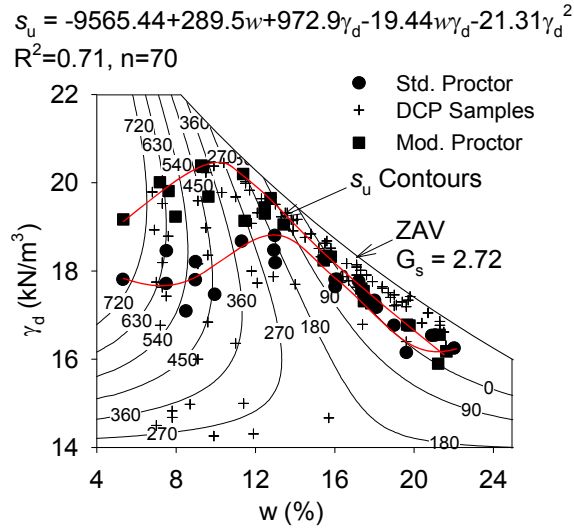


Figure 5.44.  $s_u$  contours in relationship with moisture and dry unit weight – TH60 non-granular material (301, 303, and 305 combined) (USCS: CL) ( $s_u$  determined from empirical relationship with DPI)

Table 5.13. Summary of laboratory determined  $w$ - $\gamma_d$ -DPI/ $s_u/E_{LWD}$  relationships

Soil ID	USCS	Project location	Relationship	n	R <sup>2</sup>
US10	SP-SM	Staples, MN	$E_{LWD-z1} = -6568.48 + 27.60w + 693.28\gamma_d - 2.79w^2 - 18.09\gamma_d^2$	24	0.85
TH36 silty clay	ML	North St. Paul, MN	$E_{LWD-z1} = -388.05 + 27.01w + 27.84\gamma_d - 1.84w\gamma_d$	17	0.93
TH60 soil 301	CL	Bigelow, MN	$E_{LWD-z1} = 43.67 - 6.09w + 3.86\gamma_d - 1.87(\gamma_d - 17.82)(w - 13.93)$	28	0.88
			$DPI = 146.74 - 27.70w - 0.20w\gamma_d + 1.71w^2$	18	0.95
$s_u = -1964.84 + 163.09w + 140.90\gamma_d - 10.95w\gamma_d$			18	0.97	
$E_{LWD-z1} = -56.2 - 4.69w + 8\gamma_d$			28	0.74	
TH60 soil 303			$DPI = 125.2 - 18.03w - 2.89\gamma_d + 1.22w^2$	20	0.98
			$s_u = -1825.04 + 167.39w + 131.44\gamma_d - 11.05w\gamma_d$	20	0.89
TH60 soil 305			$E_{LWD-z1} = -298.49 + 17.90w + 22.44\gamma_d - 1.27w\gamma_d$	32	0.82
			$DPI = 0.27 + 7.71w - 4.07\gamma_d$	32	0.79
			$s_u = -4922.31 + 383.82w + 344.98\gamma_d - 25.48w\gamma_d$	32	0.79
TH60 subgrade clay (combining 301, 303 and 305 soils)			$E_{LWD-z1} = -288.58 + 13.68w + 24.11\gamma_d - 1.43w\gamma_d + 0.24w^2$	88	0.84
	$DPI = 284.09 - 32.28w - 13.32\gamma_d + 1.17w\gamma_d + 0.77w^2$	70	0.79		
	$s_u = -9565.44 + 289.5w + 972.9\gamma_d - 19.44w\gamma_d - 21.31\gamma_d^2$	70	0.71		

### 5.8.3.2 Influence of Boundary Conditions on laboratory $E_{LWD}$ measurements (updated)

The materials used in evaluating the effect of boundary conditions were TH 60 non-granular (TH60-soil 306) and US 10 granular materials. Specimens were prepared using the gyratory compactor with  $\sigma_0 = 300$  kPa at 100 gyrations. The PDA continuously recorded  $\tau_G$  measurements during the compaction process. Figure 5.45 and Figure 5.46 shows  $\tau_G$  versus number of gyrations for the TH 60 non-granular and US10 granular materials, respectively. Figure 5.47 illustrates the influence of moisture content on  $\tau_G$  for the two soils.  $\tau_G$  values are shown for both the peak shear resistance and the average shear resistance for the last 10 gyrations. Results show that  $\tau_G$  for TH60 non granular material is highly sensitive to moisture content causing a significant reduction in  $\tau_G$  with increasing moisture content. Figure 5.47 also indicates that overcompaction contributes to low  $\tau_G$  with increasing number of gyrations, for samples at high moisture contents ( $w > 16\%$  for this material). For US10 granular material, results show that  $\tau_G$  increases with increasing gyrations and is relative less sensitive to moisture content compared to TH60 non-granular material.

Figure 5.48 and Figure 5.49 shows relationships between LWD measurements and moisture content for four different boundary conditions (i.e., no confinement, “stiff”, “soft” and rigid). Results indicate that  $E_{LWD}$  values are relatively higher for rigid boundary condition compared to other boundary conditions. The results are for “stiff” “soft” and no confinement conditions were grouped within a similar range. Relationships between LWD and  $\tau_G$  measurements produced good correlations for TH60 non-granular material with  $R^2$  values  $> 0.7$ .

Figure 5.50 shows the influence of the boundary condition on the LWD values for the US10 granular material, which is much more significant than the non-granular material, as expected. Results suggest that the polyurethane “stiff” and “soft” molds used do not provide significant confinement and the resulting  $E_{LWD}$  values are quite low. In the future, an intermediate sleeve stiffer than the two polyurethane sleeves could be fabricated to better capture the stiffness and field boundary conditions at the recommended testing depth of 150 mm in-situ. Other methods of confinement are also possible such as with a split mold with controlled boundary stress. Figure 5.51 indicates that a clear relationship between LWD and  $\tau_G$  was not evident with this test sequence.

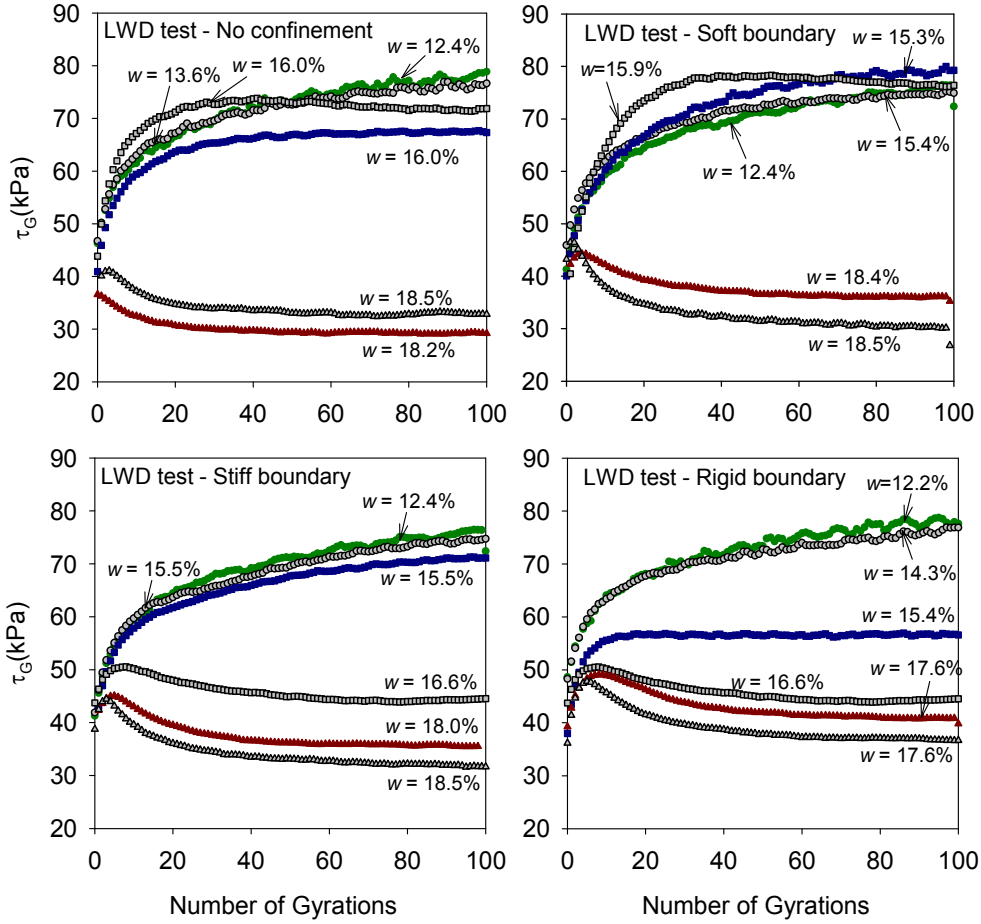


Figure 5.45. Shear resistance versus number of gyrations ( $\sigma_o = 300$  kPa) for TH 60 soil 306 (USCS: CL)

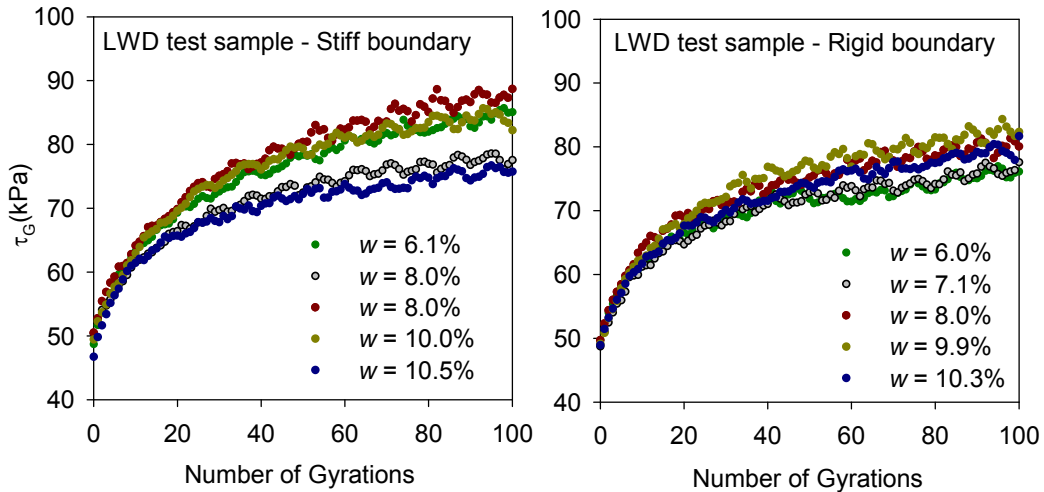


Figure 5.46. Shear resistance versus number of gyrations for US10 granular material (USCS: SP-SM) ( $\sigma_o = 300$  kPa)

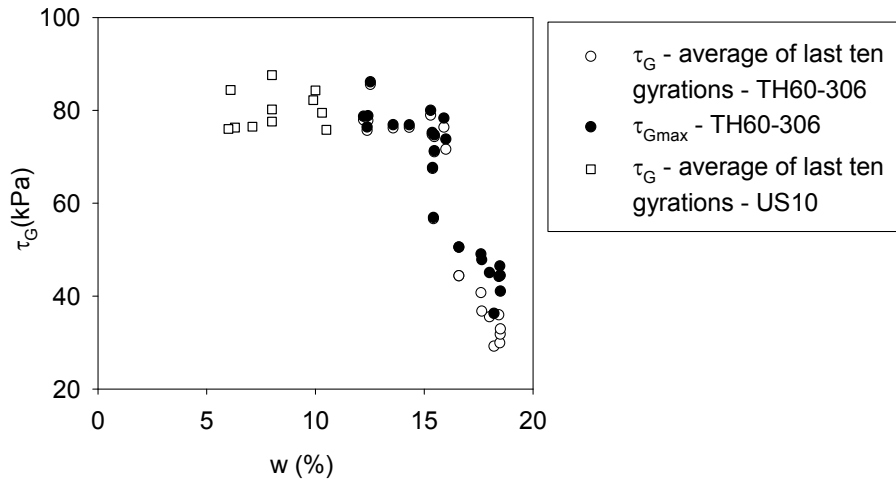


Figure 5.47. Influence of moisture content on  $\tau_G$  for TH60 – soil 306 non-granular (USCS: CL) and US 10 granular (USCS: SP-SM) materials

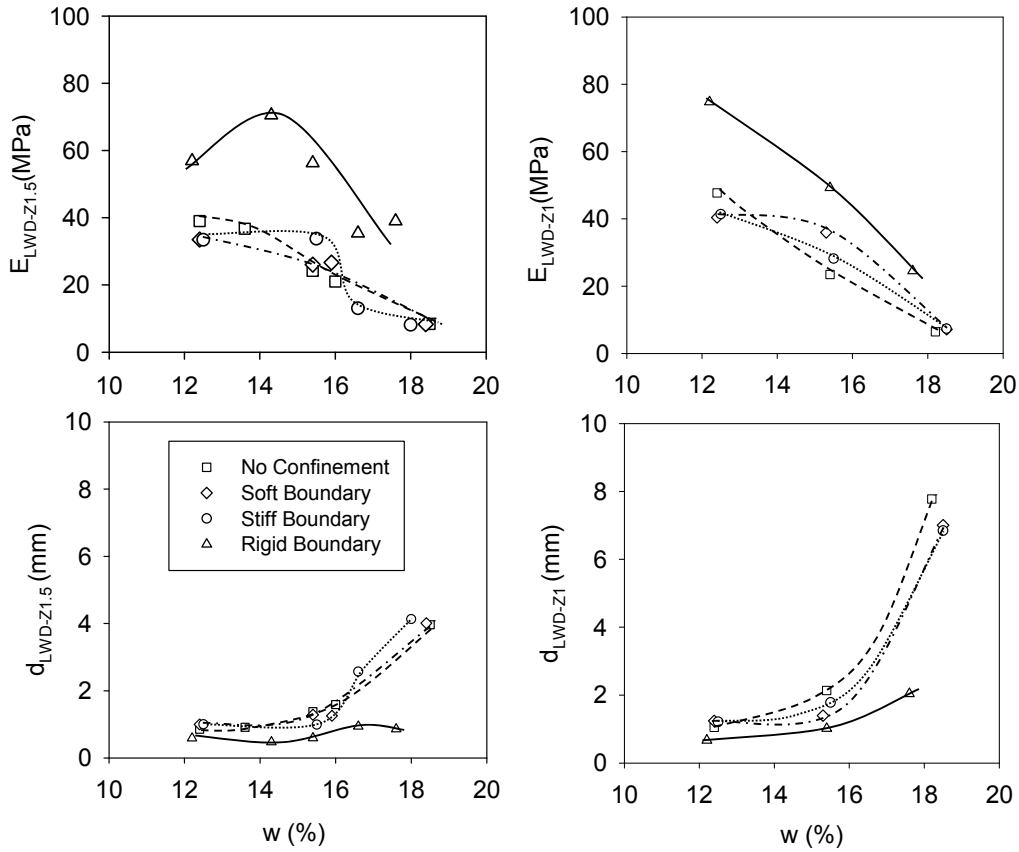


Figure 5.48. Influence of boundary conditions on LWD measurements on gyratory compacted specimens at different moisture contents – TH 60 soil 306 (USCS: CL)

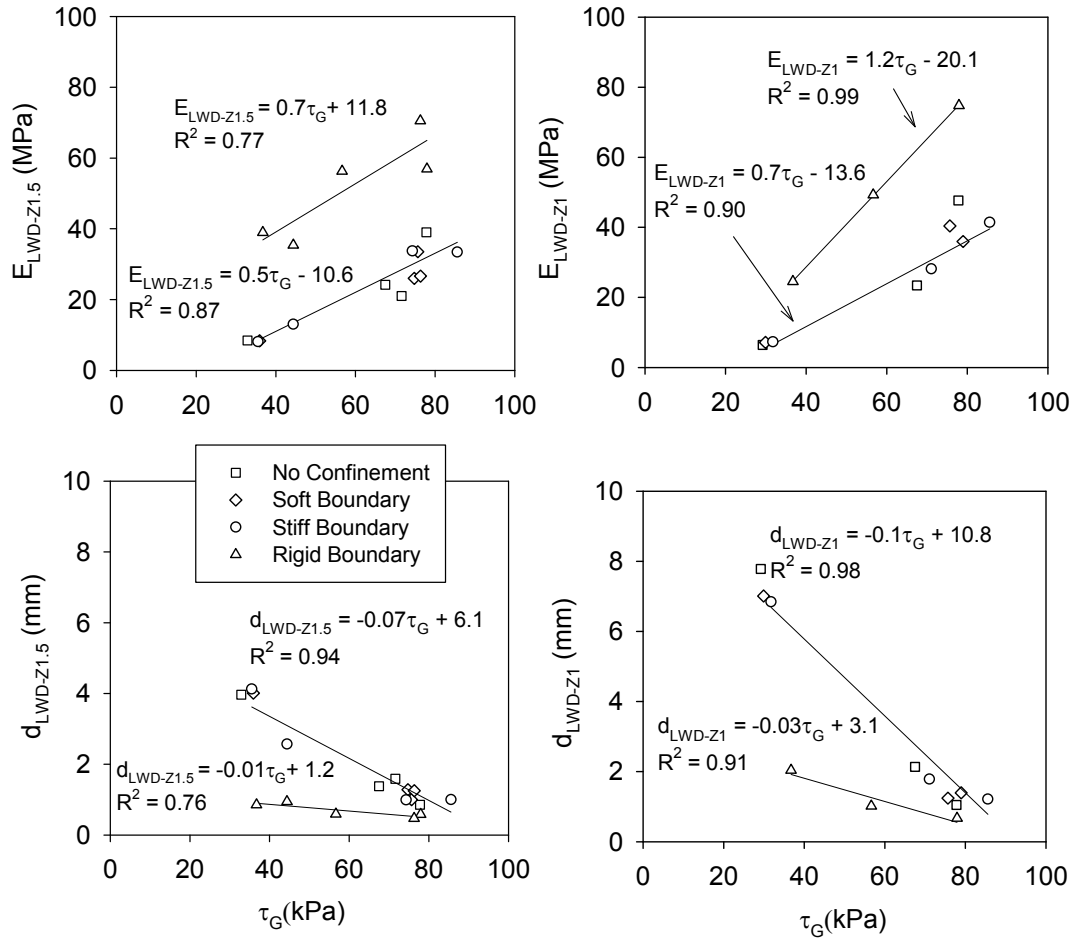


Figure 5.49. Relationships between LWD measurements and  $\tau_G$  for different boundary conditions – TH 60 soil 306 (USCS: CL)

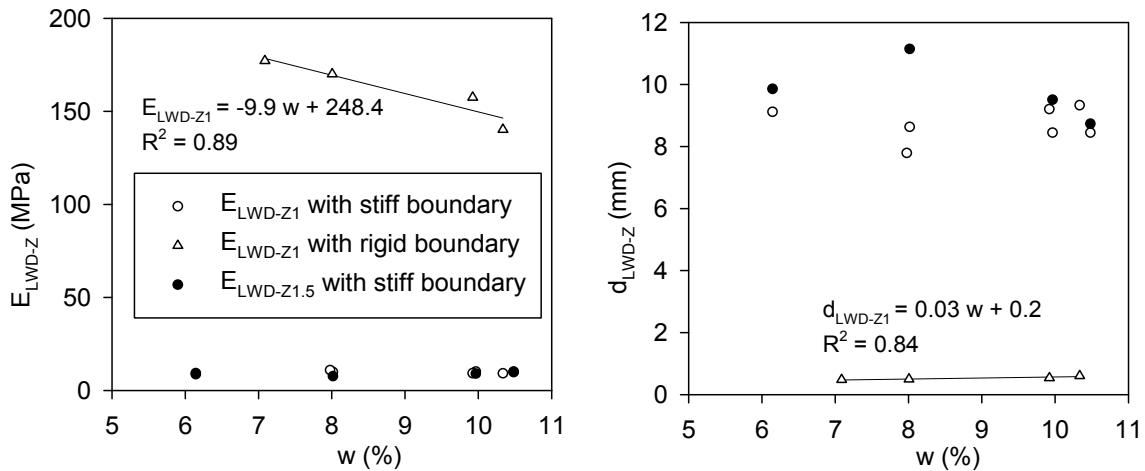


Figure 5.50. Influence of boundary conditions on LWD measurements on gyratory compacted specimens at different moisture contents – US10 granular material (USCS: SP-SM)

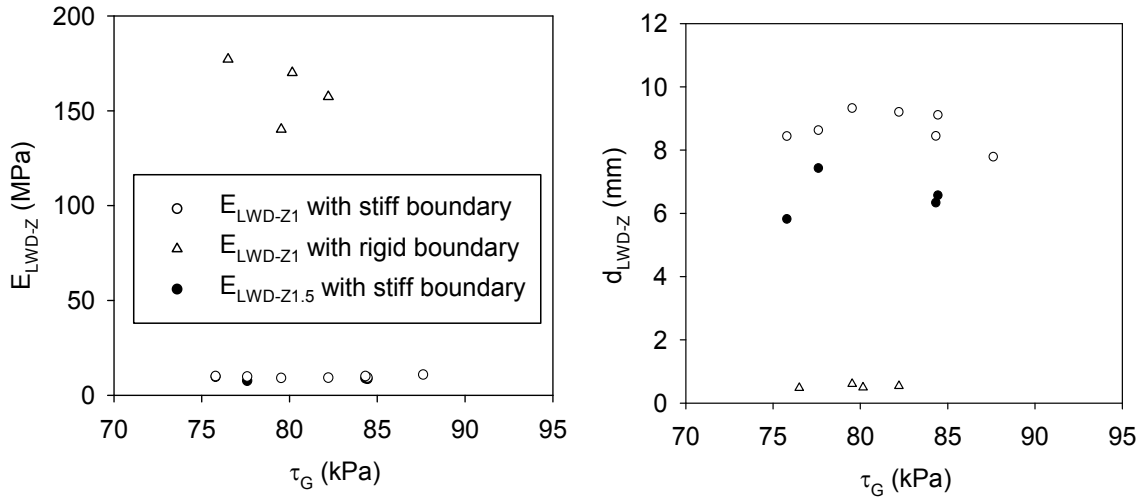


Figure 5.51. Relationship between LWD measurements and  $\tau_G$  for different boundary conditions – US10 granular material (USCS: SP-SM)

### 5.8.3.3 Relationship between PDA Shear Resistance and Undrained Shear Strength

Unconfined compression tests were conducted on gyratory compacted specimens to investigate the relationships between  $\tau_G$  and  $s_u$ . Because of the large volume of soil involved, western Iowa loess was used in this experiment at six different moisture contents. The loess material used is predominately silt (about 90%) with some clay size particles. Specimens were compacted using  $\sigma_o = 100$  kPa, 300 kPa and 600 kPa with 100 gyrations.  $\tau_G$  versus number of gyrations is presented in Figure 5.52. Results show increasing shear resistance with increasing number of gyrations up to about 15 gyrations and then no increase to slight increase in shear resistance up to 100 gyrations for samples with  $w < 17\%$ . Although not to the degree of the TH 60 non-granular material described above, some shear softening was observed at high moisture contents ( $w > 18\%$ ) with increasing number of gyrations. Figure 5.53 shows the relationship between change in  $\tau_G$  and  $s_u$  with changes in moisture content. Figure 5.54 demonstrates a strong linear correlation between the two measurements with  $R^2=0.94$ . On average, the  $s_u$  is about 1.8 times the measured  $\tau_G$ . Additional testing at other gyration angles is suggested to further explore this relationship. Presumably, increasing gyrations angles increases the shear stress development.

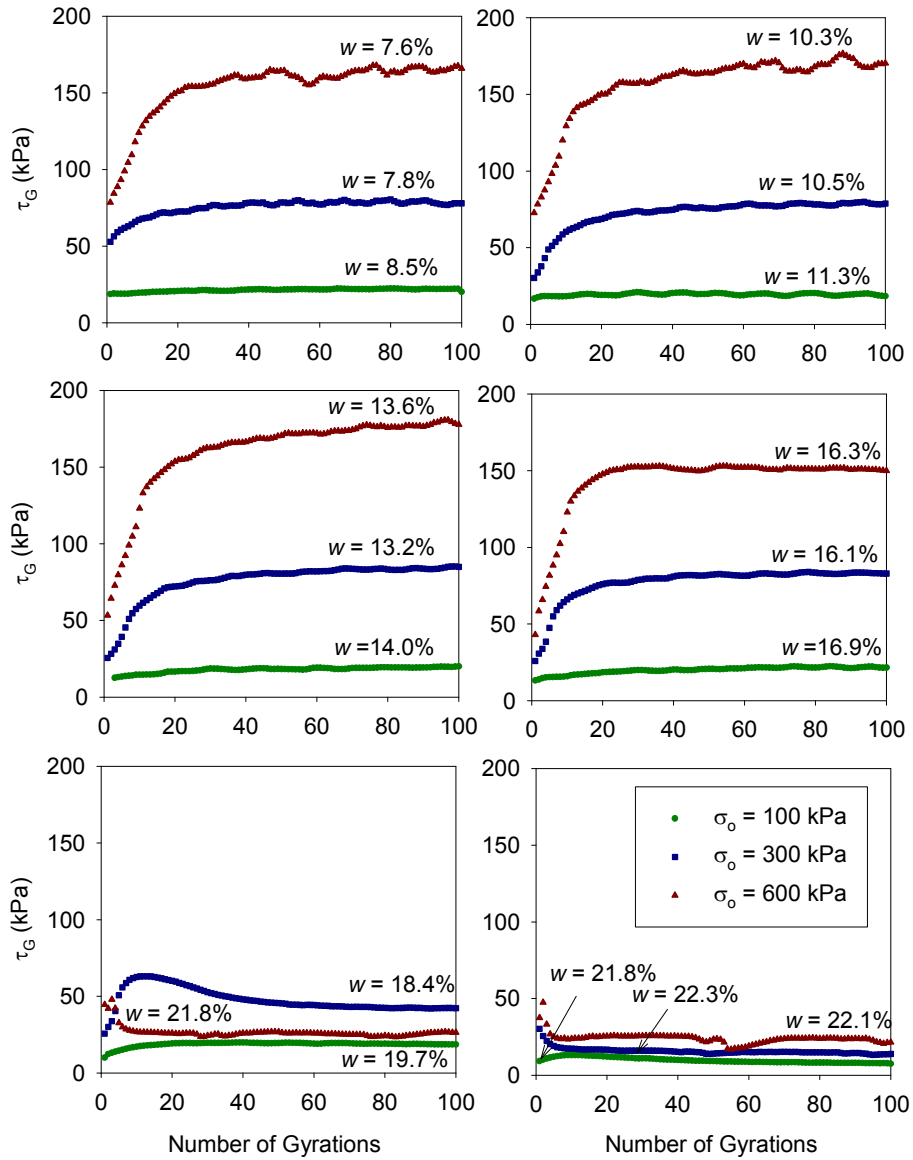


Figure 5.52.  $\tau_G$  versus number of gyrations for loess (USCS: ML)

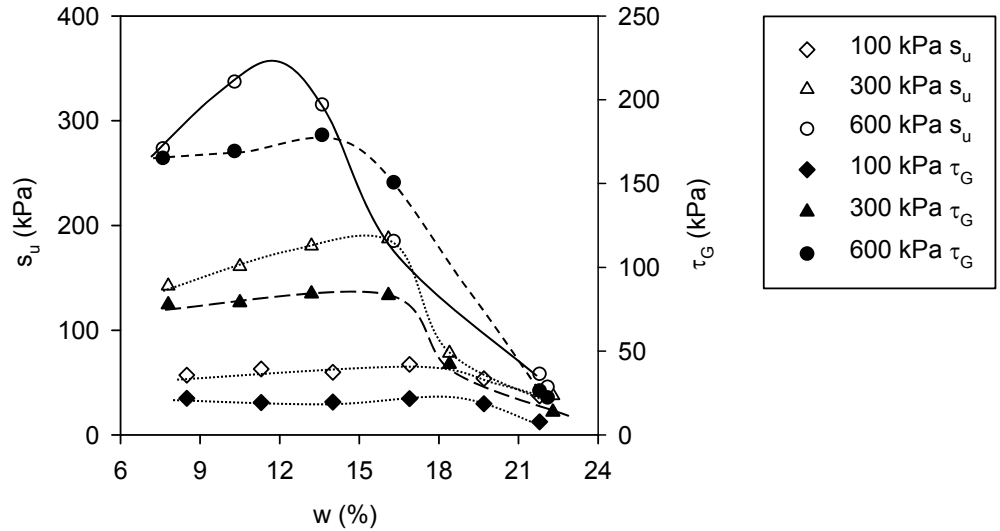


Figure 5.53.  $s_u$  and  $\tau_G$  versus moisture content for gyratory compacted specimens after 100 gyrations at  $\sigma_o = 100, 300,$  and  $600$  kPa for loess (USCS: ML)

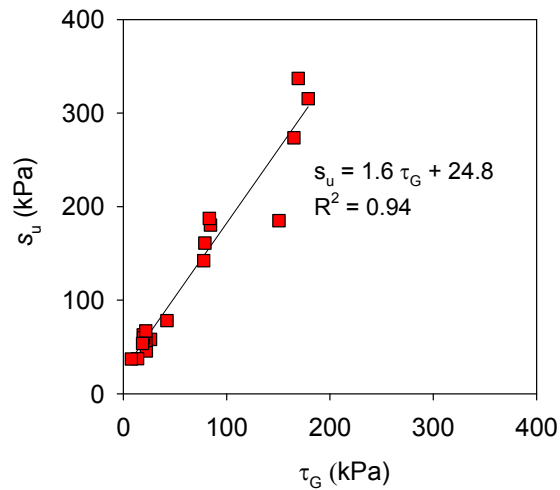


Figure 5.54. Relationship between  $s_u$  and  $\tau_G$  for loess (USCS: ML)

#### 5.8.3.4 Relationship between PDA Shear Resistance and Resilient Modulus

$M_r$  and UU tests were conducted on gyratory compacted specimens with the height to diameter ratio  $H/D=1:1$  and  $H/D=2:1$ . The  $H/D=1:1$  specimens were directly produced from the gyratory compactor, while the  $H/D=2:1$  specimens were trimmed from the gyrator samples using a tube sample to reduce the diameter. TH 60 non-granular material (#306) was prepared at the optimum moisture content based on the standard Proctor test ( $w_{opt}=18\%$ ). The mean  $M_r$  value was calculated from fifteen different loading sequences. The Witczak and Uzan (1988) model

that combines deviator and bulk stress affects (equation 5.7), was used in the interpretation of results.

$$M_r = k_1 P_a \left( \frac{\theta}{P_a} \right)^{k_2} \left( \frac{\sigma_d}{P_a} \right)^{k_3} \quad (5.7)$$

where:  $k_1, k_2, k_3$  = regression coefficients, with  $k_1 > 0$ ,  $k_2 \geq 0$ , and  $k_3 \leq 0$ ,  $\theta$  = sum of principle stresses or bulk stress ( $\sigma_1 + \sigma_2 + \sigma_3$ ),  $P_a$  = atmospheric pressure, same units as  $M_r$  and  $\theta$ ,  $\sigma_d$  = deviator stress, same units as  $M_r$  and  $\theta$ .

Model coefficients  $k_1, k_2, k_3$  and  $R^2$  values from the tests are summarized in Table 5.14. Plots of  $\sigma_d$  versus  $M_r$  for the samples tested are provided in Figure 5.55. Comparison between  $M_r$  results obtained at different testing sequences for the H/D = 1:1 and 2:1 samples is presented in Figure 5.56. With exception of samples compacted at  $\sigma_o = 300$  kPa, the results show that H/D=1:1 and 2:1 samples sizes produce similar or slightly lower  $M_r$  results.

$\tau_G$  measurements for  $M_r$  test specimens are shown in Figure 5.57. Figure 5.58 shows  $\tau_G$ -  $s_u$  and  $\tau_G$ -  $M_r$  regression relationships for H/D = 1:1 and 2:1 samples.  $\tau_G$ -  $s_u$  results obtained for loess soil are also included in the regression. The  $\tau_G$ -  $s_u$  results from TH60 non-granular material show similar trends as loess material and there was no influence of sample size on the relationship. The  $\tau_G$ -  $M_r$  relationship showed separate trends for H/D = 1:1 and 2:1 samples. Although the data is limited, the correlations show promise in terms of using the PDA  $\tau_G$  measurements which are relatively less time consuming to obtain than  $s_u$  or  $M_r$  testing. .

Table 5.14. Comparison of  $M_r$  for 2:1 and 1:1 height to diameter ratio specimens – TH-60 soil 306 (USCS: CL)

Gyratory pressure (kPa)	Sample size H×D (mm)	w (%)	$\gamma_d$ (kN/m <sup>3</sup> )	Average* $M_r$ (MPa) [range** in MPa]	Model coefficients	$\tau_G$ (kPa)	$s_u$ (kPa)	$s_u$ @ $\varepsilon=1\%$ (kPa)	$s_u$ @ $\varepsilon=5\%$ (kPa)	$\varepsilon_f$ (%)
600	142.7×72.4	19.8	17.2	19.9 [11.3 to 43.6]	$k_1=83.5$ $k_2=0.64$ $k_3=-0.67$ $R^2=0.72$	27.4	91.1	27.6	62.1	17.8
	151.7×149.9	17.5	17.9	20.7 [15.7 to 35.5]	$k_1=114.6$ $k_2=0.62$ $k_3=-0.43$ $R^2=0.88$	44.6	148.9	34.5	110.3	11.7
300	148.6×72.4	18.0	17.6	29.9 [18.6 to 48.4]	$k_1=167.3$ $k_2=0.19$ $k_3=-0.49$ $R^2=0.88$	30.9	130.0	34.5	93.1	14.6
	153.1×149.9	17.2	17.7	21.1 [15.5 to 28.7]	$k_1=139.2$ $k_2=0.36$ $k_3=-0.32$ $R^2=0.80$	33.7	137.6	44.8	120.7	11.2
100	142.5×71.9	21.8	16.3	12.7 [7.1 to 26.6]	$k_1=45.2$ $k_2=0.39$ $k_3=-0.81$ $R^2=0.93$	9.1	56.3	25.9	44.8	20.2
	160.4×149.9	20.3	16.5	15.2 [10.6 to 25.8]	$k_1=80.0$ $k_2=0.40$ $k_3=-0.52$ $R^2=0.95$	13.6	66.1	20.7	60.3	14.1

\*Average of  $M_r$  determined from 15 load sequences; \*\*range of  $M_r$  values from the 15 load sequences (see Table 2.4 for loading sequences).

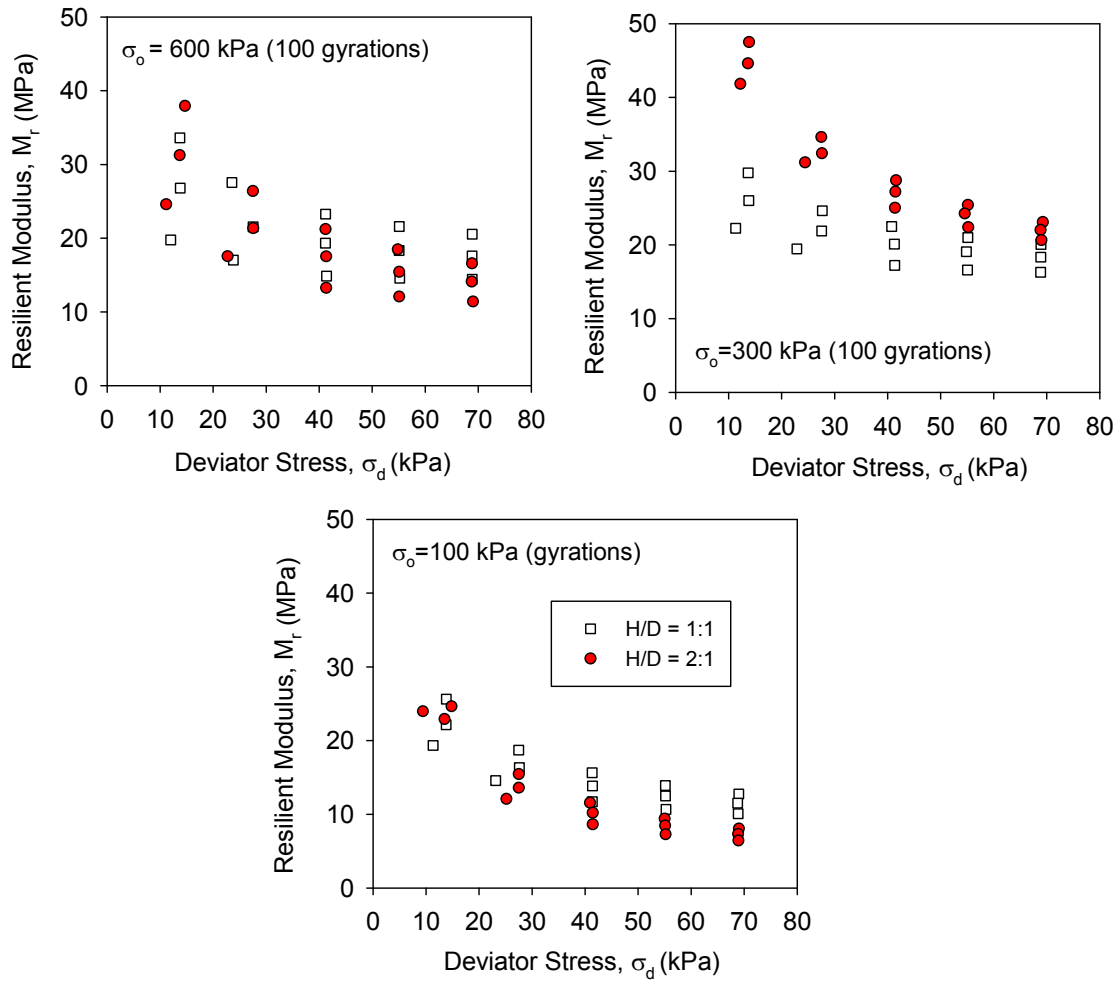


Figure 5.55. Effect of height to diameter ratio ( $H/D = 1$  and  $2$ ) on  $M_r$  of gyrotory compacted specimens at  $\sigma_o = 100, 300$  and  $600$  kPa at 100 gyrations –TH-60 soil 306 (USCS: CL)

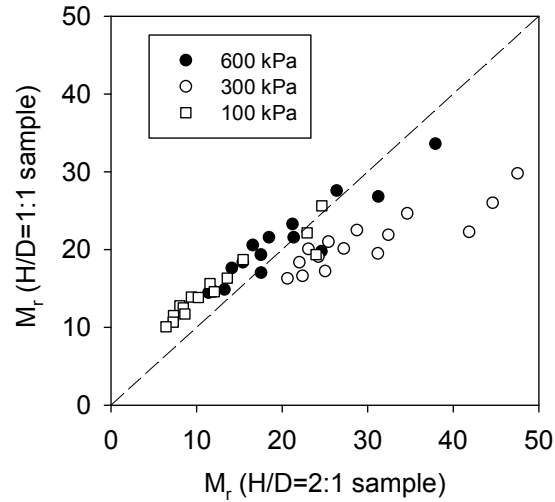


Figure 5.56. Relationship between H/D = 2:1 and 1:1  $M_r$  results on gyratory compacted specimens – TH60 soil 306 (USCS: CL)

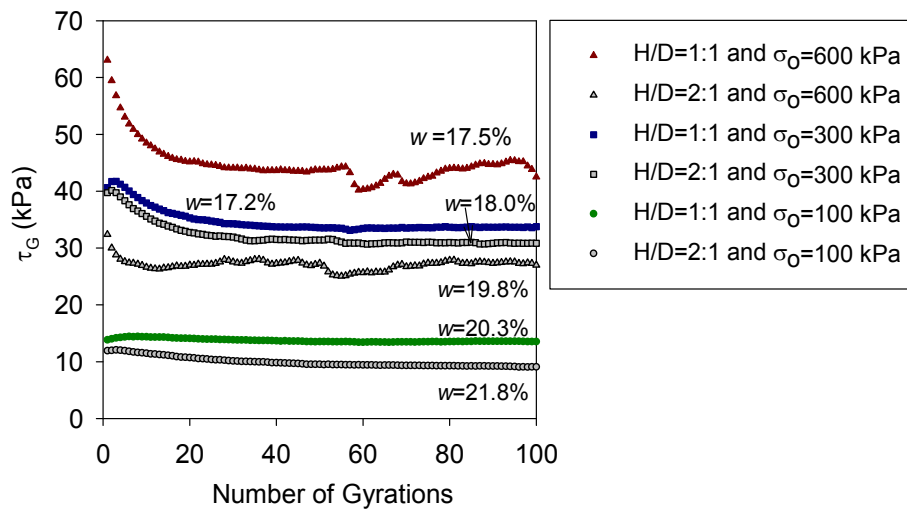


Figure 5.57.  $\tau_G$  versus number of gyrations for  $\sigma_o = 100, 300,$  and  $600$  compacted specimens TH60 soil 306 (USCS: CL)

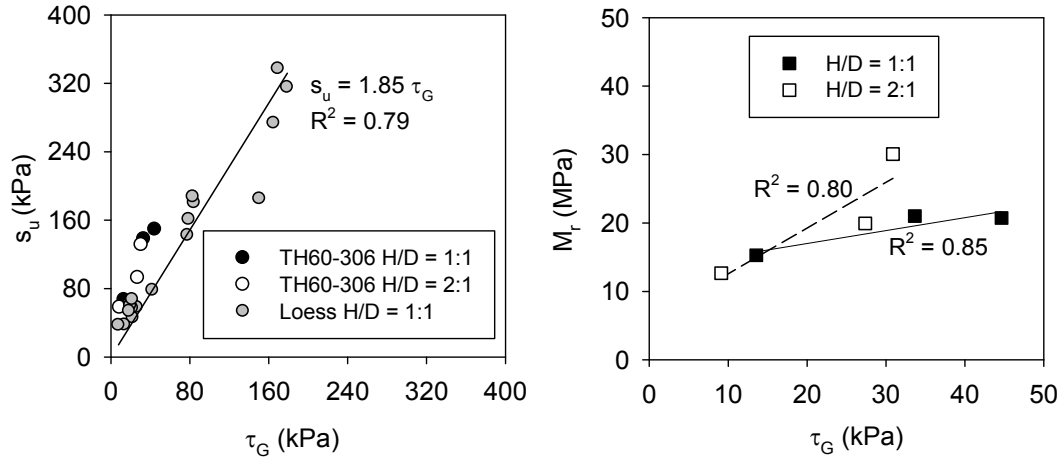


Figure 5.58. Correlation between  $s_u$ ,  $M_r$  and  $\tau_G$  for samples with H/D = 1 and 2 – TH 60 soil 306 (USCS: CL)

#### 5.8.4 Field Approach to Target Value Determination

As part of this study, 200 mm plate Zorn LWD tests were conducted at several locations on uncompacted material with the idea that with multiple hammer drops the soil would compact and the  $E_{LWD}$  value would reach an asymptote thus establishing a field target value. Results are presented in Figure 5.59 for field tests at TH 60 in non-granular soil (TH60 project test strip 4). Results indicated that with increasing number of drops  $E_{LWD}$  increases and  $d_{LWD}$  decreases to approach an asymptotic value. Moisture contents are provided for each test point and were in the range of 9.5 to 12.4%.  $E_{LWD}$  values ranged from about 6 MPa to 16 MPa. These values are lower than the average value (about 27 MPa) measured after roller compaction (see Chapter 3 discussions in TH60 test strip 4). It must be noted that the compaction stresses under the roller are much higher than that are generated under the 200 mm LWD plate by a factor of 3 to 4 (see section 3.3.4). No trend was observed in the  $E_{LWD}$  or  $d_{LWD}$  values with moisture content.

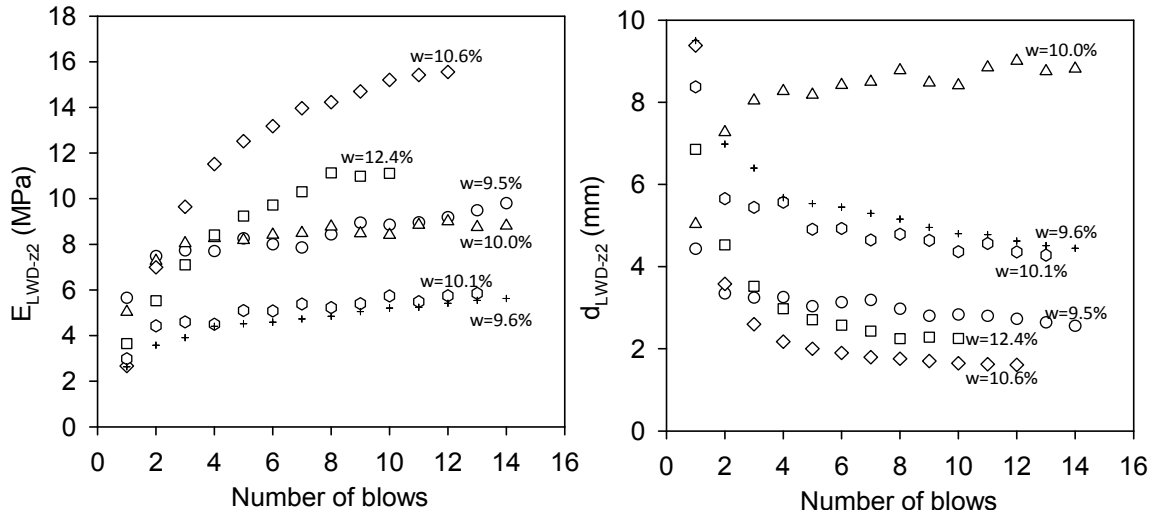


Figure 5.59. Results from in-situ LWD tests showing  $E_{LWD}$  increase and  $d_{LWD}$  decrease with number of blows at locations with different in-situ moisture contents – TH60 soil 306 (test strips 4 and 5 of Chapter 3 TH60 project)

### 5.8.5 Linking Laboratory LWD-TVs to In-Situ LWD Measurements

The approach of developing  $w-\gamma_d-E_{LWD}/DPI$  contours described above is useful in determining target  $E_{LWD}$  or  $d_{LWD}$  values for a specified moisture range and target minimum density in-situ. Mn/DOT recently developed target in-situ  $d_{LWD-ZZ}$  values based on plastic limit and estimated optimum moisture content of the material (see Siekmeier et al. 2009). These two approaches are compared with actual measured in-situ test data from TH60 project in the following discussion. First, the approach using laboratory test results to develop target  $E_{LWD-ZZ}$  and  $d_{LWD-ZZ}$  values are described and then comparisons to in-situ test measurements and Mn/DOT target values are made.

Gyratory compacted specimens of TH60 non-granular soil 306 were prepared and tested using 100-mm plate and 150-mm plate Zorn LWD, and DCP under “stiff” boundary conditions. PDA  $\tau_G$  measurements were obtained during gyratory compaction process for all the samples. Contours of  $E_{LWD-Z1.5}$ ,  $E_{LWD-Z1.0}$ , DPI,  $s_u$  (determined from DPI- $s_u$  relationships in Chapter 3) and  $\tau_G$  are presented in Figure 5.60, Figure 5.61, and Figure 5.62. Multiple regression models for the “stiff” boundary condition tests are presented on the contour plots.

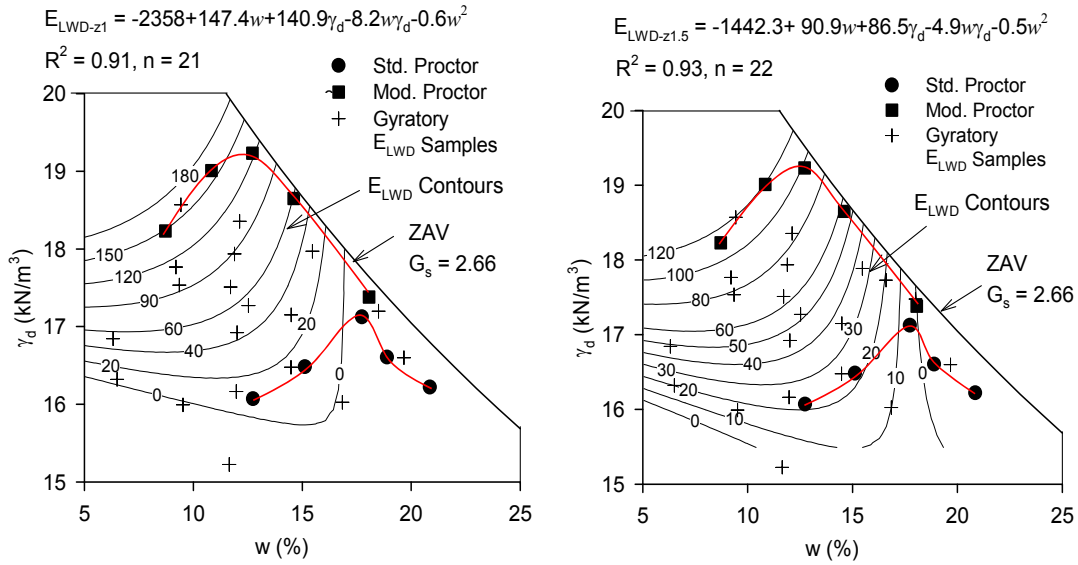


Figure 5.60.  $E_{LWD-Z1}$  and  $E_{LWD-Z1.5}$  contours in relationship with moisture and dry unit weight with stiff boundary conditions – TH60 soil 306 material (USCS: CL)

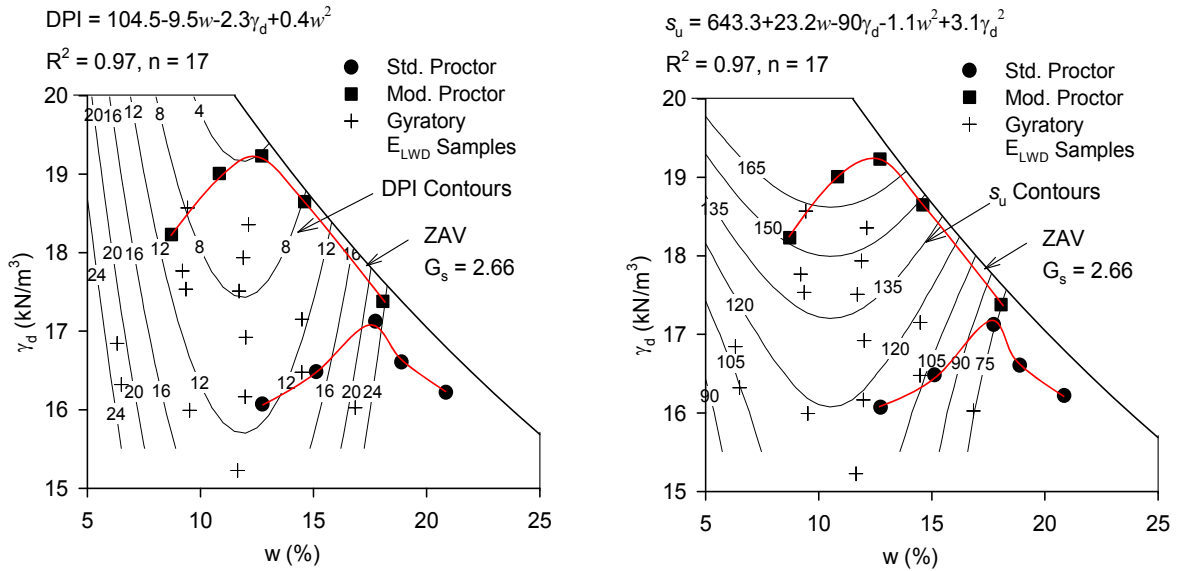


Figure 5.61. DPI and  $s_u$  contours in relationship with moisture and dry unit weight with stiff boundary conditions – TH60 soil 306 material (USCS: CL)

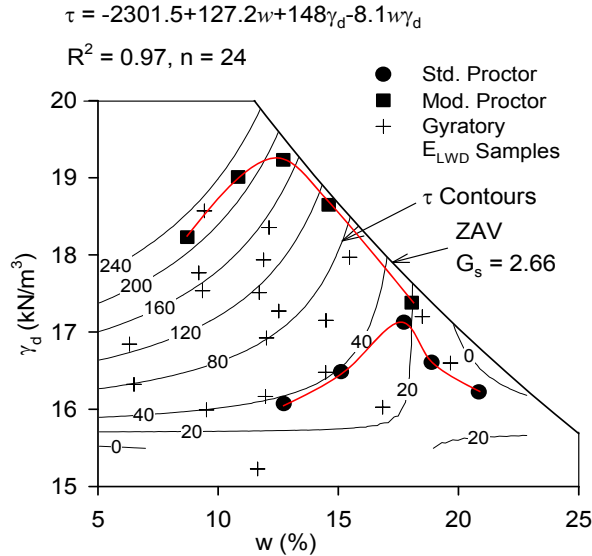


Figure 5.62.  $\tau_G$  contours in relationship with moisture and dry unit weight with stiff boundary test – TH60 soil 306 material (USCS: CL)

Regression relationships between  $\tau_G$  and LWD/DCP test measurements are presented in Figure 5.63. The regression relationships show strong correlations with  $R^2$  values  $> 0.7$ . The  $\tau_G$  and  $s_u$  predicted from DPI showed encouraging trend in the data.

Comparison between  $E_{LWD-Z1.5}$  and  $E_{LWD-Z1.0}$  measurements is presented in Figure 5.64. A line based on Terzaghi's theoretical relationships (see Figure 5.10) is also shown in Figure 5.64. Results indicate that the best fit regression line for the measurements is in close agreement with Terzaghi's theoretical relationship.

Figure 5.65 shows  $w$ - $\gamma_d$  relationship and  $E_{LWD}$  contours obtained from the "stiff" boundary model for TH60 soil 306 ( $w_{opt} = 17.3\%$ , USCS: CL) in comparison with in-situ  $w$ - $\gamma_d$  at  $E_{LWD}$  test locations from TH60 test strip 3 with similar material characteristics ( $w_{opt} = 17.3\%$ , USCS: CL).  $E_{LWD-Z2}$  and  $d_{LWD-Z2}$  values for in-situ  $w$ - $\gamma_d$  values were predicted from the laboratory-determined  $E_{LWD-Z1.5}$  using Terzaghi's theoretical relationship (see Figure 5.64). The predicted values are compared with actual in-situ measurement values in Figure 5.65. Only in-situ measurements that are in the range of moisture and density of laboratory samples are considered for the comparison. Only two in-situ test measurements were present within the range of laboratory test measurements.

Multiple regression model with rigid boundary conditions developed for TH60 soils combining 301, 303, and 305 materials (average  $w_{opt} = 14\%$ ) are used to compare in-situ  $w$ - $\gamma_d$  measurements at  $E_{LWD}$  test locations from TH60 test strips 1, 4, and 5 (average  $w_{opt} = 13.8\%$ ) in Figure 5.66. The in-situ test measurements showed  $w$  values in the range of 65% to 140% of  $w_{opt}$ .  $E_{LWD-Z2}$  and  $d_{LWD-Z2}$  values for in-situ  $w$ - $\gamma_d$  values were predicted from the laboratory-determined  $E_{LWD-Z1}$  using Terzaghi's theoretical relationship (see Figure 5.64). The predicted values are compared

with actual in-situ measurement values in Figure 5.66. The regression relationships indicate positive relationships and predicted  $E_{LWD-Z2}$  values are about 0.6 times the actual in-situ  $E_{LWD-Z2}$  measurements.

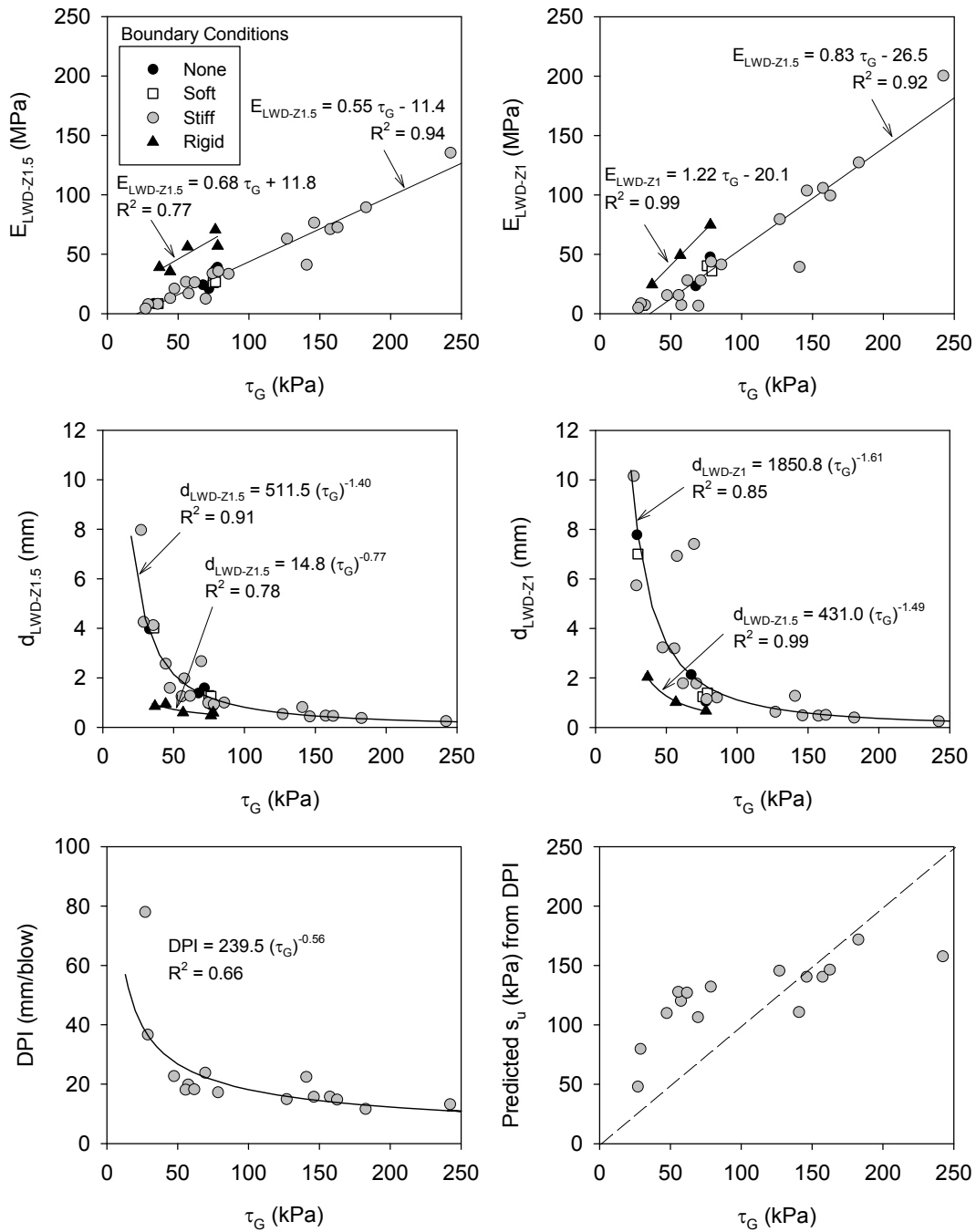


Figure 5.63. Correlations between  $\tau_G$  and LWD/DPI measurements with different boundary conditions – TH60 soil 306 material (USCS: CL)

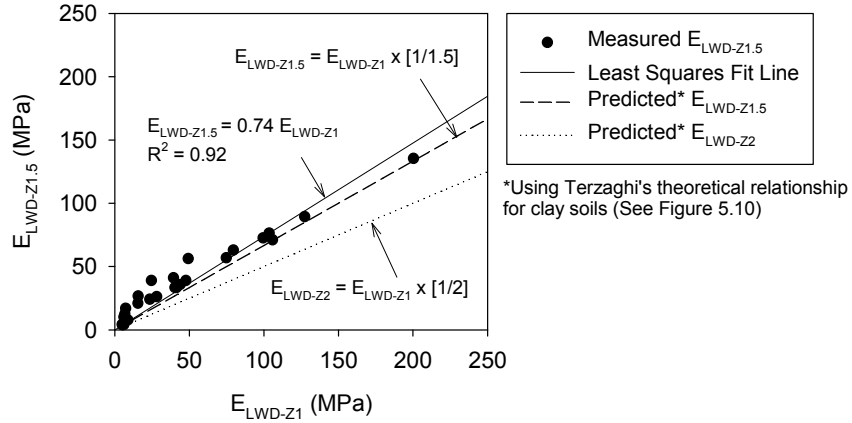


Figure 5.64. Relationships between laboratory  $E_{LWD-Z1}$  and  $E_{LWD-Z2}$  measurements in comparison with Terzaghi's theoretical relationships – TH60 soil 306 material (USCS: CL)

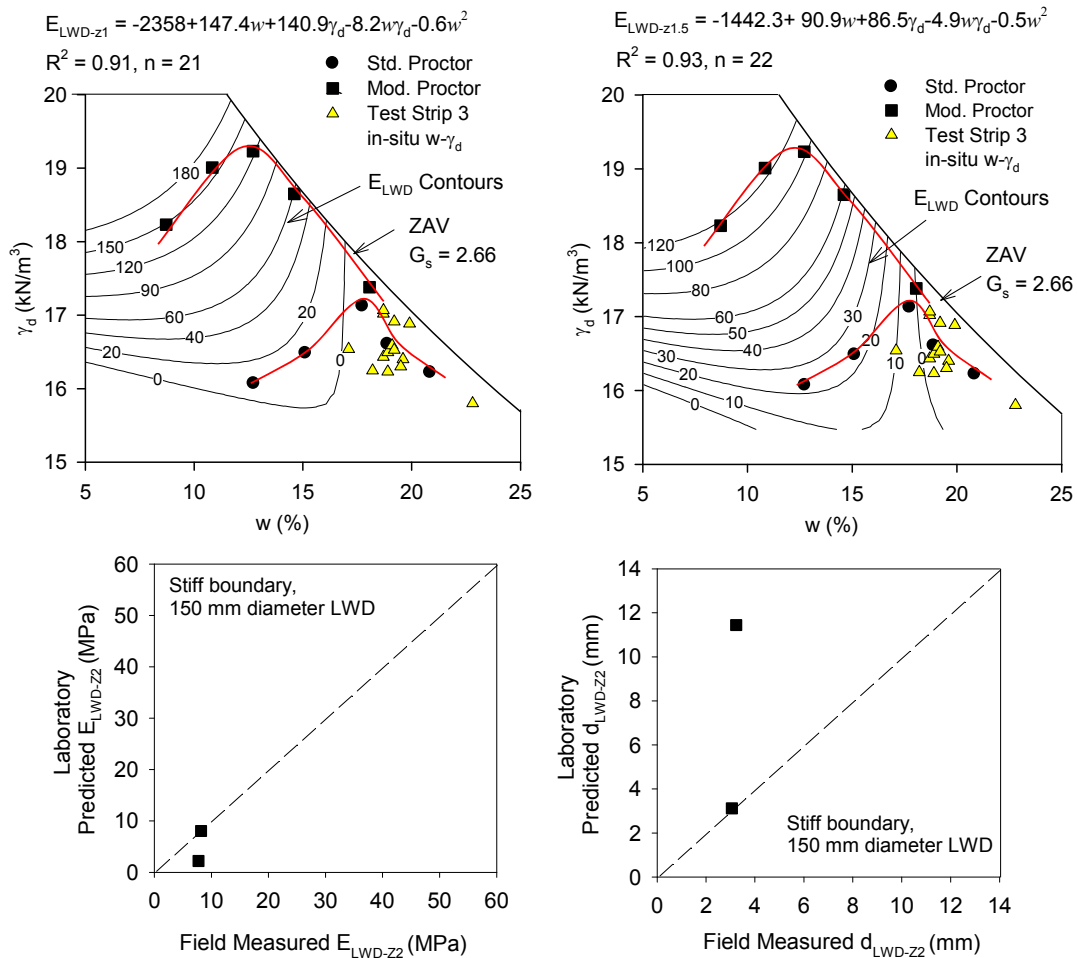


Figure 5.65. Comparison between in-situ LWD measurements (from TH60 project test strip 3) and laboratory predicted LWD target values (TH60 soil 306 “stiff” boundary model)

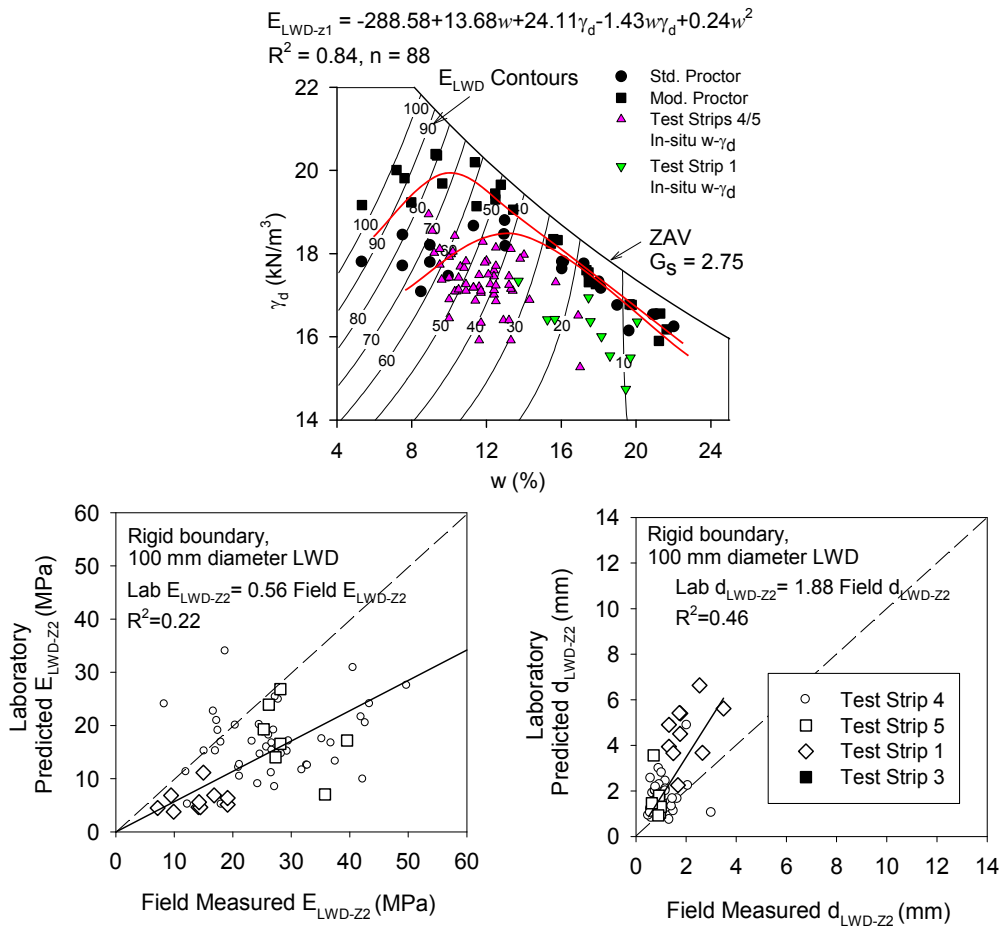


Figure 5.66. Comparison between in-situ LWD measurements (from TH60 project test strips 1 and 4/5) and laboratory predicted LWD target values (TH60 soil 301, 302, 303 combined rigid boundary model)

Mn/DOT target values in comparison with in-situ  $E_{LWD}$  measurement statistics (mean  $\mu$  and standard deviation  $\sigma$ ) and laboratory determined target values at different moisture content ranges (as percentage of  $w_{opt}$ ) are presented in Table 5.15 and Table 5.16. The laboratory determined target values are based on achieving a 95% to 110% standard Proctor maximum density. The in-situ  $w$  at most of the test locations on TH60 test strips 1, 2, and 3 was above 95%  $w_{opt}$ . Test strips 4 and 5 contained data within 65% to 140% of  $w_{opt}$ . The LWD target value ranges determined from laboratory multiple regression models and Mn/DOT procedures in comparison with in-situ LWD measurements are graphically presented for test strips 4/5 in Figure 5.67. The figure indicates that laboratory-determined target values using contour approach from the rigid boundary model are mostly within the range of Mn/DOT target values. Lower limit of in-situ measurements (within  $\mu \pm 1\sigma$  range) were lower than the minimum target values obtained from both Mn/DOT and laboratory-determined methods for 70% to 79%  $w_{opt}$ . For >80% of  $w_{opt}$ , the lower limit of in-situ measurements (again within  $\mu \pm 1\sigma$  range) were

greater than the minimum target values obtained from both Mn/DOT and laboratory-determined methods.

Table 5.15. In-situ  $d_{LWD}$  measurements (TH60 project test strips 1 to 5) for Mn/DOT moisture content target limits

Description	Test Strip 1			Test Strip 2			Test Strip 3			Test Strips 4/5		
<i>Soil Properties</i>												
Plastic Limit, PL (%)	16			27			20			19		
Standard Proctor $w_{opt}$ (%)	14.2			19.3			17.3			13.3		
<i>Mean (<math>\mu</math>) and standard deviation (<math>\sigma</math>) of <math>d_{LWD-Z2}</math> (mm) measured in-situ [in-situ <math>\gamma_d \geq 95\% \gamma_{dmax}</math>]</i>												
In-situ $w$ as percent of $w_{opt}$	n	$\mu$	$\sigma$	n	$\mu$	$\sigma$	n	$\mu$	$\sigma$	n	$\mu$	$\sigma$
70% to 74%	—			1	0.95	NA	—			3	1.1	0.3
75% to 79%	—			—			—			8	1.0	0.6
80% to 84%	—			—			—			2	0.8	0.3
85% to 89%	—			1	0.97	NA	—			3	0.9	0.2
90% to 94%	—			—			—			7	1.1	0.3
95% to 99%	—			—			—			1	1.2	NA
100% to 140%	—			1	1.87	NA	10	2.5	0.3	2	1.0	< 0.1
<i>Mean (<math>\mu</math>) and standard deviation (<math>\sigma</math>) of <math>d_{LWD-Z2}</math> (mm) measured in-situ [in-situ <math>\gamma_d &lt; 95\% \gamma_{dmax}</math>]</i>												
In-situ $w$ as percent of $w_{opt}$	n	$\mu$	$\sigma$	n	$\mu$	$\sigma$	n	$\mu$	$\sigma$	n	$\mu$	$\sigma$
70% to 74%	—			—			—			—		
75% to 79%	—			—			—			7	1.1	0.3
80% to 84%	—			—			—			4	0.8	0.1
85% to 89%	—			—			—			6	1.0	0.3
90% to 94%	—			—			—			5	0.9	0.2
95% to 99%	—			—			—			3	1.0	0.3
100% to 140%	16	1.9	0.7	6	1.9	0.3	5	3.2	0.6	7	1.5	1.1

Table 5.16. In-situ  $E_{LWD}$  measurements (TH60 project test strips 1 to 5) for Mn/DOT moisture content target limits

Description	Test Strip 1			Test Strip 2			Test Strip 3			Test Strips 4/5					
<i>Mean (<math>\mu</math>) and standard deviation (<math>\sigma</math>) of <math>E_{LWD-Z2}</math> (MPa)* measured in-situ [in-situ <math>\gamma_d \geq 95\% \gamma_{dmax}</math>]</i>															
In-situ $w$ as percent of $w_{opt}$	n	$\mu$	$\sigma$	n	$\mu$	$\sigma$	n	$\mu$	$\sigma$	n	$\mu$	$\sigma$			
70% to 74%	—			1	24	NA	—			3	24	7			
75% to 79%				—						8	24	13			
80% to 84%				—						2	34	13			
85% to 89%				1	24	NA				3	29	9			
90% to 94%				—						7	25	6			
95% to 99%				—						1	21	NA			
100% to 140%				1	13	NA				10	10	1	2	25	< 1
<i>Mean (<math>\mu</math>) and standard deviation (<math>\sigma</math>) of <math>E_{LWD-Z2}</math> (MPa)* measured in-situ [in-situ <math>\gamma_d &lt; 95\% \gamma_{dmax}</math>]</i>															
In-situ $w$ as percent of $w_{opt}$	n	$\mu$	$\sigma$	n	$\mu$	$\sigma$	n	$\mu$	$\sigma$	n	$\mu$	$\sigma$			
70% to 74%	—			—			—			—					
75% to 79%										7	25	7			
80% to 84%										4	31	6			
85% to 89%										6	26	6			
90% to 94%										5	29	6			
95% to 99%										3	26	8			
100% to 140%	16	14		4	6	14	2	5	8	2	7	22	11		

Table 5.17. Comparison between Mn/DOT and laboratory-determined  $d_{LWD}$  and  $E_{LWD}$  target values for different moisture ranges for materials from TH60 project test strips 1 to 5

<i>Laboratory-determined <math>d_{LWD-Z2}</math> (mm)*</i>								
In-situ $w$ as percent of $w_{opt}$	Min.	Max.	Min.	Max.	Min.	Max.	Min.	Max.
70% to 74%	0.6	0.9	Laboratory test materials not representative		1.2	3.9	0.6	0.9
75% to 79%	0.7	1.0		1.6	4.3	0.6	1.0	
80% to 84%	0.7	1.0		2.2	5.1	0.7	1.0	
85% to 89%	0.8	1.2		4.0	7.3	0.8	1.2	
90% to 94%	0.9	1.3		>10.0		0.9	1.3	
95% to 99%	1.1	1.5			1.1	1.5		
100% to 140%	1.6	> 10			1.6	> 10		
<i>Mn/DOT target range of <math>d_{LWD-Z2}</math> (mm) (Siekmeier et al. 2009)</i>								
In-situ $w$ as percent of $w_{opt}$	Min.	Max.	Min.	Max.	Min.	Max.	Min.	Max.
70% to 74%	0.5	1.1	1.0	1.7	0.8	1.4	0.5	1.1
75% to 79%	0.6	1.2	1.2	1.9	0.9	1.6	0.6	1.2
80% to 84%	0.7	1.3	1.4	2.1	1.0	1.7	0.7	1.3
85% to 89%	0.8	1.4	1.6	2.3	1.2	1.9	0.8	1.4
90% to 94%	1.0	1.6	1.8	2.6	1.4	2.1	1.0	1.6
<i>Laboratory-determined <math>E_{LWD-Z2}</math> (MPa)<sup>†</sup></i>								
In-situ $w$ as percent of $w_{opt}$	Max	Min.	Max	Min.	Max	Min.	Max	Min.
70% to 74%	42	29	Laboratory test materials not representative		20	6	42	29
75% to 79%	39	26		16	6	39	26	
80% to 84%	34	24		12	5	34	24	
85% to 89%	31	22		6	3	31	22	
90% to 94%	28	20		< 2			28	20
95% to 99%	24	17			24	17		
100% to 140%	16	1			16	1		
<i>Mn/DOT target range for <math>E_{LWD-Z2}</math> (MPa)**</i>								
In-situ $w$ as percent of $w_{opt}$	Max	Min.	Max	Min.	Max	Min.	Max	Min.
70% to 74%	50	23	25	15	31	18	50	23
75% to 79%	42	21	21	13	28	16	42	21
80% to 84%	36	19	18	12	25	15	36	19
85% to 89%	31	18	16	11	21	13	31	18
90% to 94%	25	16	14	10	18	12	25	16

\* laboratory  $d_{LWD-Z2}$  values predicted from estimated  $E_{LWD-Z1}$  contours [rigid boundary model for test strips 1, 4/5 and “stiff” boundary model for test strip 3]; † laboratory  $E_{LWD-Z2}$  values predicted from estimated  $E_{LWD-Z1}$  contours [rigid boundary model

for test strips 1, 4/5 and “stiff” boundary model for test strip 3];\*\*calculated using Eq. 5.1 for Poisson’s ratio  $\eta = 0.4$ , shape factor  $F = \pi/2$ , drop height  $h = 50$  mm;

Table 5.18. In-situ Mn/DOT QA  $d_{LWD}$  and  $E_{LWD}$  measurements at different moisture contents from the TH60 project

<i>Mean (<math>\mu</math>) and standard deviation (<math>\sigma</math>) of Mn/DOT QA <math>d_{LWD-Z2}</math> (mm) measurements*</i>			
In-situ $w$ as percent of $w_{opt}^*$	n	$\mu$	$\sigma$
70% to 74%	—		
75% to 79%	5	1.6	1.4
80% to 84%	5	0.9	0.2
85% to 89%	6	1.4	0.5
90% to 94%	5	1.2	0.4
95% to 99%	15	1.5	0.6
100% to 140%	24	2.6	1,7
<i>Mean (<math>\mu</math>) and standard deviation (<math>\sigma</math>) of Mn/DOT QA <math>E_{LWD-Z2}</math> (mm) measurements*</i>			
In-situ $w$ as percent of $w_{opt}^*$	n	$\mu$	$\sigma$
70% to 74%	—		
75% to 79%	5	34	25
80% to 84%	5	32	8
85% to 89%	6	21	7
90% to 94%	5	23	7
95% to 99%	15	21	9
100% to 140%	24	14	8

\* $w_{opt} = 13.2\%$  was provided in the QA testing data from Mn/DOT.

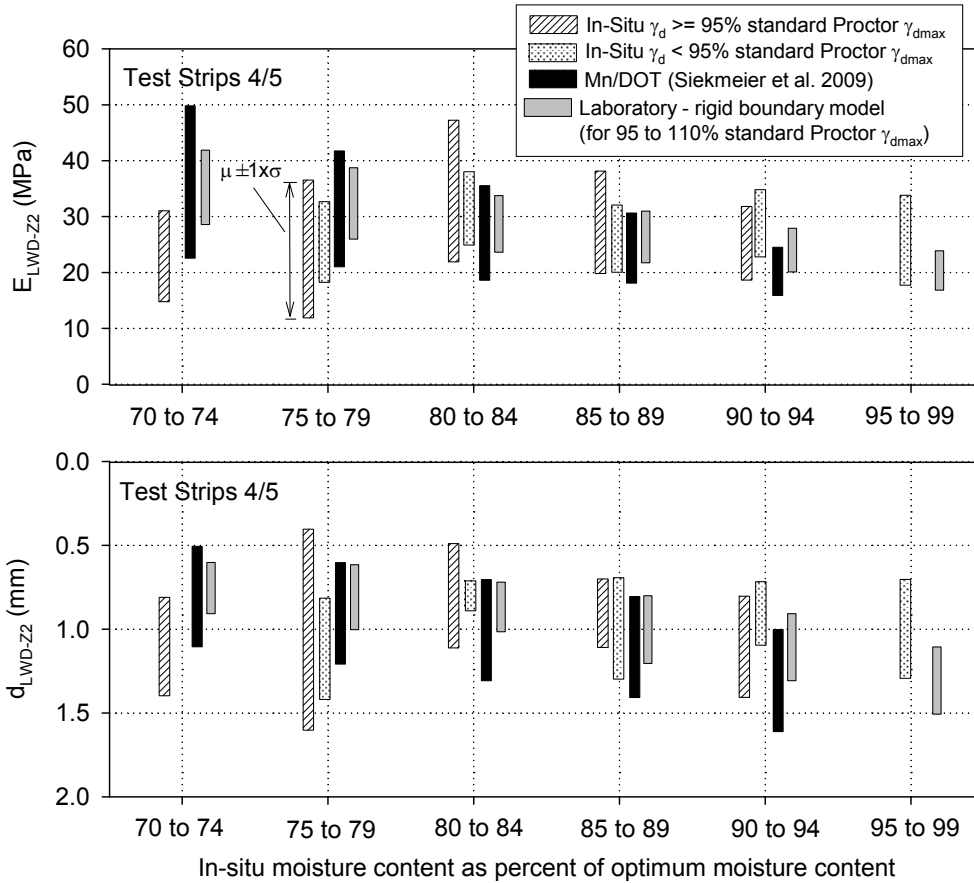


Figure 5.67. Comparison between  $E_{LWD}$  Mn/DOT and laboratory determined target values, and in-situ values (see Tables above for number of observations for each dataset)

### 5.8.6 Summary of Laboratory Target Value Determination Study

The results presented above from laboratory target value determination study demonstrate the application of gyratory compacted samples to develop relationships between moisture content, density,  $E_{LWD}$ , DCP index, and PDA  $\tau_G$  for non-granular and granular soils. These relationships are presented in terms of contour graphs overlaid on laboratory Proctor moisture-density relationships of the soils. The advantage of presenting results in that manner is that target values can be tied to both target moisture and density values.  $E_{LWD}$ , DCP index, and PDA  $\tau_G$  were found to be sensitive to moisture content for non-granular soils. Moisture content influenced the granular materials less than the non-granular materials.

New relationships were developed between the PDA  $\tau_G$  values and other soil engineering parameters (e.g.,  $E_{LWD}$ ,  $M_r$ ,  $s_u$ ). Those relationships showed good correlation coefficients ( $R^2$  values generally  $> 0.7$ ). A significant advantage with using the PDA device is that it is less time consuming than other test methods (i.e.,  $E_{LWD}$ , UU, UC, or  $M_r$  tests).

LWD and DCP tests performed on specimens within a rigid gyratory mold produced generally high stiffness/strength values. This is specifically an issue with granular materials that are more sensitive to confinement compared to non-granular materials. Two different polyurethane molds with different stiffnesses (“stiff” and “soft”) were used in this study to investigate the effects of confinement. The two polyurethane molds did not provide adequate confinement for the granular materials and did not show any noticeable difference with unconfined condition.

The laboratory-determined  $E_{LWD}$  target values (based on rigid boundary testing) for one TH60 non-granular soil were compared to Mn/DOT target values (Siekmeier et al. 2009) and in-situ  $E_{LWD}$  test results. This comparison revealed that the laboratory-determined target values are mostly within the range of Mn/DOT proposed target values. Some of the in-situ  $E_{LWD}$  measurements were lower than the minimum Mn/DOT and laboratory-determined target values for  $w = 70\%$  to  $79\%$   $w_{opt}$  range. For  $w > 80\%$  of  $w_{opt}$ , the lower limit of in-situ  $E_{LWD}$  measurements were generally greater than the minimum target values obtained from both Mn/DOT and laboratory-determined methods.

The approach presented in this section to develop target values using gyratory testing and trends presented in the relationships show promise. However, additional research with developments to the laboratory approach in terms of better simulating the actual field boundary conditions and for a wide range of soil types is warranted. The challenge is to develop a simple approach that adds value to the process without becoming too expensive or equipment intensive.

## **Chapter 6**

### **IC Verification and Specification Options**

#### **6.1 Verification Procedures for IC Equipment**

One of the tasks of this research project involved identifying alternatives for calibration/verification for IC technologies. The discussion that follows is oriented towards verification and quantifying measurement error rather than sensor calibration, which the authors considered the responsibility of the manufacturer. The outcome from this investigation resulted in (1) a statistical approach for evaluating the error associated with the roller IC-MVs in terms of repeatability and reproducibility for a given set of field and roller operation conditions, (2) an approach that would make use of a dedicated test bed with controlled and variable conditions at the centrally located MnROAD facility, and (3) a conceptual idea that would involve a mechanical system to simulate a range of soil conditions to verify IC-MVs.

##### **6.1.1 Determining IC-MV Measurement Error**

The procedure for calculating reproducibility and repeatability errors is presented in the Appendix and was discussed with example data in Chapter 3. The calculated errors have the same units as the IC-MVs and are dependent upon the roller operating conditions and “white noise” in the measurement system. Generally, a 100 m long well-compacted test section representative of the production area is suitable for testing. At least four roller passes are recommended for a given roller operation parameter (speed, theoretical vibration amplitude, vibration frequency, and travel direction). The roller passes should be performed capture the planned operating conditions on the project. The total number of passes can be determined as follows:

- Number of Passes = 4 x machine operation variables (i.e., amplitude, speed, direction, frequency, etc.). For example, the total number of passes required to evaluate just the influence of speed at two different settings, then the total number of passes required =  $4 \times 2 = 8$  passes.

Table 6.1 provides a summary of the pass-by-pass process for collecting the data needed for the measurement error analysis. It should be noted that the measurement error should be expected to increase with increasing number of variables in the analysis. Variants of this process can also provide acceptable results and depends on the desired roller operating conditions. As discussed later, the IC roller measurement error is an input parameter that is required as part of statistical QA/QC assessment.

Table 6.1 Suggested pass sequence to assess measurement error

Pass	Amplitude	Speed	Direction
<i>Assess Influence of Change in Amplitude</i>			
1	low	constant	constant
2	low	constant	constant
3	low	constant	constant
4	low	constant	constant
5	high	constant	constant
6	high	constant	constant
7	high	constant	constant
8	high	constant	constant
<i>Assess Influence of Change in Speed</i>			
1	constant	low	constant
2	constant	low	constant
3	constant	low	constant
4	constant	low	constant
5	constant	high	constant
6	constant	high	constant
7	constant	high	constant
8	constant	high	constant
<i>Assess Influence of Change in Amplitude and Speed</i>			
1	low	low	constant
2	low	low	constant
3	low	low	constant
4	low	low	constant
5	low	high	constant
6	low	high	constant
7	low	high	constant
8	low	high	constant
9	high	low	constant
10	high	low	constant
11	high	low	constant
12	high	low	constant
13	high	high	constant
14	high	high	constant
15	high	high	constant
16	high	high	constant

Pass	Amplitude	Speed	Direction
<i>Assess Influence of Change in Amplitude, Speed, and Direction*</i>			
1	low	low	forward
2	low	low	forward
3	low	low	forward
4	low	low	forward
5	low	high	forward
6	low	high	forward
7	low	high	forward
8	low	high	forward
9	high	low	forward
10	high	low	forward
11	high	low	forward
12	high	low	forward
13	high	high	forward
14	high	high	forward
15	high	high	forward
16	high	high	forward
17	low	low	reverse
18	low	low	reverse
19	low	low	reverse
20	low	low	reverse
21	low	high	reverse
22	low	high	reverse
23	low	high	reverse
24	low	high	reverse
25	high	low	reverse
26	high	low	reverse
27	high	low	reverse
28	high	low	reverse
29	high	high	reverse
30	high	high	reverse
31	high	high	reverse
32	high	high	reverse

\*direction mean roller direction of travel – not gear

### 6.1.2 Dedicated IC Verification Test Facility at MnROAD

Dedicated and controlled test beds at MnROAD facility are proposed as one alternative to verify IC-MVs. Figure 6.1 is an example of a test bed that could be used to obtain detailed correlations between different IC-MVs and mechanistic-based pavement design parameters (e.g.,  $E_{FWD}$ ,  $E_{LWD}$ , etc). The test beds would consist of different non-granular and granular material types that are commonly used in pavement foundation layers, underlain by variable support conditions to capture a wide measurement range. In addition to developing a database of correlations, the test beds could also be used to accept IC rollers at the beginning of a project and for periodic verification. Correlations to mechanistic-based parameters would give confidence in specifying roller MVs for use with performance-based specifications and for using IC-MVs for QA. This option would require an investment in the facility and personnel to regularly monitor the test bed values and performance maintenance as needed. The facility could also be used for training and certification.

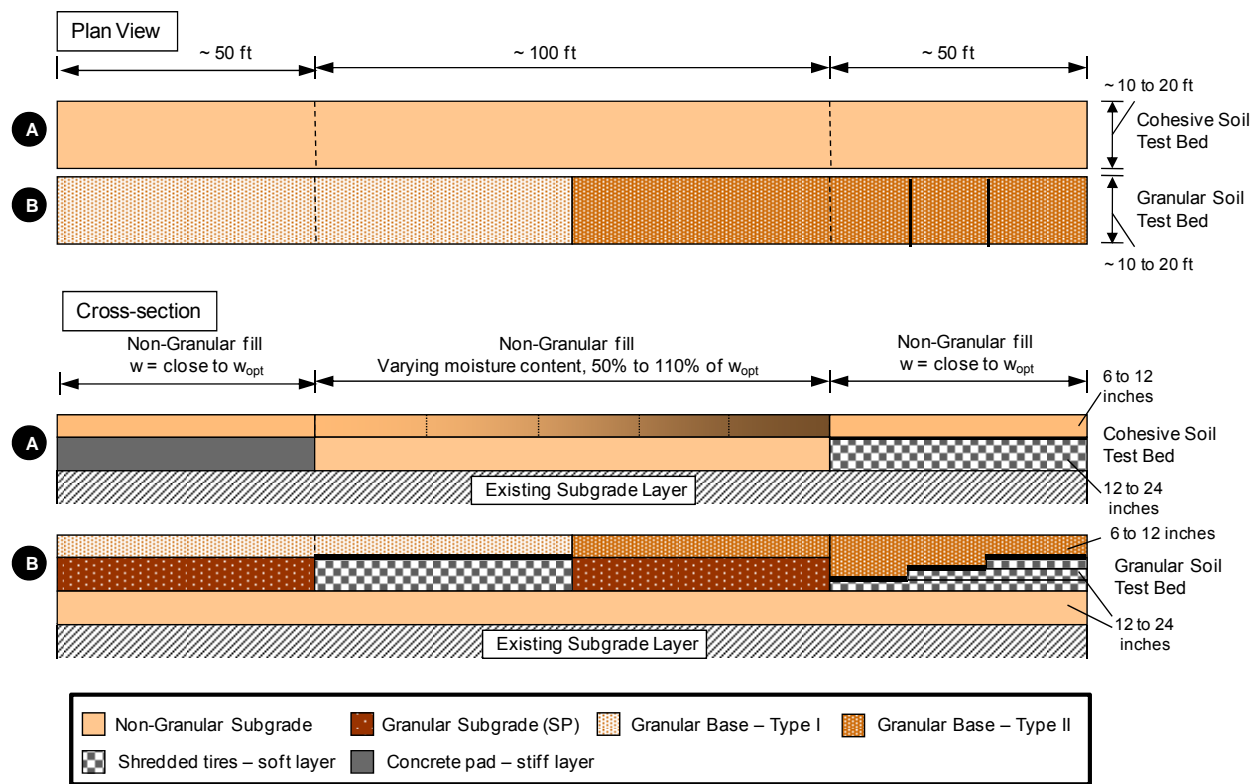


Figure 6.1. Proposed verification test beds with granular and non-granular materials

### 6.1.3 Mechanical System to Simulate Ground Conditions

An alternative to the dedicated test beds might be to develop a highly mobile mechanical system that could simulate the range of soil conditions expected to be encountered on a project. The

device could be transported to a project periodically to verify the output. Development of the components of such a system is beyond the scope of this research.

## **6.2 Recommendations for Future IC Specifications and Implementation Strategies**

In the previous report by White et al. (2007a), a summary of IC related specifications was provided and common attributes were identified. The purpose of this section is not to revisit the various specifications in detail, but rather to build on the experiences learned from implementation of IC technologies on Mn/DOT projects and suggest improvements and ideas for future consideration. Key attributes of IC specifications typically include the following:

- Descriptions of the rollers and configurations,
- Guidelines for roller operations (speed, vibration frequency, vibration amplitude, and roller overlap),
- Records to be reported (time of measurement, roller operations/mode, soil type, moisture content, layer thickness, etc.),
- Repeatability and reproducibility measurements for IC-MVs (see discussion above),
- Ground conditions (smoothness, levelness, isolated soft/wet spots)
- Calibration procedures for rollers and selection of calibration areas,
- Simple linear regression analysis between IC-MV's and point measurements,
- Number and locations of QC and QA tests,
- Operator training, and
- Acceptance procedures/corrective actions based on achievement of minimum IC-TVs and associated variability.

Although the existing IC specifications have common language for many of these attributes, it is in the use of IC-MVs for acceptance where the largest dissimilarities exist. As a comparison, the ISSMGE (2005) and the Mn/DOT (2007) target value determination approaches and acceptance criteria are summarized in Table 6.2. The ISSMGE (2005) specification links the IC-MVs to in-situ point measurements based on a linear correlation relationship with nine point measurements in low, medium and stiff areas based on the IC-MVs. Acceptance is then based on achievement of the IC-TV and associated variability. The Mn/DOT approach relies on the distribution of IC-MVs after thorough compaction of a calibration strip and then a percent limits approach for acceptance. Both approaches have the advantage of defining minimum target values and maximum allowable variability. These approaches make significant advancements over traditional point measurement QA/QC practices. However, shortcomings might be that the acceptance criteria are dependent on the specific IC technology (assuming differences exists between technologies MVs) and with no direct quantifications of risk in terms of whether or not the final site meets the established level of quality (although traditional earth specifications also do not quantify risk). What proceeds is a discussion that provides ideas that, in some cases are more rigorous, could provide a consistent means for specifying IC-MVs to define quality. The approaches presented could provide a link to performance-based specifications and quantitative mechanism to define incentive-based pay scales for earthwork compaction.

Three possible options are identified for use of IC-MVs in compaction of non-granular and granular soils with no on-site calibration. The premise of these options is to better assist the roller operator to target areas that need more compaction or re-work and the field engineer to target areas for QA testing. In addition, a conceptual statistical-framework for a more robust QA/AC evaluation of IC-MVs is presented.

Table 6.2 Summary comparison between different specifications

Specification	Target MV	Acceptance Criteria	QA/QC Test Frequencies
ISSMGE (2005)	MV-TV = MV at 1.05% QA-TV from calibration (with $r > 0.7$ )	<ul style="list-style-type: none"> <li>• Average MV <math>\geq</math> MV-TV</li> <li>• If minimum MV <math>\geq</math> MV at 0.95 x QA-TV, MV-COV shall be <math>\leq</math> 20%</li> <li>• Minimum MV for a measuring pass shall not be <math>\leq</math> MV at 0.95 x QA-TV for a maximum length of 10% of track length</li> <li>• Minimum MV for a measuring pass shall not be <math>&lt;</math> 80% of 0.95 x QA-TV</li> <li>• Maximum MV <math>\leq</math> 150% of MV at 0.95 QA-TV</li> </ul>	—
Mn/DOT (2007)	IC-TV = 90% of IC-MVs within 90%-120% of a trial IC-TV at point of no significant increase in compaction*	<ul style="list-style-type: none"> <li>• MV for 90% of area within 90% to 120% of MV-TV</li> <li>• Localized areas IC <math>&lt;</math> 80% of MV-TV reworked until MV <math>\geq</math> 90% MV-TV</li> </ul>	1 per 300 m for the entire width of embankment

\*IC-TV is established using an iterative method by grouping the calibration MV data into distribution limits (i.e.,  $>120\%$ ,  $90\%-120\%$ ,  $<80\%$  of MV-TV) based on a trial MV-TV. If a significant portion of the grade is more than 20% in excess of the selected IC-TV, a new control strip may be needed.

### 6.2.1 Option 1 – Use of IC-MV Map to Target In-situ QA Measurements

This option can be implemented relatively easily by using the final pass IC-MV map of a production area to identify “weak” areas. Following production compaction, the IC-MV map should be obtained at constant roller operation settings (i.e., speed, amplitude and frequency). The scale of the roller MV map is adjusted to highlight the “weak” areas to select for in-situ QA testing. Acceptance of the production area is based on in-situ QA test measurements in the “weak” areas.

Generally, IC-MVs have the ability to detect “weak” layers that are below the compaction layer. Results from TH60 project (see Chapter 3), however, indicated that MDP based IC-MVs at the project were not affected by soft/uncompacted zones below the compaction layer (about 250+ mm below surface). Measurement influence depths vary between different IC measurement

systems. Regardless, proper construction methods in using appropriate lift thicknesses relative to the ability of the compaction equipment and effective moisture control are important for implementing this option. In-situ QC measurements can be performed during intermediate processes for process control as to help optimize the construction sequence by focusing compaction efforts in areas that do not meet the QA requirement.

### **6.2.2 Option 2 – Assessment of IC-MV Change to Target In-situ QA Testing**

This specification option requires evaluating the change in IC-MVs between successive passes over a production area. With proper process control measures (i.e., material placed with appropriate moisture control and lift thickness), as the number of roller passes increase the change in roller MV between successive passes generally decrease. This change can fluctuate with decompaction and recompaction. As a reference point, production compaction should be performed until 90% of the production area achieves a percent change in IC-MV of  $\leq 5\%$ . These percentages may be adjusted based on field conditions and experience. Following production compaction, areas of low roller MVs are selected for QA test locations.

IC-MVs are dependent on the machine operation settings (i.e., amplitude, frequency, and speed); therefore, percent change between successive passes should be assessed only when MVs are obtained with similar operation settings. This option is more effective for controlled field conditions with relatively uniform materials, moisture content, and underlying support conditions and serves as a good QC process for the roller operator.

Results obtained from a test strip with plan dimensions of about 8 ft (one roller lane wide) wide x 140 ft long from TH60 project (test strip 3) are presented in Figure 6.2 and Figure 6.3 as an example analysis approach for this option. Percent change in roller MV can be assessed when repeated measurements are made at one particular location. The roller MVs are, however, not reported to an exact spatial location for each pass. To overcome this problem, the output data was processed in such a way that an averaged data is assigned to a preset grid point spaced along the roller path using a customized visual basic (VB) program developed at Iowa State University for this purpose. For this case, each grid point was spaced at 1 ft representing an average MV data over a window size of 0.5 ft in forward and backward directions. Figure 6.2 shows IC-MV compaction growth with pass and percent change in IC-MV between successive passes, and Figure 6.3 shows change in IC-MV spatial map with successive pass. The roller MV compaction growth shows decompaction and recompaction from pass 7 to 12. The requirement of 90% of the area achieving percent change in MV of  $\leq 5\%$  was met at pass 7 (see Table 6.3). A similar analysis approach can be applied over larger production areas. For some manufacturer systems, the roller operator can rely on the on-board computer display to assess percent change in roller MVs and determine when the requirement has been achieved. The data can be processed and analyzed using commercially available software packages (e.g., ArcGIS) with aid of kriging interpolation techniques (see White et al. 2007a) to evaluate percent change in MVs over a production area.

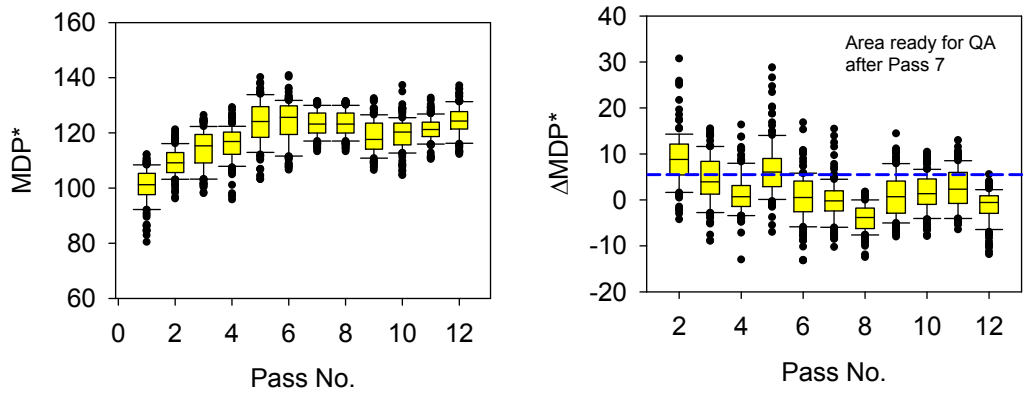


Figure 6.2. IC-MV compaction growth (left) and  $\Delta$ IC-MV (right) between successive passes for non-granular subgrade soil test strip 3 – TH 60

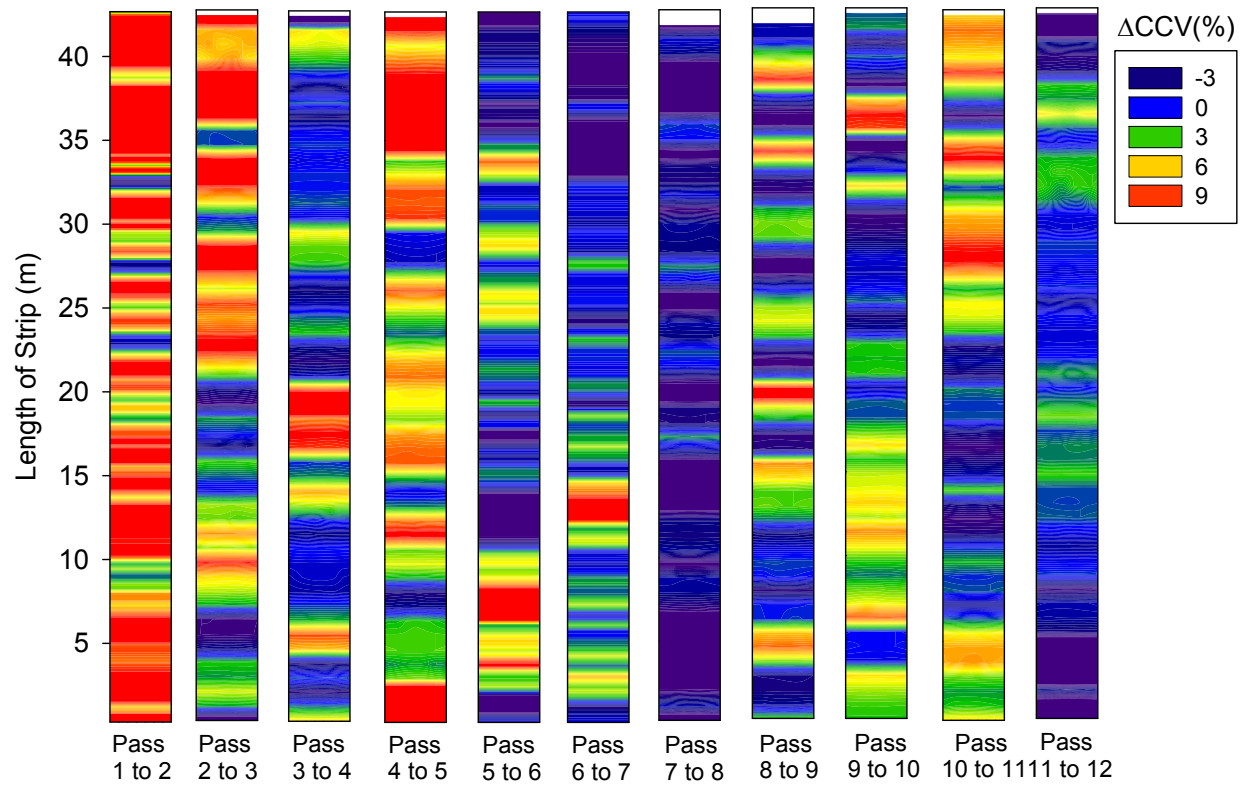


Figure 6.3. Spatial map of  $\Delta$ CCV between successive passes on non-granular subgrade soil test strip 3 – TH 60

Table 6.3. Summary of change in CCV between successive passes for non-granular subgrade soil (USCS classification: CL) test strip 3 – TH 60

Pass	Average $\Delta$ CCV	Percent Area with $\leq 5\% \Delta$ CCV
1 to 2	9	23
2 to 3	5	56
3 to 4	1	81
4 to 5	7	42
5 to 6	2	82
6 to 7	0	93
7 to 8	-4	100
8 to 9	1	82
9 to 10	2	78
10 to 11	3	65
11 to 12	-1	99

**6.2.3 Option 3 – Pre-selected IC-TVs and Mechanistic-Related QA-TVs**

IC and QA target values for this option are pre-selected, which can be derived from a database of correlations from current study/literature, information from local projects, and calibration tests on test beds of known engineering properties. The contractor would use the pre-selected IC-TVs for QC, and QA is evaluated using a combination of IC-MVs and in-situ QA test measurements.

**6.2.4 Option 4 – Concept for Statistically-Framed QA/QC Assessment Approach**

This section presents an approach that, although more rigorous mathematically, could provide a new way of characterizing compacted soils. This approach should be considered a concept and will require detailed pilot testing from multiple projects and conditions, but has the advantage of creating a consistent metric between different technologies and for defining quality.

When pavement foundation layers are compacted, there is a need to assure that the resulting soil engineering properties are satisfactory for the intended purposes (e.g. provide adequate support capacity to the pavement surface layer under traffic loads). This is achieved by performing point measurements or by evaluating IC-MVs as part of the QA procedure. Two formal goals are established below that are considered desirable following the compaction process on fill materials, which will further be used in the proposed statistical framework for QA/QC using both point measurement and IC-MV data:

- A. The overall level of critical soil engineering properties, over the entire site, achieve at least some specified minimal value (e.g., IC-TV, LWD-TV), and

- B. The variability of critical soil engineering properties, over the entire site, is no more than some specified maximal amount (e.g., %COV).

In this discussion, QA and QC are treated as distinct but closely related entities. QA refers to a formal site-wide certification process meant to constitute the standard by which the overall quality of site preparation is established. In contrast, QC is to designate an “interim” or “local” activity meant to guide operations during the compaction operations, or to determine sub-regions within which additional compaction operations are needed. The formal process of QA is primarily addressed in this discussion, and where QC is addressed as though it were being conducted as an independent activity, even though in practice the two processes generally rely on the same or related data. This is not a problem that can be easily ignored in the long run as the iterative collection of measurements for QC (e.g. collection of additional data in regions where early measurements are suspect) can lead to a data set that is very difficult to use for objective QA.

QA/QC procedures are developed for two different kinds of data. Traditional monitoring methods result in *point measurement* data whereas IC measurements result in *continuous measurement* data. Point measurements are taken independently from the compaction process, and each measurement results in a value reflecting soil properties at a single location in the site. The “locations” are considered as points within the site, even though such measurement processes do involve some physical integration of the measured soil property over a small volume (e.g., LWD test with 200 mm plate diameter measuring to a depth of about 200 mm). The time and expense associated with these measurements is such that, in most cases, fewer can be collected across the site than might be desired. But these measurement methods are generally regarded as relatively “mature” in that their relationship to the soil engineering properties of interest are fairly well-established. In practice, the lack of widespread point measurement data as part of the QA program is often counter balanced with experienced field personnel that are familiar with quality compaction operations and observational techniques. This level of qualitative observation is not considered in the proposed statistical framework that follows.

The IC-MVs are spatially “continuous” even though there is generally some granularity in the data record produced, ordinarily on the scale of several centimeters, but for practical purposes such data may be thought of as continuous relative to the much more granular data that can be acquired by point measurements . Again, each data value is associated with a GPS point location, even though it actually reflects soil properties physically integrated over the width of the roller drum (about 2 m) and perhaps up to 1.5 m (see Chapter 3). At present, IC-MVs may be regarded as “less direct” than some well-established point measurement techniques, since these data must be calculated correcting for other characteristics of machine performance, operation, etc. Generally, the relationships between IC-MVs–to–soil engineering properties of interest are less well-understood than the point measurement–to–soil engineering properties relationship.

A close examination of any measurement system reveals several sources of uncertainty that must be faced in documenting site-wide soil engineering properties. Herein three of those will be discussed:

1. The incomplete coverage problem with point measurement data,
2. The intrinsic measurement error, independent of actual soil properties, encountered in using any system, and
3. The incompletely understood relationship between IC-MVs-to-point measurement values or the actual soil engineering properties themselves.

When using point measurement values for site characterization, point (1) may be the greatest source of uncertainty in trying to extrapolate to site-wide soil properties. With continuous monitoring, point (3) may be more dominant. In general terms, each of these will be discussed to show how each kind of data may be used as the basis of QA/QC.

#### 6.2.4.1 Formal Goals for QA

The goals for QA (goals A and B) in soil compaction process are stated above in section 6.2.1. For simplicity and specificity, it is assumed that there is one well-defined soil engineering property that can, in principle, be attributed to every location in the site, and denote this property by  $Z(t)$ , where  $t$  is any (point) location within the site, denoted as  $R$ . QA goals are formalized by saying that, with respect to uniform weighting over all sites in  $R$ , the average value of  $Z$  should be no less than some specified value as indicated in Equation 6.1, and the standard deviation of  $Z$  should be no greater than some (other) specified value as indicated in Equation 6.2:

$$E(Z) = \mu = A(R)^{-1} \int_t Z(t) dt > Q_1 \tag{6.1}$$

$$SD(Z) = \sigma = \sqrt{A(R)^{-1} \int_t (Z(t) - \mu)^2 dt} < Q_2 \tag{6.2}$$

where  $A(R)$  is the area of  $R$ , for given values of  $Q_1$  = target value of  $Z$  for compliance, and  $Q_2$  = target standard deviation of  $Z$  for compliance. These statements can be modified to reflect non-uniform averaging over the site if that is appropriate. Other formal goals could, for example, be based on quantiles of the distribution of  $Z$  over  $R$ , e.g. that at least 80% (as used in ISSMGE specifications (see Table 6.1) of the locations in  $R$  have  $Z$  greater than some specified value.

Decisions are often based on data that are uncertain representations of the actual soil properties, and this leads to two points that should be made:

1. As noted, the nature of uncertainty inherent in the two kinds of measurement systems can be substantially different. In order to arrive at a unified, coherent framework for QA/QC, it is best to stipulate requirements apart from a specific kind of measurement technology.

Hence goals should be stated in terms of the actual soil engineering property  $Z$ , rather than of its measured values.

2. Due to the uncertainty inherent in any measurement system, there will always be some degree of uncertainty involved in knowing whether the goals have been met. Hence, some degree of acceptable risk should be specified, i.e. some nonzero-but-acceptable probability that a decision will be made that the site meets QA requirements when, in fact, it does not, and vice versa.

From an operational standpoint, point (1) can be addressed through repeatability and reproducibility testing and analysis (i.e., by quantifying the repeatability and reproducibility errors) as described elsewhere in this report.

#### 6.2.4.2 Risk Control

Along with the form of stated goals defined in terms of  $Z$ , two kinds of *risks* must be stipulated for each goal, namely:

1. The *risk* (or probability) that a site which actually meets the goal is erroneously declared as not meeting the goal based on data, and
2. The *risk* that a site which actually does not meet the goal is erroneously declared as meeting the goal based on the data.

The first kind of error is a “type I error” following the standard statistical nomenclature from statistical hypothesis testing, where the null hypothesis would state that the site does meet the goal. The probability,  $\alpha$ , of making this kind of error should be specified in advance. (Selection of  $\alpha$  will be determined from closely examining project level data and different soil types and could provide the basis for an incentive-based pay scale. Over time  $\alpha$  could be linked to performance records.)

The second kind of error, a “type II error”, requires a bit more specification. Suppose a site does not, in fact, meet the goal A, but its site-wide average of  $Z$  is very, very close to  $Q_1$ . The probability of a type II error will clearly be much larger than would be the case for a site in which the average value of  $Z$  is much, much larger than  $Q_1$ , for any reasonable decision rule. Hence in order to specify the acceptable risk of a type II error, the degree to which the site does not (hypothetically) meet the goal must be specified. To do this, specify  $\Delta_1$  and  $\Delta_2$ , as well as an acceptably small probabilities  $\beta$ , and say that risk shall be controlled so that:

1. The probability of erroneously declaring that a site qualifies for meeting goal A is only  $\beta$  if, in fact,  $\mu = Q_1 - \Delta_1$
2. The probability of erroneously declaring that a site qualifies for meeting goal B is only  $\beta$  if, in fact,  $\sigma = Q_2 (1+\Delta_2)$

In the statements above, note that nonconformance of the mean is stated in terms of an additive term (or “shift”), while nonconformance of the standard deviation is stated in terms of a multiplicative factor.

It should be noted that these risks could also be formulated based on using nonconformance as the null hypothesis. The practical impact of this would be that the site acceptance criteria would be much more difficult to satisfy. In effect, such rules would require that data convincingly contradict an assumption that goals are not satisfied, rather than simply being consistent with an assumption that they are. This approach would ideally be used where the “agency’s risk” (the risk of making an accident when the site actually does not conform) is more important than the “contractor’s risk” (the risk that a site that meets the QA rules is accidentally ruled as noncompliant).

#### 6.2.4.3 Data Model

At a given location  $t$ , it is stipulated that there is a well-defined (but not precisely known) value of the soil engineering property of interest,  $Z(t)$ . The model for data obtained at a location is shown for point measurement and IC-MVs in Equations 6.3 and 6.4, respectively:

$$\text{Point measurement: } X(t) = Z(t) + e_X(t) \quad (6.3)$$

$$\text{Continuous monitoring: } Y(t) = a + b Z(t) + e_Y(t) \quad (6.4)$$

where  $e_X(t)$  and  $e_Y(t)$  are measurement errors of  $X$  and  $Y$ , respectively (which can be determined from repeatability test data) and are regarded as random. These errors will be modeled as “white noise”, each with mean zero, and standard deviation that is characteristic of the measurement method. The respective standard deviations are  $SD(e_X)$  and  $SD(e_Y)$  which are assumed as known quantities (can be obtained from repeatability test data). An important assumption is that the measurement errors associated with point measurement and continuous monitoring data are statistically independent which means that each measurement contains a random noise component that is unrelated to the noise of any other measurement taken by either method. The data model is written to represent  $X$  as a “noisy” but accurate representation of the underlying soil engineering property of interest,  $Z$ . In contrast the structural component of  $Y$  contains a possible non-zero location off-set ( $a$ ) and a possible non-one scale off-set ( $b$ ). Two observations should be made. The first is that a more complicated structural relationship between  $X$  and  $Z$  could be stipulated, but unless it is completely known, this would add little practical generality to the model. Second, a more complicated relationship between  $Y$  and  $Z$  could be specified, e.g. to include quadratic or nonlinear aspects. So long as a functional form can be specified, this can generally be accommodated. A linear relationship is maintained here primarily because it likely does suffice in many situations, and to make the ideas specific. However, multiple regression analysis including soil properties from underlying layers and moisture content has been identified as a realistic approach to improving the regression models (see White and Thompson 2008, Thompson and White 2008). Currently no IC specification allows for multiple regression analysis as part of calibration – presumably due to perceived computational challenges. Multiple regression analysis has the potential advantage of creating a mechanism for site wide IC-MV calibration that can be updated as new information is collected, which would be a major advantage over current practices.

#### 6.2.4.4 A Framework for Point Measurements

The primary mission here is to discuss a framework within which defensible QA/QC procedures could be constructed for IC continuous monitoring systems. However, many of the standards that are in use for point measurement systems are based on rules that while generally well-defined and objective, are not easily interpreted statistically. Since QA/QC rules should ideally be framed in terms of risks, a notion is developed here for how these might be developed for data taken as point measurements, primarily as a “baseline” against which to compare IC-MVs.

##### *Site-Wide QA*

As noted above, a (and perhaps the) primary source of uncertainty associated with point measurement data stems from the incomplete coverage character of the information – the fact that only a small number of discrete sites  $t$  in  $R$  can be evaluated. It is now considered how QA can be formulated when  $N$  locations are randomly selected from  $R$ , and a point measurement is taken at each location. By randomly sampling locations, the point measurement data collected are in fact randomly taken from the (conceptually infinite) population of measurements that could, in principle, be taken throughout  $R$ . The average and sample variance of  $N$  point measurements be denoted by  $\bar{X}$ , and  $S_X^2$ , respectively. It follows, based on the assumptions concerning  $Z$  and the properties of  $e_X$ , and given values of  $\alpha$ ,  $\beta$ ,  $Q_1$ ,  $\Delta_1$ ,  $Q_2$  and  $\Delta_2$ , that

(i.)  $\bar{X}$  is an unbiased estimate of  $\mu$ , with standard deviation  $\sqrt{\sigma^2 + \text{SD}^2(e_X)}$

(ii.)  $S_X^2$  is an unbiased estimate of  $\sigma^2 + \text{SD}^2(e_X)$

(iii.) Goal A should be deemed to be satisfied if  $\bar{X} > C_1 = Q_1 - t_{N-1,1-\alpha} S_X / \sqrt{N}$

(iv.) Goal B should be deemed to be satisfied if

$$S_X < C_2 = \sqrt{Q_2^2 + \text{SD}^2(e_X)} \sqrt{\chi_{N-1,1-\alpha}^2 / (N-1)}$$

(v.) To control risks at stated levels for Goal A,  $N$  should be selected such that

$$N = \frac{Q_2^2 + \text{SD}^2(e_X)}{\Delta_1^2 (z_{1-\alpha} + z_{1-\beta})^2}$$

(vi.) To control risks at stated levels for Goal B,  $N$  should be selected such that

$$\chi_{N-1,1-\alpha}^2 / \chi_{N-1,\beta}^2 = \frac{Q_2^2 (1 + \Delta_2)^2 + \text{SD}^2(e_X)}{Q_2^2 + \text{SD}^2(e_X)}$$

In some cases, it may be desirable to partition  $R$  into sub-areas, and perform a specified amount of sampling in each sub-area. This technique, usually referred to as stratification in the statistical literature, often helps to ensure that all regions of  $R$  receive at least some sampling. More importantly, if  $R$  can be divided into sub-areas that are known to be relatively homogeneous

compared to the site as a whole, stratification can lead to improved information relative to simple random sampling. Analogous rules to those cited above are fairly easy to construct when a specified number of sites in each stratum (or sub-area) are randomly selected. Color-coded IC-MV maps can provide information for defining stratum boundaries.

#### *Local QC*

Because point measurement data is, in application, sampled “sparsely” throughout  $R$ , it is difficult to use as the basis of a broadly effective QC program. For example, if measurements are made at 10 randomly selected locations in a site of  $10,000 \text{ m}^2$ , the probability that a substandard sub-region of much less than  $1000 \text{ m}^2$  will be detected is obviously quite small. The most effective basis for developing the ability to detect local problems using point measurement data is simply through large numbers of samples, either in the initial/standard sampling stage (perhaps using defined stratum boundaries from IC-MV maps to ensure uniform coverage) or by reasonable iterative rules that call for additional, more spatially intensive, sampling in sub-regions that appear to produce the lowest average or most variable point measurements. With additional assumptions about the spatial distribution of  $Z$ , kriging methods could also be employed to interpolate relatively sparse point measurements for purposes of QC, but kriging cannot usually be counted on to identify spatial features of finer scale than the sampling grid.

#### 6.2.4.5 Framework for IC Continuous Monitoring

Recall that the assumption is that the point measurement system has been developed to be an accurate (if not entirely precise) reflection of the underlying soil engineering property of interest, and that the structural relationship between the IC continuous monitoring data and  $Z$  involves potential location and scale off-sets (see Equation 6.4). We further assume that these off-sets ( $a$  and  $b$  in Equation 6.4) are site-specific and are developed for the local conditions. This requires a calibration of  $Y$  using  $X$ , where  $X$  is the accepted “standard” for measurement, which should be a part of the formal QA program.

#### *Calibration*

Calibration requires that a paired sample of point measurement and IC-MV data be collected. One way to accomplish this would be to collect  $M$  spatially paired values of  $X$  and  $Y$ , using regression analysis to fit a functional form to  $Y$  as a function of  $X$ . However, this does not produce a “clean” estimate of the correct calibration curve because  $X$  and  $Z$  are not equivalent (except in the unusual case in which  $X$  contains no measurement error). A better practical option is to match each  $Y$  value with several closely spaced  $X$  values. In our context, this might be done by collecting  $m$  point measurement values across the roller drum width, i.e. so that they all represent soil that is being evaluated simultaneously in the physically integrated IC-MV. The  $m$  point measurement values in each such set are then averaged to “filter” the measurement error associated with  $Z$ . This average value of  $X$  is denoted as  $\bar{X}$ . If  $M$  such sets of data are collected, the result will be  $M$  pairs of single IC-MV data paired with averaged point measurement values. A linear regression is then computed by considering IC-MV data as a dependent variable (i.e., on y-axis) and the point measurement data as an independent variable (i.e., on x-axis) as shown in

Equation 6.5 which is associated with a mean squared error (MSE). The estimated intercept  $\hat{a}'$  and slope  $\hat{b}'$  obtained from this the linear regression are biased estimates of  $a$  and  $b$ , but the bias is small if  $SD(e_y)/\sqrt{m}$  is small relative to  $\sigma$ :

$$Y = \hat{a}' + \hat{b}' \bar{X} \quad (6.5)$$

Hence  $m$  should be selected with this in mind (typically,  $m = 3$  should be sufficient?). The overall sample size,  $M$ , should be at least 10, so that the regression estimates are not overly sensitive to the data values collected at any one location. In any case, there is some bias in this analysis, resulting in  $\hat{a}'$  somewhat overestimating  $a$ , and  $\hat{b}'$  somewhat underestimating  $b$ . Standard errors of these two estimates,  $SE(\hat{a}')$  and  $SE(\hat{b}')$  respectively, can be calculated as usual from the regression.

In production operation (after the calibration study), “calibrated” IC-MVs can be produced using Equation 6.6:

$$\tilde{Y}(t) = (Y(t) - \hat{a}') / \hat{b}' \quad (6.6)$$

QA decision rules for IC-MV data can be based on the same general idea used for point measurement sampling as described above, but here the additional uncertainty involved in the estimates  $\hat{a}'$  and  $\hat{b}'$  also needs to be incorporated. In this case, we have  $N$  values of  $\tilde{Y}(t)$  taken uniformly and densely from across  $R$ . For practical purposes, we view this as being a “noisy” but spatially complete collection of the effectively infinite collection of points in  $R$ . In effect, this means that the uncertainty in the average of calibrated values  $\bar{\tilde{Y}}$ , is essentially all due to the uncertainty in the calibration exercise associated with  $\hat{a}'$  and  $\hat{b}'$ . It follows, based on our assumptions described thus far, that:

- (i.)  $\bar{\tilde{Y}}$  is an approximately unbiased estimate of  $\mu$ , with approximate standard deviation  $SD(\bar{\tilde{Y}}) = \frac{1}{b} \sqrt{SD^2(\hat{a}') + \mu^2 SD^2(\hat{b}') + 2\mu CV(\hat{a}', \hat{b}')}$ , which can be estimated by replacing each unknown quantity with its estimate from the regression; denote this estimate by  $S\hat{D}(\bar{\tilde{Y}})$ .
- (ii.)  $S_{\tilde{Y}}^2$  is an approximately unbiased estimate of  $\sigma^2 + \frac{1}{b^2} SD^2(e_y)$
- (iii.) Goal A should be deemed to be satisfied if  $\bar{\tilde{Y}} > C_1 = Q_1 - z_{1-\alpha} S\hat{D}(\bar{\tilde{Y}})$

(iv.) Goal B should be deemed to be satisfied if

$$S_{\tilde{Y}} < C_2 = \sqrt{Q_2^2 + \frac{SD^2(e_Y)}{b^2}} \sqrt{2z_{1-\alpha} \frac{SD(\hat{b})}{b} + 1}$$

(v.) To control risks at stated levels for Goal A,  $M$  should be selected so as to be at least as large as the solution to:  $SD(\tilde{Y}) = \frac{\Delta_1}{z_{1-\alpha} + z_{1-\beta}}$ . ( $M$  enters this equation through the standard deviations and covariance of regression coefficients in the left side of the equation.)

(vi.) To control risks at stated levels for Goal B,  $M$  should be selected so as to be at

least as large as the solution to:

$$\frac{2z_{1-\alpha} \frac{SD(e_Y)}{\sqrt{Mb}} + Q_2}{\frac{SD^2(e_Y)}{b^2} + Q_2^2(1 + \Delta_2)^2} = \frac{2z_{\beta} \frac{SD(e_Y)}{\sqrt{Mb}} + Q_2}{\frac{SD^2(e_Y)}{b^2} + Q_2^2}$$

Note that  $M$  (the size of the calibration experiment), rather than  $N$ , must be selected to control risk in this case. For practical purposes, IC-MV data results in  $N$  that is effectively infinite; essentially all the uncertainty comes from the much more limited sample size available for calibration. Also, the quantities in (6) are derived under the assumption that the variability of  $Z$  encountered in the calibration experiment is typical of that seen across the site  $R$ .

### Local QC

IC-MV data is potentially more useful for local QC than point measurements because they effectively represent the entire spatial extent of  $R$  (even with “noise” at each location). IC data obtained during production can be used for local QC, but this requires consideration of both the uncertainty in calibration curve coefficients and the uncertainty involved in obtaining IC-MVs. That is, in screening individual locations, the very large sample associated with continuous monitoring cannot necessarily be depended upon to eliminate physical spatial variability because spatially individual values of  $\tilde{Y}(t)$  are being evaluated.

For a particular location  $t$ , the data value acquired via continuous monitoring can be used as the basis of a statistical *prediction interval* for  $Z$  at that location. Prediction intervals are often similar in form to confidence intervals, but are constructed so as to include a single value of an unobservable variable, rather than a statistical model parameter such as a mean or standard deviation.

In most cases, the primary concern of QC would likely be in detecting locations at which compaction has not resulted in a large enough  $Z$  value. It might be reasonable to use only a one-sided prediction bound, the upper bound for  $Z$  constructed using the lower prediction band of the regression, if firm evidence is required that a location needs more work, or the lower bound for  $Z$

constructed using the upper prediction band of the regression, if firm evidence is required that a location has been sufficiently compacted.

### **6.3 Summary**

Integrating IC-MVs into QC/QA operations will benefit from standard protocols for verification procedures and quantifying measurement errors. Verification builds confidence in the IC-MVs; and specifications that link IC-MV's to traditional point measurements should be done with knowledge of measurement errors. Procedures were discussed on both of these accounts. Three possible options for use of IC-MVs with no on-site calibration are proposed. The premise of these options is to better assist the roller operator to target areas that need more compaction or re-work and the field engineer to target areas for QA testing. A statistically rigorous concept was presented which has a potential in the future to create a new way of defining quality of compacted fill materials. A next step to fully develop these ideas will be to create contract specifications and pilot projects. Four options were presented for consideration. Figure 6.4 illustrates an idea that would combine multiple options to target more stringent compaction criteria (including uniformity) perhaps in the upper part of the embankment where it is more critical. In the long term, it is the author's view, however, that option 4 is the approach that holds the most promise for specification development because it will be more easily linked to performance of the compacted materials than the other approaches. From a practice standpoint though, option 4 will take the most effort and training to implement.

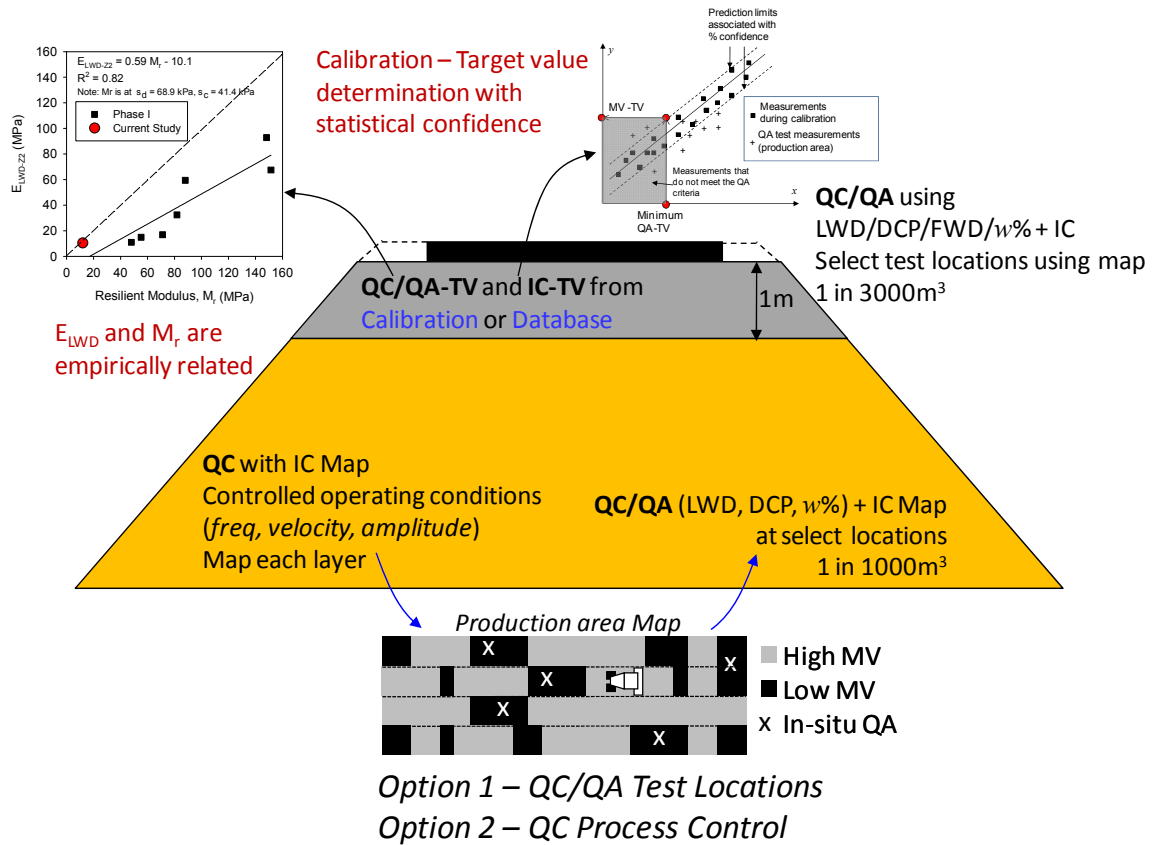


Figure 6.4. Illustration of combined specification options: lower portion IC-MVs used primarily for QC; upper 1 m with more stringent calibrations and use of IC-MVs for QC and QA



## **Chapter 7**

### **Summary and Conclusions**

#### **7.1 Summary**

This report documents the field measurements from IC field project sites, summarizes results comparing test rolling rut measurements to various IC and in-situ point measurements, provides a detailed summary of LWD measurements and an approach to determine target values, includes recommendations for IC specification and verification procedures, and finally provides summary/conclusions and further recommendations for implementation of IC and LWD technologies. Some of the key findings and conclusions from each of the topic areas are summarized in the following.

#### **7.2 Key Findings from Field Projects**

Results and observations from the field studies indicate that IC technology has significant potential to improve construction process control and resulting quality of compacted granular and non-granular materials. Detailed test results and project level findings and conclusions are provided in Chapter 3. Key findings from the field studies and their significance with respect to specifications and implementation of IC on earthwork projects with granular and non-granular materials are provided below. Results obtained from TH36 and US10 field projects are considered for granular soils and results obtained from TH60 and Olmsted County field projects are considered for non-granular soils.

##### **7.2.1 Granular Soils**

- Results indicated positive correlations between IC-MVs and modulus based in-situ test measurements (i.e.,  $E_{LWD}$ ,  $E_{FWD}$ , etc.)/strength (i.e., DPI). Correlations between dry unit weight and IC-MVs (US10 project) showed poor correlations.
- Modulus measurements obtained on granular subgrade materials (i.e., fine sand as encountered in US10 project) correlated well with IC-MVs when tests are performed in a carefully excavated trench of about 100 to 150 mm depth. Similarly, compaction layer DPI measurements obtained on granular subgrade materials correlated well with IC-MVs when the first DCP drop is regarded as a seating drop. For granular base materials (i.e., aggregate base material as encountered in TH36 project), modulus/strength based in-situ measurements obtained at the surface correlated well with the IC-MVs. These are important practical aspects of in-situ LWD and DCP testing to note when correlating with IC-MVs.
- CMV is correlated with a linear regression relationship with modulus values, while it is correlated with a non-linear power relationship with LWD deflection values. This is of

consequence as Mn/DOT is currently considering implementing  $d_{LWD}$  as part LWD QC/QA specification instead of  $E_{LWD}$  values. It must be noted that the current 90% to 120% of target values criteria needs to be reviewed for implementing  $d_{LWD}$  values due to the potential non-linear nature in the relationship with CMV.

- The primary factors contributing to low  $R^2$  values and scatter observed in the regression relationships is believed to be due to (a) differences in measurement influence depths, (b) stress state during loading and applied stresses, and (c) roller jumping (only for data obtained at high amplitude settings).
- Results from TH36 project demonstrated significantly different stress paths for loading under roller, FWD, and LWD loading which is a likely contributor to scatter in relationships between IC-MVs and  $E_{LWD}$  measurements.
- Using criteria for characterizing measurement influence depth as the depth at 10% of the maximum stresses at the surface, the measurement influence depths under the roller = 0.9 m (TH36 project) and 1.5 to 1.6 m (US10 project), 300-mm FWD plate = 0.6 m (TH36 project), and 200-mm LWD = 0.3 m (TH36 project) are determined. No significant difference was observed in the influence depth with change in amplitude under roller or increasing dynamic load under the FWD plate. The measurement influence depths under roller varied between TH36 and US10 projects due to variation in soil stiffness and layering conditions.
- Roller jumping (as measured by high RMV measurements) affected the CMV values and consequently the correlations. Influence of RMV in CMV-point measurement correlations can be accounted for through multiple regression analysis. However, for practical purposes, it is recommended to perform calibration testing in low amplitude setting (about less than 1 mm) to avoid complex interpretation and analysis of results.
- Field observations and discussion with contractor indicated that scraper traffic contributes to compaction of fill materials. EPC measurements from the US10 project indicated that stresses under scraper tire can be higher (2.2 to 2.6 times greater) than stresses observed under roller vibratory loading. Results presented by White et al. (2008) from TH64 granular subgrade project showed high CMV values in areas with construction traffic.
- CMV data obtained from repeated passes indicated that the measurements are repeatable (CMV measurement error < 3), but are not reproducible with change amplitude. The measurements obtained at different amplitudes must be treated separately. Effect of speed on CMV was not evaluated as part of this study. However, a study conducted by White et al. (2009) indicated that CMV is reproducible with variation in nominal speeds between 3.2 and 4.8 km/h.

### 7.2.2 Non-Granular Soils

- Results and observations from TH60 project showed instances where IC-TV (MDP\* = 138) established at the project being met and not the  $E_{LWD}$ -TV at many test locations.

- Relationships between MDP\* measurements with surface  $E_{LWD}$  and compaction layer DPI measurements showed positive correlations, however, with varying degree of uncertainty (i.e.,  $R^2$  values varied from about 0.3 to 0.8). Relationships between MDP\* and dry density generally showed relatively poor correlations. Soft or uncompacted zones at depths below about 0.25 m on some test strips did not affect the MDP\* measurements.
- Regression relationships showed improved  $R^2$  values in predicting MDP\* from  $E_{LWD}$  and DPI when moisture content is included in the regression analysis. This demonstrates the sensitivity of soil moisture content in interpreting MDP\* values.
- Separate trends were observed in MDP\*- $E_{LWD}$  correlations for MDP\* values  $< 140$  and  $> 140$ . This presents a challenge in implementing the QA requirement of production area meeting 90% to 120% of IC-TV as the limits are applicable only with one linear trend in the data with increasing compaction.
- Results from some test strips indicated that wrong throttle and gear settings used during roller operations produce invalid IC-MVs. The roller manufacturer recommendation is that the roller should be operated at a high throttle and low gear setting during compaction operations.
- MDP\* results obtained from repeated passes indicated that MDP\* values are repeatable with measurement error in the range of 2 to 4 when operated at a nominal speed of 3.2 km/h. The results showed relatively high measurement error in the range of 10 to 15 when operated at 6.4 km/h nominal speed.
- MDP\* results from TH60 project indicated that the values are reproducible with change in amplitude (from  $a = 0.85$  to 1.87 mm) (note that the material was mostly at wet of optimum moisture content). In contrast, the results from Olmsted County project indicated that the values are not reproducible with change in amplitude (from  $a =$  static to 1.80 mm). A study conducted by White et al. (2009) also indicated that MDP values are influenced by change in amplitude.
- MDP\* results from Olmsted County indicated that the values are affected by driving grade slope and therefore are not reproducible with change in direction of travel.
- CMV-  $E_{LWD-Z2}$  and CMV-  $d_{LWD-Z2}$  relationships derived from two test strips on the TH60 project showed good correlations but with separate trends. Statistically significant correlations were not found with DPI and dry density.
- Roller jumping (as measured by high RMV measurements) occurred at locations with very stiff conditions which affected the CMV values. It is recommended that the CMV measurement values be evaluated in conjunction with RMV values.

### 7.3 Guidance for Test Roller Specification Modification

Use of IC-MVs (CMV and MDP) and DCP/LWD point measurements to evaluate the bearing capacities of non-granular and granular subgrade layers in-situ were studied at field sites. Comparisons were made to test roller rut depth QA criteria specified by Mn/DOT for the upper subgrade layer of a pavement foundation. Correlations developed between CMV and MDP and point measurements show positive trends but with varying degrees of uncertainty in relationships. Scatter in the relationships is partly attributed to differences in measurements influence depth.

At one project site involving compaction of non-granular soils, DCP- $s_u$  profiles showed significant vertical non-uniformity. Test rolling identified soft layers at and below the surface (rut depths  $\geq 50$  mm). Based on this finding, a chart solution using layered bearing capacity analysis was developed and linked to target shear strength values to predict test rolling rut failures. It was concluded that the IC-MVs and point measurements can serve as a reliable indicator of compaction quality of non-granular and granular subgrades and as an alternative to test rolling. It is recommended however, that development of a correlation database continue with future projects to improve confidence.

### 7.4 LWD Evaluation and Target Value Determination

#### 7.4.1 Experimental Comparison of LWD Devices and Influencing Factors

Several issues need to be considered when interpreting an  $E_{LWD}$  value to successfully implement the use of the LWD devices in earthwork QA/QC testing. The following are some of the key aspects:

- $E_{LWD}$  values are influenced by size of the loading plate, plate contact stress, type and location of deflection transducer, plate rigidity, loading rate, buffer stiffness, and to some extent the measurement of load versus assumption of a constant load based on laboratory calibration.
- LWD devices that determine deflection of the plate (e.g. Zorn) are expected to measure larger deflections compared to devices that measure deflections on the ground with a geophone (e.g. Keros/Dynatest and Prima).
- The Keros  $E_{LWD}$  is on average 1.75 and 2.16 times greater than Zorn  $E_{LWD}$  with 200-mm and 300-mm plate diameters, respectively. The Dynatest  $E_{LWD}$  is on average 1.7 times greater than Zorn  $E_{LWD}$  with 200-mm plate diameter. The constant applied force of 6.69 kN in the 200-mm Zorn device is comparable with average loads by 200-mm Keros device (6.56 kN) for a drop height of 63 mm. The primary contributor to differences in calculated  $E_{LWD}$  is the difference in deflections (on average, Zorn deflections are about 1.5 times greater than Keros).

- The COV of Zorn  $E_{LWD}$  is observed to be generally lower compared to Keros or Dynatest  $E_{LWD}$  values. Some field studies showed considerable differences in the COV. To achieve good reliability and confidence in the test measurements, it is important to plan and calculate the number of tests depending on the variability of the measurements.
- Due to variations in buffer stiffnesses, differences in applied contact stresses should be expected between Keros and Dynatest 3031 devices set up with similar drop heights. Despite the differences in applied stresses, the  $E_{LWD-D2(50)}$  and  $E_{LWD-K2(50)}$  showed comparable results with a slope of linear regression equation close to 1 and  $R^2$  value of 0.94.
- In general, the  $E_{LWD}$  values increase with decreasing plate diameters, which is consistent with observations by other researchers (e.g., Chaddock and Brown 1995; Lin et al. 2006). The ratio of  $E_{LWD}$  from 150-mm and 100-mm plates to  $E_{LWD}$  from 300-mm plate showed some considerable differences with difference in material stiffness; i.e., the ratio generally tends to increase with increase in material stiffness.
- For the granular materials tested, the Zorn  $E_{LWD}$  increases with increasing plate contact stresses with stiffer material presenting a greater increase in  $E_{LWD}$ . The Keros and Dynatest devices showed an opposite trend. However, the effect of applied stress on Keros and Dynatest  $E_{LWD}$  appear to have less influence (by about 10%) for increase in contact stresses above 100 kPa.
- Variations observed in  $E_{LWD-D}$  and  $E_{LWD-K}$  by modifying the buffer stiffnesses are insignificant when the results are compared at similar applied contact stresses

#### 7.4.2 Variability of $E_{LWD}$ Measurements and Measurement Error

Key findings from the test results to quantify LWD test variability are as follows:

- An advantage of LWD testing is that many tests can be performed in a short period of time – perhaps as many as 10 or more compared to conventional sand cone density tests in the same time period. Simple and rapid field tests allow for better utilization of field personnel, and also have the advantage of better characterizing soil variability.
- Some field studies showed considerable differences in the COV between  $E_{LWD-Z2}$  and  $E_{LWD-D2}$  measurements. From analyzing the variability of LWD measurement values, increasing the number of test measurements improves the statistical confidence in the limits. A laboratory study was performed on the LWD devices to specifically evaluate the test variability of the measurements.
- For the five Zorn LWD devices evaluated in this study,  $\sigma_{\text{repeatability}}$  in the  $d_{LWD-Z2}$  and  $E_{LWD-Z2}$  measurements increased with increasing measurement value, e.g.,  $\sigma_{\text{repeatability}}$  range for  $d_0$  for soft pad = 0.06 to 0.08 mm whereas for stiff pad  $\sigma_{\text{repeatability}}$  is around 0.01 mm. The COV values show that  $d_0$  and  $E_{LWD-Z2}$  values for both stiff and soft pads are in the range of 2 to 3%. The contribution of variation attributed due to change in device on

the  $d_0$  measurement values has low significance as the  $\sigma_{\text{reproducibility}}$  is less than  $\sigma_{\text{repeatability}}$  values (or in other words percent contribution less than 50%).

- For the three Dynatest LWD devices evaluated in this study,  $\sigma_{\text{repeatability}}$  in  $E_{\text{LWD-D2}}$  measurements increased with increasing measurement value, whereas no statistically significant trend was observed for  $d_0$  measurements. The COV values summarized in that  $d_{\text{LWD-D2}}$  and  $E_{\text{LWD-D2}}$  values for soft pads are in the range of 2 to 4%, while for stiff pads they are in the range of 18 to 72%. The contribution of variation attributed due to change in device on the measurement values is significant for  $d_0$  and  $\sigma_0$  measurements due to higher  $\sigma_{\text{reproducibility}}$  than  $\sigma_{\text{repeatability}}$  values.

### 7.4.3 Guidance for a Standard Test Protocol

Following are some of the key points for LWD verification tests:

- Quantify repeatability of LWD measurements prior to use on a project site. This is performed using the following procedure: Select at least three test materials – low, medium, and stiff within the limits of measurement of the device. Perform three seating drops followed by nine consecutive measurement drops and record deflection, applied stress, and  $E_{\text{LWD}}$  measurements. The COV in the measurements at each test location should be less than a specified value (a detailed laboratory investigation is warranted to develop specifications on acceptable COV for the measurements).
- Quantify reproducibility of LWD measurements. This should be done in a context of change in operator and device, especially if multiple operators and devices are utilized for a project. The procedure to quantify reproducibility is as follows and can be combined with the repeatability measurements: Select at least three materials with varying stiffness for LWD testing following the procedure described under step 1. Tests should be performed by each operator on at least one device for the three materials, and by one operator on all the devices for the three materials. Perform three seating drops followed by nine consecutive measurement drops and record deflection, applied stress, and  $E_{\text{LWD}}$  measurements. Compute repeatability and reproducibility variations. The reproducibility standard deviation should be similar or less than the repeatability standard deviation.

Following are some of the key points during in-situ LWD testing:

1. The test surface should be level and smooth. Levelness can be checked with a bubble level. The LWD plate should not translate laterally with successive drops.
2. Tests on cohesionless materials (e.g., USCS: SW, SP, SM), should be performed in a test pit by excavating surficial loose material. Based on experience, the excavation depth may vary between 100 to 150 mm. As a rule-of-thumb, the diameter of the test pit should be approximately 2 times the plate diameter (i.e. 400 mm for 200 mm plate).

3. Tests on non-granular materials (e.g., CL, CH) compacted with padfoot rollers should be at or lower than the bottom of the padfoot penetration. (Preparation of a quality test surface often requires more time than performing the LWD test.)
4. Tests on granular base/stabilization layer materials should be at the surface of the compaction layer and may require a thin layer of leveling sand to ensure uniform contact of plate with the testing surface. Excess sand can cause seating problems, especially with geophones and should be minimized.
5. Perform three seating drops before collecting data for consistent measurements. If noticeable deflection or bearing capacity failure occurs, the material needs further compaction or is too wet. For stiff materials, one or two seating drops may be sufficient and can be determined by collecting data and demonstrating that successive seating drops do not increase the  $E_{LWD}$  by more than about 5%.
6. Following the seating drops, perform three measurement drops of the falling weight for a given drop height recording data for each drop. If  $d_{LWD}$  values successively decrease with each drop exceeding 10% of the previous measurement, additional compaction is likely needed (this criteria will be helpful to the field engineer to quickly identify problem areas).
7. Record  $d_{LWD}$  from the last three measurement drops and compute the average.
8. If desired, record  $E_{LWD}$  by using appropriate shape factor,  $F$  in the calculation ( $F = \pi/2$  for non-granular materials,  $F = 8/3$  for granular materials, and  $F = 2$  for intermediate materials). A Poisson's ratio value of 0.4 is suggested.
9. Report the following from each test location:
  - a. Material/Layer
  - b. Test location identification (e.g., station, offset, etc.)
  - c. Excavation depth if tested on granular materials
  - d. Air temperature
  - e.  $d_{LWD}$  measurements from three measurement drops
  - f. Applied stress measurements (if provided in the output)
  - g. Assumptions used in  $E_{LWD}$  calculation, if  $E_{LWD}$  values are reported (i.e., Poisson's ratio and shape factor used)

#### 7.4.4 Comparison between $E_{LWD}$ and CIV Measurements

Results from comparison testing between the Clegg Impact Hammer and the LWD are as follows:

- Advantages of CIV over LWD testing would be that the Clegg device is relatively simply to operate, the cost is lower than the LWD, the results generally correlate to CBR and  $E_{LWD}$ , and the ASTM standard provides guidance on selecting target values. Further, the maximum measurable CIV is about 100 (or 1000g), which is representative of a soil with an elastic modulus of about 2000 MPa for the 20-kg Clegg hammer. On the other hand, the maximum measurable  $E_{LWD-Z}$  is about 120 MPa for 200 mm diameter plate (with drop height of 50 cm). To be brief, for materials with high stiffness (e.g. stabilized materials) the Clegg device would still be within the measurement range.
- Some disadvantages would be that the maximum particle size of the material tested will be limited by the smaller plate diameter of the Clegg device, and multiple devices of different drop weight may be needed to test the range of strengths and stiffnesses in the field, especially for soft materials, whereas the drop height can be adjusted for the LWD. In addition, more detailed and statistically reliable empirical correlations between CIV and mechanistic parameter values are warranted for a range of soil types as further evaluation. The LWD provides a mechanistic measurement values whereas the CIV is an index.

#### 7.4.5 Laboratory Target Value Determination Study

- Results demonstrating the application of gyratory compacted samples to develop relationships between moisture content, density,  $E_{LWD}$ , DCP index, and PDA  $\tau_G$  for non-granular and granular soils are presented. These relationships are presented in terms contour graphs overlaid on laboratory Proctor moisture-density relationships of the soils. The advantage of presenting results in that manner is that target values can tied to both target moisture and density values.
- $E_{LWD}$ , DCP index, and PDA  $\tau_G$  were found to be sensitive to moisture content for non-granular soils. Moisture content was relatively less significant for granular soils.
- New relationships were developed between the PDA  $\tau_G$  values and other soil engineering parameters (e.g.,  $E_{LWD}$ ,  $M_r$ ,  $s_u$ ). Those relationships showed good correlations coefficients ( $R^2$  values generally  $> 0.7$ ). A significant advantage with using PDA device is that it is less time consuming than other test methods (i.e.,  $E_{LWD}$ , UU, UC, or  $M_r$  tests).
- Rigid boundary condition for LWD/DCP testing in gyratory mold is an issue with granular materials that are more sensitive to confinement compared to non-granular materials. Two different polyurethane molds with different stiffnesses (“stiff” and “soft”) used in this study did not provide adequate confinement for the granular materials and did not show any noticeable difference with unconfined condition.

- The laboratory-determined  $E_{LWD}$  target values (based on rigid boundary testing) for one TH60 non-granular soil were compared to Mn/DOT target values (Siekmeier et al. 2009) and in-situ  $E_{LWD}$  test results. This comparison revealed that the laboratory-determined target values are mostly within the range of Mn/DOT proposed target values. Some of the in-situ  $E_{LWD}$  measurements were lower than the minimum Mn/DOT and laboratory-determined target values for  $w = 70\%$  to  $79\%$   $w_{opt}$  range. For  $w > 80\%$  of  $w_{opt}$ , the lower limit of in-situ  $E_{LWD}$  measurements were generally greater than the minimum target values obtained from both Mn/DOT and laboratory-determined methods.
- The approach presented to develop target values using gyratory testing and trends presented in the relationships show promise. However, additional research with developments to the laboratory approach in terms of better simulating the actual field boundary conditions and for a wide range of soil types is warranted.

## 7.5 IC Verification and Specification Options

Integrating IC-MVs into QC and QA operations will benefit from standard protocols for verification procedures and quantifying measurement errors. Verification builds confidence in the IC-MVs; and specifications that link IC-MV's to traditional point measurements should be done with knowledge of measurement errors in both the traditional and new performance based measurement. Procedures suggested for verification of IC-MVs and quantifying measurement error are briefly discussed below.

Three possible options for use of IC-MVs with no on-site calibration are proposed. The premise of these options is to better assist the roller operator to target areas that need more compaction or re-work and the field engineer to target areas for QA testing. A statistically rigorous concept was presented which has a potential in the future to create a new way of defining quality of compacted fill materials. These options are briefly discussed below.

### 7.5.1 Verification

Three ideas were briefly discussed that would contribute to verification of IC-MVs and quantification of measurement error associated with specific technologies. A brief summary of these procedures are as follows:

1. A statistical approach for evaluating the measurement error associated with the roller IC-MVs in terms of the repeatability and reproducibility for a given set of field conditions and roller operations. The calculated errors have the same units at the IC-MVs and are dependent upon the roller operating conditions and “white noise” in the measurement system. Generally, a 100 m long test section representative of the production area is suitable for testing. As discussed later, the IC roller measurement error is an input parameter that is required as part of statistically valid QA/QC assessment.

2. A plan for construction of dedicated and controlled test beds at MnROAD facility is proposed as one alternative to verify IC-MVs. Figure 6.1 is an example of a test bed that could be used to obtain detailed correlations between different IC-MVs and mechanistic-based pavement design parameters (e.g.,  $E_{FWD}$ ,  $E_{LWD}$ , etc). The test beds would consist of different non-granular and granular material types that are commonly used in pavement foundation layers underlain by variable support conditions to capture a wide measurement range. In addition to developing a database of correlations, the test beds could also be used to accept IC roller at the beginning of a project and for periodic verification. Correlations to mechanistic-based parameters would give confidence in specifying roller MVs for use with performance based specifications and for using roller MVs for QA. This option would require an investment in the facility and personnel to regularly monitor the test bed values and performance maintenance as needed.
3. An alternative to the dedicated test beds might be to develop a highly mobile mechanical system that could simulate the range of soil conditions expected to be encountered on a project. The device could be transported to a project periodically to verify the output. Development of the components of such a system is beyond the scope of this research.

### 7.5.2 Specifications

Some key features of options 1 to 3 that do not require on-site calibration and option 4 with a statistical framework for a more robust QC/QA specification are as follows:

- Option 1 – The final pass roller MV map of a production area is used to identify “weak” areas. The weak areas are targeted for in-situ QA testing. Acceptance of the production area is based on in-situ QA test measurements in the “weak” areas.
- Option 2 – This option requires evaluating the change in roller MV between successive passes over a production area. Production compaction should be performed until 90% of the production area achieves a percent change in MV of  $\leq 5\%$ . These percentages may be adjusted based on field conditions and experience.
- Option 3 – IC and QA target values for this option are pre-selected, which can be derived from a database of correlations from current study/literature, information from local projects, and calibration tests on test beds of known engineering properties. The contractor would use the pre-selected roller MV target values for QC, and QA is evaluated using a combination of roller data and in-situ QA test measurements.
- Option 4 – This specification approach is based on two goals: (1) that the overall level of critical soil engineering properties, over the entire site, achieve at least some specified minimal value (IC-TV), and (2) that the variability of critical soil engineering properties, over the entire site, is no more than some specified maximal amount (e.g., %COV). These statements are quantified by determining the nature of uncertainty inherent in the measurement systems and then writing rules for defining degree of acceptable risk, (i.e., risk that a site which actually does not meet the goal is erroneously declared as meeting the goal based on the data.) The approach requires calibration of IC-MVs and point measurements. Site wide QA is then based on achievement of the defined critical soil

engineering property based on the IC results. The advantage of this approach is that it allows for the assignment of acceptable risk and creates a framework for incentive-based pay. Although more rigorous mathematically, this option could provide a new way of characterizing compacted soils. This approach should be considered a concept and will require detailed pilot testing from multiple projects and conditions, but has the advantage of creating a consistent metric between different technologies and for defining quality.

A concept is presented combining these options to target more stringent compaction criteria (including uniformity) perhaps in the upper part of the embankment where it is more critical. In the long term, it is the author's view, however, that option 4 is the approach that holds the most promise for specification development because it will be more easily linked to performance of the compacted fill materials than the other approaches. From a practice standpoint though, option 4 will take the most effort and training to implement.

## **Chapter 8**

### **Recommendations for Implementation**

The results of this research study provided further evidence that IC technology has the potential to significantly improve construction process control and the resulting quality of granular and non-granular compacted fill materials. To further make advancements and add value to the process there are three recommendations suggested as outcomes of this study with respect to:

1. Specifications
2. Training
3. Data Analysis/Archiving

#### **8.1 Recommendations for Specification Development**

The statistically-framed specification option for calibration and statistical analysis of risk is viewed as the building block of a future more robust and complete specification that is independent of IC machine and point measurement technologies. The advantage of this approach is that it allows for the assignment of acceptable risk, provides a link to performance-based measurements, and creates a framework for incentive-based pay. Although the basic framework has been established, some of the operational aspects of this specification will need to be developed. A next step to fully develop these ideas will be to create contract specifications and pilot projects. It is recommended that a specification task force take on the role to more fully developing the operational aspects of the specification.

#### **8.2 Development of Training/Certification Program**

The response from field inspectors and roller operators is generally that the IC technology brings value to projects and that it will improve construction efficiency and quality. Much has been gained over the last few years in terms of experience and knowledge from the field/pilot projects. This knowledge should be captured in the form of a formal training program for field inspectors and roller operators. A field inspector's guide should be developed for quick reference on roller operations, in-situ testing, data reporting, data analysis, and corrective actions.

#### **8.3 Data Analysis/Report/Archiving**

Finally, challenges still exist with making use of the field data during the construction process and archiving the data for future analysis and use during pavement design and performance evaluation. A critical next step in the implementation process is to develop tools that make it easier to provide real-time data analysis in terms of the specification criteria. This will benefit both the contractor and the field inspectors. It is recommended that the data analysis aspect be tied to the IC specification options and done external to the IC manufacturers' software.

## References

- AASHTO. (1999). *Standard method of test for determining the resilient modulus of soils and aggregate materials T-307*, American Association of State Highway and Transportation Officials, Washington, D.C.
- ASTM. (1983). "Test method for compaction and shear properties of bituminous mixtures by means of the U.S. Corps of Engineers gyratory testing machine." *Annual book of ASTM Standards, ASTM D3387*, West Conshohocken, PA.
- ASTM. (2000). "Test method for laboratory compaction characteristics of soils using standard effort." *Annual book of ASTM Standards, ASTM D698*, West Conshohocken, PA.
- ASTM. (2000). "Test method for laboratory compaction characteristics of soils using modified effort." *Annual book of ASTM Standards, ASTM D1557*, West Conshohocken, PA.
- ASTM. (2000). "Standard classification of soils for engineering purposes (Unified Soil Classification System)." *Annual book of ASTM Standards, ASTM D2487*, West Conshohocken, PA.
- ASTM. (2002). "Test method for determination of the impact value (IV) of a soil." *Annual Book of ASTM Standards, ASTM D5874*, West Conshohocken, PA.
- ASTM. (2003). "Test method for use of the dynamic cone penetrometer in shallow pavement applications." *Annual Book of ASTM Standards, ASTM D6951*, West Conshohocken, PA.
- ASTM. (2005). "Test method for density of soil and soil aggregate in place by nuclear methods (shallow depth)." *Annual Book of ASTM Standards, ASTM D2922*, West Conshohocken, PA.
- ASTM. (2005). "Test methods for liquid limit, plastic limit, and plasticity index of soils." *Annual Book of ASTM Standards, ASTM D4318*, West Conshohocken, PA.
- ASTM. (2006). "Test method for unconfined compressive strength of cohesive soil." *Annual Book of ASTM Standards, ASTM D2166*, West Conshohocken, PA.
- Adam, D. (1997). "Continuous compaction control (CCC) with vibratory rollers." *Proc., 1st Australia-New Zealand Conf. on Environmental Geotechnics – GeoEnvironment 97*, Melbourne, 26-28 November, Australia.
- Adam, D., and Kopf, F. (2004). "Operational devices for compaction optimization and quality control (Continuous Compaction Control & Light Falling Weight Device)." *Proc., of the Intl. Seminar on Geotechnics in Pavement and Railway Design and Construction*, December, Athens, Greece, 97-106.

- Bekker, M.G. (1960). *Off the Road Locomotion*, University of Michigan Press, Ann Arbor, MI.
- Beyer, M., Camargo, F., Davich, P. (2006). *Light weight deflectometer (LWD) user's guide*. Draft Report, Minnesota Department of Transportation, St. Paul, MN.
- Brandl, H., and Adam, D. (2004). "Continuous compaction control (CCC) for fill dams and roller compacted concrete dams." *New Developments in Dam Engineering – Proc., 4th Intl. Conf. on Dam Engineering*, October, Nanjing, China.
- Browne, M. J. (2006). *Feasibility of using a gyratory compactor to determine compaction characteristics*, MS Thesis, Montana State University, Bozeman, MT.
- Chai, G., and Roslie, N. (1998). "The structural response and behavior prediction of subgrade soils using falling weight deflectometer in pavement construction." *Proc., 3rd Intl. Conf. on Road and Airfield Pavement Technology*, Beijing, China.
- Chen, D.H., Lin, D.F., Liau, P.H., and Bilyeu, J. (2005). "A correlation between dynamic cone penetrometer values and pavement layer moduli," *Geotech. Test. J.*, 28(1), 42-49.
- Clark, I., and Harper, W. (2002). *Practical geostatistics 2000*, 3rd reprint, Ecosse North America Llc, Columbus, OH.
- Coyle, H. M., and West, E. C. (1956). *Laboratory compaction of a silty clay to simulate field density curves*, MS Thesis, Massachusetts Institute of Technology, MA.
- Davich, P., Camargo, F., Larsen, B., Roberson, R., and Siekmeier, J. (2006). *Validation of DCP and LWD moisture specifications for granular materials*, Final Report MN/RC-2006-20, Minnesota Department of Transportation, St. Paul, MN.
- Duncan, J.M., and Seed, R.B. (1986). Compaction-induced earth pressures under  $K_0$ -conditions, *J. of Geotech. Eng.*, ASCE, 112(1), 1-22.
- Dynatest. (2004). *Keros portable FWD – Instruction manual for use and maintenance*, Issue No. 010704, Denmark.
- Floss, R., Bräu, G., Gahbauer, M., Gruber, N., and Obermayer, J. (1991). "Dynamische Verdichtungsprüfung bei Erd- und Straßenbauten." *Prüfamt für Grundbau, Boden- und Felsmechanik Technische Universität München*, Heft 612, München, Germany (in German).
- Florida DOT. (2003). *Test report – FHWA GeoGauge study SPR-2(212) Validation of depth of influence*, Florida Department of Transportation, Gainesville, FL.

- Fleming, P. R., Frost, M.W., and Rogers, C. (2000). "A comparison of devices for measuring stiffness in-situ." *Proc., Unbound Aggregates in Road Construction – UNBAR 5*, Dawson, A. R., ed., Balkema, Rotterdam, 193-200.
- Fleming, P. R., Lambert J. P., Frost M. W., and Rogers, C. (2002). "In-situ assessment of stiffness modulus for highway foundations during construction." *Proc., 9th Intl. Conf. on Asphalt Pavements*, Copenhagen, Denmark.
- Geodynamik ALFA-030. *Compactometer, compaction meter for vibratory rollers*, Internal Report, Geodynamik, Stockholm, Sweden.
- Guler, M, Bahia, H.U., Bosscher, P.J., and Plesha, M.E. (1996). "Device for measuring shear resistance of hot-mix asphalt in gyratory compaction," *Transportation Research Record: Journal of the Transportation Research Board*, No. 1723, 119-124.
- Gupta, S., Ranaivoson, A., Edil, T., Benson, C., and Sawangsuriya, A. (2007). *Pavement Design Using Unsaturated Soil Technology*. Final Report MN/RC-2007-11 Minnesota Department of Transportation, St. Paul, Minnesota, May.
- Gupta, S., Kang, D.H., Ranaivoson, A. (2009). *Hydraulic, Mechanical, and Leaching Characteristics of Recycled Materials*. Draft Report submitted Minnesota Department of Transportation, St. Paul, MN.
- Hambleton, J.P., and Drescher, A. (2008). *Development of improved test rolling methods for roadway embankment construction*, Final Report MN/RC 2008-08. Minnesota Department of Transportation, St. Paul, MN.
- Hildebrand, G. (2003). "Comparison of various types of bearing capacity equipment." *Nordic Road and Transportation Research*, 15(3), Danish Road Directorate, 12-14.
- Hilf, J.W. (1991). "Chapter 8: Compacted fill." *Foundation engineering handbook by H. Fang*, Van Nostrand Reinhold, New York.
- Humboldt Mfg. Co. (2000). *Geogauge (soil stiffness/modulus) user guide*. Ver. 3.8.
- ISSMGE. (2005). *Geotechnics for pavements in transportation infrastructure, roller-integrated continuous compaction control (CCC)*, Technical Contractual Provisions – Recommendations, International Society for Soil Mechanics and Geotechnical Engineering.
- Kudla, W., Floss, R., and Trautmann, C. (1991). "Dynamic test with plate – Quick method of quality assurance of road layers without binder (Dynamischer plattendruckversuch – Schnellprüfverfahren für die qualitätssicherung von ungebundenen schichten)." *Streets and Highways (Strasse and Autobahn)*, Vol. 2, Bonn, 66-71 (in German).

- Kim, W., and Labuz, J. (2006). *Resilient modulus and strength of base course with recycled bituminous material*, Final Report MN/RC 2007-05. Minnesota Department of Transportation, St. Paul, MN.
- Konrad, J., and Lachance, D. (2001). "Use of in-situ penetration tests in pavement evaluation." *Can. Geotech. J.*, 38 (5), 924–935.
- Lambe, T. W., and Whitman, R. V. (1969). *Soil mechanics*, John Wiley & Sons, New York.
- Larsen, B.W., White, D.J., and Jahren, C.T. (2008). "Pilot project to evaluate dynamic cone penetration QA/QC specification for non-granular soil embankment construction." *Transportation Research Record*, No. 2081, 92-100.
- McElvaney, J., and Djatnika, I. (1991). "Strength evaluation of lime-stabilized pavement foundations using the dynamic cone penetrometer." *Australian Road Research*, 21(1), 40-52.
- McRae, J. L. (1965). *Gyratory testing machine technical manual for bituminous mixtures, soils, and base course materials*, Engineering Developments Company, Inc., Vicksburg, MA.
- Meyerhof, G.G., and Hanna, A.M. (1978). "Ultimate bearing capacity of foundations on layered soil under inclined load." *Can. Geotech. J.*, 15(4), 565–572.
- Mn/DOT. (2005). *Standard specifications for construction – Specification 2111 test rolling*, Minnesota Department of Transportation (Mn/DOT), St. Paul, MN.
- Mn/DOT. (2008). *Developing improved test rolling methods for roadway embankment construction – Technical Summary*, Minnesota Department of Transportation, St. Paul, MN.
- NCHRP. (2004). *Harmonized test methods for laboratory determination of resilient modulus for flexible pavement design – NCHRP 1-28A*, National Cooperative Highway Research Program, Transportation Research Board, Washington, D.C.
- NCHRP. (2009). *Intelligent soil compaction systems – NCHRP 21-09*, National Cooperative Highway Research Program, Transportation Research Board, Washington, D.C. (in review).
- Newsletter 14. (1995), *Clegg hammer modulus (CHM)*. Dr Baden Clegg Pty Ltd, Western Australia, <[http://www.clegg.com.au/information\\_list3.asp](http://www.clegg.com.au/information_list3.asp)>, Date Accessed: March 2009.
- Oman, M. (2004). *Advancement of grading and base material testing*, Final Report, Minnesota Department of Transportation, St. Paul, MN.
- Petersen, D.L., Erickson, M.L., Roberson, R., and Siekmeier, J. (2007). "Intelligent soil compaction: Geostatistical data analysis and construction specifications," *Proc., 86th Annual Transportation Research Board Meeting*, Washington, D.C.

- Ping, W. V., Xing, G., Leonard, M., and Yang, Z. (2003). *Evaluation of laboratory compaction techniques for simulating field soil compaction – Phase II*, Report No. FL/DOT/RMC/BB – 890 (F), Florida State University, Tallahassee, FL.
- Robertson, P.K., and Campanella, R.G (1983), “Interpretation of cone penetration tests – Part I (sand).” *Can. Geotech. J.*, 20(4), 718-733.
- Sandstrom, A., and Pettersson, C. (2004). “Intelligent systems for QA/QC in soil compaction.” *Proc., 83rd Annual Transportation Research Board Meeting*, Washington, D.C.
- Schmertmann, J. H. (1970). “Static cone to compute static settlement over sand.” *J. Soil Mech. and Found. Div.*, ASCE, 96, No. SM3, 1011-1043.
- Siekmeier, J., Pinta, C., Merth, S., Jensen, J., Davich, P., Camargo, F., and Beyer, M. (2009). *Using the dynamic cone Penetrometer and light weight deflectometer for construction quality assurance*, Final Report MN/RC 2209-12, Minnesota Department of Transportation, St. Paul, MN.
- Srivastava, R. M. (1996). “Describing spatial variability using geostatistical analysis.” *Geostatistics for Environmental and Geotechnical Applications, ASTM STP 1283*, R. M. Srivastava, S. Rouhani, M. V. Cromer, A. J. Desbarats, A. I. Johnson, eds., ASTM, West Conshohocken, PA, 13–19.
- Terzaghi, K., and Peck, R. B. (1967). *Soil mechanics in engineering practice*, 2nd ed., John Wiley & Sons, Inc., New York.
- Turner, H., and Sandström, Å. (1980). “A new device for instant compaction control.” *Proc. Intl. Conf. on Comp.*, Vol II, 611 – 614, Paris.
- Thompson, M., and White, D.J., (2008). “Estimating compaction of non-granular soils from machine drive power.” *J. Geotech. and Geoenv. Engrg.*, ASCE, 134(12), 1771-1777.
- Thompson, M., White, D.J., Gieselman, H., and Siekmeier, J. (2007). “Variable feedback control intelligent compaction to evaluate subgrade and granular pavement layers – field study at Minnesota US14.” *Proc., 87th Annual Transportation Research Board Meeting*, January, Washington, D.C.
- Vardeman, S., and Jobe, M. (1999). *Statistical quality assurance methods for engineers*, John Wiley & Sons, Inc., New York, NY.
- Vertek. (2005). *ProDAT CPT data processing instruction manual*, Vertek Quality Products, Applied Research Associates, South Royalton, VT.

- Vennapusa, P., and White, D. J. (2009a). "Comparison of light weight deflectometer measurements for pavement foundation materials." *Geotechnical Testing Journal*, ASTM (to appear in Vol. 32, Issue 3, May).
- Vennapusa, P., and White, D. J. (2009b). "Geostatistical analysis of spatially referenced roller-integrated compaction measurements." *Journal of Geotechnical and Geoenvironmental Engineering*, ASCE (in review).
- Vennapusa, P., White D.J., and Gieselman, H. (2009). "Influence of support conditions on roller-integrated machine drive power measurements for granular base." *Intl. Foundation Congress & Equipment Expo '09 (IGCEE'09)*, March 15-19, Lake Buena Vista, FL.
- Weiler, W.A., and Kulhawy, F.H. (1982). "Factors affecting stress cell measurements in soil." *J. of Geotech. Engrg. Div.*, 108(12), 1529-1548.
- White, D. J, Jaselskis, E. J, Schaefer, V. R., and Cackler, E. T. (2005). "Real-time compaction monitoring in non-granular soils from machine response." *Transportation Research Record*, No. 1936, 173-180.
- White, D.J., Thompson, M. and Vennapusa, P. (2007a). *Field validation of intelligent compaction monitoring technology for unbound materials*. Final Report MN/RC-2007-10, Minnesota Department of Transportation, St. Paul, MN.
- White, D.J, Thompson, M., and Vennapusa, P. (2007b). *Field study of compaction monitoring systems: self-propelled non-vibratory 825G and vibratory smooth drum CS-533 E rollers*, Final Report, Center of Transportation Research and Education, Iowa State University, Ames, IA.
- White, D.J., Thompson, M.J., Vennapusa, P., and Siekmeier, J. (2008). "Implementing intelligent compaction specification on Minnesota TH 64: Synopsis of measurement values, data management, and geostatistical analysis." *Transportation Research Record*, No. 2045, 1-9.
- White, D.J., and Thompson, M. (2008). "Relationships between in-situ and roller-integrated compaction measurements for granular soils." *J. Geotech. and Geoenv. Engrg.*, ASCE, 134(12), 1763-1770.
- White, D.J., Vennapusa, P., and Gieselman, H. (2009). *Investigation of dual roller integrated MDP/CMV compaction monitoring technologies and measurement influence depth*, Center for Transportation Research and Education, Iowa State University, Ames, IA.
- Yoon, S., and Salgado, R. (2002). *Dynamic cone penetration test (DCPT) for subgrade assesment*, FHWA/IN/JTRP – 2002/30, Joint Transportation Research Program, Purdue University, West Lafayette, IN.

Zorn, G. (2000). *Operating manual: Light drop-weight tester ZFG2000*, Zorn Stendal, Germany.

**Appendix A: Repeatability and Reproducibility Analysis Procedure and  
Example Calculations for LWD and Roller Measurement Data**

## Repeatability and Reproducibility Analysis using Two-Way Analysis of Variance (ANOVA)

Consider a data set consisting of  $m$  repeated measurements at a test location at  $I$  different locations under each condition of operation  $J$ .

*For roller measurement values:*

- $m$ : number of passes on a test strip
- $I$ : number of data points across the test strip
- $J$ : change in operator, amplitude, speed, direction, etc.

*For LWD measurement values:*

- $m$ : number of measurements at a location
- $I$ : number of test locations
- $J$ : change in operator, device, material tested, etc.

The two-way random effects model and the three quantities of interest are provided below:

$$Y_{ijk} = \mu + \alpha_i + \gamma_j + \alpha\gamma_{ij} + \epsilon_{ijk}$$

$$\sigma_{\text{repeatability}} = \sigma$$

$$\sigma_{\text{reproducibility}} = \sqrt{\sigma_{\gamma}^2 + \sigma_{\alpha\gamma}^2}$$

$$\sigma_{\text{R&R}} = \sqrt{\sigma_{\text{reproducibility}}^2 + \sigma_{\text{repeatability}}^2}$$

Estimates of these from Two-Way ANOVA Results are shown below and the parameters of the equations are shown in an example table below with ANOVA results.

$$\sigma_{\text{repeatability}} = \sigma = \sqrt{MSE}$$

For LWD measurements,  $\sigma_{\text{repeatability}}$  is simply the standard deviation of repeated measurements obtained at a given location. To calculate,  $\sigma_{\text{R&R}}$  and  $\sigma_{\text{reproducibility}}$ , **Condition** (i.e., operator, device, material tested, etc.) variables are considered as nominal variables in Two-Way ANOVA. A typical ANOVA table is provided below.

For roller measurements,  $\sigma_{\text{repeatability}}$  is computed by considering **Pass** and **Location** as nominal variables in Two-Way ANOVA – accounting for the systematic pass effect. To calculate,  $\sigma_{\text{R&R}}$  and  $\sigma_{\text{reproducibility}}$ , **Condition** (i.e., amplitude, speed, direction, etc.) and **Location** variables are considered as nominal variables in Two-Way ANOVA. A typical ANOVA table is provided below. Pass effect on the measurement values in this case should be

statistically insignificant (as assessed by student's  $t$ -ratio and  $p$ -value) (As a rule-of-thumb, in a simple linear regression analysis between pass and roller measurement values, if  $t$ -ratio is  $< -2$  or  $> 2$  and  $p$ -value is  $< 0.05$ , the effect of pass can be considered statistically significant). To conclude that there is no effect of change in **Condition** or **Location**, the reproducibility standard deviation should be similar or less than the repeatability standard deviation.

$$\sigma_{\text{reproducibility}} = \sqrt{\max\left(0, \frac{MSC}{mI} + \frac{(I-1)MSAC}{mI} - \frac{MSE}{m}\right)}$$

$$\sigma_{\text{R\&R}} = \sqrt{\sigma_{\text{reproducibility}}^2 + \sigma_{\text{repeatability}}^2}$$

Table A.1. Typical Two-Way ANOVA Table

Source	SS (sum of square)	DOF (degree of freedom)	MS (mean square)
Location ( $I$ )	$SSA$	$I-1$	$MSA = SSA/(I-1)$
Operating Condition ( $J$ )	$SSC$	$J-1$	$MSC = SSA/(J-1)$
$I \times J$ (interaction term)	$SSAC$	$(I-1)(J-1)$	$MSAC = SSAC/(I-1)(J-1)$
Error	$SSE$	$IJ(m-1)$	$MSE = SSE/IJ(m-1)$
Total	$SSTot$	$IJm - 1$	—

A two-way ANOVA Table such as indicated above can be generated using any standard statistical analysis software (e.g., JMP, SPSS) or using Add-ins in EXCEL. An example step-by-step procedure of repeatability and reproducibility analysis using JMP statistical analysis software for roller and  $E_{LWD}$  measurement values are presented below.

## Example Calculation of Repeatability and Reproducibility Analysis for LWD Measurements [Outputs from JMP Statistical Analysis Software]

The following analysis is for LWD measurements obtained on polyurethane pads of two different stiffness (i.e., two different material conditions) using four different Zorn LWD devices.

- For this data set:
  - $m$ : number of measurements on each polyurethane pad = 33
  - $I$ : number of polyurethane pads = 2
  - $J$ : number of LWD devices = 4
- The data set is summarized as shown in Tables A.2 to A.6 below. First, the repeatability ( $\sigma_{\text{repeatability}}$ ) of each device is assessed separately, which is simply the standard deviation of the measurements obtained from each device:
  - $\sigma_{\text{repeatability}} = \text{standard deviation} = \sqrt{\sum (X - \mu)^2}$   
where  $X$  – individual measurement value, and  $\mu$  – average of the measurements
- For reproducibility analysis, the data should be pasted into JMP as shown in Figure A.1. The drop number, LWD Device Number, and Polyurethane Pad Number columns have to be selected as **Nominal** (it is highlighted as red histogram, see Figure A.1) while the measurement values (in this case deflection and modulus) have to be selected as **Continuous** (it is highlighted as blue triangle, see Figure A.1) variables.
- Then select “Fit Model” as shown in Figure A.2 which opens a “Model Specification” window. Select the measurement value as “Y”, and ADD Polyurethane Pad Number ( $I$ ), LWD Device Number ( $J$ ), and Polyurethane Pad Number \* LWD Device Number ( $I*J$ ) interaction terms as “Construct Model Effects” as shown in Figure A.2. Then select “Run Model”.
- The Two-Way ANOVA Table and  $\sqrt{MSE} = \sigma_{\text{repeatability}}$  results are shown in Figure A.3. Using the SSC, SSAC, and corresponding degree of freedom numbers calculate:

$$\sigma_{\text{reproducibility}} = \sqrt{\max\left(0, \frac{MSC}{mI} + \frac{(I-1)MSAC}{mI} - \frac{MSE}{m}\right)}$$

$$\sigma_{\text{R\&R}} = \sqrt{\sigma_{\text{reproducibility}}^2 + \sigma_{\text{repeatability}}^2}$$

- Using data in Figure A.2 and the above equations (for deflection measurements), the  $\sigma_{\text{repeatability}} = 0.044$  mm and  $\sigma_{\text{reproducibility}} = 0.034$  mm and  $\sigma_{\text{R\&R}} = 0.055$  mm.

Table A.2. LWD test measurements from device # 1 on the two polyurethane pads

Polyurethane Pad # 1				Polyurethane Pad # 2			
Number	Deflection	Modulus	Device No.	Number	Deflection	Modulus	Device No.
1	2.49	9.5	1	1	0.39	60.9	1
2	2.6	9.1	1	2	0.40	59.4	1
3	2.61	9.1	1	3	0.40	59.4	1
4	2.51	9.5	1	4	0.39	60.9	1
5	2.60	9.1	1	5	0.39	60.9	1
6	2.62	9.1	1	6	0.39	60.9	1
7	2.50	9.5	1	7	0.40	59.4	1
8	2.58	9.2	1	8	0.39	60.9	1
9	2.62	9.1	1	9	0.38	62.6	1
10	2.50	9.5	1	10	0.40	59.4	1
11	2.59	9.2	1	11	0.39	60.9	1
12	2.64	9	1	12	0.40	59.4	1
13	2.50	9.5	1	13	0.38	62.6	1
14	2.59	9.2	1	14	0.40	59.4	1
15	2.63	9	1	15	0.39	60.9	1
16	2.55	9.3	1	16	0.40	59.4	1
17	2.65	9	1	17	0.40	59.4	1
18	2.66	8.9	1	18	0.40	59.4	1
19	2.29	10.4	1	19	0.38	62.6	1
20	2.49	9.5	1	20	0.38	62.6	1
21	2.54	9.4	1	21	0.39	60.9	1
22	2.44	9.7	1	22	0.38	62.6	1
23	2.54	9.4	1	23	0.39	60.9	1
24	2.59	9.2	1	24	0.38	62.6	1
25	2.45	9.7	1	25	0.38	62.6	1
26	2.55	9.3	1	26	0.38	62.6	1
27	2.56	9.3	1	27	0.40	59.4	1
28	2.47	9.6	1	28	0.38	62.6	1
29	2.55	9.3	1	29	0.38	62.6	1
30	2.50	9.5	1	30	0.40	59.4	1
31	2.48	9.6	1	31	0.37	64.2	1
32	2.56	9.3	1	32	0.39	60.9	1
33	2.58	9.2	1	33	0.40	59.4	1
$\sigma_{\text{repeatability}}$	0.08	0.29		$\sigma_{\text{repeatability}}$	0.01	1.44	

Table A.3. LWD test measurements from device # 2 on the two polyurethane pads

Polyurethane Pad # 1				Polyurethane Pad # 2			
Number	Deflection	Modulus	Device No.	Number	Deflection	Modulus	Device No.
1	2.33	10.2	2	1	0.4	59.4	2
2	2.44	9.7	2	2	0.38	62.6	2
3	2.46	9.7	2	3	0.4	59.4	2
4	2.38	10	2	4	0.39	60.9	2
5	2.48	9.6	2	5	0.38	62.6	2
6	2.49	9.5	2	6	0.39	60.9	2
7	2.37	10	2	7	0.4	59.4	2
8	2.46	9.7	2	8	0.39	60.9	2
9	2.48	9.6	2	9	0.39	60.9	2
10	2.38	10	2	10	0.39	60.9	2
11	2.47	9.6	2	11	0.38	62.6	2
12	2.51	9.5	2	12	0.39	60.9	2
13	2.33	10.2	2	13	0.38	62.6	2
14	2.46	9.7	2	14	0.38	62.6	2
15	2.48	9.6	2	15	0.39	60.9	2
16	2.38	10	2	16	0.38	62.6	2
17	2.49	9.5	2	17	0.4	59.4	2
18	2.53	9.4	2	18	0.39	60.9	2
19	2.41	9.9	2	19	0.39	60.9	2
20	2.51	9.5	2	20	0.38	62.6	2
21	2.52	9.4	2	21	0.38	62.6	2
22	2.39	9.9	2	22	0.39	60.9	2
23	2.52	9.4	2	23	0.39	60.9	2
24	2.53	9.4	2	24	0.38	62.6	2
25	2.43	9.8	2	25	0.38	62.6	2
26	2.51	9.5	2	26	0.38	62.6	2
27	2.53	9.4	2	27	0.37	64.2	2
28	2.41	9.9	2	28	0.38	62.6	2
29	2.49	9.5	2	29	0.37	64.2	2
30	2.55	9.3	2	30	0.38	62.6	2
31	2.42	9.8	2	31	0.38	62.6	2
32	2.51	9.5	2	32	0.38	62.6	2
33	2.53	9.4	2	33	0.38	62.6	2
$\sigma_{\text{repeatability}}$	0.06	0.25		$\sigma_{\text{repeatability}}$	0.01	1.29	

Table A.4. LWD test measurements from device # 3 on the two polyurethane pads

Polyurethane Pad # 1				Polyurethane Pad # 2			
Number	Deflection	Modulus	Device No.	Number	Deflection	Modulus	Device No.
1	2.48	9.6	3	1	0.4	59.4	3
2	2.57	9.2	3	2	0.4	59.4	3
3	2.58	9.2	3	3	0.41	58	3
4	2.48	9.6	3	4	0.41	58	3
5	2.56	9.3	3	5	0.42	56.6	3
6	2.6	9.1	3	6	0.4	59.4	3
7	2.49	9.5	3	7	0.39	60.9	3
8	2.57	9.2	3	8	0.39	60.9	3
9	2.61	9.1	3	9	0.4	59.4	3
10	2.48	9.6	3	10	0.4	59.4	3
11	2.59	9.2	3	11	0.39	60.9	3
12	2.6	9.1	3	12	0.4	59.4	3
13	2.48	9.6	3	13	0.4	59.4	3
14	2.57	9.2	3	14	0.39	60.9	3
15	2.59	9.2	3	15	0.4	59.4	3
16	2.5	9.5	3	16	0.4	59.4	3
17	2.57	9.2	3	17	0.39	60.9	3
18	2.61	9.1	3	18	0.4	59.4	3
19	2.5	9.5	3	19	0.39	60.9	3
20	2.58	9.2	3	20	0.4	59.4	3
21	2.6	9.1	3	21	0.4	59.4	3
22	2.5	9.5	3	22	0.4	59.4	3
23	2.59	9.2	3	23	0.4	59.4	3
24	2.64	9	3	24	0.4	59.4	3
25	2.51	9.5	3	25	0.4	59.4	3
26	2.61	9.1	3	26	0.4	59.4	3
27	2.61	9.1	3	27	0.4	59.4	3
28	2.53	9.4	3	28	0.39	60.9	3
29	2.61	9.1	3	29	0.39	60.9	3
30	2.62	9.1	3	30	0.39	60.9	3
31	2.53	9.4	3	31	0.38	62.6	3
32	2.6	9.1	3	32	0.39	60.9	3
33	2.62	9.1	3	33	0.39	60.9	3
$\sigma_{\text{repeatability}}$	0.05	0.19		$\sigma_{\text{repeatability}}$	0.01	1.13	

Table A.5. LWD test measurements from device # 4 on the two polyurethane pads

Polyurethane Pad # 1				Polyurethane Pad # 2			
Number	Deflection	Modulus	Device No.	Number	Deflection	Modulus	Device No.
1	2.47	9.6	4	1	0.41	58	4
2	2.56	9.3	4	2	0.41	58	4
3	2.59	9.2	4	3	0.41	58	4
4	2.48	9.6	4	4	0.41	58	4
5	2.57	9.2	4	5	0.41	58	4
6	2.6	9.1	4	6	0.41	58	4
7	2.49	9.5	4	7	0.42	56.6	4
8	2.6	9.1	4	8	0.42	56.6	4
9	2.6	9.1	4	9	0.41	58	4
10	2.5	9.5	4	10	0.41	58	4
11	2.59	9.2	4	11	0.43	55.3	4
12	2.63	9	4	12	0.4	59.4	4
13	2.51	9.5	4	13	0.4	59.4	4
14	2.61	9.1	4	14	0.42	56.6	4
15	2.61	9.1	4	15	0.4	59.4	4
16	2.51	9.5	4	16	0.41	58	4
17	2.6	9.1	4	17	0.4	59.4	4
18	2.63	9	4	18	0.42	56.6	4
19	2.52	9.4	4	19	0.4	59.4	4
20	2.63	9	4	20	0.4	59.4	4
21	2.64	9	4	21	0.39	60.9	4
22	2.49	9.5	4	22	0.39	60.9	4
23	2.61	9.1	4	23	0.41	58	4
24	2.65	9	4	24	0.41	58	4
25	2.5	9.5	4	25	0.41	58	4
26	2.56	9.3	4	26	0.41	58	4
27	2.62	9.1	4	27	0.42	56.6	4
28	2.49	9.5	4	28	0.43	55.3	4
29	2.59	9.2	4	29	0.43	55.3	4
30	2.65	9	4	30	0.41	58	4
31	2.52	9.4	4	31	0.41	58	4
32	2.64	9	4	32	0.41	58	4
33	2.64	9	4	33	0.4	59.4	4
$\sigma_{\text{repeatability}}$	0.06	0.21		$\sigma_{\text{repeatability}}$	0.01	1.39	

Table A.6. LWD test measurements from device # 5 on the two polyurethane pads

Polyurethane Pad # 1				Polyurethane Pad # 2			
Number	Deflection	Modulus	Device No.	Number	Deflection	Modulus	Device No.
1	2.47	9.6	5	1	0.4	59.4	5
2	2.57	9.2	5	2	0.39	60.9	5
3	2.6	9.1	5	3	0.39	60.9	5
4	2.59	9.2	5	4	0.37	64.2	5
5	2.58	9.2	5	5	0.38	62.6	5
6	2.61	9.1	5	6	0.38	62.6	5
7	2.48	9.6	5	7	0.37	64.2	5
8	2.5	9.5	5	8	0.38	62.6	5
9	2.6	9.1	5	9	0.38	62.6	5
10	2.5	9.5	5	10	0.38	62.6	5
11	2.59	9.2	5	11	0.37	64.2	5
12	2.61	9.1	5	12	0.37	64.2	5
13	2.49	9.5	5	13	0.37	64.2	5
14	2.59	9.2	5	14	0.38	62.6	5
15	2.61	9.1	5	15	0.38	62.6	5
16	2.51	9.5	5	16	0.37	64.2	5
17	2.6	9.1	5	17	0.37	64.2	5
18	2.62	9.1	5	18	0.37	64.2	5
19	2.47	9.6	5	19	0.4	59.4	5
20	2.59	9.2	5	20	0.39	60.9	5
21	2.62	9.1	5	21	0.39	60.9	5
22	2.5	9.5	5	22	0.38	62.6	5
23	2.57	9.2	5	23	0.38	62.6	5
24	2.63	9	5	24	0.4	59.4	5
25	2.51	9.5	5	25	0.38	62.6	5
26	2.61	9.1	5	26	0.38	62.6	5
27	2.63	9	5	27	0.39	60.9	5
28	2.51	9.5	5	28	0.39	60.9	5
29	2.64	9	5	29	0.38	62.6	5
30	2.66	8.9	5	30	0.39	60.9	5
31	2.53	9.4	5	31	0.37	64.2	5
32	2.61	9.1	5	32	0.38	62.6	5
33	2.64	9	5	33	0.39	60.9	5
$\sigma_{\text{repeatability}}$	0.06	0.21		$\sigma_{\text{repeatability}}$	0.01	1.53	

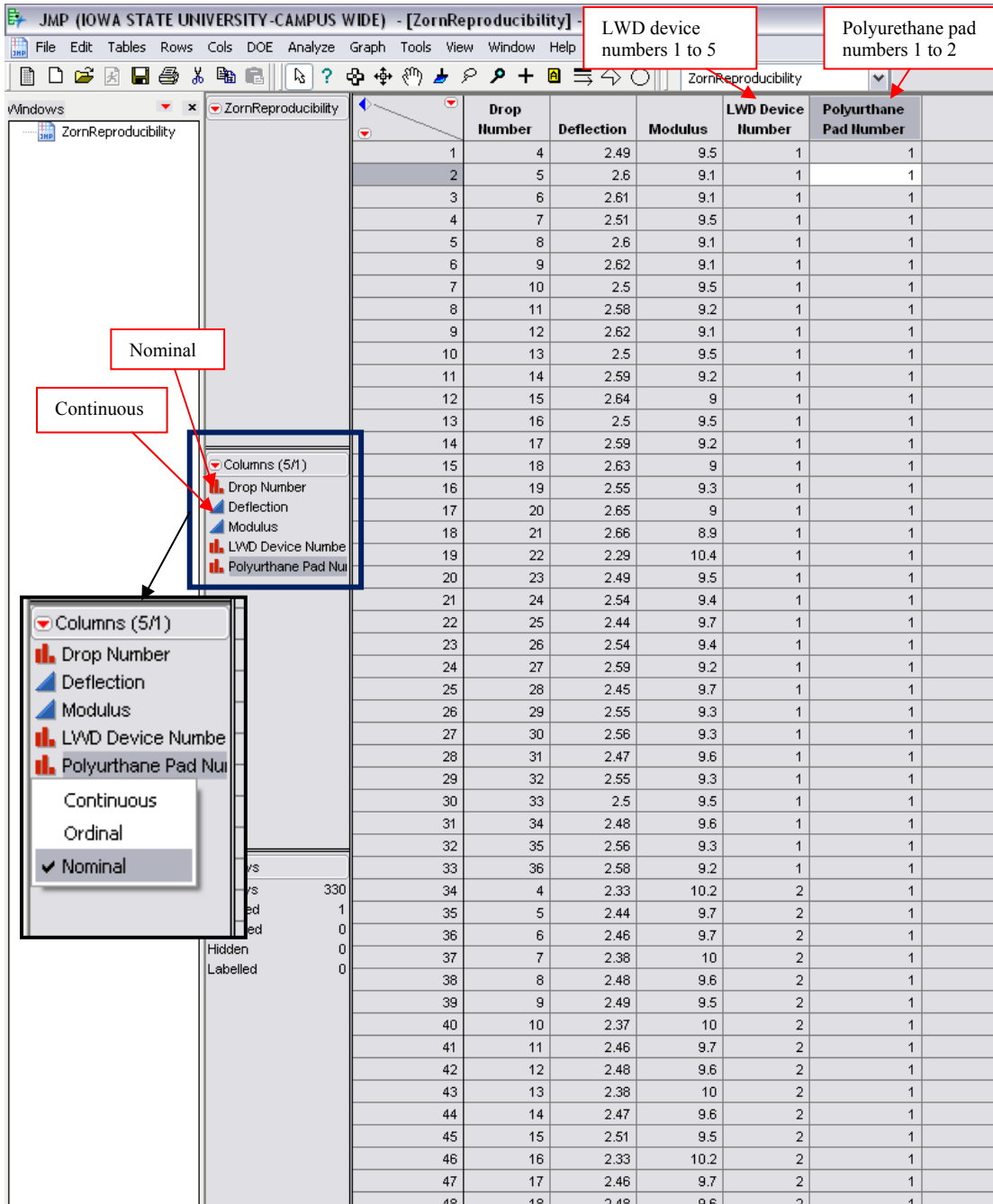


Figure A.1: Data organization in JMP for reproducibility analysis

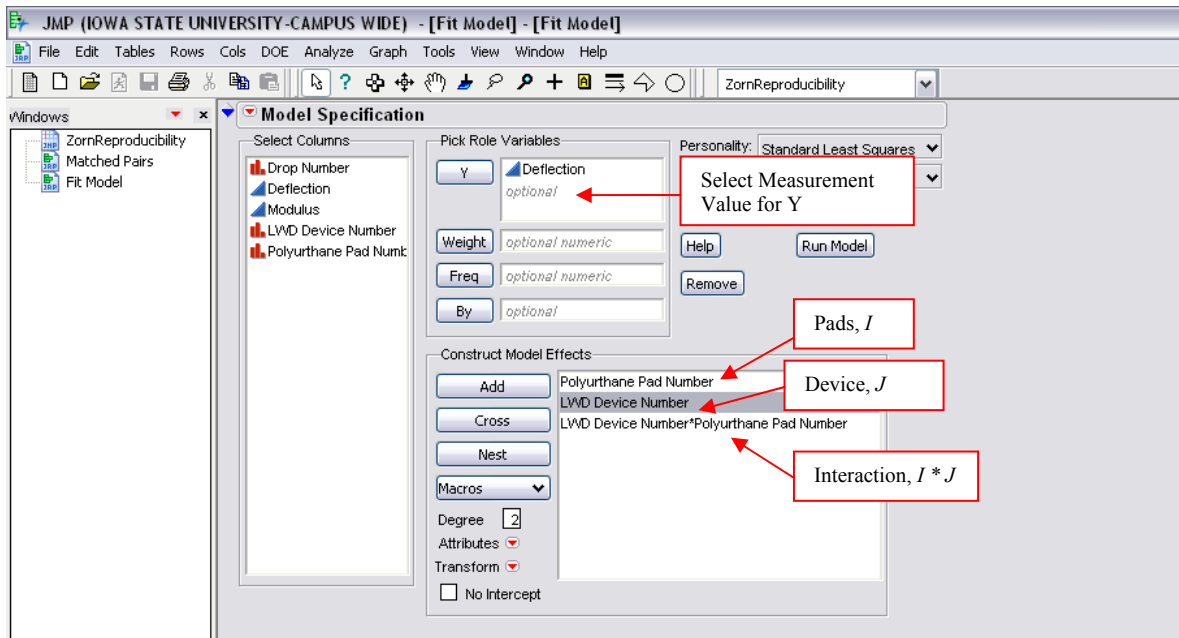
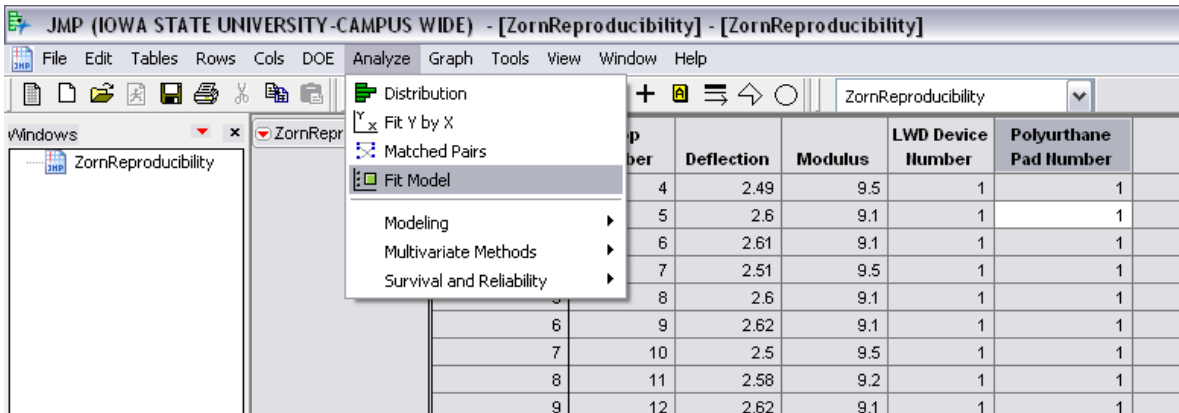


Figure A.2: Steps for model fitting and selection of X and Y variables for analysis in JMP

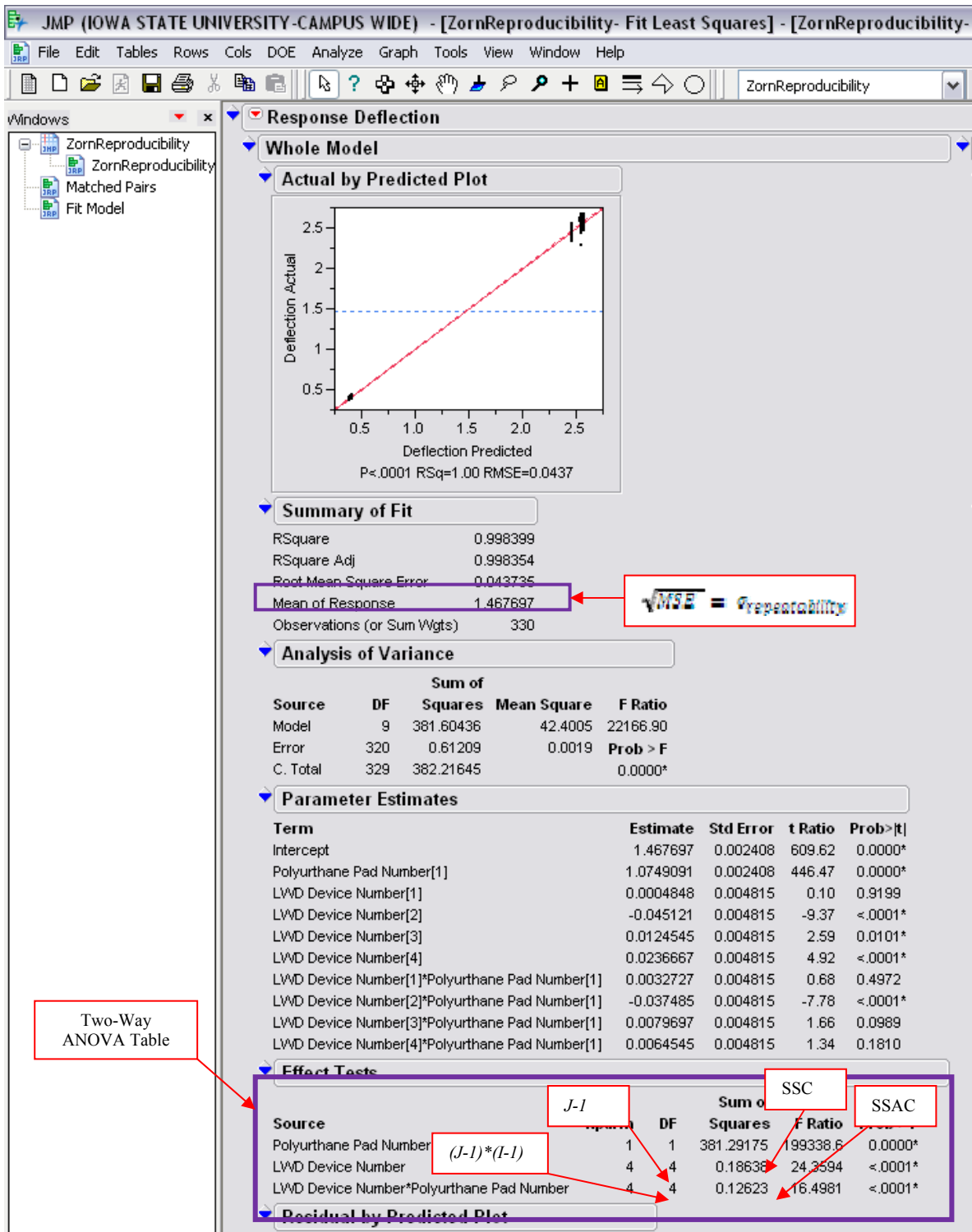


Figure A.3: Two-Way ANOVA table output in JMP

## Example Calculation of Repeatability and Reproducibility Analysis for Roller Measurements [Outputs from JMP Statistical Analysis Software]

The following analysis is for roller measurements (MDP\*) obtained over a 50 m long compacted test strip with variable stiffness in two different speeds (nominal 3.2 km/h and 6.4 km/h) at a constant amplitude setting ( $a = 0.9$  mm). The data is analyzed for repeatability of MDP\* at constant speed settings and reproducibility of MDP\* with change in speed.

- For this data set:
  - $m$ : number of passes on the test strip in each setting = 5
  - $I$ : number of data points across the test strip = 164
  - $J$ : total number of speed settings = 2
- First, the repeatability ( $\sigma_{\text{repeatability}}$ ) of MDP\* at each speed setting is computed. As explained earlier, number of **Passes** and **Location** are considered as nominal variables and a Two-Way ANOVA is performed accounting for any systematic pass effect, to compute  $\sigma_{\text{repeatability}}$ . The data must be organized into columns of Pass, Location [location represents data points across the test strip], and Measurement Values as shown in Figure A.4. One challenge with organizing the Location column is that the data points obtained from different passes are not collected at the exact same location. To overcome this problem, the data should be processed in such a way that an average data is assigned to a preset grid point (e.g., 0.3 m as used in this report) along the roller path. The grid point along the roller path represents an average of IC-MVs that falls within a window of size that is half the size of the grid length (in this case it is 0.15 m) in forward and backward directions. The approach is validated in the report (see Chapter 3).
- The Pass and Location columns have to be selected as **Nominal** (it is highlighted as red histogram, see Figure A.4) while the measurement values (in this case MDP\*) have to be selected as **Continuous** (it is highlighted as blue triangle, see Figure A.4) variables.
- Then select “Fit Model” as shown in Figure A.5 which opens a “Model Specification” window. Select the measurement value as “Y”, and ADD Pass and Location Number as “Construct Model Effects” as shown in Figure A.4. Then select “Run Model”. The Two-Way ANOVA Table and  $\sqrt{MSE}$  ■  $\sigma_{\text{repeatability}}$  results are shown in Figure A.5.
- For reproducibility analysis, select at least three passes data that has statistically negligible effect of pass. Organize the data as shown in Figure A.6 in columns of Pass, Location, Measurement Value (in this case MDP\*) and Speed. The Pass, Location, and Speed columns have to be selected as **Nominal** while the measurement value column have to be selected as **Continuous** (see Figure A.6).
- Then select “Fit Model” and select the measurement value as “Y”, and ADD Location ( $I$ ), Speed ( $J$ ) and Location \* Speed ( $I*J$ ) interaction terms as “Construct Model Effects” as shown in Figure A.7. Then select “Run Model”.

- The Two-Way ANOVA Table and  $\sqrt{MSE} = \sigma_{\text{repeatability}}$  results are shown in Figure A.3. Using the SSC, SSAC, and corresponding degree of freedom numbers calculate:

$$\sigma_{\text{repeatability}} = \sqrt{\max\left(0, \frac{MSC}{ml} + \frac{(I-1)MSAC}{ml} - \frac{MSE}{m}\right)}$$

$$\sigma_{\text{R\&R}} = \sqrt{\sigma_{\text{repeatability}}^2 + \sigma_{\text{reproducibility}}^2}$$

- Using data in Figure A.6 and the above equations (for MDP\*), the  $\sigma_{\text{repeatability}} = 5.9$ ,  $\sigma_{\text{reproducibility}} = 18.2$  mm and  $\sigma_{\text{R\&R}} = 19.1$  mm.
- Results indicate that the contribution of  $\sigma_{\text{repeatability}}$  to the overall variability  $\sigma_{\text{R\&R}}$  is greater than the contribution of  $\sigma_{\text{reproducibility}}$ . For this data set, the impact of change in speed on MDP\* is considered statistically significant.

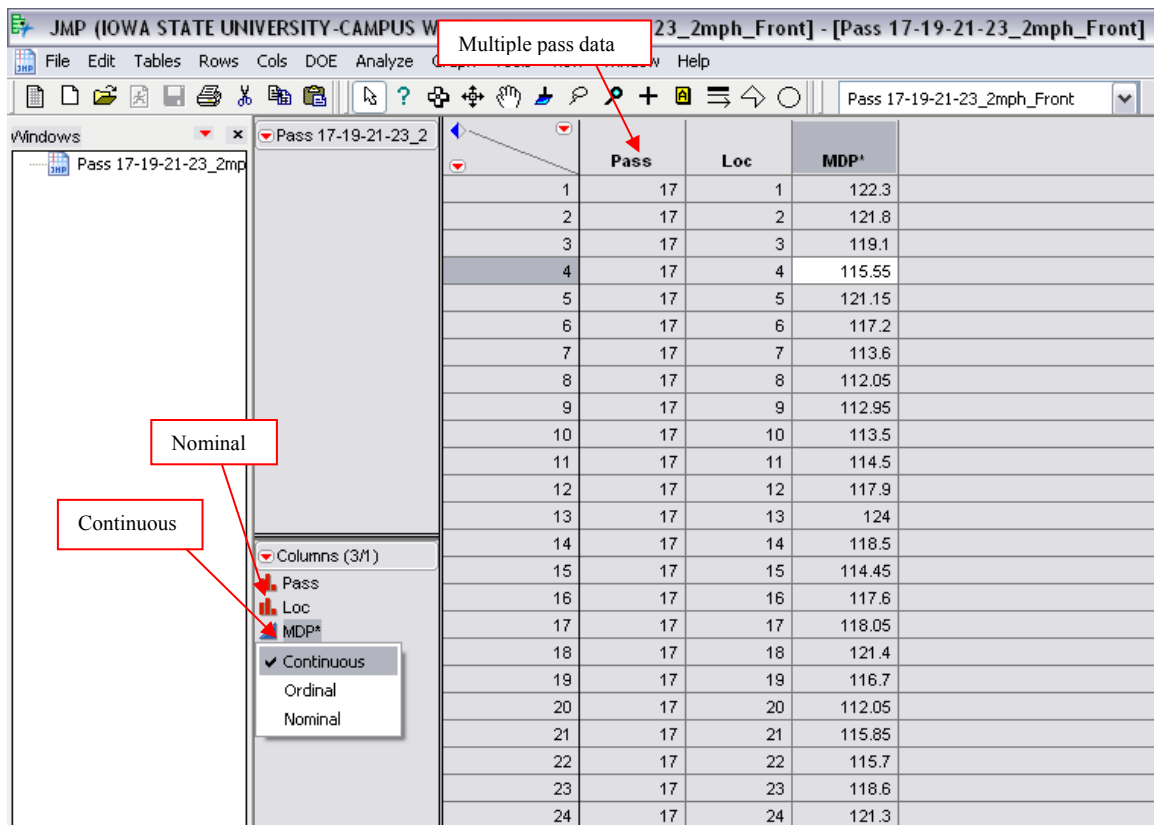


Figure A.4: Data organization in JMP for repeatability analysis of roller measurement values

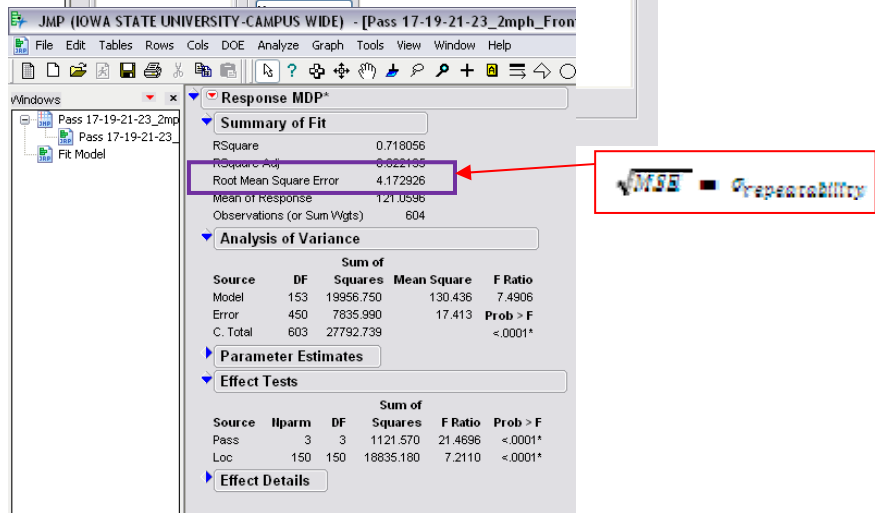
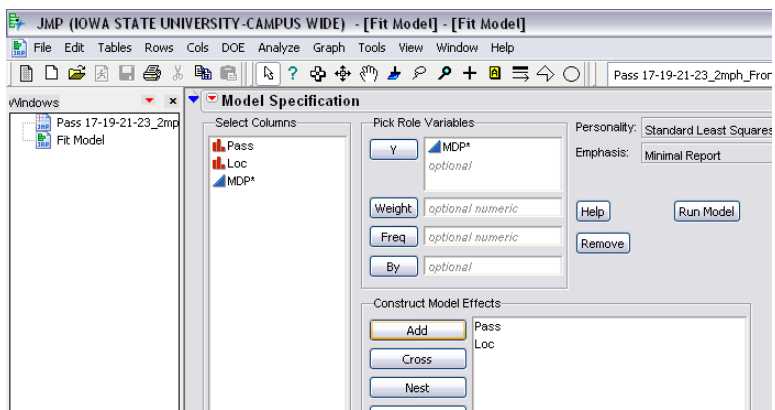
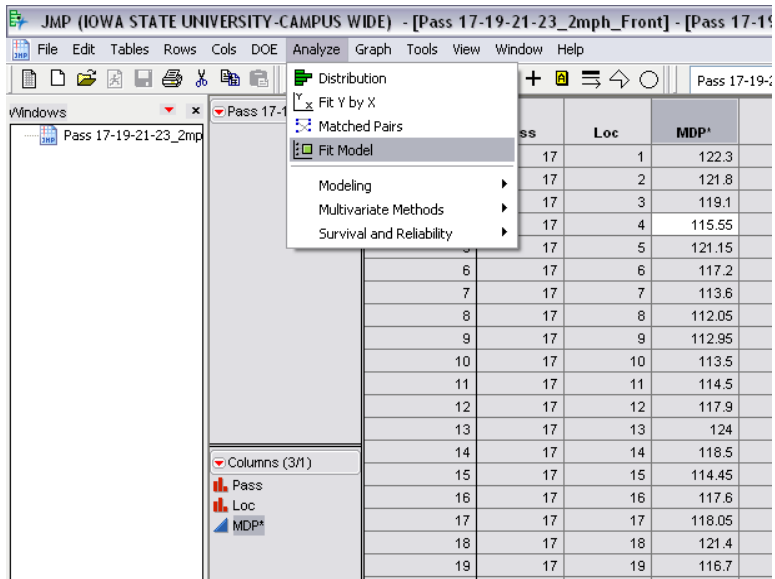


Figure A.5: Repeatability analysis procedure in JMP

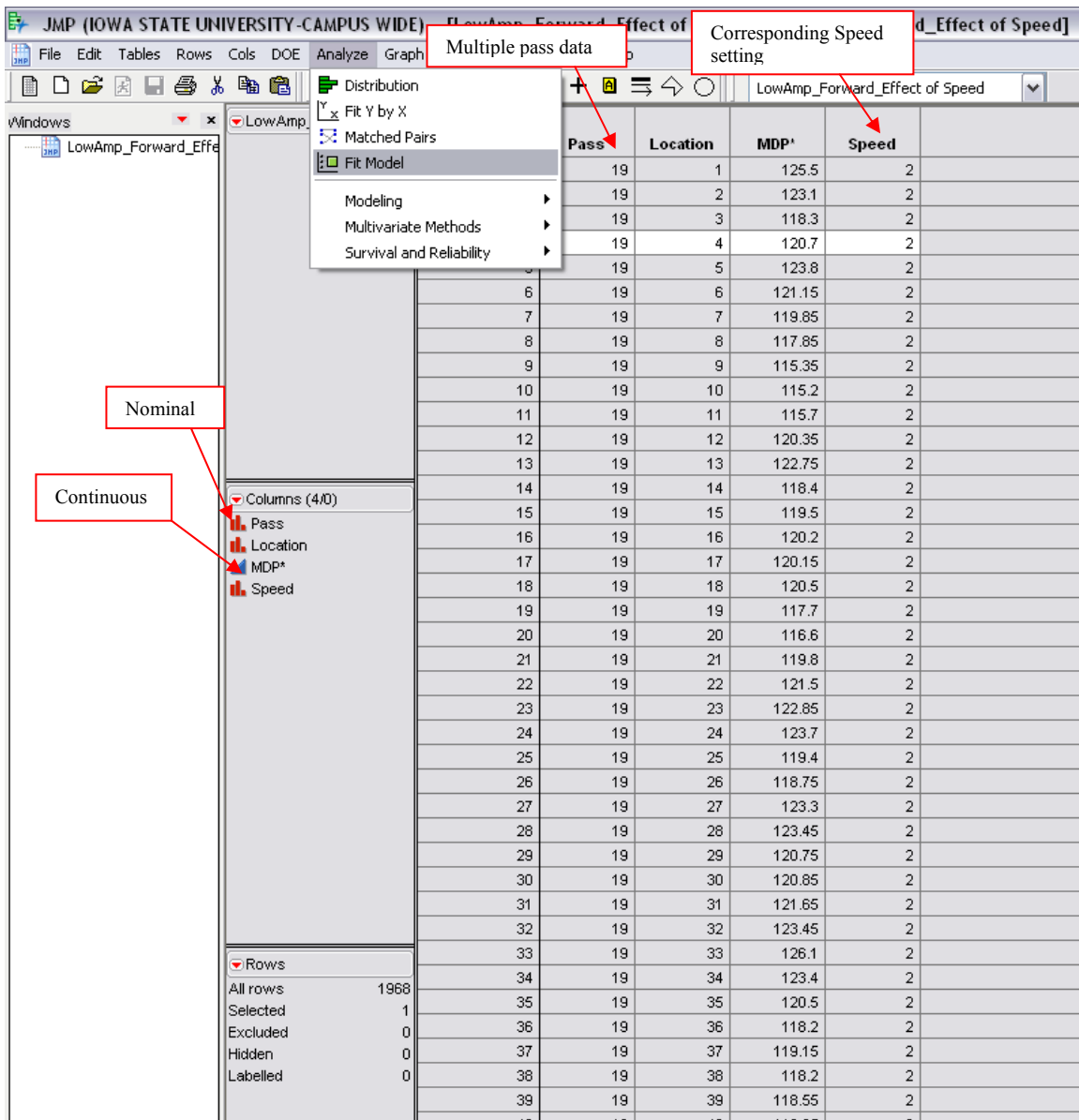


Figure A.6: Data organization in JMP for reproducibility analysis

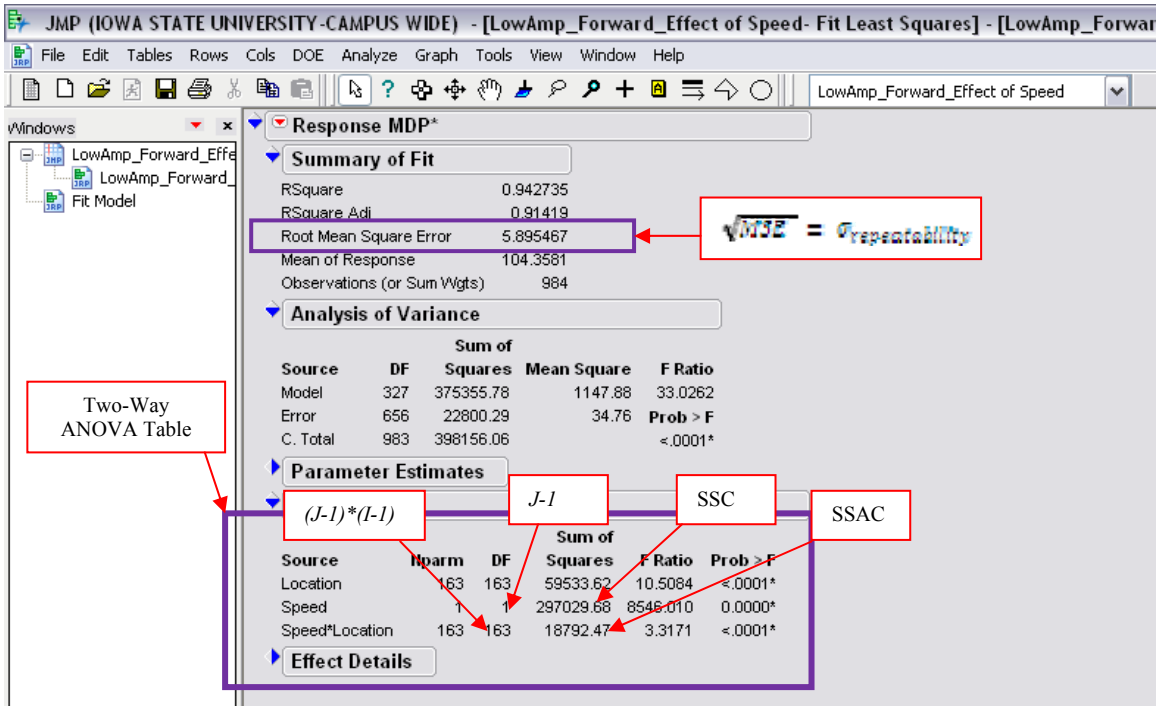
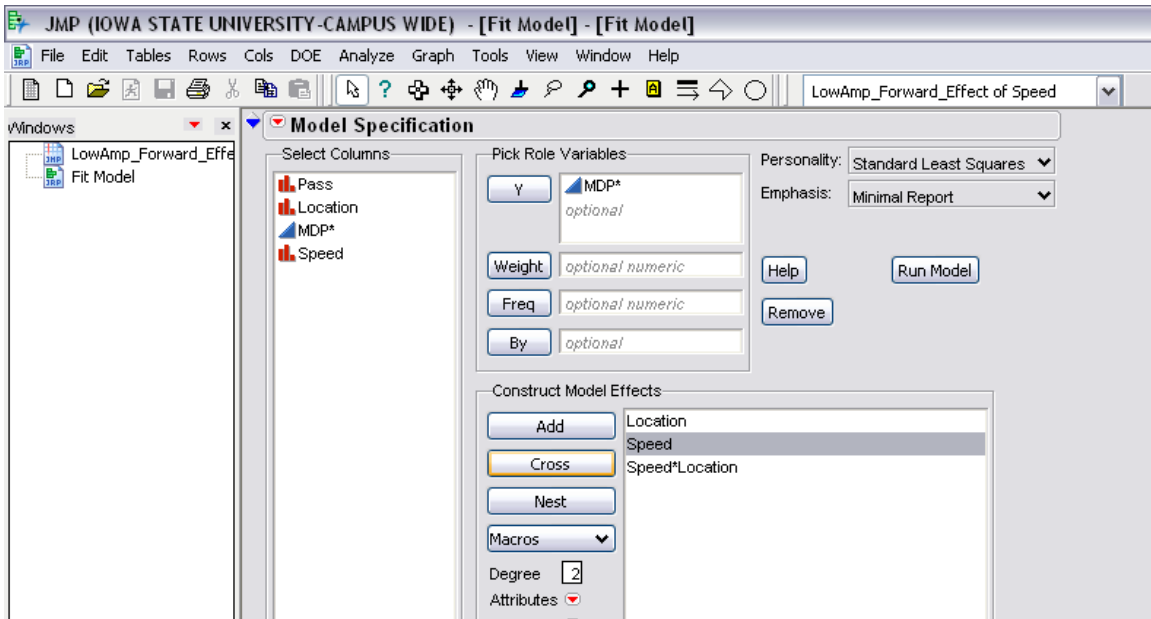


Figure A.7: Results of Two-Way ANOVA for roller measurement reproducibility analysis